Dissertation
submitted to the
Combined Faculty of Natural Sciences and Mathematics
of the Ruprecht-Karls-Universität of Heidelberg, Germany
for the degree of
Doctor of Natural Sciences

Put forward by
Gonzalo Alonso Álvarez
born in Zaragoza, Spain
Oral examination: 20.07.2020

Axions and other light dark matter candidates

Referees: Prof. Dr. Joerg Jaeckel
Prof. Dr. Arthur Hebecker

Zusammenfassung

Die Entschlüsselung des Rätsels der dunklen Materie ist eines der wichtigsten Ziele der modernen Physik. In dieser Dissertation werden neue Ansätze erforscht, die die Hypothese, dass dunkle Materie aus leichten Skalarteilchen besteht, mit anderen offenen Fragen der Teilchenphysik und der Kosmologie in Verbindung setzen.

Im ersten Teil werden Szenarien betrachtet, in denen die dunkle Materie eine Teilchen-Antiteilchen-Asymmetrie enthält. Exemplarisch wird untersucht, wie eine solche Asymmetrie im Fall skalarer dunkler Materie erzeugt werden kann. Daraufhin wird ein Modell vorgestellt, in welchem Baryogenese und asymmetrische dunkle Materie einen gemeinsamen Ursprung haben, der mit der Physik neutraler B-Mesonen zusammenhängt.

Im zweiten Teil wird der Schwerpunkt auf Axionen gelegt.Hierzu wird zunächst die kosmologische Stabilität axionartiger Teilchen sichergestellt und dann gezeigt, wie ein nicht-kanonischer kinetischer Term die Produktion dieser Art von dunkler Materie verstärken kann. Schließlich wird die Phänomenologie von Axionen in Teilchenbeschleunigern sowie ihre Kopplung an elektroschwache Eichbosonen untersucht.

Der dritte und letzte Teil befasst sich mit dem Zusammenhang zwischen der Produktion leichter Bosonteilchen und kosmologischer Inflation. Eine nicht-minimale Kopplung zwischen derartigen Teilchen und dem Gravitationsfeld führt zu einer vielseitigen Dynamik während der Inflation und resultiert in vorhersagbaren Eigenschaften der subgalaktischen Verteilung dunkler Materie.

Abstract

Unveiling the mystery of dark matter is one of the most sought-after goals of modern physics. Working towards this aim, this thesis explores new links between the possibility that dark matter is made up of light scalar particles and other open questions in particle physics and cosmology.

In the first part of the thesis, scenarios in which the dark matter contains a particle-antiparticle asymmetry are considered. As an example, the production of such an asymmetry in a model of scalar dark matter is studied. Furthermore, a setup is presented where baryogenesis and asymmetric dark matter have a common origin linked to the dynamics of neutral B mesons.

In the second part, the emphasis is put on axions. After assuring the cosmological stability of general axion-like particles, a non-canonical kinetic term is introduced, which leads to an enhanced production of this kind of dark matter. Finally, the collider phenomenology of axions and their coupling to electroweak gauge bosons is scrutinized.

The third and final part is devoted to the production of light bosons during inflation. A non-minimal coupling to gravity leads to rich inflationary dynamics and precise predictions regarding the properties of the sub-galactic distribution of dark matter.

Contents

II Dark matter and axions

III Dark matter and inflation

Preface

The research presented in this thesis was conducted predominantly at the Institute for Theoretical Physics at Heidelberg University from September 2016 to May 2020.

The contents of Chapters 2 to 8 are result of work in collaboration with other authors as listed below and have previously been published as [1, 2, 3, 4, 5, 6, 7]. They are reproduced here with permission from the publishers and the coauthors.

My role in the first two of the articles [1, 2] is that of the sole principal author, while in the rest principal authorship is shared with other coauthors. A statement containing a detailed description of my contribution to each multi-authored paper is provided at the beginning of each chapter. These statements have been shared with and agreed upon by all of the coauthors.

[1] Gonzalo Alonso-Álvarez and Joerg Jaeckel. "Exploring axionlike particles beyond the canonical setup". *Phys. Rev.* D98.2 (2018), 023539. arXiv: 1712.07500 [hep-ph]

[2] Gonzalo Alonso-Álvarez and Joerg Jaeckel. "Lightish but clumpy: scalar dark matter from inflationary fluctuations". *JCAP* 1810.10 (2018), 022. arXiv: 1807.09785 [hep-ph]

[3] G. Alonso-Álvarez, M.B. Gavela, and P. Quilez. "Axion couplings to electroweak gauge bosons". *Eur. Phys. J. C* 79.3 (2019), 223. arXiv: 1811.05466 [hep-ph]

[4] Gonzalo Alonso-Álvarez, Joerg Jaeckel, and Thomas Hugle. "Misalignment & Co.: (Pseudo-)scalar and vector dark matter with curvature couplings". *JCAP* 02 (2020), 014. arXiv: 1905.09836 [hep-ph]

[5] Gonzalo Alonso-Álvarez et al. "Very Light Asymmetric Dark Matter". *JCAP* 09 (2019), 003. arXiv: 1906.00969 [hep-ph]

[6] Gonzalo Alonso-Álvarez et al. "A Supersymmetric Theory of Baryogenesis and Sterile Sneutrino Dark Matter from B Mesons". *JHEP* 03 (2020), 046. arXiv: 1907.10612 [hep-ph]

[7] Gonzalo Alonso-Álvarez et al. "On the Wondrous Stability of ALP Dark Matter". *JCAP* 03 (2020), 052. arXiv: 1911.07885 [hep-ph]

Chapter 1

Introduction and background

Over the past few decades, our understanding of the dynamics of the Universe has rapidly grown to become comparable to that of the subatomic constituents of matter. The similarities are outstanding - both in the successes of the respective theories and in their shortcomings. The field of cosmology has developed its own *Standard Model*, following the example of particle physics. Both Standard Models represent an effort to achieve a self-consistent description of the physical processes that we observe in the cosmos and in the laboratory. This is not to say that these models can encompass all that there is: they come with limitations in their scope and completeness. In particular, current understanding favors the interpretation of the Standard Model of particle physics as an effective description of the physics above a certain length scale, rather than as a complete theory. Similarly, the Standard Model of cosmology gives an effective description of many phenomena, recurring to phenomenological equations of state for the different fluids that populate the Universe, rather than explaining the fundamental nature of such substances.

In this situation, there is a clear first way forward: to convert these effective theories into more fundamental ones, either by extending the range of validity of their descriptions or by identifying the underlying physical nature of their constituents. It is on this aim that the main purpose of this thesis focuses: to unveil the particle nature of one of the main unidentified components of the Universe, the dark matter.

However, this is not the only possible course of action. The established Standard Models as they are contain a number of apparent contradictions and incompletenesses, especially when confronted with each other. Many of them stem from unexpected experimental observations, like the overabundance of matter versus antimatter in the Universe or the lack of violation of time reversal symmetry in the strong interactions. Aside from being inconsistencies of the theory with respect to experiments that deserve a resolution of their own, they may constitute invaluable hints as to what lies beyond the Standard Models. In this thesis, we follow this line of thought and set to study potential connections between some of these quandaries and the nature of dark matter.

After presenting and motivating our general approach, in the remainder of this chapter we introduce some of the particular puzzles that are addressed in the main body of the work. This is done by reviewing the established knowledge that sets the stage for the later studies, making an emphasis on the particular questions that are addressed by the novel results of this thesis.

1.1 Dark matter

The overarching physics goal of all the research presented in this thesis is to identify the particle nature of the dark matter. To the level that is presently understood, dark matter is an effective explanation for a series of gravitational observations that are consistent with the existence of a pressureless, non-relativistic fluid that currently makes up about 25% of the energy density of the Universe. The upside of this definition is that it frees us from any prejudice regarding its particle (or non-particle) nature or its origin. At the same time, it motivates us to briefly review the cosmological and astrophysical observables on which grounds the existence of dark matter is postulated.

Probably, the most robust evidence for the existence of dark matter comes from the largest cosmological scales to which we have access, which are the ones encoded in the cosmic microwave background [8, 9] (or CMB for short). The CMB is composed of photons which freely propagate to us since the time when protons and electrons combined intro neutral atoms, causing the Universe to became transparent to most of the electromagnetic radiation. It therefore contains information about the conditions of the Universe at this early stage. In particular, it is sensitive to the dynamics of the oscillations of the primordial plasma made up of baryons and photons, which are driven by two opposing forces: gravity, which causes infall and therefore compression of the plasma, and radiation pressure, which counteracts the collapse and produces rarefaction. The balance between these two forces produces a distinctive pattern of peaks and valleys in the typical amplitude of the temperature anisotropies of the CMB as a function of their spatial size.

By measuring the relative height of these *acoustic peaks*, one can deduce the amount of gravitational matter that was present in the early Universe. The measurements [10, 11, 12] show that, in addition to the gravitational potential of baryons and photons, there needs to exist a large extra collapsing force that enhances the compressions with respect to the rarefactions. This can be produced by a fluid that contributes to the gravitational infall but not to the pressure, and so dark matter fulfills these requirements by definition. The CMB data is so rich that it allows for a very precise estimation of the amount of dark matter that needs to be present [12],

$$\Omega_c = 0.2589 \pm 0.0057, \tag{1.1.1}$$

meaning that about 1/4 of the energy density of the Universe is in the form of dark matter, which is about 5 times more abundant than ordinary baryonic matter. The imprint of dark matter in these compressions and rarefactions of the primordial plasma has also been observed

in the distribution of baryons at very large scales, which features the so-called *baryon acoustic oscillations* [13].

In agreement with the CMB, a large number of other large-scale cosmological observables require the existence of an additional gravitational component. The *large scale structure* of the Universe, that is, the distribution of galaxies and galaxy clusters in it, has been (partially) mapped with a combination of surveys, like the Sloan Digital Sky Survey [14], the Dark Energy Survey [15], and many more. The hierarchical nature of the structures observed cannot be reproduced in simulations (e.g. [16, 17]) without the existence of dark matter.

A more direct evidence is obtained from gravitational lensing: the light of distant sources, like quasars or galaxies, reaches us traveling through geodesics which are modified by the presence of gravitating energy density (see e.g. [18]). Once more, the existence of a large fraction of dark matter is required to explain the observed light patterns.

Confirmation of the existence of dark matter has also been found in smaller environments, like galaxies and galaxy clusters. The study of dynamics of galaxies within a cluster [19] (see [20] for recent results) consistently show that a large amount of dark matter is present in these environments. Similar studies have been made at the level of individual galaxies [21] (see also [22]) by observing the motion of individual stars or star clusters, throwing the same conclusion: virtually every galaxy is embedded within a halo of dark matter that significantly outweighs the visible matter.

All these observations, and more that have not been mentioned here, give extremely robust evidence for the existence of dark matter over many length and time scales. They also delineate its main properties: it needs to be sufficiently cold, that is, to behave as a non-relativistic and pressureless fluid for all gravitational processes; it needs to be dark, i.e. to only interact very weakly with ordinary matter; and it needs to be stable on cosmological time scales. This effective description is precisely what has been accepted as part of the cosmological Standard Model, and is summarized in the term "cold dark matter" [23, 24, 25, 26].

This thesis aims to supersede this effective description and identify suitable microscopic models that can explain the fundamental nature of dark matter. In order to achieve this task, it is necessary to go beyond the general characterization and examine the detailed properties of dark matter.

Of particular importance for this thesis is the question of whether dark matter enjoys any non-gravitational interaction. All the evidence delineated above only requires that dark matter gravitates, and furthermore, numerous experiments aiming for direct [27] and indirect [28] detection of dark matter, together with terrestrial experiments [29] and astrophysical observations [30], rule out the possibility that dark matter has sizable long-range interactions of other kinds. While Parts I and II of this thesis assume that the dark matter has at least some feeble interaction with ordinary matter, Part III explores the possibility that non-gravitational couplings are completely absent. As we will see, even in this most minimal scenario, interesting cosmological phenomenology arises on the account of purely gravitational interactions. In particular, a connection between the physics of dark matter production during inflation and its current distribution in small sub-galactic scales emerges.

Other questions that are investigated throughout this work are:

- Is dark matter absolutely stable or only very long lived compared to the age of the Universe? In the absence of absolute stability, a sufficiently long lifetime may be achieved in non-trivial ways, either by the protection of a conserved charge as in Chapter 2, perhaps aided by kinematic relations as in Chapter 3, or by a conspiracy of effects like in Chapter 6. Furthermore, pairwise annihilation of dark matter particles is generally possible and can lead to indirect signals, as is exemplified in Chapter 3.

- How is dark matter distributed on small sub-galactic scales? Although, as pointed out above, the role of dark matter in the formation of the large-scale structure of the Universe is well established, the clustering properties of dark matter in smaller environments, like inside galaxies, remain to be mapped and understood. Dark matter could be distributed in a homogeneous and diffuse manner, but it could also form dense clumps. This is exactly what happens in the models of Chapters 7 and 8, in which the inflationary origin of dark matter contributes to enhance its density fluctuations at small scales.

- Is there any relevant interplay between dark matter and astrophysical bodies like neutron stars? Astrophysical objects can serve as enormous "detectors" for dark matter that interacts with nucleons or leptons, as is the case of the model presented in Chapter 3. What is more, light dark matter particles can be produced in stellar bodies and affect their internal dynamics, as is discussed in Chapter 6 for the case of axions and axion-like particles.

- Can dark matter be produced in terrestrial experiments like particle colliders? If that is the case, then the properties of the dark matter particles can be studied in laboratory experiments in order to complement cosmological observations. We take advantage of this possibility in Chapters 2, 3 and 6 to nail down some of the features of the models discussed that would otherwise be difficult to test in astrophysical environments.

In order to answer all of these questions, in this thesis we construct physically realistic particle physics models for dark matter and explore their properties. Of course, this is a futile task without some sort of guiding principle, as there are many more potential models than there are answers to the above questions. We therefore focus on dark matter models that are well motivated because they can address other shortcomings in our understanding of cosmology or particle physics. In the remainder of the introduction, we present some of these shortcomings and motivate how they can be interpreted as guidelines for constructing dark matter models.

1.2 Dark matter and particle asymmetries

Much of the underlying physics behind the dark matter models discussed in this thesis have to do with discrete spacetime symmetries: parity, charge conjugation, time reversal, and

combinations thereof. In addition to the very direct connections in Part I, much of the interest in light dark matter particles in general is motivated by considerations regarding these symmetries. As is explained in Section 1.3, axions are a prime example of this. We therefore devote some time to present the basic implementation of these discrete symmetries in quantum field theory and some of their most important phenomenological consequences.

1.2.1 Discrete symmetries

Parity ($\mathcal{P}$) and time reversal ($\mathcal{T}$) are special cases of Lorentz transformations. The Lorentz group L is composed of coordinate transformations that leave the Minkowski metric tensor η invariant, i.e. that satisfy $\eta = \Lambda^T \eta \, \Lambda$. It is divided into four disconnected parts, depending on whether $\det \Lambda = \pm 1$ (proper/improper transformations) and $\Lambda^0_0 \geq 1$ or $\Lambda^0_0 \leq -1$ (orthochronous/antichronous transformations). Proper orthochronous transformations form the subgroup $L^\uparrow_+$, and all other transformations in the Lorentz group can be obtained from $L^\uparrow_+$ by using two discrete transformations: parity and time reversal, respectively given by

$$\mathcal{P} = \begin{pmatrix} 1 & 0 & 0 & 0 \\ 0 & -1 & 0 & 0 \\ 0 & 0 & -1 & 0 \\ 0 & 0 & 0 & -1 \end{pmatrix}, \qquad \text{and} \qquad \mathcal{T} = \begin{pmatrix} -1 & 0 & 0 & 0 \\ 0 & 1 & 0 & 0 \\ 0 & 0 & 1 & 0 \\ 0 & 0 & 0 & 1 \end{pmatrix}. \tag{1.2.1}$$

Physically, parity can be identified with spatial reflections, while time reversal corresponds to running the flow of time backwards. As we later discuss, it is remarkable that nature is invariant under the proper orthochronous Lorentz group but not the full Lorentz group, as parity and time reversal have both been experimentally observed to be violated [31, 32, 33, 34].

Charge conjugation ($\mathcal{C}$) is more difficult to formally define in a general way. Heuristically, we want to identify charge conjugation symmetry with the exchange of particles and their antiparticles, which can also be understood as shifting to the conjugate representation of all symmetry groups under which a field transforms (including gauge, global, and Lorentz symmetries). This definition will be sufficient for all of our purposes, but it is important to remark that formally, $\mathcal{C}$ (and so also the product $\mathcal{CP}$) can be rigorously defined from $\mathcal{CPT}$ symmetry, which can be defined on general grounds for any quantum field theory (see [35] for a pedagogical discussion). Indeed, $\mathcal{CPT}$ is a fundamental symmetry which is proved to be conserved in any Lorentz-invariant and local quantum field theory with a hermitian Hamiltonian [36].

In quantum field theory, symmetries are understood to be transformations $\psi \to \psi'$ of elements of some Hilbert space under which the physics is invariant. As was shown by Wigner [37], any symmetry can be represented as an operator W such that $\psi' = W\psi$. Furthermore, the operator is either linear and unitary, or anti-linear and anti-unitary. We will denote the parity, time reversal, and charge conjugation operators as $\hat{P}$, $\hat{T}$, and $\hat{C}$, respectively. It is easy to see that $\hat{P}$ and $\hat{C}$ are unitary, while $\hat{T}$ is anti-unitary.

Taking all the above into account, the transformation properties of quantum fields under these discrete symmetries can be readily derived (see, for instance, [38]). Given the fact that this thesis mostly deals with scalar fields, we focus on them in what follows, and point the interested reader to [38] for the transformation rules of vector and spinor fields.

- *Parity.* Under $x \to x_P = (x^0, -\vec{x})$, a scalar field transforms as

$$\phi^P(x) \equiv \hat{P}\,\phi(x)\,\hat{P}^{-1} = \eta_P\,\phi(x_P), \tag{1.2.2}$$

  where η_P satisfies $|\eta_P| = 1$ and is therefore a phase that determines the intrinsic parity of ϕ. If ϕ is a real field, it is clear that $\eta_P = \pm 1$ and the field is either a *scalar* (for $\eta_P = 1$) or a *pseudoscalar* (for $\eta_P = -1$). On the other hand, if ϕ is a complex field, η_P could in principle take any value. However, given that $\mathcal{P}^2$ behaves like an internal symmetry transformation, we are free to combine it with any conserved internal symmetry operator without changing the selection rules. In particular, it is possible[1] to redefine the parity operator so that $\hat{P}^2 = 1$, in which case the intrinsic parities of a complex scalar field can only take the values $\eta_P = \pm 1$, as for scalar fields.

- *Charge conjugation.* Under particle-antiparticle exchange, the transformation is

$$\phi^C(x) \equiv \hat{C}\,\phi(x)\,\hat{C}^{-1} = \eta_C\,\phi^\dagger(x). \tag{1.2.3}$$

  For a real field, $\phi^\dagger = \phi$ and the intrinsic charge-conjugation parity η_C takes the values $\eta_C = \pm 1$. As an example, the neutral pion π^0 has $\eta_C = 1$, which means that it cannot decay into an odd number of photons, which have $\eta_C = -1$. For a complex field, however, η_C has no physical meaning as it can always be reabsorbed using a global $U(1)$ transformation.

- *Time reversal.* Under $x \to x_T = (-x^0, \vec{x})$, the transformed scalar field is

$$\phi^T(x) \equiv \hat{T}\,\phi(x)\,\hat{T}^{-1} = \eta_T\,\phi(x_T). \tag{1.2.4}$$

  As with parity, a real scalar field can only have $\eta_T = \pm 1$ and is thus either $\mathcal{T}$-odd or $\mathcal{T}$-even. For complex scalar fields, the anti-unitarity of $\hat{T}$ always ensures that $\hat{T}^2 = 1$ and the intrinsic phase η_T is not restricted.

Using the transformation laws above, together with the ones for vector and spinor fields, one can easily check whether a given Lagrangian respects $\mathcal{C}$, $\mathcal{P}$, $\mathcal{T}$, and combinations thereof. That said, in order to judge whether the physics is truly invariant under a symmetry transformation,

[1] This is not always the case for fermions. Fermionic fields can have internal discrete symmetries that are not part of a continuous symmetry group of phase transformations. An example is a theory with Majorana neutrinos, for which fermion number cannot be embedded into baryon or lepton number. In general, intrinsic parities can be taken to assume the values ± 1, $\pm i$ [38].

one needs to look at observable processes rather than Lagrangians. For that, the symmetries have to be tested at the level of the S-matrix

$$S = T \exp\left(-i \int_{-\infty}^{\infty} \mathrm{d}t\, V(t)\right), \tag{1.2.5}$$

where T denotes the time-ordered product. The potential term V of the Hamiltonian contains the relevant interaction Lagrangian $\mathcal{L}_I$,

$$V(t) = -\int \mathrm{d}^3x\, \mathcal{L}_I(x). \tag{1.2.6}$$

For parity and charge conjugation, it is straightforward to deduce that the S-matrix is invariant as long as the interaction Lagrangian is invariant too. For time reversal, there is a subtlety related to the anti-unitary nature of the operator implementing the symmetry. Indeed, by expanding the exponential one sees that $S_T = S^\dagger$, which naively indicates that the S-matrix is not invariant. However, in this case one needs to carefully keep track of the ingoing and outgoing states. Assuming that $\hat{T}\mathcal{L}_I(x)\hat{T}^{-1} = \mathcal{L}_I(x_T)$, one has

$$\langle i_T |\, S\, | f_T \rangle = \langle f |\, S\, | i \rangle\,, \tag{1.2.7}$$

which means that if time reversal is a symmetry of the interaction Lagrangian, the S-matrix elements are equal for time-reversed processes in which initial and final states are exchanged. This actually matches our physical intuition regarding the invariance of physics when the flow of time is run backwards.

A discrete symmetry that is of particular importance to this thesis is the product of parity and charge conjugation. Formally and following the discussion made for charge conjugation, a $\mathcal{CP}$ transformation can be defined univocally using the $\mathcal{CPT}$ and time reversal operators. Furthermore, because of the $\mathcal{CPT}$ theorem [36], $\mathcal{CP}$-invariance is equivalent to $\mathcal{T}$-invariance in a local, Lorentz invariant quantum field theory.

The Standard Model, defined to contain any operator with dimension 4 or less involving the well-known particle content and respecting the gauge symmetry $SU(3) \times SU(2) \times U(1)$, allows for $\mathcal{CP}$ violation in two different ways. The first one comes from a combination of complex phases in the Yukawa couplings of quarks and leptons or, equivalently, from the single physical phase of the CKM [40] matrix, and the corresponding one in the PMNS [41, 42] matrix. The second one involves field strength tensors of any of the three gauge groups in the following gauge-invariant combination

$$\mathcal{L}_{\mathrm{SM}} \supset -\epsilon^{\mu\nu\rho\sigma} \mathrm{tr} F_{\mu\nu} F_{\rho\sigma}, \tag{1.2.8}$$

and will be discussed in depth in Section 1.3.1.

In Part I of this thesis we investigate ways in which nature can provide sources of $\mathcal{CP}$ violation aside from the previously mentioned ones. Two distinct scenarios are studied. In Chapter 2 and drawing inspiration from the Affleck-Dine model of baryogenesis [43], we show how a small $\mathcal{CP}$-violating seed in the self-couplings of a scalar field can be amplified by its

motion in field space during its cosmological evolution. Then, a supersymmetric scenario is presented in Chapter 3, in which $\mathcal{CP}$ violation is generated by couplings between quarks and their scalar superpartners. Although this is a well-known source of $\mathcal{CP}$ violation in supersymmetric extensions of the Standard Model [44], our model presents some features, like the existence of a continuous $U(1)_R$ symmetry [45] and Dirac gauginos [46], that shift the relative importance of the different contributions involved.

There are numerous phenomenological arguments that point towards the existence of yet-to-be discovered sources of $\mathcal{CP}$ violation in nature, and which constitute the motivation for the studies of the first part of this thesis. The strongest indication is probably the existence of particle-antiparticle asymmetries in our Universe, which cannot be explained within the Standard Model, as we now discuss.

1.2.2 Baryogenesis and asymmetric dark matter

One of the most important features of discrete symmetries is the role that they play in controlling the generation of particle-antiparticle asymmetries in the Universe. Two exemplifications of this are studied in this thesis: baryogenesis, which is the cosmological production of baryonic matter in excess of its antimatter counterpart, and asymmetric dark matter, which explores the possibility that the dark matter also contains a particle-antiparticle asymmetry. In both situations, there are three conditions, first stated by Sakharov [47], that need to be satisfied for these imbalances to arise:

1. Particle number violation. This is usually connected with a continuous $U(1)$ symmetry, as is baryon number in the case of baryogenesis. Clearly, for an asymmetry to arise there has to exist a process between two states X and Y that can produce a net baryon number (B) excess
$$X \to Y + B. \tag{1.2.9}$$

2. Departure from equilibrium. This condition is required so that the inverse (i.e. $\mathcal{CPT}$-conjugate) process
$$Y + B \to X \tag{1.2.10}$$
has a different rate and the particle number-violating transition (1.2.9) is not undone.

3. $\mathcal{C}$ and $\mathcal{CP}$ violation. It is clear that charge conjugation has to be violated, otherwise the process
$$\bar{X} \to \bar{Y} + \bar{B} \tag{1.2.11}$$
would occur at the same rate as (1.2.9), generating as many antibaryons as baryons. One way to understand why $\mathcal{CP}$ violation is also necessary for baryogenesis is to take into account that baryons are made of quarks, which come in left- and right-handed chiralities. Given that under a $\mathcal{CP}$ transformation $q_L \to \bar{q}_R$, conservation of $\mathcal{CP}$ enforces the equality of the rates
$$\Gamma(X \to Y + q_L) + \Gamma(X \to Y' + q_R) = \Gamma(\bar{X} \to \bar{Y} + \bar{q}_R) + \Gamma(\bar{X} \to \bar{Y}' + \bar{q}_L), \tag{1.2.12}$$

which would preclude a net baryon number from being generated.

The Standard Model *a priori* provides all the ingredients listed above to generate a baryon asymmetry. Departure from thermal equilibrium can occur in an expanding and cooling Universe, and $\mathcal{C}$ and $\mathcal{CP}$ violation are present in the weak interactions as already pointed out. Finally, baryon number violation can occur through electroweak sphalerons [48], which are non-perturbative processes that only conserve $B - L$, that is, the difference between baryon and lepton numbers [49, 50], but break both quantities regarded separately. Sphaleron-driven conversions are only efficient at sufficiently high temperatures. Because of this, they tend to erase any baryon asymmetry[2] generated before the electroweak phase transition [52]. That said, if the electroweak phase transition is of first order, the departure from equilibrium is strong enough and a net baryon asymmetry can be generated near the wall that separates the broken and unbroken phases [53]. This putative process is usually known as *electroweak baryogenesis* [54].

In practice, there are two main caveats that preclude electroweak baryogenesis from actually occurring in the Standard Model as it is. The first one is that the amount of $\mathcal{CP}$ violation, which can be measured by the Jarlskog invariant [55], is too small to explain the observed baryon asymmetry [56, 57, 58]. The second one is that the measured value of the Higgs mass [59, 60] is compatible with a crossover, rather than a strong first-order, electroweak phase transition [61, 62]. These shortcomings entail that new physics are necessary to explain the cosmological excess of matter over antimatter, in which extra sources of $\mathcal{CP}$ violation are a necessary (though not sufficient) requirement. Following this line of thought, Chapter 3 presents an extension of the Standard Model that can accommodate the generation of the observed baryon asymmetry.

Although the Sakharov conditions have been exemplified here for the case of baryogenesis, they easily generalize to other particle-antiparticle asymmetries. For instance, in asymmetric dark matter models the dark sector contains a matter asymmetry just as the visible sector does [63, 64, 65, 66]. A novel example of an asymmetric dark matter model is studied in Chapter 2, in which the particle number is identified with the $U(1)$ symmetry associated with the phase of a complex scalar field. Finally, baryogenesis and asymmetric dark matter can be combined to give a single origin for both particle-antiparticle asymmetries. This allows some of the Sakharov conditions to be circumvented: for example, in the scenario of Chapter 3, baryogenesis proceeds even if baryon number is globally conserved, as a negative asymmetry that compensates the visible one is stored in the dark matter.

1.3 Dark matter and axions

Axions are a paradigmatic example of light scalar particles that, should they exist, generally contribute to the dark matter of the Universe. What is more, their existence is well motivated

[2] They can however be useful to transform a lepton asymmetry into a baryon one, as is proposed in models of leptogenesis [51].

by different particle physics arguments. Axions constitute one of the main focus of this thesis and Part II is entirely devoted to them. We therefore now review the most important theoretical reasonings that lead to the belief that axions may indeed exist, and delineate the main characteristics that make them good dark matter candidates.

1.3.1 The strong CP problem

The QCD axion is a byproduct [67, 68] of the mechanism proposed by R. Peccei and H. Quinn [69] to explain the experimental observation that QCD respects the product of charge conjugation and parity symmetries to a very high degree [70]. This is commonly known as the *strong CP problem*. A simplistic argument to motivate why such a problem exists is that, as long as $\mathcal{CP}$ symmetry is not imposed by hand [3] in the Lagrangian of QCD, a dimension-four term

$$\mathcal{L}_{\text{QCD}} \supset -\theta_{\text{QCD}} \frac{g_s^2}{16\pi^2} \text{tr} F^{\mu\nu} \tilde{F}_{\mu\nu} \tag{1.3.1}$$

is allowed by gauge symmetry. Here, $\tilde{F}_{\mu\nu} = \frac{1}{2}\epsilon_{\mu\nu\rho\sigma}F^{\rho\sigma}$ is the dual field-strength tensor and θ_{QCD} is an *a priori* undetermined parameter. It is easy to see [4] that while charge conjugation is preserved, parity is violated if $\theta_{\text{QCD}} \neq 0$, and therefore the product $\mathcal{CP}$ is violated too. One thus expects this term to contribute to $\mathcal{CP}$-violating observables in processes involving strong interactions, like hadronic electric dipole moments [71]. The non-observation of such effects [70] then leads to the requirement that θ_{QCD} is very close to zero, in contradiction with the general expectation that dimensionless parameters in the Lagrangian should be $\mathcal{O}(1)$.

Although the above argumentation is helpful to get a simple understanding of the issue, a few caveats arise once one looks into the details. The most important one is that the term in Equation (1.3.1) can be rewritten as a divergence of a current. We usually discard total derivatives in the Lagrangian on the grounds that they give no contribution to the action for fields that vanish at infinity, and we therefore may be tempted to do the same with the θ_{QCD} term. The only reason why we cannot do this is the fact that non-abelian gauge theories allow for *instantons*[72, 73, 74]. Instantons are solutions to the Euclidean classical equation of motion with gauge field configurations that are topologically inequivalent to zero and generate non-trivial boundary terms (see [75] for a nice introduction to the topic). In four spacetime dimensions, instanton solutions arise from $SU(2)$ embeddings into the gauge group of interest, in our case $SU(3)$, and can be labelled by their *winding number* $k \in \mathbb{Z}$, given by

$$k = \frac{1}{16\pi^2} \int \text{d}^4x \, \text{tr} F^{\mu\nu} \tilde{F}_{\mu\nu}. \tag{1.3.2}$$

[3] As discussed in the previous section, it is experimentally well stablished that $\mathcal{CP}$ is not a preserved symmetry in the electroweak sector, so it seems natural to assume that QCD is not different in this regard. We will be more explicit about this later.

[4] It is helpful to make the analogy with electromagnetism, in which a term of the form $F\tilde{F}$ corresponds to $\vec{E} \cdot \vec{B}$, which is clearly $\mathcal{P}$ (and $\mathcal{CP}$)-odd.

The Hamiltonian admits ground states with different values of the winding number but the same energy, which therefore correspond to inequivalent vacuum states. Because quantum effects associated with instantons allow for tunneling between these vacua [73], the true vacuum is a superposition of states of definite winding number,

$$|\text{vac}\rangle = \sum_n \mathrm{e}^{i\varphi} |n\rangle \,, \tag{1.3.3}$$

where φ is some phase. Expanding around the superposition of vacua $|\text{vac}\rangle$ is equivalent to working with the ordinary vacuum $|0\rangle$ and an extra term in the action

$$\mathcal{L} \supset -\varphi \frac{g_s^2}{16\pi^2} \,\mathrm{tr} F^{\mu\nu} \tilde{F}_{\mu\nu}, \tag{1.3.4}$$

which, after identifying $\varphi \equiv \theta_{\text{QCD}}$, is exactly the term that we introduced on symmetry grounds in Equation (1.3.1). But we now know that it generates a contribution to the action proportional to θ_{QCD} for any state with nonzero winding number.

Another important point is that θ_{QCD} is not observable by itself: the physical θ angle receives a contribution from the electroweak sector, coming from the phase of the quark mass matrix [40]. It originates from the fact that chiral rescalings are needed in order to rotate the weak interaction eigenstates into physical (propagating) eigenstates after quarks become massive at the electroweak symmetry breaking. The Jacobian of these chiral transformations produces a term in the action analogous to Equation (1.3.1) but with a new phase θ_{EW}, which corresponds to the $U(1)$ axial phase of the quark mass matrix. With this, the physical angle becomes

$$\theta \equiv \theta_{\text{QCD}} + \theta_{\text{EW}}. \tag{1.3.5}$$

A priori, there is no reason to believe that θ should be small. However, experimental data strongly constrain the existence of $\mathcal{CP}$-violating effects involving the strong interactions. In particular, the non-observation of a sizable electric dipole moment of the neutron [70] sets the extraordinary limit [71]

$$\theta \lesssim 10^{-10}. \tag{1.3.6}$$

We would like to find an explanation for such a small parameter. Anthropic arguments by themselves [76] are not useful in this situation because our Universe would look the same even if θ were orders of magnitude larger than required by Equation (1.3.6). The strong CP problem is thus a genuine fine-tuning problem motivated by precise experimental data.

The Peccei-Quinn solution to the strong CP problem.

If we are not willing to accept a severe fine-tuning for θ, we are led to searching for dynamical solutions that may explain its smallness. The simplest one is probably to postulate the existence of a massless quark, and therefore the existence of an axial $U(1)$ symmetry that is exact at the classical Lagrangian level and only broken by the quantum effects associated to instantons as

described above. In this situation, the θ phase can be identified with the phase of the massless quark and is completely unphysical [77, 78]. This minimal solution does however not seem to be realized in nature, given that lattice QCD calculations [79] strongly disfavor the possibility that any of the Standard Model quarks is massless[5].

In spite of that, the idea that there exists an axial symmetry that is classically exact at the Lagrangian level is a fruitful one. R. Peccei and H. Quinn noticed that this possibility can still be realized as long as the symmetry is spontaneously broken at some high scale [69, 82]. The minimal requirement is thus a complex scalar field whose phase implements the global *Peccei-Quinn* $U(1)_{\rm PQ}$ symmetry and which spontaneously acquires a vacuum expectation value. As was appreciated by S. Weinberg and F. Wilczek [67, 68], this entails the appearance of a pseudo Nambu-Goldstone boson in the spectrum, which was baptized as the *axion*[6]. At the classical level, the axion inherits the axial $U(1)$ as a shift symmetry $a \to a + \text{const.}$, which is only broken by QCD instanton effects. This explains the form of the low energy effective Lagrangian of the QCD axion,

$$\mathcal{L}_a = \frac{1}{2}\partial_\mu a \partial^\mu a - \frac{a}{f_a}\frac{g_s^2}{16\pi^2}\text{tr}F^{\mu\nu}\tilde{F}_{\mu\nu}. \tag{1.3.7}$$

Here, f_a denotes the QCD axion *decay constant*, which is closely related to the scale of Peccei-Quinn symmetry breaking. Note that instanton effects reduce the continuous shift symmetry to a discrete one, $a \to a + 2\pi f_a k$, $k \in \mathbb{Z}$. We can thus use the $U(1)_{\rm PQ}$ symmetry to rotate away the θ angle, and in this way trade it for the QCD axion field $\theta \to a/f_a$. It is then necessary to make sure that the vacuum expectation value of the QCD axion does not restore the strong CP problem. The key observation here is that the energy of the vacuum as defined in Equation (1.3.3) depends on the value of θ. Using a dilute instanton gas, it is possible to show (see e.g. [83]) that

$$E(\theta) \propto \text{e}^{-\frac{8\pi^2}{g^2}}\cos\theta. \tag{1.3.8}$$

This is consistent with a theorem due to C. Vafa and E. Witten [84] that states that in the absence of other $\mathcal{CP}$-violating sources, the energy of the QCD vacuum is minimized at $\theta = 0$. Because the θ parameter has been promoted to the axion field a/f_a, it can dynamically evolve and settle at the $\mathcal{CP}$-conserving value $\theta = 0$, thus satisfactorily solving the strong CP problem.

The Peccei-Quinn mechanism has a profound phenomenological implication: the appearance of the QCD axion, a very light and weakly interacting pseudoscalar particle. The mass of the QCD axion comes from the only source of breaking of its shift symmetry, i.e. QCD instantons. At low energies, its potential can be reliably computed using chiral perturbation

[5] Some interesting possibilities [80, 81] exist in which one (or more) of the quark masses are generated by non-perturbative effects so that the axial $U(1)$ symmetry is only broken spontaneously and $\theta_{\rm QCD}$ remains unphysical. These models generally predict the existence of a QCD axion as a composite state rather than a fundamental one, but with similar phenomenological properties.

[6] We will use the term *QCD axion* to make it explicit that its existence is linked to the solution to the strong CP problem.

theory (ChPT) [85], which yields [86, 87]

$$m_a = 5.89(10)\,\mu\text{eV}\left(\frac{10^{12}\,\text{GeV}}{f_a}\right). \tag{1.3.9}$$

Aside from its $F\tilde{F}$ coupling, the QCD axion can feature pseudoscalar couplings to other gauge bosons, as well as derivative couplings to fermions. All the interactions of the QCD axion share a common feature, owing to its Nambu-Goldstone boson nature: they are suppressed by the decay constant f_a. Aside from this, the precise strength of the interactions are largely model-dependent, as was recently reviewed in [88]. Axions have a very rich phenomenology: they can be searched for at colliders (e.g. [89]) as well as at dedicated experiments [90], and have profound astrophysical implications [91]. At this point, we refer to Section 6.2 in Chapter 6 for a detailed study of the experimental and observational landscape of axions, with a focus on their couplings to electroweak gauge bosons.

1.3.2 Axions and axion-like particles

The QCD axion is a particularly well-motivated example of a broad class of putative new particles, which by extension are commonly known as axion-like particles (ALPs for short), or often simply as axions. The distinctive feature that characterizes ALPs is the existence of a shift symmetry which severely restricts their possible interactions. This shift symmetry can be explicitly broken, usually by quantum effects (e.g. by instantons), thus allowing the axion-like particle to acquire a potential and other non shift-symmetric couplings. Effectively, this results in a very generic family of particles that are typically light and weakly interacting, but that span a large range of masses and couplings.

In quantum field theory, axion-like particles typically arise as pseudo Nambu-Goldstone bosons [92, 93, 94] of global symmetries of the classical Lagrangian. They can be scalars if the symmetry is vectorial, pseudoscalar if it is axial, and may not have a definite chirality if the symmetry is chiral but not purely axial. The axion-like particle is associated with an angular degree of freedom $\phi/f_\phi \in [0,\, 2\pi]$ after spontaneous symmetry breaking at the scale f_ϕ. If the global symmetry is exact also at the quantum level, the axion-like particle remains massless. However, it is usual that at least quantum effects result in some explicit breaking of the symmetry. If these effects occur at some particular scale Λ_ϕ, then the axion-like particle acquires a potential $V(\phi/f_\phi)$, and therefore generically a mass

$$m_\phi \sim K\frac{\Lambda_\phi^2}{f_\phi}, \tag{1.3.10}$$

where K is some dimensionless coefficient. In many realizations, the source of the breaking is non-perturbative and $K \sim \mathrm{e}^{-S_{\text{inst}}}$ is exponentially suppressed by an instanton action [74, 95, 96, 73], and thus potentially very small. Given that couplings of the axion-like particle are also always inversely proportional to the ALP decay constant f_ϕ, at the effective level the

axion-like particle can essentially be described by two parameters: its mass m_ϕ and its decay constant f_ϕ, which sets the strength of its interactions.

There is another way to obtain axion-like particles that is conceptually different: they arise as Kaluza-Klein zero modes [97, 98, 99] of antisymmetric tensors in compactified extra dimensions [100]. The prime example of an extra-dimensional model is string theory, which predicts the existence of a total of 10 or 11 spacetime dimensions [101], most of which have to be compactified to reproduce our effectively 4-dimensional world. In compactification scenarios that allow for some unbroken supersymmetry and chiral matter [102], the compact manifold is of Calabi-Yau type and generically produces tens or hundreds of this kind of axion-like particles, which are referred to as "closed string axions" [7] [103]. In addition to that, axions similar to the field theory ones previously discussed (i.e. phases of matter fields related to spontaneously broken global symmetries) can also appear in string theory, and are known as "open string axions".

Although we do not describe here the details of closed string axions, it is interesting to briefly mention what the general parametric expectations regarding these particles are, following the discussion of [104]. The number of axions depends on the topology of the compact manifold, more precisely on the number of homologically inequivalent p-cycles that it admits. As stated above, in standard scenarios this typically means $\mathcal{O}(10-100)$ axions. The decay constant of a given axion is set by the size of its associated p-cycle, which is controlled by a scalar modulus field σ_i, called the "saxion". Under certain standard assumptions, it can be estimated as

$$f_i \sim \frac{\mathrm{M_P}}{\sigma_i} \lesssim \mathrm{M_P}, \tag{1.3.11}$$

where σ_i can be thought of as the dimensionless size of the p-cycle (its volume measured in string units). The inequality follows from the requirement that this size is larger than one, as the effective field theory description otherwise breaks down. Closed string axions enjoy a shift symmetry which is inherited from gauge symmetries of their parent antisymmetric tensors. They are thus massless up to exponentially suppressed explicit breakings of the shift symmetry caused by non-perturbative effects, similarly to the case of pseudo Nambu-Goldsone bosons. The most common non-perturbative effects are instantons, which generate masses of the form

$$m_i \sim \frac{m_{\mathrm{SUSY}}\Lambda_{\mathrm{inst}}}{f_i}\mathrm{e}^{-S_{\mathrm{inst}}}. \tag{1.3.12}$$

In addition to the instanton scale Λ_{inst}, which may be the Planck scale, the masses depend on the scale of supersymmetry breaking m_{SUSY}. In standard compactification scenarios, the gauge coupling of the relevant instanton group at each p-cycle is related to the saxion field as $g^2 \sim 1/\sigma$. Given that $S_{\mathrm{inst}} = 8\pi^2/g^2$, this makes the axion masses exponentially sensitive

[7] In string theory (and other fields), the word axion refers to what we have so far called an axion-like particle. In this sense, the choice of the word "axion" or "ALP" tells more about the field of study of the authors than about the physical properties of the particle. We will use both terms interchangeably.

to the scalar moduli, $m_i \propto \mathrm{e}^{-c\,\sigma_i}$ (with some constant c). This observation leads to the most important feature of closed string axions: while their decay constants have a power-law dependence on scalar moduli and therefore all lie close below the Planck scale, their masses are exponentially sensitive to σ_i and can be distributed over many orders of magnitude, generating what some authors have coined the "string axiverse" [105].

For phenomenological applications one can often stay agnostic about the origin of axion-like particles and consider an effective two-dimensional parameter space of mass m_ϕ and decay constant f_ϕ. This is the approach that is followed in Chapters 4 and 5. In contrast, QCD axion models are usually considered to belong to a single-parameter family, as the relation $m_\phi f_\phi \sim \Lambda^2_{\mathrm{QCD}}$ fixes the mass given a decay constant. This is however not always the case: as is studied in Chapter 6, models containing additional confining groups can lead to "heavy axions" [106], which are axions that solve the strong CP problem but whose mass is not necessarily fixed by the QCD scale.

1.3.3 Axions as dark matter

The previous sections make it clear that there are strong motivations to believe that axions may appear in our theory of nature. The question that immediately follows is: can we hope to find experimental or observational evidence of their existence? At first sight, their very low mass and feeble interactions with ordinary matter pose a difficult challenge. However, the putative existence of axions has extremely rich phenomenological consequences for laboratory experiments [90], as well as for astrophysical systems [91] and cosmology [104]. Observational and experimental perspectives are reviewed throughout the main body of Part II of this work, e.g. in Sections 5.1 and 6.4. In this introduction, we focus on what is probably the most interesting implication: the possibility that axions make up the dark matter of the Universe [107, 108, 109].

Axions fulfill all the requirements that a good dark matter candidate needs to satisfy. First of all, they are by nature extremely weakly interacting, both with other particles and with themselves, as their interactions are suppressed by the large energy scale f_ϕ. The second question, that of their cosmological stability, is a more interesting one. Although it may seem guaranteed given their weak interactions and small masses, parametrically enhanced decays can occur due to the bosonic nature of axions. This is explored in detail in Chapter 4, in which the conclusion is that the cosmological stability is assured for axions with the masses and decay constants of interest.

This leaves a final requirement to be checked, namely that axions behave like a pressureless fluid for all purposes related to gravitation. Something that is easy to realize is that axion dark matter with a mass $m_\phi \lesssim 1\,\mathrm{eV}$ cannot be produced thermally [110], as otherwise axions are too relativistic at the onset of structure formation [8]. As a consequence, axions have to be produced non-thermally. As a matter of fact, there is a very general way of non-thermally producing

[8] The strongest bounds on warm dark matter are derived from observations of the Lyman-α forest [111] and disfavor thermal dark matter candidates with masses below $\sim 1\,\mathrm{keV}$.

very light scalar particles in the early Universe: the misalignment mechanism [107, 108, 109] (see also [112]), which is discussed in detail in Section 5.3. The misalignment mechanism produces a coherent state of axions that can be described using classical field equations[9]. The produced cosmological axion field is very homogeneous, which corresponds to a population of zero-momentum axions. As a consequence, its stress-energy tensor is that of a perfect fluid with zero pressure, and the axion field therefore behaves as extremely cold dark matter.

A significant fraction of this thesis is devoted to the study of axions and axion-like particles as dark matter and the dynamics of the misalignment mechanism. In fact, Chapter 5 goes beyond the simplest models and considers the effects of a non-canonical kinetic term for the axion in its cosmological dynamics. Interestingly, the main conclusion is that such a generalized setup allows for axions to be efficiently produced by the misalignment mechanism in regions of parameter space that otherwise produce too little dark matter. It is precisely in this region of parameter space where the cosmological stability of axions is found to be guaranteed in Chapter 4. This contributes to motivate experimental searches for axions with low masses and low decay constants.

To end this section, note that the main features of axions as dark matter candidates can be generalized to other light bosonic particles. Indeed, in addition to focusing on axions in Part II of this thesis, in Chapters 2, 7 and 8 we deal with more general scalars or pseudoscalars, and with massive vector fields. The particularities and similarities for each of these are discussed in detail in each of the corresponding chapters.

1.4 Dark matter and inflation

One of the main emphases of this thesis lies on the origin of light scalar dark matter at the dawn of the cosmological history. To set up the stage for the discussion, we now briefly describe the picture that is currently more accepted with regards to the physics of the very early Universe, focusing on inflation. The physics of inflation is of uttermost importance for Part III, but also relevant for the first two parts of the thesis due to the existence of isocurvature fluctuations, which are a very generic feature of light bosonic particles behaving as dark matter.

1.4.1 Inflation

With the inclusion of a few ingredients like baryogenesis, dark matter and a cosmological constant, it is possible to construct a self-contained theory to describe the history of the entire observable Universe. This Standard Model of cosmology is usually known as ΛCDM or the Big Bang model, and gives a dynamical description of the evolution of the Universe. However, when trying to fully explain all cosmological and astrophysical observations, the model runs into a problem of initial conditions. Or rather a few problems, to be precise.

[9] Some authors have raised the question of whether quantum or Bose-Einstein condensation effects may be important in axion dark matter physics [113, 114, 115, 116, 117]. Although this could entail surprising phenomenological consequences, the debate is at the moment still not completely settled.

Firstly and in agreement with the cosmological principle, observations unanimously show that the Universe is homogeneous and isotropic [118] on all large scales to which we have access. In particular, the CMB has an almost perfect black body spectrum irrespective of the direction from which it is coming [10, 11, 119]. That said, the Standard Model of cosmology predicts that the early Universe was made of many casually disconnected patches, which would have no reason to be so precisely homogeneized. Secondly, a flat Universe corresponding to zero curvature is unstable with respect to small perturbations around the critical energy density. Given that current observations show that the curvature is vanishing within experimental uncertainties [12], we conclude that it must have been extremely flat at earlier stages (for instance, 1 part in 10^{14} during Big Bang nucleosynthesis [120]). Finally, some of the most popular high-energy particle physics models predict the existence of exotic relics that would have been produced in the early Universe, whose traces have however not been found.

We conclude that the Universe started its life in what seems a very particular state, and unless we are willing to accept this, we need to find a dynamical explanation for it. This is precisely what the theory of cosmological inflation [121, 122, 123, 124, 125, 126] provides. By postulating a period of quasi de Sitter [127] expansion at the beginning of the Big Bang model, the initial conditions described in the previous paragraph are dynamically attained. Although current observational evidence cannot give a definitive answer regarding the precise details of this event, it is widely accepted that something like[10] inflation must have occurred in the very early Universe.

This thesis assumes that the early Universe experienced an early phase of accelerated expansion, but does not deal with the details of the inflationary dynamics. Rather, we are interested in the ways that inflation can impact the physics of light dark matter candidates. For this, the most important aspect of inflation is its ability to generate a spectrum of density perturbations from quantum fluctuations, as we briefly review in the next section.

1.4.2 Adiabatic and isocurvature dark matter fluctuations

In the standard inflationary picture, the quantum fluctuations of the inflaton serve as seeds for the density perturbations that give rise to the growth of large-scale structure in the late Universe [130, 131, 132, 133, 134, 135]. This process occurs as follows [136, 137]. Small quantum fluctuations in the field that drives inflation, the *inflaton*, are closely related (in fact, gauge equivalent) to fluctuations in the metric that source perturbations in the curvature of spacetime, which can be thought of as a gravitational potential. In the inflationary background, the wavelengths of these fluctuations grow until they exceed the size of a patch where causal contact is possible; they are then said to have become *super-Hubble* or to have *left the horizon*. At this point, the perturbation become classical statistical fluctuations and they *freeze*, i.e. they stop evolving. After inflation has ended and the Universe is radiation- or matter-dominated, the fluctuations of the gravitational potential induce temperature and density perturbations through the Poisson equation $\nabla^2\Psi = 4\pi G\,\delta\rho$. These density fluctuations later on become

[10] Alternative possibilities include bouncing [128] and string gas [129] cosmologies.

self-gravitating and grow to give rise to the large-scale structure of the Universe that we observe today.

As we know, our present Universe can be regarded as a thermodynamic system that contains a mix of different components: radiation, dark matter, baryonic matter, neutrinos... In this situation, two kind of perturbations are possible: *adiabatic* and *isocurvature* perturbations [138]. Adiabatic perturbations are perturbations in the total energy density of the system, and are thus the ones that source the curvature perturbations. Because of this, adiabatic perturbations are also known as curvature perturbations. In contrast, isocurvature (or entropy) perturbations correspond to relative fluctuations between the different components of the system, but which do not perturb the total energy density. Clearly, there can be different isocurvature modes, corresponding to relative fluctuations between different components.

In the picture described above, the inflaton fluctuations are by construction adiabatic, since the inflaton dominates the energy density of the Universe during inflation. If all the contents of the Universe originate from the decay of the inflaton, the adiabatic nature of the fluctuations is inherited by all the components and there are no isocurvature perturbations. However, if one or more of the components have an independent production mechanism, isocurvature perturbations are possible. This is the case for some of the scenarios studied in this thesis, in which dark matter is assumed to be a light scalar field which is present during inflation and is therefore bound to acquire its own quantum fluctuations [139, 140, 141, 142], unrelated to the inflaton ones. As the dark matter field is energetically subdominant during inflation, its fluctuations do not originally contribute in a significant manner to the total energy density and can be considered to be purely isocurvature. In the late Universe, when the dark matter becomes energetically relevant, these isocurvature modes can have important phenomenological consequences, as is discussed in the main body of the thesis.

Let us now flesh out a bit more this heuristic description by introducing the relevant quantities that are useful to describe the perturbations[11]. As we anticipated, perturbations in the fields result in perturbations in their stress-energy tensors, which in turn induce perturbations in the metric via the Einstein's equations. These perturbations are defined with respect to a reference (or background) spacetime, which in this case has the spatially flat Friedmann-Lemaître-Robertson-Walker metric $\mathrm{d}s^2 = a^2(\tau)\left(-\mathrm{d}\tau^2 + \mathrm{d}\vec{x}^2\right)$. However, because general relativity is the gauge theory of coordinate transformations (or diffeomorphisms), we have the freedom to choose any coordinate system in the real spacetime. A choice of coordinates can also be viewed, in an "active" perspective, as a mapping between the reference and the real spacetime. Choosing a mapping is usually referred to as *fixing a gauge*, which in practice corresponds to *slicing* the spacetime into hypersufaces of fixed time τ and *threading* it into lines of fixed spatial coordinates $\vec{x}$. Clearly, a physical perturbation is independent of the choice of slicing and should ultimately be described using gauge-invariant quantities.

Once a gauge is fixed and a particular slicing of spacetime is chosen, the perturbed metric

[11] We restrict ourselves to the study of scalar perturbations. Tensor perturbations, associated with primordial gravitational waves, are also possible and are a topic of much interest [143].

can be written as [144]

$$\mathrm{d}s^2 = -\mathcal{N}^2\,\mathrm{d}t^2 + a^2(t)\,\mathrm{e}^{2\psi}\,\gamma_{ij}\left(\mathrm{d}x^i + \beta^i\,\mathrm{d}t\right)\left(\mathrm{d}x^j + \beta^j\,\mathrm{d}t\right), \tag{1.4.1}$$

where the lapse function $\mathcal{N}$ and the shift vector β^i define the slicing, γ_{ij} and $a(t)$ denote the spacial metric and background scale factor, respectively, and ψ is the curvature perturbation. A very useful gauge-invariant quantity to define is [145]

$$\zeta \equiv \psi + H\frac{\delta\rho}{\dot{\rho}}, \tag{1.4.2}$$

which corresponds to the curvature perturbation ψ calculated in the uniform-density slicing in which the total energy density has no perturbation ($\delta\rho = 0$). Similarly, for each component fluid, we define ζ_i as the curvature perturbation on a slicing in which the fluid i is uniform ($\delta\rho_i = 0$),

$$\zeta_i \equiv \psi + H\frac{\delta\rho_i}{\dot{\rho}_i}. \tag{1.4.3}$$

Crucially, each ζ_i can be proven to be conserved on super-horizon scales for non-interacting fluids [146]. These definitions are convenient because they allow to measure the isocurvature perturbation between the fluids i and j in a gauge invariant fashion. It is conventional to define it as

$$S_{ij} \equiv 3\left(\zeta_i - \zeta_j\right), \tag{1.4.4}$$

such that it can be identified with the perturbation in the ratio of the number densities of the two species. In the case of interest here, the isocurvature perturbation between dark matter (c) and radiation (r), which we denote just by S, can be written as

$$S \equiv 3\left(\zeta_\mathrm{c} - \zeta_\mathrm{r}\right) = 3H\left(\frac{\delta\rho_\mathrm{c}}{\dot{\rho}_\mathrm{c}} - \frac{\delta\rho_\mathrm{r}}{\dot{\rho}_\mathrm{r}}\right). \tag{1.4.5}$$

We assume that the curvature perturbation in the radiation-dominated Universe is sourced solely by the inflaton, so that the difference between θ_c and θ_r can be traced back to the fluctuations in the dark matter field (which we denote by ϕ) during inflation. In this case, the dark matter-radiation isocurvature perturbation is simply given by

$$S = \frac{\delta\rho_\phi}{\rho_\phi}, \tag{1.4.6}$$

where we have used the continuity equation. At this point, we note that the adiabatic or isocurvature nature of the perturbations is in general not time-invariant. This is clearly exemplified by the case of dark matter isocurvature, in which the primordial isocurvature perturbation also contributes to the curvature perturbation once the dark matter comes to

dominate the energy density of the Universe. Indeed, from Eq. (1.4.4) we see that the total curvature perturbation during the matter era is

$$\zeta^{\rm MD} = \zeta^{\rm inf} + \frac{1}{3}S, \tag{1.4.7}$$

where $\zeta^{\rm inf}$ is the total curvature perturbation during the radiation era. Given this ambiguity in tagging a perturbation as adiabatic or isocurvature, it is important to clarify that we implicitly assume the label to correspond to the initial state of the perturbations, deep in the radiation era.

Isocurvature perturbations are a generic prediction of scenarios of light bosonic dark matter that was present during inflation, and are therefore a topic of much study in this thesis. The generation of such fluctuations during inflation is examined in detail in Chapters 7 and 8, and their consequences for the misalignment mechanism in axion models are studied in Chapter 5.

To finish this section, we qualitatively comment on the main phenomenological differences between adiabatic and isocurvature perturbations, focusing on their imprint in the CMB. There are two main effects by which dark matter isocurvature distorts the CMB temperature spectrum:

- There is an enhancement of the CMB temperature fluctuations on very large scales, induced at the transition from a radiation-dominated Universe into a matter-dominated one right before the emission of the CMB. When the dark matter becomes energetically dominant, the isocurvature mode is effectively "transferred" to the photon fluid, generating a boost in its anisotropy on large angular scales. This manifests itself in an enhancement of the Sachs-Wolfe plateau [147] with respect to the acoustic peaks of about a factor of 6 in the pure isocurvature scenario compared to the adiabatic one. Such a large effect was used very early on [148] (see also [149, 150, 151]) to rule out the possibility of a purely isocurvature dark matter model.

- There is a shift of $\pi/2$ in the phase of the acoustic oscillations that moves the temperature spectrum to smaller scales with respect to the adiabatic case [152, 153, 154, 155]. The cause of this effect is that in order to keep the perturbations isocurvature, there has to be a compensation between the dark matter fluctuations and the radiation density perturbations. This anticorrelation means that photons originally rarefy inside potential wells, as opposed to the adiabatic case, in which they compress: the result is a sine, rather than a cosine, oscillation. Importantly, this phase shift is also present in the (E-type) polarization spectrum and the temperature-polarization cross-spectrum. This is because polarization tracks the baryon velocity, which itself undergoes acoustic oscillations $\pi/2$ out of phase with the density (and therefore the temperature).

On the observational side, the temperature and polarization spectra of the CMB, measured in most detail by the Planck mission [156], are compatible with purely adiabatic fluctuations. As a consequence, dark matter can only have a small admixture of isocurvature perturbations,

but its perturbations are mostly of curvature type. This means that axions and general models of light bosonic dark matter have to face strong constraints in conjunction with the energy scale of inflation, as is discussed in depth in Chapters 5, 7 and 8. Nevertheless, there are ways in which isocurvature perturbations, even very large ones, could be "hiding" from observations. Indeed, one of the main goals of this thesis is to motivate a scenario in which dark matter originates from purely isocurvature perturbations. This possibility is discussed in detail in Chapters 7 and 8, and relies on the fact that the CMB isocurvature limits only apply to very large cosmological scales, while the amplitude of isocurvature perturbations at intermediate and small scales is virtually unconstrained.

1.5 This thesis

This work explores well-motivated new physics scenarios and their potential connection with the dark matter problem. The previous introduction has presented a series of open questions in particle physics and cosmology and hinted at possible links between them and the origin of the dark matter that we observe in the Universe. In the main body of the thesis, we focus on concrete models that can realize this connection and study their phenomenology. The key question that is asked throughout is how potentially measurable properties of dark matter can inform our knowledge about what lies beyond the Standard Models of particle physics and cosmology.

Part I describes how particle asymmetries can be important in generating dark matter and setting its abundance, and how a dark matter asymmetry can be connected to other imbalances, like the baryon-antibaryon asymmetry of the Universe. In Chapter 2, a model of coherent scalar dark matter of asymmetric nature is presented for the first time. The particle-antiparticle asymmetry is generated in the very early Universe through the dynamics of a complex scalar field in a $U(1)$ symmetry-breaking potential, in analogy to Affleck-Dine models of baryogenesis. The phenomenological consequences of the scenario are studied, focusing in the differences with the common symmetric setups. The following Chapter 3 also deals with asymmetric scalar dark matter, but focusing on heavier particles and exploring a common origin of the asymmetry in the dark sector and the baryon one. This connection is made possible by assuming that the dark matter carries an overall negative baryon number, and is implemented by postulating the existence of new physics in neutral B meson oscillations and decays. Importantly, we show how a simple supersymmetric extension of the Standard Model contains all the necessary ingredients to realize this novel scenario.

Part II discusses the physics of axions and axion-like particles, concentrating on their potential role as dark matter but also considering searches for these particles in other environments, like collider experiments. As a starting point, Chapter 4 studies the cosmological stability of axions as dark matter, which is endangered by Bose-enhanced decays into photons. After taking into account the expansion of the Universe and in-medium plasma effects in the propagation of the produced photons, we conclude that the decay is sufficiently slow in the

interesting regions of parameter space. This observation, together with a quickly-developing experimental scene, motivates the search for axion models that can generate a large fraction of dark matter in the region of large couplings and small masses, a task that is undertaken in Chapter 5. For the first time, the effects of a non-canonical kinetic term in the misalignment mechanism are studied, paying special attention to isocurvature constraints and allowing for a temperature-dependent potential. Finally and in a complementary direction, in Chapter 6 we delve into the collider phenomenology of axions with a coupling to gluons, which is required to solve the strong CP problem. The novelty of our approach is to allow for the simultaneous coexistence of multiple axion couplings, as opposed to previous analyses which were based on single couplings. This new paradigm allows to obtain a more realistic picture of the behavior of axions in high-energy experiments.

In Part III, potential connections between the origin of dark matter and the putative inflationary epoch in the very early Universe are studied, with a focus on light scalar and vector particles with generalized gravitational interactions. In a first study that is reproduced in Chapter 7, the focus is on the production of light scalar dark matter from inflationary fluctuations. Allowing for a non-minimal coupling of the field to gravity is shown to have remarkable phenomenological consequences, leading to the production of dark matter independently of any initial conditions and predicting the existence of rich structure at sub-galactic scales. As a follow-up, Chapter 8 enlarges the scope to also accommodate for (massive) vector dark matter, and provides a general discussion of various production mechanisms: misalignment, inflationary fluctuations and the stochastic scenario.

Finally, all these ingredients and scenarios are combined in the final Chapter 9 that serves as a global analysis of the physics explored in this thesis. We provide a detailed summary of each publication in Section 9.1, highlighting the main ideas and the most important results. Then, an in-depth discussion of those results, with a focus on their embedding in the broader picture of particle physics and cosmology, is presented in Section 9.2. We finish in Section 9.3 with an outlook of potential future directions motivated by the physics demonstrated in this thesis.

The following Chapters 2 to 8 are a compilation of articles published by the author of the thesis and a number of collaborators in peer-reviewed journals. The references to the articles are listed in the Preface and are also given before each of the publications, together with a detailed description of the contributions of the author to each multi-authored paper.

Part I

Dark matter and particle asymmetries

Chapter 2

Very light asymmetric dark matter

Authors:
Gonzalo Alonso-Álvarez, Julia Gehrlein, Joerg Jaeckel,
and Sebastian Schenk

Published in *JCAP 09 (2019) 003*,
also available at arXiv:1906.00969

Principal authorship of this article is shared on an equal footing by Julia Gehrlein, Sebastian Schenk, and Gonzalo Alonso-Álvarez. The original idea for the project was conceived by Joerg Jaeckel and was further developed by the four authors. The principal authors contributed equally to the calculations and the writing of the manuscript, and the figures were produced by Sebastian Schenk. All four authors contributed with corrections and suggestions to the manuscript, as well as with improvements during the review process.

Journal of Cosmology and Astroparticle Physics
An IOP and SISSA journal

Very light asymmetric dark matter

Gonzalo Alonso-Álvarez,[a] **Julia Gehrlein,**[b,c] **Joerg Jaeckel**[a] **and Sebastian Schenk**[a]

[a]Institut für Theoretische Physik, Universität Heidelberg,
Philosophenweg 16, 69120 Heidelberg, Germany
[b]Instituto de Física Teórica UAM/CSIC,
Calle Nicolás Cabrera 13-15, Cantoblanco E-28049 Madrid, Spain
[c]Departamento de Física Teórica, Universidad Autónoma de Madrid,
Cantoblanco E-28049 Madrid, Spain

E-mail: alonso@thphys.uni-heidelberg.de, julia.gehrlein@uam.es,
jjaeckel@thphys.uni-heidelberg.de, schenk@thphys.uni-heidelberg.de

Received June 25, 2019
Revised August 7, 2019
Accepted August 7, 2019
Published September 2, 2019

Abstract. Very light dark matter is usually taken to consist of uncharged bosons such as axion-like particles or dark photons. Here, we consider the prospect of very light, possibly even sub-eV dark matter carrying a net charge that is (approximately) conserved. By making use of the Affleck-Dine mechanism for its production, we show that a sizable fraction of the energy density can be stored in the asymmetric component. We furthermore argue that there exist regions of parameter space where the energy density contained in symmetric particle-antiparticle pairs without net charge can to some degree be depleted by considering couplings to additional fields. Finally, we make an initial foray into the phenomenology of this scenario by considering the possibility that dark matter is coupled to the visible sector via the Higgs portal.

Keywords: dark matter theory, baryon asymmetry, particle physics - cosmology connection

ArXiv ePrint: 1906.00969

https://doi.org/10.1088/1475-7516/2019/09/003

JCAP09(2019)003

Contents

1 Introduction

Very light bosons such as axion(-like) particles or dark photons are increasingly popular dark matter candidates (see, e.g., [1, 2] for reviews). Currently, a significant and growing experimental community is set to hunt down these very weakly interacting particles [1, 3–17]. Due to their low mass, production of very light dark matter must be non-thermal, as thermal relics with masses significantly below keV are too warm and disrupt structure formation (see, e.g., [18, 19]). The most prominent non-thermal production mechanism is the misalignment mechanism [20–27], but other possibilities, such as the decay of cosmological defects [28] or precursor particles [29–34], and production from inflationary perturbations [27, 35–46] may contribute to part or even all of the observed dark matter density.

All the aforementioned scenarios have one thing in common: the final dark matter density does not carry any conserved global charge. As a matter of fact, light dark matter candidates are most commonly considered to be real scalar or vector bosons, which cannot possibly carry any such charge.

In this paper, we consider an alternative situation where most or at least a sizable fraction of the dark matter is asymmetric in the sense that it carries a non-vanishing (approximately) conserved global charge. This kind of scenario has of course been widely studied under the name of "asymmetric dark matter" [47–57]. However, in the standard asymmetric dark matter models the particle mass is usually assumed to be in the GeV range, motivated

JCAP09(2019)003

by the fact that a $\sim 5\,\mathrm{GeV}$ asymmetric dark matter particle would have a (dark) charge asymmetry equal to the baryon asymmetry of the Universe. We are interested in much lighter particles,[1] typically below an MeV and possibly even sub-eV, which due to their high occupation numbers can be described as coherently oscillating classical fields. Consequently, the asymmetric net charge density is orders of magnitude larger than the baryon asymmetry (and the two charges may not be related to each other at all). Indeed, for sufficiently small masses, such light dark matter would most likely be carrying the largest charge asymmetry density in the Universe.[2]

The dark matter and corresponding charge density need to be created in the early Universe. The low mass of the particles precludes any purely thermal or even mildly warm production mechanism. A suitable mechanism — in spirit very much coherent with the misalignment mechanism — is the Affleck-Dine mechanism [60] (cf. [61] for a review and [57, 62, 63] for its application to asymmetric dark matter). In this setup, charge is created during the evolution of a field displaced from its minimum in a (slightly) asymmetric potential. In section 3, we argue that through this mechanism a sufficient amount of charge can be generated even for very light particles.[3]

Beyond these principal considerations, our main motivation is phenomenological. Asymmetric dark matter carrying a conserved charge is much harder to detect than its uncharged counterpart, and it requires different methods to do so. One reason for this is that interactions of dark bosons carrying a conserved charge with the Standard Model are usually of higher dimension than those of a real scalar (or vector) field. A real scalar field can always couple linearly to any Standard Model singlet operator, $\phi_{\mathrm{real}}\,\mathcal{O}_{\mathrm{SM}}$. Coupling a charged scalar to the same operator requires $\phi^\dagger\phi\,\mathcal{O}_{\mathrm{SM}}$, which is one mass dimension higher and therefore typically more suppressed in the sense of effective field theory.

More important is, perhaps, the fact that many experimentally relevant processes are forbidden by charge conservation. This is the case too for the standard, comparatively heavy, asymmetric dark matter. For example and due to the conserved charge, any indirect detection method based on decay or annihilation of dark matter will be suppressed. At low masses, the effect is even more dramatic. Since the signal of elastic scattering off Standard Model particles is too small to be detected, essentially all direct detection experiments looking for sub-eV dark matter particles are effectively based on (coherent) absorption of dark matter particles inside the experiment. For example, the famous axion haloscope [3] aims to use a strong magnetic field to convert axions into photons, which are then absorbed by the detector. This, however, is not possible if charge is to be conserved.

This unsuitability of traditional experimental setups leaves us with three options, all of them challenging. Firstly, there remains the possibility to search directly for the symmetric dark matter fraction, which carries no charge and effectively consists of particle-antiparticle pairs. Secondly, we can hope that there exist sufficiently unsuppressed charge violating operators that could be exploited in suitably designed experimental searches. Finally, we can search for other subtle effects that do not require charge violation or even an absorption, e.g. variations in fundamental constants related to spatial or temporal changes in the dark

[1] See [58, 59] for discussions of lighter asymmetric dark matter candidates, that however, do not discuss the origin of the asymmetry.

[2] For masses $\ll$ meV, this charge density would be larger than any one potentially carried by neutrinos (or any other fermions), because the energy density of such a fermion gas would exceed the dark matter density due to Pauli blocking, even if the particles were massless.

[3] An interesting construction where the role of the Affleck-Dine field is played by a pseudo-Nambu-Goldstone boson was recently suggested in [64].

JCAP09(2019)003

matter density. A few initial attempts for the example of a Higgs portal interaction are discussed in section 5. Nevertheless, clearly more work is needed to develop effective search strategies for the challenging case of very light asymmetric dark matter.

The structure of the remainder of this work is as follows. Below, we briefly introduce our model and discuss some of its main features and model building considerations. In section 2, we review the cosmological dynamics of a (homogeneous) self-interacting scalar field in an FLRW background. Then, in section 3, we describe how a net charge density can be generated in coherent oscillations of the classical field. Section 4 considers possible effects that can reduce the energy density stored in the uncharged component of the field while preserving the charge asymmetry, like the resonant annihilation of the symmetric part into an additional scalar field. In section 5, we discuss the phenomenology of our scenario focusing on potentially observable effects induced by very light particles with a large charge asymmetry. The Higgs portal scenario is studied as an interesting example. Finally, we conclude in section 6.

1.1 A simple model for very light asymmetric dark matter

Let us introduce the model under study before going into more detail about its cosmological dynamics in the following sections. We consider a complex scalar field theory with an approximate U(1) symmetry to play the role of the dark matter,

$$\mathcal{L} = \partial_\mu \phi^\dagger \partial^\mu \phi - m^2 \phi^\dagger \phi - \lambda \left(\phi^\dagger \phi\right)^2 - \epsilon \left(\phi^4 + \phi^{\dagger\,4}\right) . \tag{1.1}$$

The first three terms on the right hand side preserve the U(1) symmetry, which is broken explicitly by the quartic term proportional to ϵ. Without loss of generality, ϵ can be chosen to be real and positive.

Explicit U(1) breaking terms are necessary in order to generate some amount of conserved charge in a cosmological background. The reason is that an inflationary epoch in the early Universe dilutes any preexisting U(1) conserved number density. Therefore, in order to survive until the present day, the charge needs to be replenished after inflation. As is shown in section 3, a conserved charge is automatically generated as long as the breaking terms are active at any point after inflation. This is known as the Affleck-Dine mechanism [60], by which the initially homogeneous scalar field at rest acquires a non-vanishing angular momentum due to the asymmetry in the shape of the potential caused by the symmetry breaking terms.

The charge generation is most effective when the quartic terms of the potential are relevant. However, in this regime also other effects due to the self-interaction of the field may become important. Indeed, when self-interactions are dominating, the dark matter cosmology is affected in two ways. First, the energy density of a scalar field governed by a quartic term dilutes like radiation. Second, fluctuations, e.g. those unavoidably generated during inflation, can grow and cause a fragmentation of the field [61, 65–70]. We recall both effects in section 2.

In principle, all U(1) symmetry breaking operators up to fourth order in the fields could be included along with the one in the Lagrangian (1.1). We however only consider the operator $\epsilon\left(\phi^4 + \phi^{\dagger 4}\right)$ in this work. The practical reason for this is that in order for the charge to be conserved at late times, the symmetry breaking has to be switched off at some point during the cosmological evolution. This is achieved when the field value becomes small and the quartic interaction terms are subdominant to the quadratic ones, which are taken to be completely U(1) preserving. Other quartic terms like $\phi^3\phi^\dagger$ can be introduced

JCAP09(2019)003

without qualitatively changing any of our conclusions, and are kept out of the discussion in the interest of simplicity.

From a theoretical point of view, the choice of the potential (1.1) can be motivated by symmetry arguments. Indeed, the Lagrangian as presented above features an exact $\mathbb{Z}_4$ symmetry. It has been argued that such discrete symmetries can be preserved even if the global continuous symmetry is broken by quantum gravity effects [71, 72]. Similar arguments can allow to suppress the symmetry breaking terms even further, e.g. a $\mathbb{Z}_6$ symmetry would only allow some particular operators of dimension six or higher. In this sense, our potential is only one instance of this class of models.

The existence of an exact $\mathbb{Z}_4$ symmetry has additional phenomenological consequences, as it severely restricts the possible interaction terms with other particles, most importantly Standard Model ones. In this case, only symmetry breaking interactions that involve at least four powers of the dark matter field are allowed. The lowest dimension interactions with Higgs bosons or photons would then be of the form

$$\frac{1}{M^2}\phi^4 H^\dagger H \quad \text{or} \quad \frac{1}{M^4}\phi^4 F^2\,, \tag{1.2}$$

respectively. In contrast, U(1) symmetric operators are less suppressed by the energy scale M,

$$|\phi|^2 H^\dagger H \quad \text{or} \quad \frac{1}{M^2}|\phi|^2 F^2\,. \tag{1.3}$$

As long as M is large, U(1) conserving operators are expected to lead to stronger effects. We will investigate the phenomenology associated to the Higgs interaction in section 5.

2 Cosmological dynamics of a U(1) symmetric field

Let us start with the equations of motion for the complex scalar field (1.1) in an expanding background. It is convenient to decompose the field into the radial and the angular degree of freedom, $\phi = \varphi\exp(i\theta)/\sqrt{2}$. In these coordinates, the equations of motion for a spatially homogeneous[4] field read

$$\ddot{\varphi} + 3H\dot{\varphi} - \varphi\dot{\theta}^2 + \frac{\partial V}{\partial\varphi} = 0\,, \tag{2.1}$$

$$\ddot{\theta} + (3H + 2\partial_t \log\varphi)\,\dot{\theta} + \frac{1}{\varphi^2}\frac{\partial V}{\partial\theta} = 0\,, \tag{2.2}$$

where $H = \dot{a}/a$ is the Hubble parameter.

Even though the main focus of this work is the generation of a global U(1) charge density due to an explicit symmetry breaking, we first want to recall the dynamics of the U(1) symmetric case, i.e. $\epsilon = 0$, corresponding to the potential

$$V(\phi) = m^2\phi^\dagger\phi + \lambda\left(\phi^\dagger\phi\right)^2\,. \tag{2.3}$$

Looking at (2.1), it is clear that the dynamics of a complex field in the above potential can be described using a massive, self-interacting real scalar φ and a massless mode θ. For simplicity,

[4] The assumption of homogeneity of the field at cosmological scales is well motivated. The situation is very similar to that of the misalignment mechanism, since any sufficiently light field present during inflation is homogenized on scales larger than today's horizon.

in this section we will assume trivial dynamics of the angular component, $\dot{\theta} = 0$, and focus on the radial mode. This is justified by the fact that during inflation[5] any initial $\dot{\theta} \neq 0$ and the corresponding conserved charge is diluted, $\dot{\theta} \propto a^{-3}$, therefore quickly becoming negligible.

2.1 A self-interacting real scalar field

Once the dynamics of the angular mode are assumed to be trivial, i.e. $\theta(t) = \text{const}$, the equation of motion for the radial field simplifies to

$$\ddot{\varphi} + 3H\dot{\varphi} + m^2\varphi + \lambda\varphi^3 = 0\,, \tag{2.4}$$

which is exactly that of a massive and self-interacting real scalar (as studied originally in [73]). The existence of the self-interaction causes significant deviations from the usual cosmological evolution of a free scalar field. The general solution of (2.4) is complicated, but in a similar way to what is commonly done for the misalignment mechanism [20–25], we can separate the evolution into distinct regimes where solutions are easily found.

At early times, when the Hubble friction is very large compared to the mass and self-coupling terms, eq. (2.4) has a dominant constant solution, i.e. the field is stuck at a certain value, $\varphi(t) = \varphi_0$. As the Hubble parameter monotonically decreases with time, there comes a point t_0 when the friction is not strong enough and the field starts to oscillate around the minimum of its potential. The Hubble scale at which this transition happens can be estimated as (cf. [74])

$$3H(t_0) \simeq \left|\frac{\partial^2 V}{\partial\varphi^2}\right|^{\frac{1}{2}}\,. \tag{2.5}$$

Assuming a radiation dominated universe, this corresponds to

$$t_0 = \frac{3}{2}\left|m^2 + 3\lambda\varphi_0^2\right|^{-\frac{1}{2}}\,. \tag{2.6}$$

For the rest of this work and unless stated otherwise, the scale factor in the radiation dominated universe will be normalized to $a(t) = \sqrt{t/t_0}$.

In the equation of motion (2.4), there is a competition between the mass and the self-coupling of the field. In the following, we can distinguish two regimes: the *quartic-dominated* regime when $\lambda\varphi^2 \gg m^2$, and the *mass-dominated* regime, characterized by $\lambda\varphi^2 \ll m^2$. Given a large enough initial field value, the evolution is at first dominated by the quartic term. Later on, the mass-dominated regime is eventually reached once the amplitude of the oscillations of the field is sufficiently damped by the expansion of the universe. If initially $\lambda\varphi_0^2 \ll m^2$, the quartic-dominated regime is skipped and the quartic terms are irrelevant for the cosmological evolution. As we are interested in studying the effect of the self-interactions, in the following we assume that $\lambda\varphi_0^2 \gtrsim m^2$.

Let us now be more quantitative. In the quartic-dominated regime, the equation of motion of φ can be written as

$$\ddot{\varphi} + 3H\dot{\varphi} + \lambda\varphi^3 = 0\,. \tag{2.7}$$

It is solved by the Jacobi elliptic cosine function with modulus $k^2 = 1/2$,

$$\varphi(\eta) = \frac{\varphi_0}{a}\,\mathrm{cn}\left(\sqrt{\lambda}\varphi_0\eta, \frac{1}{\sqrt{2}}\right) \approx \frac{\varphi_0}{a}\cos\left(\frac{3}{4}\sqrt{\lambda}\varphi_0\eta\right)\,, \tag{2.8}$$

[5] We assume that the inflation scale $H_\mathrm{I} \gg m$.

JCAP09(2019)003

where we use conformal time $\eta = 2t_0(a(t)-1)$ (i.e. $\eta(t_0) = 0$) and impose the initial condition $\varphi(0) = \varphi_0$.

The time t_1 when the transition from the quartic- to the mass-dominated regime occurs is given by the condition $\lambda\Phi^2(t_1) \simeq m^2$ (where Φ denotes the amplitude of the oscillations), yielding

$$t_1 = \frac{\lambda\varphi_0^2}{m^2} t_0 \,. \tag{2.9}$$

In the mass-dominated regime, the eq. (2.4) reduces to the well-known damped harmonic oscillator,

$$\ddot{\varphi} + 3H\dot{\varphi} + m^2\varphi = 0 \,, \tag{2.10}$$

which is solved to an excellent approximation by

$$\varphi(t) = \varphi_1 \left(\frac{a_1}{a(t)}\right)^{3/2} \cos\left(m(t-t_1)\right) \,. \tag{2.11}$$

Here, φ_1 and a_1 are evaluated at time t_1.

From the evolution of the field in both regimes, we can obtain the scale factor dependence of the energy density of the field. In the quartic-dominated regime and averaging over oscillations, the scalar field redshifts as radiation, $\langle\rho\rangle \propto a^{-4}$. In the mass-dominated regime, the energy density dilutes as $\langle\rho\rangle \propto a^{-3}$, making a massive scalar field a good dark matter candidate.[6]

The main consequences of the discussed evolution are summarized in figure 1. There, we show the initial field value needed to explain the full dark matter density observed in the universe today, $\rho_{\rm DM} = 1.3\,\mathrm{keV/cm^3}$ [75], as a function of the mass and the self-coupling. Outside of the yellow-shaded region, the field goes through a quartic-dominated phase as described above. This significantly increases the required size of the initial field value[7] to produce the full dark matter density today, up to the point that above the black dashed line, the initial field value would need to be larger than the Planck scale. A stronger bound on the initial field value can be obtained from requiring that, during inflation, the energy density stored in the complex field is much smaller than that of the inflaton. This is satisfied as long as

$$\lambda\varphi_0 \ll 3M_{\rm Pl}H_I^2 \,, \tag{2.12}$$

where H_I is the Hubble scale of inflation. For a choice of $H_I = 10^4\,\mathrm{GeV}$, we obtain the bound shown in white in figure 1.

Furthermore, requiring that the scalar field is sufficiently non-relativistic at the onset of structure formation prevents the quartic-dominated regime from lasting too long. The corresponding limit is shown in red in figure 1. A robust bound (solid line) was derived in [77], where a detailed analysis of the effects in the CMB power spectrum and the matter power spectrum at linear scales was performed. Note that this results in a more stringent

[6] Note that both results can also be obtained easily by using the virial theorem, instead of explicitly solving the equations of motion.

[7] In principle, the initial field value could be generated dynamically by the inclusion of a suitable coupling to the Ricci scalar [76] of the form $\xi R\phi^\dagger\phi$. This can induce a tachyonic mass during inflation, causing the field to evolve towards its effective minimum. However, for this minimum to be located at the necessary initial field value, the smallness of λ in our setup requires the coupling ξ to be extremely small unless inflation happens at a very low scale. This in turn also requires an extremely long period of inflation for the field to reach its effective minimum. Alternatively, if the number of e-folds is not too large, the field could attain a suitable initial condition while still evolving towards the effective minimum for somewhat larger values of ξ.

JCAP09(2019)003

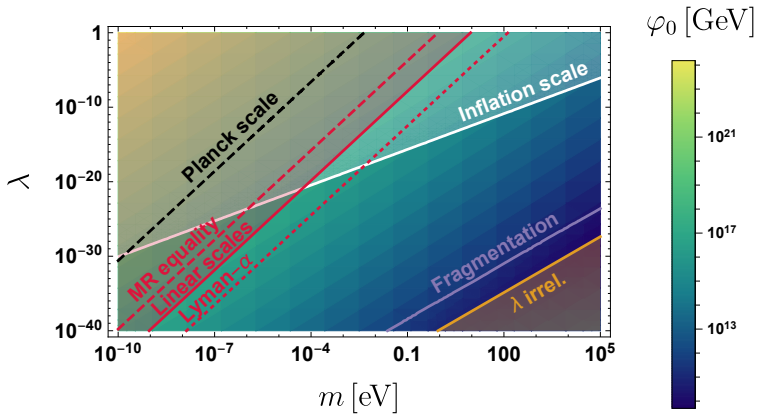

Figure 1. Initial field value φ_0 of the real scalar field that yields the observed relic abundance of dark matter, shown as a function of the mass m and the self-coupling λ. The black dashed line illustrates the Planck scale, while the white-shaded region is excluded, because the energy density in the complex field during inflation exceeds that of the inflaton (this bound depends on the inflation scale, for this figure we use $H_{\rm I} = 10^4\,{\rm GeV}$). In the yellow region the field skips the quartic-dominated regime, such that the self-coupling has no cosmological relevance. The red-shaded region is excluded because the field is still behaving like radiation at the onset of structure formation (more details, including an explanation of the different lines, are given in the main text). Above the purple line the homogeneous field fragments into fluctuations (this again mildly depends on the scale of inflation).

constraint than the one coming from the requirement that the field be non-relativistic at the time of matter-radiation equality (dashed line). An even stronger limit could potentially be placed by using Lyman-α forest observations [78]. This, however, would require a dedicated analysis of the non-linear regime which is beyond the scope of this paper. Instead, here we merely indicate the region where the field is still relativistic at the time when the smallest scale accessible to Lyman-α observations, $k \sim 40\,{\rm Mpc}^{-1}$, enters the horizon (dotted line).

Finally, let us briefly comment on the generation of isocurvature fluctuations in this scenario. The fluctuations in the dark matter density originate from the quantum fluctuations that ϕ acquires during inflation. Being uncorrelated with the inflaton ones, they are subject to isocurvature constraints. The density contrast power spectrum at CMB scales has an amplitude $\mathcal{P}_\delta \sim (H_I/\varphi)^2$. For the parameter region where $\lambda\varphi_0^2 \gtrsim m^2$, the observational bound $\mathcal{P}_\delta \lesssim 10^{-10}$ [79] is not an issue as long as $H_I \lesssim 10^6\,{\rm GeV}$, but becomes problematic for larger values of the inflation scale.

2.2 Fragmentation of the coherent field

Any coherently oscillating, self-interacting scalar field is generically prone to experiencing "fragmentation" into inhomogeneous fluctuations that carry non-vanishing momentum [61, 65–70]. This effect can be interpreted as explosive (self-)particle production via a parametric resonance [65–67, 70] (whose arguments we follow). In order to assess the relevance of this process, we study the evolution of the fluctuations $\delta\varphi$ in the homogeneous background field φ. Working to linear order in perturbations, $\bar{\varphi}(x) = \varphi(t) + \delta\varphi(\vec{x}, t)$, the fluctuations obey

JCAP09(2019)003

the mode equation

$$\ddot{\delta\varphi}_k + 3H\dot{\delta\varphi}_k + \left(\frac{k^2}{a^2} + 3\lambda\varphi^2\right)\delta\varphi_k = 0\,, \tag{2.13}$$

which is valid in the quartic-dominated regime. The dependence of eq. (2.13) on the expansion of the Universe can be removed by using conformal coordinates, $\hat{\varphi}_k = a\,\delta\varphi_k$ and $\mathrm{d}\eta = a^{-1}\mathrm{d}t$, in terms of which the mode equation becomes

$$\frac{\mathrm{d}^2\hat{\varphi}_k}{\mathrm{d}\eta^2} + \left(k^2 + 3\lambda a^2\varphi^2\right)\hat{\varphi}_k = 0\,. \tag{2.14}$$

Using the expression eq. (2.8) for the background field in the quartic-dominated regime, eq. (2.14) can be transformed into the following Mathieu equation,

$$\frac{\mathrm{d}^2\hat{\varphi}_k}{\mathrm{d}z^2} + \left(A_k - 2q\cos(2z)\right)\hat{\varphi}_k = 0\,, \tag{2.15}$$

with $q = 4/3$ and

$$z = \frac{3}{2}\sqrt{\lambda}\varphi_0\, t_0\,(a(t) - 1) \pm \frac{\pi}{2}\,, \tag{2.16}$$

$$A_k = \left(\frac{4}{3}\right)^2 \frac{k^2}{\lambda\varphi_0^2} + 2q\,. \tag{2.17}$$

A detailed discussion of the solutions to this equation is given in section 4 (see also [65–67, 70]). Here, and in order to avoid repetitions, we just state the main conclusions. Floquet's theorem implies that the solution to (2.15) contains an exponential factor,

$$\varphi_k \propto \exp\left(\mu_k z\right)\,. \tag{2.18}$$

For our case with characteristic parameter $q = 4/3$, the dominant contribution to the Floquet exponent μ_k comes from the second resonance band of the (in)stability chart of the Mathieu equation. The largest exponent corresponds to the mode with momentum $k_\star \sim \sqrt{\lambda}\varphi_0$, for which $\mu \approx 0.1$ [80]. Note that $\sqrt{\lambda}\varphi_0 \gtrsim m$ in the quartic-dominated regime, which means that the modes that experience the most rapid growth are relativistic at the time of production. We can express eq. (2.18) in terms of physical time t to obtain the fragmentation rate

$$\Gamma_{\mathrm{frag}}(t) \sim \frac{3\mu}{2}\sqrt{\lambda}\,\frac{\varphi_0}{a(t)}\,. \tag{2.19}$$

If the fluctuations grow too large, most of the energy density that was stored in the homogeneous oscillations is transferred to inhomogeneous and relativistic modes. Given that our treatment later on relies on the assumption of homogeneity of the field, a complete fragmentation of the field is to be avoided in order to retain analytic control of the dynamics. Indeed, the linear expansion of the perturbations around the background breaks down even before the mode functions become of size comparable to that of the homogeneous field, i.e. $\langle\delta\varphi^2\rangle \sim \varphi^2$. We expect this to happen at approximately

$$t_{\mathrm{frag}} \sim \Gamma_{\mathrm{frag}}^{-1}\,\log\left(\frac{\varphi}{H_I}\right)\,. \tag{2.20}$$

The logarithm takes into account the initial conditions for the growth of the perturbations, which are given by inflationary quantum fluctuations, i.e. $\delta\varphi_k \sim H_I/k^{3/2}$, where H_I is the

JCAP09(2019)003

Hubble scale of inflation. The dependence on the initial conditions is relatively weak because of the exponential nature of the fragmentation process.

If fragmentation is significant before the quartic-dominated regime ends, that is, if $t_{\rm frag} \lesssim t_1$, the linear approximation as well as the description in terms of essentially homogeneous fields breaks down. The range of parameters where this happens lies above the purple line in figure 1. The estimates of the charge generation done in section 3 are therefore only directly applicable between the purple and yellow lines in figure 1. We note, however, that this does not necessarily mean that the mechanism is not viable outside of this region. Proceeding into the non-linear regime would require suitable methods such as classical statistical field theory simulations (cf. e.g. [81, 82]), which are beyond the scope of the present paper. However, the fragmented regime is not necessarily unsuitable for dark matter. Indeed, we expect that in large regions of the parameter space the field is still sufficiently cold, but exhibits fluctuations on small yet macroscopic length scales, similar to what was found in [83] for an uncharged field. For overall attractive interactions, interesting phenomena such as the formation [68, 69] (see also [61] for an overview) of Q-balls [84] that can also be dark matter [68] may arise. In the repulsive case, highly non-trivial effects may also occur [85]. A detailed study of these effects for the very light fields of interest to us would be very interesting.

After understanding the basics of the cosmological evolution of the self-interacting real scalar field, in the next sections we shift the focus to the dynamics of a complex scalar field.

3 Affleck-Dine dynamics and generation of charge

In this section, we study the generation of a net U(1) charge during the cosmological evolution of the complex scalar field with explicit U(1) symmetry breaking terms. The creation of an effective charge density occurs via the Affleck-Dine mechanism, which was originally proposed as a baryogenesis scenario [60], but has also been used to link baryogenesis and dark matter [57, 62, 63]. Therefore and in contrast to the previous section, we now include the symmetry breaking terms in the potential and take the dynamics of the angular degree of freedom into account. To be concrete, we consider the model from eq. (1.1), i.e. a massive scalar field with quartic self-interactions of Affleck-Dine type [60],

$$V(\phi) = m^2\phi^\dagger\phi + \lambda\left(\phi^\dagger\phi\right)^2 + \epsilon\left(\phi^4 + \phi^{\dagger\,4}\right) . \tag{3.1}$$

The coupling ϵ explicitly breaks the U(1) symmetry.[8] The charge density is produced in the early Universe when this term is active, and is conserved at late times when the field value drops below the threshold at which the quartic interaction becomes inefficient and the U(1) symmetry is effectively restored. Our goal in what follows is to compute the energy density associated with this U(1)-protected charge density.

3.1 Charge generation

Let us now turn to the dynamics of the charge generation for the dark matter field via the Affleck-Dine mechanism, which are essentially unaltered from the case of baryogenesis (see, e.g., [61]). Importantly, however, we directly consider the homogeneous scalar field as our dark matter candidate.

[8] If we were to take into account other quartic symmetry breaking terms such as $\phi^\dagger\phi^3$, the results would be qualitatively similar.

JCAP09(2019)003

Similar to the case of a real scalar, it is convenient to decompose the field into the radial and the angular degree of freedom, $\phi = \varphi \exp(i\theta)/\sqrt{2}$. In these coordinates, the scalar potential reads

$$V(\varphi, \theta) = \frac{m^2}{2}\varphi^2 + \frac{\lambda}{4}\varphi^4 + \frac{\epsilon}{2}\cos(4\theta)\,\varphi^4\,. \tag{3.2}$$

Explicitly, the equations of motion for the radial and angular components are

$$\ddot{\varphi} + 3H\dot{\varphi} - \varphi\dot{\theta}^2 + m^2\varphi + \lambda\varphi^3 + 2\epsilon\cos(4\theta)\,\varphi^3 = 0\,, \tag{3.3}$$

$$\ddot{\theta} + (3H + 2\partial_t \log\varphi)\,\dot{\theta} - 2\epsilon\varphi^2 \sin(4\theta) = 0\,. \tag{3.4}$$

The overall evolution of the complex field ϕ is similar to the real case. First, the field is stuck at its initial value and phase due to the Hubble friction. At a later point, it starts to roll down the potential, probing the quartic self-interactions of the potential that now in addition drive the angular motion via the U(1) symmetry breaking terms. During this epoch, a significant amount of energy density can be transferred to the angular degree of freedom, creating a net charge asymmetry. As the Universe expands, the amplitude of the oscillations becomes small enough so that the mass term comes to dominate the evolution and the field acts as dark matter. In this regime, the effective U(1) symmetry of the theory is restored, finally stabilizing the charge density.

The net U(1) charge density is mostly governed by the dynamics of the angular component θ,

$$n = \varphi^2\dot{\theta}\,. \tag{3.5}$$

Upon the use of the equations of motion, n satisfies the differential equation

$$\dot{n} + 3Hn + \frac{\partial V}{\partial\theta} = 0\,. \tag{3.6}$$

From eq. (3.6) it is easy to see that the non-conservation of charge density is proportional to the symmetry breaking coupling,

$$\frac{1}{a^3}\frac{\mathrm{d}}{\mathrm{d}t}\left(a^3 n\right) = -\frac{\partial V}{\partial\theta} = 2\epsilon\varphi^4 \sin(4\theta)\,. \tag{3.7}$$

Therefore, in the U(1) symmetric case, $\epsilon = 0$, the charge density is comovingly conserved. From eq. (3.7) we can get a qualitative understanding of the behavior of $n(t)$. The symmetry breaking term on the right hand side sources the charge generation. Depending on θ it can be positive or negative. As soon as θ moves significantly, charge will be continuously created and destroyed for as long as the quartic terms are active. When the mass term starts to dominate, the field behaves like $\varphi \sim a^{-3/2}$ and the right hand side falls off as $\sim a^{-6}$, effectively restoring the U(1) symmetry. From then on the previously generated charge density is comovingly conserved.

According to our earlier discussion for the real scalar field, a long enough period of time spent in the quartic-dominated regime can lead to fragmentation of the coherent field. As shown in figure 1, the quartic-dominated regime has to be rather short in order to prevent this from happening. This is possible if the quartic couplings are not much larger than m^2/φ_0^2. In this scenario, the generation of the charge has to be sufficiently fast in order to occur before fragmentation becomes sizeable. This can be achieved in the band between the purple and yellow regions of figure 1. But even when fragmentation is important, there is no reason to believe that charge generation is completely inefficient. However, our estimations

JCAP09(2019)003

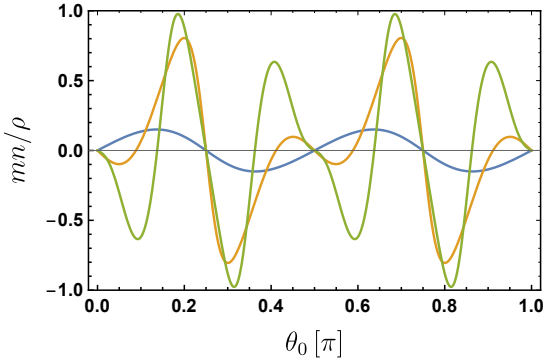

Figure 2. Final fraction of the energy density stored in the charged particles with respect to the total energy density of the coherent oscillations of ϕ as a function of the initial misalignment angle θ_0. The initial radial field value is chosen to give the correct relic abundance of dark matter. As a benchmark, we choose the parameters $m = 1\,\text{eV}$ and $\lambda = 10^{-39}$, which fall in the region between the yellow and purple lines in figure 1. The U(1) breaking coupling ϵ is set to $0.01\,\lambda$ (blue), $0.1\,\lambda$ (yellow) and $0.2\,\lambda$ (green). As we can see, a sizeable fraction of the energy density can be stored in the charge asymmetry, e.g. for $\epsilon = 0.2\,\lambda$ (green), we observe values in excess of 95%.

are not applicable in this case, which requires a full non-perturbative treatment along the lines of [69, 81, 82, 85]. Indeed, interesting non-trivial effects such as a formation of Q-balls or other inhomogeneous structures are expected [68, 69, 84, 85]. Yet, this lies beyond the scope of the present work.

In practice, to obtain n, we solve the equations of motion for the radial and angular mode numerically and then use eq. (3.5) for the charge density. The final amount of net charge is illustrated in figure 2, where we show the fraction of energy density stored in the charge asymmetry, $m\,n$, compared to the total energy density of the field ρ, as a function of the initial misalignment angle θ_0 for different values of ϵ. For simplicity, we estimate the initial field value φ_0 by considering the real scalar field case illustrated in figure 1. For small ϵ values, the created charge exhibits a simple oscillatory pattern with respect to the initial angle. The reason is that in this case θ only traverses a small range of values during the time when the quartic term is active. Thus, the right hand side of eq. (3.7) is always of the same sign and the asymmetry is driven in a single direction. However, as ϵ becomes larger, θ changes more quickly, and leads to a continuous creation and destruction of charge that makes the behavior more complicated.

Remarkably, figure 2 shows that it is possible to obtain a sizable fraction close to unity for a suitable choice of parameters without invoking any significant fine tuning. As already pointed out in the introduction and as will be discussed in section 5, detecting the part of dark matter that carries a conserved U(1) charge is challenging. Therefore, if most of the dark matter is charged, current detection techniques may be significantly less sensitive than in purely symmetric scenarios.

3.2 Charged dark matter

For later use, we now compile some expressions describing the late time behavior of the field. After the U(1) symmetry is restored, the dynamics are governed by the mass term of the potential. In this situation, the general solution for the complex field rotates on an ellipse

JCAP09(2019)003

(see, e.g., [86] for useful formulas) in the complex plane,

$$\phi = \left(\frac{a_1}{a}\right)^{\frac{3}{2}} \Psi_1 \left[\cos(\vartheta)\cos(mt+\delta) + i\sin(\vartheta)\cos(mt)\right]. \tag{3.8}$$

Here, Ψ_1 is a complex amplitude and δ is a phase, both fixed at a suitable time t_1 or scale factor a_1.

From eq. (3.8), we can easily compute the charge density as

$$n = m\left(\frac{a_1}{a}\right)^3 |\Psi_1|^2 \sin(2\vartheta)\sin(\delta)\,. \tag{3.9}$$

Similarly, the total energy density is given by

$$\rho_{\rm CDM} = m^2\left(\frac{a_1}{a}\right)^3 |\Psi_1|^2 = \rho_{\rm a} + \rho_{\rm s} + \mathcal{O}\left(\frac{H}{m}\right), \tag{3.10}$$

where we neglect small terms arising from the Hubble evolution. Moreover, we take the opportunity to define the energy densities in the asymmetric and symmetric parts,

$$\rho_{\rm a} = mn\,, \qquad \rho_{\rm s} = \rho_{\rm CDM} - \rho_a\,. \tag{3.11}$$

From this, it is also convenient to introduce the asymmetric and symmetric fractions of the energy density,

$$\eta_{\rm a} = \frac{\rho_{\rm a}}{\rho_{\rm CDM}}\,, \qquad \eta_{\rm s} = \frac{\rho_{\rm s}}{\rho_{\rm CDM}}\,, \tag{3.12}$$

which in the quadratic-dominated regime are independent of time.

Later, in section 5 we mostly consider charge conserving interactions. Those usually involve the combination

$$\phi^\dagger\phi = \frac{1}{2}\frac{\rho_{\rm CDM}}{m^2}\left[\mathcal{A} + \mathcal{B}\cos^2(mt+\alpha)\right], \tag{3.13}$$

where,

$$\mathcal{A} = 1 - \sqrt{1-\eta_{\rm a}^2}, \qquad \mathcal{B} = 2\sqrt{1-\eta_{\rm a}^2}, \tag{3.14}$$

and α is a phase related to ϑ and δ, which is however not important for our discussions.

In order to get a better physical understanding of the quantites defined above, let us consider some extreme cases. The combination in eq. (3.13) is constant if the whole density is stored in the charge asymmetry ($\eta_{\rm a} = 1$), whereas in the completely symmetric case ($\eta_{\rm a} = 0$) it is purely oscillatory. More insights can be gained by considering the slightly more general cases $1 - \eta_{\rm a} = \eta_{\rm s} \ll 1$ and $\eta_{\rm a} = 1 - \eta_{\rm s} \ll 1$. In the first case, we have

$$\mathcal{A} \approx 1 - \sqrt{2}\sqrt{\eta_{\rm s}\eta_{\rm a}}\,, \qquad \mathcal{B} \approx 2\sqrt{2}\sqrt{\eta_{\rm s}\eta_a}\,, \qquad \text{for} \quad (1-\eta_{\rm a}) = \eta_{\rm s} \ll 1\,. \tag{3.15}$$

In other words, there is a large constant part ~ 1 while the oscillations are suppressed $\sim \sqrt{\eta_{\rm s}}$.

In the opposite limit, we have

$$\mathcal{A} \approx \frac{\eta_{\rm a}^2}{2}\,, \qquad \mathcal{B} \approx 2 - \eta_{\rm a}^2\,, \qquad \text{for} \quad \eta_{\rm a} = 1 - \eta_{\rm s} \ll 1\,. \tag{3.16}$$

This corresponds to oscillations with a small constant component.

4 Depletion of the uncharged component via annihilations

In contrast to the asymmetric component of the dark matter, the symmetric part is not protected by the U(1) symmetry, so there is the possibility that it depletes, e.g. via annihilation of the effective[9] particle-antiparticle pairs. In this section, we consider such a possibility in order to determine the fraction of the symmetric part of the dark matter that can be lost. For example, if the annihilation is into massless particles, the energy density stored in them dilutes as radiation and therefore quickly becomes redshifted.[10] The result is an effective increase in the fraction of the energy density stored in the charged component compared to the uncharged part.

The specific interaction that we consider in the following does not lead to a full depletion of the uncharged component, as the annihilations stop when the charged and uncharged energy densities are roughly of the same order. As a consequence, even in situations where the initial charge asymmetry is relatively small, the present day asymmetry can still be significant. More generally, our discussion provides a proof of principle that a sizable depletion is possible, motivating the thorough investigation of depletion mechanisms.

4.1 Annihilation into a second (uncharged) scalar

As a concrete realization of the ideas above, we consider the depletion of the symmetric component by an additional coupling of the complex scalar field ϕ to another scalar field χ. For concreteness, we focus on the interaction

$$\mathcal{L}_I = g\,|\phi|^2\,\chi^2\,. \tag{4.1}$$

In order to study the transfer of energy from the field ϕ to χ, we consider the dynamics of the quantum field χ in the oscillating background ϕ. Such a situation has been intensely studied in the context of reheating after inflation [65–67, 70] (cf. also [88]), and we base our discussion on the findings of these works.

The interaction term (4.1) induces an oscillating mass term for the field χ, i.e. the frequencies of the mode functions of χ are modified as

$$\ddot{\chi}_k + 3H\dot{\chi}_k + \left(\frac{k^2}{a^2} + m_\chi^2 + 2g\,|\phi|^2\right)\chi_k = 0\,. \tag{4.2}$$

It is then possible that some momentum modes are enhanced by resonance effects. Since the mode functions determine the occupation number, this enhancement can be viewed as a resonant production of χ-particles. This process is known as *parametric resonance* [65–67, 70].

Let us therefore study the parametric resonance induced by the coherent oscillations of ϕ in more detail. For simplicity, we take χ to be massless, such that the mode functions obey

$$\ddot{\chi}_k + 3H\dot{\chi}_k + \left(\frac{k^2}{a^2} + g\varphi^2\right)\chi_k = 0\,, \tag{4.3}$$

where we use the polar decomposition of ϕ. From the above equation of motion it is clear that the oscillating nature of φ can drive the χ-modes into a resonance, inducing rapid (as we will shortly see, exponential) growth of the mode functions.

[9] As long as we are dealing with coherently oscillating fields, one cannot strictly speak of pair annihilation, but it serves as an intuitive picture.

[10] This generally has to happen long enough before matter-radiation equality, but as it was recently shown [87], a small component of dark matter decaying at late times can help alleviate the H_0 tension.

JCAP09(2019)003

The total number density of χ-particles is given by a summation over all modes,

$$n_\chi = \frac{1}{(2\pi a)^3}\int \mathrm{d}^3k\, n_k = \frac{1}{2\pi^2 a^3}\int \mathrm{d}k\, k^2 n_k\,. \tag{4.4}$$

The corresponding energy density of the generated χ-particles can be computed similarly,

$$\rho_\chi = \frac{1}{(2\pi a)^3}\int \mathrm{d}^3k\, \omega_k n_k = \frac{1}{2\pi^2 a^3}\int \mathrm{d}k\, k^2 \omega_k n_k\,, \tag{4.5}$$

where ω_k denotes the energy of the mode. The comoving occupation numbers can be obtained from the mode functions via [67],

$$n_k = \frac{\omega_k}{2}\left(\frac{|\dot{\chi}_k|^2}{\omega_k^2} + |\chi_k|^2\right) - \frac{1}{2}. \tag{4.6}$$

Proceeding in a similar way as we did in section 2, we study separately the evolution of the occupation numbers governed by (4.3) in the two different regimes of the evolution of the radial mode φ: the quartic- and mass-dominated regimes. In the following, for simplicity, we neglect the asymmetric part of the field and only consider the symmetric contribution. That is, we focus on the depletion of the symmetric part of ϕ (cf. section 3.2). We comment on the effects of a non-vanishing asymmetric part at the end of this section.

4.2 Quartic-dominated epoch

In the regime where the quartic self-interaction dominates the evolution of the field, the theory is essentially scale invariant. Hence it is useful to use conformal coordinates $x_k = a\chi_k$ and $\mathrm{d}\eta = a^{-1}\mathrm{d}t$, in which the equation of motion reads,

$$\frac{\mathrm{d}^2 x_k}{\mathrm{d}\eta^2} + \left(k^2 + g a^2 \varphi^2\right) x_k = 0\,. \tag{4.7}$$

Importantly, we assume that the evolution of the radial mode is governed by the U(1) symmetric interactions only, i.e. it is given by (2.8). Under this assumption, the equation of motion for the mode functions (4.7) can be rewritten as a Mathieu equation,

$$\frac{\mathrm{d}^2 x_k}{\mathrm{d}z^2} + \left(A_k - 2q\cos(2z)\right) x_k = 0\,, \tag{4.8}$$

where we have defined

$$z = \frac{3}{2}\sqrt{\lambda}\varphi_0 t_0\left(a(t) - 1\right) \pm \frac{\pi}{2}\,, \tag{4.9}$$

$$A_k = \left(\frac{4}{3}\right)^2 \frac{k^2}{\lambda\varphi_0^2} + 2q\,, \tag{4.10}$$

$$q = \frac{4}{9}\frac{g}{\lambda}\,. \tag{4.11}$$

Without the need to solve the differential equation for the mode functions explicitly, we know by Floquet's theorem that the solution contains an exponential factor,

$$x_k \propto \exp\left(\mu_k z\right)\,, \tag{4.12}$$

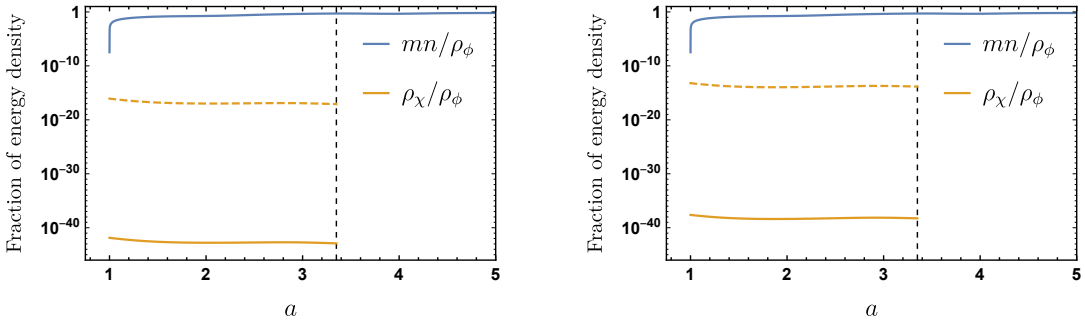

Figure 3. Fraction of energy density stored in charged particles compared to the fraction of the energy transferred to the field χ as a function of the scale factor a for the quartic-dominated epoch. The end of the quartic-dominated regime is indicated by a dashed vertical line. As a benchmark for the coherent oscillations of ϕ, we chose the parameters $m = 1\,\mathrm{eV}$, $\lambda = 10^{-39}$, $\epsilon = 0.1\,\lambda$ and $\theta_0 = 0.2\,\pi$. Furthermore, the initial field value is chosen to give the correct relic abundance of dark matter. The left panel corresponds to a narrow resonance, $g = 0.1\,\lambda$, while the right panel shows a broad resonance, $g = 10^4\,\lambda$. The solid yellow line assumes that the initial occupation numbers are just the minimal quantum $n_k = 1/2$, whereas the dashed line uses inflationary fluctuations $n_k \sim (H_\mathrm{I}/k)^2$, with $H_\mathrm{I} = 10^4\,\mathrm{GeV}$. We note that our estimate accounts only for the exponential growth of the mode functions and does not take into account polynomial pre-factors. This causes the slight decrease in both panels.

with Floquet exponent μ_k. The Floquet exponents characterize the different solutions of the Mathieu equation. For instance, if μ_k is imaginary, x_k is an oscillatory function, falling into the class of stable solutions of the Mathieu equation. We are however interested in the unstable solutions, i.e. solutions with real and positive μ_k, which correspond to exponential growth of the mode functions and thus rapid particle production. The Floquet exponents are in turn characterized by so-called (in)stability bands of the Mathieu equation for different values of A_k and q. These stability bands determine the rate of resonant production of χ-particles in the unstable regions, see, e.g., [80].

The Floquet exponent μ_k for each mode is essentially set by q, i.e. the ratio between the couplings g and λ of the theory. This ratio is therefore the defining quantity that controls the production rate of χ-particles. Semi-analytic estimates for the Floquet exponent exist for two different limits, $q \ll 1$ and $q \gg 1$. These two regimes are coined *narrow* and *broad* resonance, respectively.

In figure 3 we show an example of the energy transfer from the coherent oscillations of the symmetric part of ϕ to the field χ for both types of resonance as a function of the scale factor. A detailed discussion of how to arrive at these results is given in appendix A. The fraction of energy density stored in the created charged particles (shown in blue) is computed taking the full dynamics of the oscillations into account. However, the result for the resonant production of χ-particles (shown in yellow) is only valid in a purely quartic-dominated regime for the radial oscillations. For the chosen benchmark point, we observe that the generation of charge stops at $a \sim \mathcal{O}(10)$, before the creation of χ-particles becomes significant. In fact, our description of energy transfer is only applicable up to $a \sim \mathcal{O}(3)$, which is the point where the purely quartic-dominated regime ends and the mass term takes over. That is, during the quartic-dominated epoch, the transfer of the energy to χ cannot reach a significant amount, such that the depletion of the uncharged component of the dark matter

JCAP09(2019)003

is neither efficient in narrow resonance, $g \ll \lambda$, nor in the broad resonance regime, $g \gg \lambda$. Furthermore, this implies that the induced backreaction on the dynamics of ϕ due to the creation of χ-particles[11] can be neglected as long as the quartic interaction terms dominate the evolution of ϕ. This assures that the mechanism of charge production described in the previous section is not affected.

4.3 Mass-dominated epoch

Once the mass term starts to dominate the evolution of the field, the U(1) symmetry of the theory is restored and the generated charge density is (approximately) conserved. However, similar to the quartic-dominated regime, the uncharged component of ϕ is still subject to annihilation into χ-particles.

After a convenient field redefinition, $x_k = a^{3/2}\chi_k$, the equation of motion for the modes reads

$$\ddot{x}_k + \left(\frac{k^2}{a^2} + \frac{3}{4}H^2 + g\varphi^2\right) x_k = 0\,. \tag{4.13}$$

In contrast to the quartic-dominated epoch, the explicit dependence on the Hubble scale of the expansion does not drop out.[12]

As pointed out in the beginning of this section, we assume that the evolution of the radial mode is entirely governed by U(1) symmetric interactions, i.e. it is given by eq. (2.11). Using this, the equation of motion is of quasi Mathieu form,

$$\frac{\mathrm{d}^2 x_k}{\mathrm{d}z^2} + (A_k - 2q\cos(2z))\, x_k = 0\,, \tag{4.14}$$

where we have defined

$$z = mt\,, \tag{4.15}$$

$$A_k = \frac{k^2}{a^2 m^2} + \frac{3}{4}\frac{H^2}{m^2} + 2q\,, \tag{4.16}$$

$$q = \frac{g\Phi^2}{4m^2}\,. \tag{4.17}$$

Here, Φ denotes the amplitude of the radial oscillations of the symmetric component. The term involving the Hubble parameter appears as a shift of the momentum in each mode by $k^2 \to k^2 + 3/4a^2H^2$. As we will later see, this shift is small and can be neglected.

Eq. (4.14) is not precisely a Mathieu equation, because the characteristic parameters A_k and q explicitly depend on time through the scale factor. Depending on the coupling g, the system might start out in a broad resonance, but, as time evolves, q continuously decreases until it eventually ends up in a narrow resonance. In addition, q might significantly vary within a few oscillations of the field, such that the analysis based on the static stability chart of the Mathieu equation is not applicable anymore. Instead, the dominant process in this setting will be the so-called *stochastic resonance* [67]. In this regime, the occupation number n_k typically increases, but may sometimes decrease instead. The reason for this is that the frequency of the modes χ_k changes drastically with each oscillation of φ. Consequently, the phases of χ_k are practically uncorrelated at the successive stages of particle production,

[11] In particular, the resonant production of χ-particles effectively contributes an additional friction term $\sim \Gamma\dot{\phi}$ to the equations of motion of ϕ, where Γ denotes the rate of particle production.

[12] Note that in a universe dominated by matter instead of radiation, the term involving H^2 would disappear.

mildly diminishing the resonant effect. For a detailed discussion of the stochastic resonance phenomenon, we refer the reader to the seminal work [67]. Here, we closely follow their derivation in order to estimate the rate of resonant production of χ-particles during the mass-dominated epoch.

A necessary condition for the resonance to be active is given by $q^2 m \gtrsim H$ [67]. Given the typical scale of the Hubble parameter in the mass-dominated regime, this roughly translates into $\sqrt{g}\Phi \gtrsim m$. This condition equivalently reads $q \lesssim 1/4$, which means that we expect particle production to stop in the narrow resonance regime. The same condition, in turn, allows us to estimate the time scale t_f or the number of oscillations N_f after which the resonance terminates.

Rapid production of χ-particles occurs whenever the adiabaticity condition for the mode frequencies of χ is violated,

$$\omega_k^2 \lesssim \frac{\mathrm{d}\omega_k}{\mathrm{d}t}\,, \tag{4.18}$$

with the frequency given by $\omega_k^2 = \frac{k^2}{a^2} + \frac{3}{4}H^2 + g\varphi^2$. Due to the oscillations of the driving field, the resonance is only active for a short period of time in the vicinity of each zero crossing $\varphi(t) = 0$. This period is typically of order inverse to the characteristic momenta involved in the resonance, $\Delta t \sim k_\star^{-1}$. These, in turn, can be estimated by

$$\frac{k^2}{a^2} \lesssim k_\star^2(t) \equiv \sqrt{g} m \Phi(t)\,. \tag{4.19}$$

Since $k_\star^2 \gg a^2 H^2$, the momentum shift induced by the Hubble scale is completely negligible, as claimed above.

Similar to what we did in the quartic-dominated epoch, we turn to the rate of the exponential growth of the occupation numbers,

$$n_k \sim \exp\left(2\mu_k m t\right)\,. \tag{4.20}$$

That is, we want to estimate the Floquet exponent μ_k for the total duration of the resonance. As worked out in detail in [67], this exponent is given during each zero crossing t_j by,

$$\mu_k^j = \frac{1}{2\pi} \ln\left(1 + 2e^{-\pi\kappa_j^2} - 2\sin\hat{\theta} e^{-\frac{\pi}{2}\kappa_j^2}\sqrt{1 + e^{-\pi\kappa_j^2}}\right)\,, \tag{4.21}$$

with $\kappa_j^2 = k^2/(a_j^2\sqrt{g} m \Phi_j)$. Here, each index labels an evaluation at t_j. Furthermore, $\hat{\theta}$ denotes a random phase, implementing the fact that the phases of the modes are uncorrelated at successive moments of particle production. For simplicity, we drop the term involving the random phase in eq. (4.21) for the remaining part of this work.

Each short burst of particle production contributes with a growth exponent $\mu_k^j \Delta t_j$. In order to define an effective Floquet exponent, we average over the oscillations of φ,

$$\mu_k = \frac{1}{t_f - t_i} \sum_{j=1}^{N_f} \mu_k^j \Delta t_j\,, \tag{4.22}$$

where t_i and t_f denote the start and the end of the resonance, respectively. Using this averaged Floquet exponent (4.22), the computation of the energy density that is transferred to the field χ proceeds as in the quartic-dominated regime (cf. (4.5)).

JCAP09(2019)003

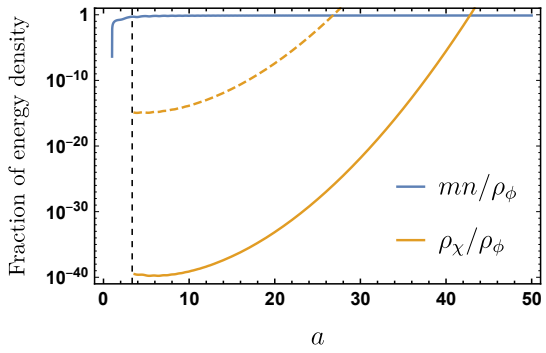

Figure 4. As in figure 3, fraction of energy density stored in charged particles compared to the fraction of the energy transferred to the field χ as a function of the scale factor a but for the mass-dominated regime, which starts at the vertical dashed line.

In figure 4 we illustrate an example of the energy transfer from the coherent oscillations of ϕ to the field χ as a function of the scale factor for a broad resonance, $g = 10^4\,\lambda$. Similar to figure 3, the generation of charge density (shown in blue) takes the full dynamics into account, while for the resonant production of χ-particles (shown in yellow) we assume a pure mass-dominated regime for the radial oscillations. For the chosen benchmark point, in contrast to the quartic-dominated era, we observe that the energy transfer from ϕ to χ can be very efficient in the mass-dominated regime.

In the last few paragraphs of this section, we would like to point some relevant caveats to our estimations. As it is, figure 4 seems to indicate that the symmetric part of the dark matter is entirely depleted before the resonance terminates, which for our particular choice of parameters is estimated to happen at $a_f \sim \mathcal{O}(70)$. This picture is however not complete for two reasons. Firstly, at the point where the energy transfer becomes an order one effect, our simplifications of neglecting backreaction break down and computational control is lost, preventing us from making precise statements about the exact amount of remaining symmetric abundance. Secondly, we recall that so far we have only considered the U(1) conserving terms for the evolution of ϕ. Including the asymmetric component (i.e. the angular motion of the field) effectively introduces an additional mass term for χ that can act to either drive or even terminate the resonance, as we now discuss.

Indeed, taking into account the symmetric and asymmetric contributions to the radial mode (cf. section 3.2),[13] we have

$$\varphi^2 = \frac{\rho_{\rm CDM}}{m^2}\left[\mathcal{A} + \mathcal{B}\cos^2(mt)\right] , \tag{4.23}$$

where $\mathcal{A}$ grows with the asymmetric fraction of the energy density and $\mathcal{B}$ with the symmetric one. The oscillating driving term is now proportional to $\mathcal{B}$. In addition, we have a new constant part given by $\mathcal{A}$. Inserting this into the condition (4.18) the numerator is $\sim \mathcal{B}$, whereas in the denominator we get a momentum shift by $k^2 \to k^2 + g\mathcal{A}\rho_{\rm CDM}/m^2$. The reason for this is that the field squared is always displaced from the minimum at least by an amount proportional to $\mathcal{A}$, and the effective mass of χ is therefore always positive. Evaluating

[13] Here, we drop the phase α which is irrelevant for our discussion.

at the time when φ^2 is minimal, we find for the range of momenta that fulfill this condition,

$$\left(\left(\frac{\mathcal{B}}{2}\right)^{\frac{2}{3}} c^{\frac{2}{3}} - \mathcal{A}c\right) \gtrsim \frac{k^2}{a^2 m^2} \gtrsim 1\,, \quad \text{where} \quad c = g\frac{\rho_{\rm CDM}}{m^2} \sim \frac{1}{a^3}\,. \tag{4.24}$$

Here, the condition on the right hand side of k^2 corresponds to the need for the instability to be active over a sufficient momentum range. Since $\mathcal{B} \lesssim 2$, the left hand side requires $c \gtrsim 1$ for the resonance to be active. Looking now at the second term on the left hand side we see that the resonance is hindered by the asymmetric part. When $\mathcal{A} \sim 1$ the resonance stops for all values of $c \gtrsim 1$. Using eq. (3.14) we find that this happens when $\eta_{\rm a} \sim \eta_{\rm s}$. In practice, this mechanism therefore does not allow to effectively deplete the symmetric part far beyond the halfway point.

In summary, we conclude that for suitable values of the portal coupling, the energy transfer can be negligible during the quartic-dominated regime, but very efficient during the mass-dominated epoch. This means that while the generation of the charge density is not affected, part of the energy density stored in the radial oscillations can be efficiently depleted, at least up to reaching the level where $\eta_{\rm a} \sim \eta_{\rm s}$. Another interesting possibility would be to consider a negative portal coupling g, which can induce a tachyonic mass term for the χ field. Such a tachyonic instability allows for the annihilation channel to be always kinematically open, in principle enabling a much more efficient depletion of the symmetric dark matter component. As a matter of fact, this case can be treated with the same methods of parametric resonance that we presented in this section. In line with [89], we find indications that the energy transfer from ϕ to χ can be tremendously increased already in the quartic-dominated epoch, as the resonance bands are much broader and the corresponding Floquet exponents are orders of magnitude larger, even for moderate values of the coupling. The details of this interesting possibility for an efficient depletion of the energy density stored in the uncharged component of ϕ would require a dedicated study.

5 Phenomenology of light dark matter with a net charge

As already outlined in the introduction, detection of very light dark matter carrying a non-vanishing charge density is made more challenging mainly by two effects.

The first one is that only the combination $\phi^\dagger\phi$ can appear in couplings, instead of just $\phi_{\rm real}$ as would be the case for a real scalar field $\phi_{\rm real}$. This severely limits the available interactions between the dark matter and the Standard Model. Indeed, at the renormalizable level there is only one "portal" coupling

$$\mathcal{L}_H = \kappa\,|\phi|^2\,H^\dagger H \tag{5.1}$$

which is the one that will be considered in more detail in the next subsection.

The challenges that arise due to the U(1) symmetry are perhaps more obvious for higher dimensional operators. For example, the usual two-photon coupling of an axion-like particle is replaced by[14]

$$\frac{1}{M}\phi_{\rm real}F\tilde{F} \quad \hookrightarrow \quad \frac{1}{M^2}\,|\phi|^2\,F^2. \tag{5.2}$$

[14] A CP even scalar would couple to F^2, while allowing for CP violation the coupling to $F\tilde{F}$ could be the relevant one. This does not affect our dimensional argument.

JCAP09(2019)003

We see that higher dimensional operators generically feature an extra suppression by the potentially large energy scale M.

The second challenge, which is closely related to the first one, is that charged particles cannot be absorbed, an effect that is used in most experiments for the detection of very light dark matter particles.

Let us have a more careful look at this effect. Very light dark matter particles have very high occupation numbers and can be conveniently described by using classical field equations (as we have done in this paper). For a real scalar field and neglecting velocity effects,[15] the effect of dark matter in a typical experimental setup corresponds to a spatially constant oscillating field,

$$\phi_{\rm real} \sim \Phi_{\rm real} \sin(mt)\,. \tag{5.3}$$

Considering typical interactions with the Higgs boson or photons we have

$$b\,\Phi_{\rm real} \sin(mt) H^\dagger H \quad \text{or} \quad \frac{\Phi_{\rm real}}{M} \sin(mt) F\tilde{F}\,. \tag{5.4}$$

where b denotes the coupling constant of the real Higgs portal that has mass dimension 1. In other words, an oscillating term appears in front of the operators involving Standard Model fields. This implies that, from the point of view of the visible sector, time translation invariance is broken and the Standard Model fields can gain energy. Under suitable conditions, the absorption of unconserved dark matter particles can take the form of oscillating driving forces. For example, the Higgs interaction leads to oscillating mechanical forces on test masses [8] whereas the photon interaction can drive an electromagnetic resonator [3].

Let us now see how the situation changes for the case of charged scalar fields. As discussed in section 3.2 the charge conserving interaction term can be readily expressed in terms of the density as in eq. (3.13). Let us consider the case, when most of the energy density is stored in the asymmetric component, i.e. $1 - \eta_{\rm a} = \eta_{\rm s} \ll 1$. In this case eq. (3.13) reads,[16]

$$\phi^\dagger \phi = \frac{1}{2} \frac{\rho_{\rm CDM}}{m^2} \left[1 + 2\sqrt{2\eta_{\rm s}\eta_{\rm a}} \cos^2(mt)\right]. \tag{5.5}$$

If there is no symmetric part, $\eta_{\rm s} = 0$, there is no oscillating term and the Standard Model fields cannot gain energy in this way. This can be understood because any absorption can only proceed as a pairwise particle-antiparticle annihilation, and if there is only one species, this cannot happen. Indeed, the oscillating terms are proportional to $\sqrt{\eta_{\rm s}}$, showing that an uncharged, symmetric component is needed. The power absorbed is typically proportional to the square of the oscillating term and therefore $\sim \eta_{\rm a}\eta_{\rm s}$. This can be roughly understood as the probability of a particle meeting a suitable antiparticle at each interaction.

5.1 The Higgs portal

Let us briefly illustrate our general considerations above for the concrete example of the only renormalizable portal for a charged dark matter particle, i.e. the Higgs portal coupling given in eq. (5.1).

[15] This is a good approximation within the coherence length $\sim 1/(mv)$, since the velocity is very non-relativistic.

[16] We again drop the irrelevant phase α.

Fine tuning. The Higgs portal coupling induces a contribution to the mass of ϕ,

$$m^2 = m_0^2 + \kappa v_0^2/2\,, \tag{5.6}$$

where $v_0 = 246\,\mathrm{GeV}$ is the measured value of the Higgs vacuum expectation value (vev). If the field ϕ is to remain light and without invoking a precise cancellation between the two different contributions to the mass, we require that

$$\kappa \lesssim 3 \cdot 10^{-35} \left(\frac{m}{\mu\mathrm{eV}}\right)^2 . \tag{5.7}$$

This should however be seen as a purely fine tuning argument rather than a strict limit.[17] In the following, we want to turn to direct experimental tests and observations.

Higgs decays. If the dark matter is much lighter than the Higgs, $m \ll m_H/2$, the current experimental constraint on the branching ratio $\mathrm{BR}(H \to \mathrm{inv.}) < 0.24$ [90] bounds κ to be

$$\kappa \lesssim 0.0036\,, \tag{5.8}$$

which is in line with, e.g., [91]. This is a relatively weak constraint, but importantly does not rely on ϕ being dark matter.

Varying fermion masses. The Higgs portal coupling (5.1) also leads to a shift of the mass parameter μ^2 of the Higgs potential or, equivalently, to a shift of the Higgs vev,

$$v = \sqrt{\frac{\mu^2 - \kappa\,|\phi|^2}{\lambda}} \approx v_0 \left(1 - \frac{\kappa\,|\phi|^2}{2\mu^2}\right) , \tag{5.9}$$

where we define $v_0 = \sqrt{\mu^2/\lambda}$, which corresponds to the unperturbed ($\kappa = 0$) Higgs vev. The latter expression assumes that the shift is small, and is valid as long as $\kappa\,|\phi|^2 \ll \mu^2$. Clearly, a modified Higgs vev translates into a shift of the Standard Model fermion masses,

$$m_f \approx m_f^0 \left(1 - \frac{\kappa\,|\phi|^2}{2\mu^2}\right) . \tag{5.10}$$

The correction to the mass is hence $\Delta m_f = m_f^0 \kappa\,|\phi|^2\,/(2\mu^2)$, which can be positive or negative depending on the sign of the coupling κ.

Since in our setup we assume that the totality of the dark matter is explained by the scalar field, the relative modification of the fermion masses can be rewritten in terms of the dark matter density,

$$\frac{\Delta m_f}{m_f^0} = \frac{\kappa}{4\mu^2}\frac{\rho_{\mathrm{DM}}}{m^2}\,. \tag{5.11}$$

In this form, the dependence of the correction on the mass of ϕ is also made explicit. Parametrically, the relative change in the fermion masses is

$$\frac{\Delta m_f}{m_f^0} \simeq 10^{-16}\kappa \left(\frac{\rho_{\mathrm{DM}}^{\mathrm{local}}}{0.4\ \mathrm{GeV/cm^3}}\right)\left(\frac{\mu\mathrm{eV}}{m}\right)^2 , \tag{5.12}$$

[17] The Higgs vev is in general a dynamical quantity that varies during the history of the Universe. In order not to experience a dramatic change in the cosmological evolution of ϕ (or avoid a dynamical fine tuning), we can assume that the reheating temperature never exceeds the electroweak scale so that the Higgs vev is fixed to its current value during the whole postinflationary epoch.

JCAP09(2019)003

where we have used the measured value for the Higgs mass $m_H \simeq 125\,\text{GeV}$ [90, 92, 93]. An absolute shift in the fermion masses is of course hard to observe, but the fact that eq. (5.12) depends on the (local) dark matter density opens up interesting possibilities. The change in the fermion mass can for example affect the frequency of atomic transitions. Current limits coming from atomic clocks bound the time variation of the ratio $\mu = m_p/m_e$ to be [94]

$$\frac{\dot{\mu}}{\mu} = (0.2 \pm 1.1) \cdot 10^{-16}\text{yr}^{-1} \,. \tag{5.13}$$

Similar bounds have also been derived in [95]. In our setup, variations of μ can arise if the dark matter density at the experimental locations (i.e. the Earth) changes over time due to, for instance, the presence of very small scale dark matter substructure. Assuming an observation time of 1 year, κ could be constraint to be

$$\kappa \lesssim 2 \cdot 10^{-1} \left(\frac{0.4\ \text{GeV/cm}^3}{\rho_{\text{DM}}^{\text{local}}}\right) \left(\frac{m}{\mu\text{eV}}\right)^2 \left(\frac{\Delta\rho_{\text{DM}}}{\rho_{\text{DM}}^{\text{local}}}\right)^{-1} \,, \tag{5.14}$$

where $\Delta\rho_{\text{DM}}$ denotes the typical change in the local dark matter density over the appropriate observation time.

Big Bang nucleosynthesis. Apart from generating a shift in the fermion masses,[18] the modification of the Higgs vev also affects the Fermi constant,

$$G_F = \frac{1}{\sqrt{2}v^2} = G_F^0 \left(1 - \frac{\kappa}{4\mu^2}\frac{\rho_{\text{DM}}}{m^2}\right)^{-2} \,. \tag{5.15}$$

Hence, the DM-Higgs coupling alters all weak interaction rates. A powerful probe of weak interactions and the Fermi constant in the early universe around $T \approx 1\,\text{MeV}$ is provided by Big Bang nucleosynthesis (BBN). Detailed studies of the effect of a shift in the Fermi constant on BBN have been conducted in, e.g., [98, 99]. Here, we quote their results and apply them to our setup. The observed abundance of ^{4}He sets lower and upper bounds on the ratio of Fermi constant at BBN compared to the value measured today,

$$0.78 < G_F^{\text{BBN}}/G_F^0 < 1.01 \,. \tag{5.16}$$

The lower bound increases to 0.85 when the limits on ^{7}Li production are also included. We can translate the constraints into a bound on κ by taking into account the redshift of the dark matter density.[19] This gives

$$-4 \cdot 10^{-9} \lesssim \kappa \left(\frac{\mu\text{eV}}{m}\right)^2 \left(\frac{\rho_{\text{DM}}^{\text{av}}}{1.3\ \text{keV/cm}^3}\right) \lesssim 2 \cdot 10^{-10} \,. \tag{5.17}$$

The lower bound changes to $-3 \cdot 10^{-9}$ if the effect on ^{7}Li production is taken into account. Despite the measurement itself being way less precise, this constraint is much stronger than the one coming from atomic clocks. The reason for this is that the dark matter density at the time of BBN was about 20 orders of magnitude larger than the present (local) one, and therefore the shift in eq. (5.15) benefits from this huge enhancement.

[18] In spirit, the limit derived here from BBN is similar to the one obtained in [96, 97] for the very low mass limit $m \ll 10^{-16}\,\text{eV}$ of a real scalar quadratically coupled to fermions. There, the field value is not oscillating during BBN either.

[19] For $m \lesssim 10^{-16}\,\text{eV}$, the field does not start rolling until after BBN and the redshift dependence assumed here is not directly applicable [100].

Astrophysical observations. Some astrophysical observables can also be used to constrain variations in G_F. For example, the agreement between the redshift determined from the 21 cm line and the redshift determined from optical resonance lines of the same object constrains the electron-to-proton mass ratio m_e/m_p, the fine structure constant α as well as the product $\alpha^2 g_p m_e/m_p$ [101, 102], where g_p denotes the gyromagnetic moment of the proton. Since the bulk of m_p does not come from the Higgs mechanism, its relative change in the proton mass is negligible compared to the electron one. The strongest limits come from a quasar absorption system at $z = 1.77$, which constrain the product $\Delta \ln\left(\alpha^2 g_p m_e/m_p\right) < 2 \times 10^{-4}$ [103]. This implies that G_F varies less than 0.04% from today to that redshift. Furthermore, from the agreement between optical and radio redshifts of a distant galaxy at $z = 3.4$, it has been determined that G_F varies less than 0.2% back to a redshift of $z = 3.4$ [104]. Translating these constraints into bounds on κ gives

$$|\kappa| \lesssim 2 \cdot 10^{12} \left(\frac{m}{\mu\text{eV}}\right)^2 \left(\frac{0.4\ \text{GeV/cm}^3}{\rho_{\text{DM}}^{\text{local}}}\right) \left(\frac{\Delta\rho_{\text{DM}}}{\rho_{\text{DM}}^{\text{local}}}\right)^{-1}, \text{ at } z = 1.77\,, \tag{5.18}$$

$$|\kappa| \lesssim 1 \cdot 10^{13} \left(\frac{m}{\mu\text{eV}}\right)^2 \left(\frac{0.4\ \text{GeV/cm}^3}{\rho_{\text{DM}}^{\text{local}}}\right) \left(\frac{\Delta\rho_{\text{DM}}}{\rho_{\text{DM}}^{\text{local}}}\right)^{-1}, \text{ at } z = 3.4\,. \tag{5.19}$$

This result depends on the difference between the dark matter density of the observed galaxy to the local one at Earth, which is denoted by $\Delta\rho_{\text{DM}}$.

6 Conclusions

In this work, we have studied a model of very light (even sub-eV) asymmetric dark matter. In our setup, dark matter is produced non-thermally via the Affleck-Dine mechanism. The final energy density is a combination of a symmetric component, i.e. one that contains an equal number of particles and antiparticles, and an asymmetric one only constituted of particles (or antiparticles). These two components can naturally be of the same size if the symmetry breaking terms in the potential are comparable to the symmetric self-interactions, and for particular initial conditions the asymmetric component can contribute in excess of $\sim 95\%$ to the total dark matter abundance.

We have also described how a coupling $|\phi|^2 \chi^2$ of the charged field ϕ to an additional (massless) scalar field χ with a positive coupling constant allows to deplete the symmetric part of the energy density via a parametric resonance effect. The symmetric component cannot completely disappear in this way, as this mechanism becomes inefficient when the two components are of the same size. Therefore, if such couplings are present, the present-day dark matter abundance is generically expected to be evenly distributed between a symmetric and an asymmetric population. A negative coupling constant leading to a tachyonic instability would make the depletion more efficient, but also cause a breakdown of the approximations on which our results rely. We leave a more complete study of this situation to future work. A promising way forward could be an approach, e.g., based on classical statistical field theory simulations. Such an approach would also automatically include the effects of fragmentation, i.e. the disintegration of the homogeneous field into inhomogeneous fluctuations. This effect generally occurs in a large part of parameter space where the self-interactions are somewhat larger than the ones we study here (which correspond to the minimal values required to efficiently produce a charge asymmetry). Sufficiently large self-interactions could also have other consequences such as the formation of Q-balls or other macroscopic, inhomogeneous

JCAP09(2019)003

configurations that may have interesting effects for phenomenology. These possibilities merit further investigation.

A crucial feature of such light asymmetric dark matter is the change in the resulting phenomenology and, in particular, of the expected experimental signatures. Direct detection of sub-eV dark matter usually proceeds via an effective absorption of the dark matter particles. The existence of a comovingly conserved particle number in the dark matter however forbids the asymmetric component from being absorbed, making this detection strategy much less sensitive. Further suppression arises from the restrictions on the interaction with Standard Model particles due to the requirement of charge conservation.

As an application of this idea, we study the simple example of a Higgs portal coupling interaction. Instead of the usual oscillatory time variations of constants of nature (such as fermion masses or G_F), in the asymmetric scenario effects only arise due to variations in the dark matter density, therefore hindering the sensitivity of the traditional experimental setups. To overcome this limitation, we study alternative probes based on variations arising from redshift evolution as well as local fluctuations of the dark matter field.

It is of course also possible to look for the symmetric component of the dark matter, which generically appears in our model but can be comparatively subdominant to the asymmetric one. In any case, this symmetric component is susceptible to the usual resonant search approaches looking for oscillations at a fixed frequency,[20] as the ones that are employed to look for dark matter made from light uncharged bosons. Similar effects would also arise from suppressed charge violating couplings to the Standard Model.

Finally, we would like to point out that, since the sensitivity of direct detection searches is reduced for very light asymmetric dark matter, its couplings to the visible sector are allowed to be larger than is commonly assumed in the usual uncharged scenario. This opens up the opportunity to search for such particles in laboratory or astrophysical environments that can directly produce them.

Acknowledgments

We are grateful to Doddy Marsh for useful discussions on structure formation. J.G. thanks Heidelberg University for kind hospitality in the early stages of the project. G.A. receives support from the Fundación "la Caixa" via a "la Caixa" postgraduate fellowship. S.S. gratefully acknowledges financial support by the Heidelberg Graduate School for Physics during which major parts of this work were carried out. This project has received support from the European Union's Horizon 2020 research and innovation programme under the Marie Sklodowska-Curie grant agreement No. 674896 and No. 690575.

A Parametric resonance and the Mathieu equation

The resonant production of particles in an oscillating background field is described by the Mathieu equation,

$$\frac{\mathrm{d}^2 x_k}{\mathrm{d}z^2} + (A_k - 2q\cos(2z))\, x_k = 0\,. \tag{A.1}$$

[20] More precisely, this would look similar to the real scalar case with quadratic fermion couplings studied, e.g., in [96, 97].

Floquet's theorem implies that the solutions to the Mathieu equation contain an exponential factor,

$$x_k \sim \exp\left(\mu_k z\right) . \tag{A.2}$$

The Floquet exponents μ_k are characterized by so called (in)stability bands of the Mathieu equation for different values of A_k and q, see, e.g., [80].

We want to discuss two different regimes, $q \ll 1$ and $q \gg 1$, i.e. the *narrow* and *broad* resonance. Both are important to determine the rate of resonant χ-particle production in the classical background field ϕ. The equations of motion for the mode functions x_k are given in section 4.

A.1 Narrow resonance

In the regime of narrow resonance, $q \ll 1$, the dominant contribution to the unstable solution comes from the first resonance band[21] of the Mathieu equation. In this band, the Floquet exponent is given by [67, 80]

$$\mu_k = \sqrt{\left(\frac{q}{2}\right)^2 - \left(\frac{k}{\Lambda} - 1\right)^2} , \tag{A.3}$$

where we defined $\Lambda^2 \equiv (3/4)^2 \lambda \varphi_0^2$. It is maximal at its center, $\mu_{k_\star} = q/2$, which corresponds to the momentum $k_\star^2 \sim \lambda \varphi_0^2$. In this sense, the resonance is narrow, because only very few, distinct momentum modes are enhanced — in this case it is the specific mode $k_\star$. Integrating over the narrow momentum band (cf. eq. (4.5)) yields the transfer of energy from ϕ to χ. It occurs at a rate

$$\Gamma \sim \frac{2}{3} \frac{g\varphi_0}{\sqrt{\lambda}} \frac{1}{a(t)} . \tag{A.4}$$

Note that this rate is larger than the naive expectation from a perturbative approach. In particular, treating the interaction term (4.1) as an effective (time dependent) trilinear coupling $g\langle\varphi\rangle\varphi\chi^2$, one can perturbatively study the decay $\varphi \to \chi\chi$. Parametrically, the corresponding rate is given by $\Gamma \sim \frac{g^2\varphi_0}{\sqrt{\lambda}} \frac{1}{a(t)}$, which is suppressed by an additional factor of the coupling compared to the parametric resonance. On the one hand, this additional factor can be recovered by also taking Bose enhancement into account, see, e.g., [88]. On the other hand, from the perspective of parametric resonance one can in principle also recover the perturbative result, when considering the (properly normalized) energy transfer from ϕ to χ at early times. In this sense, both methods describe the same outcome from different perspectives.

A.2 Broad resonance

The broad resonance regime corresponds to $q \gg 1$. As its name suggests, in contrast to the narrow resonance, it corresponds to a regime where a broader spectrum of modes is enhanced. Therefore, particle production is typically more efficient compared to a narrow resonance.

The dynamics of the Mathieu equation are less under control in the broad resonance case compared to the narrow resonance regime. Still, especially if $q \gg 1$, we can make use of an analytic approximation of the Floquet exponents given in [105],

$$\mu_k = \frac{1}{\pi} \log\left(\sqrt{x} + \sqrt{x-1}\right) , \tag{A.5}$$

[21] See, for instance, the stability chart of the Mathieu equation in [80].

JCAP09(2019)003

where we define

$$x = \left(1 + e^{-\pi\sqrt{q}\epsilon}\right) \cos^2 \Psi \,, \tag{A.6}$$

$$\Psi = \left(\frac{\pi^2}{2} + \epsilon \log\left(\pi q^{1/4}\right)\right) \sqrt{q} + \frac{1}{2}\Im\left[\frac{\Gamma\left(\left(1 - i\sqrt{q}\epsilon\right)/2\right)}{\Gamma\left(\left(1 + i\sqrt{q}\epsilon\right)/2\right)}\right] . \tag{A.7}$$

In terms of the parameters of the Mathieu equation, we furthermore define $\epsilon \equiv \frac{A_k}{2q} - 1$. Here, we consider the case $\epsilon > 0$. For the regime $\epsilon < 0$, see [106].

Using the analytic approximation of μ_k, it is straightforward to compute the energy density stored in the creation of particles by numerically evaluating the momentum integral given in eq. (4.5).

References

[1] R. Essig et al., *Working group report: new light weakly coupled particles*, in *Proceedings, 2013 community summer study on the future of U.S. particle physics: snowmass on the Mississippi (CSS2013): Minneapolis, MN, U.S.A., July 29–August 6, 2013* (2013), arXiv:1311.0029 [INSPIRE].

[2] D.J.E. Marsh, *Axion cosmology*, *Phys. Rept.* **643** (2016) 1 [arXiv:1510.07633] [INSPIRE].

[3] P. Sikivie, *Experimental tests of the invisible axion*, *Phys. Rev. Lett.* **51** (1983) 1415 [*Erratum ibid.* **52** (1984) 695] [INSPIRE].

[4] D. Horns, J. Jaeckel, A. Lindner, A. Lobanov, J. Redondo and A. Ringwald, *Searching for WISPy cold dark matter with a dish antenna*, *JCAP* **04** (2013) 016 [arXiv:1212.2970] [INSPIRE].

[5] D. Budker, P.W. Graham, M. Ledbetter, S. Rajendran and A. Sushkov, *Proposal for a cosmic axion spin precession experiment (CASPEr)*, *Phys. Rev.* **X 4** (2014) 021030 [arXiv:1306.6089] [INSPIRE].

[6] J. Jaeckel and J. Redondo, *An antenna for directional detection of WISPy dark matter*, *JCAP* **11** (2013) 016 [arXiv:1307.7181] [INSPIRE].

[7] W. Chung, *CULTASK, the coldest axion experiment at CAPP/IBS in Korea*, PoS(CORFU2015)047.

[8] P.W. Graham, D.E. Kaplan, J. Mardon, S. Rajendran and W.A. Terrano, *Dark matter direct detection with accelerometers*, *Phys. Rev.* **D 93** (2016) 075029 [arXiv:1512.06165] [INSPIRE].

[9] Y. Kahn, B.R. Safdi and J. Thaler, *Broadband and resonant approaches to axion dark matter detection*, *Phys. Rev. Lett.* **117** (2016) 141801 [arXiv:1602.01086] [INSPIRE].

[10] MADMAX Working Group collaboration, *Dielectric haloscopes: a new way to detect axion dark matter*, *Phys. Rev. Lett.* **118** (2017) 091801 [arXiv:1611.05865] [INSPIRE].

[11] D. Alesini, D. Babusci, D. Di Gioacchino, C. Gatti, G. Lamanna and C. Ligi, *The KLASH proposal*, arXiv:1707.06010 [INSPIRE].

[12] A. á. Melcón et al., *Axion searches with microwave filters: the RADES project*, *JCAP* **05** (2018) 040 [arXiv:1803.01243] [INSPIRE].

[13] ADMX collaboration, *A search for invisible axion dark matter with the axion dark matter experiment*, *Phys. Rev. Lett.* **120** (2018) 151301 [arXiv:1804.05750] [INSPIRE].

[14] J. Jaeckel and A. Ringwald, *The low-energy frontier of particle physics*, *Ann. Rev. Nucl. Part. Sci.* **60** (2010) 405 [arXiv:1002.0329] [INSPIRE].

[15] J.L. Hewett et al., *Fundamental physics at the intensity frontier*, technical report ANL-HEP-TR-12-25.

JCAP09(2019)003

[16] P.W. Graham, I.G. Irastorza, S.K. Lamoreaux, A. Lindner and K.A. van Bibber, *Experimental searches for the axion and axion-like particles*, *Ann. Rev. Nucl. Part. Sci.* **65** (2015) 485 [arXiv:1602.00039] [INSPIRE].

[17] I.G. Irastorza and J. Redondo, *New experimental approaches in the search for axion-like particles*, *Prog. Part. Nucl. Phys.* **102** (2018) 89 [arXiv:1801.08127] [INSPIRE].

[18] S. Colombi, S. Dodelson and L.M. Widrow, *Large scale structure tests of warm dark matter*, *Astrophys. J.* **458** (1996) 1 [astro-ph/9505029] [INSPIRE].

[19] P. Bode, J.P. Ostriker and N. Turok, *Halo formation in warm dark matter models*, *Astrophys. J.* **556** (2001) 93 [astro-ph/0010389] [INSPIRE].

[20] J. Preskill, M.B. Wise and F. Wilczek, *Cosmology of the invisible axion*, *Phys. Lett.* **B 120** (1983) 127 [INSPIRE].

[21] L.F. Abbott and P. Sikivie, *A cosmological bound on the invisible axion*, *Phys. Lett.* **B 120** (1983) 133 [INSPIRE].

[22] M. Dine and W. Fischler, *The not so harmless axion*, *Phys. Lett.* **B 120** (1983) 137 [INSPIRE].

[23] P. Sikivie, *Axion cosmology*, *Lect. Notes Phys.* **741** (2008) 19 [astro-ph/0610440] [INSPIRE].

[24] A.E. Nelson and J. Scholtz, *Dark light, dark matter and the misalignment mechanism*, *Phys. Rev.* **D 84** (2011) 103501 [arXiv:1105.2812] [INSPIRE].

[25] P. Arias, D. Cadamuro, M. Goodsell, J. Jaeckel, J. Redondo and A. Ringwald, *WISPy cold dark matter*, *JCAP* **06** (2012) 013 [arXiv:1201.5902] [INSPIRE].

[26] J. Jaeckel, *A family of WISPy dark matter candidates*, *Phys. Lett.* **B 732** (2014) 1 [arXiv:1311.0880] [INSPIRE].

[27] G. Alonso-Álvarez, T. Hugle and J. Jaeckel, *Misalignment & Co.: (Pseudo-)scalar and vector dark matter with curvature couplings*, arXiv:1905.09836 [INSPIRE].

[28] A. Ringwald and K. Saikawa, *Axion dark matter in the post-inflationary Peccei-Quinn symmetry breaking scenario*, *Phys. Rev.* **D 93** (2016) 085031 [arXiv:1512.06436] [INSPIRE].

[29] R.T. Co, L.J. Hall and K. Harigaya, *QCD axion dark matter with a small decay constant*, *Phys. Rev. Lett.* **120** (2018) 211602 [arXiv:1711.10486] [INSPIRE].

[30] P. Agrawal, N. Kitajima, M. Reece, T. Sekiguchi and F. Takahashi, *Relic abundance of dark photon dark matter*, arXiv:1810.07188 [INSPIRE].

[31] J.A. Dror, K. Harigaya and V. Narayan, *Parametric resonance production of ultralight vector dark matter*, *Phys. Rev.* **D 99** (2019) 035036 [arXiv:1810.07195] [INSPIRE].

[32] R.T. Co, A. Pierce, Z. Zhang and Y. Zhao, *Dark photon dark matter produced by axion oscillations*, *Phys. Rev.* **D 99** (2019) 075002 [arXiv:1810.07196] [INSPIRE].

[33] M. Bastero-Gil, J. Santiago, L. Ubaldi and R. Vega-Morales, *Vector dark matter production at the end of inflation*, *JCAP* **04** (2019) 015 [arXiv:1810.07208] [INSPIRE].

[34] A.J. Long and L.-T. Wang, *Dark photon dark matter from a network of cosmic strings*, *Phys. Rev.* **D 99** (2019) 063529 [arXiv:1901.03312] [INSPIRE].

[35] P.J.E. Peebles and A. Vilenkin, *Noninteracting dark matter*, *Phys. Rev.* **D 60** (1999) 103506 [astro-ph/9904396] [INSPIRE].

[36] P.W. Graham, J. Mardon and S. Rajendran, *Vector dark matter from inflationary fluctuations*, *Phys. Rev.* **D 93** (2016) 103520 [arXiv:1504.02102] [INSPIRE].

[37] S. Nurmi, T. Tenkanen and K. Tuominen, *Inflationary imprints on dark matter*, *JCAP* **11** (2015) 001 [arXiv:1506.04048] [INSPIRE].

JCAP09(2019)003

[38] K. Kainulainen, S. Nurmi, T. Tenkanen, K. Tuominen and V. Vaskonen, *Isocurvature constraints on portal couplings*, *JCAP* **06** (2016) 022 [arXiv:1601.07733] [INSPIRE].

[39] O. Bertolami, C. Cosme and J.G. Rosa, *Scalar field dark matter and the Higgs field*, *Phys. Lett.* **B 759** (2016) 1 [arXiv:1603.06242] [INSPIRE].

[40] C. Cosme, J.G. Rosa and O. Bertolami, *Scale-invariant scalar field dark matter through the Higgs portal*, *JHEP* **05** (2018) 129 [arXiv:1802.09434] [INSPIRE].

[41] G. Alonso-Álvarez and J. Jaeckel, *Lightish but clumpy: scalar dark matter from inflationary fluctuations*, *JCAP* **10** (2018) 022 [arXiv:1807.09785] [INSPIRE].

[42] T. Markkanen, A. Rajantie and T. Tenkanen, *Spectator dark matter*, *Phys. Rev.* **D 98** (2018) 123532 [arXiv:1811.02586] [INSPIRE].

[43] P.W. Graham and A. Scherlis, *Stochastic axion scenario*, *Phys. Rev.* **D 98** (2018) 035017 [arXiv:1805.07362] [INSPIRE].

[44] F. Takahashi, W. Yin and A.H. Guth, *QCD axion window and low-scale inflation*, *Phys. Rev.* **D 98** (2018) 015042 [arXiv:1805.08763] [INSPIRE].

[45] S.-Y. Ho, F. Takahashi and W. Yin, *Relaxing the cosmological moduli problem by low-scale inflation*, *JHEP* **04** (2019) 149 [arXiv:1901.01240] [INSPIRE].

[46] T. Tenkanen, *Dark matter from scalar field fluctuations*, *Phys. Rev. Lett.* **123** (2019) 061302 [arXiv:1905.01214] [INSPIRE].

[47] S.M. Barr, R.S. Chivukula and E. Farhi, *Electroweak fermion number violation and the production of stable particles in the early universe*, *Phys. Lett.* **B 241** (1990) 387 [INSPIRE].

[48] S.M. Barr, *Baryogenesis, sphalerons and the cogeneration of dark matter*, *Phys. Rev.* **D 44** (1991) 3062 [INSPIRE].

[49] D.B. Kaplan, *A Single explanation for both the baryon and dark matter densities*, *Phys. Rev. Lett.* **68** (1992) 741 [INSPIRE].

[50] S.B. Gudnason, C. Kouvaris and F. Sannino, *Towards working technicolor: effective theories and dark matter*, *Phys. Rev.* **D 73** (2006) 115003 [hep-ph/0603014] [INSPIRE].

[51] S.B. Gudnason, C. Kouvaris and F. Sannino, *Dark matter from new technicolor theories*, *Phys. Rev.* **D 74** (2006) 095008 [hep-ph/0608055] [INSPIRE].

[52] R. Kitano and I. Low, *Dark matter from baryon asymmetry*, *Phys. Rev.* **D 71** (2005) 023510 [hep-ph/0411133] [INSPIRE].

[53] R. Kitano and I. Low, *Grand unification, dark matter, baryon asymmetry and the small scale structure of the universe*, hep-ph/0503112 [INSPIRE].

[54] D.E. Kaplan, M.A. Luty and K.M. Zurek, *Asymmetric dark matter*, *Phys. Rev.* **D 79** (2009) 115016 [arXiv:0901.4117] [INSPIRE].

[55] H. Davoudiasl and R.N. Mohapatra, *On relating the genesis of cosmic baryons and dark matter*, *New J. Phys.* **14** (2012) 095011 [arXiv:1203.1247] [INSPIRE].

[56] K. Petraki and R.R. Volkas, *Review of asymmetric dark matter*, *Int. J. Mod. Phys.* **A 28** (2013) 1330028 [arXiv:1305.4939] [INSPIRE].

[57] K.M. Zurek, *Asymmetric dark matter: theories, signatures and constraints*, *Phys. Rept.* **537** (2014) 91 [arXiv:1308.0338] [INSPIRE].

[58] A. Aguirre and A. Diez-Tejedor, *Asymmetric condensed dark matter*, *JCAP* **04** (2016) 019 [arXiv:1502.07354] [INSPIRE].

[59] S. HajiSadeghi, S. Smolenski and J. Wudka, *Asymmetric dark matter with a possible Bose-Einstein condensate*, *Phys. Rev.* **D 99** (2019) 023514 [arXiv:1709.00436] [INSPIRE].

JCAP09(2019)003

[60] I. Affleck and M. Dine, *A new mechanism for baryogenesis*, *Nucl. Phys.* **B 249** (1985) 361 [INSPIRE].

[61] M. Dine and A. Kusenko, *The origin of the matter - antimatter asymmetry*, *Rev. Mod. Phys.* **76** (2003) 1 [hep-ph/0303065] [INSPIRE].

[62] N.F. Bell, K. Petraki, I.M. Shoemaker and R.R. Volkas, *Pangenesis in a baryon-symmetric universe: dark and visible matter via the affleck-dine mechanism*, *Phys. Rev.* **D 84** (2011) 123505 [arXiv:1105.3730] [INSPIRE].

[63] C. Cheung and K.M. Zurek, *Affleck-dine cogenesis*, *Phys. Rev.* **D 84** (2011) 035007 [arXiv:1105.4612] [INSPIRE].

[64] K. Harigaya, *Nambu-Goldstone Affleck-Dine baryogenesis*, arXiv:1906.05286 [INSPIRE].

[65] L. Kofman, A.D. Linde and A.A. Starobinsky, *Reheating after inflation*, *Phys. Rev. Lett.* **73** (1994) 3195 [hep-th/9405187] [INSPIRE].

[66] Y. Shtanov, J.H. Traschen and R.H. Brandenberger, *Universe reheating after inflation*, *Phys. Rev.* **D 51** (1995) 5438 [hep-ph/9407247] [INSPIRE].

[67] L. Kofman, A.D. Linde and A.A. Starobinsky, *Towards the theory of reheating after inflation*, *Phys. Rev.* **D 56** (1997) 3258 [hep-ph/9704452] [INSPIRE].

[68] A. Kusenko, V. Kuzmin, M.E. Shaposhnikov and P.G. Tinyakov, *Experimental signatures of supersymmetric dark matter Q balls*, *Phys. Rev. Lett.* **80** (1998) 3185 [hep-ph/9712212] [INSPIRE].

[69] K. Enqvist, A. Jokinen, T. Multamaki and I. Vilja, *Numerical simulations of fragmentation of the Affleck-Dine condensate*, *Phys. Rev.* **D 63** (2001) 083501 [hep-ph/0011134] [INSPIRE].

[70] J. Berges and J. Serreau, *Parametric resonance in quantum field theory*, *Phys. Rev. Lett.* **91** (2003) 111601 [hep-ph/0208070] [INSPIRE].

[71] L.M. Krauss and F. Wilczek, *Discrete gauge symmetry in continuum theories*, *Phys. Rev. Lett.* **62** (1989) 1221 [INSPIRE].

[72] J.E. Kim, *Abelian discrete symmetries Z_N and Z_{nR} from string orbifolds*, *Phys. Lett.* **B 726** (2013) 450 [arXiv:1308.0344] [INSPIRE].

[73] P.J.E. Peebles, *Fluid dark matter*, *Astrophys. J.* **534** (2000) L127 [astro-ph/0002495] [INSPIRE].

[74] G. Alonso-Álvarez and J. Jaeckel, *Exploring axionlike particles beyond the canonical setup*, *Phys. Rev.* **D 98** (2018) 023539 [arXiv:1712.07500] [INSPIRE].

[75] PLANCK collaboration, *Planck 2018 results. VI. Cosmological parameters*, arXiv:1807.06209 [INSPIRE].

[76] M. Dine, L. Randall and S.D. Thomas, *Baryogenesis from flat directions of the supersymmetric standard model*, *Nucl. Phys.* **B 458** (1996) 291 [hep-ph/9507453] [INSPIRE].

[77] J.A.R. Cembranos, A.L. Maroto, S.J. Núñez Jareño and H. Villarrubia-Rojo, *Constraints on anharmonic corrections of fuzzy dark matter*, *JHEP* **08** (2018) 073 [arXiv:1805.08112] [INSPIRE].

[78] M. Viel, J. Lesgourgues, M.G. Haehnelt, S. Matarrese and A. Riotto, *Constraining warm dark matter candidates including sterile neutrinos and light gravitinos with WMAP and the Lyman-alpha forest*, *Phys. Rev.* **D 71** (2005) 063534 [astro-ph/0501562] [INSPIRE].

[79] PLANCK collaboration, *Planck 2018 results. X. Constraints on inflation*, arXiv:1807.06211 [INSPIRE].

[80] N.W. McLachlan, *Theory and application of Mathieu functions*, Clarendon Press, Oxford (1951).

[81] G.N. Felder and I. Tkachev, *LATTICEEASY: a program for lattice simulations of scalar fields in an expanding universe*, *Comput. Phys. Commun.* **178** (2008) 929 [hep-ph/0011159] [INSPIRE].

JCAP09(2019)003

[82] J. Berges, *Nonequilibrium quantum fields: from cold atoms to cosmology*, arXiv:1503.02907 [INSPIRE].

[83] J. Berges, A. Chatrchyan and J. Jaeckel, *Foamy dark matter from monodromies*, arXiv:1903.03116 [INSPIRE].

[84] S.R. Coleman, *Q balls*, *Nucl. Phys.* **B 262** (1985) 263 [*Erratum ibid.* **B 269** (1986) 744] [INSPIRE].

[85] G.D. Moore, *Condensates in relativistic scalar theories*, *Phys. Rev.* **D 93** (2016) 065043 [arXiv:1511.00697] [INSPIRE].

[86] L.D. Landau and E.M. Lifshitz, *The classical theory of fields*, Pergamon Press, Oxford (1971).

[87] Z. Berezhiani, A.D. Dolgov and I.I. Tkachev, *Reconciling planck results with low redshift astronomical measurements*, *Phys. Rev.* **D 92** (2015) 061303 [arXiv:1505.03644] [INSPIRE].

[88] D. Baumann, *The physics of inflation: a course for graduate students in particle physics and cosmology*, lecture notes.

[89] B.R. Greene, T. Prokopec and T.G. Roos, *Inflaton decay and heavy particle production with negative coupling*, *Phys. Rev.* **D 56** (1997) 6484 [hep-ph/9705357] [INSPIRE].

[90] Particle Data Group collaboration, *Review of particle physics*, *Phys. Rev.* **D 98** (2018) 030001 [INSPIRE].

[91] G. Arcadi, A. Djouadi and M. Raidal, *Dark Matter through the Higgs portal*, arXiv:1903.03616 [INSPIRE].

[92] ATLAS collaboration, *Observation of a new particle in the search for the standard model Higgs boson with the ATLAS detector at the LHC*, *Phys. Lett.* **B 716** (2012) 1 [arXiv:1207.7214] [INSPIRE].

[93] CMS collaboration, *Observation of a new boson at a mass of 125 GeV with the CMS experiment at the LHC*, *Phys. Lett.* **B 716** (2012) 30 [arXiv:1207.7235] [INSPIRE].

[94] R.M. Godun, P.B.R. Nisbet-Jones, J.M. Jones, S.A. King, L.A.M. Johnson, H.S. Margolis et al., *Frequency ratio of two optical clock transitions in Yb+171 and constraints on the time variation of fundamental constants*, *Phys. Rev. Lett.* **113** (2014) 210801 [arXiv:1407.0164] [INSPIRE].

[95] N. Huntemann, B. Lipphardt, C. Tamm, V. Gerginov, S. Weyers and E. Peik, *Improved limit on a temporal variation of m_p/m_e from comparisons of Yb^+ and Cs atomic clocks*, *Phys. Rev. Lett.* **113** (2014) 210802 [arXiv:1407.4408] [INSPIRE].

[96] Y.V. Stadnik and V.V. Flambaum, *Can dark matter induce cosmological evolution of the fundamental constants of Nature?*, *Phys. Rev. Lett.* **115** (2015) 201301 [arXiv:1503.08540] [INSPIRE].

[97] Y.V. Stadnik and V.V. Flambaum, *Constraining scalar dark matter with Big Bang nucleosynthesis and atomic spectroscopy*, arXiv:1504.01798 [INSPIRE].

[98] E.W. Kolb, M.J. Perry and T.P. Walker, *Time variation of fundamental constants, primordial nucleosynthesis and the size of extra dimensions*, *Phys. Rev.* **D 33** (1986) 869 [INSPIRE].

[99] R.J. Scherrer and D.N. Spergel, *How constant is the Fermi coupling constant?*, *Phys. Rev.* **D 47** (1993) 4774 [INSPIRE].

[100] K. Blum, R.T. D'Agnolo, M. Lisanti and B.R. Safdi, *Constraining axion dark matter with big bang nucleosynthesis*, *Phys. Lett.* **B 737** (2014) 30 [arXiv:1401.6460] [INSPIRE].

[101] J.N. Bahcall and M. Schmidt, *Does the fine-structure constant vary with cosmic time?*, *Phys. Rev. Lett.* **19** (1967) 1294 [INSPIRE].

[102] A.M. Wolfe, R.L. Brown and M.S. Roberts, *Limits on the variation of fundamental atomic quantities over cosmic time scales*, *Phys. Rev. Lett.* **37** (1976) 179 [INSPIRE].

JCAP09(2019)003

[103] A.M. Wolfe and M.M. Davis, *Detection of 21-cm absorption at Z of approximately 1.8 in the quasi-stellar object 1331+170*, *Astron. J.* **84** (1979) 699.

[104] J.M. Uson, D.S. Bagri and T.J. Cornwell, *Radio detections of neutral hydrogen at redshift $Z = 3.4$*, *Phys. Rev. Lett.* **67** (1991) 3328 [INSPIRE].

[105] H. Fujisaki, K. Kumekawa, M. Yamaguchi and M. Yoshimura, *Particle production and gravitino abundance after inflation*, *Phys. Rev.* **D 54** (1996) 2494 [hep-ph/9511381] [INSPIRE].

[106] H. Fujisaki, K. Kumekawa, M. Yamaguchi and M. Yoshimura, *Particle production and dissipative cosmic field*, *Phys. Rev.* **D 53** (1996) 6805 [hep-ph/9508378] [INSPIRE].

JCAP09(2019)003

Chapter 3

A supersymmetric theory of baryogenesis and sterile sneutrino dark matter from B mesons

Authors:
Gonzalo Alonso-Álvarez, Gilly Elor, Ann E. Nelson,
and Huangyu Xiao

Published in *JHEP 03 (2020) 046*,
also available at arXiv:1907.10612

Principal authorship of this article is shared on an equal footing by the four authors. The original idea for the project was conceived by Ann Nelson and was further developed by the four authors. The calculations in Sections 3, 4, and 5 were performed predominantly by Gonzalo Alonso-Álvarez, and those in Sections 2, 6, and 7 were performed with equal participation from the three authors. All figures were produced by Gonzalo Alonso-Álvarez. Sections 2, 3, 4, 5 were written predominantly by Gonzalo Alonso-Álvarez, and Sections 1, 6, 7, and 8 were written with equal participation from the four authors. All four authors contributed with corrections and suggestions to the manuscript, as well as with improvements during the review process.

Published for SISSA by Springer

Received: October 16, 2019
Revised: February 17, 2020
Accepted: February 19, 2020
Published: March 9, 2020

A supersymmetric theory of baryogenesis and sterile sneutrino dark matter from B mesons

Gonzalo Alonso-Álvarez,[a] **Gilly Elor,**[b] **Ann E. Nelson**[b,1] **and Huangyu Xiao**[b]

[a] *Institut für Theoretische Physik, Universität Heidelberg, Philosophenweg 16, 69120 Heidelberg, Germany*

[b] *Department of Physics, University of Washington, Box 1560, Seattle, WA 98195, U.S.A.*

E-mail: alonso@thphys.uni-heidelberg.de, gelor@uw.edu, huangyu@uw.edu

Abstract: Low-scale baryogenesis and dark matter generation can occur via the production of neutral B mesons at MeV temperatures in the early Universe, which undergo CP-violating oscillations and subsequently decay into a dark sector. In this work, we discuss the consequences of realizing this mechanism in a supersymmetric model with an unbroken $\mathrm{U}(1)_R$ symmetry which is identified with baryon number. B mesons decay into a dark sector through a baryon number conserving operator mediated by TeV scale squarks and a GeV scale Dirac bino. The dark sector particles can be identified with sterile neutrinos and their superpartners in a type-I seesaw framework for neutrino masses. The sterile sneutrinos are sufficiently long lived and constitute the dark matter. The produced matter-antimatter asymmetry is directly related to observables measurable at B factories and hadron colliders, the most relevant of which are the semileptonic-leptonic asymmetries in neutral B meson systems and the inclusive branching fraction of B mesons into hadrons and missing energy. We discuss model independent constraints on these experimental observables before quoting predictions made in the supersymmetric context. Constraints from astrophysics, neutrino physics and flavor observables are studied, as are potential LHC signals with a focus on novel long lived particle searches which are directly linked to properties of the dark sector.

Keywords: Supersymmetry Phenomenology

ArXiv ePrint: 1907.10612

[1] Ann Nelson passed away after this manuscript was written. Her contribution made this work possible, particle physics a richer field and the whole world a little bit brighter. We are forever grateful for her kindness and inspiration.

https://doi.org/10.1007/JHEP03(2020)046

JHEP03(2020)046

Contents

JHEP03(2020)046

1 Introduction

The nature and genesis of dark matter (DM) and the dynamical origin of the matter-antimatter asymmetry of the Universe are two outstanding mysteries that the Standard Model of Particle Physics (SM) cannot explain. Meanwhile, the SM also suffers from aesthetic or fine-tuning problems, especially the gauge hierarchy problem. The hope of solving these puzzles has driven theorists and experimentalists alike to search for new physics (NP).

Many particle physics models have been proposed to explain the origin of the DM relic abundance, measured to be $\Omega_{\rm DM}h^2 = 0.1200 \pm 0.0012$ [1], i.e. roughly 26% of the critical energy density of the Universe [1, 2]. However, searches for DM at colliders and at designated direct detection experiments together with studies of the possible indirect effects of DM in astrophysical observations have yet to shed light on its nature, thereby severely constraining many scenarios.

The origin of the primordial matter-antimatter asymmetry $Y_B \equiv (n_B - n_{\bar{B}})/s = (8.718 \pm 0.004) \times 10^{-11}$, inferred from measurements of the Cosmic Microwave Background (CMB) [1, 2] and Big Bang Nucleosynthesis (BBN) [3, 4], requires a dynamical explanation: *baryogenesis*. Many mechanisms of baryogenesis (satisfying the three Sakharov conditions [5]: C and CP Violation (CPV), baryon number violation, and departure from thermal equilibrium) have been proposed, but remain experimentally challenging to verify due to the inaccessibly high scales and very massive particles involved.

A new mechanism for low-scale baryogenesis and DM production was introduced in [6].[1] Contrary to the standard lore that baryogenesis is difficult to test experimentally, the mechanism of [6] predicts distinct signals at B factories and hadron colliders. In particular, a large positive enhancement of the charge/semileptonic-leptonic asymmetry in neutral B meson oscillation systems is required, as are new decay modes of charged and neutral B mesons into baryons and missing energy together with exotic decays of b-flavored baryons.

Weak scale supersymmetry (SUSY) offers a theoretically well motivated solution to the gauge hierarchy problem with a plethora of implications for LHC searches. However, the lack of discoveries at the LHC has pushed the Minimal Supersymmetric Standard Model (MSSM) to ever more tuned corners of parameter space [13], prompting theorists to introduce new variations of weak scale SUSY where experimental constraints may be evaded or relaxed. For instance, supersymmetric models with Dirac gauginos [14, 15] and

[1] Many models and mechanisms that simultaneously generate a baryon asymmetry and produce the DM abundance in the early Universe have been proposed. For instance, in models of Asymmetric Dark Matter [7–12], DM carries a conserved charge just as baryons do.

JHEP03(2020)046

an exact $\mathrm{U}(1)_R$ symmetry (R-SUSY) [16, 17] are phenomenologically appealing [18]. Exact $\mathrm{U}(1)_R$ symmetries — under which particles within the same supersymmetric multiplet carry different charges — are motivated by top down constructions. By forbidding Majorana gaugino masses and supersymmetric a-terms, the majority of collider constraints are circumvented in models of R-SUSY. Therefore, such extensions of the MSSM are intriguing in their own right, but are arguably even more motivated if the deviation from minimality accommodates a solution to other outstanding problems of the SM, such as DM and baryogenesis.

In the present work, we realize the mechanism of baryogenesis and DM production introduced in [6] in an R-SUSY setup where an exact $\mathrm{U}(1)_R$ symmetry is identified with $\mathrm{U}(1)_B$ baryon number.[2] In this baryogenesis scenario, neutral B mesons are produced at MeV temperatures in the early Universe, undergo CP-violating oscillations and subsequently decay to a Dirac gaugino (which is charged under the R-symmetry and therefore baryon number) through a four-fermion interaction obtained by integrating out heavy squarks. Successful baryogenesis requires at least one squark to have a mass of $\mathcal{O}(1\,\mathrm{TeV})$, and critically a Dirac gaugino with mass of a few GeV (typically smaller than $4\,\mathrm{GeV}$ in order for B meson decay to be kinematically allowed). Current constraints do not allow the existence of so light gluinos or charginos, but the bounds do not apply to the color neutral bino [13].

The collider phenomenology of various R-SUSY setups has been greatly studied [21–27], along with constraints from low energy flavor observables and electric dipole moments [28]. However, previous work on R-SUSY models focused on scenarios with heavy Dirac gauginos (for instance [18] considers flavor constraints on a model where all the gauginos share the same mass scale of order $500\,\mathrm{GeV}$–TeV). Realizing the mechanism of [6] motivates us to study the phenomenology of a complementary region of R-SUSY parameter space — one where multiple gaugino mass scales are present. This allows the bino to be light enough for baryogenesis purposes while the other gauge superpartners are heavier and avoid collider constraints. This scenario can be realized, for instance, if different SUSY breaking scales are assumed [29].

In the present work we further extend the R-SUSY setup to include a sterile neutrino and sneutrino with GeV scale masses, and discuss their role in providing a mass for SM neutrinos via a type-I seesaw [30–33]. In this scenario, the bino decays predominantly into a sterile neutrino-sneutrino pair. The sterile neutrino decays are generically long lived and may be searched for at SHiP [34], FASER [35], CODEX-b [36], MATHUSLA [37] and in the ATLAS muon tracker [38], while the sneutrino is stable on cosmological time scales and constitutes the DM. This opens up a variety of astrophysical constraints and signals which are discussed and assessed.

While the existence of an R-symmetry is theoretically well motivated, it is generically expected that this symmetry is not realized exactly, as supergravity considerations lead

[2] R-SUSY models can accommodate diverse baryogenesis scenarios [19, 20], sometimes at the cost of breaking the R-symmetry [21]. In this regard, realizing the mechanism of [6] is a novel application of such ingredients and, as will be discussed, motivates a rather unstudied region of parameter space: a light (GeV mass scale) Dirac bino.

JHEP03(2020)046

to a gravitino whose mass is not $\mathrm{U}(1)_R$ symmetric. Supergravity breaking of the $\mathrm{U}(1)_R$ symmetry introduces, for instance, Majorana sparticle masses generated from the conformal anomaly along with $a$terms and small soft squark masses, resulting in additional constraints (see [39] for a detailed discussion). We quantify the degree to which the R-symmetry can be broken while still being able to accommodate the baryogenesis and DM production mechanism from B mesons.

This paper is organized as follows: in section 2 we review the key ingredients and results of [6], i.e. the generic model and parameter space needed to achieve baryogenesis and DM from B mesons. In section 3 we present new model independent constraints on the experimental observables within our framework. Next, section 4 introduces the model of R-SUSY with Dirac gauginos and right-handed neutrino multiplets, in addition to discussing the degree to which we require the R-symmetry to be exact. In section 5 we present our results for flavor observables within the SUSY model — namely the contributions to the semileptonic-leptonic asymmetries in neutral B meson oscillations and various other flavor constraints. Next, in section 6 we discuss what region of parameter space is able to generate the observed matter-antimatter asymmetry and the DM relic abundance. This is followed by a discussion of additional constraints on the model parameters arising from neutrino physics, DM stability, supersymmetry breaking and neutron stars. In section 7 various signals at colliders and B factories that can probe this model are discussed. Finally, we conclude in section 8 by summarizing the allowed parameter space of the model that realizes baryogenesis. Some further details of the computations are given in the appendices.

2 Baryogenesis and dark matter from B mesons

Here we review the mechanism of low scale baryogenesis and DM production from the oscillations and subsequent decay of neutral B mesons, which was proposed in [6]. An inflaton-like[3] field Φ with mass m_Φ decays out of thermal equilibrium in the early Universe, at temperatures of order $T_R \sim 1-100\,\mathrm{MeV}$. The main decay products are assumed to be quarks and antiquarks that hadronize producing neutral $B^0_{q=s,d} = |\bar{b}\,q\rangle$ mesons and antimesons $\bar{B}^0$, which then undergo CP-violating oscillations before decaying partially into a dark sector.[4]

A minimal set of four new particles is required to generate the necessary interactions between the visible and dark sectors (see [6, 39] for details). First consider an electrically charged ($Q_e = -1/3$), baryon number carrying ($B = -2/3$), color triplet scalar which couples to SM quarks — foreshadowing, we denote this particle by $\tilde{q}_R$. Such a particle couples to the SM quarks through the fully $\mathrm{SU}(3)_c$ antisymmetric term $\tilde{q}^*_R\,\bar{u}\,b^c$, and various other flavor combinations. Additionally, we introduce a Dirac fermion ψ carrying baryon number -1, so that couplings of the form $\tilde{q}_R\bar{\psi}\,s^c$ are allowed. To avoid collider constraints, the new colored scalar is assumed to have a mass around the TeV scale (see section 7.3

[3]The details of an inflation model are beyond the scope of this work. This role can also be played by a modulus or any other late-time decaying particle.

[4]Additional mesons may also be produced, but are uninteresting for the current setup as only B mesons can give rise to baryogenesis in this way due to kinematic considerations.

JHEP03(2020)046

for a more detailed discussion), allowing us to integrate it out arriving at an effective Hamiltonian valid a low energies:

$$\mathcal{H}_{\text{eff}} \;=\; \frac{\lambda_{\text{eff}}}{m_{\tilde{d}}^2} u\, s\, b\, \psi\,. \tag{2.1}$$

To simplify the notation, we have chosen a particular combination of light quark flavors to showcase the mechanism, and have parametrized the effective coupling by λ_{eff}. It will however be true that any other combination of couplings that yields an effective four-fermion interaction involving b and ψ and two other light quarks[5] is equally suitable.

For a sufficiently light ψ, with mass smaller than about 4 GeV, the effective operator in eq. (2.1) allows the $\bar{b}$ quark within the B meson to decay; $B_q^0 \to \psi + \text{Baryon} + X$, where X parametrizes mesons or other additional SM particles. Since ψ carries baryon number, this decay is baryon number conserving. However, an asymmetry $n_\psi - \bar{n}_\psi$ can be generated due to the CP-violating nature of the neutral meson oscillations. If ψ is allowed to decay back into visible sector particles, the generated asymmetry will be erased. However, the asymmetry may be preserved if ψ dominantly decays into stable DM particles. This is made possible by the existence of a dark scalar baryon ϕ with baryon number -1 and a dark Majorana fermion ξ. If a discrete $\mathbb{Z}_2$ symmetry is assumed under which the dark sector particles transform as $\psi \to \psi$, $\phi \to -\phi$ and $\xi \to -\xi$, we can write a Yukawa operator

$$\mathcal{L} \;\supset\; -\lambda_N\, \bar{\psi}\, \phi\, \xi\,, \tag{2.2}$$

mediating the decay of ψ into the dark sector, where an overall negative baryon number is stored. A positive baryon asymmetry is thus produced in the visible sector without globally breaking baryon number. Note that the scalar ϕ carries baryon number and as such its mass is constrained to be greater than $\sim 1.2\,\text{GeV}$ [40].[6] In this paper we consider a scenario in which the scalar constitutes the DM (the fermion will turn out to be long lived but unstable on cosmological time scales). The combination of kinematics, proton decay, dark matter stability, and neutron star stability leads us to consider a parameter space where

$$m_B - m_n > m_\psi > m_\phi + m_\xi > 1.5\,\text{GeV} \quad \text{and} \quad m_\xi + m_n > m_\phi > 1.2\,\text{GeV}\,, \tag{2.3}$$

where m_n is the neutron mass and m_B is the B meson mass.

The asymmetry and DM abundance can be determined by solving a system of coupled Boltzmann equations [6, 41]. Doing this, the comoving baryon asymmetry is found to

[5] More precisely, any up- plus down-type pair of first or second generation quarks, in order to preserve hypercharge and for the B meson to be able to decay through the effective operator. We refer to table III in [6] for an exhaustive list of options.

[6] The authors of [40] showed that the observation of neutron stars with masses greater than $2M_\odot$ constrains the mass of a dark particle carrying baryon number to be greater than the neutron chemical potential inside the star, which is about 1.2 GeV. Otherwise, if a light dark baryon did exist, a process such as $n + n \to \text{DM} + \text{DM}$ could occur within the star. As a consequence, neutrons would be replaced by DM particles and the neutron Fermi pressure would diminish. This would destabilize the neutron star, leading to gravitational collapse.

JHEP03(2020)046

scale as

$$Y_B \;\propto\; \mathrm{Br}\left(B^0 \to \mathcal{B} + X\right) \sum_{q=s,d} \alpha_q \left(T_R, \Delta m_{B_q}\right) \times a^q_{\ell\ell}\,. \tag{2.4}$$

Here, $\mathrm{Br}(B^0 \to \mathcal{B} + X)$ is the branching fraction of the B^0 meson to a baryon $\mathcal{B}$ and X, which stands for the dark sector particles plus potentially other mesons or SM particles. The "reheat temperature" T_R is taken to be the temperature at which the Φ decays become significant, that is, when $3H(T_R) = \Gamma_\Phi$, where Γ_Φ is the decay width of Φ. Furthermore, $a^q_{\ell\ell}$ is the leptonic charge asymmetry (which in this set-up is effectively equivalent to the semileptonic-leptonic asymmetry a^q_{sl}), an experimental observable which parametrizes CP violation in the $B^0_{s,\,d}$ systems. An important point is that, as in neutrino physics, neutral B meson oscillations can only occur in a coherent system. Additional interactions with the mesons can act to decohere the oscillations [42, 43] by "measuring" the system, thereby suppressing the CP violation and diminishing the potential to generate an asymmetry. In the early Universe, decoherence is caused by the scattering of $e^\pm$ off B^0 mesons due to their charge asymmetry. For CP violation to effectively happen, B mesons must oscillate at a rate similar to or faster than the $e^\pm B^0_q \to e^\pm B^0_q$ scattering in the plasma. The factor of $\alpha_q \left(T_R, \Delta m_{B_q}\right)$ in eq. (2.4) is a measure of decoherence at the temperature T_R for each of the $q = s, d$ systems.

The kinematically allowed and currently experimentally unconstrained parameter space that accommodates the measured baryon asymmetry and DM relic abundance was mapped out in [6]. In order to reproduce the observed value of $Y_B \sim 8.7 \times 10^{-11}$, the experimental observables in eq. (2.4) must, after scanning over the (m_Φ, Γ_Φ) parameter space, lie within the ranges

$$\mathrm{Br}(B^0 \to \mathcal{B} + X) \sim 2 \times 10^{-4} - 10^{-1}\,, \quad \text{and} \quad \sum_{q=s,d} a^q_{\mathrm{sl}} \sim 10^{-5} - 10^{-3} > 0\,. \tag{2.5}$$

If we compare with the SM predictions [44]

$$a^{s,\,\mathrm{SM}}_{\mathrm{sl}} = (2.22 \pm 0.27) \times 10^{-5} \quad \text{and} \quad a^{d,\,\mathrm{SM}}_{\mathrm{sl}} = (-4.7 \pm 0.6) \times 10^{-4}\,, \tag{2.6}$$

we conclude that the amount of CP violation predicted by the SM is typically not enough for successful baryogenesis. However, given the current experimental constraints [4]

$$a^{s,\,\mathrm{exp}}_{\mathrm{sl}} = (-0.6 \pm 2.8) \times 10^{-3} \quad \text{and} \quad a^{d,\,\mathrm{exp}}_{\mathrm{sl}} = (-2.1 \pm 1.7) \times 10^{-3}\,, \tag{2.7}$$

we see that there is room for new physics to enhance the CP violation and accommodate the required values in eq. (2.5). We will explore this in more detail in section 3. The other relevant quantity is the branching ratio of B mesons into a baryon and dark sector states which would contribute to missing energy in an experiment. To the best of our knowledge, to the date an inclusive search for such a decay has not been performed. Given the experimental constraints on similar processes like $B \to K\nu\nu$, which are in the $\mathcal{O}(10^{-5})$ level, we expect that existing and future data from BaBar, Belle (-II) and LHCb may be in position to fully test the parameter range that allows for successful baryogenesis.

JHEP03(2020)046

The symmetric component of the DM is generally overproduced in this set-up. Therefore, additional interactions allowing the DM to annihilate are required in order to deplete its abundance. The results of [6] show that an annihilation cross section

$$\langle \sigma v \rangle_{\rm dark} = (6-20) \times 10^{-25}\,{\rm cm}^3/{\rm s} \tag{2.8}$$

is needed in order to reproduce the observed DM density $\Omega_{\rm DM}h^2 \sim 0.12$.

One of the main appeals of this mechanism is its susceptibility to be tested in terrestrial experiments such as flavor facilities and accelerators. Indeed, experimental constraints on $a_{\rm sl}$ can directly constrain the mechanism. We explore this model-independent bounds in section 3. Next, we construct a realization of this mechanism, i.e. (2.1) and (2.2), in a supersymmetric framework. Having a full model will allow us to consistently calculate the new physics contributions to $a_{\rm sl}$ and the branching fraction ${\rm Br}(B^0 \to \mathcal{B} + X)$, together with any other related flavor observables that the new particles and couplings may modify. In doing so, we will be able to identify the phenomenologically viable region of parameter space where baryogenesis can successfully be achieved, and develop the best approach to experimentally test the mechanism in high and low energy experiments.

3 Model independent constraints

We now conduct a model independent study to further quantify the required new physics (NP) contributions to realize baryogenesis and DM from B mesons. This will set the stage for successfully embedding this mechanism in a full model. As seen in (2.4), the baryon asymmetry depends critically on the semileptonic asymmetres $a_{\rm sl}^q$ and the branching fraction ${\rm Br}\left(B^0 \to \mathcal{B} + X\right)$ of neutral B mesons to baryons and dark sector states. As discussed above, the SM prediction for the semileptonic asymmetries is not enough to generate the observed baryon asymmetry required for baryogenesis, and in this section we study the ability for general NP contributions to enhance this asymmetry, taking into account all the relevant experimental constraints. The amount of NP introduced is constrained by measurements of different B_q^0 oscillation parameters, in turn limiting the size of the enhancement of the semileptonic-leptonic asymmetry which is consistent with experimental data. As a consequence of these bounds, we obtain a lower limit on the required branching fraction in order to generate the measured baryon asymmetry of the Universe. In this section we remain agnostic about the origin of the NP contributions and perform the study in a data driven and model independent way.

3.1 The semileptonic asymmetries

Experimental measurements of the oscillation parameters in neutral B meson mixing constrain the size of NP effects that introduce new CP violation into these systems. We now quantify such constraints. Recall that the evolution of the neutral $B_q^0 - \bar{B}_q^0$ system is described by

$$i\frac{\rm d}{{\rm d}t}\begin{pmatrix} |B_q^0(t)\rangle \\ |\bar{B}_q^0(t)\rangle \end{pmatrix} = \left(\mathcal{H}_{\rm osc}^q\right)\begin{pmatrix} |B_q^0(t)\rangle \\ |\bar{B}_q^0(t)\rangle \end{pmatrix}, \tag{3.1}$$

JHEP03(2020)046

where the Hamiltonian 2×2 matrix $\mathcal{H}^q_{\rm osc} = M^q - i\Gamma^q$ contains off diagonal terms which result in CP violation in the neutral meson mixing. Writing the off-diagonal elements as

$$M^q_{12} = |M^q_{12}|\, e^{i\phi^q_M} \quad \text{and} \quad \Gamma^q_{12} = |\Gamma^q_{12}|\, e^{i\phi^q_\Gamma}\,, \tag{3.2}$$

the mass and decay rate differences between the two propagation eigenstates are given by

$$\Delta M^q \simeq 2\,|M^q_{12}| \quad \text{and} \quad \Delta\Gamma^q \simeq 2\,|\Gamma^q_{12}|\cos\phi^q_{12}\,, \tag{3.3}$$

where we have defined

$$\phi^q_{12} = \arg\left(-\frac{M^q_{12}}{\Gamma^q_{12}}\right) = \pi + \phi_M - \phi_\Gamma\,. \tag{3.4}$$

To get to eq. (3.3) we have assumed that $|\Gamma^q_{12}| \ll |M^q_{12}|$, which is well established experimentally. Note that although both M^q_{12} and Γ^q_{12} can be complex, only the phase difference between the two is physical. This phase is the main quantity controlling the CP violation in the system. In the SM, where the off-diagonal elements of the oscillation Hamiltonian are generated by box diagrams, nonzero ϕ^q_M and ϕ^q_Γ arise from the phase in the CKM matrix [45–48].

The NP contributions that are relevant for baryogenesis only modify M^q and leave Γ^q unchanged from its SM value. In particular, there is no extra source of *direct CP violation*, which measures differences in the tree-level decay of $B^0 \to f$ with respect to the CP conjugate $\bar{B}^0 \to \bar{f}$. In addition, no new common final state to which both B^0 and $\bar{B}^0$ can decay is introduced. Therefore, the CP-violating observables that may be modified by NP contributions are:

- *CP violation in mixing*, which is described by the mixing phase ϕ^q_{12}. CP violation in mixing can be measured via the *semileptonic CP asymmetries*, also known as CP asymmetries in flavor-specific decays. The asymmetry is defined as

$$a^q_{\rm sl} = \frac{\Gamma\left(\bar{B}^0_q \to f\right) - \Gamma\left(B^0_q \to \bar{f}\right)}{\Gamma\left(\bar{B}^0_q \to f\right) + \Gamma\left(B^0_q \to \bar{f}\right)} = {\rm Im}\left(\frac{\Gamma^q_{12}}{M^q_{12}}\right) = \left|\frac{\Gamma^q_{12}}{M^q_{12}}\right| \sin\phi^q_{12}, \tag{3.5}$$

  where the final state is such that the decays $B^0_q \to f$ and $\bar{B}^0_q \to \bar{f}$ are forbidden.

- *Mixing-induced CP violation*, also known as *CP violation in interference*, which arises from interference between mixing and decay. Here, we consider a final state f to which in principle both B^0 and $\bar{B}^0$ can decay, and define

$$A^q_{CP,f}(t) = \frac{\Gamma\left(\bar{B}^0_q \to f\right) - \Gamma\left(B^0_q \to f\right)}{\Gamma\left(\bar{B}^0_q \to f\right) + \Gamma\left(B^0_q \to f\right)}. \tag{3.6}$$

  This form of CP violation is controlled by the phase ϕ^q, which is defined as

$$\phi^q = -\pi + \phi^q_M + \arg\left(\frac{\bar{\mathcal{A}}_f}{\mathcal{A}_f}\right), \tag{3.7}$$

  where $\mathcal{A}_f$ ($\bar{\mathcal{A}}_f$) denotes the decay amplitude of B^0 ($\bar{B}^0$) to f.

In order to assess the extent to which NP can impact these observables, it is customary to define [44]

$$M_{12}^q = M_{12}^{q,\mathrm{SM}} \cdot \Delta^q \equiv M_{12}^{q,\mathrm{SM}} \cdot |\Delta^q| \, \mathrm{e}^{i\phi_\Delta^q}, \quad \Gamma_{12}^q = \Gamma_{12}^{q,\mathrm{SM}}. \tag{3.8}$$

We reiterate that we are only allowing modifications in M_{12}^q, but not Γ_{12}^q, which is fixed to its SM value. The complex parameter Δ^q is a measure of the effects of NP. This parametrization has the advantage that each of Δ^q and ϕ_Δ^q are individually related to the observables ΔM^q and ϕ^q. It also allows to write a simple expression for the semileptonic asymmetries in the $B_{s,d}^0$ systems. For each $q = s, d$ we have

$$a_{\mathrm{sl}}^q = \frac{\left|\Gamma_{12}^{q,\mathrm{SM}}\right|}{\left|M_{12}^{q,\mathrm{SM}}\right|} \frac{\sin\left(\phi_{12}^{q,\mathrm{SM}} + \phi_\Delta^q\right)}{|\Delta^q|}. \tag{3.9}$$

It is however more convenient for us to parametrize $M_{12}^{q,\mathrm{NP}}$ in a way that makes the relation with the parameters of the NP model more transparent. For that purpose, we define

$$M_{12}^{q,\mathrm{NP}} = M_{12}^{q,\mathrm{SM}} \cdot \alpha^q = M_{12}^{q,\mathrm{SM}} \cdot |\alpha^q| \, \mathrm{e}^{i\phi_\alpha^q}. \tag{3.10}$$

Note that $\Delta = 1 + \alpha$. The NP effects are thus normalized with respect the SM values as

$$\alpha^q = \frac{\left|M_{12}^{q,\mathrm{NP}}\right|}{\left|M_{12}^{q,\mathrm{SM}}\right|}, \qquad \phi_\alpha^q = \phi_M^{q,\mathrm{NP}} - \phi_M^{q,\mathrm{SM}}. \tag{3.11}$$

The sign of the contribution to a_{sl}^q depends on the relative alignment of the NP phase with respect to the SM one (recall that a positive contribution is required for successful baryogenesis, see section 2). In the SM, the CP violation can be traced back to the single physical complex phase in the CKM matrix. Using the Wolfenstein parametrization, we obtain the SM predictions for the phases of the mass splittings,

$$\phi_M^{d,\mathrm{SM}} \simeq \arctan \frac{2\eta(1-\rho)}{(1-\rho)^2 - \eta^2} \simeq 0.768\,\mathrm{rad}, \quad \text{and} \quad \phi_M^{s,\mathrm{SM}} \simeq \arctan \frac{-2\lambda^2\eta}{1-\lambda^4\eta^2} \simeq -0.036\,\mathrm{rad}. \tag{3.12}$$

The experimental measurements of the oscillation period of neutral B mesons (which constraints ΔM^q) and the CP violation in interference (which constrains ϕ^q) can be turned into exclusion limits on the size of NP contributions. We use the most up-to-date averages by the HFLAV group [49] to derive our constraints. A key ingredient for the analysis are the SM predictions for the values of the relevant quantities $\Delta M^{q,\mathrm{SM}}$, $\Delta\Gamma^{q,\mathrm{SM}}$, $\phi_{12}^{q,\mathrm{SM}}$, $\phi^{q,\mathrm{SM}}$ and $a_{\mathrm{sl}}^{q,\mathrm{SM}}$, which we obtain from [44].

The results of our analysis are shown in figure 1 for the B_d and B_s systems. The main conclusion is that the combination of measurements pushes the absolute value of any NP contributions to be roughly one order of magnitude smaller than the SM values. This statement is slightly dependent on the phase of the NP contributions. Additionally, for

JHEP03(2020)046

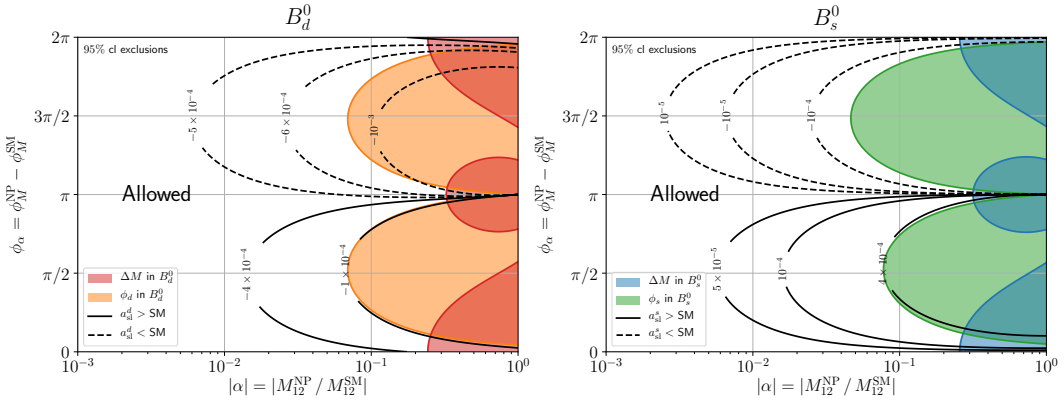

Figure 1. Bounds on the NP contributions to the absolute value (horizontal axis) and the phase (vertical axis) of M_{12}, assuming Γ_{12} is given by the SM value. The left panel corresponds to the B_d^0 system, and the right panel to B_s^0. Colored contours are excluded by measurements of ΔM and mixing-induced CP violation. The contour levels give the values of the semileptonic asymmetry, with solid (dashed) lines corresponding to values larger (smaller) than the SM ones.

small enough values of $\left|M_{12}^{q,\rm NP}\right|$, the phase $\phi_M^{q,\rm NP}$ is essentially unconstrained. In figure 1, we have also overlaid contours showing the value of the $a_{\rm sl}^q$ arising from the NP parameters. As expected, phases in the $(0,\pi)$ range enhance $a_{\rm sl}^q$ with respect to its SM value, whereas phases in the $(\pi,2\pi)$ range give a negative contribution to the asymmetry. It is important to note that in the B_d^0 system the asymmetry is bound to be negative, while in the B_s^0 system it can be positive. More precisely, we obtain the following 95% cl ranges for the semileptonic asymmetries:[7]

$$a_{\rm sl}^d \in \left[-8.9\times10^{-4},\,-9.0\times10^{-5}\right], \quad \text{and} \quad a_{\rm sl}^s \in \left[-2.1\times10^{-4},\,4.1\times10^{-4}\right]. \tag{3.13}$$

This is a much tighter region than the one quoted in eq. (2.7), which is an average of only direct measurements of the asymmetries. Of course, the one we have derived here is reliant on the extra assumptions mentioned above regarding the NP contributions.

3.2 The branching fraction Br$(B^0 \to \mathcal{B} + X)$

Taking the values in eq. (3.13) as reference for the maximum positive asymmetry that can be accommodated by NP contributions, we may use (2.4) to set a limit on the possible branching fraction of neutral B mesons to baryons and dark sector states Br $\left(B^0 \to \mathcal{B} + X\right)$ that is required to reproduce the observed baryon asymmetry of the Universe.

The baryon asymmetry is solved for by evolving a set of coupled Boltzmann equations [6, 39, 41] governing the evolution of the number densities of the relevant particles Φ, B, $\bar{B}$ and the DM. The solution may be found numerically, and factorizes into the

[7] Our limits differ by up to a factor of 2 from the ones derived in [50] (see http://www.utfit.org for up-to-date results), which are extracted from a global fit of all SM+NP parameters including all relevant constraints.

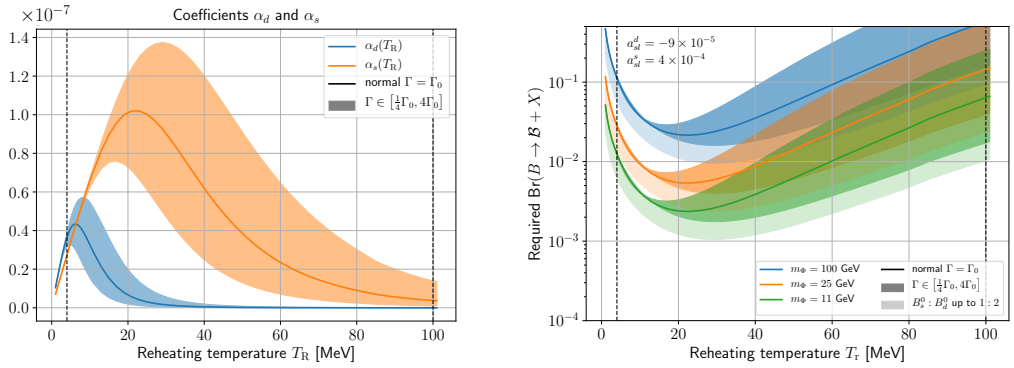

Figure 2. *Left:* values of the numerically determined functions α_d and α_s as a function of the reheating temperature over the range of interest 4–100 MeV, computed following the prescription of [41]. In order to account for the uncertainty in the calculation coming from the lack of precise knowledge of the scattering rate Γ of $e^\pm$ off B mesons in the primordial plasma, we conservatively allow for up to a factor of 4 uncertainty in Γ. This uncertainty mostly stems to the lack of knowledge about the charge radius of the neutral B mesons. *Right:* branching ratio of B mesons to visible baryons and dark antibaryons necessary to reproduce the baryon asymmetry of the Universe, also as a function of the reheating temperature. We use the largest experimentally allowed values for the semileptonic asymmetries and give the results for 3 different values of the mass of Φ. We use different shades of the colors to highlight uncertainties coming from the scattering rate as explained above and, additionally, from potential variations in the fragmentation ratio of b quarks to B_s^0 and B_d^0 mesons [4] (we use a benchmark ratio of 1 : 4 but to be conservative allow it to be as large as 1 : 2). In this range of parameters, branching ratios in the 0.001–0.1 range can lead to successful baryogenesis.

following form:

$$Y_B = \left(\frac{\mathrm{Br}\left(B^0 \to \mathcal{B} + X\right)}{10^{-2}}\right)\left(\frac{100\,\mathrm{GeV}}{m_\Phi}\right)\left(\alpha_d(T_R)\, a_{\mathrm{sl}}^d + \alpha_s(T_R)\, a_{\mathrm{sl}}^s\right) . \tag{3.14}$$

In addition to the branching fraction and the semileptonic asymmetry, the asymmetry depends on m_Φ and Γ_Φ. The Φ width may be related to the late era reheating temperature in the usual way $\Gamma_\Phi = 3H(T_R)$. Following the prescription of [41], the value of the asymmetry is simply inversely proportional to m_Φ and depends on the decay width through a numerically determined polynomial denoted by $\alpha_q(T_R)$ for the $B^0_{q=s,d}$ systems, whose dependence on T_R is depicted in figure 2. Roughly speaking, α_q acts to parametrize the decoherence effects of the system.

In analogy with neutrino oscillations, additional interactions with the B mesons can "measure" the state of the meson and decohere the oscillating system through the Zeno effect [51]. Such decoherence will spoil the oscillations and therefore prevent a baryon asymmetry from being generated. For the setup at hand, the only possible source of dechorence is the $e^\pm$ scattering off the neutral B meson in the early Universe plasma. To a good approximation, decoherence becomes important when the scattering rate exceeds the oscillation lengths of the B_s^0 or B_d^0 system, which are measured to be $\Delta M_s = 1.17 \times$

JHEP03(2020)046

$10^{-11}\,\mathrm{GeV}$ and $\Delta M_d = 3.34 \times 10^{-13}\,\mathrm{GeV}$. The temperature-dependent scattering rate is roughly $\Gamma_{e^\pm B \to e^\pm B} \sim 10^{-11}\,\mathrm{GeV}\,(T/20\,\mathrm{MeV})^5$ up to uncertainties in the charge radius of $B^0_{s,d}$ mesons. Therefore, decoherence becomes more relevant at high temperatures. More specifically, the oscillations decohere for $T \gtrsim (15,\, 30)\,\mathrm{MeV}$ for the B_d and B_s systems, respectively. Decoherence effects may be properly treated in the Boltzmann equations through the prescription of [43]. Results are displayed on the left panel of figure 2, for which we assume that reheating occurs between $\sim 4 - 100\mathrm{MeV}$, that is, *between BBN and hadronization*. To avoid excessive decoherence, baryogenesis favors reheating temperatures in the range $T_R \sim 15 - 50\,\mathrm{MeV}$.

The behavior of the numerical results for $\alpha_q(T_R)$ can be understood as follows: at high reheat temperatures ($T_R \gtrsim 50\mathrm{MeV}$), the B mesons formed from the decay of the Φ do not oscillate coherently and asymmetry production is therefore highly suppressed. As we consider lower values of T_R, the scattering rate for $e^\pm B \to e^\pm B$ drops such that the B^0_s mesons are produced and oscillate coherently thereby producing a baryon asymmetry. At even lower temperatures, $B^0_d - \bar{B}^0_d$ coherent oscillations will also contribute to the asymmetry. The change of behavior of $\alpha_{s,d}(T_R)$ at very low T_R is the result of dilution by a greater entropy density.

Recall that for baryogenesis to proceed through B meson oscillations and subsequent decay to the dark sector, a large positive net semileptonic-leptonic asymmetry is favored. As we saw above, the NP contributions to the neutral B meson oscillating systems can enhance the semileptonic-leptonic asymmetry in B^0_s decays to at most $a^s_{\mathrm{sl}} = 8.80 \times 10^{-4}$ while not being in conflict with measurements in B physics. Meanwhile, $a^d_{\mathrm{sl}} < 0$ in all regions of parameter space, so that maximizing the produced baryon asymmetry favors the smallest possible value of this negative contribution, namely $a^d_{\mathrm{sl}} = -4 \times 10^{-4}$. At the same time, figure 2 shows that the maximal values of α_s occurs for a reheat temperature of about 30 MeV. Taking everything into account, we conclude that in order to reproduce the observed value of $Y = (8.718 \pm 0.004) \times 10^{-11}$, a sizable inclusive branching ratio of B mesons to baryons is needed. The required value for this branching ratio is displayed on the right panel of figure 2 for extremal values of $a^{s,q}_{\mathrm{sl}}$, therefore representing a lower limit on the size of the branching fraction. The relatively large branching ratio is a robust prediction of the mechanism and provides a unique opportunity for high-energy experiments like LHCb [52] and Belle-II [53] to test this baryogenesis scenario.

4 A supersymmetric realization

The model independent analysis presented above allows to place constraints on the observables that play a direct role in the baryogenesis mechanism considered here. However, it is expected that other related observables can be used to indirectly test the scenario once the required minimal NP content is embedded in a consistent framework. With this aim, we construct a complete realization of the model in a supersymmetric context. The key ingredients of the theory which allow for baryogenesis to be realized are an unbroken $\mathrm{U}(1)_R$ symmetry [16, 17] and the presence of Dirac gauginos [14, 15]. Supersymmetric models with Dirac gauginos and $\mathrm{U}(1)_R$ symmetries are phenomenologically appealing [18]. By

forbidding Majorana gaugino masses and supersymmetric a-terms, the majority of collider constraints that push the MSSM into ever more fine tuned regions of parameter space are avoided. Their collider phenomenology has been greatly studied [21–26], along with flavor considerations [28]. Among other applications, these models can accommodate diverse baryogenesis scenarios [19, 20], sometimes at the cost of breaking the R-symmetry [21]. In this regard, realizing the mechanism of [6] is a novel application of such ingredients and, as will be discussed, motivates a rather unstudied region of parameter space: a light (GeV mass scale) Dirac bino.

Let us briefly summarize the main ideas behind our supersymmetric theory for baryogenesis and DM from B mesons. R-symmetries are known to arise naturally in supersymmetric constructions [14–18, 28]. Supercharges and their conjugates transform in opposite ways under an R-symmetry, allowing for particles within the same supermultiplet to carry different R-charges. Although $\mathrm{U}(1)_R$ is usually taken to be broken at low energies, an interesting possibility is for it to remain exact[8] and be identified with baryon number. Following this avenue leads to quarks and squarks having different baryon number assignments, as shown in tables 1 and 2. In this way, a right-handed down-type squark $\tilde{d}_R$ has the required charge assignments to play the role of the heavy colored scalar in eq. (2.1). We may also identify an adequate candidate for the neutral GeV scale Dirac baryon ψ in the form of the Dirac bino. After integrating out the heavy squark, the effective four-fermion operator in eq. (2.1) arises from a combination of R-parity violating and gauge interactions. Furthermore, the Dirac partner of the bino is by definition a singlet under the SM gauge group, allowing it to naturally couple to a dark sector. The dark sector can be minimally accommodated by introducing a generic new singlet chiral multiplet. More interestingly, this new singlet can be identified with a right-handed neutrino multiplet. In this way, the bino mediates the decay of B mesons into dark sector states. The complete set of superfield charge assignments is summarized in table 1, and the corresponding particle fields and their properties are given in table 2. In what follows, we will further elaborate upon the ingredients of this model needed to realize baryogenesis.

4.1 An exact $\mathrm{U}(1)_R$ symmetry

The model is similar to the one studied in [21, 22]. An exact R-symmetry requires a superpotential with R-charge of 2 (superspace derivatives $\mathcal{D}_\alpha$ have R-charge -1). Given the $\mathrm{U}(1)_R$ charges of superfields (see table 1), only the following terms respect the R-symmetry:

$$\mathbf{W} \supset y_u \mathbf{Q}\mathbf{H}_u\mathbf{U}^c - y_d \mathbf{Q}\mathbf{H}_d\mathbf{D}^c - y_e \mathbf{L}\mathbf{H}_d\mathbf{E}^c + \frac{1}{2}\lambda''_{ijk}\mathbf{U}^c_i\mathbf{D}^c_j\mathbf{D}^c_k + \mu_u \mathbf{H}_u\mathbf{R}_d + \mu_d \mathbf{R}_u\mathbf{H}_d \tag{4.1}$$

The first four terms of eq. (4.1) constitute the usual MSSM superpotential, with the addition of the "R-parity violating" (RPV) term $\mathbf{U}^c_i\mathbf{D}^c_j\mathbf{D}^c_k$ (the subscripts denote generation

[8] It is however difficult to argue against the existence of some amount of breaking due to supergravity, we will discuss this in section 4.7.

JHEP03(2020)046

Superfield	R-Charge (B no.)	L no.
$\mathbf{U}^c, \mathbf{D}^c$	2/3	0
$\mathbf{Q}$	4/3	0
$\mathbf{H}_u, \mathbf{H}_d$	0	0
$\mathbf{R}_u, \mathbf{R}_d$	2	0
$\mathbf{S}$, $\mathbf{T}$, $\mathbf{O}$	0	0
$\mathbf{L}$	1	1
$\mathbf{E}^c$, $\mathbf{N}^c_R$	1	−1

Table 1. Summary of superfields with their R-charge (baryon number) and lepton number assignments. Each antichiral superfield has R-charge opposite to that of the corresponding chiral superfield.

indices) which is now allowed.[9] The rest describe the Higgs sector; the $\mathbf{R}_{u,d}$ multiplets are added to generate μ terms which are forbidden in models with R-symmetry. Electroweak symmetry breaking proceeds as usual when the scalars of $\mathbf{H}_u$ and $\mathbf{H}_d$ acquire vacuum expectation values, while the VEVs of $\mathbf{R}_{u.d}$ remain zero.

Given the $\mathrm{U}(1)_R$ charge assignments of the matter content (see table 1), $\mathbf{U}^c$ and $\mathbf{D}^c$ have an R-charge of 2/3. If we explicitly write out the decomposition of the multiplets, e.g. $\mathbf{D}^c = \tilde{d}^*_R + \sqrt{2}\theta d^\dagger_R + \theta^2 F_d$, we see that the d-type right-handed squarks have R-charge $-2/3$ while the quarks[10] have R-charge 1/3 (recall that θ has R-charge 1). Since we identify baryon number with R-charge, $\tilde{d}_R$ has the appropriate charge assignments to be identified with the heavy colored scalar that mediates the effective interaction of eq. (2.1). At the quark/squark level, the $\mathbf{U}^c\mathbf{D}^c\mathbf{D}^c$ term in the superpotential produces the interactions

$$\mathcal{L} \supset \lambda''_{123}\left(\tilde{u}^*_R s^\dagger_R b^\dagger_R + \tilde{s}^*_R b^\dagger_R u^\dagger_R + \tilde{b}^*_R u^\dagger_R s^\dagger_R\right). \tag{4.2}$$

As in section 2, we have chosen a particular combination of quark flavor to keep the notation simple. In general, the role of $\tilde{d}_R$ can be played by any first or second generation up- or down-type squark, which means that any of the couplings λ''_{ij3} with $i, j = 1, 2$ can be relevant for the baryogenesis mechanism.

4.2 Dirac gauginos

In Wess-Zumino gauge, the field strength of a vector superfield can be written in the usual way as

$$\mathbf{W}^{\tilde{B}}_\alpha = \tilde{B}_\alpha + \left[D_1\delta^\beta_\alpha + \frac{i}{2}(\sigma^\mu\bar{\sigma}^\nu)^\beta_\alpha B_{\mu\nu}\right]\theta_\beta + i\theta^2\sigma^\mu_{\alpha\dot{\beta}}\nabla_\mu\tilde{B}^{\dagger\dot{\beta}}, \tag{4.3}$$

[9] Note that although the λ'' couplings are R-parity violating, they preserve the $\mathrm{U}(1)_R$ symmetry (i.e. they do not break baryon number). As it is a very extended convection in the SUSY literature, we will henceforth refer to λ'' as the RPV couplings. Other R-parity violating couplings, like the ones usually denoted by λ, λ' or μ' (see e.g. [54]) are not allowed by the R-symmetry.

[10] We use the notation of [54] to denote $d^\dagger_R$ as the Weyl spinor in the chiral superfield $\mathbf{D}^c$.

Particle	Description	Spin	Q_{EM}	Baryon no.	Lepton no.	Mass
Φ	"Inflaton-like" scalar	0	0	0	0	11–100 GeV
$\tilde{q}_R \in \mathbf{D}^c\,, \mathbf{U}^c$	Squark	0	$-1/3$	$-2/3$	0	$\mathcal{O}$(TeV)
$\tilde{B} \in \mathbf{W}_\alpha$ $\lambda_s^\dagger \in \mathbf{S}$	Dirac bino	1/2	0	-1	0	$\mathcal{O}$(GeV)
$\nu_R \in \mathbf{N}_R$	Sterile neutrino	1/2	0	0	1	$\mathcal{O}$(GeV)
$\tilde{\nu}_R \in \mathbf{N}_R$	Sterile sneutrino DM	0	0	-1	1	$\mathcal{O}$(GeV)

Table 2. Summary of the component fields and their charge assignments, properties, and the superfield in which they are embedded. We work in terms of Weyl spinors so that the Dirac bino consists of two components $\psi = (\tilde{B}, \lambda_s^\dagger)$. Here, Φ is an "inflaton-like" field that decays out of equilibrium producing b and $\bar{b}$ quarks. The heavy colored squark $\tilde{q}_R$ is integrated out to mediate quark-bino four fermion interactions (note that various flavors of squarks may generate this interaction, as will be discussed further below). The Dirac bino mediates decays of hadrons into the dark sector. The dark sector is embedded into a right-handed neutrino supermultiplet where the sneutrino is stable and represents our DM candidate, while the sterile neutrino generally decays on time scales of interest for collider searches.

where fields are expressed in terms of the $y^\mu = x^\mu - i\bar{\theta}\sigma^\mu\theta$ coordinates. The hypercharge $\mathrm{U}(1)_Y$ field strength tensor is $B_{\mu\nu} = \partial_\mu B_\nu - \partial_\nu B_\mu$, and $\tilde{B}$ is the bino, that is, a left handed 2-component Weyl spinor. One may construct a 4-component Dirac gaugino by adding another 2-component Weyl spinor to the theory. Concretely, let us introduce a new $\mathbf{S}$ superfield

$$\mathbf{S}(y^\mu) = \phi_s + \sqrt{2}\lambda_s^\alpha\theta_\alpha + \theta^\alpha\theta_\alpha F_s. \tag{4.4}$$

Gauge invariance requires the new field to transform in the adjoint representation, while the R-symmetry fixes its R-charge to vanish. Multiplets for the other SM gauge fields (a triplet T and an octet O) are added in a similar way.[11]

With the addition of the new superfields, Dirac gaugino mass terms can be generated [18, 55]. Consider the following superpotential terms:

$$\mathcal{L}_{\text{mass}} = \sqrt{2}\int d^2\theta\ \mathbf{W}'^\alpha\left[\frac{c_1}{\Lambda_1}\mathbf{W}_\alpha^{\tilde{B}}\mathbf{S} + \frac{c_2}{\Lambda_2}\mathbf{W}_\alpha^{\tilde{W}i}\mathbf{T}^i + \frac{c_3}{\Lambda_3}\mathbf{W}_\alpha^{\tilde{g}a}\mathbf{O}^a\right] + \text{h.c.}\,. \tag{4.5}$$

SUSY breaking is introduced through a D-term spurion $\mathbf{W}'^\alpha = D\theta^\alpha$. Here, c_i are $\mathcal{O}(1)$ coefficients, and in general we allow the SUSY breaking scale for each gauge group Λ_i to be different. From eqs. (4.3) and (4.4) together with eq. (4.5), we see that upon SUSY breaking, Dirac mass terms

$$\mathcal{L}_{\text{mass}}^{\tilde{B}} \supset \sqrt{2}c_1\frac{D}{\Lambda_1}\tilde{B}^\alpha\lambda_{s,\alpha} + c_1\frac{DD_1}{\Lambda_1}\phi_s \tag{4.6}$$

[11] The existence of these adjoint superfields can be motivated by imposing a $\mathcal{N} = 2$ supersymmetry in the gauge sector, as was done in [18].

JHEP03(2020)046

are generated (the second term of (4.6) vanishes on-shell when $D_1 = 0$). We denote the 4-component Dirac bino and its corresponding Dirac mass as

$$\psi = \begin{pmatrix} \tilde{B} \\ \lambda_s^\dagger \end{pmatrix} \quad \text{and} \quad m_\psi = \sqrt{2} c_1 \frac{\langle D \rangle}{\Lambda_1} \,, \tag{4.7}$$

in consonance with eq. (2.1). Similar expressions are obtained for the other gauginos, which acquire masses $m_{\psi_{2,3}} = \sqrt{2} c_{2,3} D/\Lambda_{2,3}$. In order to reproduce the spectrum required for baryogenesis, m_ψ needs to be a few GeV. At the same time, collider [13] and flavor [56, 57] constraints generically push charginos and gluinos to lie above the TeV scale. If no other source of mass for gauginos is present, this implies that there must exist a hierarchy $(c_1/\Lambda_1)/(c_{2,3}/\Lambda_{2,3}) \lesssim 10^{-3}$. Such hierarchy can be explained either by invoking some tuning of the c_i coefficients or by allowing for at least two separate sources of SUSY breaking [29] so that $\Lambda_1 \ll \Lambda_{2,3}$.

4.3 Squark masses and couplings

Soft masses for squarks (and other superpartners) can be generated through an F-term SUSY breaking spurion $\mathbf{X} = \theta F$ [28] at a scale Λ_F, which produces squark masses $m_{\tilde{q}} \sim F^* F/\Lambda_F$. Given the experimental constraints [21, 26, 28] and depending on the scale of gluino and chargino masses, squarks as light as a few 100 GeV can be feasible.[12]

As discussed above, the role of the colored scalar participating in the baryogenesis mechanism is played by a right-handed squark, which can be up- or down-type and belong to any of the first two generations. The squark mass is assumed to be in the TeV range so that it can be safely integrated out at the GeV scale where the baryogenesis dynamics happen. It is straightforward to see how the $\tilde{q}_R \bar{\psi} s$ term in eq. (2.1) is generated in the supersymmetric setup. Interacting chiral matter theories have gauge interactions of the form

$$\mathcal{L}_{\text{gauge}} \supset -\sqrt{2} g' Q_{q_R} (\tilde{q}_R^* q_R \tilde{B}^\dagger) + \text{h.c.} \,, \tag{4.8}$$

where Q_{q_R} and $g' = e/\cos\theta_W$ denote the charge assignment and hypercharge gauge coupling (as customary, e is the electromagnetic charge quantum and θ_W is the weak mixing angle). When $\tilde{s}_R$ is integrated out, the effective four-fermion interaction $\tilde{B}\, u\, s\, b$ is recovered. Of course, other flavor combinations for the operator are possible: they are summarized in table 3 along with the resulting coefficient of the effective interaction. It is worth noting that the gauge coupling being fixed, the only unknown parameter that sets the strength of the effective interaction is λ''_{ij3}.

4.4 The Higgs sector and neutralino mixing

The number of neutral fermions in R-symmetric models is larger than in the MSSM due to the presence of the new SU(2) doublets $R_{u,d}$ and the singlet and triplet fields S and T. Here

[12] Dirac gaugino masses produce a *supersoft* [18] scenario where radiative corrections to the squark masses are finite. This allows for squarks to be much lighter than gauginos, thus alleviating many of the collider and flavor constraints. For this reason, this paradigm is sometimes referred to as *supersafe*.

four-fermion operator	Effective coupling	$\tilde{q}_R$ particle
$\psi\, b\, u\, d$	$\lambda''_{113}\sqrt{2}\, g' \left(\frac{Q_u}{m^2_{\tilde{u}}} + \frac{Q_d}{m^2_{\tilde{d}}} - \frac{Q_d}{m^2_{\tilde{b}}}\right)$	$\tilde{u}_R$, $\tilde{d}_R$, $\tilde{b}_R$
$\psi\, b\, u\, s$	$\lambda''_{123}\sqrt{2}\, g' \left(\frac{Q_u}{m^2_{\tilde{u}}} + \frac{Q_d}{m^2_{\tilde{s}}} - \frac{Q_d}{m^2_{\tilde{b}}}\right)$	$\tilde{u}_R$, $\tilde{s}_R$, $\tilde{b}_R$
$\psi\, b\, c\, d$	$\lambda''_{213}\sqrt{2}\, g' \left(\frac{Q_u}{m^2_{\tilde{c}}} + \frac{Q_d}{m^2_{\tilde{d}}} - \frac{Q_d}{m^2_{\tilde{b}}}\right)$	$\tilde{c}_R$, $\tilde{d}_R$, $\tilde{b}_R$
$\psi\, b\, c\, s$	$\lambda''_{223}\sqrt{2}\, g' \left(\frac{Q_u}{m^2_{\tilde{c}}} + \frac{Q_d}{m^2_{\tilde{s}}} - \frac{Q_d}{m^2_{\tilde{b}}}\right)$	$\tilde{c}_R$, $\tilde{s}_R$, $\tilde{b}_R$

Table 3. Exhaustive list of all the possible operators contribution to the baryogenesis mechanism in a $\mathrm{U}(1)_R$ supersymmetric setup with Dirac gauginos.

JHEP03(2020)046

we follow [26] to investigate the mixing between all these states after electroweak symmetry breaking. The relevant terms in the Higgs sector, allowed by gauge and R-Symmetries, are given by

$$\mathbf{W} \supset \mu_u \mathbf{H}_u \mathbf{R}_u + \mu_d \mathbf{H}_d \mathbf{R}_d + \mathbf{S}\Big(\lambda_u^{\tilde{B}} \mathbf{H}_u R_u + \lambda_d^{\tilde{B}} \mathbf{H}_d \mathbf{R}_d\Big) + \mathbf{T}\Big(\lambda_u^{\tilde{W}} \mathbf{H}_u \mathbf{R}_u + \lambda_d^{\tilde{W}} \mathbf{H}_d \mathbf{R}_d\Big). \quad (4.9)$$

Recall that $\mathbf{R}_{u,d}$ are added to generate the otherwise R-symmetry forbidden μ-terms. Electroweak symmetry breaking proceeds as usual when the scalars of $\mathbf{H}_u$ and $\mathbf{H}_d$ acquire vacuum expectation values v_u and v_d (the VEVs of $\mathbf{R}_{u.d}$ remain zero). The terms in (4.9), together with the Dirac gaugino masses and the gauge potential, generate the Dirac mass mixing matrix

$$M_{\tilde{N}} = \begin{pmatrix} m_\psi & 0 & g' v_u/\sqrt{2} & -g' v_d/\sqrt{2} \\ 0 & m_{\tilde{W}} & -g v_u/\sqrt{2} & g v_d/\sqrt{2} \\ \lambda_u^{\tilde{B}} v_u/\sqrt{2} & -\lambda_u^{\tilde{W}} v_u/\sqrt{2} & \mu_u & 0 \\ -\lambda_d^{\tilde{B}} v_d/\sqrt{2} & \lambda_d^{\tilde{W}} v_d/\sqrt{2} & 0 & \mu_d \end{pmatrix}, \quad (4.10)$$

which is written in the $(\tilde{B},\, \tilde{W},\, \tilde{R}_u,\, \tilde{R}_d) \times (\lambda_S,\, \lambda_T,\, \tilde{H}_u,\, \tilde{H}_d)$ basis. As usual, $g = e/\sin\theta_W$ and we require that $v_u^2 + v_d^2 = v^2/2 = (174\,\mathrm{GeV})^2$. In the large $\tan\beta \equiv v_u/v_d$ limit, the mass matrix simplifies to

$$M_{\tilde{N}} \simeq \begin{pmatrix} m_\psi & 0 & g' v/\sqrt{2} & 0 \\ 0 & m_{\tilde{W}} & -g v/\sqrt{2} & 0 \\ \lambda_u^{\tilde{B}} v/\sqrt{2} & -\lambda_u^{\tilde{W}} v/\sqrt{2} & \mu_u & 0 \\ 0 & 0 & 0 & \mu_d \end{pmatrix}, \quad (4.11)$$

showing that one of the states with mass μ_d decouples. It is clear that if $\lambda_u^{\tilde{B}} = \lambda_u^{\tilde{W}} = 0$, there is no mixing between the bino, the neutral weakino and the higgsinos. Even if $\lambda_u^{\tilde{B},\tilde{W}}$ are nonzero, in the limit where $m_\psi \ll v \ll m_{\tilde{W}},\, \mu_u$, the lightest state is mostly bino with mass m_ψ. This is the case of interest to us, as we are dealing with a GeV bino but other gauginos and higgsinos are at or above the TeV scale. In this limit, the mixings of the bino are approximately given by

$$\theta_{\tilde{B}\tilde{W}} \simeq \frac{1}{2} \frac{\lambda_u^{\tilde{B}}\, g\, v^2}{m_{\tilde{W}}\, \mu}, \qquad \theta_{\tilde{B}\tilde{H}_u} \simeq \frac{1}{\sqrt{2}} \frac{\lambda_u^{\tilde{B}}\, v}{\mu}. \quad (4.12)$$

Although not relevant for the baryogenesis dynamics, these mixings can play a role in constraining the model using flavor observables such as $\mu \to e\gamma$, which are discussed in section 5.2.

4.5 A dark chiral multiplet

As was highlighted in section 2, the crucial step to generate a baryon asymmetry in the visible sector without incurring into global baryon number violation is to allow ψ to decay into a dark sector where the corresponding antibaryon number is stored. In this way, a DM abundance is generated in parallel to the baryon asymmetry.

Thus far, the model we have introduced cannot accommodate DM. However, being uncharged under the SM gauge group, the singlet S offers a natural portal to a dark sector. Given that the fermion in S is the Dirac partner of the bino, such a coupling allows ψ to decay to the dark sector. The minimal extension to take advantage of this portal includes a new chiral multiplet $\boldsymbol{\phi}$ where the $B = -1$ dark scalar ϕ and the $B = 0$ Majorana spinor ξ can both be embedded,

$$\boldsymbol{\phi} = \phi^* + \sqrt{2}\theta^\alpha \xi_\alpha + \theta^2 F_\phi. \tag{4.13}$$

The only superpotential terms allowed by gauge and $\mathrm{U}(1)_R$ symmetries are precisely

$$W \supset \int \mathrm{d}^2\theta \, (y_s \mathbf{S}\boldsymbol{\phi}\boldsymbol{\phi} + m_\phi \boldsymbol{\phi}\boldsymbol{\phi}) \, . \tag{4.14}$$

The former generates the coupling $\lambda_s \, \phi^* \, \xi$ while the latter gives masses to the dark states. Note that the invariance of (4.14) under $\boldsymbol{\phi} \leftrightarrow -\boldsymbol{\phi}$ acts to stabilize the DM (corresponding to the $\mathbb{Z}_2$ symmetry introduced in [6]).

This most economic and generic extension contains all the ingredients to produce the baryon asymmetry and an asymmetric DM component. However, given that the dark states ϕ and ξ and the mediator ψ are rather light, a symmetric relic abundance tends to be overproduced [6] in this minimal setup. In order to partially deplete the symmetric abundance, new interactions have to be added to allow for the excess DM to annihilate.[13] In our case, there exists an attractive solution to this problem: to identify the dark sector states with a right-handed neutrino supermultiplet.

4.6 Sterile sneutrino dark matter

In order to accommodate neutrino masses in the $\mathrm{U}(1)_R$ symmetric model, the minimum requirement is the presence of a right-handed sterile neutrino multiplet $\mathbf{N}_R$ with R-charge $+1$,

$$\mathbf{N}_R^c = \tilde{\nu}_R^* + \sqrt{2}\theta \nu_R^\dagger + \theta^2 F_{\nu_R}^* \, . \tag{4.15}$$

Identifying $\mathrm{U}(1)_R$ with $\mathrm{U}(1)_B$ leads to the right-handed sneutrino $\tilde{\nu}_R$ carrying baryon number -1, while the right-handed neutrino remains uncharged under baryon number. At the same time, $\mathbf{N}_R^c$ has to carry -1 lepton number. The following operators, allowed by

[13] This problem is recurrent in asymmetric DM scenarios that identify the dark sector and baryon asymmetries. See [58] for other examples of how the symmetric DM component can be depleted.

JHEP03(2020)046

all the symmetries (but including a $\Delta L = 2$ Majorana neutrino mass term), can be added to the superpotential:

$$\mathbf{W} \supset \frac{\lambda_N}{4}\mathbf{S}\mathbf{N}_R^c\mathbf{N}_R^c + \mathbf{H}_u\mathbf{L}^I y_N^{IJ}\mathbf{N}_R^{J\,c} + \frac{1}{2}\mathbf{N}_R^c M_M \mathbf{N}_R^c + \text{h.c.}\,. \tag{4.16}$$

To keep the discussion general, we allow for three flavors of sterile neutrinos ($I = e, \nu, \tau$; $J = 1, 2, 3$). Note that the first and third terms are equivalent to the ones in (4.14), so the identification of N_R^c as the DM multiplet is direct. The first term of (4.16) may be expanded in component fields as

$$\frac{\lambda_N}{4}\int \mathrm{d}^2\theta\ \mathbf{S}\mathbf{N}_R^c\mathbf{N}_R^c \supset \frac{1}{2}\lambda_N\left(\lambda_s\nu_R^\dagger\tilde{\nu}_R^* + \phi_s\nu_R^\dagger\nu_R^\dagger\right) + \text{h.c.}\,. \tag{4.17}$$

This operator generates the three point interaction (2.2) that mediates the decay of the Dirac bino (through its right-handed partner λ_s) into the dark sector states ν_R and $\tilde{\nu}_R$. The second term in (4.16) generates Dirac neutrino masses. The $\mathrm{SU}(2)_L$ multiplets can be expanded out as

$$\begin{aligned}
&\int \mathrm{d}^2\theta\left(\mathbf{H}_u^0\mathbf{N}_L^I y_N^{IJ}\mathbf{N}_R^{J\,c} - \mathbf{H}_u^+\mathbf{E}_L^I y_N^{IJ}\mathbf{N}_R^{J\,c}\right) + \text{h.c.} \\
&= 2y_N^{IJ}\left(h_u^0\nu_L^I\nu_R^{J\dagger} + \tilde{h}_u^0\tilde{\nu}_L^I\nu_R^{J\dagger} + \tilde{h}_u^0\nu_L^I\tilde{\nu}_R^{J*}\right) \\
&\quad - 2y_N^{IJ}\left(h_u^+\ell_L^I\nu_R^{J\dagger} + \tilde{h}_u^+\tilde{\ell}_L^I\nu_R^{J\dagger} + \tilde{h}_u^+\ell_L^I\tilde{\nu}_R^{J*}\right) + \text{h.c.}\,,
\end{aligned} \tag{4.18}$$

where $\ell^I = e,\, \mu,\, \tau$. Upon electroweak symmetry breaking, $\langle h_u^0\rangle = v_u$ produces a Dirac mass for the neutrino,

$$\mathcal{L} \supset m_D\left(\nu_L^i{\nu_R^j}^\dagger + {\nu_L^i}^\dagger\nu_R\right), \tag{4.19}$$

with $m_D = 2y_N v_u = 2y_N v\sin\beta$. For simplicity, we have assumed a diagonal flavor structure and suppressed generation indices. This simple setup reproduces the type-I seesaw mechanism [30–33], whereby the light neutrinos obtain masses $m_\nu \simeq m_D^2/M_M$, as long as $m_D \ll M_M$. For the baryogenesis mechanism to be viable, at least one of the right-handed neutrinos needs to have a mass in the GeV range so that ψ can decay into it. In order to obtain a neutrino mass of $m_\nu \lesssim 0.1\,\text{eV}$, a small Yukawa $y_N \lesssim 10^{-8}$ is required, as will be further discussed in section 6.3.

Aside from generating Dirac neutrino masses, the second term in (4.16) also provides the interactions necessary to avoid the overproduction of a symmetric DM component. The crucial difference to the generic case discussed in the previous section is the fact that the DM particles, being identified with sterile neutrino and sneutrino, now carry lepton number. The annihilation of right-handed sneutrinos into left-handed neutrinos can occur via t-channel exchange of a bino or a higgsino. We will study this in more detail in section 6.2.

4.7 $\mathrm{U}(1)_R$ symmetry breaking from supergravity

The model presented above relies on an exact global $\mathrm{U}(1)_R$ symmetry which is identified with baryon number. While R-symmetries are motivated by top down constructions, we

JHEP03(2020)046

do generically expect them to be broken at low scales. Supersymmetry breaking effects coming from supergravity are generically always present (however see [59] for a possible alternative), and these generate a tiny Majorana mass for the gauginos through the conformal anomaly (as well as soft squark masses and a-terms). The order parameter is the gravitino mass $m_{3/2}$ so that gaugino Majorana masses

$$M_1 \propto m_{3/2} = \frac{\langle F_\phi \rangle}{M_{\rm Pl}} \tag{4.20}$$

appear. Here, $M_{\rm Pl}$ denotes the Planck mass. In particular, Anomaly Mediated Symmetry Breaking (AMSB) [60, 61] produces a small Majorana mass term for the bino

$$M_a = \frac{\beta_{g_a}}{g_a} m_{3/2} \quad \Rightarrow \quad M_1 = \frac{g'^2}{16\pi^2}\frac{33}{5} m_{3/2}\,. \tag{4.21}$$

Additionally, soft squark masses $(m^2)^i_j = \frac{1}{2}|m_{3/2}|^2 \frac{d}{dt}\gamma^i_j$ and non-zero a-terms $a^{ijk} = -m_{3/2}\beta_{y^{ijk}}$ will be generated. Clearly, the introduction of (even tiny) a-terms, soft squark masses and Majorana gaugino masses from AMSB can spoil the phenomenological advantages of R-SUSY. Therefore, it is interesting to quantify the degree to which the R-symmetry must be exact, i.e. the size of the gravitino mass and couplings λ''_{ijk} of eq. (4.1) that still accommodate a phenomenologically viable model. This will be further discussed in section 6.5, where we will see that the most stringent constraints come from the AMBS Majorana gaugino masses that lead to dinucleon decay.

5 Flavor phenomenology

After having outlined a complete model with a field content that realizes the mechanism of [6], we may begin to preform calculations within this framework in order to identify the phenomenologically viable parameter space. As we will see, generating the observed baryon asymmetry and the DM relic abundance of the Universe requires a precise range of model parameters and observables, which are summarized in table 5. A key prediction of this scenario is the modification of some of the oscillation parameters of the neutral B meson system with respect to the values expected in the SM. Because of this, sufficiently precise measurements of the B meson system can *directly* probe the baryogenesis dynamics. Any NP inducing such modifications is also expected to have an effect on other $\Delta F = 2$ observables, like oscillations in the B, K, and D neutral meson systems; and on $\Delta F = 1$ processes such as $\mu \to e\gamma$ and $b \to s\gamma$. Making use of the supersymmetric model, these effects can be quantified within a consistent framework.

It is common lore that SUSY models with an R-Symmetry are not too severely constrained by flavor observables (see e.g. [28]). However, due to the presence of the $\mathcal{O}(\text{GeV})$ bino and the λ''_{ijk} as the only RPV couplings, our mechanism highlights a different slice of parameter space from what has been previously considered. It is therefore important to re-evaluate the constraints and apply them to the relevant parameter space, as well to assess whether the model prediction for the semileptonic-leptonic asymmetry in the B_s and B_d systems lies within the range that can accommodate baryogenesis.

The RPV couplings $\lambda''_{ijk}\mathbf{U}^c_i\mathbf{D}^c_j\mathbf{D}^c_k$ are an obvious source of flavor violation, and may also produce CP violation through complex phases. A comprehensive study of the phenomenological implications of RPV couplings was made in [62]. The main particularity of our setup is that the most constraining processes, i.e. proton decay and nucleon-antinucleon oscillations, are forbidden as long as the $R-$symmetry remains exact (we discuss the implications of $R-$symmetry breaking in section 6.5). As a consequence, the flavor violating observables described below give the strongest constraints for all the RPV couplings.

Soft masses for SM fermion superpartners can also be sources of flavor and CP violation. A particularity of the unbroken $\mathrm{U}(1)_R$ is that left-right squark and slepton mixing is forbidden by the R-symmetry [16]. The soft scalar mass matrices can be parametrized as usual by dimensionless ratios $\delta^{ij}_{LL} \equiv (m^2_{\tilde{q}})^{ij}/|m^2_{\tilde{q}}|$ of the off-diagonal elements to the diagonal ones $m^2_{\tilde{q}}$, where i, j are quark or lepton flavor indices (analogously for δ^{ij}_{RR}). As we will see, CP violation can arise if these ratios have complex phases.

5.1 $\Delta F = 2$ meson oscillations

In addition to the flavor violation already present in the SM, our setup allows for new processes contributing to neutral meson-antimeson oscillations, where flavor is violated by two units. For baryogenesis, a NP contribution in the B^0-$\bar{B}^0$ system is desirable. At the same time, experimental constraints, which are strongest in the K^0-$\bar{K}^0$ system, must be satisfied. Studies in general supersymmetric extensions of the SM [56, 57], in RPV contexts [62, 63] and in $\mathrm{U}(1)_R$ models with Dirac gauginos [28] have been performed. Here we extend and adapt those results to our scenario.

The physics of neutral meson oscillations, as well as the relevant observables, have been described in section 3.1 in a model independent way. We now link such observables to the NP model at hand. Firstly, the modification of the mass splitting between meson and antimeson can be computed as

$$\Delta M^{\mathrm{NP}} = 2\left(\sum_{i=1}^{5} C_i M_i + \sum_{i=1}^{3} \tilde{C}_i \tilde{M}_i\right). \tag{5.1}$$

Here, $\overset{(\sim)}{C}_i$ encode the model-specific partonic processes, which are discussed below. $\overset{(\sim)}{M}_i$ correspond to the matrix elements of the resulting effective four-fermion operators $\overset{(\sim)}{Q}_i$, that is, $\overset{(\sim)}{M}_i = \langle \bar{B}^0 | \overset{(\sim)}{Q}_i | B^0 \rangle$ and similarly for K^0 and B^0_s. The operators are numbered following [57]. The ones relevant for us are $Q_1 = \bar{b}^\alpha_L \gamma_\mu d^\alpha_L \, \bar{b}^\beta_L \gamma_\mu d^\beta_L$, $\tilde{Q}_1 = \bar{b}^\alpha_R \gamma_\mu d^\alpha_R \, \bar{b}^\beta_R \gamma_\mu d^\beta_R$, $Q_4 = \bar{b}^\alpha_R d^\alpha_L \, \bar{b}^\beta_L d^\beta_R$ and $Q_5 = \bar{b}^\alpha_R d^\beta_L \, \bar{b}^\beta_L d^\alpha_R$, where α and β are color indices. The corresponding matrix elements are

$$\begin{aligned} M_1 &= \tilde{M}_1 = \frac{1}{3} f_B^2 m_B B_1, \\ M_4 &= \left[\frac{1}{24} + \frac{1}{4}\left(\frac{m_B}{m_b + m_d}\right)^2\right] f_B^2 m_B B_4\,, \\ M_5 &= \left[\frac{1}{8} + \frac{1}{12}\left(\frac{m_B}{m_b + m_d}\right)^2\right] f_B^2 m_B B_5. \end{aligned} \tag{5.2}$$

In our calculations, we use the values obtained in [64] for the bag parameters B_i.

JHEP03(2020)046

The decay rate difference $\Delta\Gamma$ is not modified in our setup, as there is no new common state to which both meson and antimeson can decay. Its value can therefore be set to the SM prediction as was done in section 3. As a consequence, the previous expression eq. (5.1) also allows to calculate CP-violating observables, which depend on the complex phase of $\overset{(\sim)}{C}_i$ with respect to the SM counterpart, as made explicit in eq. (3.11). We are particularly interested in contributions to the semileptonic asymmetries in the $B^0_{s,d}$ systems, as these are the key observables that enter the baryogenesis mechanism.

At the partonic level, the meson oscillations arise from box diagrams. In the SM they are mediated by W bosons, but in our supersymmetric scenario new contributions arise, which can be classified into two groups depending on the origin of the flavor violation.

Contributions from RPV couplings. The corresponding Feynman diagrams are shown in figure 7 in appendix A. The first two contain four RPV vertices with λ'' couplings, while the lower two diagrams involve mixed contributions with two RPV vertices and two gauge/Higgs vertices with the corresponding CKM factors. These diagrams were calculated in [63] for the (s)top couplings λ''_{3jk}, here we generalize the computation to include also contributions from first two generation (s)quarks. The explicit analytic expressions are given in (A.1). Flavor changing squark mass mixing is neglected for this computation.

As can be seen in eq. (A.1), one-loop diagrams involving RPV interactions generate the operators $\tilde{Q}_1$, Q_4 and Q_5. The former is associated with the box diagram involving four λ'' couplings and therefore scales as $\tilde{C}_1 \sim \lambda''^4/m^2_{\tilde{q}}$, where λ''^4 symbolizes the appropriate product of four potentially different $\lambda''^{(\star)}_{ijk}$ couplings (see eq. (A.1) for the explicit combinations that arise). For simplicity, we assume universal squark masses and compute the loop integrals in the limit where $m_{\tilde{q}}$ is much larger than any other mass.[14] The other two operators are associated with diagrams with only two RPV couplings, while the other two vertices correspond to weak interactions where flavor violation is due to CKM insertions. Therefore, they both scale as $C_{4,5} \sim \lambda''^2 V^2/m^2_{\tilde{q}}$, where V^2 represents the appropriate CKM factors (see eq. (A.1) for explicit expressions). These diagrams also carry a factor of $m_{u_i} m_{u_j}/m^2_W$, which introduces an extra suppression unless only top quarks run in the loop (i.e. $i = j = 3$). Note that the RPV couplings generically source CP violation in the neutral meson mixing because the λ'' couplings can be complex.

Using the experimental measurements of the neutral meson oscillation parameters, $(\Delta M, \phi^{d,s})$ for $B^0_{d,s}$ and $(\Delta M, \epsilon_K)$ for K^0, together with the SM predictions for such observables,[15] we can obtain constraints on the products of RPV couplings. The resulting limits are compiled in table 4. For all of them, we assume a value of $m_{\tilde{q}} = 1\,\text{TeV}$. The limits on the diagonal of each table are dominated by the $\tilde{C}_1$ contribution with four λ'' factors, which means that they scale with $m_{\tilde{q}}$. However, the off-diagonal entries in the tables,

[14] We do not take into account renormalization group running effects for the operators $\overset{(\sim)}{Q}_i$ from the squark scale down to the hadronic scale. We estimate this approximation to be good within a factor of ~ 2 for the coefficients $\overset{(\sim)}{C}_i$ and therefore do not expect a large effects on the limits presented in table 4 and figure 3.

[15] The SM predictions in the K^0 sector have large uncertainties and we therefore assume that the SM values saturate the experimental bounds to obtain conservative limits.

JHEP03(2020)046

K^0	λ''^*_{113}	λ''^*_{213}	λ''^*_{313}
λ''_{123}	3.7×10^{-3} / 3.0×10^{-4}	– / 9.0×10^{-2}	2.5 / 1.6×10^{-2}
λ''_{223}	– / 2.5	3.7×10^{-3} / 3.0×10^{-4}	0.25 / 1.6×10^{-3}
λ''_{323}	– / 0.29	0.22 / 1.4×10^{-3}	2.8×10^{-3} / 4.8×10^{-5}

B^0_d	λ''^*_{112}	λ''^*_{212}	λ''^*_{312}
λ''_{123}	3.8×10^{-3} / 2.0×10^{-3}	– / –	4.0 / 1.1
λ''_{223}	– / –	3.8×10^{-3} / 2.0×10^{-3}	0.40 / 0.11
λ''_{323}	– / –	– / –	3.3×10^{-3} / 1.5×10^{-3}

B^0_s	λ''^*_{112}	λ''^*_{212}	λ''^*_{312}
λ''_{113}	1.8×10^{-2} / 1.0×10^{-2}	– / –	– / –
λ''_{213}	– / –	1.8×10^{-2} / 1.0×10^{-2}	2.3 / 0.73
λ''_{313}	– / –	– / –	1.6×10^{-2} / 8.1×10^{-3}

Table 4. Constraints on products of RPV couplings from neutral meson oscillations. Each of the K^0, B^0_d and B^0_s systems constrain different combinations of couplings. For each product, the first limit assumes that the NP contribution is aligned with the SM one, while the second one assumes maximal CP-violating phase. A line indicates that the derived limit is above the unitarity bound on the couplings. The limits are computed assuming a universal squark mass $m_{\tilde{q}} = 1\,\text{TeV}$, and scale with $m_{\tilde{q}}$ (diagonal ones) or $m^2_{\tilde{q}}$ (off-diagonal ones).

which rely on the $C_{4,5}$ contributions, scale with $m^2_{\tilde{q}}$ and are weaker due to the CKM and/or quark mass suppressions explained in the previous paragraph. The exception are the bottom right entries of the tables, which correspond to diagrams mediated by top quarks for which the contributions from $\tilde{C}_1$ and $C_{4,5}$ are of similar size for $m_{\tilde{q}} = 1\,\text{TeV}$. Each of the entries in the table quotes two limits: the left one corresponds to the case where the phase of the NP contribution to M_{12} is aligned with the SM one; the limit in that case comes from measurements of ΔM. The right one assumes that the NP phase is orthogonal to the SM one and therefore enhances CP violation, the limits in that case come from $\phi^{d,s}$ and ϵ_K. For the general case where the phases are neither aligned nor orthogonal, the limit lies between the two extremal values quoted in table 4.

In the general case where the RPV couplings are complex and source CP violation, contributions to the semileptonic asymmetries in the B^0_d and B^0_s are expected. Indeed, as figure 1 shows and was discussed in section 3.1, NP effects can significantly enhance $a^{d,s}_{\text{sl}}$ with respect to their SM value while satisfying all other constraints. For instance, the benchmark values used for the baryogenesis calculations are obtained if *any* one product of complex RPV couplings saturates the corresponding limit in table 4.

Contributions from squark mass mixings. Off-diagonal terms in the squark mass matrix can also induce neutral meson oscillations. The bino-mediated diagrams are shown

JHEP03(2020)046

in figure 9 (appendix A) for the B_d^0 system, the cases of B_s^0 and K^0 are analogous. For Dirac gauginos, the number of contributing diagrams is smaller than in the MSSM, as the Dirac partners do not couple to quarks and thus chirality flips in the internal gaugino propagators are not possible.[16] Furthermore, the $\mathrm{U}(1)_R$ symmetry prohibits the presence of a-terms, i.e. no left-right squark mass mixing is allowed.

The authors of [28] considered the $\Delta F = 2$ flavor constraints arising from box diagrams with gluinos, which due to the stronger coupling give the largest contribution if the masses of all gauginos are assumed to be similar. This is not necessarily the case in the regime where $m_\psi \sim 1\,\mathrm{GeV}$ is much lighter than gluinos and winos. The analytic expressions for the contribution of a light bino to the oscillation parameters defined in section 3 are given in appendix A. Parametrically, the contribution of a light GeV bino to ΔM is of the same order as that of a gluino which is about 10 times heavier than the squarks.

CP violation arises when ΔM^{NP} is a complex quantity. This happens if the off-diagonal elements of the squark mixing matrix are complex, and thus so are δ_{LL} and δ_{RR}. The CP-violating observables defined in section 3 can thus receive NP contributions. With this, the experimental constraints detailed in section 3, together with the analogous ones for the kaon system (ΔM_K and ϵ_K, see [44]) can be used to constraint squark mixing. Figure 3 shows the excluded ranges of values for the diagonal and (generally complex) off-diagonal elements $m_{\tilde{q}}$ and δ. The non-trivial dependence of the constraints on the phase of δ comes from interference with the SM contributions, i.e. the alignment between the NP effects and their SM counterparts.

The values of the semileptonic asymmetries as a function of the model parameters are shown as contour lines in figure 3. For squark masses in the TeV scale and $\mathcal{O}(1)$ absolute values of the mixings δ_{sb} and δ_{bd}, a broad interval of phases lead to semileptonic asymmetries compatible with baryogenesis. At the same time, the stringent bounds in the kaon sector restrict δ_{ds} to be $\lesssim 10^{-2}$ unless its phase is close to zero (or $\pi/2$). This is compatible with baryogenesis, as δ_{ds} does not play a role in B meson oscillations, but points towards some flavor structure that particularly suppresses any flavor violation which does not involve the third generation; see for instance [65, 66] for constructions where such flavor structures arise.

5.2 $\Delta F = 1$ observables

Processes in which flavor is violated by one unit can also probe model parameters relevant for baryogenesis. We limit the discussion to two observables, $b \to s\gamma$ and $\mu \to e\gamma$, as they offer the best experimental prospects. Although the latter is the best tested experimentally, the former is directly related to parameters relevant for the baryogenesis mechanism. For this study we mainly adapt the results of [28] to our setup.

[16] For heavy gauginos that can be integrated out, effective dimension five operators like $\tilde{d}_R^\star \tilde{s}_L^\star \, d_R^\dagger s_L$ are absent, and the transition happens through dimension six operators like $\tilde{d}_L \partial_\mu \tilde{s}_L^\star \, d_L^\dagger \gamma^\mu s_L$. For a light bino this does not result in extra suppression, but the chirality structure of the diagrams is in any case different than for Majorana gauginos.

JHEP03(2020)046

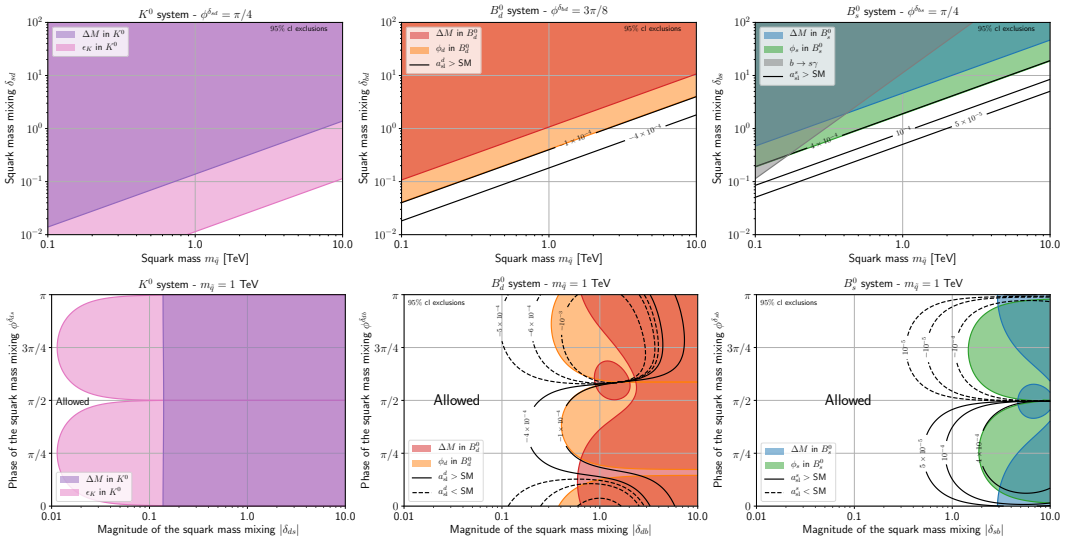

Figure 3. Constraints on the soft squark masses coming from the bino contribution to mixing in neutral meson K, B_d^0 and B_s^0 systems. The shaded areas are excluded by the CP conserving and violating observables indicated in the labels, which are explained in section 3. For simplicity, we assume an approximately universal value $m_{\tilde{q}}$ for the diagonal elements of the mass matrix. The dependence on the bino mass drops out as long as $m_{\tilde{B}} \ll m_{\tilde{q}}$. The upper panels show constraints assuming maximal CP violation, while the lower ones show the dependence on the phases of the squark mass matrix elements. The contour lines in the B_d^0 and B_s^0 cases represent values of the semileptonic asymmetry in each system. As expected, the kaon sector measurements gives the strongest limits, showcasing the need for some flavor structure to produce sizeable contributions to the semileptonic asymmetries.

Contributions from RPV couplings. The diagrams contributing to the $b \to s\gamma$ decay are shown in figure 8 in appendix A, along with the full analytic expression for the decay rate, given in eq. (A.3). Assuming a universal squark mass $m_{\tilde{q}}$, we obtain

$$\text{Br}(b \to s\gamma) \simeq 4.2 \cdot 10^{-7} \left(\frac{\text{TeV}}{m_{\tilde{q}}}\right)^4 \left|\sum_{i=1}^{3} \lambda''^{*}_{i12}\lambda''_{i13}\right|^2 . \tag{5.3}$$

Comparing with the experimental measurement [67] $\text{Br}(\bar{B} \to X_s\gamma) = (3.55 \pm 0.24 \pm 0.09) \times 10^{-4}$ and the SM prediction [68] $\text{Br}(\bar{B} \to X_s\gamma) = (3.15 \pm 0.23) \times 10^{-4}$, we see that this process does not place any meaningful constraint on the RPV couplings for squark masses around or above the TeV scale.

Contributions from squark and slepton mass mixings. Flavor violating decays can also be triggered by off-diagonal elements in the mass matrix of squarks (for $b \to s\gamma$) or sleptons (for $\mu \to e\gamma$). Given the particularities of the R-symmetric model, i.e. the absence of $L - R$ sfermion mixing and the inert nature of the Dirac partner of the gauginos, the bino can only mediate two kind of diagrams contributing to this process. They are depicted in figure 10 for $b \to s\gamma$, the ones for $\mu \to e\gamma$ are analogous. The first diagram requires an

JHEP03(2020)046

external chirality flip while the second one involves mixing between the appropriate Dirac higgsino and the bino, as discussed in section 4.4.

The flavor-violating decay of the b quark is most important because it directly probes the couplings relevant for baryogenesis. Evaluating eq. (A.9) in the small $\tan\beta$ limit, we obtain a branching ratio

$$\mathrm{Br}(b \to s\gamma) = \Gamma(b \to s\gamma)\tau_B \;\simeq\; 8.4 \times 10^{-8} \left(\frac{\mathrm{TeV}}{m_{\tilde{q}}}\right)^4 \left(\left(\frac{7}{8}\right)^2 \delta_{LL}^2 + \delta_{RR}^2\right). \tag{5.4}$$

This should be compared with the experimental measurement [67] $\mathrm{Br}(\bar{B} \to X_s\gamma) = (3.55 \pm 0.24 \pm 0.09) \times 10^{-4}$, which is compatible with the SM prediction [68] $\mathrm{Br}(\bar{B} \to X_s\gamma) = (3.15 \pm 0.23) \times 10^{-4}$. The corresponding exclusion on the $b - s$ squark mixing is shown in the top right panel of figure 3.

The computation of the flavor-violating muon decay is analogous to the $b \to s\gamma$ one with the obvious substitutions, see eq. (A.14) for the corresponding expression. Evaluating it again in the small $\tan\beta$ limit, we find

$$\mathrm{Br}(\mu \to e\gamma) \simeq 3.4 \times 10^{-8} \left(\frac{\mathrm{TeV}}{m_{\tilde{\ell}}}\right)^4 \left(\left(\frac{7}{8}\right)^2 \delta_{LL}^2 + \delta_{RR}^2\right). \tag{5.5}$$

This process is extremely suppressed in the SM, so this contribution is constrained by the stringent experimental upper limit $\mathrm{Br}(\mu^+ \to e^+\gamma) < 4.2 \times 10^{-13}$ (90% cl) set by the MEG experiment [69]. For sleptons at the TeV scale, the mass mixing in the $e-\mu$ sector is bound to be $\delta_{e\mu} < 4 \times 10^{-3}$, which again indicates that any flavor violation that only involves the first two generations should be suppressed.

6 Theoretical and phenomenological considerations

We now discuss constraints on the model parameters that arise from the requirement of achieving the measured matter-antimatter asymmetry and DM abundance. The model independent results of section 3 are applied to the R-SUSY model of section 4, as is the analysis of flavor observables performed in section 5. With this, we find that successful baryogenesis requires squark masses in the scale of $1 - 4\,\mathrm{TeV}$ and at least one of the λ''_{ij3} RPV couplings to be $\mathcal{O}(1)$. Both these requirements stem from the necessity for a large branching fraction of (visible) baryon number violating decays of neutral B mesons. The observed DM abundance is easily accounted for with order one couplings of ψ to the sterile neutrino multiplet. We further discuss constraints that apply to parameters that do not directly control baryogenesis. Such effects are rather a byproduct of realizing the mechanism in the R-SUSY model. At the phenomenological level, we discuss bounds coming from neutrino physics and astrophysics. On the more theoretical side, supergravity considerations on the size of R-symmetry breaking constrain the gravitino mass and some RPV couplings.

JHEP03(2020)046

6.1 Baryogenesis

As was highlighted in section 3.2, successful baryogenesis requires a relatively large branching ratio of B mesons into final states containing a single baryon and dark sector particles. In the supersymmetric setup, such decays can be mediated by any of the four-fermion operators listed in table 3. Assuming that the decay is dominated by a single one of them yields a branching ratio

$$\mathrm{Br}\left(B^0 \to \mathcal{B} + X\right) \sim 10^{-3} \left(\frac{\Delta m}{2\,\mathrm{GeV}}\right)^4 \left((1.9\,\mathrm{TeV})^2 \lambda''_{ij3}\sqrt{2}\, g' \left(\frac{Q_u}{m^2_{\tilde{u}_i}} + \frac{Q_d}{m^2_{\tilde{d}_j}} - \frac{Q_d}{m^2_{\tilde{b}}}\right)\right)^2 , \tag{6.1}$$

where $\Delta m = m_{B^0} - m_{\mathcal{B}} - m_X$ is the mass splitting between B meson and final states, and X represents the dark particles together with any other mesons. Note that eq. (6.1) is computed using a spectator approximation [39], which breaks down when the mass splitting $\Delta m \lesssim 2\,\mathrm{GeV}$. In general, given the hadron spectrum of interest here, we expect $2\,\mathrm{GeV} \lesssim \Delta m \lesssim 3\,\mathrm{GeV}$ for the operators of interest. For final states involving charm quarks, Δm may be too small to reliably use the spectator quark approximation and an analytic estimation of the branching ratio is not feasible.

For hypercharge coupling $g'(m_b) \sim 0.34$ and assuming degenerate squark masses, achieving a large enough branching fraction for baryogenesis

$$\mathrm{Br}\left(B^0 \to \mathcal{B} + X\right) \gtrsim 10^{-3} \quad \text{requires} \quad m_{\mathrm{squark}} \lesssim 1\,\mathrm{TeV}\sqrt{\lambda''_{ij3}}\frac{\Delta m}{2\,\mathrm{GeV}}\,, \tag{6.2}$$

where we have used the maximum positive value of $(a^s_{\mathrm{sl}})_{\mathrm{max}} = 4.1 \times 10^{-4}$ and the minimum negative of $(a^d_{\mathrm{sl}})_{\mathrm{min}} = -9.0 \times 10^{-5}$ to maximize the asymmetry. It is also important to take into account the lower bound on squark masses of $\sim 1\,\mathrm{TeV}$, which is discussed in more detail in section 7.3. Because of this, it is clear that attaining a large enough branching fraction to accommodate the observed baryon asymmetry favors at least one of the RPV couplings being large, together with (at least one) squark mass in the TeV scale,[17] that is

$$\mathrm{Max}\left[\lambda''_{ij3}\right] \sim \mathcal{O}(1)\,, \quad \text{for} \quad i,\, j = 1, 2 \quad \text{and} \quad m_{\tilde{q}_R} = 1 - 4\,\mathrm{TeV}\,. \tag{6.3}$$

Here the range in the allowed squark mass parameter space takes into account enhancement to the coupling from the renormalization group running of the anomaly dimension of the 4 fermi operator.[18]

6.2 Dark matter relic abundance

The mechanism of [6] tends to generically overproduce a symmetric DM component, therefore requiring additional dark sector interactions to deplete its abundance. This is the case when the DM is constituted by the lightest dark sector particle. However, if the dark

[17] The parameter space for squark masses can be opened up a little by increasing λ''_{ij3} up to where perturbativity begins to break down (for instance [62] computes the renormalization group running in R-SUSY models and obtains $\lambda''_{123} < 1.25$).

[18] A detailed RGE study is beyond the scope of the current work.

JHEP03(2020)046

sector states are identified with a right-handed neutrino multiplet, the sneutrino is stable on cosmological time scales even if it is slightly heavier than the right-handed neutrino. This is due to the fact that the R-symmetry is exact and baryon number remains conserved. The sterile sneutrino carries baryon number -1 while the right-handed neutrino has zero baryon number, so as long as the mass difference $m_{\nu_R} - m_{\tilde{\nu}_R}$ is smaller than the neutron mass, sneutrinos cannot kinematically decay to right-handed neutrinos and remain cosmologically stable.

In the situation where $m_{\tilde{\nu}_R} > m_{\nu_R}$, a sneutrino-antisneutrino pair can annihilate into right-handed neutrinos. After that, the ν_R decays as usual into SM leptons, thus contributing to the depletion of the symmetric component of DM. The annihilation cross section for $\tilde{\nu}_R\tilde{\nu}_R^\star \to \nu_R\nu_R$ is dominated by the exchange of light binos. The thermally averaged cross section is given by

$$\langle\sigma v\rangle = \frac{\lambda_N^4 m_{\nu_R}^2 \sqrt{m_{\tilde{\nu}_R}^2 - m_{\nu_R}^2}}{32\pi m_{\tilde{\nu_R}}(m_{\tilde{\nu_R}}^2 - m_{\nu_R}^2 + m_\psi^2)^2}\,. \tag{6.4}$$

With this, we can easily leverage the results of [6] to find that the observed DM relic abundance is reproduced for values of the superpotential coupling λ_N of the order

$$\lambda_N \sim \mathcal{O}(10^{-1}) \quad \Rightarrow \quad \Omega_{\rm DM}h^2 = 0.12\,. \tag{6.5}$$

In what follows we take this as the benchmark value for λ_N. It is worth emphasizing once again that this requires the sneutrino to be heavier than right-handed neutrino. Otherwise, the kinematic suppression of the annihilation rate by a factor of $e^{-\Delta m/T}$, where $\Delta m = m_{\nu_R} - m_{\tilde{\nu_R}}$ makes this annihilation channel inefficient. Therefore, if right-handed neutrinos are heavier than sneutrinos, additional dark sector interactions are generally needed to reproduce the correct relic abundance.

6.3 Generation of neutrino masses

As was discussed in section 4.6, the SM neutrinos ν acquire a tiny mass through their Dirac mass mixing with the Majorana right-handed neutrinos ν_R. This is nothing but the well-known type-I seesaw mechanism [30–33]. As usual, diagonalization of the neutrino mass matrix with terms from eq. (4.19) and eq. (4.18) leads to a large eigenvalue $m_{\nu_R} \sim M_M$ and a small one $m_\nu = 4\,y_N^2\,v^2\,\sin^2\beta/m_{\nu_R}$, as long as the Yukawa $y_N \sin\beta$ is sufficiently small. Successful baryogenesis requires the existence of at least one right-handed neutrino with a mass $m_{\nu_R} \sim$ GeV. At the same time, current experimental data constrain the mass of any of the SM neutrinos to be $m_\nu \lesssim 0.12\,\text{eV}$ [34, 70, 71]. Fulfilling these two conditions bounds ν_R's contribution to the seesaw, constraining the sterile neutrino Yukawa coupling to be[19]

$$y_N\,\sin\beta \lesssim 2\cdot 10^{-8}\sqrt{\frac{m_{\nu_R}}{1\,\text{GeV}}}\,. \tag{6.6}$$

[19] Baryogenesis only requires the existence of one GeV-scale right-handed neutrino, but additional sterile neutrinos may be present and play a role in the generation of SM neutrino masses. We are therefore unable to make more precise statements regarding the spectrum of neutrino masses and Yukawa couplings.

This translates into an upper limit for the mixing between the active and the sterile neutrino, which is given as usual by the ratio of the Dirac to Majorana mass terms, corresponding to $|U| \equiv y_N\, v\, \sin\beta/m_{\nu_R}$ in terms of our model parameters. We find

$$|U|^2 \lesssim 10^{-10}\, \frac{m_{\nu_R}}{1\,\mathrm{GeV}}\,. \tag{6.7}$$

The usual phenomenological constraints for type-I seesaw models with GeV-scale right-handed neutrinos apply to our scenario. The strongest limits come from a combination of beam dump, LEP and B factory searches (see [72] for a recent review). Meaningful bounds can also be obtained from displaced vertices searches at LHC [73]. In the most simplistic scenario which we discuss here, the mixing between sterile and active neutrino flavors is expected to be small, $|U|^2 \sim 10^{-11}$, which is beyond the reach of current experimental setups.

As a particular feature, our model predicts that a relatively large number of sterile neutrinos are produced in B meson decays. As was discussed in section 6.1, a new decay channel for B mesons with branching ratio of $\gtrsim 10^{-3}$ is required for baryogenesis. The bino produced in this process decays predominantly to a right-handed neutrino and sneutrino pair, constituting a large new production cross section for sterile neutrinos. Experiments like LHCb and other B factories and SHiP [34], where $\sim 7 \cdot 10^{13}$ B mesons are expected to be produced, are best posed to take advantage of this production channel, potentially allowing to place meaningful constraints in the parameters of the model. We leave a more detailed investigation of this interesting possibility for future work.

6.4 Dark matter stability

The stability of the right-handed sneutrino DM is a consequence of kinematic relations and the action of a stabilizing symmetry which is a combination of baryon and lepton number. This stability is however not absolute, as decays into three light (anti)quarks and a SM neutrino are possible via a higher dimensional operator. The diagram for the process is shown in figure 4. The first vertex corresponds to the coupling of the Dirac bino to the dark sector sterile neutrino multiplet through eq. (4.17). The second is an effective four-fermion operator analogous to the ones shown in table 3, but with a different flavor combination, namely

$$\mathcal{O} = \sqrt{2} g' \lambda''_{112} \left(\frac{Q_u}{m^2_{\tilde{u}}} + \frac{Q_d}{m^2_{\tilde{d}}} - \frac{Q_d}{m^2_{\tilde{s}}} \right) \psi\, u\, d\, s\,. \tag{6.8}$$

The decay is thus induced by the λ''_{112} RPV coupling, which is not directly relevant for baryogenesis. The full process $\tilde{\nu}_R \to \psi^* + \nu_R^{(*)} \to \bar{u} + \bar{d} + \bar{s} + \nu_{\mathrm{SM}}$ is mediated by an off-shell bino and is further suppressed by the small mixing between the active and the sterile neutrino, so the decay rate is expected to be very small. Let us nevertheless estimate it to obtain a constraint on the RPV coupling to light quarks from the requirement of DM stability.

The hadronized final state must contain a baryon and a strange quark, so the lowest mass final state in the decay contains a Λ baryon, which has a mass $m_\Lambda \simeq 1.1\,\mathrm{GeV}$. As

JHEP03(2020)046

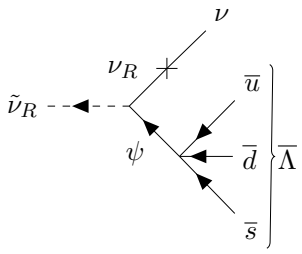

Figure 4. Decay of the right-handed sneutrino DM particle into three light (anti)quarks (which hadronize into i.e. a $\bar{\Lambda}$ baryon) and a neutrino. The process is mediated by an off-shell bino and right-handed neutrino, as well as the RPV coupling λ''_{112}. Propagator arrows indicate the flow of baryon number.

the DM mass is constrained to be in the range 1.2–2.7 GeV, the maximum momentum for any final state particle is around 1.1 GeV. This is too small for the simple approximation of considering 3 free light quarks as decay products to be good. However, we can leverage the fact that the available energy is low enough so that final states with fewer particles, perhaps only one hadron, should dominate the width. We therefore compute the rate for the decay $\tilde{\nu}_R \to \overline{\Lambda} + \nu$. A rough estimate can be obtained by using dimensional analysis to match $uds \leftrightarrow 4\pi f_\pi^3\,\Lambda$. The lifetime for the two-body decay is then

$$\tau_{\tilde{\nu}_R \to \bar{\Lambda}\,\nu} \sim 4.3\times 10^{17}\text{sec}\,\frac{10^{-11}}{|U|^2}\left(\frac{4.2\times 10^{-5}}{\lambda''_{112}}\right)^2\left(\frac{0.1}{\lambda_N}\right)^2 \frac{\left(\frac{m_\psi}{3\,\text{GeV}}\right)^2\left(\frac{m_{\tilde{\nu}_R}}{2\,\text{GeV}}\right)\left(\frac{3\,\text{GeV}^2}{\Delta m^2}\right)}{\left(\text{TeV}^2\left(\frac{Q_u}{m_{\tilde{u}}^2}+\frac{Q_d}{m_{\tilde{d}}^2}-\frac{Q_d}{m_{\tilde{s}}^2}\right)\right)^2}\,, \tag{6.9}$$

where $\Delta m^2 = m^2_{\tilde{\nu}_R} - m^2_\Lambda$ and the rest of the notation is as described in previous sections. A most conservative bound can be obtained by requiring that this lifetime is larger than the age of the Universe, 4.3×10^{17} sec. Using the benchmark parameter values indicated in eq. (6.9), we obtain a constraint on the RPV coupling,

$$\lambda''_{112} \lesssim 10^{-5}\,. \tag{6.10}$$

The operator of eq. (6.8) also leads to a (visible) baryon number non-conserving decay of the sterile neutrino, $\nu_R \to \tilde{\nu}_R\,\bar{u}\,\bar{d}\,\bar{s}$. As one sterile neutrino is produced for each DM antibaryon during baryogenesis, such a process could washout the generated baryon asymmetry if its rate is too large. However, the width of this decay channel is set by the same RPV coupling which is bound to be small by DM stability in eq. (6.9). Because of this, its rate is negligible compared to the usual baryon number preserving SM right-handed neutrino decays.

Even if the bound eq. (6.10) is satisfied and the DM is cosmologically stable, the sneutrino may have a non-negligible decay width into antiquarks and a neutrino. As discussed above, the most likely decay mode is expected to be into $\overline{\Lambda} + \nu$. If such process occurs inside a large volume detector such as as Super-Kamiokande [74], the pions and the annihilation of the $\bar{p}$ and $\bar{n}$ from the $\overline{\Lambda}$ decay could produce a detectable signal. Furthermore, observations of the antiproton flux in cosmic rays can be used to the constrain the rate of

DM annihilation or decay into antimatter [75–79]. However, the antiprotons produced in our setup have very low energies, which makes modelling their propagation in the galactic medium a difficult task. On top of that, the background contribution to the low-energy antiproton flux from astrophysical sources is hard to model [80, 81]. A careful analysis would therefore be needed to apply any such constraint to our scenario.

6.5 How exact must the R-symmetry be?

As discussed in section 4.7, AMSB [60, 61] effects coming from supergravity generate small Majorana gaugino Masses, soft squark masses and a-terms (trilinear scalar couplings), all of order the gravitino mass $m_{3/2}$. While other supergravity scenarios exist in which these contributions are suppressed (see e.g. [59]), it is interesting to study generic constraints on the gravitino mass and associated bounds on the RPV couplings.

The Majorana mass term in eq. (4.21) allows for two neutrons to decay into 2 kaons (dinucleon decay) or neutron-antineutron oscillations via a Majorana mass insertion. In a nuclear environment, the antineutrons annihilate with other nucleons leading to the decay of the nucleus. This process is severely constrained by the lack of observation of such decays. Flavor structure may also severely suppress this process [39], with the most constrained operators involving only up, down and strange quarks. Such operators are generated via the combination of the λ''_{112} operator and a Majorana mass for the bino, or by any of the other λ''_{ijk} in combination with a Majorana bino mass and flavor violation from the weak interactions or squark mixing parameters. Among the RPV couplings, λ''_{112} is the most constrained as it can lead to dinucleon decay without any squark mixing or weak interaction insertion. Adapting the results of [39], where the dinucleon decay bound is translated into the $\Lambda - \overline{\Lambda}$ mixing rate $\delta_{\Lambda\Lambda}$, to the R-SUSY setup presented here, we find

$$\delta_{\Lambda\Lambda} \simeq (2 \times 10^{-2}\,\mathrm{GeV}^3)^2 \frac{M_1}{m_\psi^2 - m_n^2} \left(\frac{g'\,\lambda''_{112}}{m^2_{\tilde{q}_R}} \right)^2 \lesssim 10^{-30}\,\mathrm{GeV}\,, \tag{6.11}$$

where m_ψ is the Dirac mass of the bino given in eq. (4.7), λ''_{112} is the RPV coupling as defined in eq. (4.1) and M_1 is the bino Majorana mass, e.g. generated by AMSB (see eq. (4.21)). Given that in our model the R-symmetry is identified with baryon number, the gravitino is a baryon and therefore subject to the constraints coming from neutron stars as discussed in section 6.6, i.e. it must satisfy $m_{3/2} \gtrsim 1.2\,\mathrm{GeV}$. Taking this into account and using the vanilla AMSB scenario without any additional suppression, eq. (6.11) implies the bound

$$\lambda''_{112} \lesssim 5 \times 10^{-6} \tag{6.12}$$

for $\mathcal{O}(1\,\mathrm{TeV})$ squark masses. Note that this is similar to the bound from DM stability discussed in section 6.4. Additionally, the squark mass matrix receive a contribution from AMSB as discussed in section 4.7. This effect should comply with the limits obtained in section 4.3. Finally, AMSB generates non-zero a-terms which can also contribute to dinucleon decay. This effect is however sub-leading to the one discussed above arising from the Majorana bino mass. All in all, in the scenario where the R-symmetry is slightly broken

JHEP03(2020)046

by supergravity effects, avoiding a too large dinucleon decay rate places strong constraints on some combinations of RPV and flavor violating couplings.

6.6 Dark matter capture in neutron stars

The extremely dense environment found inside neutron stars has been utilized as a laboratory for constraining DM interactions and properties. Neutron stars, the remnants of a collapsed core of a giant star, are prevented from further gravitational collapse into a black hole by Fermi pressure of neutrons and electrons. DM that interacts with neutrons and electrons can upset this balance leading to destabilization of the star. Many studies have been conducted to investigate such effects and the constraints they imply [82–88]. As an example of an application, in section 2 we have used the results of [40] to restrict our parameter space to dark baryon masses greater than $\sim 1.2\,\text{GeV}$, as lighter dark baryons would lead to a process that would deplete the neutrons (and therefore the Fermi pressure) via conversion into DM within the star.

We now examine constraints on our model arising from the possibility that DM is captured inside the core of a neutron star. Scattering processes of DM on electrons or neutrons within the neutron star imparts the DM's kinetic energy on the target such that the emitted DM particle may not have enough energy to escape the star. DM that accumulates within the core of a neutron star due to this loss of kinetic energy will begin to self gravitate, eventually overcoming the Fermi pressure, thereby destabilizing the star and leading to gravitational collapse [89, 90].

In our framework, DM-neutron scattering proceeds through two higher dimensional four-fermion operators coupling to light quarks, and as such has a negligible rate. However, DM-electron scattering $e^-\tilde{\nu}_R \to e^-\tilde{\nu}_R$ occurs via a one loop diagram involving a bino, W boson and sterile neutrinos. The cross section for this process is given approximately by

$$\sigma_{e\,\tilde{\nu}_R} \sim \frac{1}{16\pi}\left(\frac{g^2\, m^2_{\tilde{\nu}_R}\, \lambda^2_N\, y^2_N\, v^2\, \sin^2\beta}{m_\psi\, m^2_{\nu_R}\, m^2_W}\right)^2 \sim 10^{-64}\,\text{cm}^2\left(\frac{y_N \sin\beta}{10^{-8}}\right)^4 , \tag{6.13}$$

where on the right hand side we have fixed GeV mass dark sector particles and TeV scale squarks along with other benchmark values as discussed above. Note that since we consider bosonic DM there is no contribution to the Fermi pressure from the captured DM, and we simply recast the bound from [91] on the scattering cross section that would result in enough DM being captured to cause it to self gravitate. To avoid this, the DM-electron cross-section needs to be smaller than $\sim 10^{-58}\,\text{cm}^2$ (for 1 GeV DM mass). Therefore, black hole formation is avoided for small enough sterile neutrino oscillation parameters,

$$\sigma_{e\,\tilde{\nu}_R} \lesssim 10^{-64}\text{cm}^2 \quad \Rightarrow \quad y_N \sin\beta \;\lesssim\; 3\times 10^{-7}\,. \tag{6.14}$$

Recall from eq. (6.6) that in a type-I seesaw framework, $y_N \sin\beta$ should not exceed $\sim 10^{-8}$ in order to accommodate constraints on the maximal size of SM neutrino masses. Therefore, in the simplest type-I seesaw framework DM capture in neutron stars proceeds at a low enough rate and does not induce the collapse of the star.

JHEP03(2020)046

The accumulation of DM in the core of the neutron star is even less constrained in our framework, as the captured DM carries antibaryon number and can therefore annihilate with neutrons within the star. Such annihilation process may proceed through several different channels in our model. Let us consider as an example the annihilation to a sterile neutrino and a kaon, which is kinetically favored and proceeds through t-channel exchange of a Dirac bino. We estimate the cross section for the parton level process $\tilde{\nu}_R + udd \to \nu_R + d\bar{s}$ as

$$\sigma_{\rm annh} \sim \frac{1}{8\pi}\frac{(4\pi f_\pi^2)^2(m_{\tilde{\nu}_R}^2 + m_n^2 - m_{K^0}^2 - m_{\nu_R}^2)}{m_\psi^2(m_{\tilde{\nu}_R}^2 + m_n^2)}\lambda_N^2\left(\lambda''_{112}\sqrt{2}\,g'\left(\frac{Q_u}{m_{\tilde{u}}^2} + \frac{Q_d}{m_{\tilde{d}}^2} - \frac{Q_d}{m_{\tilde{b}}^2}\right)\right)^2$$
$$\sim 10^{-48}\,{\rm cm}^2\,{\lambda''_{112}}^2, \tag{6.15}$$

where we have used our usual benchmark values. For given annihilation and capture rates C_a and C_c, which measure the probability of a single particle annihilating or being captured over a unit time interval, the number $N_{\tilde{\nu}_R}$ of DM particles captured by a neutron star evolves according to

$$\frac{dN_{\tilde{\nu}_R}}{dt} = C_c - C_a N_{\tilde{\nu}_R}\,. \tag{6.16}$$

The capture rate C_c depends on the scattering rate of DM with neutron star constituents. As shown above, in our case the scattering with electrons dominates over the one with neutrons. Using eq. (6.13) and the results of [89], the capture rate is estimated to be

$$C_c \;\sim\; 10^{23}\,{\rm yr}^{-1}\,\left(\frac{\sigma_{e\,\tilde{\nu}_R}}{10^{-55}\,{\rm cm}^2}\right). \tag{6.17}$$

Assuming that DM particles at the core of the neutron star are relativistic and that the density of surrounding neutrons is similar to nuclear density n_s, the annihilation rate is simply given by $C_a \sim \sigma_{\rm annh}^{\rm inc}\, n_s$, where $\sigma_{\rm annh}^{\rm inc}$ is the inclusive cross section for DM annihilation with neutrons, which receives a large contribution from eq. (6.15). The number of DM particles that is required for bosonic DM to form a black hole [89] is about $N_{\tilde{\nu}_R} \approx 10^{38}$. To avoid the accumulation of too many DM particles inside the neutron star, we can simply require $C_a N_{\tilde{\nu}_R} > C_c$. This condition translates into a lower bound on the annihilation cross section, which in our case reads

$$\sigma_{\rm annh}^{\rm inc} \gtrsim 10^{-80}\,{\rm cm}^2\,\left(\frac{y_N\sin\beta}{10^{-8}}\right)^4. \tag{6.18}$$

This condition is easily satisfied by the annihilation process described above.

7 Signals at colliders and B factories

In this section we identify the main features of the model that are likely to be tested in current and upcoming terrestrial experiments, with focus on colliders and B factories. As we will see, a rich phenomenology including exotic B decays and long lived particle searches provides an opportunity to fully test this baryogenesis scenario. More precisely, the large $\sim 10^{-3}$ branching ratio of B mesons to baryons and missing transverse energy ($E_T^{\rm miss}$)

JHEP03(2020)046

eq. (6.1), along with the requirement of $1 - 4\,\text{TeV}$ squark masses (eqs. (6.2) and (6.3)), result in multiple correlated signals arising from processes occurring at different vertices within LHC detectors.

7.1 Semileptonic asymmetries

An avenue to probe the baryogenesis scenario is through the semileptonic asymmetries. As was discussed in section 3.1, an enhancement of a_{sl}^s and/or a_{sl}^d with respect to their SM values is required to reproduce the observed baryon asymmetry. This amplification of the CP violation in the B meson system can be tested as the still relatively loose experimental bounds tighten up on the SM predictions. Given stronger constraints on the semileptonic asymmetries, larger values of the branching ratio of B to a baryon and missing energy than the ones quoted in eq. (6.2) would be required for the viability of the baryogenesis mechanism, strengthening the signals of the searches described below. Therefore, experimental efforts in this direction complement the searches proposed below in testing the dynamics of the model.

7.2 Exotic B meson decays at B factories

As was discussed in section 6.1, successful baryogenesis requires a new decay mode of B mesons with a relatively large branching ratio of $\sim 10^{-3}$. The decay products include a single baryon and dark sector states (a sneutrino DM particle and a sterile neutrino) carrying baryon number, potentially along with some mesons. This apparently baryon number violating decay can be looked for in B factories like BABAR, Belle [92] and Belle II [53]. Depending on what precise combination of coupling and light squark dominates the process (see eq. (6.1)), different baryons and mesons are expected to appear as decay products. Generically, protons and strange or charmed baryons will be produced. A more experimentally challenging situation would arise if a large fraction of decays occurs into a neutron and dark particles, as such a virtually invisible final state would be extremely difficult to detect. However, all of the possible operators contributing to the decay contain either an up quark or a charm quark, and either a down quark or a strange quark. The only operator that would not produce either charmed or strange particles in the final state is isospin symmetric, so averaging over both the B^0 and B^+ decays it is valid to assume an equal number of decays containing protons and neutrons.

A dedicated search for exotic B decays with a final state containing a baryon and missing energy has not been performed to this date. However, an inclusive branching ratio $\text{Br}\,(B \to \mathcal{B} + \text{anything}) = 6.8 \pm 0.6\%$ was reported in [93] (see also [4]), which is large compared to the known exclusive modes. A loose limit $\text{Br}\,(B \to \mathcal{B} + X) \lesssim 1 - 2\,\%$ can be derived assuming that the (also reported [94, 95]) modes $\text{Br}\,(B \to p\bar{p} + \text{anything}) = 2.47 \pm 0.23\%$ and $\text{Br}\left(B \to \Lambda\bar{p}/\bar{\Lambda}p + \text{anything}\right) = 2.5 \pm 0.4\,\%$ do not contain any invisible fermion in the final state. A dedicated search in BABAR or Belle II is highly desirable and has the potential to probe the full parameter space, given the sensitivity[20] of similar searches like $\text{Br}\,(B \to \Lambda\bar{p}\nu\bar{\nu}) < 3 \cdot 10^{-5}$ (90% cl) using BABAR data [96]. An additional

[20] We thank S. Robertson for his input on this matter.

signal of interest arises in the case when the mixing of the sterile neutrino with SM neutrinos is large enough for it to decay into SM states within the detection volume. This possibility is discussed in section 7.6.

7.3 LHC searches for heavy colored scalars

As highlighted in eq. (6.3), the mass of at least one of the squarks must to be $\mathcal{O}(\text{TeV})$, in order for it to mediate a large enough $B^0 \to \mathcal{B}+X$ branching ratio. In this mass range, such colored scalars can potentially be produced at the LHC. Let us therefore briefly discuss the existing constraints on the mass of the squarks arising from collider searches. Our discussion is based on that of [39]. Studies in similar setups have been performed in [21, 26, 27], but are not applicable to our setup as they focus on binos which are significantly heavier than the ones of interest here.

If kinematically possible, squarks can be pair produced through the usual QCD processes. Additionally, resonant production of a single squark can occur through the $\lambda''_{ijk}\mathbf{U}^c_i\mathbf{D}^c_j\mathbf{D}^c_k$ operator. The latter channel can constrain larger masses due to the lower kinematic threshold of the single production process. Once produced, a squark $\tilde{q}_R$ can decay either to a pair of quarks (through the aforementioned coupling) or to a quark and a bino (through the gauge coupling in eq. (4.8)). The bino decays mostly into dark sector states and therefore contributes to missing energy.

Searches for dijet resonances and monojet events containing missing energy are best suited to place constrains on the mass of $\tilde{q}_R$. The limits were computed in [39]; although the detailed limits depend on the values and flavor structure of the couplings λ''_{ijk}, the reach of the searches does not extend beyond $1-1.2\,\text{TeV}$. In this work we therefore conservatively assume that squarks lie above this scale, in which case no limits from LHC searches for colored scalars exist. Note however that this is not strictly necessary, as lighter squarks are allowed providing λ''_{ijk} are small enough. A detailed study of the flavor structure and comparison with the requirement in eq. (6.3) is left for future work.

7.4 Exotic decays of b hadrons at the LHC

At the LHC, $b\bar{b}$ pairs are copiously produced via strong interactions. These b-quarks subsequently hadronize and decay. Through the effective four-fermion operators in table 3, one of the b-quarks may undergo the visible baryon number violating decay $b \to \bar{u}\bar{d}\psi$ (or $b \to \bar{u}\bar{s}\psi$). Recall that ψ is the Dirac bino (eq. (4.7)), which subsequently decays into two dark sector states: a stable sneutrino DM particle and a sterile neutrino. If the sterile neutrino is sufficiently long-lived, both particles leave the detector contributing to missing transverse energy of the event. The rate for this exotic b decay is directly related to the baryogenesis dynamics (see eq. (6.1)) and is expected to be significant, corresponding to a branching fraction of $\sim 10^{-3}$.

At the partonic level, the process of interest is shown in figure 5 (*left*) and can be summarized as

$$\bar{b}\,b \to \bar{b}\,\bar{u}\,\bar{q}\,\psi\,, \quad \text{where} \quad q = s\,, b\,, \tag{7.1}$$

JHEP03(2020)046

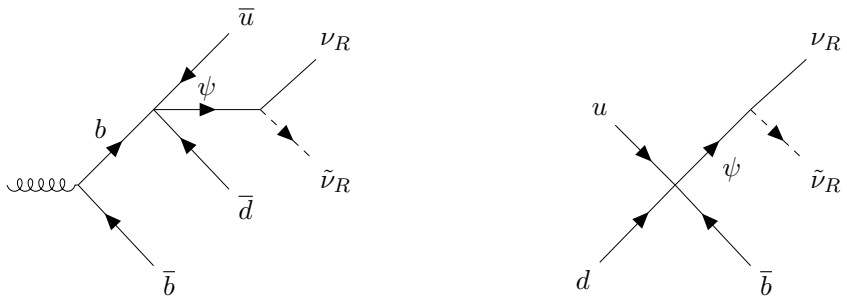

Figure 5. Production channels of the bino at the LHC, also showing its decay into a neutrino/sneutrino pair. The left diagram schematically shows the decay of a b quark in a $b\bar{b}$ pair through the effective four-fermion operator $\psi\, u\, d\, b$ (this is a parton level diagram, the b quark would hadronize before decaying). The right one corresponds to direct production of the bino through the same effective four-fermion operator. Propagator arrows indicate the flow of baryon number.

and ψ subsequently decays into a DM particle and a sterile neutrino, both of which are assumed to be stable at detector scales (the possibility of the sterile neutrino decaying before leaving the detector is discussed in section 7.6). The corresponding signature at the LHC is an event with a single jet along with significant missing transverse energy (E_T^{miss}) [97]. The fact that the single jet is produced from a b-quark allows for the use of b-tagging [98], which provides a further distinctive feature of the process.

7.5 LHC searches for $j + E_T^{\text{miss}}$

A similar final state to the one discussed in section 7.4 can be generated through $2 \to 2$ processes in pp collisions. Assuming that the squark mediator is too heavy to be produced on-shell,[21] we may calculate the rate using the effective four-fermion operators given in table 3. As an example, we consider the process $u\, d \to \psi\, \bar{b}$, which involves couplings relevant for baryogenesis. The corresponding diagram is shown in figure 5 (*right*). At the partonic level, we can estimate the production cross section as

$$\sigma_{ud\to\psi\bar{b}} \sim \text{pb}\, {\lambda''_{113}}^2 \left(\frac{1\,\text{TeV}}{m_{\tilde{q}}}\right)^4 \left(\frac{\sqrt{s_{ud}}}{1\,\text{TeV}}\right)^2 , \tag{7.2}$$

where $\sqrt{s_{ud}}$ is the partonic center-of-mass energy and we have neglected all fermion masses. Similarly to the exotic b-hadron decay, this process results in a distinctive final state consisting of a single b-jet plus missing transverse energy corresponding to the decay of the bino into dark sector particles. The generalization to the other RPV operators λ''_{ijk} is straightforward and motivates more general mono-jet searches [97].

[21] Close to the squark threshold deviations from eq. (7.2) are expected, but the order of magnitude estimate remains valid. The careful analysis required to obtain a more precise expression lies beyond the scope of this work.

JHEP03(2020)046

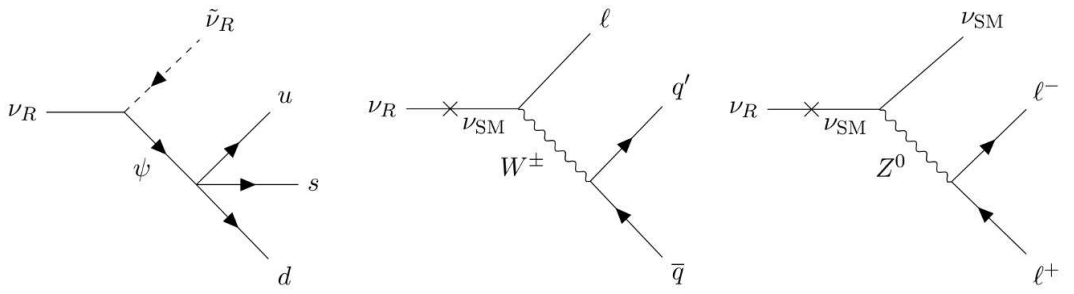

Figure 6. Decays of the right-handed neutrino through an RPV coupling (left) and charged (center) and neutral (center) current interactions after a Dirac mass insertion. Propagator arrows indicate the flow of baryon number.

7.6 LHC searches for long lived particles

In the discussion of the previous section we have assumed the Dirac bino to decay into dark sector states which leave the detector as missing transverse energy, but this might not always be the case. In fact, in the model presented above the dark sector particles are identified with a sneutrino and a right-handed neutrino. The sneutrino is sufficiently stable to be a good DM candidate and therefore invisible in any high energy experiment. The sterile neutrino ν_R is however unstable and expected to decay back into SM particles. Interestingly, for the range of parameters of interest for baryogenesis, the sterile neutrino can decay with a lifetime that is long on collider time scales, thereby providing exciting implications for long lived particle searches at MATHUSLA [37], FASER [35], CODEX-b [36], and the ATLAS muon tracker [38].

The right-handed neutrino can in principle decay into DM and three light quarks through an off-shell bino and an RPV coupling as shown in figure 6 (*left*). However, this process is related to the same coupling that is required to be small by DM stability (as discussed in section 6.2). As a consequence, this decay channel is constrained to have a rate that is too small for detection purposes.[22] Nevertheless, the neutral and charged current decay of the sterile neutrinos through a mass mixing to SM neutrinos may in general be long lived.[23] In particular, the processes $\nu_R \to q'\,\bar{q}\,l$ and $\nu_R \to l^+\,l^-\,\nu$ (see the center and left diagrams in figure 6) are long lived with decay lengths of order $1-10^6$ meters for values of the Yukawa couplings that lie within the requisite range to accommodate SM neutrino masses. Therefore, depending on the exact parameters and experimental setup, the sterile neutrino might either leave the detector as missing energy or decay in a displaced vertex, motivating the use of long lived particle detection techniques.

[22] Additional frameworks of low-scale baryogenesis through meson and baryon oscillations contain decays which are long lived on collider time scales and can produce three light quarks. For instance, in the set-up of [39], baryogenesis proceeds through the oscillation of charmed and beautiful baryons which creates an asymmetry in a Majorana fermion χ. χ can be produced at the LHC, and would be relatively long lived before decaying into light quarks $\chi \to u\,d\,s$. Note that this scenario does however *not* accommodate DM.

[23] Constructing models which produce collider signals from long-lived sterile neutrino decays is a subject of much study [99].

JHEP03(2020)046

In the framework presented here, the prompt production and subsequent long lived decay of the sterile neutrino would produce novel signals at the LHC. Let us exemplify the particular case involving b quarks, which is the interesting one for baryogenesis. As discuss in the previous sections, two different production channels are possible, each one of them producing a signature with some distinctive features.

Firstly, the creation of a b quark and a Dirac bino from a pp collision can proceed as in figure 5 (*right*) through the $\psi\, u\, d\, b$ operator in table 3. The cross section estimated in eq. (7.2). The bino then promptly decays into a sterile neutrino and DM through the operator in eq. (4.17). This is followed by the long lived decay of the sterile neutrino as discussed above, resulting in a lepton jet (for the CC case). The parton-level process is therefore

$$u\, d \to b\, \psi \;\to b\, \nu_R\, \tilde{\nu}_R \;\to b\, q'\, \bar{q}\, l\, \tilde{\nu}_R \;\text{ ,or }\; b\, l^+\, l^-\, \nu\, \tilde{\nu}_R\,. \tag{7.3}$$

In this case, the long lived particle is centrally produced. A potential study in, for instance, the ATLAS detector would involve a mono-jet signal (as discussed in section 7.5) and an associated long lived decay leading to a lepton jet [100]. Note that our signal is novel in that it contains a single lepton within the jet.

Secondly, QCD production of a $b\bar{b}$ pair can be followed by the decay of one of the quarks through the same four-fermion operator $\psi\, u\, d\, b$, resulting in a forward production of quarks, DM and a sterile neutrino as shown in figure 5 (*left*). The prompt b decay signal can be searched for as discussed in section 7.4 by triggering on the associately produced b quark. The long lived sterile neutrino decays through the charged or neutral current channels just discussed. At the partonic level, this corresponds to the process

$$b \to \bar{u}\, \bar{d}\, \psi \to \bar{u}\, \bar{d}\, \tilde{\nu_R}\, \nu_R \to \bar{u}\, \bar{d}\, \tilde{\nu_R}\, q\, \bar{q}\, l \;\text{ ,or }\; \bar{u}\, \bar{d}\, \tilde{\nu_R}\, l^+\, l^-\, \nu\,. \tag{7.4}$$

The kinematics of these decays would be primed for forward searches such as FASER. We leave a detailed analysis of all these interesting collider signals to future work.

8 Summary and outlook

In this work we have constructed a supersymmetric realization of the mechanism proposed in [6], where the baryon asymmetry and the DM abundance of the Universe are produced from neutral B meson oscillation and subsequent decay into a dark sector. We have introduced a model of R-SUSY in which an exact $\mathrm{U}(1)_R$ symmetry is identified with $\mathrm{U}(1)_B$ baryon number (such that particles within the same multiplet are charged differently under baryon number). Heavy squarks of mass $1-2\,\mathrm{TeV}$ are integrated out to generate baryon number conserving four-fermion operators coupling SM quarks to a light Dirac bino (about 2-4 GeV in mass) which carries baryon number.

The existence of an exact R-symmetry forbids the existence of Majorana masses for gauginos, which are instead of Dirac type. This is a crucial feature of the model, as the Majorana gauginos and the absence of R-parity allow for neutron-antineutron oscillations and dinucleon decays, both of which processes are very tightly constrained experimentally. That said, it is well known that supergravity effects generically break the R-symmetry and

generate Majorana gaugino masses (along with soft squark masses and a-terms). Taking this into account, we have quantified the degree to which the R-symmetry needs to be exact in the face of the experimental constraints.

The baryogenesis mechanism starts when b-quarks and antiquarks are produced from the late decay of an "inflaton-like" TeV scale particle at temperatures $T_R \sim 10 - 50\,\mathrm{MeV}$. The quarks then hadronize into neutral $B^0_{s,d}$ mesons which oscillate and quickly decay into a baryon and a Dirac bino via the aforementioned operator. The Dirac bino further decays into dark sector particles, which are identified with a right-handed sterile neutrino and its baryon number carrying superpartner — a sterile sneutrino which is stable on cosmological time scales and and therefore constitutes the DM.

We have shown that the R-SUSY model presented here reproduces the measured baryon asymmetry and DM abundance of the Universe while being consistent with experimental constraints from colliders and flavor observables. In particular, this mechanisms motivates a study of a yet unexplored region of the R-SUSY model parameter space — that of a light Dirac bino. Indeed, this work represents the first excursion into the exploration of this slice of parameter space.

Focusing first on the flavor observables that are relevant for the baryogenesis dynamics, we have shown that the NP modifications to the semileptonic-leptonic asymmetries $a^{s,d}_{\mathrm{sl}}$ in the neutral $B^0_{s,d} - \bar{B}^0_{s,d}$ systems can be large enough to generate a sufficient baryon asymmetry while being allowed by current experimental constraints. In our model, the extra CP violation that enhances the semileptonic asymmetries can be traced back to complex phases in the RPV couplings λ''_{ijk} or in the off-diagonal elements of the squark mass matrix. Another robust prediction of the mechanism is the existence of a new decay channel of B mesons into a baryon and dark sector states, which needs to have a large branching fraction $\gtrsim 10^{-3}$. In the supersymmetric setup, this is only possible if at least one of the squarks has a mass close to 1 TeV while the RPV couplings λ''_{ij3} have a flavor structure that allows at least one of the combinations 11, 12, 21 or 22 to be $\mathcal{O}(1)$. The R-SUSY NP modifications to additional flavor observables (most notably $K^0 - \bar{K}^0$ oscillations and the branching ratio of $b \to s\gamma$ and $\mu \to e\gamma$) further constrain couplings that, while not directly relevant for baryogenesis, give a hint towards the flavor structure of the model. The values of the parameters for which R-SUSY successfully realizes baryogenesis are summarized in table. 5.

As a new feature of the supersymmetric model, the dark sector particle content may be elegantly realized as a sterile neutrino supermultiplet. The Dirac bino then decays predominantly into the sterile neutrino and the cosmologically stable sterile (scalar) sneutrino, which carries baryon number -1 and constitutes the DM. In this way, equal and opposite matter-antimatter asymmetries are generated in the visible and dark sectors without violating the global baryon number of the Universe. Dark sector interactions between the sneutrino and neutrino act to deplete the otherwise overproduced symmetric abundance of the sneutrino DM. These partially invisible decays of the bino (and, by extension, of b-flavored hadrons) can be looked for at B-factories like Babar and Belle II or at the LHC, by exploiting mono-jet searches and b-tagging techniques. In addition to that, the decays of the sterile neutrino into SM fermions may be long lived on collider time scales and can be

JHEP03(2020)046

Parameter	Description	Achieve Baryogenesis and DM	Reference
m_Φ	Φ mass	11–100 GeV	-
T_R	reheat temperature	10–50 MeV	fig. 2, sec. 3.2
$m_{\tilde{q}_R}$	squark mass	1–4 TeV	fig. 2, sec. 6.1, sec. 7.3
m_ψ	Dirac bino mass	1.2–4.2 GeV	sec. 2, see also [6]
m_{ν_R}	Majorana neutrino mass	1.2–2.7 GeV	sec. 2, see also [6]
$m_{\tilde{\nu_R}}$	sneutrino mass	1.2–2.7 GeV	sec. 2, see also [6]
Br	Br of $B \to \nu\tilde{\nu} + \text{Baryon}$	$4 \times 10^{-4} - 0.1$	fig. 2, sec. 3.2, sec. 6.1
$a^d_{\rm sl}$	asymmetry in B^0_d	$\left[-8.9\times10^{-4},\, -9.0\times10^{-5}\right]$	fig. 1, sec. 3.1, fig. 3, sec. 5.1
$a^s_{\rm sl}$	asymmetry in B^0_s	$\left[-2.1\times10^{-4},\, +4.1\times10^{-4}\right]$	fig. 1, sec. 3.1, fig. 3, sec. 5.1
$\text{Max}\left[\lambda''_{ij3}\right]$	RPV coupling	$\gtrsim 1$	sec. 6.1
λ''_{112}	RPV coupling $u\,d\,s$	$\lesssim 10^{-5}$	sec. 6.4
λ_N	coupling for $\lambda_s\,\tilde{\nu}_R\,\nu_R$	$\mathcal{O}(0.1)$	sec. 6.2

Table 5. Ranges of parameters relevant for generating the observed baryon asymmetry ($Y_B = 8.7 \times 10^{-11}$) and DM abundance ($\Omega_{\rm DM}h^2 = 0.12$) of the Universe and which are consistent with all experimental constraints. For convenience, in the third column we provide a link to the relevant section in this paper where each result is discussed.

searched for at experiments like SHiP, MATHUSLA, FASER, CODEX-b, and the ATLAS and CMS muon trackers. Additional constraints on model parameters are derived from measurements of neutrino oscillations and by exploiting astrophysical observations, most importantly the existence of stable neutron stars.

To conclude, we have presented a supersymmetric model that can achieve low-scale baryogenesis and DM production without baryon number violation. In contrast to the standard lore of high scale baryogenesis, our setup enjoys a plethora of possible experimental signatures ranging from measurements of flavor observables to long lived decays at colliders. Such exciting possibilities leave the door open to fully test this baryogenesis scenario in the not too distant future.

Acknowledgments

We thank Shih-Chieh Hsu and Henry Lubatti for useful discussions regarding long lived decay searches at the LHC. We also thank Shih-Chieh Hsu for useful comments on the draft. GA thanks the University of Washington for kind hospitality during the early stages of the project. GA receives support from the Fundación "la Caixa" via a "la Caixa" postgraduate fellowship. AEN is supported in part by the Kenneth K. Young Chair in Physics. AEN, GE and HX are supported in part by the U.S. Department of Energy Award DE-SC0011637. This project has received support from the European Union's Horizon 2020 research and innovation programme under the Marie Sklodowska-Curie grant agreement No 674896.

A Analytic expressions for flavor violating observables

Here we give the analytic expressions and some more details on the evaluation of the NP contributions to the flavor violating observables discussed in section 5. We distinguish two kinds of contributions depending on whether the light bino plays a role in the process or not.

A.1 Contributions from RPV couplings

The $R-$parity violating couplings λ''_{ijk} can mediate flavor changing transitions and induce CP-violating effects through their complex phases. A comprehensive study of RPV SUSY phenomenology was done in [62], to which we refer for any further details not discussed here.

$\Delta F = 2$ processes. Neutral meson oscillation parameters are modified by the existence of diagrams like the ones depicted in figure 7 for the case of the B_d^0 system. The corresponding box diagrams were computed in [63] for the (s)top couplings, here we generalize the results including the two lighter generations. One important difference in our setup is the absence of left-right squark mass mixing, which is forbidden by the R-symmetry. Taking this into account, we find

$$\tilde{C}_1 = \sum_{i,j=1}^{3} \frac{1}{4\pi^2}\, \lambda''^{*}_{i12}\lambda''_{i23}\lambda''^{*}_{j12}\lambda''_{j23}\, \left[I_4\left(m_s^2, m_s^2, m^2_{\tilde{u}_{i,R}}, m^2_{\tilde{u}_{j,R}}\right) + I_4\left(m^2_{u_i}, m^2_{u_j}, m^2_{\tilde{s}_R}, m^2_{\tilde{s}_R}\right)\right], \tag{A.1}$$

$$\begin{aligned}
C_4 &= -C_5, \\
C_5 &= \sum_{i,j=1}^{3} \frac{g^2}{4\pi^2}\, \lambda''^{*}_{i12}\lambda''_{j23}\, V_{i1}V^{\star}_{j3}\, m_{u_i} m_{u_j} \left[I_2\left(m^2_{\tilde{s}_R}, m^2_W, m^2_{u_i}, m^2_{u_j}\right) \right. \\
&\quad \left. + \frac{1}{4m_W^2} I_4\left(m^2_{\tilde{s}_R}, m^2_W, m^2_{u_i}, m^2_{u_j}\right) + \frac{1}{4m_W^2 \tan^2\beta} I_4\left(m^2_{\tilde{s}_R}, m^2_{H^+}, m^2_{u_i}, m^2_{u_j}\right) \right] \\
&\quad + \sum_{i,j=1}^{3}\sum_{r=1}^{2} \frac{g^2}{8\pi^2}\, \lambda''^{*}_{i12}\lambda''_{j23}\, V_{i1}V^{\star}_{j3}\, \frac{m_{u_i} m_{u_j}}{2m_W^2 \sin^2\beta}\, |C_{r2}|^2\; I_4\left(m_b^2, m^2_{\tilde{\chi}_r^+}, m^2_{\tilde{u}_i}, m^2_{\tilde{u}_j}\right).
\end{aligned}$$

Here, V_{ij} denotes the corresponding CKM matrix element and C_{rs} refers to the mixing matrix of positive charginos. The loop integrals are given by

$$I_n(m_1^2, m_2^2, m_3^2, m_4^2) = \int_0^\infty \frac{k^n \mathrm{d}k^2}{\left(k^2+m_1^2\right)\left(k^2+m_2^2\right)\left(k^2+m_3^2\right)\left(k^2+m_4^2\right)}. \tag{A.2}$$

In the limit where one of the masses M is much larger than the others, we have $I_4 \sim 1/M^2$ and $I_2 \sim 1/(M\mu)^2$, where μ is some combination of the remaining masses. Additionally, logarithmic factors with quotients of masses can appear in the expressions. Therefore, squark masses dominate the integrals and the coefficients C_i are always suppressed by $1/m_{\tilde{q}}^2$.

$\Delta F = 1$ processes. The RPV couplings alone can induce the flavor-violating decay $b \to s\gamma$ through the diagrams shown in figure 8. Summing all contributions, the resulting

JHEP03(2020)046

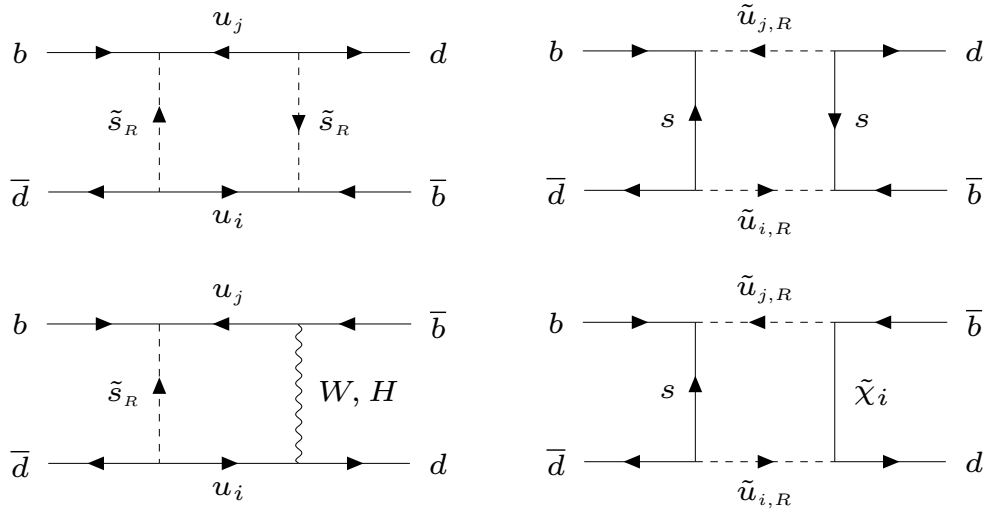

Figure 7. Diagrams involving the RPV couplings λ''_{ijk} and contributing to the neutral meson oscillations. The case of the B^0_d system is shown as an example, the K^0 and B^0_s are analogous with the obvious substitutions. Propagator arrows indicate the flow of baryon number.

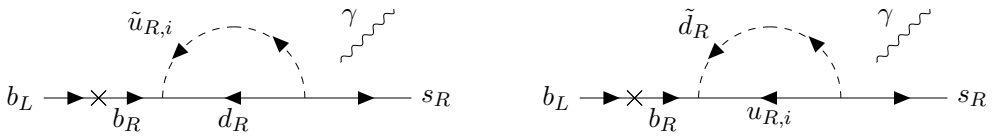

Figure 8. Diagrams for the flavor-violating decay $b \to s\gamma$ mediated by RPV interactions. The photon can be attached to any charged line. Propagator arrows indicate the flow of baryon number.

branching ratio is

$$\mathrm{Br}(b \to s\gamma) = \frac{2N_C\,\alpha_{\mathrm{em}}\,m_b^5}{4} \cdot \tau_B \left(\left| \sum_{i=1}^{3} B_{R1}^{\mathrm{RPV}} + \tilde{B}_{R1}^{\mathrm{RPV}} \right|^2 \right), \tag{A.3}$$

where

$$B_{R1}^{\mathrm{RPV}} = -\frac{\lambda''^{*}_{i12}\lambda''_{i13}}{864\pi^2} \frac{1}{m^2_{\tilde{u}_{R,i}}} G_1\left(x_d\right), \tag{A.4}$$

$$\tilde{B}_{R1}^{\mathrm{RPV}} = -\frac{\lambda''^{*}_{i12}\lambda''_{i13}}{864\pi^2} \frac{1}{m^2_{\tilde{d}_R}} G_1\left(x_{u_i}\right),$$

The loop function G_1 is defined in eq. (A.12) and is evaluated at $x_d = m_d^2/m^2_{\tilde{u}_{R,i}}$ or $x_{u_i} = m^2_{u_i}/m^2_{\tilde{d}_R}$. For heavy squarks, we have $G_1(x \ll 1) \simeq 1/2$.

A.2 Contributions from squark mass mixing

Here we compute the contribution of a light Dirac bino to the meson oscillation parameters, following the spirit of [28]. The flavor violation is generated in this case by off diagonal

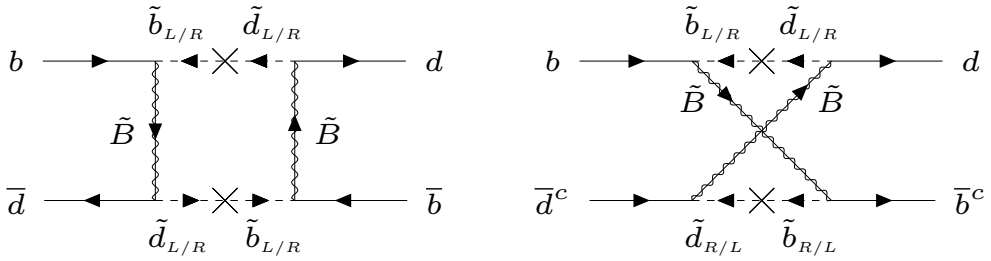

Figure 9. Diagrams mediated by Dirac binos and involving squark mass mixing which contribute to neutral meson oscillations. The case of the B_d^0 system is shown as an example, the K^0 and B_s^0 are analogous with the obvious substitutions. Note that only $L-L$ or $R-R$ (and not $L-R$) squark mixing is allowed by the R-symmetry. Propagator arrows indicate the flow of baryon number.

elements in the squark soft mass mixing matrix. To be specific, we give the expressions for consider B_d^0, but the computations for B_s^0 and K are analogous. The relevant diagrams are shown in figure 9. With the notation of eq. (5.1), we obtain

$$C_1 = \left(\frac{1}{6}\right)^4 \frac{\alpha_Y^2}{m_{\tilde{q}}^2} \delta_{LL}^2 \tilde{f}_6(\lambda_{\tilde{B}}), \tag{A.5}$$

$$\tilde{C}_1 = \left(\frac{1}{6}\right)^4 \frac{\alpha_Y^2}{m_{\tilde{q}}^2} \delta_{RR}^2 \tilde{f}_6(\lambda_{\tilde{B}}), \tag{A.6}$$

$$C_4 = \left(\frac{1}{6}\right)^4 \frac{\alpha_Y^2}{m_{\tilde{q}}^2} 4\delta_{LL}\delta_{RR}\, \tilde{f}_6(\lambda_{\tilde{B}}), \tag{A.7}$$

Comparing with [28], we see that binos give rise to fewer operators than gluinos due to the more restricted color structure of the diagrams. The loop function depends on the ratio $\lambda_{\tilde{B}} = m_{\tilde{B}}^2/m_{\tilde{q}}^2$ and is given by

$$\tilde{f}_6(\lambda_{\tilde{B}}) = \frac{6\lambda_{\tilde{B}}(1+\lambda_{\tilde{B}})\log\lambda_{\tilde{B}} - \lambda_{\tilde{B}}^3 - 9\lambda_{\tilde{B}}^2 + 9\lambda + 1}{3(1-\lambda_{\tilde{B}})^5}\,, \tag{A.8}$$

which approaches $\tilde{f}_6 \to 1/3$ when $m_{\tilde{B}} \ll m_{\tilde{q}}$. To get this result we have neglected the momentum of the external quarks and applied Fierz rearrangements to obtain the desired color structures. In general, $\Delta M^{\rm NP}$ is a complex quantity because the off-diagonal elements of the squark mixing matrix can be complex, and thus so are δ_{LL} and δ_{RR}. Effects in the CP-violating observables defined in section 3 are therefore expected. Note however that C_1 is always real because it only depends on the absolute value of the squark mixing parameters $\delta^2 = \delta \cdot \delta^\star$. Analogous formulas, with the obvious substitutions, hold for the B_s^0 and K^0 systems.

$\Delta F = 1$ processes. The calculation of these processes are done following the conventions of [28]. The diagrams for $b \to s\gamma$ are shown in figure 10. Summing contributions from both diagrams, the decay width of a b quark to a s quark and a photon mediated by

JHEP03(2020)046

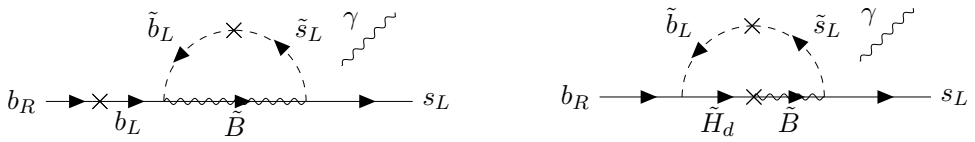

Figure 10. Diagrams for the flavor-violating decay $b \to s\gamma$ mediated by a light bino, with external (left) and internal (right) chirality flip. The flavor violation arises through off-diagonal terms in the squark mass matrix. The photon can be attached to any charged line. Propagator arrows indicate the flow of baryon number.

a light bino can be written as

$$\mathrm{Br}(b \to s\gamma) = \frac{N_c\, \alpha_{\mathrm{em}}\, m_b^5}{4} \cdot \tau_B \left(|B_{L1} + B_{L2}|^2 + |B_{R1} + B_{R2}|^2 \right), \tag{A.9}$$

where $B_{L1,R1}$ correspond to diagrams with an external chirality flip,

$$\begin{aligned} B_{L1} &= -\frac{\alpha_Y}{432\pi} \frac{\delta_{LL}}{m_{\tilde{q}}^2} G_1(x_{\tilde{B}}), \\ B_{R1} &= -\frac{\alpha_Y}{108\pi} \frac{\delta_{RR}}{m_{\tilde{q}}^2} G_1(x_{\tilde{B}}), \end{aligned} \tag{A.10}$$

while $B_{L2,R2}$ come from the diagrams with internal bino-higgsino mixing,

$$\begin{aligned} B_{L2} &= -\frac{\alpha_Y}{144\pi} \cos^2\beta \frac{\delta_{LL}}{m_{\tilde{q}}^2} G_2(x_{\tilde{B}}), \\ B_{R2} &= \frac{\alpha_Y}{72\pi} \cos^2\beta \frac{\delta_{RR}}{m_{\tilde{q}}^2} G_2(x_{\tilde{B}}). \end{aligned} \tag{A.11}$$

The loop functions G_1 and G_2, which are to be evaluated at $x = m_{\tilde{B}}^2/m_{\tilde{q}}^2$, are given by

$$\begin{aligned} G_1(x) &= \frac{17x^3 - 9x^2 - 9x + 1 - 6x^2(x+3)\log x}{2(1-x)^5}, \\ G_2(x) &= \frac{-5x^2 + 4x + 1 + 2x(x+2)\log x}{(1-x)^4}. \end{aligned} \tag{A.12}$$

In the case where the bino is much lighter than the squarks, we have $G_1(x_{\tilde{B}}) \simeq 1/2$ and $G_2(x_{\tilde{B}}) \simeq 1$.

The computation of the flavor-violating muon decay $\mu \to e\gamma$ is very similar to the $b \to s\gamma$ transition, with the obvious substitutions. We therefore directly give the result

$$\mathrm{Br}(\mu \to e\gamma) = \frac{48\alpha_{\mathrm{em}}\pi^3}{G_F^2} \left(|A_{L1} + A_{L2}|^2 + |A_{R1} + A_{R2}|^2 \right), \tag{A.13}$$

where

$$A_{L1} = -\frac{\alpha_Y}{48\pi}\frac{\delta_{LL}}{m_{\tilde{\ell}}^2}G_1(x_{\tilde{B}}), \tag{A.14}$$

$$A_{R1} = -\frac{\alpha_Y}{12\pi}\frac{\delta_{RR}}{m_{\tilde{\ell}}^2}G_1(x_{\tilde{B}}),$$

$$A_{L2} = -\frac{\alpha_Y}{16\pi}\cos^2\beta\frac{\delta_{LL}}{m_{\tilde{\ell}}^2}G_2(x_{\tilde{B}}),$$

$$A_{R2} = \frac{\alpha_Y}{8\pi}\cos^2\beta\frac{\delta_{RR}}{m_{\tilde{\ell}}^2}G_2(x_{\tilde{B}}).$$

The loop functions as defined above should now be evaluated at $x = m_{\tilde{B}}^2/m_{\tilde{\ell}}^2$.

References

[1] Planck collaboration, *Planck 2018 results. VI. Cosmological parameters*, arXiv:1807.06209 [INSPIRE].

[2] Planck collaboration, *Planck 2015 results. XIII. Cosmological parameters*, *Astron. Astrophys.* **594** (2016) A13 [arXiv:1502.01589] [INSPIRE].

[3] R.H. Cyburt, B.D. Fields, K.A. Olive and T.-H. Yeh, *Big Bang Nucleosynthesis: 2015*, *Rev. Mod. Phys.* **88** (2016) 015004 [arXiv:1505.01076] [INSPIRE].

[4] Particle Data Group collaboration, *Review of Particle Physics*, *Phys. Rev.* **D 98** (2018) 030001 [INSPIRE].

[5] A.D. Sakharov, *Violation of CP Invariance, C asymmetry and baryon asymmetry of the universe*, *Pisma Zh. Eksp. Teor. Fiz.* **5** (1967) 32 [INSPIRE].

[6] G. Elor, M. Escudero and A. Nelson, *Baryogenesis and Dark Matter from B Mesons*, *Phys. Rev.* **D 99** (2019) 035031 [arXiv:1810.00880] [INSPIRE].

[7] S. Nussinov, *Technocosmology: could a technibaryon excess provide a 'natural' missing mass candidate?*, *Phys. Lett.* **B 165** (1985) 55.

[8] S. Dodelson and L.M. Widrow, *Baryogenesis in a Baryon Symmetric Universe*, *Phys. Rev.* **D 42** (1990) 326 [INSPIRE].

[9] S.M. Barr, R.S. Chivukula and E. Farhi, *Electroweak Fermion Number Violation and the Production of Stable Particles in the Early Universe*, *Phys. Lett.* **B 241** (1990) 387 [INSPIRE].

[10] D.B. Kaplan, *A Single explanation for both the baryon and dark matter densities*, *Phys. Rev. Lett.* **68** (1992) 741 [INSPIRE].

[11] G.R. Farrar and G. Zaharijas, *Dark matter and the baryon asymmetry*, *Phys. Rev. Lett.* **96** (2006) 041302 [hep-ph/0510079] [INSPIRE].

[12] D.E. Kaplan, M.A. Luty and K.M. Zurek, *Asymmetric Dark Matter*, *Phys. Rev.* **D 79** (2009) 115016 [arXiv:0901.4117] [INSPIRE].

JHEP03(2020)046

[13] M.E. Cabrera, J.A. Casas and A. Delgado, *Upper Bounds on Superpartner Masses from Upper Bounds on the Higgs Boson Mass*, *Phys. Rev. Lett.* **108** (2012) 021802 [arXiv:1108.3867] [INSPIRE].

[14] P. Fayet, *Supergauge Invariant Extension of the Higgs Mechanism and a Model for the electron and Its Neutrino*, *Nucl. Phys.* **B 90** (1975) 104 [INSPIRE].

[15] P. Fayet, *Fermi-Bose Hypersymmetry*, *Nucl. Phys.* **B 113** (1976) 135 [INSPIRE].

[16] L.J. Hall and L. Randall, $\mathrm{U}(1)_R$ *symmetric supersymmetry*, *Nucl. Phys.* **B 352** (1991) 289 [INSPIRE].

[17] L. Randall and N. Rius, *The Minimal* $\mathrm{U}(1)_R$ *symmetric model revisited*, *Phys. Lett.* **B 286** (1992) 299 [INSPIRE].

[18] P.J. Fox, A.E. Nelson and N. Weiner, *Dirac gaugino masses and supersoft supersymmetry breaking*, *JHEP* **08** (2002) 035 [hep-ph/0206096] [INSPIRE].

[19] R. Fok, G.D. Kribs, A. Martin and Y. Tsai, *Electroweak Baryogenesis in R-symmetric Supersymmetry*, *Phys. Rev.* **D 87** (2013) 055018 [arXiv:1208.2784] [INSPIRE].

[20] S. Ipek and J. March-Russell, *Baryogenesis via Particle-Antiparticle Oscillations*, *Phys. Rev.* **D 93** (2016) 123528 [arXiv:1604.00009] [INSPIRE].

[21] H. Beauchesne, K. Earl and T. Gregoire, *LHC phenomenology and baryogenesis in supersymmetric models with a* $\mathrm{U}(1)_R$ *baryon number*, *JHEP* **06** (2017) 122 [arXiv:1703.03866] [INSPIRE].

[22] C. Frugiuele, T. Gregoire, P. Kumar and E. Ponton, *'*$L = R$*' -* $\mathrm{U}(1)_R$ *as the Origin of Leptonic 'RPV'*, *JHEP* **03** (2013) 156 [arXiv:1210.0541] [INSPIRE].

[23] J. Kalinowski, *SUSY with R-symmetry: confronting EW precision observables and LHC constraints*, *Acta Phys. Polon.* **B 47** (2016) 203 [arXiv:1510.06652] [INSPIRE].

[24] P. Diessner, W. Kotlarski, S. Liebschner and D. Stöckinger, *Squark production in R-symmetric SUSY with Dirac gluinos: NLO corrections*, *JHEP* **10** (2017) 142 [arXiv:1707.04557] [INSPIRE].

[25] C. Alvarado, A. Delgado and A. Martin, *Constraining the R-symmetric chargino NLSP at the LHC*, *Phys. Rev.* **D 97** (2018) 115044 [arXiv:1803.00624] [INSPIRE].

[26] J. Gehrlein, S. Ipek and P.J. Fox, *Biνo Phenomenology at the LHC*, *JHEP* **03** (2019) 073 [arXiv:1901.09284] [INSPIRE].

[27] G. Chalons, M.D. Goodsell, S. Kraml, H. Reyes-González and S.L. Williamson, *LHC limits on gluinos and squarks in the minimal Dirac gaugino model*, *JHEP* **04** (2019) 113 [arXiv:1812.09293] [INSPIRE].

[28] G.D. Kribs, E. Poppitz and N. Weiner, *Flavor in supersymmetry with an extended R-symmetry*, *Phys. Rev.* **D 78** (2008) 055010 [arXiv:0712.2039] [INSPIRE].

[29] T. Cohen, G.D. Kribs, A.E. Nelson and B. Ostdiek, *750 GeV diphotons from supersymmetry with Dirac gauginos*, *Phys. Rev.* **D 94** (2016) 015031 [arXiv:1605.04308] [INSPIRE].

[30] R.N. Mohapatra and G. Senjanović, *Neutrino Mass and Spontaneous Parity Nonconservation*, *Phys. Rev. Lett.* **44** (1980) 912 [INSPIRE].

[31] M. Gell-Mann, P. Ramond and R. Slansky, *Complex Spinors and Unified Theories*, *Conf. Proc.* **C 790927** (1979) 315 [arXiv:1306.4669] [INSPIRE].

JHEP03(2020)046

[32] P. Minkowski, *$\mu \to e\gamma$ at a Rate of One Out of 10^9 Muon Decays?*, *Phys. Lett.* **B 67** (1977) 421.

[33] J. Schechter and J.W.F. Valle, *Neutrino Masses in* SU(2) × U(1) *Theories*, *Phys. Rev.* **D 22** (1980) 2227 [INSPIRE].

[34] SHiP collaboration, *A facility to Search for Hidden Particles (SHiP) at the CERN SPS*, arXiv:1504.04956 [INSPIRE].

[35] J.L. Feng, I. Galon, F. Kling and S. Trojanowski, *ForwArd Search ExpeRiment at the LHC*, *Phys. Rev.* **D 97** (2018) 035001 [arXiv:1708.09389] [INSPIRE].

[36] V.V. Gligorov, S. Knapen, M. Papucci and D.J. Robinson, *Searching for Long-lived Particles: A Compact Detector for Exotics at LHCb*, *Phys. Rev.* **D 97** (2018) 015023 [arXiv:1708.09395] [INSPIRE].

[37] MATHUSLA collaboration, *MATHUSLA: A Detector Proposal to Explore the Lifetime Frontier at the HL-LHC*, 2019, http://mathusla.web.cern.ch [arXiv:1901.04040] [INSPIRE].

[38] ATLAS collaboration, *Search for long-lived particles produced in pp collisions at $\sqrt{s} = 13$ TeV that decay into displaced hadronic jets in the ATLAS muon spectrometer*, *Phys. Rev.* **D 99** (2019) 052005 [arXiv:1811.07370] [INSPIRE].

[39] K. Aitken, D. McKeen, T. Neder and A.E. Nelson, *Baryogenesis from Oscillations of Charmed or Beautiful Baryons*, *Phys. Rev.* **D 96** (2017) 075009 [arXiv:1708.01259] [INSPIRE].

[40] D. McKeen, A.E. Nelson, S. Reddy and D. Zhou, *Neutron stars exclude light dark baryons*, *Phys. Rev. Lett.* **121** (2018) 061802 [arXiv:1802.08244] [INSPIRE].

[41] A.E. Nelson and H. Xiao, *Baryogenesis from B Meson Oscillations*, *Phys. Rev.* **D 100** (2019) 075002 [arXiv:1901.08141] [INSPIRE].

[42] M. Cirelli, P. Panci, G. Servant and G. Zaharijas, *Consequences of DM/antiDM Oscillations for Asymmetric WIMP Dark Matter*, *JCAP* **03** (2012) 015 [arXiv:1110.3809] [INSPIRE].

[43] S. Tulin, H.-B. Yu and K.M. Zurek, *Oscillating Asymmetric Dark Matter*, *JCAP* **05** (2012) 013 [arXiv:1202.0283] [INSPIRE].

[44] M. Artuso, G. Borissov and A. Lenz, *CP violation in the B_s^0 system*, *Rev. Mod. Phys.* **88** (2016) 045002 [arXiv:1511.09466] [INSPIRE].

[45] A. Lenz and U. Nierste, *Numerical Updates of Lifetimes and Mixing Parameters of B Mesons*, in *CKM unitarity triangle. Proceedings, 6th International Workshop, CKM 2010, Warwick, UK, September 6-10, 2010*, 2011, arXiv:1102.4274 [INSPIRE].

[46] A. Lenz, *Theoretical update of B-Mixing and Lifetimes*, in *2012 Electroweak Interactions and Unified Theories: Proceedings of the 47th Rencontres de Moriond on Electroweak Interactions and Unified Theories*, La Thuile Italy (2012) [arXiv:1205.1444] [INSPIRE].

[47] F.J. Botella, G.C. Branco, M. Nebot and A. Sánchez, *Mixing asymmetries in B meson systems, the D0 like-sign dimuon asymmetry and generic New Physics*, *Phys. Rev.* **D 91** (2015) 035013 [arXiv:1402.1181] [INSPIRE].

[48] T. Gershon and V.V. Gligorov, *CP violation in the B system*, *Rept. Prog. Phys.* **80** (2017) 046201 [arXiv:1607.06746] [INSPIRE].

[49] HFLAV collaboration, *Averages of b-hadron, c-hadron and τ-lepton properties as of summer 2016*, *Eur. Phys. J.* **C 77** (2017) 895 [arXiv:1612.07233] [INSPIRE].

JHEP03(2020)046

[50] UTfit collaboration, *Model-independent constraints on $\Delta F = 2$ operators and the scale of new physics*, *JHEP* **03** (2008) 049 [arXiv:0707.0636] [INSPIRE].

[51] A. Venugopalan and R. Ghosh, *Decoherence and the quantum Zeno effect*, quant-ph/9503014 [INSPIRE].

[52] A. Hicheur, *Review of recent LHCb results and prospects for Run II*, in *International School on High Energy Physics: Session C: Workshop in HEP (LISHEP 2015)*, Manaus Brazil (2015) [arXiv:1509.07708] [INSPIRE].

[53] Belle-II collaboration, *The Belle II Physics Book*, *PTEP* **2019** (2019) 123C01 [arXiv:1808.10567] [INSPIRE].

[54] S.P. Martin, *A Supersymmetry primer*, hep-ph/9709356 [INSPIRE].

[55] K. Benakli, *Dirac Gauginos: A User Manual*, *Fortsch. Phys.* **59** (2011) 1079 [arXiv:1106.1649] [INSPIRE].

[56] F. Gabbiani, E. Gabrielli, A. Masiero and L. Silvestrini, *A Complete analysis of FCNC and CP constraints in general SUSY extensions of the standard model*, *Nucl. Phys.* **B 477** (1996) 321 [hep-ph/9604387] [INSPIRE].

[57] J.A. Bagger, K.T. Matchev and R.-J. Zhang, *QCD corrections to flavor changing neutral currents in the supersymmetric standard model*, *Phys. Lett.* **B 412** (1997) 77 [hep-ph/9707225] [INSPIRE].

[58] H. Davoudiasl, D.E. Morrissey, K. Sigurdson and S. Tulin, *Hylogenesis: A Unified Origin for Baryonic Visible Matter and Antibaryonic Dark Matter*, *Phys. Rev. Lett.* **105** (2010) 211304 [arXiv:1008.2399] [INSPIRE].

[59] M.A. Luty, *Weak scale supersymmetry without weak scale supergravity*, *Phys. Rev. Lett.* **89** (2002) 141801 [hep-th/0205077] [INSPIRE].

[60] L. Randall and R. Sundrum, *Out of this world supersymmetry breaking*, *Nucl. Phys.* **B 557** (1999) 79 [hep-th/9810155] [INSPIRE].

[61] G.F. Giudice, M.A. Luty, H. Murayama and R. Rattazzi, *Gaugino mass without singlets*, *JHEP* **12** (1998) 027 [hep-ph/9810442] [INSPIRE].

[62] R. Barbier et al., *R-parity violating supersymmetry*, *Phys. Rept.* **420** (2005) 1 [hep-ph/0406039] [INSPIRE].

[63] P. Slavich, *Constraints on R-parity violating stop couplings from flavor physics*, *Nucl. Phys.* **B 595** (2001) 33 [hep-ph/0008270] [INSPIRE].

[64] Fermilab Lattice, MILC collaboration, *$B^0_{(s)}$-mixing matrix elements from lattice QCD for the Standard Model and beyond*, *Phys. Rev.* **D 93** (2016) 113016 [arXiv:1602.03560] [INSPIRE].

[65] R. Barbieri, G.R. Dvali and L.J. Hall, *Predictions from a* U(2) *flavor symmetry in supersymmetric theories*, *Phys. Lett.* **B 377** (1996) 76 [hep-ph/9512388] [INSPIRE].

[66] V.A. Kuzmin, *Might fast b violating transitions be found soon?*, in *Future prospects of baryon instability search in p decay and $n \to \bar{n}$ oscillation experiments: Proceedings of International workshop*, Oak Ridge U.S.A. (1996), pg. 89 [hep-ph/9609253] [INSPIRE].

[67] Heavy Flavor Averaging Group collaboration, *Averages of B-Hadron, C-Hadron and tau-lepton properties as of early 2012*, arXiv:1207.1158 [INSPIRE].

JHEP03(2020)046

[68] M. Misiak and M. Poradzinski, *Completing the Calculation of BLM corrections to $\bar{B} \to X_s\gamma$*, *Phys. Rev.* **D 83** (2011) 014024 [arXiv:1009.5685] [INSPIRE].

[69] MEG collaboration, *Search for the lepton flavour violating decay $\mu^+ \to e^+\gamma$ with the full dataset of the MEG experiment*, *Eur. Phys. J.* **C 76** (2016) 434 [arXiv:1605.05081] [INSPIRE].

[70] M. Drewes, *The Phenomenology of Right Handed Neutrinos*, *Int. J. Mod. Phys.* **E 22** (2013) 1330019 [arXiv:1303.6912] [INSPIRE].

[71] K.N. Abazajian et al., *Light Sterile Neutrinos: A White Paper*, arXiv:1204.5379 [INSPIRE].

[72] S. Alekhin et al., *A facility to Search for Hidden Particles at the CERN SPS: the SHiP physics case*, *Rept. Prog. Phys.* **79** (2016) 124201 [arXiv:1504.04855] [INSPIRE].

[73] I. Boiarska et al., *Probing baryon asymmetry of the Universe at LHC and SHiP*, arXiv:1902.04535 [INSPIRE].

[74] SUPER-KAMIOKANDE collaboration, *The Super-Kamiokande detector*, *Nucl. Instrum. Meth.* **A 501** (2003) 418 [INSPIRE].

[75] L. Bergstrom, J. Edsjo and P. Ullio, *Cosmic anti-protons as a probe for supersymmetric dark matter?*, *Astrophys. J.* **526** (1999) 215 [astro-ph/9902012] [INSPIRE].

[76] M. Garny, A. Ibarra and D. Tran, *Constraints on Hadronically Decaying Dark Matter*, *JCAP* **08** (2012) 025 [arXiv:1205.6783] [INSPIRE].

[77] A. Ibarra, D. Tran and C. Weniger, *Indirect Searches for Decaying Dark Matter*, *Int. J. Mod. Phys.* **A 28** (2013) 1330040 [arXiv:1307.6434] [INSPIRE].

[78] N. Fornengo, L. Maccione and A. Vittino, *Constraints on particle dark matter from cosmic-ray antiprotons*, *JCAP* **04** (2014) 003 [arXiv:1312.3579] [INSPIRE].

[79] M. Cirelli and G. Giesen, *Antiprotons from Dark Matter: Current constraints and future sensitivities*, *JCAP* **04** (2013) 015 [arXiv:1301.7079] [INSPIRE].

[80] C. Evoli, I. Cholis, D. Grasso, L. Maccione and P. Ullio, *Antiprotons from dark matter annihilation in the Galaxy: astrophysical uncertainties*, *Phys. Rev.* **D 85** (2012) 123511 [arXiv:1108.0664] [INSPIRE].

[81] R. Cowsik, *Positrons and Antiprotons in Galactic Cosmic Rays*, *Ann. Rev. Nucl. Part. Sci.* **66** (2016) 297 [INSPIRE].

[82] A. Gould, B.T. Draine, R.W. Romani and S. Nussinov, *Neutron Stars: Graveyard of Charged Dark Matter*, *Phys. Lett.* **B 238** (1990) 337 [INSPIRE].

[83] A. de Lavallaz and M. Fairbairn, *Neutron Stars as Dark Matter Probes*, *Phys. Rev.* **D 81** (2010) 123521 [arXiv:1004.0629] [INSPIRE].

[84] S.D. McDermott, H.-B. Yu and K.M. Zurek, *Constraints on Scalar Asymmetric Dark Matter from Black Hole Formation in Neutron Stars*, *Phys. Rev.* **D 85** (2012) 023519 [arXiv:1103.5472] [INSPIRE].

[85] N.F. Bell, A. Melatos and K. Petraki, *Realistic neutron star constraints on bosonic asymmetric dark matter*, *Phys. Rev.* **D 87** (2013) 123507 [arXiv:1301.6811] [INSPIRE].

[86] J. Bramante, K. Fukushima and J. Kumar, *Constraints on bosonic dark matter from observation of old neutron stars*, *Phys. Rev.* **D 87** (2013) 055012 [arXiv:1301.0036] [INSPIRE].

JHEP03(2020)046

[87] M.I. Gresham and K.M. Zurek, *Asymmetric Dark Stars and Neutron Star Stability*, *Phys. Rev.* **D 99** (2019) 083008 [arXiv:1809.08254] [INSPIRE].

[88] R. Garani, Y. Genolini and T. Hambye, *New Analysis of Neutron Star Constraints on Asymmetric Dark Matter*, *JCAP* **05** (2019) 035 [arXiv:1812.08773] [INSPIRE].

[89] T. Güver, A.E. Erkoca, M. Hall Reno and I. Sarcevic, *On the capture of dark matter by neutron stars*, *JCAP* **05** (2014) 013 [arXiv:1201.2400] [INSPIRE].

[90] G. Bertone and M. Fairbairn, *Compact Stars as Dark Matter Probes*, *Phys. Rev.* **D 77** (2008) 043515 [arXiv:0709.1485] [INSPIRE].

[91] B. Bertoni, A.E. Nelson and S. Reddy, *Dark Matter Thermalization in Neutron Stars*, *Phys. Rev.* **D 88** (2013) 123505 [arXiv:1309.1721] [INSPIRE].

[92] BaBar and Belle collaborations, *The Physics of the B Factories*, *Eur. Phys. J.* **C 74** (2014) 3026 [arXiv:1406.6311] [INSPIRE].

[93] ARGUS collaboration, *Measurement of inclusive baryon production in B meson decays*, *Z. Phys.* **C 56** (1992) 1 [INSPIRE].

[94] ARGUS collaboration, *Measurement of Inclusive B Meson Decays Into Baryons*, *Z. Phys.* **C 42** (1989) 519 [INSPIRE].

[95] CLEO collaboration, *Measurement of baryon production in B meson decay*, *Phys. Rev.* **D 45** (1992) 752 [INSPIRE].

[96] BaBar collaboration, *Search for the rare decay $B \to \Lambda\bar{p}\nu\bar{\nu}$*, in *39th International Conference on High Energy Physics (ICHEP2018)*, Seoul South Korea (2018).

[97] LHC Dark Matter Working Group collaboration, *LHC Dark Matter Working Group: Next-generation spin-0 dark matter models*, *Phys. Dark Univ.* (2018) 100351 [arXiv:1810.09420].

[98] ATLAS and CMS collaborations, *b tagging in ATLAS and CMS*, in *5th Large Hadron Collider Physics Conference (LHCP 2017)*, Shanghai China (2017) [arXiv:1709.01290] [INSPIRE].

[99] A. Atre, T. Han, S. Pascoli and B. Zhang, *The Search for Heavy Majorana Neutrinos*, *JHEP* **05** (2009) 030 [arXiv:0901.3589] [INSPIRE].

[100] ATLAS collaboration, *A search for prompt lepton-jets in pp collisions at $\sqrt{s} = 8$ TeV with the ATLAS detector*, *JHEP* **02** (2016) 062 [arXiv:1511.05542] [INSPIRE].

JHEP03(2020)046

Part II

Dark matter and axions

Chapter 4

On the wondrous stability of ALP dark matter

Authors:
Gonzalo Alonso-Álvarez, Rick S. Gupta, Joerg Jaeckel,
and Michael Spannowsky

Published in *JCAP 03 (2020) 052*,
also available at arXiv:1911.07885

Principal authorship of this article is shared on an equal footing by the four authors. The original idea for the project was conceived by all authors. The calculations in Section 4 were performed predominantly by Gonzalo Alonso-Álvarez. All figures were produced by Gonzalo Alonso-Álvarez. The manuscript was written predominantly by Rick S. Gupta and Gonzalo Alonso-Álvarez. All four authors contributed with corrections and suggestions to the manuscript, as well as with improvements during the review process.

Journal of Cosmology and Astroparticle Physics
An IOP and SISSA journal

On the wondrous stability of ALP dark matter

Gonzalo Alonso-Álvarez,[a] **Rick S. Gupta,**[b] **Joerg Jaeckel**[a] **and Michael Spannowsky**[b]

[a]Institut für theoretische Physik, Universität Heidelberg,
Philosophenweg 16, 69120 Heidelberg, Germany
[b]Institute for Particle Physics Phenomenology,
South Road, Durham DH1 3LE, United Kingdom

E-mail: alonso@thphys.uni-heidelberg.de, sandeepan.gupta@durham.ac.uk,
jjaeckel@thphys.uni-heidelberg.de, michael.spannowsky@durham.ac.uk

Received January 9, 2020
Accepted March 4, 2020
Published March 24, 2020

Abstract. The very low mass and small coupling of axion-like particles (ALPs) is usually taken as a guarantor of their cosmological longevity, making them excellent dark matter candidates. That said, Bose enhancement could stimulate decays and challenge this paradigm. Here, we analyze and review the cosmological decay of ALPs into photons, taking Bose enhancement into account, thereby going beyond the usual naive perturbative estimate. At first glance, this calculation seems to yield an exponentially growing resonance and therefore an extremely fast decay rate. However, the redshifting of the decay products due to the expansion of the Universe as well as the effective plasma mass of the photon can prevent an efficient resonance. While this result agrees with existing analyses of the QCD axion, for more general ALPs that can feature an enhanced photon coupling, stability is only ensured by a combination of the expansion and the plasma effects.

Keywords: axions, dark matter theory

ArXiv ePrint: 1911.07885

JCAP03(2020)052

 https://doi.org/10.1088/1475-7516/2020/03/052

Contents

1 Introduction

Axions, axion-like particles (ALPs), as well as other very light, weakly coupled bosons are promising and popular dark matter candidates [1–4]. Usually lacking a conserved charge,[1] they can in principle decay, and generally do. However, both their weak couplings as well as their low mass contribute to the decay rate being extremely small, and decays are often of little concern to the model builder.

Let us illustrate the situation at hand with the paradigmatic example of an ALP ϕ with a two-photon coupling,

$$\mathcal{L} = \frac{1}{2}\left(\partial_\mu \phi\right)^2 - \frac{1}{2} m_\phi^2 \phi^2 - \frac{1}{4} g_{\phi\gamma\gamma} \phi F^{\mu\nu} \tilde{F}_{\mu\nu}. \tag{1.1}$$

The perturbative decay rate is then given by

$$\Gamma_{\text{pert}} = \frac{g_{\phi\gamma\gamma}^2 m_\phi^3}{64\pi}. \tag{1.2}$$

The region where ϕ becomes cosmologically unstable corresponds to $\Gamma_{\text{pert}} > H_0$, where H_0 is the present-day Hubble parameter, and is indicated as the solid black line labelled "Perturbative decay" in figure 1. As expected, the decay is only relevant for large masses $\gtrsim 1\,\text{keV}$.

The estimate above showcases the fact that the interactions are very small and the corresponding rate is tiny. So why have another look and reconsider the cosmological relevance of decay processes? The reason lies in the generation of the dark matter ALPs, which, as is well known, are produced coherently via the misalignment mechanism [1–3]. The key feature to highlight is the coherent nature of the produced particles. Indeed, if the ALP is present during inflation, the field is completely homogenized within the horizon. Therefore, all ALPs are in the same state, i.e. their occupation number is enormous,

$$N_\phi \sim \frac{\rho_\phi}{m_\phi H^3} \sim 10^{40} \left(\frac{\text{eV}}{m_\phi}\right)^2 \left(\frac{\Phi}{10^{11}\,\text{GeV}}\right)^2 \left(\frac{m_\phi}{H}\right)^3, \tag{1.3}$$

[1] See [5] for an example of very light dark matter particles featuring a conserved charge.

JCAP03(2020)052

where $H = \dot{a}/a$ denotes the Hubble constant, m_ϕ the mass of the ALP field and Φ the typical field amplitude. Such a large occupation number makes Bose enhancement effects seem plausible. Yet, this by itself does not necessarily result in an enhanced decay rate. Bose enhancement also requires large occupation numbers in the final state, in our case populated by photons. Interestingly, since the decay into two photons is a two body decay and therefore all produced photons have equal energy, they can quickly accumulate a high occupation number, allowing for Bose enhancement to set in. As we will see in more detail below, it is here that the crux of the matter, which saves the perturbative estimate in all standard cases, lies. In the expanding Universe, the produced photons redshift, thereby moving out of the momentum range required for them to take part in the Bose enhancement and generally making ALPs cosmologically stable. Furthermore, the fact that the Universe is permeated by an ionized plasma that generates an effective mass for the photons also contributes to hinder the decay.

The problem of the potential instability of coherent bosonic dark matter is as old as axion dark matter itself [1–3]. Indeed, the authors of [1, 2] already realized that coherent decay of QCD axion dark matter into either relativistic axions or photons is ineffective due to expansion and plasma effects — the two effects that we will reconsider here for more general ALPs. A non-equilibrium QFT calculation of the photon production from coherent QCD axion dark matter oscillations was performed in [6] and reached the same conclusion, albeit plasma effects were not included in the computation. The decay of the condensate into relativistic axion modes can also be described as a growth of quantum fluctuations caused by anharmonicities in the potential. This was done in [1, 7], once more finding that the effect is negligible in an expanding background, unless extreme misalignment angles occur [8].

As the situation is well-stablished in the case of QCD axions, in this work we consider the more general case of axion-like particles, where the mass and the decay constant (and therefore the photon coupling) are independent parameters. The question of stability is of particular interest for ALPs with larger couplings and/or larger initial field values, which are theoretically motivated by monodromies [9, 10], clockwork constructions [11–13] and string theory expectations [14]. On the more experimental side, the (m_ϕ, $g_{a\gamma\gamma}$) parameter space will be tested by many future ALP dark matter experiments such as ABRACADABRA [15], ADMX [16], BRASS [17], CULTASK [18] HAYSTAC [19], KLASH [20], MadMax [21], ORGAN [22], QUAX [23], or RADES [24]. In addition, experiments like IAXO [25] will look for ALPs with photon couplings independently of whether they constitute the dark matter. As we will see, it is a non-trivial conspiracy of expansion and plasma effects that allow the ALP to be sufficiently stable and therefore a viable dark matter candidate in the region of parameter space probed by these experiments.

Before returning to the main topic of this note, let us point out that even if the cosmological stability is not threatened, interesting effects related to ALP-photon interactions can take place. For instance, decays in dark matter-rich environments can lead to observable radio signals [26, 27]; while photon propagation in an axion background can exhibit parametric resonance-driven conversions [28, 29]. The associated signals would be enhanced if axion structures exist in our galaxy, be it in the form of axion stars [30–32], miniclusters [33–37], condensates [38, 39], or superradiant clouds around black holes [40–42]. On a different direction, it has been recently suggested that dark matter axions could be detected by looking for an electromagnetic "echo" [43]. Finally, the ALP condensate could also suffer similar tachyonic or parametric instabilities that can lead to a rapid decay into dark photons. The authors of [44] argued that this effect could help deplete an excess of dark matter axions.

JCAP03(2020)052

This idea was further developped in [45], while [46, 47] used the instability to generate dark photon dark matter.[2] This violent decay process can lead to the production of gravitational waves, as was pointed out in [54].

In this work we focus on the effect of a photon coupling, as it is the only bosonic Standard Model particle that is lighter than the typical dark matter ALPs. However, modifications of the simplest pseudo-Goldstone scenario for ALPs can also increase the effect of other couplings. An important example are the self couplings. While these effects are small for simple pseudo-Goldstones [1, 7], they can become important in a monodromy setup where the initial field values are large [10]. This can lead to a fragmentation of the condensate and a significant density fluctuations at small scales [55]. Moreover, if the ALP exhibits couplings to other light bosonic dark sector particles, similar effects to what we discuss in the following may become relevant.

This brief note presents a detailed study of the cosmological stability of generic light pseudoscalar dark matter. The discussion in the previous paragraphs sets the plan for the rest of the manuscript. In the following section 2, we use classical equations of motion to account for coherent effects, i.e. Bose enhancement, in the decay. This naively suggests an enormously enhanced decay rate. Then, in sections 3 and 4, the effects of expansion and in-medium photon dispersion are consecutively taken into account. This generally prevents the Bose enhanced regime from being reached. Finally, we conclude in section 5.

2 Bose enhanced decay rates

An alternative to the usual perturbative calculation of the decay rate $\phi \to \gamma\gamma$ is to consider the growth of the photon field in the time-dependent ALP background. We first study this in Minkowski space where the alternative approach may be expected to yield the same result as the perturbative one. The equation of motion (EoM) in Fourier space reads (see, e.g. [44])

$$\ddot{A}_\pm + \left(k^2 \pm g_{\phi\gamma\gamma}\, k\, \dot{\phi}\right) A_\pm = 0, \tag{2.1}$$

where k is the momentum of the photon mode and $A_\pm$ represent the two helicity modes for the photon. For brevity, we will consider only the mode $A \equiv A_-$, but A_+ can be treated analogously. The ALP dark matter field, which is taken to be homogeneous, performs oscillations with frequency m_ϕ and amplitude Φ and is therefore given by

$$\phi(t) = \Phi \sin(m_\phi t), \tag{2.2}$$

corresponding to the solution to its free EoM.[3] Using the definitions

$$x = \frac{m_\phi}{2} t, \qquad \lambda = \frac{4k^2}{m_\phi^2}, \qquad \text{and} \qquad q = 2 g_{\phi\gamma\gamma} \Phi \frac{k}{m_\phi}, \tag{2.3}$$

the EoM of the photon field has the form of a standard Mathieu equation [59],

$$\frac{\mathrm{d}A}{\mathrm{d}x} + (\lambda - 2q\cos(2x))A = 0. \tag{2.4}$$

[2] See [4, 48–53] for other scenarios for the production of light vector dark matter.

[3] In our calculation, we neglect the backreaction of the decay photons on the ALP field. This is a good approximation as long as only a small number of photons is produced. Once photon production becomes significant enough for backreaction effects to matter, the stability is already compromised.

JCAP03(2020)052

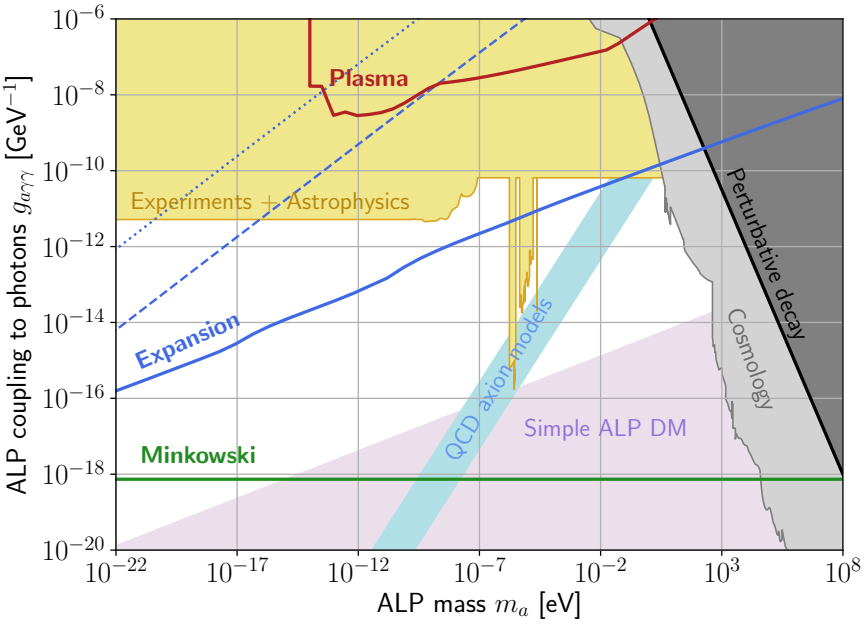

Figure 1. Parameter space for ALPs in the mass vs. two-photon coupling plane (adapted from [4, 56–58]). The shaded regions indicate experimental and observational limits as labelled. The green line indicates the stability bound that would arise from Bose enhanced decay, neglecting expansion and plasma effects. The blue lines shows how the expansion of the Universe ameliorates this constraint. The dotted line corresponds to evaluating the stability condition today, the dashed one corresponds to matter-radiation equality and the solid line is obtained by evaluating it at the earliest possible time, when the field just starts to oscillate, i.e. when $H \sim m_\phi/3$. Finally, the red line additionally takes into account the plasma effects that prevent decay. We conclude that stability is ensured in all regions that are not already excluded by experiments or observations.

The crucial result is that this differential equation admits exponentially growing solutions

$$A \sim \exp\left(\eta_k t\right), \tag{2.5}$$

with a rate

$$\eta_k = \beta_k \, g_{\phi\gamma\gamma} \Phi \, m_\phi, \tag{2.6}$$

where β_k is an $\mathcal{O}(1)$ coefficient. Such growing solutions appear for k-modes satisfying the condition

$$\left| k - \frac{m_\phi}{2} \right| < \delta k, \tag{2.7}$$

where the effective width of the resonance band is (see e.g. [60] for an analytical derivation)

$$\delta k \sim g_{\phi\gamma\gamma} \Phi \, m_\phi / 2. \tag{2.8}$$

The coefficient β_k reaches its maximum $\beta_{k_\star} = 1/4$ at the center of the band $k = k_\star = m_\phi/2$, and decreases to zero at the edges. This is nothing but the well-known phenomenon of parametric resonance [61–66].

The (dominant[4]) resonance occurs around $k_\star = m_\phi/2$ as one would expect for a perturbative two-photon decay. The puzzling observation is however that both the width, δk, and the effective growth rate of the photon field, η_k, given in eq. (2.6), are parametrically different from the perturbative decay rate given in eq. (1.2). Crucially, the rate obtained from the EoM is proportional to only one power of the coupling constant, and it also depends on the ALP field amplitude and therefore on the ALP density. For example, let us consider the QCD axion with $f = 10^{12}\,\mathrm{GeV}$, for which the perturbative decay time

$$\Gamma_{\mathrm{pert}}^{-1} \sim 10^{51}\ \mathrm{s} \tag{2.9}$$

is comfortably larger than the age of the Universe. However, the decay time obtained from the EoM,

$$\eta_{k_\star}^{-1} \sim 10^{-7}\ \mathrm{s}, \tag{2.10}$$

is dramatically smaller. For a generic ALP, the region of parameter space where the lifetime obtained from the EoM in eq. (2.1) is smaller than a Hubble time is indicated by the green line labelled "Minkowski" in figure 1. The enhanced rate thus seems to affect huge areas in parameter space. However, as we will see in the next section, this instability does not become effective in a large part of this region once we take proper account of the expansion of the Universe and the effective plasma mass of the photon.

Before going on to discuss these effects, let us nevertheless try to understand the origin of the huge discrepancy between the classical and the standard perturbative calculations. As already mentioned in the introduction, we are dealing with bosonic systems featuring very large occupation numbers. In such a situation (cf., e.g., [67]) the decay rate receives a Bose enhancement via the photon occupation number N_k,

$$\Gamma = \Gamma_{\mathrm{pert}}(1 + 2N_k). \tag{2.11}$$

For $N_k \gg 1$, the second term can lead to an exponential growth in the photon number. This can easily be seen by writing the Boltzmann equation for photons with momentum $k_\star = m_\phi/2$ (we denote number densities by lowercase n and occupation numbers by uppercase N),

$$\dot{n}_\gamma = 2\Gamma n_\phi = 2\Gamma_{\mathrm{pert}}(1 + 2N_k)n_\phi. \tag{2.12}$$

This rate equation can be rewritten using the relations

$$\Gamma_{\mathrm{pert}} = \frac{g_{\phi\gamma\gamma}^2 m_\phi^3}{64\pi}\,, \quad n_\phi = \frac{1}{2} m_\phi \Phi^2\,, \quad \text{and} \quad N_k \sim \frac{n_\gamma/2}{4\pi k_\star^2\, \delta k\,/(2\pi)^3}\,, \tag{2.13}$$

where we have divided the photon number density by the corresponding phase-space volume to obtain the expression for the photon occupation number. For now we will simply insert eq. (2.8) for the width of the momentum shell δk (which is derived from the EoM eq. (2.1)). Below we will justify this from a perturbative argument based on the uncertainty principle. Doing this, we can solve eq. (2.12) in the $N_k \gg 1$ limit to obtain a number density

$$n_\gamma \propto \exp\left(\beta g_{\phi\gamma\gamma}\Phi m_\phi t\right), \tag{2.14}$$

and so the result from the classical EoM is recovered. The fudge factor β takes into account the $\mathcal{O}(1)$ uncertainty in the expression for N_k in eq. (2.13).

[4]The Mathieu equation also features a number of sub-dominant resonances. These are, however, parametrically weaker [60].

JCAP03(2020)052

The assumption that $N_k \gg 1$ needs justification, as initially no photons may be present in the relevant phase-space region. Let us estimate the time needed for the photon occupation number to grow beyond 1 via the perturbative decay. To evaluate this, we start from eq. (2.12) in the regime where $N_k \ll 1$, and therefore ignore the second term to obtain

$$\Delta n_\gamma = 2\Gamma_{\rm pert} n_\phi \Delta t. \tag{2.15}$$

If the decay happens within a short time Δt, the momentum of the photons has an indetermination Δk due to the uncertainty principle $\Delta E\, \Delta t \geq 1/2$. Therefore, the corresponding growth in the occupation number after a time Δt is

$$\Delta N_k \sim \frac{\Delta n_\gamma}{4\pi k_\star^2/(2\pi)^3} \cdot \Delta t\,. \tag{2.16}$$

In consequence, the Bose-enhanced regime is reached on a time-scale

$$\frac{1}{\Delta t} \sim \frac{\sqrt{\pi}}{2\sqrt{2}}\, g_{\phi\gamma\gamma} \Phi\, m_\phi, \tag{2.17}$$

which corresponds to the time-scale for the exponential growth obtained in eq. (2.6) using the equations of motion. The corresponding width $\delta k \sim 1/\Delta t$ parametrically matches eq. (2.8), justifying its use above. At later times, when $N_k \gtrsim 1$, the width is also of the same parametric size. This is due to the fact that after each subsequent time $\sim \Delta t$, the newly created photons from the stimulated decay dominate the occupation number and "reinitialize" the uncertainty principle.

A more careful numerical analysis of the EoM reveals that, for arbitrary initial conditions, the typical time needed to reach the regime of exponential growth is given by this same time-scale. In this sense, the perturbative calculation and the results from the EoM are consistent.

3 Expansion prevents growth

As already indicated, so far a crucial effect has been neglected: the expansion of the Universe. This can be incorporated into the EoM, most conveniently by using conformal time (see appendix A for the precise expressions). However, the effect that is relevant for our purposes is just the fact that the photon k-modes are redshifted due to the expansion and therefore move out of the resonance band. This allows for a physical and intuitive approach to the problem, which we follow in this section.

After a time $\Delta t \ll H$, where H is the Hubble rate of expansion, the physical momentum of the photon modes changes by an amount

$$\frac{\Delta k}{k} \simeq H\, \Delta t\,. \tag{3.1}$$

For Bose enhancement to be effective, the exponential growth of the photon number, which is proportional to $|A|^2$, has to set in on a short time-scale compared to the one at which modes are redshifting out of the resonance. This requires

$$\Delta t_{\rm growth} \sim \frac{1}{2\eta_{k_\star}} \lesssim \frac{\delta k}{k_\star} \frac{1}{H} \sim \Delta t_{\rm redshift}. \tag{3.2}$$

The actual condition for instability is slightly stronger: the resonance has to be effective for a long enough time to allow the ALP condensate to decay. Decay of the dark matter field happens when a sizeable fraction of its energy density is lost. The energy density in the exponentially growing photon modes is given by

$$\rho_\gamma(t) = \frac{1}{\pi^2}\int \mathrm{d}k\, k^2 \omega_k N_k(t), \tag{3.3}$$

where ω_k is the frequency of a (single helicity) mode and N_k is its occupation number,

$$N_k = \frac{\omega_k}{2}\left(|\dot{A}_k|^2/\omega_k^2 + |A_k|^2\right). \tag{3.4}$$

Given that the resonance has a very narrow bandwidth $\delta k \ll k$, the integral can be approximated using the method of steepest descent to give

$$\rho_\gamma(t) \simeq \frac{1}{\pi^2}\, k_\star^3\, \delta k \sqrt{\frac{\pi}{\eta_{k_\star} t}}\, N_{k_\star}(t), \tag{3.5}$$

where the rate $\eta_{k_\star}$ at centre of the resonance band $k_\star = m_\phi/2$ is given in eq. (2.6), and thus

$$N_{k_\star}(t) = N^0_{k_\star} \mathrm{e}^{2\eta_{k_\star} t}. \tag{3.6}$$

Here, $N^0_{k_\star}$ denotes the initial occupation number of the mode. As discussed in the previous section, the exponential enhancement sets in when $2\eta_{k_\star}\,\Delta t \gtrsim 1$. After that point, the ratio of the energy density in the produced photon population with respect to that stored in the ALP field, $\rho_\phi \simeq m_\phi^2\Phi^2/2$, can be approximated by

$$\frac{\rho_\gamma}{\rho_\phi} \sim \frac{g_{\phi\gamma\gamma}\, m_\phi^2}{\Phi}\, N^0_{k_\star} \mathrm{e}^{2\eta_{k_\star} t}. \tag{3.7}$$

The initial condition can correspond to vacuum fluctuations, $N^{\mathrm{vac}}_{k_\star} = 1/2$, or to CMB photons with a corresponding occupation number

$$N^{\mathrm{CMB}}_{k_\star} = \frac{1}{\exp\left(m_\phi/(2T_{\mathrm{CMB}})\right) - 1} \sim \frac{2T_{\mathrm{CMB}}}{m_\phi}, \tag{3.8}$$

valid for $m_\phi \ll T_{\mathrm{CMB}}$, using the CMB temperature at the time at which the resonance is active. In both cases, the prefactor of the exponential in eq. (3.7) is very small. Therefore, for a sizeable fraction of the DM ALPs to decay the resonance has to be active for many growth times,

$$\Delta t_{\mathrm{decay}} \sim \zeta \Delta t_{\mathrm{growth}} \sim \zeta/(2\eta_{k_\star}) \tag{3.9}$$

where

$$\zeta \sim \max\left\{\log\left(\frac{\Phi}{g_{\phi\gamma\gamma} m_\phi^2}\right), \log\left(\frac{\Phi}{g_{\phi\gamma\gamma} m_\phi T_{\mathrm{CMB}}}\right)\right\}. \tag{3.10}$$

Thus, the final condition for stability, $\Delta t_{\mathrm{decay}} \lesssim \Delta t_{\mathrm{redshift}}$, can be recast as

$$g^2_{\phi\gamma\gamma}\Phi^2(t) \lesssim 2\zeta \frac{H(t)}{m_\phi}, \tag{3.11}$$

JCAP03(2020)052

which is required to hold at any time during the evolution of the Universe. ζ amounts to a factor of $\mathcal{O}(10\text{–}100)$ for the parameters of interest.

As shown in appendix A, the condition in eq. (3.11) can also be derived by an investigation of the EoM for the photon field in a Friedmann-Robertson-Walker (FRW) background. The analysis in appendix A also shows that other effects related to expansion, namely the damping of the amplitude of the photon field and the ALP oscillations, are not as effective in curbing the exponential growth as the one discussed above.

The requirement for stability in eq. (3.11) must hold at all times. In figure 1, the dotted and dashed blue lines correspond to it being evaluated today and at matter-radiation equality, respectively. We clearly see that the constraint becomes stronger when evaluated at earlier times. The reason for this is that the left hand side of eq. (3.11) falls with the scale factor as $1/a^3$, whereas the right hand side falls only as $1/a^2$. The stability condition is therefore most restrictive when evaluated at the earliest possible time. This corresponds to the time $t_{\rm osc}$ when the ALP field oscillations start, given by $H(t_{\rm osc}) \sim m_\phi/3$. Assuming standard cosmology, this produces the solid blue line labelled as "Expansion" in figure 1.

The QCD axion and simple ALPs that arise as Goldstone bosons inhabit regions which are below the blue line in figure 1. These are thus stable even without taking into account plasma effects (this was already understood in the original works [1, 2]). The reason for this is that a sufficient condition for the stability condition in eq. (3.11) to be obeyed is for the product $g_{\phi\gamma\gamma}\Phi(t_{\rm osc})$ to be smaller than unity. This is automatically satisfied for simple pseudo-Goldstone bosons, as in this case the field value is bounded by [68]

$$\Phi \lesssim \pi f. \tag{3.12}$$

At the same time, the photon coupling can be written as

$$g_{\phi\gamma\gamma} = \frac{C_{\phi\gamma\gamma}\alpha_{\rm em}}{4\pi f}, \tag{3.13}$$

where $C_{\phi\gamma\gamma}$ summarizes the model dependence (e.g. due to charge assignments of fermions mediating the interaction). In simple models, this constant is not expected to be much larger than unity and therefore $g_{a\gamma\gamma}\Phi \lesssim 1$. However, there is a renewed interest in ALP models that can accommodate larger values of this product. Recently, it has been realised that this part of the parameter space can be populated by monodromy [9, 10] or clockwork constructions [11–13], and by string theory expectations [14]. In these situations, the relation $g_{a\gamma\gamma}\Phi \lesssim 1$ is violated by either having an initial field value that is larger than that of a naive Goldstone boson or by directly enhancing the photon coupling over its usually expected value.

4 Plasma effects prevent early decay

There is still a critical observation that we have ignored in our analysis so far: the early Universe is filled with a dense plasma that has a severe impact on the propagation of photons. Following [69], the coherent interactions with the background can be described with a modified dispersion relation and a wavefunction renormalization for the photon.

Importantly, a photon propagating in a medium acquires an extra polarization degree of freedom, that can be identified as a longitudinal excitation in the Lorentz gauge. However, the homogeneous ALP field does not couple to this degree of freedom. This can be seen

JCAP03(2020)052

by explicitly writing down the terms in the photon EoM arising from the $\phi F\tilde{F}$ term in the Lagrangian,

$$\frac{1}{4}g_{a\gamma\gamma}\phi F_{\mu\nu}\tilde{F}^{\mu\nu} \quad \xrightarrow{\text{EoM}} \quad g_{a\gamma\gamma}\left(\dot{\phi}\,\nabla\times\mathbf{A}-\nabla\phi\times(\dot{\mathbf{A}}-\nabla A_0)\right), \tag{4.1}$$

where $A=(A^0,\mathbf{A})$ and A^0 is completely determined by the Lorentz gauge condition $\partial\cdot A=0$. As in this work are only dealing with a spatially homogeneous ALP field, only the first term in the above equation is non-vanishing. This term only sources transverse photons and accordingly we do not further discuss longitudinal modes.

As discussed in appendix B, the most relevant effect[5] for our purposes is the fact that the dispersion relation of transverse modes is modified in such a way that the medium does not allow modes with frequency below a certain cutoff to be excited. The lowest frequency that can propagate is known as the *plasma frequency*, ω_P. In practice, this is equivalent to considering an effective in-medium mass[6] $m_\gamma=\omega_P$ for the photons. The immediate consequence is that the decay of the ALP cannot take place at all as long as its mass is below the $2m_\gamma$ threshold [1]. This can be seen by adding a term $m_\gamma^2 A_\pm$ in the left hand side of the EoM in eq. (2.1), so that the condition for parametric resonance becomes

$$\left|\sqrt{k^2+m_\gamma^2}-\frac{m_\phi}{2}\right|<\delta k, \tag{4.2}$$

in terms of physical momenta. If $m_\phi<2m_\gamma$, the effective mass prevents the resonance and thus the decay of the ALP from happening. This effect turns out to be efficient in stabilizing the ALP in a large part of the parameter space.

In order to quantitatively evaluate this effect, an expression for the effective photon mass (or *plasma mass*) throughout the relevant epochs of the history of the Universe is required. To obtain it, we use the results of [69, 70] and apply them to our setup. The result is presented in figure 2 as a function of the Hubble parameter, while the corresponding dependencies on the temperature and redshift, together with the details of the calculation, are given in appendix B.

The shape of the curves in figures 2 and 3 can be qualitatively understood as follows. At high temperatures $T\gg 1\,\text{MeV}$, relativistic electron-positron pairs dominate the dispersion relation of photons and generate a large effective mass $m_\gamma\propto T$. The effective mass sharply drops during the e^+e^- annihilation at $T\sim m_e$, after which the dominant contribution comes from scatterings off the leftover electrons and the ionized hydrogen and helium atoms. At even lower temperatures $T\sim 0.1\,\text{eV}$, electrons and protons combine to form neutral atoms causing another drop in the effective mass. Finally, the first stars reionize the medium at around $z\sim 1$–10, which explains the increase in the plasma mass at $T\sim$ meV. Today, the effective photon mass in the intergalactic medium[7] is expected to be $m_\gamma\sim 10^{-14}$–$10^{-13}\,\text{eV}$, which sets an absolute lower bound on the mass of the (background) ALPs that can be subject to decay.

[5] The wavefunction renormalization constant of the transverse mode is always very close to one and does not play a role in our analysis [69].

[6] Strictly, only modes with wavenumber $k\gg\omega_\text{P}$ have a dispersion relation that approaches that of a massive particle (see appendix B and [69] for more details).

[7] The space between galaxies is thought to be permeated by an ionized plasma with electron densities $n_e\sim 10^{-6}$–$10^{-4}\,\text{cm}^{-3}$ and temperatures $T\sim 10^5$–$10^7\,\text{K}$, known as the warm-hot intergalactic medium or WHIM [71].

JCAP03(2020)052

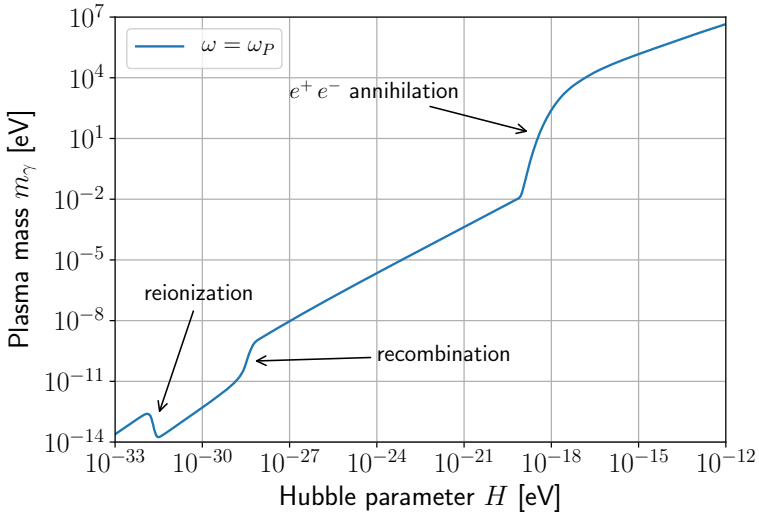

Figure 2. Effective mass of the photon (in the sense explained in the text) in the early Universe as a function of the Hubble parameter (see figure 3 for m_γ as a function of temperature and redshift). For this figure, we fix $\omega = \omega_P$.

As soon as the plasma is dilute enough such that $m_\gamma < m_\phi/2$, the ALP decay is allowed and the discussion in the previous section becomes valid. Given that the condition in eq. (3.11) is stronger earlier on, it must be imposed at the first moment that it becomes applicable. Two requirements are needed: that the ALP field is oscillating (i.e. that $3H \lesssim m_\phi$) and that the photon plasma mass falls beyond the threshold $m_\gamma \lesssim m_\phi/2$. By looking at figure 2, one immediately concludes that the latter is the most restrictive of the two. This means that it is the plasma effects that set the earliest time at which the resonance can be active, and ultimately the region of parameter space where the ALP dark matter field is cosmologically unstable.

Numerically, the region of ALP parameter space where Bose enhancement can be relevant is delineated by the red line labelled "Plasma" in figure 1. It is obtained by imposing eq. (3.11) as soon as $2m_\gamma < m_\phi$. As discussed above, there is no bound on ALPs lighter than present-day photons in the intergalactic medium, i.e. for $m_\phi \lesssim 10^{-14}\,\text{eV}$. We conclude that when plasma effects are considered, the region that is prone to instabilities is much smaller due to the delay of the ALP decay. As advertised in the introduction, it is therefore crucial to take into account both the expansion of the Universe and the in-medium dispersion effects to absolutely establish the stability of ALP dark matter.

Let us conclude this section by commenting on the possibility of photon production due to spinodal or tachyonic instabilities [6, 44]. As soon as the temperature is low enough such that the photon plasma mass can be ignored, one can see from eq. (2.1) and eq. (A.1) that the frequency of certain modes of the photon field can become imaginary if they lie in the band $\lambda - 2q < 0$. The mode remains tachyonic only as long as the sign of the cosine does not change. Requiring that the timescale of the energy growth is smaller than the time that the cosine preserves its sign, in addition to the tachyonic condition, gives [44]

$$m_\phi < \frac{k}{a} < g_{\phi\gamma\gamma}\Phi m_\phi, \tag{4.3}$$

which clearly requires $g_{\phi\gamma\gamma}\Phi > 1$. It is easy to see that the condition for photon production due to a tachyonic instability is not satisfied anywhere in the stable region below the red line in figure 1. Indeed, from eq. (3.11), we see that the product $g_{\phi\gamma\gamma}\Phi$ is at most of the order of $\sqrt{H/m_\phi}$, which is much smaller than unity by the time the photon mass becomes smaller than the ALP mass (see figure 2).

5 Conclusions

Axion-like particles (ALPs) are dark matter candidates that often enjoy a $\phi F\tilde{F}$ coupling, through which the ALP can decay into two photons. That said, the cosmological stability of this kind of dark matter seems to be nearly trivial at first sight due to its low mass and incredibly weak coupling. However, if the ALP field exists already during inflation, the rapid expansion creates an extremely homogeneous and therefore coherent initial state. Given the low mass of the ALPs, this effectively corresponds to a bosonic state with incredibly high occupation numbers, suggesting the possibility of a Bose enhancement of the dark matter decay. Indeed, in an otherwise empty and non-expanding Universe, the resulting stimulated emission would lead to an extremely rapid decay of ALPs into photons, invalidating most of the interesting parameter space. However, as already found in the original papers [1–3], there are two effects that prevent this catastrophe: the expansion of the Universe and the plasma effects that modify the propagation of photons. For QCD axions, the former is already sufficient to prevent the evaporation of the dark matter; however, for ALPs with larger couplings significant non-excluded areas of parameter space would still be subject to decay. Here the plasma effects are crucial, as they generate an effective photon mass which kinematically forbids the decay of ALPs lighter than this plasma mass. This opens up the full parameter space not yet excluded by past experiments or astrophysical observations (which do not rely on ALPs being the dark matter). In this sense, the full region is viable to be explored by current and near future ALP dark matter experiments [15–24].

It may be interesting to think of additional observable effects caused by the Bose enhanced decay stimulated by the CMB photons. Even if the ALP condensate is not significantly depleted, this leads to an additional number of photons of frequency $\sim m_\phi/2$ being injected. Usually this effect is bigger at relatively small masses where, however, it seems challenging to detect. The interplay of the condensate with primordial magnetic fields can also lead to interesting phenomena [72]. Although first estimates suggest that the cosmological stability of the ALPs is not threatened under standard assumptions regarding the magnetic field strength, this is a topic worth studying in more detail.

For ALP couplings other than the photon one, similar Bose enhanced effects may become important and therefore the viability of the ALP as a DM candidate needs careful verification. Indeed, while self-couplings have been found to be safe for QCD axions [1, 7], they can be relevant in models that go beyond the simplest pseudo-Goldstone ALP. Among other effects, they can lead to a fragmentation of the condensate [55].[8] Similarly, some care is needed when couplings, e.g. to other light dark sector bosons, are stronger than expected for naive pseudo-Goldstone bosons as suggested by recent theoretical constructions [9–14].

[8]The fragmentation does not invalidate these light scalars as dark matter candidates, but can significantly modify their cosmological and astrophysical phenomenology.

JCAP03(2020)052

Acknowledgments

We thank S. Davidson for very useful discussions and J. Redondo for sharing his wisdom and his personal notes on the topic with us. JJ would like to thank the IPPP for hospitality during the time this project was started and support within the DIVA fellowship programme. GA is a grateful recipient of a "la Caixa" postgraduate fellowship from the Fundación "la Caixa".

A Equation of motion of the photon in an expanding Universe

The condition in eq. (3.11) can be derived by investigating the photon EoM in an FRW background,

$$\frac{\mathrm{d}^2 A}{\mathrm{d}x^2} + \frac{2H}{m_\phi}\frac{\mathrm{d}A}{\mathrm{d}x} + \left(\lambda\frac{1}{a^2} - 2q\frac{1}{a^{5/2}}\cos(2x)\right)A = 0, \tag{A.1}$$

where we set the scale factor a to be 1 at $t = t_0$, and define $x = m_\phi t/2$, $\lambda = 4k^2/m_\phi^2$ and $q = 2g_{\phi\gamma\gamma}\Phi k/m_\phi$ such that they coincide with their flat space definitions. Taking $a \sim t^n \sim x^n$, with $n = 1/2$ (2/3) for radiation (matter) domination, we can replace factors of $1/a$ by factors of $(x_0/x)^n$, where $x_0 = x(t_0)$.

Here, we focus on the regime where the photon plasma mass is much smaller than the ALP mass, i.e. $m_\gamma \ll m_\phi$, so that the exponentially enhanced decay is possible. From figure 2, we see that this implies $x = m_\phi t/2 = n m_\phi/(2H) \gg 1$. We thus choose an initial time point such that $x_0 \equiv 1/\xi \ll 1$, and make a change of variables $y = x - x_0$ to obtain

$$\frac{\mathrm{d}^2 A}{\mathrm{d}y^2} + \left(\frac{\xi n}{1+\xi y}\right)^{2n}\frac{\mathrm{d}A}{\mathrm{d}y} + \left(\lambda\left(\frac{1}{1+\xi y}\right)^{2n} - 2q\left(\frac{1}{1+\xi y}\right)^{5n/2}\cos(2y+\delta)\right)A = 0. \tag{A.2}$$

Note that for $\xi = 0$ we recover the Mathieu equation in eq. (2.4). For non-zero ξ, exponential growth may not take place if, as explained above, the k-modes get redshifted out of the unstable band. The redshifting causes λ/a^2 to decreases with time as

$$\lambda\left(\frac{1}{1+\xi y}\right)^{2n} \approx \lambda\left(1 - 2n\xi y\right), \tag{A.3}$$

so that the time it takes for k-modes to move out of the unstable band $|\lambda - 1| < q$ is

$$\Delta y_{\mathrm{redshift}} = \frac{q}{2n\xi}. \tag{A.4}$$

Demanding this to be smaller than the time scale of exponential growth, $\Delta y_{\mathrm{decay}} = \zeta/q$, we again find

$$q^2 \lesssim 2\zeta n\xi \quad \Rightarrow \quad (g_{\phi\gamma\gamma}\Phi)^2 \lesssim 2\zeta\frac{H}{m_\phi}. \tag{A.5}$$

where ζ is defined in eq. (3.10).

It is worth noting that there are two other effects that can potentially curb the exponential enhancement. The first is the Hubble friction (second term in eq. (A.1)) and the second is the damping of the ALP oscillations (that is, the decrease in $q/a^{5/2}$ with time). These effects, however, are subdominant compared to the redshifting discussed above. While the first effect becomes relevant only for $\xi \sim q$, the second is not important because the change in q in the time $\Delta t_{\mathrm{redshift}}$ is $\mathcal{O}(q^2)$ and thus marginal.

B Dispersion relation of the photon in the primordial plasma

Here we briefly review the most relevant dispersion effects that affect the propagation of photons in the early Universe plasma. The discussion is based on [69, 70] whom we closely follow. Other references where similar studies are made are [73–75], among others.

A photon propagating through a plasma is subject to scattering with the charged constituents of the medium. The coherent accumulation of such interactions can be macroscopically described by a modification of the dispersion relation of the photon, which becomes

$$-\omega^2 + k^2 + \pi_a(\omega, k) = 0. \tag{B.1}$$

The index $a = \{T(\pm), L\}$ labels the different polarizations of the field, now also including a longitudinal degree of freedom that is not present in vacuum. Thus, the key quantities are π_L and π_T, the longitudinal and transverse components of the polarization tensor $\Pi^{\mu\nu}$. In an ionized plasma, the dominant contribution to the polarization tensor is that of the free electrons and positrons. At lowest order in QED [69, 70],

$$\pi_L = \omega_P^2 \left(1 - G(v_\star^2 k^2/\omega^2)\right) + (v_\star^2 - 1)k^2, \tag{B.2}$$

$$\pi_T = \omega_P^2 \left(1 + G(v_\star^2 k^2/\omega^2)/2\right), \tag{B.3}$$

with

$$G(x) = \frac{3}{x}\left(1 - \frac{2x}{3} - \frac{1-x}{2\sqrt{x}} \log\left(\frac{1+\sqrt{x}}{1-\sqrt{x}}\right)\right). \tag{B.4}$$

In the above expression, $v_\star = \omega_1/\omega_P$ depends on the *plasma frequency* ω_P and ω_1,

$$\omega_P^2 = \frac{4\alpha_{\rm em}}{\pi} \int_0^\infty \mathrm{d}p\, f_p\, p \left(v - \frac{1}{3}v^3\right), \tag{B.5}$$

$$\omega_1^2 = \frac{4\alpha_{\rm em}}{\pi} \int_0^\infty \mathrm{d}p\, f_p\, p \left(\frac{5}{3}v^3 - v^5\right), \tag{B.6}$$

where f_p is the sum of the phase-space distributions of e^- and e^+.

For nondegenerate systems, as appropriate in the early Universe, one has

$$\omega_P^2 \simeq \begin{cases} \frac{4\pi\alpha_{\rm em} n_e}{m_e}\left(1 - \frac{5}{2}\frac{T}{m_e}\right) & \text{Nonrelativistic,} \\ \frac{4\alpha_{\rm em}}{3\pi}\left(\mu^2 + \frac{1}{3}\pi^2 T^2\right) & \text{Relativistic,} \end{cases} \tag{B.7}$$

where T, n_e and μ are the temperature, number density and chemical potential of the electrons, respectively. This can be inserted into the dispersion relation, eq. (B.1).

In practice, we are only interested in the cutoff frequency below which no propagating modes (i.e., modes with non-vanishing real k) exist in the plasma. We focus on transverse modes, as these are the only ones that couple to the homogeneous ALP field.[9] Given that π_T is a monotonically increasing function of k, we can simply solve eq. (B.1) for $k = 0$, in which case $G = 0$. It is thus easy to see that the cutoff frequency is straightforwardly given by the plasma frequency ω_P. In analogy to the case of a massive particle, for which the mass gives a lower bound for the frequency (or energy) of the propagating states, we refer to the cutoff frequency as the *plasma mass* of the photon, and denote it by m_γ. Note, however,

[9] Longitudinal modes have a more complex behaviour that may be interesting to study in inhomogeneous situations.

JCAP03(2020)052

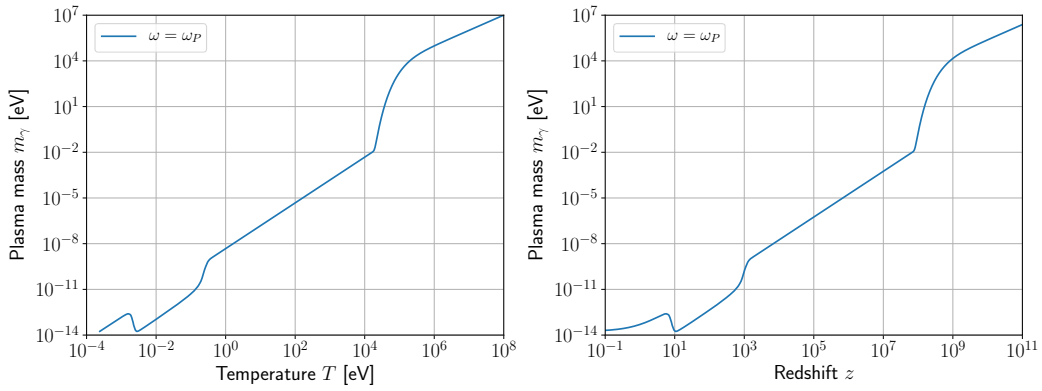

Figure 3. Effective transverse photon mass in the early Universe as a function temperature (*left*) and redshift (*right*) (see figure 2 for m_γ as a function of the Hubble parameter). For this figure, we fix the frequency to the plasma one, $\omega = \omega_P$.

that this is an abuse of nomenclature, as the dispersion relation for transverse modes only really approaches that of a massive particle for short wavelengths $k \gg \omega_P$. Our definition of m_γ differs slightly from the standard one (e.g. [69]), by up to a factor of 3/2 in the relativistic limit.

At very early times in the history of the Universe, the plasma is comprised primarily of e^+e^- pairs (before e^+e^- annihilation) and ionized hydrogen atoms (after e^+e^- annihilation). This entails that the interactions of photons with the medium are indeed dominated by Coulomb scattering with electrons and positrons. However, at lower temperatures the protons and electrons recombine to form neutral atoms and the free electron density becomes very small. As a result, the scattering off hydrogen and helium atoms cannot generally be neglected anymore and there is an additional contribution to the transverse photon mass, which becomes [74]

$$m_\gamma^2 \simeq \omega_P^2 - 2\omega^2(\mathrm{n}-1)_\mathrm{H} - 2\omega^2(\mathrm{n}-1)_\mathrm{He}. \tag{B.8}$$

Here, $\mathrm{n}_X \equiv \mathrm{n}_X(n_X)$ is the refractive index, which is proportional the density of atoms of the species X. The contribution from helium can be neglected because it is less abundant (it has a mass fraction $Y_p = m_\mathrm{He}/m_\mathrm{H} \simeq 0.25$) and its refractive index, $(\mathrm{n}-1)_\mathrm{He} = 0.36\times10^{-4}$, is much smaller than the hydrogen one, $(\mathrm{n}-1)_\mathrm{H} = 1.32\times10^{-4}$ (values for normal conditions [76]). The transverse photon mass can then be given as a function of the proton density n_p and the ionization fraction X_e as

$$m_\gamma^2 = 1.4\times10^{-21}\,\mathrm{eV}^2\left(X_e - 7.7\times10^{-3}\left(\frac{\omega}{\mathrm{eV}}\right)^2(1-X_e)\right)\frac{n_p}{\mathrm{cm}^{-3}}. \tag{B.9}$$

One may worry that during the dark ages, the negative contribution from the scattering off neutral hydrogen can drive m_γ^2 to be negative for high-frequency photons. This does however not play any role in our analysis, given that the photons produced from resonant ALP decays have frequencies only slightly above ω_P, too small for the second term in eq. (B.9) to be relevant. Putting everything together, we obtain the profile for the cosmological history of the plasma mass of the photon shown in figure 3, both as a function of temperature and redshift (figure 2 shows the corresponding line as a function of the Hubble parameter). For the calculation, we fix $\omega = \omega_P$ and use the ionization fraction profile from [74].

JCAP03(2020)052

References

[1] L.F. Abbott and P. Sikivie, *A cosmological bound on the invisible axion*, *Phys. Lett.* **B 120** (1983) 133 [INSPIRE].

[2] J. Preskill, M.B. Wise and F. Wilczek, *Cosmology of the invisible axion*, *Phys. Lett.* **B 120** (1983) 127 [INSPIRE].

[3] M. Dine and W. Fischler, *The not so harmless axion*, *Phys. Lett.* **B 120** (1983) 137 [INSPIRE].

[4] P. Arias, D. Cadamuro, M. Goodsell, J. Jaeckel, J. Redondo and A. Ringwald, *WISPy cold dark matter*, *JCAP* **06** (2012) 013 [arXiv:1201.5902] [INSPIRE].

[5] G. Alonso-Álvarez, J. Gehrlein, J. Jaeckel and S. Schenk, *Very light asymmetric dark matter*, *JCAP* **09** (2019) 003 [arXiv:1906.00969] [INSPIRE].

[6] D.-S. Lee and K.-W. Ng, *Photon production of axionic cold dark matter*, *Phys. Rev.* **D 61** (2000) 085003 [hep-ph/9909282] [INSPIRE].

[7] E.W. Kolb, A. Singh and M. Srednicki, *Quantum fluctuations of axions*, *Phys. Rev.* **D 58** (1998) 105004 [hep-ph/9709285] [INSPIRE].

[8] A. Arvanitaki, S. Dimopoulos, M. Galanis, L. Lehner, J.O. Thompson and K. Van Tilburg, *The large-misalignment mechanism for the formation of compact axion structures: signatures from the QCD axion to fuzzy dark matter*, arXiv:1909.11665 [INSPIRE].

[9] L. McAllister, E. Silverstein and A. Westphal, *Gravity waves and linear inflation from axion monodromy*, *Phys. Rev.* **D 82** (2010) 046003 [arXiv:0808.0706] [INSPIRE].

[10] J. Jaeckel, V.M. Mehta and L.T. Witkowski, *Monodromy dark matter*, *JCAP* **01** (2017) 036 [arXiv:1605.01367] [INSPIRE].

[11] K. Choi, H. Kim and S. Yun, *Natural inflation with multiple sub-Planckian axions*, *Phys. Rev.* **D 90** (2014) 023545 [arXiv:1404.6209] [INSPIRE].

[12] K. Choi and S.H. Im, *Realizing the relaxion from multiple axions and its UV completion with high scale supersymmetry*, *JHEP* **01** (2016) 149 [arXiv:1511.00132] [INSPIRE].

[13] D.E. Kaplan and R. Rattazzi, *Large field excursions and approximate discrete symmetries from a clockwork axion*, *Phys. Rev.* **D 93** (2016) 085007 [arXiv:1511.01827] [INSPIRE].

[14] J. Halverson, C. Long, B. Nelson and G. Salinas, *Towards string theory expectations for photon couplings to axionlike particles*, *Phys. Rev.* **D 100** (2019) 106010 [arXiv:1909.05257] [INSPIRE].

[15] Y. Kahn, B.R. Safdi and J. Thaler, *Broadband and resonant approaches to axion dark matter detection*, *Phys. Rev. Lett.* **117** (2016) 141801 [arXiv:1602.01086] [INSPIRE].

[16] T.M. Shokair et al., *Future directions in the microwave cavity search for dark matter axions*, *Int. J. Mod. Phys.* **A 29** (2014) 1443004 [arXiv:1405.3685] [INSPIRE].

[17] BRASS: Broadband Radiometric Axion SearcheS, http://www.iexp.uni-hamburg.de/groups/astroparticle/brass/brassweb.htm.

[18] CAPP/IBS collaboration, *Haloscope searches for dark matter axions at the center for axion and precision physics research*, *EPJ Web Conf.* **164** (2017) 01012 [arXiv:1702.03664] [INSPIRE].

[19] HAYSTAC collaboration, *HAYSTAC status, results and plans*, in *13th conference on the intersections of particle and nuclear physics (CIPANP 2018) Palm Springs, California, U.S.A., 29 May–3 June 2018*, 2019, arXiv:1901.01668 [INSPIRE].

[20] C. Gatti et al., *The Klash proposal: status and perspectives*, in *14th Patras workshop on axions, WIMPs and WISPs (AXION-WIMP 2018) (PATRAS 2018) Hamburg, Germany, 18–22 June 2018*, 2018, arXiv:1811.06754 [INSPIRE].

JCAP03(2020)052

[21] MADMAX interest Group collaboration, *MADMAX: a new road to axion dark matter detection*, *J. Phys. Conf. Ser.* **1342** (2020) 012098 [arXiv:1712.01062] [inSPIRE].

[22] B.T. McAllister, G. Flower, E.N. Ivanov, M. Goryachev, J. Bourhill and M.E. Tobar, *The ORGAN experiment: an axion haloscope above 15 GHz*, *Phys. Dark Univ.* **18** (2017) 67 [arXiv:1706.00209] [inSPIRE].

[23] D. Alesini et al., *Galactic axions search with a superconducting resonant cavity*, *Phys. Rev.* **D 99** (2019) 101101 [arXiv:1903.06547] [inSPIRE].

[24] A.A. Melcon et al., *Axion searches with microwave filters: the RADES project*, *JCAP* **05** (2018) 040 [arXiv:1803.01243] [inSPIRE].

[25] **IAXO** Collaboration, I. Irastorza et al., *The international axion observatory IAXO. Letter of intent to the CERN SPS committee*, CERN Report CERN-SPSC-2013-022.

[26] .A. Caputo, C.P. Garay and S.J. Witte, *Looking for axion dark matter in dwarf spheroidals*, *Phys. Rev.* **D 98** (2018) 083024 [*Erratum ibid.* **D 99** (2019) 089901] [arXiv:1805.08780] [inSPIRE].

[27] A. Caputo, M. Regis, M. Taoso and S.J. Witte, *Detecting the stimulated decay of axions at radiofrequencies*, *JCAP* **03** (2019) 027 [arXiv:1811.08436] [inSPIRE].

[28] D. Espriu and A. Renau, *Photon propagation in a cold axion background with and without magnetic field*, *Phys. Rev.* **D 85** (2012) 025010 [arXiv:1106.1662] [inSPIRE].

[29] D. Yoshida and J. Soda, *Electromagnetic waves propagating in the string axiverse*, *PTEP* **2018** (2018) 041E01 [arXiv:1710.09198] [inSPIRE].

[30] I.I. Tkachev, *Coherent scalar field oscillations forming compact astrophysical objects*, *Sov. Astron. Lett.* **12** (1986) 305 [inSPIRE].

[31] I.I. Tkachev, *An axionic laser in the center of a galaxy?*, *Phys. Lett.* **B 191** (1987) 41 [inSPIRE].

[32] I.I. Tkachev, *Astrophysical axionic lasers*, (1987).

[33] T.W. Kephart and T.J. Weiler, *Luminous axion clusters*, *Phys. Rev. Lett.* **58** (1987) 171 [inSPIRE].

[34] T.W. Kephart and T.J. Weiler, *Stimulated radiation from axion cluster evolution*, *Phys. Rev.* **D 52** (1995) 3226 [inSPIRE].

[35] I.I. Tkachev, *Fast radio bursts and axion miniclusters*, *JETP Lett.* **101** (2015) 1 [arXiv:1411.3900] [inSPIRE].

[36] M.P. Hertzberg and E.D. Schiappacasse, *Dark matter axion clump resonance of photons*, *JCAP* **11** (2018) 004 [arXiv:1805.00430] [inSPIRE].

[37] R.F. Sawyer, *Axion, photon-pair mixing in models of axion dark matter*, arXiv:1809.01183 [inSPIRE].

[38] A. Arza, *Photon enhancement in a homogeneous axion dark matter background*, *Eur. Phys. J.* **C 79** (2019) 250 [arXiv:1810.03722] [inSPIRE].

[39] G. Sigl and P. Trivedi, *Axion condensate dark matter constraints from resonant enhancement of background radiation*, arXiv:1907.04849 [inSPIRE].

[40] J.G. Rosa and T.W. Kephart, *Stimulated axion decay in superradiant clouds around primordial black holes*, *Phys. Rev. Lett.* **120** (2018) 231102 [arXiv:1709.06581] [inSPIRE].

[41] S. Sen, *Plasma effects on lasing of a uniform ultralight axion condensate*, *Phys. Rev.* **D 98** (2018) 103012 [arXiv:1805.06471] [inSPIRE].

[42] T. Ikeda, R. Brito and V. Cardoso, *Blasts of light from axions*, *Phys. Rev. Lett.* **122** (2019) 081101 [arXiv:1811.04950] [inSPIRE].

JCAP03(2020)052

[43] A. Arza and P. Sikivie, *Production and detection of an axion dark matter echo*, *Phys. Rev. Lett.* **123** (2019) 131804 [arXiv:1902.00114] [INSPIRE].

[44] P. Agrawal, G. Marques-Tavares and W. Xue, *Opening up the QCD axion window*, *JHEP* **03** (2018) 049 [arXiv:1708.05008] [INSPIRE].

[45] N. Kitajima, T. Sekiguchi and F. Takahashi, *Cosmological abundance of the QCD axion coupled to hidden photons*, *Phys. Lett.* **B 781** (2018) 684 [arXiv:1711.06590] [INSPIRE].

[46] P. Agrawal, N. Kitajima, M. Reece, T. Sekiguchi and F. Takahashi, *Relic abundance of dark photon dark matter*, *Phys. Lett.* **B 801** (2020) 135136 [arXiv:1810.07188] [INSPIRE].

[47] R.T. Co, A. Pierce, Z. Zhang and Y. Zhao, *Dark photon dark matter produced by axion oscillations*, *Phys. Rev.* **D 99** (2019) 075002 [arXiv:1810.07196] [INSPIRE].

[48] P.W. Graham, J. Mardon and S. Rajendran, *Vector dark matter from inflationary fluctuations*, *Phys. Rev.* **D 93** (2016) 103520 [arXiv:1504.02102] [INSPIRE].

[49] J.A. Dror, K. Harigaya and V. Narayan, *Parametric resonance production of ultralight vector dark matter*, *Phys. Rev.* **D 99** (2019) 035036 [arXiv:1810.07195] [INSPIRE].

[50] M. Bastero-Gil, J. Santiago, L. Ubaldi and R. Vega-Morales, *Vector dark matter production at the end of inflation*, *JCAP* **04** (2019) 015 [arXiv:1810.07208] [INSPIRE].

[51] G. Alonso-Álvarez, J. Jaeckel and T. Hugle, *Misalignment & Co.: (pseudo-)scalar and vector dark matter with curvature couplings*, *JCAP* **02** (2020) 014 [arXiv:1905.09836] [INSPIRE].

[52] Y. Ema, K. Nakayama and Y. Tang, *Production of purely gravitational dark matter: the case of fermion and vector boson*, *JHEP* **07** (2019) 060 [arXiv:1903.10973] [INSPIRE].

[53] K. Nakayama, *Vector coherent oscillation dark matter*, *JCAP* **10** (2019) 019 [arXiv:1907.06243] [INSPIRE].

[54] C.S. Machado, W. Ratzinger, P. Schwaller and B.A. Stefanek, *Audible axions*, *JHEP* **01** (2019) 053 [arXiv:1811.01950] [INSPIRE].

[55] J. Berges, A. Chatrchyan and J. Jaeckel, *Foamy dark matter from monodromies*, *JCAP* **08** (2019) 020 [arXiv:1903.03116] [INSPIRE].

[56] J. Redondo, *Bounds on very weakly interacting sub-eV particles (WISPs) from cosmology and astrophysics*, in *Proceedings, 4th Patras workshop on axions, WIMPs and WISPs (AXION-WIMP 2008): Hamburg, Germany, 18–21 June 2008*, pp. 23–26, (2008) [arXiv:0810.3200].

[57] J. Jaeckel and A. Ringwald, *The low-energy frontier of particle physics*, *Ann. Rev. Nucl. Part. Sci.* **60** (2010) 405 [arXiv:1002.0329].

[58] I.G. Irastorza and J. Redondo, *New experimental approaches in the search for axion-like particles*, *Prog. Part. Nucl. Phys.* **102** (2018) 89 [arXiv:1801.08127] [INSPIRE].

[59] N.W. McLachlan, *Theory and application of Mathieu functions*, Clarendon Press, (1947).

[60] I. Kovacic, R. Rand, and S.M. Sah, *Mathieu's equation and its generalizations: overview of stability charts and their features*, *Appl. Mech. Rev.* **70** (2018) 020802.

[61] J.H. Traschen and R.H. Brandenberger, *Particle production during out-of-equilibrium phase transitions*, *Phys. Rev.* **D 42** (1990) 2491 [INSPIRE].

[62] L. Kofman, A.D. Linde and A.A. Starobinsky, *Reheating after inflation*, *Phys. Rev. Lett.* **73** (1994) 3195 [hep-th/9405187] [INSPIRE].

[63] Y. Shtanov, J.H. Traschen and R.H. Brandenberger, *Universe reheating after inflation*, *Phys. Rev.* **D 51** (1995) 5438 [hep-ph/9407247] [INSPIRE].

[64] D. Boyanovsky, H.J. de Vega, R. Holman and J.F.J. Salgado, *Analytic and numerical study of preheating dynamics*, *Phys. Rev.* **D 54** (1996) 7570 [hep-ph/9608205] [INSPIRE].

JCAP03(2020)052

[65] L. Kofman, A.D. Linde and A.A. Starobinsky, *Towards the theory of reheating after inflation*, *Phys. Rev.* **D 56** (1997) 3258 [hep-ph/9704452] [INSPIRE].

[66] J. Berges and J. Serreau, *Parametric resonance in quantum field theory*, *Phys. Rev. Lett.* **91** (2003) 111601 [hep-ph/0208070] [INSPIRE].

[67] D. Baumann, *The physics of inflation: a course for graduate students in particle physics and cosmology*.

[68] R.S. Gupta, Z. Komargodski, G. Perez and L. Ubaldi, *Is the relaxion an axion?*, *JHEP* **02** (2016) 166 [arXiv:1509.00047] [INSPIRE].

[69] G.G. Raffelt, *Stars as laboratories for fundamental physics*, Chicago University Press, (1996), http://wwwth.mpp.mpg.de/members/raffelt/mypapers/199613.pdf.

[70] E. Braaten and D. Segel, *Neutrino energy loss from the plasma process at all temperatures and densities*, *Phys. Rev.* **D 48** (1993) 1478 [hep-ph/9302213] [INSPIRE].

[71] F. Nicastro et al., *Observations of the missing baryons in the warm-hot intergalactic medium*, arXiv:1806.08395 [INSPIRE].

[72] J. Ahonen, K. Enqvist and G. Raffelt, *The paradox of axions surviving primordial magnetic fields*, *Phys. Lett.* **B 366** (1996) 224 [hep-ph/9510211] [INSPIRE].

[73] J. Redondo and M. Postma, *Massive hidden photons as lukewarm dark matter*, *JCAP* **02** (2009) 005 [arXiv:0811.0326] [INSPIRE].

[74] A. Mirizzi, J. Redondo and G. Sigl, *Microwave background constraints on mixing of photons with hidden photons*, *JCAP* **03** (2009) 026 [arXiv:0901.0014] [INSPIRE].

[75] C. Dvorkin, T. Lin and K. Schutz, *Making dark matter out of light: freeze-in from plasma effects*, *Phys. Rev.* **D 99** (2019) 115009 [arXiv:1902.08623] [INSPIRE].

[76] E. Hecht, *Optics, 5th Edition*, Pearson Education, (2017).

JCAP03(2020)052

Chapter 5

Exploring ALPs beyond the canonical

Author:
Gonzalo Alonso-Álvarez and Joerg Jaeckel

Published in *Phys.Rev.D 98 (2018) 2, 023539*,
also available at arXiv:1712.07500

Gonzalo Alonso-Álvarez is the principal author of this article. The original idea for the project was conceived by Joerg Jaeckel and further developed by both authors. All the calculations were performed by Gonzalo Alonso-Álvarez and all figures were produced by Gonzalo Alonso-Álvarez. The article was originally written by Gonzalo Alonso-Álvarez, and Joerg Jaeckel contributed with corrections and suggestions. Both authors participated equally in the review process.

Exploring axionlike particles beyond the canonical setup

Gonzalo Alonso-Álvarez and Joerg Jaeckel
Institut für Theoretische Physik, Universität Heidelberg, Philosophenweg 16, 69120 Heidelberg, Germany

(Received 26 April 2018; published 27 July 2018)

Axionlike particles (ALPs) are interesting dark matter candidates from both the theoretical and the experimental perspective. Usually they are motivated as pseudo-Nambu-Goldstone bosons. In this case one of their most important features is that their coupling to other particles is suppressed by a large scale, the vacuum expectation value of the field breaking the symmetry that gives rise to them. This naturally endows them with very weak interactions but also restricts the maximal field value and therefore the regions where sufficient dark matter is produced. In this paper we investigate deviations from this simplest setup, where the potential and interactions are as expected for a pseudo-Nambu-Goldstone boson, but the kinetic term has singularities. This leads to a significantly increased area in parameter space where such particles can be dark matter and can be probed by current and near future experiments. We discuss cosmological limits and in the course of this give a simple derivation of a formula for isocurvature fluctuations in models with general anharmonic potentials. As an application of this formula we give an update of the isocurvature constraints for QCD axion dark matter models, using the most recent results for the QCD topological susceptibility and the newest Planck data.

DOI: 10.1103/PhysRevD.98.023539

I. INTRODUCTION

Axions and axionlike particles (ALPs) are a prediction of some of the best-motivated beyond the standard model physics scenarios (see, e.g., [1–3] for reviews). Many of their properties are determined by two quantities: the mass, m, and the so-called decay constant, f_a. An important feature that all these particles share is that they enjoy a shift symmetry, a discrete version of which is preserved at the quantum level. The existence of this symmetry protects their potential from quantum corrections that could otherwise be very large. In the framework of quantum field theory, such particles arise as pseudo-Nambu-Goldstone bosons of approximate global chiral symmetries [4–9]. In other setups such as supergravity or string theory, particles with similar properties appear in the spectrum. For instance, ALPs are a general consequence of the compactification of extra dimensions and string theory [10–16]. In that context, there can be dozens of such particles whose potentials, kinetic terms and interactions may contain a large number of free parameters. In an attempt to accommodate all these similar particle candidates, we will talk about ALPs in the general sense of a light (pseudo)scalar particle, and we will reserve the term "axion" to refer to ALPs that couple to the gluon field strength tensor through the QCD topological term and solve the strong CP problem.

Axionlike particles are excellent candidates to account for some or all the dark matter that we observe in the Universe [17–20]. Cosmological and astrophysical observations tell us that dark matter particles should be weakly interacting, stable at cosmological scales and cold. ALPs can naturally fulfill all these requirements. First, the discrete shift symmetry constrains their possible couplings to other fields, and those that are allowed are typically suppressed by f_a, which can be a large energy scale. This fact, together with their small mass which limits the possible number and type of decay products as well as the phase space, makes them extremely stable. Naively, the fact that they are very light might seem to contradict the requirement that the ALP dark matter population should be cold. However, it is easy to see that this is not necessarily the case. Because of their feeble interactions with other particles, ALPs are not produced thermally, but rather by the so-called misalignment mechanism, which yields a very nonrelativistic population of ALPs that behave as cold dark matter [17,19,21–23].

All in all, ALPs and axions are well-motivated dark matter candidates, but their possible mass and decay constant span many orders of magnitude, thereby providing a significant challenge for experimental tests. Fortunately, their properties, in particular their low mass, also provides for new opportunities for experimental searches and theoretical arguments that can be used to probe their parameter space (see [24] for a recent review).

Experimental tests are usually dependent on the coupling to Standard Model particles. One example is a coupling to two gluons,

$$\mathcal{L} \supset \frac{\alpha}{8\pi f_a}\phi G_{\mu\nu}\tilde{G}^{\mu\nu}. \tag{1}$$

This coupling also induces a coupling to a nucleon electric dipole moment (EDM),

$$\mathcal{L} \subset g_d \phi \bar{N}\sigma_{\mu\nu}F^{\mu\nu}N \tag{2}$$

that is particularly important for searches when ϕ is dark matter.[1] The coupling constants are related via [26,27]

$$g_d \approx \frac{2.4\times 10^{-16}}{f_a}\,\mathrm{e}\cdot\mathrm{cm} \approx 3.4\times 10^{3}\ \mathrm{GeV}^{-2}\left(\frac{\mathrm{GeV}}{f_a}\right). \tag{3}$$

Figure 1 summarizes the constraints that can be cast on the canonical ALP dark matter scenario from these interactions with the visible sector. In addition we show limits that arise from unavoidable gravitational interactions.

Unfortunately, some of the theoretically favored existing models require high decay constants for the ALPs to be able to account for all the dark matter energy density that we observe in our Universe. This means that some of the better-motivated combinations of (m, f_a) are not in the best position to be tested, be it through gravitational interactions or through couplings to gluons and nucleons or photons. It is therefore timely to search for models that can accommodate low enough values of f_a that can be in reach of these searches, while still being able to produce the required dark matter abundance. One option is to enlarge the field range by a monodromy [36–38] as done in [39].

In this paper we pursue the same goal by employing a nonstandard kinetic term for the ALP field. This is a possibility that has been exploited in the literature [40,41] in the context of inflationary models (though not so much for axion inflation), but to our knowledge such a study has not been performed for dark matter models. As we will see, a very rich phenomenology arises when this possibility is allowed. Of special interest is that this scenario will indeed be able to populate regions of the parameter space that can be tested in the near future, either with astrophysical observations or experimental searches. Focusing on the coupling to nucleons, the main motivation for us in this respect is threefold. First, as was already argued, we want to explore the possibility of building an ALP dark matter model with a larger such coupling. Second, we ask ourselves if these models could lie on the region of parameter space to the left of the QCD axion band in Fig. 1. Finally and concerning the big bang nucleosynthesis bound that seems to restrict this area of parameter space, we would like to test its robustness constraining such ALP models.

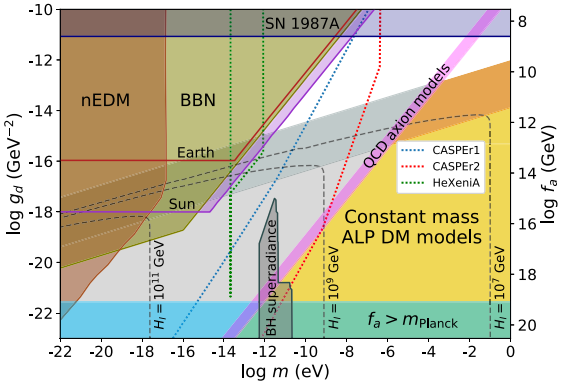

FIG. 1. Parameter space for canonical axionlike particles, considering gravitational effects and interactions derived from the QCD $G\tilde{G}$ term. On the horizontal axis we plot the mass of the ALP, while the vertical axis gives the decay constant f_a on the right and the effective coupling to nucleons $g_d \propto f_a^{-1}$ on the left. Canonical ALP models with a constant mass can only generate enough dark matter via the misalignment mechanism in the yellow and grey shaded areas. Accounting for the anharmonicities of the potential and allowing for a fine-tuned initial condition, this region can be enlarged to also include the orange band (we take the lowest viable Hubble scale of inflation, $H_I \sim 4.5\times 10^{-23}$ GeV). Note that the QCD axion models are restricted to lie on the magenta line. Taking the interaction to be given by Eq. (1), the region to the left of the QCD axion line is disfavored by the unavoidable (temperature-dependent) contribution to the mass from QCD effects [28] (see also Sec. V). This region is shown in light grey. The dark blue region is excluded by the supernova limits estimated in [29]. Shaded in brown is the area where experiments looking for a static nuclear electric dipole moment (nEDM) (see [30]) would have found the oscillating one, while the dotted lines represent sensitivity estimates for future oscillating EDM experiments [31,32]. In the dark green region "BBN" ALPs coupled to QCD are inconsistent with the production of the observed abundance of light elements during big bang nucleosynthesis [28]. The violet and dark red lines dubbed "Earth" and "Sun" correspond to constraints from the ALP field being sourced by dense astrophysical objects [33]. The dark grey area is disfavored by the observation of quickly rotating stellar black holes which would have been spun down in a superradiant process (from [34]). The area above the dashed black lines, plotted for different values of the Hubble scale of inflaton H_I, is disfavored due to the generation of too much power in isocurvature perturbations at the scales probed by the Planck satellite [35] (see more details in Sec. IV). Finally, f_a is (softly) bounded from above by the requirement that it does not exceed the Planck scale.

[1]The coupling (1) also induces tree-level P, T-violating forces between nucleons, which can give a larger contribution to atomic EDMs than the loop-induced nucleon EDMs [25]. This is relevant for EDM experiments that use atoms instead of free neutrons, like some of the ones presented in Fig. 1. For those, the limits and projections should be understood as applying directly to f_a and not g_d.

In this work we study the viability of ALPs with a noncanonical kinetic term as dark matter candidates from a purely phenomenological perspective. Let us nevertheless briefly mention some of the mechanisms that can give rise to this scenario. For instance, a nonminimal coupling of the ALP field to gravity in the so-called Jordan frame induces a noncanonical kinetic function in the usual Einstein frame. In the context of supergravity, an explicit breaking of the shift symmetry in the Kähler potential also results in nonstandard kinetic terms for the ALP. Finally, in the context of compactifications, string theory *a priori* contains all the necessary ingredients to generate axions with noncanonical kinetic terms, caused, for example, by backreaction effects. However, no explicit construction of the models that we consider in this work exists as of today, and this task is beyond the scope of this paper. We leave the study of the possibility of embedding this phenomenological study in a more complete framework for future work.

This paper is structured as follows: in Sec. II we discuss the effects of noncanonical kinetic terms and set up our explicit case study. In Sec. III we study how these modified kinetic terms affect the cosmological evolution of the ALP field, and in Sec. IV we analyze the isocurvature perturbations predicted in this setup. In Sec. V we discuss the impact of allowing for a coupling to QCD in this scenario, and we conclude in Sec. VI.

Before getting started on the details we note that, although in this paper we focus mainly on the example of gluon interactions, most of our discussion is completely general and can be applied to any other coupling. Moreover, while the structure of interactions that we consider is inspired by that of pseudo-Nambu-Goldstone bosons, the essential qualitative features should also apply in the case of more general scalars and only depends on the singularities of the noncanonical kinetic terms.

II. NONCANONICAL KINETIC TERMS

In this section we examine the effect that a nonstandard kinetic term can have on the dynamics of the ALP field. Let us start with the Lagrangian

$$\mathcal{L} = \frac{1}{2}K^2(\phi)\partial^\mu\phi\partial_\mu\phi - V(\phi), \tag{4}$$

where we have allowed for a general real scalar (and positive definite) function of ϕ, $K^2(\phi)$, to scale the kinetic term and thus render it not canonically normalized. For definiteness, we will work with the usual periodic potential for ALP fields,

$$V(\phi) = \Lambda^4\left(1 - \cos\frac{\phi}{f_a}\right). \tag{5}$$

We now proceed by performing a field redefinition to obtain the canonically normalized field. The formal solution is to define

$$\varphi(\phi) = \int K(\phi)d\phi \equiv g(\phi), \tag{6}$$

and thus the Lagrangian for φ is

$$\mathcal{L}(\varphi) = \frac{1}{2}\partial^\mu\varphi\partial_\mu\varphi - V(g^{-1}(\varphi)). \tag{7}$$

Being canonically normalized, φ is the physical (propagating) field. Let us see what kinds of functions K result in φ being a viable dark matter candidate.

The first condition is that φ behaves like cold dark matter in the late Universe. This requires that it oscillate harmonically at late times (see, e.g., [17]). Accordingly the kinetic term should not modify the dynamics close to the origin. This is automatic if the kinetic term approaches a nonvanishing constant value close to the origin,

$$K \to \text{const} = 1 \quad \text{for } \varphi \to 0. \tag{8}$$

As indicated in the equation, this constant can be chosen to be equal to 1 by a suitable choice of normalization.

So why should we now choose a nontrivial function for K and what shall we choose? As already mentioned in the Introduction, we would like to find a model with larger couplings, i.e., smaller f_a, that still gives a sufficient dark matter density. Roughly speaking the problem of obtaining a sufficient energy density can be understood as follows. For the potential Eq. (5) the maximal initial energy density is given by Λ^4. This is linked to the mass m of the particle via $\Lambda^4 = m^2 f_a^2$. If f_a is too small the initial and in consequence the final energy density is too small to make up all of the dark matter.

One way to avoid this problem would be to break the periodicity of the potential (5) such that the potential continues to grow for large field values, e.g., by exploiting a monodromy [39].

Here we will explore a different strategy. As long as the Hubble constant is sufficiently large the evolution of the field is frozen and the energy density is approximately constant. As discussed below the evolution and consequently the dilution of the energy starts when $H^2 \sim |V''(\varphi)|$. Hence, we can increase the energy density today by choosing the kinetic function K such that the potential becomes very flat for large field values.[2] A cartoon of this is shown in Fig. 2.

[2]An alternative is to start in a region of field space where $V'(\varphi)$ is very small; i.e., the field is close to a maximum. However, this is strongly limited by the existence of inflationary fluctuations [42,43] (see also Sec. IV).

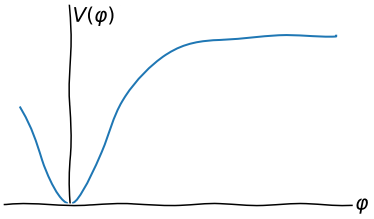

FIG. 2. Slow-roll-like potential.

Using

$$\frac{\partial V}{\partial \varphi} = \frac{\partial V}{\partial \phi} \cdot \frac{\partial \phi}{\partial \varphi} = \frac{1}{K} \frac{\partial V}{\partial \phi}, \tag{9}$$

we see that this can be easily achieved if K has a singularity at some field value $\phi = a$,

$$K \to \infty \quad \text{for } \varphi \to a. \tag{10}$$

This singular structure has an additional advantage: The noncanonically normalized field ϕ will never exceed $\phi = a$ during its evolution. Limits such as the one discussed in Sec. V D arising from big bang nucleosythesis (BBN) that are based on a sizable field value at some earlier epoch can thus be avoided if a is sufficiently small.

A simple function that satisfies the above requirements while keeping the periodic properties intact is

$$K(\phi) = \frac{1}{\cos\left(\frac{N\phi}{f_a}\right)}. \tag{11}$$

While this choice might seem rather arbitrary at first, there are some arguments that make it more general than it seems. The approach for obtaining a flattened potential for a scalar via a noncanonical kinetic term has been widely used in the context of inflationary cosmology [40,41]. Indeed over the last years, α-attractor models [44,45] have attracted special attention. In this context, the authors of [46] showed that the determining property of this class of models is the existence of a pole in the kinetic term. More precisely, it is the order and the residue of the pole that play a key role, and not so much the precise functional form of the kinetic function. We can therefore be confident that our results will not depend much on the specific choice of K. Similarly to [46], here we focus on the case of a second-order pole. As we mentioned before, this case is better motivated and may arise, for instance, as a consequence of a nonminimal coupling to gravity. Nevertheless, we check in Appendix A that our main conclusions remain unchanged if we allow for higher-order poles.

Also, recall that the shift symmetry $\phi \to \phi + \text{const}$ of the ALP field is what protects its mass from large corrections. It thus seems sensible to preserve or only slightly break this symmetry. Indeed, by our choice of potential Eq. (5), we are assuming that a small explicit breaking is present. This breaking typically occurs at the nonperturbative level [47,48] and crucially preserves the discrete shift symmetry $\phi \to \phi + 2k\pi f_a$, which allows us to retain a sufficient level of protection against quantum corrections. We would like the kinetic term to preserve, at least, this discrete shift symmetry, which requires that $K(\phi)$ be a periodic function of ϕ/f_a. These arguments quickly lead us to Eq. (11). Once again, we stress that the fact that we are writing a specific kinetic term should not be understood as a construction of a complete model, bur rather as a benchmark for our phenomenological study.

The transformation to the canonically normalized field is given by

$$\varphi(\phi) = \frac{2f_a}{N} \operatorname{arctanh}\left(\tan\frac{N\phi}{2f_a}\right). \tag{12}$$

We should note that the poles of $K(\phi)$ are located at $\phi/f_a = \pi/(2N)$. This means that, when doing the field redefinition (12), we are restricting the field space to $\phi/f_a \in (-\frac{\pi}{2N}, \frac{\pi}{2N})$. As already mentioned above this will become important when discussing the limits arising from a gluon coupling in Sec. V. In principle there exist a total of N different branches $\phi/f_a \in ((k-\frac{1}{2})\frac{\pi}{N}, (k+\frac{1}{2})\frac{\pi}{2N})$ where the field could be trapped. However, the only one which has a minimum in the potential is the one closest to the origin. In other branches, the field would slow-roll towards infinity,[3] making them unappealing for the phenomenological purposes that we have in mind. For this reason, we focus on the phenomenologically viable region around zero.

Using the field redefinition (12) the Lagrangian for the canonically normalized field is given by

$$\mathcal{L} = \frac{1}{2}\partial^\mu\varphi\partial_\mu\varphi - \Lambda^4\left[1 - \cos\left(\frac{2}{N}\arctan\left(\tanh\frac{N\varphi}{2f_a}\right)\right)\right]. \tag{13}$$

By expanding about the origin, it can be checked that we indeed recover the quadratic behavior for small field values. The potential is plotted in Fig. 3 for different values of N. It indeed looks quite similar to what we imagined in Fig. 2.

What about the equations of motion? Let us assume that we have a homogeneous and isotropic field, $\phi = \phi(t)$ and consequently $\varphi = \varphi(t)$. The Klein-Gordon equation for a homogeneous and isotropic field in an expanding spacetime is

[3]In principle one could have tunneling between different branches. If the decay time of the metastable vacuum is small enough, the field would always eventually end up in the branch closest to zero. However, a calculation of the tunneling rate is highly model dependent and beyond the scope of this work.

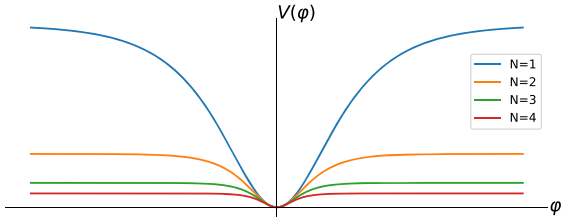

FIG. 3. Potential for the canonically normalized field, plotted for various values of N. Note that the potential is quadratic for small field values but flattens away from the origin.

$$\ddot{\varphi} + 3H\dot{\varphi} + \partial_{\varphi}V(\varphi) = 0, \tag{14}$$

where H is the Hubble expansion parameter.

For convenience we introduce the dimensionless field variable,

$$\psi = \varphi/f_a, \tag{15}$$

in analogy to how the θ angle relates to the original axion field. Thus, we will be expressing the field value in terms of f_a units. The equation of motion can then be written as

$$\ddot{\psi} + 3H\dot{\psi} + m^2 \frac{1}{\cosh N\psi} \sin\left[\frac{2}{N}\arctan\left(\tanh\frac{N\psi}{2}\right)\right] = 0, \tag{16}$$

where we define

$$m^2 = \frac{\Lambda^4}{f_a^2}, \tag{17}$$

which corresponds to the second derivative of the physical field around the minimum at $\psi = \varphi = \phi = 0$. m is the physical mass of the dark matter particles.

III. COSMOLOGICAL EVOLUTION AND DARK MATTER PRODUCTION

The goal of this section is to find an estimate for the dark matter density in the model defined above and compare it with the observed abundance. The energy density of the field depends on the parameters (f_a, m, N), as well as the initial conditions for the field and its cosmological evolution. For this purpose it is useful to briefly recall the misalignment mechanism [21–23], which gives us the basic idea of how our field evolves in a cosmological setup.

A. The misalignment mechanism

Here we briefly summarize how a misaligned light scalar field evolves in an expanding spacetime, closely following the description in [17]. Let us consider the simplified case of a real scalar field with Lagrangian

$$\mathcal{L} = \frac{1}{2}\partial_\mu\phi\partial^\mu\phi - \frac{1}{2}m_\phi^2\phi^2. \tag{18}$$

Note that our final goal is not the harmonic case but a more complicated potential with strong anharmonicities. However, solving this simplified equation will give us helpful insights to tackle the anharmonic potential. In a homogeneous setting, the equation of motion for ϕ is

$$\ddot{\phi} + 3H\dot{\phi} + m_\phi^2\phi = 0. \tag{19}$$

This is the equation of a damped harmonic oscillator. There are two distinct regimes in the evolution of ϕ. First, at very early times when $3H \gg m_\phi$, the oscillator is overdamped and so the solution is $\dot{\phi} = 0$, and the field is stuck at its initial value. At a later time t_1 such that $3H(t_1) = m_\phi$, the damping has decreased enough so that the field can start to oscillate. The equation of motion for the oscillating regime can then be solved using the WKB approximation:

$$\phi(t) \simeq \phi(t_1)\left(\frac{a(t_1)}{a(t)}\right)^{3/2}\cos\left(m_\phi(t - t_1)\right), \tag{20}$$

where $a(t)$ is the scale factor. We see that the energy density, which is proportional to the amplitude of the oscillations squared, dilutes with expansion as a^{-3}. This means that the oscillating field behaves like pressureless matter for all processes mediated by gravitation. In this simplified setup, the energy density in the axion field today is

$$\rho_\phi(t_0) \simeq 0.17\frac{\text{keV}}{\text{cm}^3}\sqrt{\frac{m_\phi}{\text{eV}}}\left(\frac{\phi_0}{10^{11}\text{ GeV}}\right)^2\mathcal{F}(T_1), \tag{21}$$

where

$$\mathcal{F}(T_1) = \frac{(g_\star(T_1)/3.36)^{\frac{3}{4}}}{(g_{\star S}(T_1)/3.91)} \tag{22}$$

is a smooth function (cf. [17]) that varies from 1 to ~0.3 when $T_1 \in (T_0, 200\text{ GeV})$. The last result assumes that the field starts oscillating during radiation domination and that the comoving entropy is conserved.

B. Analytical estimate of the dark matter density

After this small detour to explain the misalignment mechanism for the harmonic potential, let us go back to our case of interest: the ALP field with a nonstandard kinetic term. Recall that the equation of motion that we have obtained for the physical field ψ is

$$\ddot{\psi} + 3H\dot{\psi} + m^2\frac{1}{\cosh N\psi}\sin\left[\frac{2}{N}\arctan\left(\tanh\frac{N\psi}{2}\right)\right] = 0. \tag{23}$$

We see that in the limit of small ψ, when $N\psi \ll 1$, this reduces to the simplified case (19) and the evolution is exactly as we described in the simple real scalar field case. However, the situation is different in the regime $N\psi \gtrsim 1$. As we can expect by looking at Fig. 3, the flatness of the potential away from the minimum at $\psi = 0$ will have the effect of delaying the start of the oscillations. Moreover, the oscillations, once they start, will not be harmonic until the damping has made the amplitude decrease enough to be in the small field regime. This means that the WKB approximation might not be as good in this case.

Although we suspect that the WKB approximation might break down when the amplitude of the oscillations is big due to the anharmonicity of the potential, we will use it as a first approximation to solve the equation of motion and get an analytical estimate of the result. We will later contrast this to a more precise numerical computation. In the analytical approach, we will study the two regimes, where the damping is over- and undercritical, respectively, and build up the global evolution of the field by gluing together the solution for each regime. Our goal is to compute the current energy density of dark-matter-like particles given an initial condition for the physical field.

As we saw, the first thing to do is to find the time when the oscillations start. In analogy with the simple case, where the condition was $3H = m_\phi$, we use a generalization of this formula for a nonharmonic potential, namely

$$3H = |V''(\psi_0)|^{1/2}. \tag{24}$$

In Sec. III C we will see that this indeed works reasonably well to determine when the oscillations start, as it takes into account the flatness of the potential away from the origin. In the limit of large $N\psi \gg 1$, the second derivative of the potential can be written as

$$V''(\psi) \simeq -2Nm^2 \exp^{-N\psi} \sin\frac{\pi}{2N}. \tag{25}$$

This turns out to be a very good approximation for intermediate and even small values of $N\psi$. One key difference with the harmonic case is that here the point in time when oscillations begin depends on the initial field value φ_0. With this we already see that the oscillations are exponentially delayed for big $N\psi$:

$$\begin{aligned} t_s \equiv t_{\rm start} &= \frac{3}{2|V''(\psi_0)|^{1/2}} \\ &\simeq \frac{3}{2m}\left(2N\sin\frac{\pi}{2N}\right)^{-1/2} \exp^{\frac{N\psi_0}{2}} \propto \exp^{\frac{N\psi_0}{2}}, \end{aligned} \tag{26}$$

where we have assumed radiation domination so that $H = 1/(2t)$. We now use this as an initial condition for the WKB approximation. In this approximation, the energy density of the physical field φ is

$$\rho_\varphi(T) = \frac{1}{2}m^2 f_a^2 \psi_0^2 \frac{g_{\star S}(T)}{g_{\star S}(T_s)}\left(\frac{T}{T_S}\right)^3, \tag{27}$$

where we have used the conservation of comoving entropy $S = sa^3$ to express it in terms of temperatures instead of scale factors. Using the expression for the Hubble constant during radiation domination

$$H(T) = 1.66\sqrt{g_\star(T)}\frac{T^2}{m_{\rm pl}}, \tag{28}$$

we can express the current energy density of the field as a function of the initial condition ψ_0,

$$\begin{aligned} \rho_\varphi \simeq 0.17 \frac{\rm keV}{\rm cm^3}\cdot\sqrt{\frac{m}{1\ {\rm eV}}}\left(\frac{f_a}{10^{11}\ {\rm GeV}}\right)^2 \psi_0^2 \mathcal{F}(T_s) \\ \cdot\left(2N\sin\frac{\pi}{2N}\right)^{-3/4}\exp^{\frac{3}{4}N\psi_0}. \end{aligned} \tag{29}$$

We can compare this density with the one corresponding to a harmonic potential. The result is

$$\frac{\rho^{\rm anh}}{\rho^{\rm harm}} \simeq \frac{\mathcal{F}(T_1)}{\mathcal{F}(T_s)}\cdot\left(2N\sin\frac{\pi}{2N}\right)^{-3/4}\exp^{\frac{3}{4}N\psi_0} \sim \exp^{\frac{3}{4}N\psi_0}, \tag{30}$$

so the energy density is exponentially enhanced[4] for large N and initial condition ψ_0. The precise exponent that we obtain here should be taken as a very rough estimate. Indeed, a numerical computation is needed to get a precise result, which is what we will aim for in the following section.

As we can see in (30) the enhancement is exponential in $N\psi$. This implies that the field values required to yield the correct dark matter abundance are usually not too large. In the phenomenologically interesting region we usually do not need to have values for $N\psi$ that are bigger than 50. The largest initial field values happen for $N = 1$ and are of order 50 in units of f_a.

Another constraint that we have to care about is that the field is behaving like dark matter once it comes to dominate the dynamics of the Universe; i.e., we do want to avoid having an additional phase of inflationary expansion driven by ψ. A sufficient condition for this is that the field has already started to oscillate at matter radiation equality. Making use of the more precise numerical estimate that we will obtain in the next section, we can estimate what region of parameter space satisfies this condition,

$$f_a \gtrsim 10^{-6}\ {\rm GeV}\cdot N\cdot\left(\frac{\rm eV}{m}\right)^{0.81}. \tag{31}$$

[4]In Appendix A we check that a significant enhancement also exists if we allow for a kinetic function with a higher-order pole.

This condition excludes the very small values of the mass and the decay constant in the upper left corner of Fig. 1, which are already in tension with the nEDM experiment, BBN observations and the limits from [33].

C. Numerical computation

Having obtained a simple estimate of the cosmological evolution of the field, we now make use of a numerical solution of the equation of motion to have a more precise result. Our goal in this subsection is to quantify how much the solution for the nonlinear equation of motion (23) deviates from the harmonic case (19).

Following the usual practice for dealing with anharmonicities in the ALP potential (see [49–52], and [53] has a slightly different definition), we use an effective parametrization in terms of an anharmonicity function $f(\psi_0)$, such that

$$\rho^{\rm anh} = f(\psi_0)\rho^{\rm harm}, \tag{32}$$

where ρ is the energy density of the ALP field, computed late enough when it is already behaving as cold dark matter. This function only depends on the initial misalignment angle, and it should account for all the deviations from the harmonic solution. This approach is normally used to account for departures from the quadratic potential in the usual axion and ALP models. Our case is slightly different, mostly because we are dealing with an unbounded field range. As a consequence, the usual functional form for $f(\psi_0)$ does not work here. Guided by the result obtained in the analytical approximation, we work with the following ansatz for the anharmonicity function:

$$f(\psi_0) = \mathrm{e}^{bN\psi_0}, \tag{33}$$

where b is a real parameter to be determined. This ansatz accounts for the exponential enhancement in energy density that we have found analytically. The normalization needed is that $f(\psi_0) \to 1$ when $\psi_0 \to 0$, so as to recover the harmonic case in the small field limit.

The goal now is to fit the ansatz to a numerical computation of the energy density. To set the problem in a more straightforward way, we want to compare the numerical solution of

$$\ddot{\psi} + 3\tilde{H}(\tilde{t})\dot{\psi} + \tilde{m}^2 \frac{1}{\cosh N\psi} \sin\left[\frac{2}{N}\arctan\left(\tanh\frac{N\psi}{2}\right)\right] = 0 \tag{34}$$

with the solution for the damped harmonic oscillator equation

$$\ddot{\psi} + 3\tilde{H}(\tilde{t})\dot{\psi} + \tilde{m}^2\psi = 0. \tag{35}$$

In this computation we use dimensionless quantities measured in units of m, denoted with a tilde: $\tilde{H}, \tilde{t}, \tilde{m}\ldots$ In these units, the time for the start of the oscillations in the harmonic case is $\tilde{t}_1^{\rm harm} = 3/2$ (assuming radiation domination), and the period of the oscillations is 2π. We solve the equations numerically until we are well within the adiabatic regime in both cases (that is, when the amplitude of the oscillations has decreased enough so that the noncanonical potential is well approximated by the harmonic one). Then, we compute the energy density $\rho = (1/2)f_a^2\dot{\psi}^2 + V(f_a\psi)$ and extract the anharmonicity factor as the quotient of both energy densities. As we are within the adiabatic regime, ρ scales as $\rho \propto a^{-3}$ in both cases, so the quotient will stay constant. An example of the numerical solution can be seen in Fig. 4.

This process is repeated for a large number of values of ψ_0 and N and we fit the results to the ansatz (33). We obtain a very good fit with a value of $b = 0.56$, as can be seen in Fig. 5. One should note that we are fitting a two-dimensional data sample with just one parameter, so finding a good fit confirms that we have chosen an adequate ansatz.

The anharmonicity function allows us to compute the energy density of the noncanonical ALP field in a very simple way, combining the harmonic solution (21) with the anharmonicity function (33). As long as we are within the adiabatic regime, the energy density in this approximation is given by

$$\begin{aligned}\rho_\psi^{\rm anh}(t) &\simeq \frac{1}{2}f_a^2m^2f(\psi_0,N)\psi_0^2\left(\frac{a_1^{\rm harm}}{a(t)}\right)^3 \\ &= \frac{1}{2}f_a^2m^2f(\psi_0,N)\psi_0^2\frac{g_{\star S}(T)}{g_{\star S}(T_1^{\rm harm})}\left(\frac{T}{T_1^{\rm harm}}\right)^3. \end{aligned}\tag{36}$$

The key difference between this equation and (27) is that here we use the well-known solution of the harmonic equation of motion, instead of the full nonlinear one that arises in our noncanonical setup. All the information about the nonlinearity is encoded in the anharmonicity function, making it much more manageable.

In the analytical approach, we found that the quotient between noncanonical and canonical density scales as $\rho_{\rm NC}/\rho_{\rm C} \sim \mathrm{e}^{(3/4)N\psi_0}$. In the full numerical approach[5] we find a somewhat lower coefficient for the exponent of 0.56.

We have seen that a noncanonical kinetic term can indeed enhance the energy density of ALP dark matter. In the next few sections we will make use of the solutions for the cosmological evolution of the noncanonical ALP field to make predictions about its phenomenology, and to apply it to some particularly interesting cases.

[5]In this study we have limited ourselves to the homogeneous field evolution. Recently, the authors of [54] showed that potentials like the one we are considering can lead to a parametric resonance instability that can make inhomogeneous modes grow. This effect may help to alleviate some tension that has been pointed out in [55] between the existence of ultralight ALPs and Lyman α forest observations.

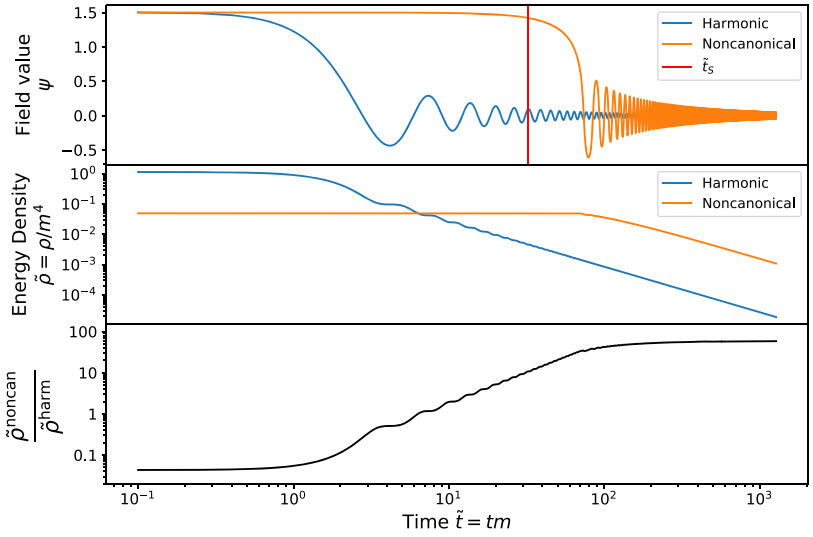

FIG. 4. Numerical solution of the noncanonical equation of motion compared to the harmonic solution, using $N = 5$ and $\psi_0 = 1.5$ as an example. The top panel shows the solution for the field as a function of time, while the middle and bottom ones show the energy density of the field and the quotient of energy densities for the harmonic and noncanonical equations of motion. Note that this quotient approaches a constant as the adiabatic regime is reached, allowing us to obtain the anharmonicity factor. As a comparison and confirmation of our analytical results, the top panel also shows the time at which the oscillations are predicted to start in our analytical approach, Eq. (26).

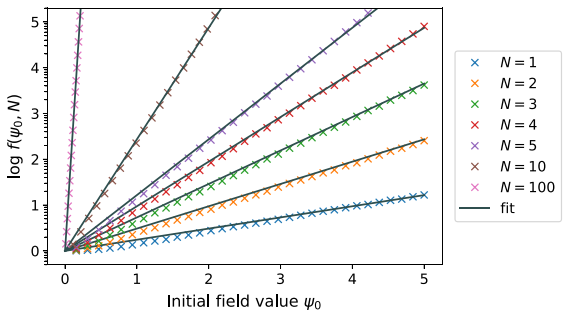

FIG. 5. Fit of the anharmonicity function to the ansatz in Eq. (33). We plot the result of the fit for a set of values of N and a range of the initial misalignment angle $\psi_0 \in (0, 5)$.

IV. ISOCURVATURE PERTURBATIONS

So far, we have assumed the initial misalignment angle $\theta_0 = f_a\phi_0$ to be a constant value all throughout the Universe, but of course we have to take into account fluctuations, e.g., those imprinted by inflation. We do this by taking the initial misalignment angle as a spatially varying quantity, and describing it in terms of its average and variance. Two very distinct scenarios arise, depending on whether the mechanism that gives rise to the ALP field turns on before or after the inflationary epoch of our Universe.

If the ALP field was established, e.g., by spontaneous symmetry breaking, after inflation, the variance of the angle can be large even within our Hubble volume. The mean value will be $\phi_0 = 0$ and the energy density is given by the fluctuations as well as other effects such as, e.g., the decay of topological defects [56,57]. In particular the latter contributions are not well understood and may also have some model dependence when going beyond the QCD axion.

To avoid this, we will focus on the scenario where the ALP field was present during inflation. Classically, if the ALP field was established before inflation, then the spatial variance of the field within a Hubble patch will be washed out as spacetime is stretched during inflation. This means that $\sigma_\phi^2 \to 0$, and the misalignment field can take any value ϕ_0 in our Hubble patch.

However, this is not completely true, as any light field present during inflation will acquire quantum fluctuations (see, e.g., [58]). The power spectrum of such fluctuations for a canonically normalized scalar field is scale invariant,

$$\langle|\delta\phi(k)|^2\rangle = \left(\frac{H_I}{2\pi}\right)^2 \frac{1}{k^3/(2\pi^2)}. \tag{37}$$

These fluctuations can be thought of as arising from a thermal spectrum at the Gibbons-Hawking temperature $T_{GH} = H_I/(2\pi)$ [59]. As long as these fluctuations do not restore the spontaneously broken symmetry that gives

rise to the ALPs, i.e., as long as[6] $T_{GH} < f_a$, this will imprint small fluctuations on top of the otherwise homogeneous ALP field. The corresponding fluctuations of the misalignment angle in Fourier space will have an amplitude of $\sigma_\phi(k) = H_I/(2\pi f_a)$. In real space, the fluctuations are of a size $\sigma_\phi = \gamma H_I/(2\pi f_a)$, where $\gamma \sim \mathcal{O}(1)$ is a dimensionless factor that effectively encodes the dispersive effect of the logarithmically divergent small k modes (see [50]). Its value depends on the length scales that we are interested in. Following [61] we will set $\gamma = 2$ for the CMB characteristic scale $k_\star = 0.05\ \mathrm{Mpc}^{-1}$.

As the ALP has a negligible contribution to the total energy density of the Universe during inflation, fluctuations in the field do not contribute to the usual curvature perturbations. Rather, they manifest themselves as fluctuations in the ratio of the number density of ALPs to the total entropy density, and they are completely uncorrelated with the curvature perturbations. This is the reason why they are called "entropy" or "isocurvature perturbations." As their interactions with other standard model particles are greatly suppressed, ALPs do not thermalize with the other species and their perturbations remain isocurvature [62]. At later stages of the cosmological evolution, the dark matter ALPs pick up a significant contribution to the energy density of the Universe, and so they contribute to the temperature and polarization fluctuations of the CMB as cold dark matter isocurvature modes.

Planck has set strong bounds on isocurvature perturbations [35],

$$\beta_{\mathrm{iso}} = \frac{\Delta^2_\phi(k_\star)}{\Delta^2_\phi(k_\star) + \Delta^2_{\mathcal{R}}(k_\star)} < 0.038 \tag{38}$$

at 95% C.L. Here, $\Delta^2_\phi(k_\star)$ and $\Delta^2_{\mathcal{R}}(k_\star)$ are the power spectrum of the axion and curvature perturbations at the pivot scale $k_\star$, respectively. Once the value of $\Delta^2_{\mathcal{R}}(k_\star)$ is set [Planck gives $\Delta^2_{\mathcal{R}}(k_\star) = 2.1(9) \times 10^{-9}$], this translates into a bound on the axion isocurvature fluctuations.

To use these limits to constrain our scenario, we have to compute our prediction for

$$\Delta^2_\phi = \left\langle \left(\frac{\delta\rho_\phi}{\rho_\phi}\right)^2 \right\rangle \Bigg|_{t_{\mathrm{CMB}}}, \tag{39}$$

that is, we need to evolve the fluctuations in the energy density until the time of emission of the CMB and compare them with the homogeneous average value.

If the evolution of the field is linear, as it is in the case of canonical ALP models with a purely quadratic potential, the power spectrum is constant during the cosmological evolution. As a consequence, one can evaluate it at any point, such as right after inflation and before the onset of the oscillations in the ALP field. However, in any model that contains anharmonicities, the evolution at early times will be nonlinear, which implies that Δ^2_ϕ will evolve nontrivially after inflation. Thus, to arrive at the correct prediction for the isocurvature perturbations, we have to track the evolution of the fluctuations until late times.

In addition to the limits from isocurvature fluctuations, the inflationary fluctuations[7] in the ALP field also forbid tuning the initial misalignment angle with arbitrary precision. In fact, there is an unavoidable limit to this tuning, and it is that our tuning precision cannot be better than the fluctuations, with $\sigma_\theta = \gamma H_I/(2\pi f_a)$, as was argued in [42]. This has two related consequences. The first is that the initial misalignment angle cannot be infinitely close to zero. The requirement that the current ALP energy density is not bigger than the measured dark matter density $\Omega_C h^2 \sim 0.12$ then sets a bound on the parameter space. This bound is model independent (as long as all the potentials are approximately quadratic for small θ) and roughly requires

$$m < \left(\frac{10^{12}\ \mathrm{GeV}}{H_I}\right)^4 \mathrm{eV}. \tag{40}$$

Secondly, if the field range is compact (as for the usual canonical ALP), an argument similar to the one above tells us that some regions of the parameter space will not yield enough energy density to account for all the dark matter. Indeed, it is not possible to tune the initial value of the field at the top of the potential with infinite precision, due to the presence of fluctuations. The requirement here is that $\pi - \theta_0 < \gamma H_I/(2\pi f_a)$. This particular limit will strongly depend on the anharmonicity of the potential, so it is not possible to give a more explicit expression. We discuss some particular cases in the next subsection. However, this last effect will not be relevant in our noncanonical model, as there we have an unbounded field range (our potential does not have a maximum).

A. Isocurvature perturbations for anharmonic potentials

We now present a general analytical expression to compute the isocurvature perturbations in general ALP models where the potential might have big anharmonicities. We do this using the anharmonicity function formalism that we presented in the previous section. An equivalent result was derived in [63] using the δN formalism. Here we provide a more straightforward derivation and extend the use of the formula to more general potentials.

To evaluate expression (39), we will use the fact that at t_{CMB} the field should already be oscillating harmonically,

[6]It is also necessary that the symmetry is not restored during reheating [60]. We will assume this to be true.

[7]Quantum fluctuations of the ALP field should also be considered, but their effect is negligible when compared to the inflationary fluctuations.

as observations require it to behave as cold dark matter already by the time of matter-radiation equality. As we are already well within the adiabatic regime, the anharmonicity function approach will work well to describe the evolution of the energy density, which means that we can use Eq. (36). As fluctuations are small, we can work to linear order in σ_ϕ to find[8]

$$\begin{aligned}\Delta_\phi^2 &= \left\langle \left(\frac{\delta\rho_\phi}{\rho_\phi}\right)^2 \right\rangle\Big|_{t_{\rm CMB}} \\ &= \left(\frac{\partial \log \rho_\phi(t_{\rm CMB})}{\partial \log \phi}\Big|_{\phi_0}\right)^2 \left\langle \left(\frac{\delta\phi_0}{\phi_0}\right)^2 \right\rangle \\ &= 4\frac{\sigma_\phi^2}{\phi_0^2}\left(1+\frac{1}{2}\frac{\mathrm{d}\log f(\theta)}{\mathrm{d}\log\theta}\Big|_{\theta_0}\right)^2 \\ &= 4\gamma^2\frac{H_I^2}{4\pi^2 f_a^2\theta_0^2}\left(1+\frac{1}{2}\frac{\mathrm{d}\log f(\theta)}{\mathrm{d}\log\theta}\Big|_{\theta_0}\right)^2. \end{aligned} \tag{41}$$

Note that even if this quantity is evaluated at $t_{\rm CMB}$, it directly depends only on the initial misalignment angle and the statistics of its fluctuations at inflation. All the information about the later evolution is encoded in the anharmonicity function.

We will now apply the formula (59) to both the case of the canonical ALP with a cosine potential and to our noncanonical model, and compare the results with the harmonic approximation.

For the harmonic case, where $f(\theta_0)=1$, we have the usual expression

$$\Delta_\phi^2 = \gamma^2\frac{H_I^2}{\pi^2 f_a^2\theta_0^2}. \tag{42}$$

The constraints that one finds, for different values of the energy scale of inflation, are presented in Fig. 6. The harmonic case in particular corresponds to the first column of plots.

Of course, the harmonic case can only be an approximation valid for small θ, as ALP models should preserve the shift symmetry $\theta+2\pi$. Among the potentials that satisfy this condition, the most commonly used is $V(\theta)=m^2(1-\cos\theta)$. The anharmonicity function that appears in this case was studied in [49–52]. After comparing with numerical simulations, we have decided to use a slightly different version of it, proposed in [53], which provides a better fit to the numerical data,

$$f(\theta_0) = \left[\log\left(\frac{e}{1-(\theta_0/\pi)^4}\right)\right]^{3/2}. \tag{43}$$

With this, it is easy to arrive at the following expression for the isocurvature perturbations,

$$\Delta_\phi^2 = \gamma^2\frac{H_I^2}{\pi^2 f_a^2\theta_0^2}\left(1+\frac{3}{f(\theta_0)^{2/3}}\cdot\frac{1}{(\pi/\theta)^4-1}\right)^2. \tag{44}$$

Note that this reduces to the harmonic result for small θ_0. However, for angles close to π, the isocurvature perturbations are greatly enhanced. As expected, this function diverges at $\theta_0=\pi$, but as we have noted before, this limit is unattainable because of the fluctuations in the field. In Fig. 6, we can see that the limits we can put on the parameter space are a bit stronger than in the harmonic case, in particular for low values of m and f_a, which correspond to large values of the initial misalignment angle.

Finally, we turn to the noncanonical case. The main difference with the canonical ALP, aside from the shape of the potential, is that here we are dealing with an unbounded field range. As the potential is asymptotically flat, it is always possible to enhance the production of ALPs by choosing a larger initial misalignment angle, as we saw in Sec. III. This means that this model can always evade the limits related to underproduction of dark matter. Using the anharmonicity function that we derived in the previous section, we find that the isocurvature power spectrum generated in this scenario is

$$\Delta_\phi^2 = \gamma^2\frac{H_I^2}{\pi^2 f_a^2\theta_0^2}\left(1+\frac{1}{2}bN\theta_0\right)^2, \tag{45}$$

where $b=0.56$. Again, this reduces to the harmonic case for small θ. The last column of plots in Fig. 6 illustrates the limits that arise from the Planck data. Note that in the harmonic and canonical model featuring a compact field range a strong restriction on the parameter space is given by the requirement to produce enough dark matter (the limits arising from this condition are shaded in purple in Fig. 6). As we have already argued, this limit is not present in our noncanonical setup, which features an unbounded field range. As a consequence, this model opens up a large region of parameter space, corresponding to low masses and decay constants, that was disfavored until now.

Finally let us remark that, as is well known, high scale inflation strongly constrains ALP models due to the generation of large isocurvature perturbations, which are not seen in the CMB. The tensor to scalar ratio r is strongly correlated with a high scale of inflation, so a detection of primordial gravitational waves would put a strong constraint on all axion and ALP dark matter models, including ours. Future experiments [64–66] are expected to increase the sensitivity in measuring r and thus the energy scale of inflation.

[8]Here we implicitly assume that the fluctuations are still superhorizon when the adiabatic regime is reached. This is indeed the case for all the large scale modes of cosmological interest, like the ones probed by the CMB.

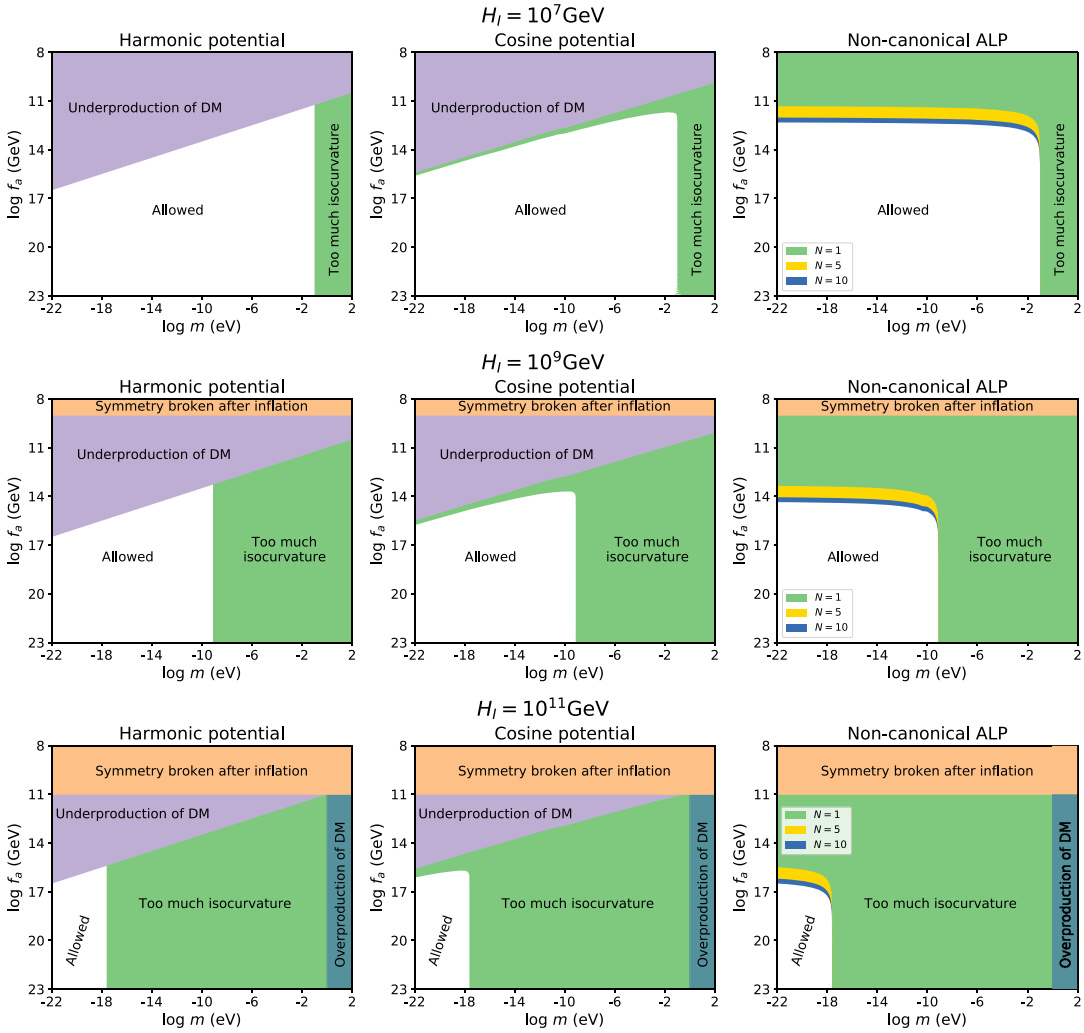

FIG. 6. Isocurvature limits arising in the three different models studied: the harmonic potential (left), the canonical ALP (center) and the noncanonical one (right). From top to bottom, we plot the limits in the (m, f_a) parameter space for different values of the energy scale of inflation H_I. Note that a higher H_I puts stronger bounds on ALP models. In fact, $H_I \gtrsim 10^{12}$ GeV rules out the complete parameter space, whereas for $H_I \lesssim 10^6$ GeV, the limits are very weak.

V. COUPLING TO QCD: TEMPERATURE-DEPENDENT MASS

So far, we have not assumed a coupling of the ALP to any other field. In what follows, we will allow for a coupling to gluons via a term $\theta G\tilde{G}$. We will study two distinct cases. First, we contemplate the possibility of having a noncanonical kinetic term in an otherwise QCD-axion model. Then, we add an extra term to the Lagrangian which, as we will see, allows us to construct a model of light ALPs that enjoys relatively strong gluon couplings.

A. The QCD axion

In this section we will focus on the QCD axion as introduced by Peccei and Quinn as a solution to the strong CP problem in quantum chromodynamics (QCD) [4–6].

The Lagrangian for the canonically normalized axion field is now

$$\mathcal{L}_\phi = \frac{1}{2}\partial^\mu\phi\partial_\mu\phi - \Lambda_{\rm QCD}^4\left(1 - \cos\frac{\phi}{f_a}\right), \qquad (46)$$

and as usual we can define the angle $\theta = \phi/f_a$, so that $\theta \in (-\pi, \pi]$. For our modification with a noncanonically normalized field, we have

$$\mathcal{L}_\phi = \frac{1}{2\cos^2\left(N\frac{\phi}{f_a}\right)}\partial^\mu\phi\partial_\mu\phi - \Lambda_{\rm QCD}^4\left(1-\cos\frac{\phi}{f_a}\right), \quad (47)$$

and after we perform a field redefinition to have it canonically normalized, we find the Lagrangian

$$\mathcal{L}_\varphi = \frac{1}{2}\partial^\mu\varphi\partial_\mu\varphi - \Lambda_{\rm QCD}^4\left[1-\cos\left(\frac{2}{N}\arctan\left(\tanh\frac{N\varphi}{2f_a}\right)\right)\right]. \quad (48)$$

There is just one difference that makes the QCD axion case particular, and it is that here the energy scale appearing in the potential is fixed by QCD to be [43]

$$\Lambda_{\rm QCD} = f_\pi m_\pi \frac{\sqrt{m_u m_d}}{m_u + m_d} \simeq 76\ \text{MeV}. \quad (49)$$

It is easy to see that the mass of the axion, m_a, is given by $f_a m_a = \Lambda_{\rm QCD}^2$. It is important to note that the numerical value quoted above is only valid at zero (or very low) temperatures. Indeed, the axion potential is affected by finite temperature effects, such that the mass of the axion varies with temperature. At low temperatures below the QCD critical temperature $T_{\rm crit} \sim 160$–170 MeV, the mass remains roughly constant.[9] That said, much of the dynamics that is of interest to us will happen in the early Universe, at temperatures close to or above $T_{\rm crit}$. There are different ways to compute the temperature dependence of the axion mass [42,43,49,52,67,68]. The function that controls the temperature dependence of the axion mass is the topological susceptibility $\chi(T)$, which is usually parametrized as a power law:

$$m_a^2(T) = \frac{\chi(T)}{f_a^2}, \quad \text{where } \chi(T) \simeq \chi_0\left(\frac{T}{T_{\rm crit}}\right)^{2\alpha}. \quad (50)$$

Here we will use $2\alpha = -7.1$ and $\chi_0 = 0.11$, from recent lattice computations [68] that are consistent with the instanton values up to an overall normalization factor.

We see that the main effect is that the mass of the axion is approximately constant until $T_{\rm crit}$, and then it drops as a power law, so that the axion is essentially massless at high temperatures. The most important implication of the temperature-dependent mass is that a smaller mass at early times can delay the start of the oscillations of the field, which in turn results in a higher energy density of axionic dark matter today. This happens both for the canonical and noncanonical axion models.

B. Anharmonicity function and isocurvature perturbations revisited: Temperature dependence

We have seen that coupling ALPs to QCD through $\phi G\tilde{G}$ results in a temperature-dependent mass for the ALP, both in the canonical and noncanonical setup. This of course has an impact on its cosmological evolution, which can be of importance in computing observables such as the isocurvature perturbations that we discussed in Sec. IV. To account for this effect, we will modify the anharmonicity function formalism that we introduced in Sec. III C to incorporate the temperature dependence. That is, we want to compute

$$F_T(\theta_0, f_a) \equiv \frac{\rho_T^{\rm anh}}{\rho^{\rm harm}}, \quad (51)$$

evaluated at a point in time late enough so that the anharmonic and temperature-dependent axion field has already entered the adiabatic regime.

For definiteness, we will use the following expression for the axion mass:

$$m_a(T) = \begin{cases} m_a\left(\frac{T}{T_{\rm crit}}\right)^\alpha & \text{if } T \geq T_{\rm crit}, \\ m_a & \text{if } T \leq T_{\rm crit}. \end{cases} \quad (52)$$

First of all, we note that this temperature dependence will only have an effect if the field starts oscillating before the QCD critical temperature $T_{\rm crit}$. In the harmonic limit, this means that if the mass is smaller than m_a^*, defined by $3H(T_{\rm crit}) = m_a^*$, the field will have acquired its late-time mass by the time it starts oscillating. Thus, the later evolution of the field will be insensitive to the temperature effects that happened earlier on. In terms of decay constants, this sets a distinct scale:

$$f_a^* \simeq 8.7 \times 10^{16}\ \text{GeV}. \quad (53)$$

If we take into account the anharmonicities of the potential, it might happen that the start of the oscillations is delayed until after $T_{\rm crit}$, even if $f_a < f_a^*$. The condition to be in this regime is that the initial misalignment angle θ_0 is larger than some value $\theta_0^*(f_a)$. This value is given for a general anharmonicity function[10] by

$$\left(\frac{f_a^*}{f_a}\right)^{3/2} = f(\theta_0^*). \quad (54)$$

[9]The small temperature dependence can be computed using chiral perturbation theory as in [43].

[10]Note the difference between $f(\theta_0)$, which is the anharmonicity function presented in Sec. III C and induced purely by the shape of the potential, and $F_T(\theta_0, f_a)$, which also includes the effects of the temperature-dependent mass.

For the case of a canonical axion with a cosine potential like in (46), we find

$$\theta_0^*(f_a) \simeq \pi\left[1-\exp\left(1-\frac{f_a^*}{f_a}\right)\right]^{1/4}, \tag{55}$$

whereas in the noncanonical case (48), we find

$$\psi_0^*(f_a, N) \simeq \frac{3}{2bN}\log\left(\frac{f_a^*}{f_a}\right). \tag{56}$$

For any set of decay constants and initial misalignment angles that satisfy $f_a < f_a^*$ and $\theta_0 < \theta_0^*$, we compute F_T for a generic anharmonic potential, finding

$$F_T(\theta_0, f_a) \simeq \left(\frac{f_a^*}{f_a}\right)^{\frac{\alpha}{2(2-\alpha)}} \cdot (f(\theta_0))^{\frac{2(3-\alpha)}{3(2-\alpha)}}. \tag{57}$$

The details of the derivation of this result are given in Appendix B. Here we see that the result depends critically on the exponent of the temperature dependence of the axion mass at high temperatures above the QCD critical temperature. To sum up, we can write the full temperature-dependent anharmonicity function as follows:

$$F_T(\theta_0, f_a) = \begin{cases} f(\theta_0) & \text{if } f_a > f_a^*, \\ f(\theta_0) & \text{if } f_a < f_a^* \quad \text{and} \quad \theta_0 > \theta_0^*, \\ \left(\frac{f_a^*}{f_a}\right)^{\frac{\alpha}{2(2-\alpha)}} \cdot (f(\theta_0))^{\frac{2(3-\alpha)}{3(2-\alpha)}} & \text{if } f_a < f_a^* \quad \text{and} \quad \theta_0 < \theta_0^*. \end{cases} \tag{58}$$

With this, we can use the same approach as in Sec. IV A to compute the isocurvature perturbations, this time using the temperature-dependent anharmonicity function,

$$\Delta_\phi^2 = 4\gamma^2 \frac{H_I^2}{4\pi^2 f_a^2 \theta_0^2}\left(1+\frac{1}{2}\frac{\mathrm{d}\log F_T(\theta)}{\mathrm{d}\log\theta}\bigg|_{\theta_0}\right)^2. \tag{59}$$

We apply this formula for both the canonical QCD axion and for our noncanonical model, and obtain the results presented in Figs. 7 and 8, respectively. For the canonical QCD axion, our results are an update from the ones obtained in [63,69], as we are using the more recent data from the Planck satellite and a better fitting anharmonicity function.

C. ALPs coupled to QCD with $f_a m \ll \Lambda_{\mathrm{QCD}}^2$

Let us now study the possibility of an ALP having a coupling to the $G\tilde{G}$ term while satisfying $f_a m \ll \Lambda_{\mathrm{QCD}}^2$. This is an interesting region of the parameter space, as ALPs that satisfy these conditions may be found by looking for an oscillating nucleon or atomic electric dipole moment.

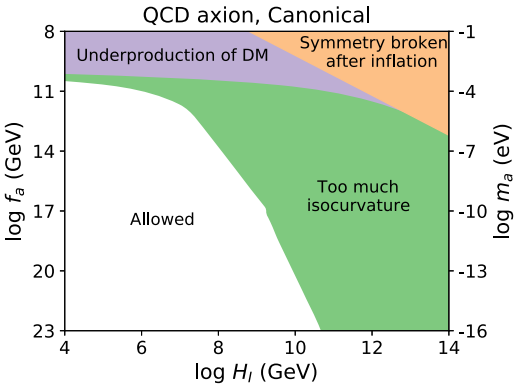

FIG. 7. Isocurvature constraints on the axion scale f_a as a function of the inflation scale H_I for the QCD axion with potential (46). Both the anharmonicities of the potential and the temperature dependence of the mass are taken into account through the anharmonicity function defined in (58). Our results differ slightly from the ones obtained in [63,69] due to the fact that we are using the more recent data from the Planck satellite and a different anharmonicity function.

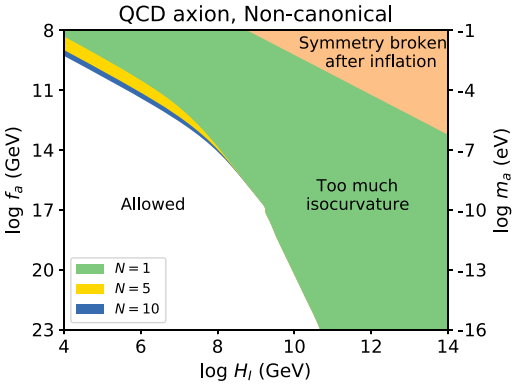

FIG. 8. Isocurvature constraints on the axion scale f_a as a function of the inflation scale H_I for the QCD axion with a noncanonical kinetic term (47). Both the anharmonicities of the potential and the temperature dependence of the mass are taken into account through the anharmonicity function defined in (58).

There exist a number of proposed laboratory searches focusing on this direction [27,31,32,70].

However, we have seen that coupling the ALP to QCD via a term proportional to $G\tilde{G}$ induces an irreducible contribution to the mass, given by (49). Explicitly this contributes

$$m_a^2(T=0) \simeq \left(5.7\times 10^{-5}\ \mathrm{eV}\left(\frac{10^{11}\ \mathrm{GeV}}{f_a}\right)\right)^2, \tag{60}$$

to the square of the axion mass as given in [43]. This contribution will also have a temperature dependence as described by (50).

A priori, this irreducible contribution to the axion mass seems irreconcilable with the condition $f_a m \ll \Lambda_{\rm QCD}^2$ [28]. The only known way of circumventing this caveat is to precisely cancel this contribution with an additional, fine-tuned term in the Lagrangian. Acknowledging the flaws of this *ad hoc* approach, we follow it and study the phenomenology of such models when allowing for a noncanonical kinetic term.

At the level of the Lagrangian, we add an extra term to the potential so that it becomes

$$V(\phi) = \Lambda_{\rm QCD}^4\left(1-\cos\frac{\phi}{f_a}\right) - \Lambda_0^4\left(1-\cos\left(\frac{\phi}{nf_a}+\alpha\right)\right). \tag{61}$$

In principle there can exist a phase difference between both contributions. For our purposes, it will be necessary to require that this phase difference vanish, so we will take $\alpha = 0$. This can be viewed as equivalent to asking for a separate solution to the strong CP problem. In principle any integer n is possible but for simplicity we will limit ourselves to the $n = 1$ case. In the small ϕ limit, this potential induces a mass for the ALP,

$$m^2 = m_a^2(T) - m_0^2, \tag{62}$$

where $m_0 f_a = \Lambda_0^2$ and recall that m_a is completely fixed by f_a as in Eq. (60). It is then possible to choose m_0 so that we get any zero-temperature mass for the ALP; i.e., we can set $m_0^2 = m_a^2(T=0) - m^2$. We are interested in the $m^2 \ll m_a^2(T=0)$ regime. The full mass can then be expressed as

$$m^2(T) = m_a^2(T) - m_a^2(0) + m^2. \tag{63}$$

Because at early times the QCD contribution is strongly suppressed, in that regime we have $m^2(T) < 0$. We will use the following simplified expression for the temperature-dependent mass of the ALP:

$$m^2(T) = \begin{cases} m^2 & \text{for } T < T_{\rm crit} \\ -m_a^2(0) & \text{for } T > T_{\rm crit} \end{cases}. \tag{64}$$

Note that the negative mass does not indicate an unstable potential but only that $\phi = 0$ is not the minimum at that time.

1. Canonical case

As a first step, we implement the mass subtraction and the resulting temperature dependence in an ALP model with a canonically normalized scalar field with potential given by

$$V(\phi) = f_a^2 m^2(T)\left(1-\cos\frac{\phi}{f_a}\right), \tag{65}$$

with $m(T)$ defined in (64). The most relevant feature of this scenario is that before the QCD phase transition, the potential is minimized at $\theta = \pi$ rather than at $\theta = 0$. Accordingly, at early times the field evolves towards its minimum at π, around which it will oscillate with damped amplitude. Then, after the QCD phase transition, the potential rapidly acquires its late-time shape, with a minimum at the origin. The field thus oscillates around its CP-conserving value $\theta = 0$ at late times. The main role of the first set of oscillations is to set the initial condition for the second one to be close to π. We refer to Fig. 9 for a cartoon explaining this evolution. It should be noted that this discussion is only valid if $f_a m \ll \Lambda_{\rm QCD}^2$, that is, if we lie to the left of the QCD axion band in Fig. 10. In the other limit, i.e., $f_a m \gg \Lambda_{\rm QCD}^2$, the contribution of the QCD mass is negligible and we recover the usual constant mass ALP scenario.

Let us now be a bit more quantitative. Initially, H is large and the field is stuck at its initial value θ_0. Then, as long as the early-time mass $m_a(0)$ overcomes the Hubble friction before the QCD phase transition, the field will oscillate around π. The condition for this to happen is roughly $f_a \gtrsim 10^{17}$ GeV, but this value can be modified by the anharmonicities depending on the initial misalignment. These oscillations continue until the temperature decreases to $T_{\rm crit}$, at which time the amplitude is approximately given by

$$(\pi - \theta_{\rm crit}) \simeq (\pi - \theta_0)\left(\frac{\mathcal{F}(T_{\rm crit})}{\mathcal{F}(T_1)}\right)^{1/2}\left(\frac{f_a}{2\times 10^{17}\ \text{GeV}}\right)^{3/4} \times f^{1/2}(\theta_0). \tag{66}$$

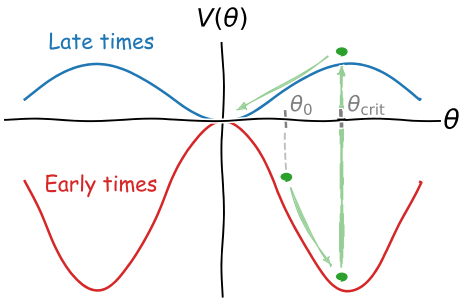

FIG. 9. Cartoon explaining the evolution of the field. The red and blue lines represent the potential before and after the QCD phase transition, respectively. The green dots and arrows represent the evolution of the field. (The oscillations are not drawn explicitly in order to simplify the figure.) The initial misalignment angle θ_0 and the value of the field at the QCD phase transition, $\theta_{\rm crit}$, are depicted.

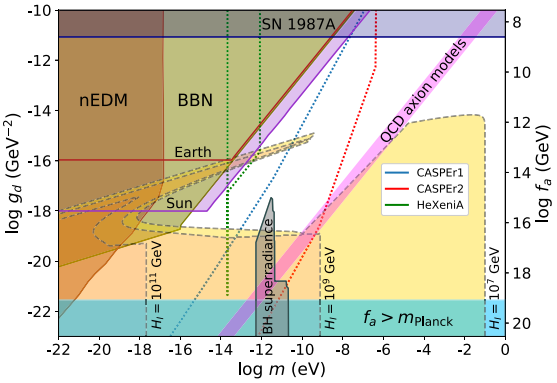

FIG. 10. Parameter space of the model defined by the potential given in (65). We present the isocurvature constraints for different values of H_I, ranging from 10^6 to 10^{11} GeV. A higher scale of inflation restricts the model to lie in the respective colored areas. For the purpose of visualization we have continuously connected the solution in the two different regimes that we have considered, i.e., to the left and to the right of the QCD axion band. All the other limits presented in Fig. 1 are also applicable in this scenario, as they only depend on the dynamics of the field after the QCD phase transition.

Here, the anharmonicity function is given by (43) and T_1 is defined by $3H(T_1) = m_a(0)$. The value of $\theta_{\rm crit}$ gives the initial condition for the oscillations that happen after the QCD phase transition, now around $\theta = 0$ and with frequency given by the late-time mass m. Typically, $\theta_{\rm crit}$ is very close to π so the anharmonicities of the potential will play a key role. Taking this into account, we can compute the energy density of the oscillating scalar field as

$$\rho \simeq 0.17 \frac{\rm keV}{\rm cm^3} \mathcal{F}(T_2) \sqrt{\frac{m}{\rm eV}} \left(\frac{f_a}{10^{11}\ {\rm GeV}}\right)^2 \theta_{\rm crit}^2 f(\theta_{\rm crit}), \quad (67)$$

where $3H(T_2) = m$.

We can then determine in what region of parameter space the right dark matter abundance can be generated with an initial misalignment angle θ_0 of order $\mathcal{O}(1)$. It is possible to either enhance or suppress the energy density given in (67) by tuning the initial misalignment angle closer to zero or π. However, due to Eq. (59), there is an enhancement of the isocurvature perturbations each time the field gets close to a maximum of the potential, where the anharmonicity function becomes large. Because of this, the available tuning of the initial misalignment angle is very limited in this scenario due to the stringent constraints on isocurvature fluctuations. Figure 10 shows how the allowed parameter space shrinks for larger values of the Hubble scale of inflation. Despite the strong isocurvature constraints, we can see that this scenario populates some unexplored regions of parameter space to the left of the QCD axion line that could be probed by upcoming experiments looking for ALPs.

2. Noncanonical case

We now want to implement the temperature-dependent potential (65) in our noncanonical ALP scenario. In terms of the cosmological evolution of the field, this is effectively done by writing

$$V(\varphi) = f_a^2 m^2(T) \left[1 - \cos\left(\frac{2}{N} \arctan\left(\tanh\frac{N\varphi}{2f_a}\right)\right)\right]. \quad (68)$$

This is the same potential as we had before, except that for high temperatures $T > T_{\rm crit}$ the mass squared will be negative and will be a function only of f_a, as given in (64). This tells us that, depending on the value of the parameters m and f_a, we will have two very different behaviors, which qualitatively can be understood as follows.

First, if the field does not start rolling until after the QCD phase transition, then all the dynamics and the observables will not be affected at all by the features of the potential at high temperatures. This is because there is no evolution while the field is frozen by Hubble friction. Only after it has acquired its late-time mass m does it start rolling, and thus the cosmological evolution is exactly as we computed in Sec. III. However, the key difference is that now the ALP is coupled to $G\tilde{G}$, so it may be tested by observables and experiments that exploit this coupling.

The other option is, of course, that the field starts rolling before the QCD phase transition. Then the dynamics can depend strongly on the initial conditions and is rather complicated. However, we will see that this scenario leads to an overproduction of ALPs whose energy density exceeds the observed CDM one. As we are only interested in ALPS as dark matter candidates, the second scenario is not interesting for us and we just need to focus on the first one.

Let us now be more quantitative and compute what region of the parameter space allows for ALP dark matter with a noncanonical kinetic term and coupled to QCD. As we have anticipated, this ALP will only be a good dark matter candidate if its evolution is frozen until after the QCD phase transition. Then, the present ALP energy density will only depend on f_a, the present mass m and the initial misalignment angle ψ_0. The latter is given by Eq. (36), and satisfies

$$\psi_0^2 e^{bN\psi_0} \simeq \frac{7.26}{\mathcal{F}(T_1)} \sqrt{\frac{\rm eV}{m}} \left(\frac{10^{11}\ {\rm GeV}}{f_a}\right)^2, \quad (69)$$

where T_1 is the temperature at which the oscillations start.

We now need to find what the region of the parameter space is where the field starts oscillating only after the QCD phase transition. The QCD phase transition happens at a temperature of around $T_{\rm crit} \sim 160$ MeV, which corresponds

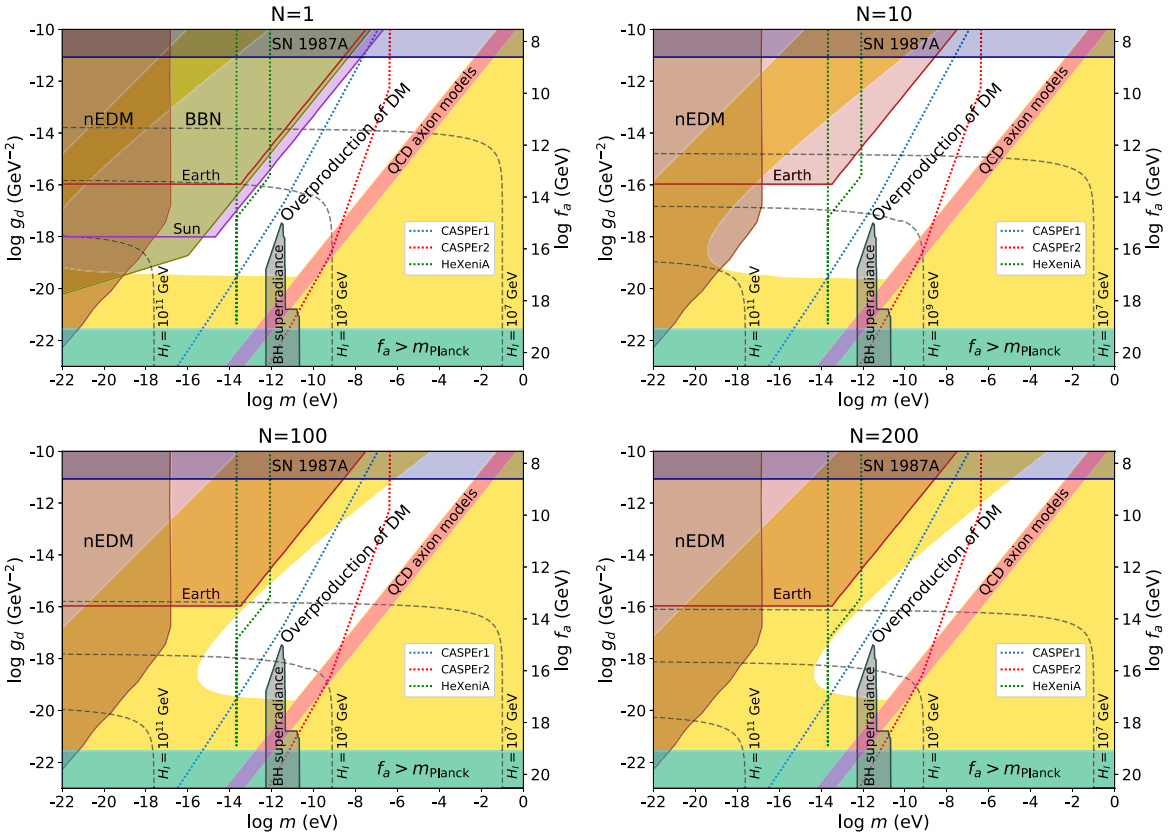

FIG. 11. Parameter space for ALPs with a noncanonical kinetic term of the form (11) coupled to QCD via a $G\tilde{G}$ term, along with constraints coming from its cosmological evolution and searches for an oscillating EDM. Each panel represents a different value of the parameter N. This scenario can provide the right dark matter density in the yellow shaded region, while the areas excluded by overproduction of dark matter or the condition (31) to avoid a second period of inflation are colored in white. The brown region is excluded by reanalyzing data originally intended to search for a static neutron EDM in order to look for an oscillating one [30]. The dark green region in the first figure is inconsistent with the production of the observed abundance of light elements during big bang nucleosynthesis [28]. This limit is effective only for $N < 4$ and absent in the other figures. Similarly, the limit from [33] corresponding to the ALP field being sourced at the Sun only applies for small values of N, while the Earth one stays valid in all cases. Finally, f_a is (softly) bounded from above by the requirement that it does not exceed the Planck scale, and from below by the supernova limits estimated in [29].

to a Hubble parameter of $H(T_{\rm crit}) \sim 10^{-11}$ eV. By asking that $3H(T_{\rm crit}) > |V''(\psi_0)|^{1/2}$, we get the condition

$$H(T_{\rm crit}) > 3.24 \times 10^{-6}\ \text{eV} \cdot \sqrt{2N \sin\frac{\pi}{2N}}\,\mathcal{F}(T_1)^{1/(2b)} \times \psi_0^{1/b} \left(\frac{m}{\text{eV}}\right)^{1/(4b)} \left(\frac{f_a}{10^{11}\ \text{GeV}}\right)^{1/b-1}. \quad (70)$$

This region is plotted in Fig. 11, together with the further cosmological and astrophysical bounds that restrict the parameter space.

Finally we still have to justify our claim that if the field starts oscillating before the QCD phase transition we always get an overproduction of ALPs. For a given (m, f_a), any initial misalignment angle bigger than the one given by (69) will lead to an energy density in ALPs greater than the observed dark matter one. But if the condition (70) is not satisfied, then the field will start rolling towards bigger ψ values, because $m^2(T) < 0$ at high temperatures. Thus, the effect of the rolling at high temperatures is to drive the field away from the required misalignment angle to give the correct dark matter abundance. This statement is independent of what misalignment angle we start with, and thus rules out ALPs in the region colored in white in Fig. 11 as dark matter candidates.[11]

[11]Such an overproduction could, e.g., be ameliorated in scenarios with two stages of inflation [71,72].

D. Big bang nucleosynthesis

Aside from a potential over (or under) production there is an additional constraint that rules out large areas of experimentally accessible parameter space. This arises from cosmology, more precisely BBN [28]. A nonvanishing θ angle at the time of BBN can spoil the production of light elements such as ^{4}He. This is due to the fact that a nonvanishing θ angle induces a difference between the mass of the proton and the neutron [73]

$$\delta Q \equiv m_n - m_p = c_+ \frac{m_d^2 - m_u^2}{\sqrt{m_u^2 + m_d^2 + 2m_u m_d \cos\theta}}, \quad (71)$$

where $c_+ \simeq 2.5$ can be determined by looking at the mass splitting $M_\Theta - M_N$ in the baryon octet [74]. A larger mass splitting means that the freeze-out abundance of neutrons with respect to protons would be lower. In addition to that, the free neutron decay rate is enhanced, which means that more neutrons decay between freeze-out and nucleosynthesis. This depletion of neutrons[12] eventually turns into an underproduction of ^{4}He. Based on the discussion in [28,75], these effects result in a shift that can be estimated as

$$\frac{\delta Y_p}{Y_p} \equiv \frac{Y_p^0 - Y_p(\theta)}{Y_p^0} = \left(1 - \frac{Y_p^0}{2}\right)\left(\frac{\delta(n/p)_{\rm fr}}{(n/p)_{\rm fr}} + \delta\Gamma_n t_{\rm nuc}\right) \simeq 0.66\theta^2. \quad (72)$$

Using the values $Y_p^0 = 0.25$ and $t_{\rm nuc} = 880$ s [76], one can now take the conservative limit $|\delta Y_p/Y_p| < 10\%$ to see that successful nucleosynthesis requires

$$\theta_{\rm BBN} < 0.39. \quad (73)$$

In our noncanonical model, the first thing we notice is that the θ angle is bounded,

$$|\theta| = |\frac{2}{N}\arctan\left(\tanh\frac{N\psi}{2}\right)| \leq \frac{\pi}{2N}, \quad (74)$$

so the BBN bound is completely avoided if $N > 4$. For smaller N we are in the region of small θ and the behavior is approximately that of a canonical ALP. Here we use the bound given in [28]. The corresponding excluded region is shaded in darker and labeled "BBN" in Fig. 11.

[12]There are other effects that play a role, like the change in the deuteron binding energy or the rise in the freeze-out temperature. We have found that the contribution of these effects is smaller than the one considered above, so we neglected them for this analysis.

VI. CONCLUSIONS

The question raised in this paper can be summarized in the following way: is it possible to have an axionlike particle with a noncanonical kinetic term as a phenomenologically viable and interesting dark matter candidate? Our study points towards an affirmative answer. Using in particular a noncanonical term with singularities similar to those used in α-attractor models for inflation we find a significantly enlarged parameter space for dark matter. In particular, regions with larger couplings—where canonical ALPs are underproduced—now become viable, offering interesting possibilities for near future experiments.

For the production via the misalignment mechanism the key feature of the noncanonical kinetic term is that today's ALP energy density is enhanced due to a delay in the start of the oscillations. This arises because the effective potential is flattened by the growing noncanonical kinetic term, which also makes the field range of the physical field unbounded. As a consequence, any combination of mass and decay constant can generate enough ALP energy density to account for all the dark matter that we observe in the Universe.

An important cosmological constraint arises from isocurvature fluctuations imprinted by inflation. To apply these constraints to our scenario we give a simple derivation of the size of isocurvature fluctuations in general models with arbitrary potential and even a temperature dependence of the potential. As a useful cross-check we have updated the isocurvature constraints [63,69] using the newest Planck data [35] and the most recent results for the QCD topological susceptibility [68]. The result can be found in Fig. 7. In our noncanonical setup the isocurvature constraints are even slightly weaker as can be seen in Fig. 8.

An interesting nontrivial situation arises if the ALP is coupled to the strong interactions, i.e., via a term $\sim\phi G\tilde{G}$. This is of particular interest since a number of experiments are currently searching for ALP dark matter with this coupling [30–32]. The coupling to gluons leads to two nontrivial features: the generation of a temperature-dependent, irreducible contribution to the ALP mass and an effective ALP-field-value-dependent nucleon mass. The former naively makes large parts of the low mass region explored by current experiments inaccessible [28]. This can be avoided by invoking a precise cancellation with an additional term in the ALP potential (with or without noncanonical terms). The latter leads to strong constraints from big bang nucleosynthesis. These are significantly weakened in our scenario with a noncanonical kinetic term. This opens up significant parameter space that can be explored in near future experiments such as Casper [31] and HeXeniA [32], as well as EDM storage rings [77].

ACKNOWLEDGMENTS

This project has received funding from the European Union's Horizon 2020 research and innovation program

under the Marie Sklodowska-Curie Grants No. 690575 (RISE InvisiblesPlus) and No. 674896 (ITN ELUSIVES).

APPENDIX A: EFFECT OF HIGHER-ORDER POLES IN THE KINETIC FUNCTION

In this appendix we briefly study how our results change if we allow our noncanonical kinetic term for the ALP field to have a pole of arbitrary (even) order. We work with the Lagrangian (4), this time with the kinetic function given by

$$K(\phi) = \frac{1}{\cos^p\left(\frac{N\phi}{f_a}\right)}, \qquad p \in \mathbb{N}. \tag{A1}$$

Note that with this definition the order of the pole is $2p$. In the main body we have focused on the $p = 1$ case. As opposed to the $p = 1$ case, for a general value of p it is not possible to find an exact analytic expression for the transformation to the canonically normalized field $\psi(\phi)$. However, we can find an approximate expression, valid close to the pole at $\phi/f_a = \pi/(2N)$, by expanding $K(\phi)$ in a Laurent series and keeping only the leading divergent term. With that, we can then proceed as in Sec. III B and obtain an estimation for the enhancement in the relic density. The result is

$$\frac{\rho^{\mathrm{anh}}}{\rho^{\mathrm{harm}}} \propto \begin{cases} \exp^{\frac{3}{4}N\psi_0}, & p = 1 \\ (N\psi_0)^{\frac{3}{2}\left(1+\frac{1/2}{k-1}\right)}, & p \neq 1 \end{cases}. \tag{A2}$$

Due to the now unbounded field range, a significant enhancement is possible. Nevertheless, it may seem that the enhancement effect is much weaker in the $p > 1$ cases, which could seem counterintuitive. However, we must note that the field redefinition $\psi(\phi)$ is different for different values of p, which means that it is not so obvious to compare the distinct cases just by looking at (A2). In order to be able to compare, we can recast (A2) in terms of the noncanonically normalized field ϕ, which avoids the problem of the p-dependent field redefinition. Doing so, we can write

$$\frac{\rho^{\mathrm{anh}}}{\rho^{\mathrm{harm}}} \propto \left(\frac{1}{\sqrt{\frac{\pi}{2N} - \theta_0}}\right)^{2p-1}, \tag{A3}$$

which is valid for all $p \in \mathbb{N}$. Looking at (A3) we can confirm that there exists an enhancement in the ALP relic density for all values of p. What is more, looking at it from the point of view of the noncanonically normalized field, the effect is stronger the higher the order of the pole, as one would naively expect.

APPENDIX B: TEMPERATURE-DEPENDENT ANHARMONICITY FUNCTION

In this section we detail how to implement the effects of the temperature dependence of the QCD axion mass into the anharmonicity function [53,69]. The approach that we follow allows us to analytically upgrade any anharmonicity function that does not include temperature effects into a full temperature-dependent anharmonicity function. The derivation that we present is valid for any scalar field whose potential can be factorized as

$$V(\phi) = m^2(T) \cdot V_0(\phi), \tag{B1}$$

where $V_0(\phi)$ is a temperature-independent potential that has a minimum around which the field can oscillate (possibly anharmonically), and the temperature dependence acts only as a scaling. This is the case for general axion models, including those we study in this paper. If there is no temperature dependence at all, then $m(T) \equiv m$ and working as in Sec. III C we can express the energy density of the field with an anharmonic potential as

$$\rho^{\mathrm{anh}} = f(\theta_0)\rho^{\mathrm{harm}}, \tag{B2}$$

where ρ^{harm} is the solution to the harmonic case described in Sec. III A and $f(\theta_0)$ is the anharmonicity function that depends on the initial value of the dimensionless field $\theta = \phi/f_a$.

At the effective level, we can think that the only effect of the anharmonicities is to change the time (or temperature) at which the oscillations start. This is of course not what actually happens, but with this approach we will be able to make a good estimate of the energy density of the field at late times. In this picture, we have that

$$f(\theta_0) = \frac{\rho^{\mathrm{anh}}}{\rho^{\mathrm{harm}}} = \left(\frac{T_{\mathrm{S}}^{\mathrm{harm}}}{T_{\mathrm{S}}^{\mathrm{anh}}}\right)^3 \frac{g_{\star S}(T_{\mathrm{S}}^{\mathrm{harm}})}{g_{\star S}(T_{\mathrm{S}}^{\mathrm{anh}})}, \tag{B3}$$

which follows from the dependence of the WKB solution (27) on the temperature at which oscillations start.[13] With this we can extend the equation for the condition of the start of the oscillations in the harmonic case, $3H(T_{\mathrm{S}}^{\mathrm{harm}}) = m$, to the anharmonic case, using an effective mass that encodes the effects of the anharmonicity. It reads

$$3H(T_{\mathrm{S}}^{\mathrm{anh}}) = m(f(\theta_0))^{-2/3}. \tag{B4}$$

This expression will be useful later on.

We now assume that there is a temperature-dependent mass that evolves as (52), as is the case for axion models.

[13] In the following equations, we will neglect all instances of quotients of effective degrees of freedom, as they only introduce a small correction and make the derivation much more cumbersome.

As was argued in the main body of the paper, if $T_S^{\rm anh} < T_{\rm crit}$, the oscillations start after the QCD phase transition, when the mass has already attained its low-temperature value, and the temperature dependence has no effect on the later evolution of the field. In the harmonic case, this happens if the zero-temperature mass is smaller than m^* given by $3H(T_{\rm crit}) = m^*$, that is,

$$m^* = 3 \cdot 1.66 \sqrt{g_\star(T_{\rm crit})} \frac{T_{\rm crit}^2}{m_{\rm Pl}} \simeq 6.6 \times 10^{-11}\ {\rm eV}. \quad \text{(B5)}$$

In terms of decay constants, this translates into a maximum value $f_a^* \simeq 8.7 \times 10^{16}$ GeV above which the temperature dependence does not play a role. In the anharmonic case, it can happen that the anharmonicities delay the start of the oscillations beyond $T_{\rm crit}$, even if $f_a < f_a^*$, if the initial misalignment angle is large enough. We can use Eq. (B3) to find an expression for this critical value θ_0^*. Writing it in terms of f_a^*, it reads

$$\left(\frac{f_a^*}{f_a}\right)^{3/2} = f(\theta_0^*), \quad \text{(B6)}$$

from where θ_0^* can be obtained once an explicit anharmonicity function is chosen.

Finally, if both $f_a < f_a^*$ and $\theta_0 < \theta_0^*$, then $T_S^{\rm anh} > T_{\rm crit}$ and the temperature-dependent evolution of the mass will have an impact on the oscillating behavior of the field. First of all, we compute how the onset of the oscillations is modified. For this purpose, we can just substitute the constant mass m for the temperature-dependent one $m(T)$ in Eq. (B4). Using the expression for $m(T)$ given in (52), we have the condition

$$3H(T_S) = m\left(\frac{T_S}{T_{\rm crit}}\right)^{\alpha} (f(\theta_0))^{-2/3}. \quad \text{(B7)}$$

To simplify the notation, we have denoted T_S the temperature at which the oscillations start if we take into account both the anharmonicities of $V_0(\phi)$ and the temperature dependence of $m(T)$. We can recast this equation in terms of decay constants, finding

$$\frac{T_S}{T_{\rm crit}} = \left(\frac{f_a^*}{f_a} \cdot (f(\theta_0))^{-2/3}\right)^{\frac{1}{2-\alpha}}. \quad \text{(B8)}$$

To continue, we use the expression for the energy density of an oscillating scalar field with a slowly varying mass, which can be found for instance in [17] and reads[14]

$$\rho(T) = \frac{1}{2} m(T) m(T_S) f_a^2 \theta_0^2 \frac{g_{\star S}(T)}{g_{\star S}(T_S)} \left(\frac{T}{T_S}\right)^3. \quad \text{(B9)}$$

At low temperatures below the QCD critical temperature, the quotient between this expression and the corresponding one for the harmonic case is

$$\frac{\rho(T)}{\rho^{\rm harm}(T)} = \frac{m(T_S)}{m} \frac{g_{\star S}(T_S^{\rm harm})}{g_{\star S}(T_S)} \left(\frac{T_S^{\rm harm}}{T_S}\right)^3. \quad \text{(B10)}$$

But this is precisely what we need to define the temperature-dependent anharmonicity function $F(\theta_0, f_a)$. Again, neglecting the quotient of effective degrees of freedom, we find

$$\begin{aligned} F(\theta_0, f_a) &\equiv \frac{\rho(T)}{\rho^{\rm harm}(T)} \\ &\simeq \frac{m(T_S)}{m} \left(\frac{T_S^{\rm harm}}{T_{\rm crit}}\right)^3 \left(\frac{T_{\rm crit}}{T_S}\right)^3 \\ &= \left(\frac{T_S}{T_{\rm crit}}\right)^{\alpha-3} \left(\frac{f_a}{f_a^*}\right)^{-3/2} \\ &= \left(\frac{f_a^*}{f_a}\right)^{\frac{\alpha}{2(2-\alpha)}} (f(\theta_0))^{\frac{2(3-\alpha)}{3(2-\alpha)}}. \end{aligned} \quad \text{(B11)}$$

It can be checked that this result agrees with the ones given in [53,69], but it can be applied in more general contexts.

[14] This expression is a generalization of the WKB approximation presented before.

[1] J. Jaeckel and A. Ringwald, The low-energy frontier of particle physics, Annu. Rev. Nucl. Part. Sci. **60**, 405 (2010).
[2] M. Cicoli, Axion-like particles from string compactifications, arXiv:1309.6988.
[3] A. Ringwald, Axions and axion-like particles, arXiv: 1407.0546.
[4] R. D. Peccei and H. R. Quinn, *CP* Conservation in the Presence of Pseudoparticles, Phys. Rev. Lett. **38**, 1440 (1977).
[5] S. Weinberg, A New Light Boson?, Phys. Rev. Lett. **40**, 223 (1978).
[6] F. Wilczek, Problem of Strong P and T Invariance in the Presence of Instantons, Phys. Rev. Lett. **40**, 279 (1978).
[7] E. Masso and R. Toldra, On a light spinless particle coupled to photons, Phys. Rev. D **52**, 1755 (1995).
[8] E. Masso and R. Toldra, New constraints on a light spinless particle coupled to photons, Phys. Rev. D **55**, 7967 (1997).

[9] E. Masso, F. Rota, and G. Zsembinszki, Planck-scale effects on global symmetries: Cosmology of pseudo-Goldstone bosons, Phys. Rev. D **70**, 115009 (2004).
[10] P. Svrcek and E. Witten, Axions in string theory, J. High Energy Phys. 06 (2006) 051.
[11] M. R. Douglas and S. Kachru, Flux compactification, Rev. Mod. Phys. **79**, 733 (2007).
[12] A. Arvanitaki, S. Dimopoulos, S. Dubovsky, N. Kaloper, and J. March-Russell, String axiverse, Phys. Rev. D **81**, 123530 (2010).
[13] B. S. Acharya, K. Bobkov, and P. Kumar, An M theory solution to the strong *CP* problem and constraints on the axiverse, J. High Energy Phys. 11 (2010) 105.
[14] T. Higaki and T. Kobayashi, Note on moduli stabilization, supersymmetry breaking and axiverse, Phys. Rev. D **84**, 045021 (2011).
[15] D. J. E. Marsh, The axiverse extended: Vacuum destabilisation, early dark energy and cosmological collapse, Phys. Rev. D **83**, 123526 (2011).
[16] M. Cicoli, M. Goodsell, and A. Ringwald, The type IIB string axiverse and its low-energy phenomenology, J. High Energy Phys. 10 (2012) 146.
[17] P. Arias *et al.*, WISPy cold dark matter, J. Cosmol. Astropart. Phys. 06 (2012) 013.
[18] A. Ringwald, Exploring the role of axions and other WISPs in the dark universe, Phys. Dark Universe **1**, 116 (2012).
[19] J. Jaeckel, A family of WISPy dark matter candidates, Phys. Lett. B **732**, 1 (2014).
[20] D. J. E. Marsh, Axion cosmology, Phys. Rep. **643**, 1 (2016).
[21] J. Preskill, M. B. Wise, and F. Wilczek, Cosmology of the invisible axion, Phys. Lett. **120B**, 127 (1983).
[22] L. F. Abbott and P. Sikivie, A cosmological bound on the invisible axion, Phys. Lett. **120B**, 133 (1983).
[23] M. Dine and W. Fischler, The not-so-harmless axion, Phys. Lett. **120B**, 137 (1983).
[24] P. W. Graham, I. G. Irastorza, S. K. Lamoreaux, A. Lindner, and K. A. van Bibber, Experimental searches for the axion and axion-like particles, Annu. Rev. Nucl. Part. Sci. **65**, 485 (2015).
[25] Y. V. Stadnik and V. V. Flambaum, Axion-induced effects in atoms, molecules and nuclei: Parity nonconservation, anapole moments, electric dipole moments, and spin-gravity and spinaxion momentum couplings, Phys. Rev. D **89**, 043522 (2014).
[26] M. Pospelov and A. Ritz, Theta-Induced Electric Dipole Moment of the Neutron via QCD Sum Rules, Phys. Rev. Lett. **83**, 2526 (1999).
[27] P. W. Graham and S. Rajendran, New observables for direct detection of axion dark matter, Phys. Rev. D **88**, 035023 (2013).
[28] K. Blum, R. T. D'Agnolo, M. Lisanti, and B. R. Safdi, Constraining axion dark matter with big bang nucleosynthesis, Phys. Lett. B **737**, 30 (2014).
[29] G. G. Raffelt, Astrophysical axion bounds, Lect. Notes Phys. **741**, 51 (2008).
[30] C. Abel *et al.*, Search for Axion-like Dark Matter through Nuclear Spin Precession in Electric and Magnetic Fields, Phys. Rev. X **7**, 041034 (2017).
[31] D. Budker, P. W. Graham, M. Ledbetter, S. Rajendran, and A. Sushkov, Cosmic Axion Spin Precession Experiment (CASPEr), Phys. Rev. X **4**, 021030 (2014).
[32] U. Schmidt (private communication).
[33] A. Hook and J. Huang, Probing axions with neutron star inspirals and other stellar processes, J. High Energy Phys. 06 (2018) 036.
[34] A. Arvanitaki, M. Baryakhtar, and X. Huang, Discovering the QCD axion with black holes and gravitational waves, Phys. Rev. D **91**, 084011 (2015).
[35] P. A. R. Ade *et al.*, Planck 2015 results. XX. Constraints on inflation, Astron. Astrophys. **594**, A20 (2016).
[36] E. Silverstein and A. Westphal, Monodromy in the CMB: Gravity waves and string inflation, Phys. Rev. D **78**, 106003 (2008).
[37] L. McAllister, E. Silverstein, and A. Westphal, Gravity waves and linear inflation from axion monodromy, Phys. Rev. D **82**, 046003 (2010).
[38] N. Kaloper and L. Sorbo, A Natural Framework for Chaotic Inflation, Phys. Rev. Lett. **102**, 121301 (2009).
[39] J. Jaeckel, V. M. Mehta, and L. T. Witkowski, Monodromy dark matter, J. Cosmol. Astropart. Phys. 01 (2017) 036.
[40] M. Alishahiha, E. Silverstein, and D. Tong, DBI in the sky, Phys. Rev. D **70**, 123505 (2004).
[41] V. Domcke, F. Muia, M. Pieroni, and L. T. Witkowski, PBH dark matter from axion inflation, J. Cosmol. Astropart. Phys. 07 (2017) 048.
[42] O. Wantz and E. P. S. Shellard, Axion cosmology revisited, Phys. Rev. D **82**, 123508 (2010).
[43] G. G. di Cortona, E. Hardy, J. P. Vega, and G. Villadoro, The QCD axion, precisely, J. High Energy Phys. 01 (2016) 034.
[44] R. Kallosh, A. Linde, and D. Roest, Superconformal inflationary alpha-attractors, J. High Energy Phys. 11 (2013) 198.
[45] R. Kallosh and A. Linde, Planck, LHC, and alpha-attractors, Phys. Rev. D **91**, 083528 (2015).
[46] M. Galante, R. Kallosh, A. Linde, and D. Roest, The Unity of Cosmological Attractors, Phys. Rev. Lett. **114**, 141302 (2015).
[47] R. D. Peccei, The strong *CP* problem and axions, Lect. Notes Phys. **741**, 3 (2008).
[48] J. E. Kim and G. Carosi, Axions and the strong *CP* problem, Rev. Mod. Phys. **82**, 557 (2010).
[49] M. S. Turner, Cosmic and local mass density of "invisible", axions, Phys. Rev. D **33**, 889 (1986).
[50] D. H. Lyth, Axions and inflation: Vacuum fluctuations, Phys. Rev. D **45**, 3394 (1992).
[51] K. Strobl and T. J. Weiler, Anharmonic evolution of the cosmic axion density spectrum, Phys. Rev. D **50**, 7690 (1994).
[52] K. J. Bae, J.-H. Huh, and J. E. Kim, Update of axion CDM energy density, J. Cosmol. Astropart. Phys. 09 (2008) 005.
[53] A. Diez-Tejedor and D. J. E. Marsh, Cosmological production of ultralight dark matter axions, arXiv:1702.02116.
[54] J. Soda and Y. Urakawa, Cosmological imprints of string axions in plateau, arXiv:1710.00305.
[55] V. Irsic, M. Viel, M. G. Haehnelt, J. S. Bolton, and G. D. Becker, First Constraints on Fuzzy Dark Matter from Lyman-Alpha Forest Data and Hydrodynamical Simulations, Phys. Rev. Lett. **119**, 031302 (2017).
[56] P. Sikivie, Cosmic global strings, Phys. Scr. **T36**, 127 (1991).

[57] C. Hagmann, S. Chang, and P. Sikivie, Axion radiation from strings, Phys. Rev. D **63**, 125018 (2001).
[58] A. Linde, Particle physics and inflationary cosmology, arXiv:hep-th/0503203.
[59] G. W. Gibbons and S. W. Hawking, Cosmological event horizons, thermodynamics, and particle creation, Phys. Rev. D **15**, 2738 (1977).
[60] M. Beltran, J. Garcia-Bellido, and J. Lesgourgues, Isocurvature bounds on axions revisited, Phys. Rev. D **75**, 103507 (2007).
[61] M. P. Hertzberg, M. Tegmark, and F. Wilczek, Axion cosmology and the energy scale of inflation, Phys. Rev. D **78**, 083507 (2008).
[62] S. Weinberg, Must cosmological perturbations remain nonadiabatic after multi-field inflation?, Phys. Rev. D **70**, 083522 (2004).
[63] T. Kobayashi, R. Kurematsu, and F. Takahashi, Isocurvature constraints and anharmonic effects on QCD axion dark matter, J. Cosmol. Astropart. Phys. 09 (2013) 032.
[64] T. Matsumura *et al.*, Mission design of LiteBIRD, J. Low Temp. Phys. **176**, 733 (2014).
[65] A. Kogut *et al.*, The Primordial Inflation Explorer (PIXIE): A nulling polarimeter for cosmic microwave background observations, J. Cosmol. Astropart. Phys. 07 (2011) 025.
[66] K. N. Abazajian *et al.*, CMB-S4 science book, arXiv:1610.02743.
[67] O. Wantz and E. P. S. Shellard, The topological susceptibility from grand canonical simulations in the interacting instanton liquid model: Chiral phase transition and axion mass, Nucl. Phys. **B829**, 110 (2010).
[68] S. Borsanyi, M. Dierigl, Z. Fodor, S. D. Katz, S. W. Mages, D. Nogradi, J. Redondo, A. Ringwald, and K. K. Szabo, Axion cosmology, lattice QCD and the dilute instanton gas, Phys. Lett. B **752**, 175 (2016).
[69] L. Visinelli and P. Gondolo, Dark matter axions revisited, Phys. Rev. D **80**, 035024 (2009).
[70] P. W. Graham and S. Rajendran, Axion dark matter detection with cold molecules, Phys. Rev. D **84**, 055013 (2011).
[71] H. Davoudiasl, D. Hooper, and S. D. McDermott, Inflatable Dark Matter, Phys. Rev. Lett. **116**, 031303 (2016).
[72] S. Hoof and J. Jaeckel, QCD axions and axion-like particles in a 2-inflation scenario, Phys. Rev. D **96**, 115016 (2017).
[73] L. Ubaldi, Effects of theta on the deuteron binding energy and the triple-alpha process, Phys. Rev. D **81**, 025011 (2010).
[74] R. J. Crewther, P. Di Vecchia, G. Veneziano, and E. Witten, Chiral estimate of the electric dipole moment of the neutron in quantum chromodynamics, Phys. Lett. **88B**, 123 (1979).
[75] Y. V. Stadnik and V. V. Flambaum, Can Dark Matter Induce Cosmological Evolution of the Fundamental Constants of Nature?, Phys. Rev. Lett. **115**, 201301 (2015).
[76] V. Mukhanov, *Physical Foundations of Cosmology* (Cambridge University Press, Cambridge, England, 2005).
[77] S. P. Chang *et al.*, Axion dark matter search with the storage ring EDM method, Proc. Sci. PSTP2017 (**2018**) 036 [arXiv:1710.05271].

Chapter 6

Axion couplings to electroweak gauge bosons

Authors:
Gonzalo Alonso-Álvarez, M. Belén Gavela, and Pablo Quílez

Published in *Eur.Phys.J.C. 79 (2019) 3, 223*,
also available at arXiv:1811.05466

Principal authorship of this article is shared on an equal footing by the three authors. The original idea for the project was conceived by Belén Gavela and was further developed by the three authors. The calculations in Section 4 were performed predominantly by Gonzalo Alonso-Álvarez, and those in Sections 2 and 3 were performed with equal participation from the three authors. Gonzalo Alonso-Álvarez produced all figures. Section 4 was written predominantly by Gonzalo Alonso-Álvarez. All three authors contributed with corrections and suggestions to the manuscript, as well as with improvements during the review process.

Eur. Phys. J. C (2019) 79:223
https://doi.org/10.1140/epjc/s10052-019-6732-5

THE EUROPEAN PHYSICAL JOURNAL C

Regular Article - Theoretical Physics

Axion couplings to electroweak gauge bosons

G. Alonso-Álvarez[1,a], **M. B. Gavela**[2,b], **P. Quilez**[2,c]

[1] Institut für Theoretische Physik, Universität Heidelberg, Philosophenweg 16, 69120 Heidelberg, Germany
[2] Departamento de Física Teórica and Instituto de Física Teórica, IFT-UAM/CSIC, Universidad Autónoma de Madrid, Cantoblanco 28049, Madrid, Spain

Received: 4 December 2018 / Accepted: 28 February 2019 / Published online: 12 March 2019

Abstract We determine the model-independent component of the couplings of axions to electroweak gauge bosons, induced by the minimal coupling to QCD inherent to solving the strong CP problem. The case of the invisible QCD axion is developed first, and the impact on W and Z axion couplings is discussed. The analysis is extended next to the generic framework of heavy true axions and low axion scales, corresponding to scenarios with enlarged confining sector. The mass dependence of the coupling of heavy axions to photons, W and Z bosons is determined. Furthermore, we perform a *two-coupling-at-a-time* phenomenological study where the gluonic coupling together with individual gauge boson couplings are considered. In this way, the regions excluded by experimental data for the axion-WW, axion-ZZ and axion-$Z\gamma$ couplings are determined and analyzed together with the usual photonic ones. The phenomenological results apply as well to ALPs which have anomalous couplings to both QCD and the electroweak bosons.

Contents

1 Introduction

The term "axion" denotes any (pseudo)Nambu–Goldstone boson (pNGB) of a global chiral $U(1)$ symmetry which is exact at the classical level but is explicitly broken only by anomalous couplings to the field strength of QCD and perhaps other confining groups.[1] Axions are the characteristic byproduct of solutions to the strong CP problem based on an anomalous $U(1)$ axial symmetry, usually called Peccei-Quinn (PQ) symmetry [1]. Whatever its mass, an axion necessarily has anomalous gluonic couplings and it only deserves that name if its presence solves the strong CP problem. When the number of axions in a given theory outnumbers the total number of distinct instanton-induced scales other than QCD, one (or more) light axions remain.

In scenarios with an axion a coupled only to QCD, two states of the spectrum have anomalous couplings, the axion and the η'. Only one eigenstate can then acquire a mass of the order Λ_{QCD}: this is identified as the physical η', while the axion would remain massless in the limit of vanishing quark masses. The latter are relevant, though, and their impact on

[a] e-mail: alonso@thphys.uni-heidelberg.de
[b] e-mail: belen.gavela@uam.es
[c] e-mail: pablo.quilez@uam.es

[1] The SM η' is excluded from this definition since the associated $U(1)_A$ symmetry is also explicitely broken by the non-zero quark masses.

the mixing of pseudoscalars results in an axion mass given by [2,3]

$$m_a^2 f_a^2 \sim m_\pi^2 f_\pi^2 \frac{m_u m_d}{(m_u + m_d)^2}, \tag{1.1}$$

where m_π, f_π, m_u, m_d denote the pion mass and decay constant, and the up and down quark masses, respectively. The axion scale to which all axion couplings are inversely proportional is denoted by f_a. The expression in Eq. (1.1) is characteristic of all usual "invisible" axion constructions, characterised by QCD being the only confining gauge group. Paradigmatic examples are the DFSZ and the KSVZ models [4–7] and their variations. These invisible axions are also called QCD axions.

The main phenomenological constraints for QCD axions are obtained from their couplings to photons, gluons and fermions. For instance, the effective coupling to photons $g_{a\gamma\gamma}$ is defined as

$$\delta\mathcal{L} \supset \frac{1}{4} g_{a\gamma\gamma}\, a\, F_{\mu\nu}\tilde{F}^{\mu\nu}, \tag{1.2}$$

$$g_{a\gamma\gamma} = -\frac{1}{2\pi f_a}\alpha_{\rm em}\left(\frac{E}{N} - 1.92(4)\right), \tag{1.3}$$

where $F_{\mu\nu}$ is he electromagnetic field strength, α_{em} the corresponding fine structure constant, and E and N denote respectively the electromagnetic and color anomaly coefficients. The ratio E/N is model-dependent and has been recently computed in Refs. [8,9] for different representations of exotic fermions in standard "invisible axion" models. This ratio contains all direct loop contributions of PQ and electrically charged fermions, including the up and down and other SM quarks if PQ charged. The second term in the parenthesis in Eq. (1.3) is instead model-independent [3,10–13]. It stems from the mixing of the axion with the η' pseudoscalar -as both couple to $G_{\mu\nu}\tilde{G}^{\mu\nu}$ with $G_{\mu\nu}$ being the QCD field strength- and also with the pion through the η'-pion mixing due to the up-down quarks mass difference. Obviously, such model-independent mixings are relevant for axions lighter than the QCD confining scale, while if the axion is much heavier this effect should become negligible.

Light enough axions (that is, below $\mathcal{O}(100\,\text{MeV})$) can participate in astrophysical phenomena [14–16]. The constraints that follow from their non-observation in photonic processes lead to very high values for the decay constant, $f_a \gtrsim 10^8$ GeV. It follows then from Eq. (1.1) that $m_a \leq 10^{-2}$ eV for QCD axions.

Nevertheless, in specific QCD axion models the coupling to photons may be suppressed [9,17] and moreover large uncertainties may hover over the purely hadronic constraints [18]. It is thus important to analyze the axion couplings to other electroweak gauge bosons, as they may become the phenomenologically dominant couplings in certain regions of the parameter space for those models. Couplings of axions and also of axion-like particles (ALPs) to heavy gauge bosons are increasingly explored [19–25] in view of present and future collider data, and also in view of rare meson decay data. For instance, in addition to LHC-related signals, recent works [26,27] consider the one-loop impact of aWW couplings on rare meson decays.

Here we first determine the model-independent components of the mixing of QCD axions with electroweak gauge bosons, which result from the mixing of the axion with the pseudoscalar mesons of the SM. In other words, we determine the equivalent of the 1.92 factor in the photonic coupling in Eq. (1.3), for the couplings of the axion to W and Z gauge bosons. A chiral Lagrangian formulation will be used for this purpose, determining the leading-order effects. The heavy electroweak gauge bosons will be introduced in that Lagrangian as external –classical– sources. Our results should impact the analyses for light axions of theories which solve the strong CP problem. They are novel and relevant in particular whenever the axion is lighter than the QCD confining scale and is on-shell in either low-energy or high-energy experiments. They also impact the comparison between the data taken at experiments at low and high-energy. For instance, a null result in NA62 data for $K \to \pi a$ does not imply the absence of a signal at high energy in an accelerator such as that from off-shell axions at LEP or at a collider. This is because model-independent contributions are present at the low momenta dominant in rare decays (and cancellations may then take place), while at high energies they are absent.

As a second step, we will extend the analysis to heavy axions which solve the strong CP problem. Axions much heavier than Λ_{QCD} and with low axion scales are possible within dynamical solutions to the strong CP problem, at the expense of enlarging the confining sector of the Standard Model (SM) beyond QCD [28–39]. These theories introduce a second and large instanton-induced scale $\Lambda' \gg \Lambda_{QCD}$ to which the axion also exhibits anomalous couplings, resulting in the bulk of its large mass. Precisely because the axion mass typically lies well above the MeV regime, these heavy axions avoid the stringent astrophysical and laboratory constraints and present and future colliders may discover them. The transition between the light and heavy axion regime will be explored for the coupling of the axion to the photon and to the electroweak gauge bosons.

Finally, the phenomenological part of the analysis will be carried out on a "two-coupling-at-a-time" basis: it will take into account the simultaneous presence of a given electroweak coupling and the axion–gluon–gluon anomalous coupling (essential to solve the strong CP problem). For the analysis of data, for the first time the experimentally excluded areas for the EW couplings g_{aWW}, g_{aZZ} and $g_{a\gamma Z}$

will be identified and depicted separately, besides the customary ones for the $g_{a\gamma\gamma}$ coupling. Furthermore, the relations among the exclusion regions stemming from electroweak gauge invariance will be determined and exploited. Model predictions will be illustrated over the experimental parameter space.

Aside from the main focus of the paper on true axions, our analysis applies to and calls for a timely extension of the ALP parameter space. Very interesting bounds on ALPs from LEP and LHC [19–25,40,41] assume often just one electroweak coupling for the axion, and no gluonic coupling. The path to consider any two (or more) couplings at a time will change the experimental perspective on ALPs.

What is the difference between a heavy axion and an ALP with both anomalous electroweak and gluonic couplings? The key distinction is that the former stems from a solution to the strong CP problem while a "gluonic ALP" may not. Both exhibit anomalous couplings to QCD and in both cases there is an external source of mass besides that induced by QCD instantons and mixing. However, for a true heavy axion that extra source of mass does not induce a shift of the θ parameter outside the CP conserving minimum (and thus the solution to the strong CP problem is preserved), while for a generic gluonic ALP such a shift may be induced. Nevertheless, this important distinction is not directly relevant for this work, as the novel aspects and phenomenological analysis developed below are valid for both true heavy axions which solve the strong CP problem and for gluonic ALPs. To sum up, all results below for heavy axions apply directly to gluonic ALPs as well. In addition, the conclusions based purely on EW gauge invariance have an even larger reach: they hold for all type of axions and for generic ALPs (that is, ALPs with or without gluonic couplings).

The structure of the paper can be easily inferred from the Table of Contents.

2 The Lagrangian for the QCD axion

Without loss of generality, the axion couplings can be encoded in a model-independent way in an effective Lagrangian. At leading order in inverse powers of the scale $f_{\rm PQ}$ at which the global PQ symmetry is broken, and at energies above the electroweak (EW) scale, it reads

$$\mathscr{L}_{\rm eff} = \mathscr{L}_{\rm SM} + \frac{1}{2}(\partial_\mu \hat{a})(\partial^\mu \hat{a}) + \delta\mathscr{L}_a, \tag{2.1}$$

where $\hat{a}$ denotes the axion eigenstate at energies well above the confinement scale and $\mathcal{L}_{\rm SM}$ is the SM Lagrangian,

$$\begin{aligned}\mathcal{L}_{\rm SM} \supset & -\frac{1}{4}G^a_{\mu\nu}G^{a\mu\nu} - \frac{1}{4}W^a_{\mu\nu}W^{a\mu\nu} \\ & -\frac{1}{4}B_{\mu\nu}B^{\mu\nu} + D_\mu\Phi^\dagger D^\mu\Phi \\ & + \sum_\psi i\bar{\psi}\not{D}\psi - \Big(\bar{Q}_L\,\mathbf{Y}_D\,\Phi D_R + \bar{Q}_L\,\mathbf{Y}_U\,\tilde{\Phi}U_R \\ & + \bar{L}_L\,\mathbf{Y}_E\,\Phi E_R + \text{h.c.}\Big).\end{aligned} \tag{2.2}$$

In this expression, $W_{\mu\nu}$ and $B_{\mu\nu}$ are respectively the $SU(2)_L$ and $U(1)_Y$ gauge field strengths, while Φ, Q_L, L_L, U_R, D_R and E_R respectively encode the Higgs doublet, the fermion and lepton doublets, the vectors of right-handed up-type, down-type quarks and right-handed charged leptons (neutrino masses will be disregarded), with ψ running over all those type of fermions and $\tilde{\Phi} \equiv i\sigma^2\Phi^*$. The three 3×3 matrices in flavour space $\mathbf{Y}_D$, $\mathbf{Y}_U$ and $\mathbf{Y}_E$ encode the Yukawa couplings for down quarks, up quarks and charged leptons, respectively. For the effective axion couplings, we first focus on the anomalous couplings of the axion and their impact on the pseudoscalar mass matrix.

We will work in the basis in which the only PQ-breaking operators in the Lagrangian, $\delta\mathscr{L}_a^{\not{\rm PQ}}$, are the anomalous couplings of axions to gauge bosons. This choice is allowed by the reparametrization invariance of the effective axion Lagrangian (see "Appendix C"). The CP-conserving and PQ-violating next-to-leading order (NLO) corrections due to axion physics then read[2]

$$\delta\mathscr{L}_a^{\not{\rm PQ}} = N_0\,\mathbf{O}_{\tilde{G}} + L_0\,\mathbf{O}_{\tilde{W}} + P_0\,\mathbf{O}_{\tilde{B}}, \tag{2.3}$$

with $\mathbf{O}_{\tilde{G}}$, $\mathbf{O}_{\tilde{W}}$ and $\mathbf{O}_{\tilde{B}}$ denoting the anomalous axion couplings to gluons, $SU(2)_L$ and $U(1)_Y$ gauge bosons, respectively,

$$\mathbf{O}_{\tilde{G}} \equiv -\frac{\alpha_s}{8\pi}\,G^a_{\mu\nu}\tilde{G}^{a\mu\nu}\frac{\hat{a}}{f_{\rm PQ}}, \tag{2.4}$$

$$\mathbf{O}_{\tilde{W}} \equiv -\frac{\alpha_W}{8\pi}\,W^a_{\mu\nu}\tilde{W}^{a\mu\nu}\frac{\hat{a}}{f_{\rm PQ}}, \tag{2.5}$$

$$\mathbf{O}_{\tilde{B}} \equiv -\frac{\alpha_B}{8\pi}\,B_{\mu\nu}\tilde{B}^{\mu\nu}\frac{\hat{a}}{f_{\rm PQ}}, \tag{2.6}$$

where α_s, α_W and α_B denote respectively the fine structure constants for the QCD, $SU(2)_L$ and $U(1)$ gauge interactions, and N_0, P_0 and L_0 are dimensionless operator coefficients. Customarily, the Lagrangian in Eq. (2.3) is rewritten as

$$\delta\mathscr{L}_a = \frac{1}{4}g^0_{agg}\,\hat{a}\,G\tilde{G} + \frac{1}{4}g^0_{aWW}\,\hat{a}\,W\tilde{W} + \frac{1}{4}g^0_{aBB}\,\hat{a}\,B\tilde{B}, \tag{2.7}$$

where the Lorentz indices of the field strengths are implicit from now on and

$$g^0_{agg} \equiv -\frac{1}{2\pi f_{\rm PQ}}\,\alpha_s\,N_0, \qquad g^0_{aWW} \equiv -\frac{1}{2\pi f_{\rm PQ}}\alpha_W\,L_0,$$

[2] The derivative operators also present in the most general basis [3,24,42,43] are PQ invariant and thus not shown.

$$g^0_{aBB} \equiv -\frac{1}{2\pi f_{\rm PQ}}\alpha_B\, P_0. \tag{2.8}$$

The model-dependent group theoretical factors can be generically written in terms of the fermionic PQ charges $\mathcal{X}_i$ as

$$\begin{aligned} N_0 &= \sum_{i=\text{heavy}} 2\,\mathcal{X}_i\, T(R_i^{SU(3)}),\\ L_0 &= \sum_{i=\text{heavy}} 2\,\mathcal{X}_i T(R_i^{SU(2)}),\\ P_0 &= \sum_{i=\text{heavy}} 2\,\mathcal{X}_i\, Y_i^2, \end{aligned} \tag{2.9}$$

where $\mathcal{X}_i$ is the difference between the right-handed and left-handed PQ charges:[3]

$$\mathcal{X}_i = \mathcal{X}_{Li} - \mathcal{X}_{Ri}. \tag{2.10}$$

In Eq. (2.9), $T(R_i^{SU(3)})$ and $T(R_i^{SU(2)})$ are respectively the Dynkin indices of the fermionic representation R_i under QCD and $SU(2)_L$, and Y_i denotes the hypercharge. The sum over "heavy" fermions and the subscript 0 indicate that the contribution to the anomalous couplings from all exotic heavy quarks, and/or heavy SM quarks (s, c, b, and t quarks) if PQ charged, is encoded in the N_0, L_0 and P_0 operator coefficients. That is, the possible contribution of the SM first generation up (u) and down (d) quarks is not included in those coefficients. Indeed, for models in which they have PQ charges an additional PQ-invariant term must be considered, replacing the u and d Yukawa couplings in Eq. (2.2) by:

$$\begin{aligned} \delta\mathscr{L}_a^{PQ} &= -\bar{Q}_{1L}\,\mathbf{Y}_d\,\Phi\, d_R\, e^{i\,\mathcal{X}_d\,\hat{a}/f_{\rm PQ}}\\ &\quad -\bar{Q}_{1L}\,\mathbf{Y}_u\,\tilde{\Phi}\, u_R\, e^{i\,\mathcal{X}_u\,\hat{a}/f_{\rm PQ}} + \text{h.c.}, \end{aligned} \tag{2.11}$$

which assumes as convention that the axion transforms under the PQ symmetry as $a \longrightarrow a + f_{\rm PQ}$. The $\mathcal{X}_{u,d}$ dependence in Eq. (2.11) will be shown below to generate extra contributions to the physical anomalous couplings. In this equation Q_1 denotes the first family doublet, and flavour-mixing effects as well as leptonic couplings are omitted from now on for simplicity. In all equations above, color and $SU(2)_L$ indices are implicit and the QCD θ angle has been removed from the Lagrangian via the PQ symmetry.

Among the most general set of purely derivative operators, additional couplings could also be considered, e.g.

$$\begin{aligned} \delta\mathscr{L}^{PQ}_{a,\text{deriv}} &= -\frac{\partial_\mu \hat{a}}{f_{\rm PQ}}\Big(\bar{Q}_L\,\gamma_\mu\, c_1^Q\, Q_L \;+\; \bar{U}_R\,\gamma_\mu\, c_1^U\, U_R\\ &\quad + \bar{D}_R\,\gamma_\mu\, c_1^D\, D_R\Big), \end{aligned} \tag{2.12}$$

where c_1^Q, c_1^U and c_1^D are matrices of arbitrary coefficients in flavour space. Nevertheless, the reparametrization invariance of the Lagrangian [44] allows to work in a basis in which these terms (which would seed pseudoscalar kinetic mixing) are absent and their impact is transferred to other axionic couplings.[4] From now on they will be disregarded all through the analysis on pseudoscalar mixing. In summary, the Lagrangian to be analyzed below when considering mixing effects reads

$$\delta\mathscr{L}_a \;=\; \delta\mathscr{L}_a^{\not PQ} \;+\; \delta\mathscr{L}_a^{PQ}. \tag{2.13}$$

Below EW symmetry breaking and above confinement

After electroweak symmetry breaking but before QCD confinement, the effective Lagrangian in Eq. (2.13) results in

$$\begin{aligned} \delta\mathscr{L}_a &= -\,\bar{u}_L\, m_u\, u_R\, e^{i\,\mathcal{X}_u\,\hat{a}/f_{\rm PQ}}\\ &\quad -\,\bar{d}_L\, m_d\, d_R\, e^{i\,\mathcal{X}_d\,\hat{a}/f_{\rm PQ}} \;+\; \text{h.c.}\\ &\quad +\frac{1}{4}g^0_{agg}\,\hat{a}\,G\tilde{G} + \frac{1}{4}g^0_{a\gamma\gamma}\,\hat{a}\,F\tilde{F} + \frac{1}{4}g^0_{aWW}\,\hat{a}\,W\tilde{W}\\ &\quad +\frac{1}{4}g^0_{aZZ}\,\hat{a}\,Z\tilde{Z} + \frac{1}{4}g^0_{a\gamma Z}\,\hat{a}\,F\tilde{Z}, \end{aligned} \tag{2.14}$$

where

$$g^0_{agg} = -\frac{1}{2\pi f_{\rm PQ}}\,\alpha_s\, N_0 \tag{2.15}$$

$$g^0_{a\gamma\gamma} = -\frac{1}{2\pi f_{\rm PQ}}\alpha_{\rm em}\, E_0, \tag{2.16}$$

$$g^0_{aWW} = -\frac{1}{2\pi f_{\rm PQ}}\frac{\alpha_{\rm em}}{s_w^2}\, L_0, \tag{2.17}$$

$$g^0_{aZZ} = -\frac{1}{2\pi f_{\rm PQ}}\frac{\alpha_{\rm em}}{s_w^2 c_w^2}\, Z_0, \tag{2.18}$$

$$g^0_{a\gamma Z} = -\frac{1}{2\pi f_{\rm PQ}}\frac{\alpha_{\rm em}}{s_w c_w}\, 2R_0. \tag{2.19}$$

In these equations s_w and c_w denote the sine and cosine of the Weinberg mixing angle and $\alpha_{em} = \alpha_W c_w^2 = \alpha_B s_w^2$.

For models in which the the first generation of SM quarks are not PQ charged, $\mathcal{X}_{u,d} = 0$. When those quarks are instead charged under PQ, their contribution to the anomalous gauge couplings has to be included in the group theory factors, which are replaced by

$$\begin{aligned} &N = N_0 + N_{u,d}, \quad E = E_0 + E_{u,d},\\ &L = L_0 + L_{u,d}, \end{aligned} \tag{2.20}$$

$$Z = Z_0 + Z_{u,d}, \quad R = R_0 + R_{u,d}, \tag{2.21}$$

[3] Obviously, only left-handed quarks may contribute to L_0; in any case, it is always possible to work in a convention in which only left-handed quarks are PQ charged.

[4] In "App. C" it will be explicitly shown that they do not have physical impact on mixing. Note that possible flavour non-diagonal couplings are not considered.

as computed further below. In all cases, only two among the four parameters E, L, Z and R are linearly independent, because of gauge invariance, see Eq. (2.3),

$$E \equiv L + P, \quad Z \equiv L c_w^4 + P s_w^4, \quad R \equiv L c_w^2 - P s_w^2. \tag{2.22}$$

A non-vanishing N is the trademark of axion models which solve the strong CP problem, while the presence of the other couplings is model-dependent. It is customary to define the physical axion scale f_a from the strength of the gluonic coupling:

$$f_a \equiv \frac{f_{PQ}}{N}. \tag{2.23}$$

2.1 The Lagrangian below the QCD confinement scale

Three pseudoscalars mix once quarks are confined: the axion, the SM singlet η_0 and the neutral pion π_3. The π_3-η_0 mixing is due to the quark mass differences which break the global flavour symmetry. At leading order in the chiral expansion and in the two quark approximation, the mass Lagrangian for the pions and η_0 reads

$$\mathcal{L} \supset B_0 \frac{f_\pi^2}{2} \mathrm{Tr}\left(\mathbf{\Sigma}\, M_q^\dagger + M_q\, \mathbf{\Sigma}^\dagger\right), \tag{2.24}$$

where B_0 can be expressed in terms of the QCD quark condensate $\langle \bar{q} q \rangle$ as $B_0 f_\pi^2 = -2\langle \bar{q} q \rangle$, and M_q denotes the quark mass matrix,

$$M_q = \begin{pmatrix} m_u & 0 \\ 0 & m_d \end{pmatrix}. \tag{2.25}$$

The matrix of pseudoscalar fields can be written as

$$\mathbf{\Sigma}(x) = \exp[i\,(2\eta_0/(f_\pi\,\sqrt{2})\,\mathbf{1}]\exp[i\,\mathbf{\Pi}/f_\pi]\,, \tag{2.26}$$

where the η_0 decay constant has been approximated by f_π and

$$\mathbf{\Pi} \equiv \begin{pmatrix} \pi_3 & \sqrt{2}\pi^+ \\ \sqrt{2}\pi^- & -\pi_3 \end{pmatrix}. \tag{2.27}$$

In the presence of the axion, the anomalous QCD current $G\tilde{G}$ couples to both the axion and the η_0 fields and mixes them. The two mixing sources combined result ultimately in an axion–pion mixing. For simplicity, we will first consider the case with $\mathcal{X}_{u,d} = 0$ in Eq. (2.11), and afterwards the case $\mathcal{X}_{u,d} \neq 0$.

2.1.1 SM light quarks not charged under PQ ($\mathcal{X}_{\mathbf{u,d}} = \mathbf{0}$)

A popular example of this class of models are KSVZ ones, in which only heavy exotic quarks are charged under PQ. For any model in which the u and d SM quarks are singlets of the PQ symmetry, their quark mass matrix in the basis here considered is that in Eq. (2.25). In this case $N = N^0$, as all contributions to the anomalous gluonic coupling are already included in N^0. The potential for the three pseudoscalars is, at first order in the pseudoscalar masses,

$$V = -B_0 f_\pi^2 \left[m_u \cos\left(\frac{\pi_3}{f_\pi} + \frac{\eta_0}{f_\pi}\right) + m_d \cos\left(\frac{\pi_3}{f_\pi} - \frac{\eta_0}{f_\pi}\right)\right] + \frac{1}{2} K \left(2\frac{\eta_0}{f_\pi} + \frac{a}{f_a}\right)^2, \tag{2.28}$$

where the last term stems from the instanton potential with $K \sim \Lambda_{QCD}^4$ [45–47]. The resulting mass matrix for the three neutral pseudoscalars is given by

$$M^2_{\{\pi_3,\,\eta_0,a\}} = \begin{pmatrix} B_0\,(m_u + m_d) & B_0\,(m_u - m_d) & 0 \\ B_0\,(m_u - m_d) & 4K/f_\pi + B_0(m_u + m_d) & 2K/(f_\pi f_a) \\ 0 & 2K/(f_\pi f_a) & K/f_a^2 \end{pmatrix}. \tag{2.29}$$

The diagonalization leads to the well-known expressions for the pseudoscalar mass terms:

$$\begin{aligned} m_\pi^2 &\simeq B_0\,(m_u + m_d), \\ m_{\eta'}^2 &\simeq \frac{4K}{f_\pi^2} + B_0\,(m_u + m_d), \\ m_a^2 &\simeq \frac{f_\pi^2 m_\pi^2}{f_a^2} \frac{m_u m_d}{(m_u + m_d)^2}. \end{aligned} \tag{2.30}$$

It follows from these expressions that K can be expressed in terms of the low-energy physical parameters as

$$K \simeq \frac{1}{4}\,(m_\eta^2 - m_\pi^2)\, f_\pi^2. \tag{2.31}$$

The corresponding mixing matrix is given by

$$\begin{pmatrix} 1 & \frac{f\,(m_d - m_u)}{2 f_a (m_d + m_u)} & \frac{f}{2 f_a} \\ -\frac{f\,(m_d - m_u)}{2 f_a (m_d + m_u)} & 1 & -\frac{m_\pi^2}{m_{\eta'}^2}\frac{(m_d - m_u)}{(m_d + m_u)} \\ -\frac{f}{2 f_a} & \frac{m_\pi^2}{m_{\eta'}^2}\frac{(m_d - m_u)}{(m_d + m_u)} & 1 \end{pmatrix}, \tag{2.32}$$

or, equivalently, the mass eigenstates are given by

$$a \simeq \hat{a} + \theta_{a\pi}\,\pi_3 + \theta_{a\eta'}\,\eta_0, \tag{2.33}$$

$$\pi^0 \simeq \pi_3 + \theta_{\pi\,a}\,a + \theta_{\pi\eta'}\,\eta_0, \tag{2.34}$$

$$\eta' \simeq \eta_0 + \theta_{\eta'\,a}\,a + \theta_{\eta'\,\pi}\,\pi_3. \tag{2.35}$$

Here, all the mixing angles are assumed small and

$$\theta_{a\pi} \simeq -\frac{f_\pi}{2f_a}\frac{m_d-m_u}{m_u+m_d}, \quad \theta_{a\eta'} \simeq -\frac{f_\pi}{2f_a}, \theta_{\pi\eta'} \simeq \frac{m_\pi^2}{m_{\eta'}^2}\frac{(m_d-m_u)}{(m_d+m_u)}, \tag{2.36}$$

$$\theta_{\pi\,a} \simeq -\theta_{a\pi}, \quad \theta_{\eta'\,a} \simeq -\theta_{a\eta'}, \quad \theta_{\eta'\,\pi} \simeq -\theta_{\pi\eta'}. \tag{2.37}$$

Only the leading terms for each mixing entry have been kept in Eqs. (2.32)–(2.37). The complete matrix to first order in $1/f_a$ and in quark masses –that is, $\mathcal{O}(m_\pi^2/m_\eta^2)$– can be found in "Appendix A": the impact of the extra terms may be comparable to that of next-to-leading operators in the chiral expansion and will thus not be retained here.

The results in Eqs. (2.33)–(2.37) illustrate that the physical low-energy axion eigenstate acquires π_3 and η_0 components and thus inherits their couplings to *all gauge bosons*, weighted down by their mixing with the axion. These results apply to any physical process in which the axion is on-shell and the axion mass is lighter than the confinement scale.

We are interested in identifying the model-independent contributions in the coupling to the electroweak gauge bosons for light axions and for the SM light pseudoscalars. We will first recover in our basis the customary axion–photon couplings, to set the framework.

Axion–photon coupling

The physical $g_{a\gamma\gamma}$ is given by

$$g_{a\gamma\gamma} = g^0_{a\gamma\gamma} + \theta_{a\pi}\,g_{\pi\gamma\gamma} + \theta_{a\eta'}\,g_{\eta'\gamma\gamma}, \tag{2.38}$$

where the last two terms are the contributions induced by the model-independent axion–pion and axion-η' QCD mixing. Denoting by q_u and q_d the electric charges of the up and down quarks, respectively, the photonic couplings of the SM light pseudoscalars are given by

$$g_{\pi\gamma\gamma} \equiv -\frac{3\,\alpha}{\pi\ f_\pi}\big(q_u^2 - q_d^2\big), \quad g_{\eta'\gamma\gamma} \equiv -\frac{3\,\alpha}{\pi\ f_\pi}\big(q_u^2 + q_d^2\big). \tag{2.39}$$

For the present case with $\mathcal{X}_{u,d} = 0$, that is $E_0 = E$ and $N_0 = N$, it follows that

$$g_{a\gamma\gamma} = g^0_{a\gamma\gamma} + \frac{\alpha}{2\pi f_a}\left(6\,\frac{q_d^2\,m_u + q_u^2\,m_d}{m_u+m_d}\right), \tag{2.40}$$

resulting in the well-known expression

$$g_{a\gamma\gamma} = -\frac{\alpha}{2\pi f_a}\left(\frac{E}{N} - \frac{2}{3}\,\frac{m_u+4\,m_d}{m_u+m_d}\right), \tag{2.41}$$

which is valid to first order in chiral perturbation theory.

2.1.2 SM light quarks charged under PQ ($\mathcal{X}_{\mathbf{u,d}} \neq \mathbf{0}$)

The quark mass matrix in Eq. (2.24) is to be replaced by

$$M_q = \begin{pmatrix} m_u & 0 \\ 0 & m_d \end{pmatrix}\begin{pmatrix} e^{i\,\mathcal{X}_u\,\hat{a}/f_{\rm PQ}} & 0 \\ 0 & e^{i\,\mathcal{X}_d\,\hat{a}/f_{\rm PQ}} \end{pmatrix}. \tag{2.42}$$

The potential in Eq. (2.28) is now generalized to

$$\begin{aligned} V = -B_0 f_\pi^2 \Bigg[& m_u \cos\left(\frac{\pi_3}{f_\pi} + \frac{\eta_0}{f_\pi} - \mathcal{X}_u\,\frac{\hat{a}}{f_{\rm PQ}}\right) \\ & + m_d \cos\left(\frac{\pi_3}{f_\pi} - \frac{\eta_0}{f_\pi} - \mathcal{X}_d\,\frac{\hat{a}}{f_{\rm PQ}}\right)\Bigg] \\ & + \frac{1}{2}\,K\left[2\frac{\eta_0}{f_\pi} + N_0\frac{\hat{a}}{f_{\rm PQ}}\right]^2, \end{aligned} \tag{2.43}$$

resulting in a pseudoscalar squared mass matrix $M^2_{\{\pi_3,\,\eta_0,a\}}$ which takes the form

$$M^2_{\{\pi_3,\,\eta_0,a\}} = \begin{pmatrix} B_0\,(m_u+m_d) & B_0\,(m_u-m_d) & -B_0\,\frac{f_\pi}{f_{\rm PQ}}\big(m_u\,\mathcal{X}_u - m_d\,\mathcal{X}_d\big) \\ B_0\,(m_u-m_d) & \frac{4K}{f_\pi} + B_0(m_u+m_d) & \frac{2\,N_0\,K}{f_\pi\,f_{\rm PQ}} + B_0\,\frac{f_\pi}{f_{\rm PQ}}\big(m_u\,\mathcal{X}_u + m_d\,\mathcal{X}_d\big) \\ -B_0\,\frac{f_\pi}{f_{\rm PQ}}\big(m_u\,\mathcal{X}_u - m_d\,\mathcal{X}_d\big) & \frac{2\,N_0\,K}{f_\pi\,f_{\rm PQ}} + B_0\,\frac{f_\pi}{f_{\rm PQ}}\big(m_u\,\mathcal{X}_u + m_d\,\mathcal{X}_d\big) & \frac{N_0^2\,K}{f_{\rm PQ}^2} + B_0\,\frac{f_\pi^2}{f_{\rm PQ}^2}\big(m_u\,\mathcal{X}_u^2 + m_d\,\mathcal{X}_d^2\big) \end{pmatrix}. \tag{2.44}$$

The mixing angles in Eqs. (2.36)–(2.37) still hold but for the pion–axion mixing which is now given by[5]

$$\theta_{a\pi} \simeq -\frac{f_\pi}{2f_{\rm PQ}}\left(\mathcal{X}_d - \mathcal{X}_u + \big(N_0 + \mathcal{X}_d + \mathcal{X}_u\big)\frac{m_d-m_u}{m_u+m_d}\right). \tag{2.45}$$

The coefficient in front of the mass-dependent term in this equation coincides with the strength of the physical gluonic couplings,[6] given by

$$N = \big(N_0 + \mathcal{X}_d + \mathcal{X}_u\big), \tag{2.46}$$

[5] This expression for the axion–pion mixing agrees with the result of Ref. [18] for the case where the only PQ charged fermions are the up and down quarks, i.e. $N_0 = 0$.

[6] As expected from the triangle diagram, all fermions (including the up and down quarks) run in the loop and contribute to $N = N_0 + \sum_{u,\,d} 2\,\mathcal{X}\,T(R) = N_0 + \mathcal{X}_d + \mathcal{X}_u$.

and in consequence

$$\theta_{a\pi} \simeq -\frac{f_\pi}{2N f_a}\left(\mathcal{X}_d - \mathcal{X}_u + N\frac{m_d - m_u}{m_u + m_d}\right). \tag{2.47}$$

The expressions for the mass of the physical pion, η' and axion are the same than those in Eq. (2.30).

Axion–photon coupling

For the case in which the up and down quarks are charged under PQ, $\mathcal{X}_{u,d} \neq 0$, N is given by Eq. (2.46) resulting in

$$g_{a\gamma\gamma} = g^0_{a\gamma\gamma} - \frac{\alpha}{2\pi f_a}\left(\frac{E_{u,d}}{N} - \frac{2}{3}\frac{m_u + 4\,m_d}{m_u + m_d}\right), \tag{2.48}$$

where

$$E_{u,d} = 6\,\mathcal{X}_u\,q_u^2 + 6\,\mathcal{X}_d\,q_d^2. \tag{2.49}$$

In consequence

$$\begin{aligned} g_{a\gamma\gamma} &= -\frac{\alpha}{2\pi f_a}\left(\frac{E_0}{N} + \frac{E_{u,d}}{N} - \frac{2}{3}\frac{m_u + 4\,m_d}{m_u + m_d}\right) \\ &= -\frac{\alpha}{2\pi f_a}\left(\frac{E}{N} - \frac{2}{3}\frac{m_u + 4\,m_d}{m_u + m_d}\right). \end{aligned} \tag{2.50}$$

In summary, the most general mass matrix leads to the same expression than for the case $\mathcal{X}_{u,d} = 0$ in Eq. (2.55) if taking into account in E also the contribution of the up and down quarks.

2.2 Axion couplings to EW gauge bosons

The description in terms of the effective chiral Lagrangian is only appropriate for energies/momenta not higher than the cutoff of the effective theory, $4\pi f_\pi$, that is, the QCD scale as set by the nucleon mass. In this context, the W and Z bosons can be considered as external currents that couple to a QCD axion whose energy/momentum is not higher than Λ_{QCD}, for instance a light enough on-shell QCD axion. In other words, the W and Z bosons enter the effective chiral Lagrangian as classical sources, alike to the treatment of baryons in the effective chiral Lagrangian.

We extend here the results of the previous section to the interactions of axions with SM heavy gauge bosons. Equation (2.55) is thus generalized for any pair of electroweak gauge bosons X, Y,

$$g_{aXY} = g^0_{aXY} + \theta_{a\pi}\,g_{\pi XY} + \theta_{a\eta'}\,g_{\eta' XY}. \tag{2.51}$$

Indeed, all axion couplings to EW bosons receive a model-independent component due to the pion-η'-axion mixings, in the regime in which the involved energy/momenta are smaller or comparable to the confinement scale. A relevant point when computing the couplings of the QCD axion to heavy EW bosons is the fact that, after confinement, a new type of $SU(2)_L$-breaking effective interaction of the form

$$\hat{a}\,W^3_{\mu\nu}\tilde{B}^{\mu\nu}, \tag{2.52}$$

is present in addition to those in Eqs. (2.4)–(2.6). It stems via axion–pion coupling from the $\pi_a W^a_{\mu\nu}\tilde{B}^{\mu\nu}$ effective interaction. The details of the computation can be found in "App. B". In terms of the physical photon, Z and W, the interaction Lagrangian for the QCD axion is then given by

$$\begin{aligned} \delta\mathscr{L}_a^{gauge} &= \frac{1}{4}g_{agg}\,a\,G\tilde{G} + \frac{1}{4}g_{aWW}\,a\,W\tilde{W} + \frac{1}{4}g_{aZZ}\,a\,Z\tilde{Z} \\ &\quad + \frac{1}{4}g_{a\gamma\gamma}\,a\,F\tilde{F} + \frac{1}{4}g_{a\gamma Z}\,a\,F\tilde{Z}, \end{aligned} \tag{2.53}$$

where

$$g_{agg} = -\frac{1}{2\pi f_a}\alpha_s, \tag{2.54}$$

$$g_{a\gamma\gamma} = -\frac{1}{2\pi f_a}\alpha_{\rm em}\left(\frac{E}{N} - \frac{2}{3}\frac{m_u + 4m_d}{m_u + m_d}\right), \tag{2.55}$$

$$g_{aWW} = -\frac{1}{2\pi f_a}\frac{\alpha_{\rm em}}{s_w^2}\left(\frac{L}{N} - \frac{3}{4}\right), \tag{2.56}$$

$$\begin{aligned} g_{aZZ} &= -\frac{1}{2\pi f_a}\frac{\alpha_{\rm em}}{s_w^2 c_w^2} \\ &\quad \times\left(\frac{Z}{N} - \frac{11s_w^4 + 9c_w^4}{12} - \frac{s_w^2(s_w^2 - c_w^2)}{2}\frac{m_d - m_u}{m_u + m_d}\right), \end{aligned} \tag{2.57}$$

$$\begin{aligned} g_{a\gamma Z} &= -\frac{1}{2\pi f_a}\frac{\alpha_{\rm em}}{s_w c_w} \\ &\quad \times\left(\frac{2R}{N} - \frac{9c_w^2 - 11s_w^2}{6} - \frac{1}{2}(c_w^2 - 3s_w^2)\frac{m_d - m_u}{m_u + m_d}\right). \end{aligned} \tag{2.58}$$

Equation (2.55) is the known leading-order result [10,13] for the photonic couplings of the QCD axion, which holds in all generality for on-shell axions lighter than the QCD confinement scale. The contributions in Eqs. (2.56)–(2.58) are new and extend that result to the couplings of heavy gauge bosons in the appropriate energy range. Indeed, the last term in the parenthesis for each of these couplings encodes the impact of the mixing of the axion with the pion and η', see Eqs. (2.15)–(2.19) for comparison with the unmixed case. These are model-independent contributions, valid for any QCD axion, i.e., for any model in which the SM strong gauge group is the only confining force and thus the only source of an instanton potential for the axion. In other words, they are valid for any axion whose mass and scale are related by Eq. (2.30). Note that those corrections hold precisely because the axion mass is smaller than the confining scale of QCD, which is the regime in which the SM pseudoscalars lighter than the QCD scale are the physical eigenstates of the spectrum and the mixing effects are meaningful.

Numerically, at leading order in the chiral expansion it follows that

$$g_{a\gamma\gamma} = -\frac{1}{2\pi f_a}\alpha_{\rm em}\left(\frac{E}{N} - 2.03\right), \tag{2.59}$$

$$g_{aWW} = -\frac{1}{2\pi f_a}\frac{\alpha_{\rm em}}{s_w^2}\left(\frac{L}{N} - 0.75\right), \tag{2.60}$$

$$g_{aZZ} = -\frac{1}{2\pi f_a}\frac{\alpha_{\rm em}}{s_w^2 c_w^2}\left(\frac{Z}{N} - 0.52\right), \tag{2.61}$$

$$g_{a\gamma Z} = -\frac{1}{2\pi f_a}\frac{\alpha_{\rm em}}{s_w c_w}\left(\frac{2R}{N} - 0.74\right). \tag{2.62}$$

The numerical value of the model-independent term in Eq. (2.59) differs from the usual one [13] of 1.92 in Eq. (1.3), as the latter includes higher order chiral corrections, a refinement out of the scope of this paper and left for future work.

The model-independent results obtained here for the coupling of light QCD axions to the SM electroweak bosons may impact axion signals in rare decays in which they participate. For instance, in low-energy processes the axion could be be photophobic at low energies [17] (or more generally, EW-phobic), in models in which the terms in parenthesis cancel approximately, unlike at higher energies at which the model-independent component disappears and only the model-dependence (encoded in E/N, M/N, Z/N and R/N) is at play.

Gauge invariance

As it was already enforced in Eq. (2.22), the couplings of the axion to the EW gauge bosons are not independent as a consequence of gauge invariance. Indeed, all four couplings stem from the two independent effective operators in Eqs. (2.5) and (2.6), plus that in Eq. (2.52) for a light QCD axion ($m_a \ll \Lambda_{QCD}$). In consequence, three physical couplings can be independent among the set $\{g_{a\gamma\gamma}, g_{aWW}, g_{aZZ}, g_{a\gamma Z}\}$, and the following relation must hold:

$$g_{aZZ} = -\left(c_w^2 + \frac{s_w^4}{c_w^2}\right) g_{aWW} + \frac{c_w^3}{s_w} g_{a\gamma\gamma} + \left(1 + c_w^2 + \frac{s_w^4}{c_w^2}\right) g_{a\gamma Z}. \tag{2.63}$$

Note that this result does not depend on the details of any particular axion model; it is independent of the presence or absence of gluonic couplings and it thus applies in all generality for a light pseudoscalar with only anomalous electroweak couplings. That is, it is also valid for generic ALPs which only have EW interactions. Furthermore, it suggests that it may be inconsistent to assume only one EW coupling: the minimum number of physical EW couplings for an axion or ALP is two. The relation in Eq. (2.63) sets an avenue to oversconstrain the parameter space which is promising. It allows to use the better constrained EW couplings to bound the fourth one.

3 Beyond the QCD axion

We discuss in this section the case of a "heavy axion": an axion whose mass is not given by the QCD axion expression in Eq. (1.1) but receives instead extra contributions. We have in mind a true axion which solves the strong CP problem, for which the source of this extra mass does not spoil the alignment of the CP conserving minimum. This is the case for instance of models in which the confining sector of the SM is enlarged involving a new force with a confining scale much larger than the QCD one [28–39]. This avenue is of particular interest as it allows to consider heavy axions and low axion scales (e.g. $\mathcal{O}$(TeV)), and still solve the SM strong CP problem. The axion mass can then expand a very large range of values. It can become much larger than the EW scale or, conversely, be in the GeV range or lower. For the purpose of this work, the latter range is to be kept in mind as a general guideline, so as to remain in the range of validity of the effective Lagragian with confined hadrons. The procedure will also serve as a template to show how the mixing effects disappear from the axion-gauge couplings as the axion mass is raised.

In practice, the analysis below applies identically to a true heavy axion which solves the strong CP problem and to a gluonic ALP, that is, any ALP which has both electroweak and gluonic anomalous couplings, even if not related to a solution to the strong CP problem. For the sake of generality, consider the addition of an extra mass term to the effective Lagrangian obtained after EW symmetry breaking but above confinement in Eq. (2.14),

$$\delta\mathcal{L}_a = \frac{1}{2} M^2 \hat{a}^2. \tag{3.1}$$

For simplicity, from now on we focus on the case in which the first generation of SM quarks carry no PQ charge, as it is straightforward to enlarge the analysis beyond this hypothesis, as shown in the previous section. After confinement, the pseudoscalar mass matrix in Eq. (2.29) is then replaced by

$$M^2_{\{\pi_3,\,\eta_0,a\}} = \begin{pmatrix} B_0\,(m_u + m_d) & B_0\,(m_u - m_d) & 0 \\ B_0\,(m_u - m_d) & 4K/f_\pi + B_0(m_u + m_d) & 2K/(f_\pi f_a) \\ 0 & 2K/(f_\pi f_a) & K/f_a^2 + M^2 \end{pmatrix}. \tag{3.2}$$

In the limit $f_a \gg K^{1/4}$ (i.e. $f_a \gg \Lambda_{QCD}$) the expressions for the π, η' and a mass eigenvalues become

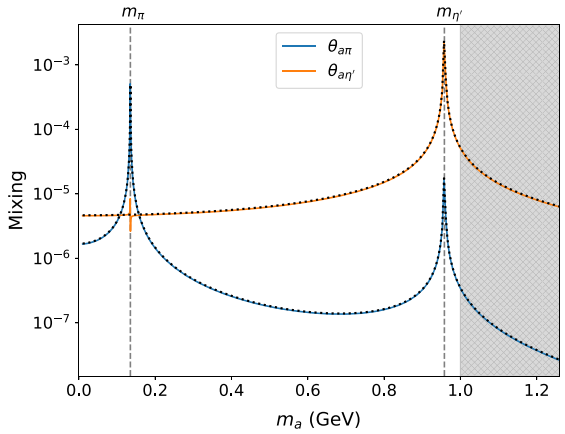

Fig. 1 Mixing angles as a function of the (heavy) axion mass m_a, for a value of $f_a = 10\,\text{TeV}$. The grey area indicates the range where the validity of the chiral expansion breaks down. The figure also applies to gluonic ALPs

$$
\begin{aligned}
m_\pi^2 &\simeq B_0\,(m_u + m_d),\\
m_{\eta'}^2 &\simeq \frac{4K}{f_\pi^2} + B_0\,(m_u + m_d),\\
m_a^2 &\simeq M^2 + \frac{f_\pi^2 m_\pi^2}{f_a^2}\frac{m_u m_d}{(m_u+m_d)^2}.
\end{aligned}
\tag{3.3}
$$

The corresponding axion–pion and axion-η' mixing angles take a very simple form in the limit $M \gg m_\pi$,

$$
\begin{aligned}
\theta_{a\pi} &\simeq -\frac{f_\pi}{2f_a}\frac{m_d - m_u}{m_u + m_d}\,\frac{1}{1-\frac{M^2}{m_\pi^2}}\,\frac{1}{1-\frac{M^2}{m_{\eta'}^2}},\quad \theta_{a\eta'}\\
&\simeq -\frac{f_\pi}{2f_a}\,\frac{1}{1-\frac{M^2}{m_{\eta'}^2}},
\end{aligned}
\tag{3.4}
$$

where again only the leading term on each entry of the mixing matrix has been retained. In fact, it can be checked that these equations hold even for small values of M, as long as M is non-degenerate with the pion or η' mass. The comparison with Eq. (2.36) ilustrates that the M-dependent corrections may be important for axion masses near the pion mass or the η' mass. The divergences in Eq. (3.4) for an axion degenerate in mass with the pion or the η' are an artifact of the approximations which in practice correspond to large mixing values, as expected in those ranges. The numerical results do not rely on that approximation and are illustrated in Fig. 1: the spikes correspond to an axion degenerate with either the pion or the η'.

3.1 Heavy axion couplings to EW gauge bosons

The couplings of the heavy axion to the electroweak gauge bosons reflect the dependence of the mixing parameters on the extra source of mass M, as follows:

$$
g_{aWW} = -\frac{1}{2\pi f_a}\frac{\alpha_{\text{em}}}{s_w^2}\left(\frac{L}{N} - \frac{3}{4}\frac{1}{1-\left(\frac{M}{m_{\eta'}}\right)^2}\right),
\tag{3.5}
$$

$$
\begin{aligned}
g_{a\gamma\gamma} = &-\frac{1}{2\pi f_a}\alpha_{\text{em}}\\
&\times\left[\frac{E}{N} - \frac{1}{1-\left(\frac{M}{m_{\eta'}}\right)^2}\left(\frac{5}{3} + \frac{m_d - m_u}{m_u + m_d}\,\frac{1}{1-\left(\frac{M}{m_\pi}\right)^2}\right)\right],
\end{aligned}
\tag{3.6}
$$

$$
\begin{aligned}
g_{aZZ} = &-\frac{1}{2\pi f_a}\frac{\alpha_{\text{em}}}{s_w^2 c_w^2}\\
&\times\left[\frac{Z}{N} - \frac{1}{1-\left(\frac{M}{m_{\eta'}}\right)^2}\left(\frac{11s_w^4 + 9c_w^4}{12}\right.\right.\\
&\left.\left. - \frac{s_w^2(s_w^2 - c_w^2)}{2}\frac{m_d - m_u}{m_u + m_d}\,\frac{1}{1-\left(\frac{M}{m_\pi}\right)^2}\right)\right],
\end{aligned}
\tag{3.7}
$$

$$
\begin{aligned}
g_{a\gamma Z} = &-\frac{1}{2\pi f_a}\frac{\alpha_{\text{em}}}{s_w c_w}\left[\frac{2K}{N} - \frac{1}{1-\left(\frac{M}{m_{\eta'}}\right)^2}\left(\frac{9c_w^2 - 11s_w^2}{6}\right.\right.\\
&\left.\left. - \frac{1}{2}(c_w^2 - 3s_w^2)\frac{m_d - m_u}{m_u + m_d}\,\frac{1}{1-\left(\frac{M}{m_\pi}\right)^2}\right)\right].
\end{aligned}
\tag{3.8}
$$

The M-dependent corrections in these couplings can be relevant for heavy axions which solve the strong CP problem as well as for gluonic ALPs, as long as their mass parametrized by Eq. (3.3) is sensibly larger than that for the QCD (i.e. invisible) axion, $M^2 > m_\pi^2 f_\pi^2/f_a^2$. These expressions hold as long as chiral perturbation theory is valid, that is $M \lesssim 1\,\text{GeV}$.

For values of M noticeably larger than the η' mass the model prediction depicted is only indicative, as the effective Lagrangian in terms of pions and η' is not really adequate and the description should the be done in terms of the couplings to quarks. At those energies ($m_a \gg m_{\eta'}$) QCD is perturbative and it would be pertinent to compute the two-loop contribution of the gluonic coupling to the EW gauge boson couplings. For the case of photons, a qualitative estimation has been performed in Ref. [21] with the result:

$$
\delta g_{a\gamma\gamma} = -\frac{3\,\alpha_{\text{em}}\,\alpha_s(m_a^2)}{\pi^2}\,g_{agg}\sum_f q_f^2 B_1(\tau_f)\log\left(\frac{f_{\text{PQ}}^2}{m_f^2}\right),
\tag{3.9}
$$

leading to a photonic axion coupling given by

$$
\begin{aligned}
g_{a\gamma\gamma} = &-\frac{1}{2\pi f_a}\alpha_{\text{em}}\\
&\times\left(\frac{E}{N} - \frac{3\,\alpha_s^2}{2\pi^2}\sum_f q_f^2 B_1(\tau_f)\log\left(\frac{f_{\text{PQ}}^2}{m_f^2}\right)\right).
\end{aligned}
\tag{3.10}
$$

The loop function $B_1(\tau)$ will be defined later in Eq. 4.6. The derivation of the equivalent formula for the coupling of axions to heavy EW gauge boson couplings is left for future work. Nevertheless, the analysis presented here conveys the qualitative behaviour expected for the transition between the low and high axion mass regimes.

Gauge invariance

For high axion masses (i.e. $M \gg \Lambda_{QCD}$ in Eq. (3.3)), the mixing of the axion with the SM pseudoscalars becomes negligible. For those scales, QCD enters the perturbative regime and Eq. (3.9) illustrates how the model-independent contributions to the EW couplings diminish. As the latter become negligible, the axion coupling to EW gauge bosons is parametrized by just the two effective interactions in Eqs. (2.5) and (2.6). In other words, the heavy axion EW couplings span a parameter space with two degrees of freedom (instead of three for light axions with $m_a \ll \Lambda_{QCD}$, see Sect. 2.2). Two independent constraints follow for heavy axions:

$$g_{aWW} = g_{a\gamma\gamma} + \frac{c_w}{2\,s_w} g_{a\gamma Z}, \tag{3.11}$$

$$g_{aZZ} = g_{a\gamma\gamma} + \frac{c_w^2 - s_w^2}{2\,s_w c_w} g_{a\gamma Z}, \tag{3.12}$$

where we have chosen to express the couplings g_{aWW}, g_{aZZ} in terms of the overall better constrained ones $g_{a\gamma\gamma}$ and $g_{a\gamma Z}$.[7] These powerful relations will be exploited in the next section to further constrain uncharted regions of the experimental parameter space.

Alike to the discussion after Eq. (2.63), the relations in Eqs. (3.11) and (3.12) apply not only to heavy axions and heavy gluonic ALPs, but also to generic ALPs which only exhibit EW interactions and are much heavier than nucleons. The corollary that at least two EW couplings –if any– must exist for any axion or ALP holds as well.

4 Phenomenological analysis

The impact of the results obtained above on present and future axion searches will be illustrated in this section. Both tree-level and loop-level effects will be taken into account. Indeed the latter are relevant when confronting data on photons, electrons and nucleons, as the experimental constraints on these channels are so strong that they often dominate the bounds on EW axion couplings.

4.1 Loop-induced couplings

The tree-level coupling of the axion to photons can be suppressed in some situations [9,17] (photophobic ALPs are also possible [25]). Additionally, many models have no tree-level couplings to leptons or suppressed couplings to nucleons [8]. However, all possible effective couplings will mix at the loop level. This affects the renormalization group (RG) evolution, via which all couplings allowed by symmetry will be generated even when assuming only a subset of couplings at some scale.

Before proceeding with the phenomenological analysis, we discuss in this subsection the loop-induced effective interactions arising from the direct coupling to electroweak gauge bosons. Because the experimental and observational limits are usually strongest for photons, electrons, and nucleons, the loop-induced contributions to these channels can give stronger constraints than those stemming from the tree-level impact on other channels.

Denoting the effective axion–fermion Lagrangian by

$$\delta\mathscr{L}_{a\,\mathrm{eff}} \supset \sum_f c^f_{1\,\mathrm{eff}}\,\frac{\partial_\mu \hat{a}}{f_{\mathrm{PQ}}}\left(\bar{f}\,\gamma_\mu\,\gamma_5\,f\right), \tag{4.1}$$

it has been shown [21] that the coefficient $c^f_{1\,\mathrm{eff}}$ receives one loop-induced corrections from electroweak couplings,

$$\begin{aligned}
\frac{c^f_{1\,\mathrm{eff}}}{f_a} &= \frac{3}{4}\left(\frac{\alpha_{\mathrm{em}}}{4\pi\,s_w^2}\frac{3}{4}g_{aWW} + \frac{\alpha_{\mathrm{em}}}{4\pi\,c_w^2}\left(Y^2_{f_L}+Y^2_{f_R}\right)g_{aBB}\right)\log\frac{f^2_{\mathrm{PQ}}}{m_W^2} \\
&\quad + \frac{3}{2}\frac{\alpha_{\mathrm{em}}}{4\pi}Q_f^2\,g_{a\gamma\gamma}\log\frac{m_W^2}{m_f^2} \\
&= \frac{9}{16}\frac{\alpha_{\mathrm{em}}}{4\pi\,s_w^2}g_{aWW}\log\frac{f^2_{\mathrm{PQ}}}{m_W^2} \\
&\quad + \frac{3}{4}\frac{\alpha_{\mathrm{em}}}{4\pi\,s_w^2c_w^2}\left(\frac{3}{4}c_W^4 + \left(Y^2_{f_L}+Y^2_{f_R}\right)s_W^4\right)g_{aZZ}\log\frac{f^2_{\mathrm{PQ}}}{m_W^2} \\
&\quad + \frac{3}{4}\frac{\alpha_{\mathrm{em}}}{4\pi\,s_wc_w}\left(\frac{3}{4}c_W^2 - \left(Y^2_{f_L}+Y^2_{f_R}\right)s_W^2\right)g_{a\gamma Z}\log\frac{f^2_{\mathrm{PQ}}}{m_W^2} \\
&\quad + \frac{3}{2}\frac{\alpha_{\mathrm{em}}}{4\pi}Q_f^2\,g_{a\gamma\gamma}\log\frac{f^2_{\mathrm{PQ}}}{m_f^2}.
\end{aligned} \tag{4.2}$$

To obtain this result, the ultraviolet scale inside the loop diagrams has been identified with the axion scale f_{PQ}, which is the cutoff of the effective theory. Note that the one-loop induced contributions to the fermion couplings are independent of the axion mass (other than a negligible dependence through the axion-gauge couplings such as $g_{a\gamma\gamma}$, see below). They are generically of order $\alpha/4\pi$ as expected, that is, over two orders of magnitude smaller than the original effective gauge coupling. Nevertheless, the experimental constraints are so strong that they will often provide the leading bounds on gauge-axion couplings.

[7] Obviously, the milder constrain in Eq. (2.63) also applies here.

The most relevant fermionic limits are those on the coupling to electrons and light quarks. While Eq. (4.2) is directly applicable to leptons and heavy quarks, at low energies light quarks form hadrons: the loop-induced coupling to nucleons have highest impact. Following Refs. [8,13], the relation between nucleon and light quark couplings can be written as

$$\begin{aligned} c_p + c_n &= 0.50(5)\left(c_1^u + c_1^d - 1\right) - 2\delta, \\ c_p - c_n &= 1.273(2)\left(c_1^u - c_1^d - \frac{1-z}{1+z}\right), \end{aligned} \tag{4.3}$$

where $z = m_u/m_d = 0.48(3)$ and c_1^u and c_1^d are defined in terms of the coefficients in Eq. (2.12) as

$$c_1^u = \frac{c_1^U - c_1^Q}{2}, \qquad c_1^d = \frac{c_1^D - c_1^Q}{2}. \tag{4.4}$$

In Eq. (4.3), δ is a combination of the heavy SM quark coefficients analogous to those in Eq. (4.4), $\delta = 0.038(5)c_1^s + 0.012(5)c_1^c + 0.009(2)c_1^b + 0.0035(4)c_1^t$.

The combination of Eqs. (4.2) and (4.3) allows to derive the coupling to nucleons induced by the coupling to electroweak bosons.

The axion–photon coupling also receives one-loop corrections in the presence of couplings of the axion to fermions or gauge bosons. For energies or masses in the loops higher than $\Lambda_{\rm QCD}$, quarks are the appropiate propagating degrees of freedom,[8] and the one-loop contributions for an on-shell axion can be expressed as [21]

$$\begin{aligned} g_{a\gamma\gamma}^{\rm eff} &= g_{a\gamma\gamma}^0 + \sum_f N_C^f Q_f^2 \frac{\alpha_{em}}{\pi} \frac{2c_1^f}{f_a} B_1(\tau_f) \\ &\quad + 2\frac{\alpha_{em}}{\pi} g_{aWW} B_2(\tau_W), \end{aligned} \tag{4.5}$$

where the subscript f runs over leptons and heavy quarks. Here, $\tau_i = 4m_i^2/m_a^2$ and

$$\begin{aligned} B_1(\tau) &= 1 - \tau f^2(\tau) \\ B_2(\tau) &= 1 - (\tau - 1) f^2(\tau), \\ f(\tau) &= \begin{cases} \arcsin \frac{1}{\sqrt{\tau}}, & \tau \geq 1 \\ \frac{\pi}{2} + \frac{i}{2} \log \frac{1+\sqrt{1-\tau}}{1-\sqrt{1-\tau}}, & \tau < 1 \end{cases}. \end{aligned} \tag{4.6}$$

Asymptotically, $B_1 \to 1$ in the limit $m_a \gg m_f$ and $B_1 \to -m_a^2/(12m_f^2)$ when $m_a \ll m_f$. This means that the contribution of fermions heavier than the axion is strongly suppressed. Similarly, $B_2 \to 1 + \pi^2/4 - \log^2 m_a/m_W$ when $m_a \gg m_W$, whereas $B_2 \to m_a^2/(6m_W^2)$ in the $m_a \ll m_W$ limit.

It is worth noting that chaining the two previous one-loop contributions gives an approximate estimation of the two-loop contribution of a given heavy gauge boson coupling to the axion–photon coupling. As an example, consider g_{aWW} in Eq. (4.2): it results in an effective fermion coupling $c_{1\,\rm eff}^f$ which, when subsequently inserted in the second term in Eq. (4.5), results in an effective axion–photon coupling. This can be compared with the third term which gives directly a one-loop contribution of g_{aWW} to $g_{a\gamma\gamma}$: for $m_a \ll m_W$, the second term in Eq. (4.5) may actually be numerically larger than the third term, that is, the two-loop contribution via fermionic couplings may dominate over the one-loop gauge one, as it was pointed out in Refs. [21,25]. Indeed, this two-loop contribution may be phenomenologically the most relevant one to constrain the axion couplings to heavy electroweak gauge bosons. A caveat is that only a true two-loop computation may settle the dominant pattern, but the analysis discussed is expected to provide an order of magnitude estimate.

4.2 Axion decay channels and lifetime

The plethora of couplings discussed, contributing either at tree or loop level, produces a rich variety of production and decay channels of the axion, depending on its mass and on the relative strength of the couplings. A quantitative evaluation of the lifetime and branching ratios is essential for assessing what experiments or searches are more adequate to test different regions of parameter space.

In order to determine the detection capabilities of a given final state channel, an important element is whether the axion can decay into it within the detector, or escapes and contributes to an "invisible" channel. For purely illustrative purposes, Fig. 2 compares the axion decay widths into different final states for a particular choice of the model-dependent parameters.[9] This figure serves to indicate the mass threshold for the different channels and is also a good indicator of the relative width of each decay channel. The determination of the areas experimentally excluded –to be developed in Sect. 4.3– will not depend on the value of the effective couplings assumed in this figure, though.[10]

In the low mass region $m_a < 3m_\pi$, only decays to pairs of electrons, muons or photons are possible. The axion typically becomes long lived enough so as to be stable at collider and

[8] For energies below the QCD scale, radiative corrections involving light quarks have to be evaluated using chiral Lagrangian methods. This was achieved in Ref. [21], the conclusion being that the results remain qualitatively right once the quarks masses are substituted by an appropriate hadronic scale, m_π for u and d and m_η for s. However, in the presence of gluonic couplings this contribution is subdominant to the one computed in the previous sections and will thus not be considered here.

[9] The value for $g_{a\gamma\gamma}$ used in this figure corresponds approximately to $f_a = 10$ TeV and $E = 1$ in axion models. Rescaling for other values of the couplings can be achieved by taking into account that $\Gamma_i \propto g_{aXY}^2$.

[10] The widths used in determining the coloured regions in Fig. 4 induced at tree-level derive directly from the effective g_{aXY} value for each point of the parameter space.

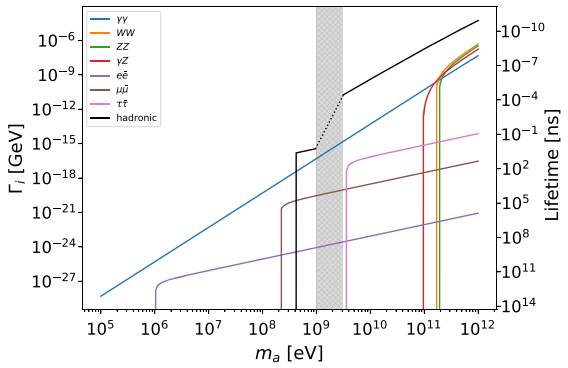

Fig. 2 Illustration of the axion (or ALP) decay widths, as a function of the axion mass for a benchmark value of $g_{a\gamma\gamma} = 10^{-7}\,\text{GeV}^{-1}$ and the rest of gauge boson couplings as in Eq. (4.8). The grey hatched region signals the 1–3 GeV "no human's land" for hadronic decays in between the chiral and the perturbative regimes, where the dots indicate that no reliable prediction is possible

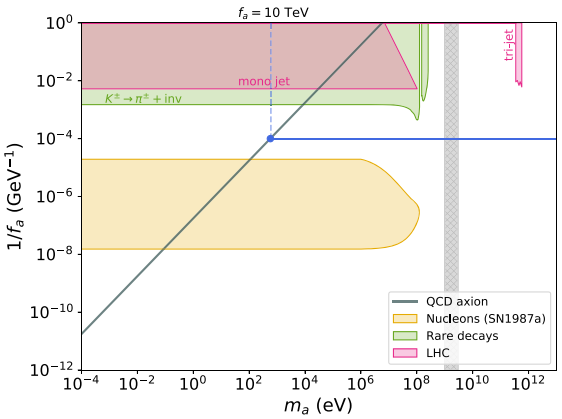

Fig. 3 Coupling to gluons. The excluded areas rely on considering exclusively the coupling g_{agg} by itself. The SN1987a limit was computed in Ref. [15], while the rare decays and LHC exclusions are obtained using the results of Ref. [49] and Refs. [20,50], respectively. Particular models are represented by the overlaid lines, the black one corresponding to the QCD axion and the blue one to heavy axion models (here for a benchmark choice of $f_a = 10\,\text{TeV}$). See Sect. 4.4 for more details. We provide exclusion plots without superimposed lines as auxiliary files

flavour experiments. Note that this region is particularly sensitive to a possible cancellation/suppression of the photonic coupling $g_{a\gamma\gamma}$ [this happens for instance in models of axions in which the model-dependent parameter E/N partially cancels the model-independent contribution, see Eqs. (2.55) and (3.6)]. This would suppress the decay width to photons and thus enhance the branching fraction to fermions, especially close to the respective mass thresholds.

The hadronic channel plays a central role as soon as it opens. It then dominates the decay of the axion due to the large gluonic coupling. The lightest possible hadronic final state is three neutral pions. At around the GeV scale many other final states become viable, but in this region chiral perturbation theory starts to break down and we refrain from making any quantitative predictions.[11] At high axion masses above 3 GeV the inclusive decay to hadrons can be safely estimated within perturbative QCD.[12]

At much higher energies, tree-level decays to pairs of EW gauge bosons become possible and, though subdominant with respect to the hadronic one, will play a relevant role in collider searches.

4.3 Experimental constraints on the (heavy) axion parameter space

We have reinterpreted a number of axion searches into our framework. Far from an in-depth review, this study primarily intends to point out the relative strength of the different observables in probing different flavours and parameter regions of axion and ALP models. Interestingly and contrary to common lore, we find that some regions of parameter space can be better tested through the axion couplings to heavy gauge bosons rather than to photons.

The coloured areas in Fig. 3 show the regions experimentally excluded if taking into account *exclusively* the axion–gluon coupling g_{agg} (which in axion models fixes the axion scale f_a). Although this work focuses on the case where also EW gauge boson couplings are present, this parameter space is also shown for reference.

The couplings of axions to EW gauge bosons ($g_{a\gamma\gamma}$ g_{aWW}, g_{aZZ} and $g_{a\gamma Z}$) will be instead explored within a two-operator framework: *the axion–gluon coupling g_{agg} and one electroweak gauge coupling are to be simultaneously considered*. In other words, for each EW axion coupling g_{aXY}, the regions experimentally excluded will be determined assuming the Lagrangian[13]

$$\delta\mathscr{L}_a = \frac{1}{4} g_{agg}\, a\, G\tilde{G} + \frac{1}{4} g_{aXY}\, a\, X\tilde{Y} + \frac{1}{2} M^2 a^2. \qquad (4.7)$$

This choice is mainly motivated by the focus on solving the strong CP problem, or alternatively as an ALP analysis which goes beyond the traditional consideration of only one operator at a time. The regions experimentally excluded for axion-EW gauge boson couplings are then depicted in Fig. 4 as coloured areas. Note that we don't discuss any cos-

[11] After this paper was completed, Ref. [48] appeared which discusses the hadronic decays of axions in this region $1\,\text{GeV} < m_a < 3\,\text{GeV}$.

[12] Note that heavy-flavour tagging can allow to distinguish final states involving heavy quarks, but this separation will not be taken into account here.

[13] The axion mass m_a is a combination of M and the instanton contribution related to the first term, as previously explained (see Eq. 3.3).

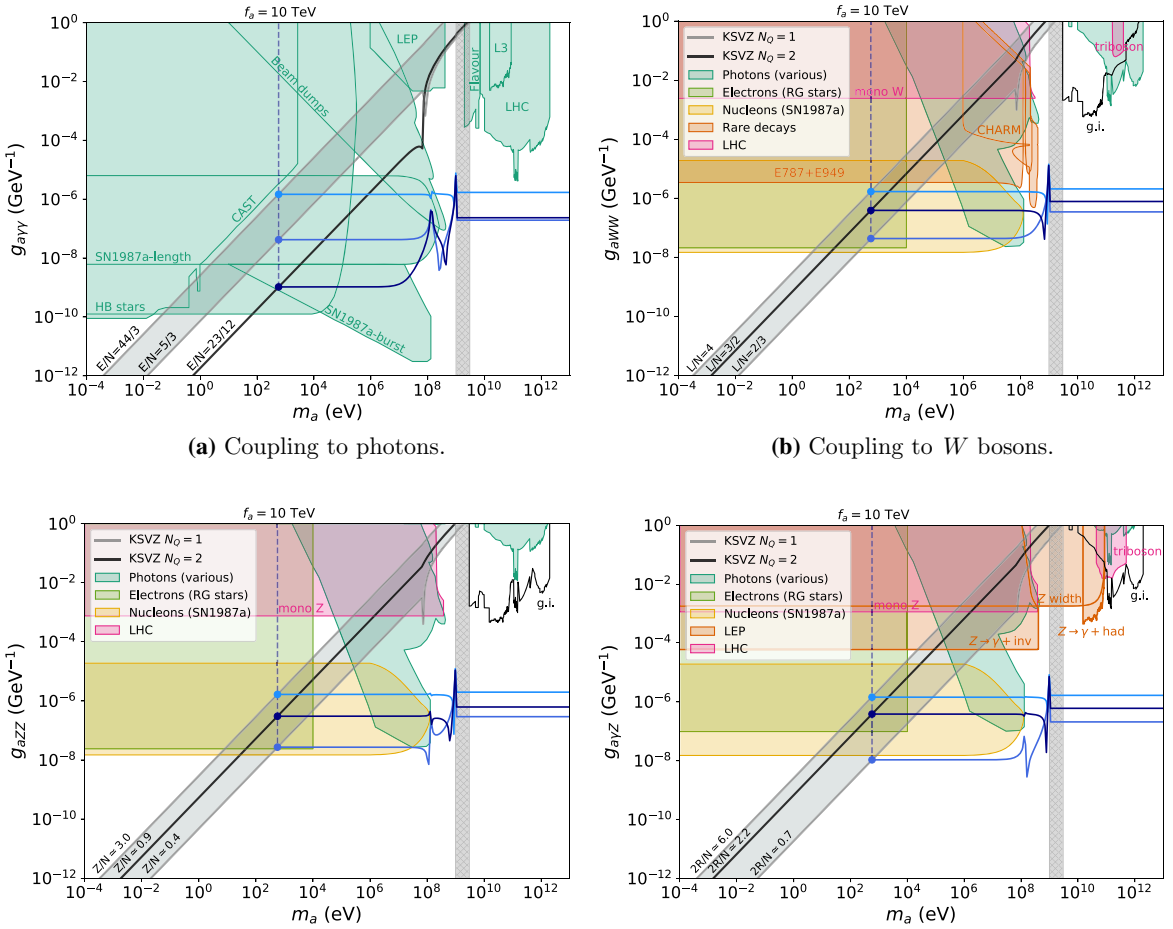

(a) Coupling to photons.

(b) Coupling to W bosons.

(c) Coupling to Z bosons.

(d) Coupling to a photon and a Z boson.

Fig. 4 Coupling to EW gauge bosons. A two-operator framework is used: each panel assumes the existence of the corresponding electroweak coupling plus the axion–gluon coupling. The coloured regions are experimentally excluded. In panels b, c and d, the loop-induced constraints labelled as "photons", "electrons" and "nucleons" depend mildly on f_a (see text). The label "g.i." illustrates the exclusion power of EW gauge invariance. The superimposed lines correspond to KSVZ-type QCD axion models (black line and grey band) and to one benchmark heavy axion model with $f_a = 10$ TeV (blue lines). The parameter space for heavy axions corresponds to moving up and down that set of blue lines, see Sect. 4.4. The results apply as well to gluonic ALPs (we provide exclusion plots without superimposed lines as auxiliary files)

mological bounds. The reason for this is that models of heavy axions, typically containing an extended confining sector, are expected to significantly alter the standard cosmological picture that is usually assumed to obtain such exclusions. The study of heavy axion cosmology thus requires a full self-consistent study which is left for future work.

The resulting greenish regions in Fig. 4a match well-known exclusion regions for $g_{a\gamma\gamma}$, although the overlap is not complete because the latter typically only take into account the effective axion–photon coupling; the additional presence in our analysis of the axion–gluon coupling g_{agg} has a particularly relevant impact in the heavy axion region (see below).

Figure 4b–d respectively for g_{WW}, g_{ZZ} and $g_{\gamma Z}$ are novel. The possibility of measuring four distinct EW observables offers a multiple window approach and a superb cross-check if a signal is detected, given the fact that for axion masses much smaller (larger) than Λ_{QCD} only three (two) couplings are independent among the set $\{g_{a\gamma\gamma}\ g_{aWW}, g_{aZZ}, g_{a\gamma Z}\}$, see Eq. (2.63) (Eqs. (3.11) and (3.12)).

For the majority of the regions excluded in Fig. 4, the experiment directly constraints certain regions of the parameter space $\{g_{aXY}, m_a\}$ and no further assumptions are required; those constraints apply then also to ALPs which have no gluonic couplings. However, for some collider searches the interplay between the particular EW coupling

g_{aXY} under analysis and the coupling to gluons plays a relevant role, and it is necessary to assume their relative strength. This will be taken as given by

$$\frac{g_{agg}}{g_{aXY}} = \frac{\alpha_s}{\alpha_{XY}}. \tag{4.8}$$

This is well motivated by pseudo Nambu–Goldstone bosons with anomalous couplings generated by the triangle diagram with $\mathcal{O}(1)$ group theory factors. In any case, the results are largely insensitive to this assumption, since in the best limits stemming from LHC searches the production cross section times branching ratio scales as

$$\begin{aligned}&\sigma(pp \to a) \times \mathrm{BR}(a \to XY)\\ &\quad \propto \frac{g_{agg}^2\, g_{aXY}^2}{8 g_{agg}^2 + g_{aXY}^2} \xrightarrow{g_{agg} \gg g_{aXY}} \frac{g_{aXY}^2}{8}.\end{aligned} \tag{4.9}$$

It is then enough to adopt the reasonable assumption that the coupling to gluons is larger than that to EW gauge bosons $g_{agg} \gtrsim g_{aXY}$. This assumption has been adopted exclusively for LHC searches in the axion mass region where the hadronic decay channels are open, i.e. $m_a > 3\, m_\pi$.

In addition, the bounds obtained via loop contributions have a logarithmic dependence on the cut-off scale f_a. A relation between f_a and g_{aXY} needs to be assumed in order to translate the bounds on fermionic or photonic couplings into bounds on EW gauge boson couplings. In these cases, Eq. (4.8) will be used again, which for axion models translates into

$$f_a = \frac{\alpha_{XY}}{2\pi\, g_{aXY}}, \tag{4.10}$$

where Eq. (2.54) has been used. In any case, as the cutoff dependence in loops is logarithmic this assumption has a minor impact on the exclusion plots.

To sum up, for each EW-axion coupling the experimentally excluded regions in Fig. 4 are depicted on the parameter space $\{g_{aXY}, m_a\}$ without any assumption, except:

A For LHC searches and $m_a > 3\, m_\pi$, Eqs. (4.8) and (4.9) were used, which for most cases is equivalent to assume $g_{agg} \gg g_{aXY}$.
B For the regions labelled as "photons", "electrons" and "nucleons" in Fig. 4b–d, the loop-induced bounds have a very mild dependence on the assumption in Eq. (4.10).

After having presented the general strategy that we use for the reinterpretation of constraints into our setup, we proceed to describe the origin of each of the exclusion regions coloured in Fig. 4.

Coupling to photons

The combination of astrophysical and terrestrial probes makes this search a particularly powerful tool to test the axion paradigm, especially for low mass axions. Even in the case of relatively large axion masses and/or situations where the coupling to photons can be suppressed, photons still place strong constraints both at tree-level and through loop-induced effects.

The experimental limits on $g_{a\gamma\gamma}$ are compiled in Fig. 4a. At the lowest axion masses considered here, $m_a \lesssim 10$ meV, the most competitive bounds come from the CAST helioscope [51], and will improve in the future with the upgrade to the IAXO experiment [52]. At slightly larger masses up to $m_a \sim 1$ keV, $g_{a\gamma\gamma}$ is constrained by an energy-loss argument applied to Horizontal Branch (HB) stars [14]. A similar argument applies to the supernova SN1987a and constrains larger masses up to the 100 MeV range, both using extra cooling arguments [53] and by the lack of observation of a photon burst coming from decaying emitted axions [54]. In the same mass range, larger couplings can be constrained using beam dump experiments, with these exclusions led at present by the NuCal [55] experiment together with the 137 [56] and 141 [57] experiments at SLAC. We adapt here the constraints compiled in Ref. [58], noting that these bounds rely solely on the photon coupling.

For yet higher axion masses, where colliders provide the best limits, the gluon coupling plays a relevant role. As long as no hadronic decay channel is open, the LEP constraints based on $Z \to \gamma\gamma$ and $Z \to \gamma\gamma\gamma$ searches obtained in [19,20] for ALPs without gluonic couplings are also applicable to heavy axions. However, for masses above $3m_\pi$, hadronic final states start to dominate and we refrain from claiming any exclusion, as a new dedicated analysis would be required to use these channels. This explains the white gap just left of the grey hatched "no human's land" region, which should be at least partially covered when the forementioned analysis is performed. It is nevertheless possible to exploit some collider searches, if a relation between the gluonic and the EW couplings is assumed. Assumption A is adopted here. Our reinterpretation of the analysis in Ref. [59], in which the $L3$ collaboration looked for hadronic final states accompanied by a hard photon, yields the limit labelled "L3" in Fig. 4a, though it is ultimately superseded by LHC exclusions. The region labelled "Flavour" is excluded by data from Babar [60] and LHCb [61], as computed in Ref. [41]. For high axion masses near the TeV scale, the limits from LHC are much stronger than those from LEP, because of the enhanced axion production via gluon-gluon fusion. We have included the limits obtained in this context in Refs. [62,63] using run 1 data. These limits are extremely strong and should improve with the addition of run 2 data, especially at higher energies.

Finally, the bounds on $g_{a\gamma\gamma}$ described above have been translated – using assumption B – into competitive bounds for the other EW axion couplings, by means of their loop-mediated impact.

Coupling to fermions

Flavour blind observables involving fermions can be used to constrain gauge boson couplings via the impact of the latter at loop level, see Eq. (4.2). In order to fix the mild logarithmic dependence on the cutoff scale, assumption B will be adopted.

The most relevant constraints on flavour-blind axion–fermion interactions are of astrophysical origin and come from either electrons or nucleons. Firstly, a coupling of the axion to electrons allows for efficient extra cooling of some stars, which allows to place a bound on the axion-electron coupling g_{aee} via the observation of Red Giants (RG) [14]. Secondly, and in a manner similar to the discussion above for photons, a too strong coupling of the axion to nucleons would have shortened the duration of the neutrino burst of the supernova SN1987a. We use the most recent evaluation of this bound calculated in Ref. [15]. These two observations (RG and SN1987a) give the strongest limits on the coupling of axions to gauge bosons for axion masses respectively below 10 keV and 10 MeV, as can be seen in Fig. 4.

In addition, the one-loop induced fermion couplings also play a role in many of the observables considered here. In particular, they open potential axion decay channels into pairs of fermions.

Rare decays

For axion masses in the MeV–GeV range, g_{aWW} is best tested by its one-loop impact on rare meson decay experiments, where axions can be produced in flavour-changing neutral current (FCNC) processes. This search was first proposed in Ref. [26] (where ALPs either stable or decaying to photons were considered). Recently, these bounds have been recomputed in Ref. [25] in the context of photophobic ALPs, considering as well the potential decays of the axion to a pair of fermions due to the one-loop induced coupling in Eq. (4.2). We reinterpret these searches, taking into account in addition the effects of the gluonic axion coupling under the assumptions A and B. The main consequence is that, for axion masses $m_a > 3m_\pi$, the sensitivity is drastically reduced because of the opening of hadronic axion decay channels.

At low axion masses below $2m_\mu$, the axion is long-lived enough so that it can be considered stable for experimental purposes. This means that in these regions the axion has to be looked for in invisible searches. The most stringent limits were placed by the E787 and E949 experiments testing the $K^+ \to \pi^+ X$ channel, with X invisible [49]. Following Ref. [26], we reinterpret this search in terms of axions coupled to W bosons, which yields the constraint shown in Fig. 4b. These bounds will be improved in the near future by the NA62 experiment.

Axions can also be produced from rare meson decays in proton beam dump experiments, where they can be looked for in searches for long-lived particles. The current best limits are set by the CHARM experiment [64], where the axion can be produced in Kaon and B meson decays and subsequently decays to a pair of electrons or muons. The framework developed in Ref. [65] has been recast to obtain the limit on g_{aWW} shown in Fig. 4b.[14]

Direct couplings to heavy gauge bosons

LEP provides the best environment to directly test the $g_{a\gamma Z}$ coupling for axion masses below m_Z, as shown in Fig. 4d. The first constraint set assuming only the $g_{a\gamma Z}$ coupling was placed in Ref. [24] exploiting the limit on the uncertainty of the total Z width [67], $\Gamma(Z \to \text{BSM}) \lesssim 2\,\text{MeV}$ at 95% C.L., which allows to set a conservative bound on the process $Z \to a\gamma$. Stronger limits can be placed by more specific searches, as studied in Ref. [25]. The best limit at axion masses low enough for the axion to be long-lived stem from the $Z \to \gamma +$ inv. search. For higher axion masses, the large hadronic branching fraction makes the $Z \to \gamma +$ had. search the more fruitful one to look for axions. Under assumption A for the relative strength of the gluonic and EW couplings, we exploit the results of the search performed by the L3 collaboration as presented in Ref. [59] to obtain strong limits for m_a in the range from 10 GeV up to the Z mass. Note that, even if the search is the same than that used to constrain the photonic axion coupling, the exclusion for $g_{a\gamma Z}$ has a larger reach due to the fact that the process is mediated by an on-shell Z boson, instead of a very virtual photon.

LHC allows to look for a plethora of processes sensitive to axions. In particular, for heavy axions it provides the best limits on the coupling to heavy EW gauge bosons. The drawback of restricting the analysis to processes that separately involve only one of the EW gauge boson couplings plus the gluon coupling is the reduced number of available searches. Nevertheless, the advantage is that it provides robust and model-independent constraints.

The authors of Ref. [24] studied the LHC phenomenology of axions that are stable on collider lengths and thus would

[14] After this work was completed, Ref. [66] appeared which revisits the CHARM exclusion contour and provides projections of the expected NA62 and SHiP sensitivities.

manifest themselves as missing energy. In particular, mono-W and mono-Z final states where an axion is radiated as missing energy/momentum can set constraints on the three couplings g_{aWW}, g_{aZZ} and $g_{a\gamma Z}$, as shown in Fig. 4. For large axion masses $m_a > m_Z$, the authors of Ref. [25] suggested that triboson final states place the strongest bounds on ALPs coupling to massive gauge bosons, though the sensitivity of this search is hindered for axions because of the large hadronic branching ratio that we take into account. Adapting their constraints –with assumption A– leads to the exclusion of regions in parameter space near the TeV range, as shown in Fig. 4b, d for g_{aWW} and $g_{a\gamma Z}$, respectively. Note that significant exclusions can also be placed through the loop-induced coupling to photons. However, the most promising LHC search is one that –to the best of our knowledge– has not been performed yet. We advocate [68] the use of $pp \to a \to VV'$ processes, which benefit from the large production cross section through the gluonic coupling together with the clean final states that the decay to EW gauge bosons produce. We foresee that this search will have a sensitivity to the couplings of axions to heavy EW gauge bosons similar to the photonic case presented in Fig. 4a. Though potentially very interesting, the detailed analysis that this study requires is beyond the scope of this work and is left for the future [68].

4.4 Impact on (heavy) axion models and gluonic ALPs

The black oblique line in Fig. 3 corresponds to the linear relation between $1/f_a$ and m_a for the QCD axion, Eq. (1.1). The horizontal blue branch is one example of how that relation changes after Eq. (3.3) for an illustrative example of a true heavy axion.

The black, grey and blue lines in Fig. 4 illustrate possible $\{m_a, f_a\}$ values for axions which have a gluonic coupling g_{agg} (and thus may solve the strong CP problem) in addition to at least one coupling to heavy gauge bosons. Those model-dependent lines are superimposed[15] on the colored/white regions excluded/allowed by experiments for each one of the couplings in the set $\{g_{a\gamma\gamma}, g_{a\gamma Z}, g_{aZZ}, g_{aWW}\}$, as determined above. The examples chosen corresponds to KSVZ-type axions: either a standard QCD axion or a heavy axion as in theories with an enlarged confining gauge sector.

In each panel, for a given value of the model-dependent coupling:

- The expectation for the pure QCD axion is depicted by grey and black lines. The bands in Fig. 4 delimited by grey lines correspond to just one exotic KSVZ fermion representation. The values of the model-dependent parameters delimiting these benchmark bands [17] are summarized in Table 1. The black line is instead an illustrative case with two fermion representations such that the coupling to photons $g_{a\gamma\gamma}$ cancels up to theoretical uncertainties [17]. The upward bending of the lines obeys the expected change of the prediction for axion masses larger than the η' mass, a regime in which the last term in the parentheses in Eqs. (2.55)–(2.58) is absent.
- The expectations for heavy axions are illustrated with blue lines. The big dots which fall on the QCD axion lines correspond to $M = 0$ in Eqs. (3.1)–(3.3). The heavy axion trajectories start on those points and the prediction moves on each blue line towards the right as M grows. As the value of the axion mass gets near the pion and the η' masses, the prediction reflects the "resonances" found in the pseudoscalar mixing angles and the physical couplings to gauge bosons. For larger values of M the mixing effects progressively vanish, as physically expected and reflected in Eqs. (3.5)–(3.8), and the predictions stabilize again. The asymptotic value of the couplings is then induced only by the model-dependent parameters (E, L, Z, R), and it is often higher than for heavy axions lighter than the pion, for which the partial cancellation between the model-dependent and model-independent mixing effects may operate.

Table 1 Maximum and minimum values of the model-dependent coefficients for the benchmark KSVZ models with only one exotic fermion representation depicted in Fig. 4

	$SU(3)_c \times SU(2)_L \times U(1)_Y$
$(E/N)_{\max} = 44/3$	$(3, 3, -4/3)$
$(E/N)_{\min} = 5/3$	$(3, 2, +1/6)$
$(L/N)_{\max} = 4$	$(3, 3, \ Y\ )$
$(L/N)_{\min} = 2/3$	$(8, 2, -1/2)$
$(Z/N)_{\max} = 2.9$	$(3, 3, -4/3)$
$(Z/N)_{\min} = 0.4$	$(8, 2, -1/2)$
$(2R/N)_{\max} = 5.9$	$(3, 3, -1/3)$
$(2R/N)_{\min} = 0.7$	$(8, 2, -1/2)$

The figures illustrate that the M-dependent corrections may be relevant even for not very large M values. For instance, two close values of the model-dependent photon couplings E/N may give a very close $g_{a\gamma\gamma}$ prediction for M values above the η' mass, while that prediction can widely differ for M values smaller than the QCD scale. This is clearly reflected by the lines corresponding to the smaller values of E/N in Fig. 4a.

The parameter space for heavy axion models spans in fact most of the region to the right of the oblique band for the QCD axion: parallel sets of horizontal lines above and below

[15] For the reader interested in generic gluonic ALPs rather than heavy axions, we provide the exclusion plots without any superimposed lines as auxiliary files.

the blue ones depicted are possible and expected for other values of the heavy axion parameters. For a given f_a, varying M (that is, varying m_a) is tantamount to move right or left on a horizontal blue line, while varying f_a displaces up or down the set of horizontal blue lines. Finally, all these considerations for heavy axion models apply as well to gluonic ALPs, as argued earlier.

Gauge invariance

For heavy axions or any type of ALP with masses $m_a \gg \Lambda_{QCD}$, couplings to EW gauge bosons are directly tested and gauge invariance imposes the two relations in Eqs. (3.11) and (3.12). Therefore, the combination of the experimental constrains on two of the operators in the set $\{g_{a\gamma\gamma},\ g_{aWW},\ g_{aZZ},\ g_{a\gamma Z}\}$ translates in model independent bounds on the other two couplings. For light masses $m_a \leq \Lambda_{QCD}$, only Eq. (2.63) applies instead. These bounds based solely on EW gauge invariance have been depicted by black curves on the upper right corner of Fig. 4b–d. They susbtantially reduce the latter parameter space, especially in the cases of g_{aWW} and g_{aZZ}, whose current direct constraints are less powerful. They are to be taken with caution, though, since in each of the exclusion plots only one EW coupling was taken into account, while the relations deduced from gauge invariance involve several non-vanishing EW couplings. Furthermore, in a future multiparameter analysis where tree-level axion–fermion couplings are included, those relations could be corrected via one-loop effects.

4.5 Implications for heavy axion models

In existing models that solve the strong CP problem with heavy axions, often either

$$M^2 \sim \Lambda'^4/f_a^2, \qquad \text{or} \qquad M^2 \sim m_{\pi'}^2 f_{\pi'}^2/f_a^2 \tag{4.11}$$

where $\Lambda' \gg \Lambda_{QCD}$ is a new strong confining scale, and the primed fields denote exotic "pions" corresponding to the exotic fermions charged under the extra confining force. Let us assume the first option as an example. In this case,[16]

$$\Lambda'^4 \sim (m_a^2 f_a^2 - m_\pi^2 f_\pi^2). \tag{4.12}$$

Assume that an experiment detects an axion–photon signal and a certain value for the axion mass which correspond to a point in the white region of Fig. 4a and located to the right of the QCD band. For instance, let us consider a point located on one of the flat sections of the blue lines depicted. The interpretation in terms of a heavy axion depends on whether the axion is heavier or lighter than the pion and η', respectively:

- $m_a \gg m'_\eta$. The model-independent effects due to the mixings with SM pseudoscalars have become negligible, and $g_{a\gamma\gamma}$ is a direct measure of the product $(1/f_a)E/N$.
- $m_a \ll m_\pi$. In this case the measured $g_{a\gamma\gamma}$ value is undistinguishable from that for the QCD axion, with the E/N and f_a dependence given by Eq. (2.55). In other words, it would indicate either a heavy axion or a QCD axion with some degree of photophobia, as in that region they become undistinguishable. This is so at least for the lowest axion masses and/or without the help of other measurements involving heavy EW gauge bosons.

In both cases, in the framework of a KSVZ model, an additional measurement of the axion coupling to heavy gauge bosons would be enough to disentangle the values of f_a and M, that is, to determine the high scale Λ'. The model-independent corrections determined in Eqs. (3.5)–(3.8) can be essential when exploiting low-energy processes (e.g. rare decays), specially when they lead to the cancellation of a given coupling. Such cancellation in a channel in general will not apply to the couplings of the axion to other gauge bosons. Overall, the fact that only two or three axion-EW couplings are independent, while four channels can be explored, will allow to overconstrain the system.

5 Conclusions

Among the novel results of this work, we have first determined at leading order in the chiral expansion the model-independent components of the coupling of the QCD axion to heavy EW gauge bosons: $g_{a\gamma Z}$, g_{aZZ} and g_{aWW}. They stem from the axion-η'-pion mixing induced by the anomalous QCD couplings of these three pseudoscalars. Our results extend to heavy EW gauge bosons the well known result for the photonic coupling of the axion $g_{a\gamma\gamma}$. They must be taken into account whenever an axion lighter than Λ_{QCD} is on-shell and/or the energy and momenta involved in a physical process are of the order of the QCD confining scale or lower. As a previous step, we re-derived pedagogically the leading contributions to $g_{a\gamma\gamma}$ for the case of the most general axion couplings ("App. C"), and then proceeded to the determination of the couplings to the SM heavy gauge bosons.

This analysis of the EW couplings of the QCD axion may have rich consequences when comparing the presence/absence of signals at two different energy regimes. For instance, the axion could be photophobic at low energies [17] or even EW-phobic (e.g. in rare meson decays) because of cancellations between the model-independent and model-dependent components, while an axion signal may appear at accelerators or other experiments at higher energies at which the model-independent component disappears.

[16] The $m_u m_d/(m_u+m_d)^2$ factor in the QCD contribution is not shown for simplicity.

We have next extended those results to the case of heavy axions which solve the strong CP problem. This has allowed to explore how the mixing of the axion with the pion and η' evolves with rising axion mass, and in consequence how the model-independent contributions to all four EW axion couplings vanish as the axion mass increases above the QCD confinement scale. We have determined the modified expression for $g_{a\gamma\gamma}$ relevant for heavy axions, which may have rich consequences: an hypothetical measurement of that coupling outside the QCD axion band could point to either a heavy axion or a photophobic QCD axion. The analogous expressions for $g_{a\gamma Z}$, g_{aZZ} and g_{aWW} have been also worked out.

On the purely phenomenological analysis, we developed a "two simultaneous coupling" approach in order to determine the regions experimentally excluded by present data for $g_{a\gamma\gamma}$, $g_{a\gamma Z}$, g_{aZZ} and g_{aWW} versus the axion mass. Each EW coupling has been considered simultaneously with the anomalous gluonic coupling essential to solve the strong CP problem. The allowed/excluded experimental areas have been depicted for each of those couplings as a function of the axion mass. This is the first such reinterpretation for $g_{a\gamma Z}$, g_{aZZ} and g_{aWW}. Even for $g_{a\gamma\gamma}$, the results of previous studies often did not apply and must be reanalysed: for instance the present bounds extracted from LEP and LHC data tend to focus on ALPs which would not have gluonic couplings, with very few exceptions [20,41,62,63]. Furthermore, we have included an estimation of the one-loop induced bounds for each EW axion coupling, which leads to supplementary constraints.

The expectations from KSVZ-type of theories have been then projected and illustrated over the obtained experimental regions, both for the QCD axion and for heavy axions. The compatibility of hypothetical *a priori* contradictory signals in high and low energy experiments in terms of a given axion has been pointed out. Furthermore, we discussed how to interpret an eventual signal (or null result) outside the QCD axion band in terms of the value of the new high confining scale generically present in heavy axion theories.

A simple point with far reaching consequences results from EW gauge invariance. In all generality, not all couplings of axions to EW gauge bosons are independent among the four physical ones in the set $\{g_{a\gamma\gamma}\ g_{a\gamma Z}, g_{aZZ}$ and $g_{aWW}\}$. In particular, the relations obtained imply that at least two EW gauge couplings –if any– must be non-vanishing for any axion or ALP. These facts have been used to project the exclusion limits for the presently best constrained couplings onto the parameter space for the less constrained ones. In particular, for axions/ALPs much heavier than Λ_{QCD}, those relations have been projected on the parameter space for g_{aWW}, g_{aZZ} and $g_{a\gamma Z}$, reinforcing their constraints. A future multiparameter analysis may correct them via loop corrections. Nevertheless, the results obtained here clear up the uncharted experimental regions and may be of use in setting a search strategy. More in general, the existence of four physical axion couplings to EW bosons at experimental reach constitutes a phenomenal tool to over-constrain the axion parameter space and to check the origin of an eventual axion signal.

Finally, all results obtained for heavy axions apply as well to ALPs which have both EW and gluonic anomalous couplings. The constraints stemming from EW gauge invariance extend even to generic ALPs which do not couple to gluons. In consequence, this work also extends automatically the usual parameter space for ALPs that do not intend to solve the strong CP problem, adding to the incipient efforts to go towards a multi-parameter strategy.

Acknowledgements We acknowledge J. Fernandez de Troconiz, R. Houtz, J. Jaeckel, J.M. No, R. del Rey, O. Sumensari and V. Sanz for very interesting conversations and comments. We also thank J. Jaeckel for his useful remarks on the manuscript. M.B.G and P. Q. acknowledge IPMU at Tokyo University, where the last part of this work was developed. G. A. thanks the IFT at the Universidad Autónoma de Madrid and the University of Washington for the hospitality during the first and last stages of this work, respectively. This project has received support from the European Union's Horizon 2020 research and innovation programme under the Marie Sklodowska-Curie Grant Agreements No. 690575 (RISE InvisiblesPlus) and No. 674896 (ITN ELUSIVES). M.B.G and P. Q. also acknowledge support from the the Spanish Research Agency (Agencia Estatal de Investigación) through the grant IFT Centro de Excelencia Severo Ochoa SEV-2016-0597, as well as from the "Spanish Agencia Estatal de Investigación" (AEI) and the EU "Fondo Europeo de Desarrollo Regional" (FEDER) through the Project FPA2016-78645-P. The work of G. A. was supported through an ESR contract of the H2020 ITN Elusives (H2020-MSCA-ITN-2015//674896-ELUSIVES) and through a "La Caixa" predoctoral Grant of Fundación La Caixa. The work of P.Q. was supported through a "La Caixa-Severo Ochoa" predoctoral grant of Fundación La Caixa.

Data Availability Statement This manuscript has no associated data or the data will not be deposited. [Authors' comment: There is no data associated with this manuscript. Exclusion plots without superimposed model lines are available at https://arxiv.org/abs/1811.05466.]

Funded by SCOAP[3].

A The neutral pseudoscalar mass matrix

In the expansion in which all terms appearing at first order in $1/f_a$ and in quark masses are kept, Eq. (2.29) becomes

$$\begin{pmatrix} 1 & \frac{f(m_d-m_u)}{2f_a(m_d+m_u)}\left(1+\frac{m_\pi^2}{m_{\eta'}^2}\frac{(m_d-m_u)^2}{(m_d+m_u)^2}\right) & \frac{f}{2f_a}\left(1-\frac{m_\pi^2}{m_{\eta'}^2}\right) \\ -\frac{f(m_d-m_u)}{2f_a(m_d+m_u)}\left(1-\frac{m_\pi^2}{m_{\eta'}^2}\frac{4m_dm_u}{(m_d+m_u)^2}\right) & 1 & -\frac{m_\pi^2}{m_{\eta'}^2}\frac{(m_d-m_u)}{(m_d+m_u)} \\ -\frac{f}{2f_a}\left(1-\frac{m_\pi^2}{m_{\eta'}^2}\frac{4m_dm_u}{(m_d+m_u)^2}\right) & \frac{m_\pi^2}{m_{\eta'}^2}\frac{(m_d-m_u)}{(m_d+m_u)} & 1 \end{pmatrix}. \tag{A.1}$$

B Anomalous couplings of the pseudoscalar mesons to the EW gauge bosons

In addition to the axion couplings in Eqs. (2.4)–(2.6), new couplings involving gauge bosons are expected as soon as the extra pseudoscalar mesons appear in the spectrum below the confinement scale. In particular, for the η_0 and the pions, the following interactions with EW gauge bosons (considered as external currents) are possible below the QCD confinement scale:

$$W^a_{\mu\nu}\tilde{W}^{a\mu\nu}\frac{\eta_0}{f_\pi}, \qquad B_{\mu\nu}\tilde{B}^{\mu\nu}\frac{\eta_0}{f_\pi},$$
$$B_{\mu\nu}\tilde{B}^{\mu\nu}\frac{\pi_3}{f_\pi}, \qquad W^a_{\mu\nu}\tilde{B}^{\mu\nu}\frac{\pi_a}{f_\pi}. \tag{B.1}$$

The lightness of pseudoscalar mesons in QCD appears as a natural consequence of the spontaneous breaking of the chiral symmetry $U(2)_L \times U(2)_R \longrightarrow U(2)_V$. The pions and eta mesons can be identified as the pseudo Nambu–Goldstone bosons of the broken symmetry. However, the chiral symmetry is only approximate. It is explicitly broken not only by the quark masses, but also by the electroweak gauge interactions. This fact famously explains the difference between charged and neutral pion masses but also allows the computation of the coupling of pseudoscalar mesons to the EW bosons through the anomaly,

$$\partial^\mu j^a_\mu = \frac{\alpha_i}{8\pi}C^{abc}_{group}F_{b\,\mu\nu}\tilde{F}^{\mu\nu}_c, \tag{B.2}$$

where $\tilde{F}^{\mu\nu} = \frac{1}{2}\epsilon^{\mu\nu\sigma\rho}F_{\sigma\rho}$, the fine structure constant of the corresponding gauge interaction is denoted by $\alpha_i = \frac{g_i^2}{4\pi}$ and the group theoretical factor C_{group} is given by

$$C^{abc}_{group} = \sum_{LH-RH} Tr\left[T^a\{t^b, t^c\}\right]. \tag{B.3}$$

Here, T^a is the generator associated to the conserved current (i.e. to the global symmetry) and t^a are the generators of the representation of the gauge group under which each fermion transforms.

Applying these formulas, the anomalous couplings of the neutral pseudoscalar mesons π^3 and η' to the EW gauge bosons can be computed. For the pion,

$$\mathcal{L} \supset \frac{1}{4}g_{\pi BB}\,\pi_3 B\tilde{B} + \frac{1}{4}g_{\pi BW}\,\pi_3 B\tilde{W^3} \longrightarrow \frac{1}{4}g_{\pi ZZ}\,\pi_3 Z\tilde{Z} + \frac{1}{4}g_{\pi\gamma\gamma}\,\pi_3 F\tilde{F} + \frac{1}{4}g_{\pi\gamma Z}\,\pi_3 F\tilde{Z}, \tag{B.4}$$

with

$$g_{\pi BB} \equiv -\frac{\alpha}{2\pi\ f_\pi}\left(\frac{1}{c_w^2}\right),$$
$$g_{\pi ZZ} \equiv -\frac{\alpha}{2\pi\ f_\pi}\left(\frac{s_w^2}{c_w^2}-1\right),$$
$$g_{\pi BW} \equiv -\frac{\alpha}{2\pi\ f_\pi}\left(\frac{1}{c_w\,s_w}\right),$$
$$g_{\pi\gamma\gamma} \equiv -\frac{\alpha}{\pi}\frac{1}{f_\pi},$$
$$g_{\pi\gamma Z} \equiv -\frac{\alpha}{2\pi\ f_\pi}\left(\frac{c_w^2-3s_w^2}{c_w\,s_w}\right).$$

Equivalently for the η meson,

$$\mathcal{L} \supset \frac{1}{4}g_{\eta' WW}\,\eta_0\,W\tilde{W} + \frac{1}{4}g_{\eta' BB}\,\eta_0\,B\tilde{B} \longrightarrow \frac{1}{4}g_{\eta' ZZ}\,\eta_0\,Z\tilde{Z} + \frac{1}{4}g_{\eta'\gamma\gamma}\,\eta_0\,F\tilde{F} + \frac{1}{4}g_{\eta'\gamma Z}\,\eta_0\,F\tilde{Z}, \tag{B.5}$$

with

$$g_{\eta' WW} \equiv -\frac{\alpha}{2\pi\ f_\pi}\left(\frac{3}{2}\frac{1}{s_w^2}\right),$$
$$g_{\eta' WW} \equiv -\frac{\alpha}{2\pi\ f_\pi}\left(\frac{3}{2}\frac{1}{s_w^2}\right),$$
$$g_{\eta' BB} \equiv -\frac{\alpha}{2\pi\ f_\pi}\left(\frac{11}{6}\frac{1}{c_w^2}\right),$$
$$g_{\eta' ZZ} \equiv -\frac{\alpha}{2\pi\ f_\pi}\left(\frac{11\,s_w^4+9\,c_w^4}{6\,s_w^2c_w^2}\right),$$
$$g_{\eta'\gamma\gamma} \equiv -\frac{\alpha}{2\pi\ f_\pi}\left(\frac{10}{3}\right),$$
$$g_{\eta'\gamma Z} \equiv -\frac{\alpha}{2\pi\ f_\pi}\left(\frac{9\,c_w^4-11\,s_w^4}{3\,s_w^2c_w^2}\right). \tag{B.6}$$

The mixing of the axion with the η' and the neutral pion will result in additional contributions to the coefficients of the

interactions in Eqs. (2.5) and (2.6), via the first three operators in Eq. B.1. The fourth one results in a neutral pion-W^3B coupling, which in turn induces a $SU(2)_L$-breaking coupling of the physical axion to W^3B . In other words, below $\Lambda_{\rm QCD}$ the operator space of axion electroweak couplings spans three degrees of freedom, instead of the two above the QCD confinement scale, with

$$\begin{aligned}\delta\mathscr{L}_a^{gauge} &= \frac{\alpha_s}{8\pi}\frac{a}{f_a}G\tilde{G} + \frac{1}{4}g_{aWW}\,a\,W\tilde{W}\\ &\quad + \frac{1}{4}g_{aBB}\,a\,B\tilde{B} + \frac{1}{4}g_{aBW}\,a\,B\tilde{W},\end{aligned} \tag{B.7}$$

where

$$\begin{aligned}g_{aWW} &= -\frac{1}{2\pi f_a}\frac{\alpha_{\rm em}}{s_w^2}\left(\frac{L}{N}-\frac{3}{4}\right),\\ g_{aBB} &= -\frac{1}{2\pi f_a}\frac{\alpha_{\rm em}}{c_w^2}\left(\frac{P}{N}-\frac{5m_u+17m_d}{12(m_u+m_d)}\right),\\ g_{aBW} &= \frac{1}{2\pi f_a}\frac{\alpha_{\rm em}}{s_w c_w}\left(\frac{1}{2}\frac{m_d-m_u}{m_u+m_d}\right)\end{aligned} \tag{B.8}$$

are obtained using the result for the mass mixing of the axion with the pseudoscalar mesons given in Eq. (2.33).

Similarly for the heavy axion case,

$$\begin{aligned}g_{aWW} &= -\frac{1}{2\pi f_a}\frac{\alpha_{\rm em}}{s_w^2}\left(\frac{L}{N}-\frac{3}{4}\frac{1}{1-\left(\frac{M}{m_{\eta'}}\right)^2}\right),\\ g_{aBB} &= -\frac{1}{2\pi f_a}\frac{\alpha_{\rm em}}{c_w^2}\left[\frac{P}{N}\right.\\ &\quad \left.-\frac{1}{1-\left(\frac{M}{m_{\eta'}}\right)^2}\left(\frac{11}{6}+\frac{1}{2}\frac{m_d-m_u}{m_u+m_d}\frac{1}{1-\left(\frac{M}{m_\pi}\right)^2}\right)\right],\\ g_{aBW} &= \frac{1}{2\pi f_a}\frac{\alpha_{\rm em}}{s_w c_w}\\ &\quad \times\left(\frac{1}{2}\frac{m_d-m_u}{m_u+m_d}\frac{1}{1-\left(\frac{M}{m_\pi}\right)^2}\frac{1}{1-\left(\frac{M}{m_{\eta'}}\right)^2}\right).\end{aligned} \tag{B.9}$$

C How general is the mass matrix in Eq. 2.29?

Let us start with the most general Lagrangian above the QCD confinement scale that is relevant for the mass and mixings of the axion:

$$\begin{aligned}\delta\mathscr{L}_a &= \frac{1}{2}\,\partial_\mu\hat{a}\,\partial_\mu\hat{a} + c_1^u\,\frac{\partial_\mu\hat{a}}{f_{\rm PQ}}\left(\bar{u}\,\gamma_\mu\,\gamma_5\,u\right) + c_1^d\,\frac{\partial_\mu\hat{a}}{f_{\rm PQ}}\left(\bar{d}\,\gamma_\mu\,\gamma_5\,d\right)\\ &\quad - \bar{u}_L\,m_u\,u_R\,e^{i\,c_2^u\,\hat{a}/f_{\rm PQ}} - \bar{d}_L\,m_d\,d_R\,e^{i\,c_2^d\,\hat{a}/f_{\rm PQ}} + \text{h.c.}\\ &\quad + c_3\,\frac{\alpha_s}{8\pi}\,\frac{\hat{a}}{f_{\rm PQ}}G\tilde{G} + \frac{1}{4}g^0_{a\gamma\gamma}\,\hat{a}\,F\tilde{F}.\end{aligned} \tag{C.1}$$

For simplicity, here we focus on the coupling to photons but the discussion is of course applicable to the other EW gauge bosons. The relation of the $c_1^{u,d}$ couplings with the corresponding ones c_1^Q, c_1^U and c_1^D in the $SU(2)\times U(1)$ gauge invariant formulation in Eq. (2.12) are given by Eq. (4.4), while $c_3 = N_0$ in that equation. Without loss of generality, PQ invariance can be imposed on all operators in the Lagrangian but the anomalous couplings. As a consequence, the couplings $c_2^{u,\,d}$ are related to the PQ charges of the up and down quarks in in Eq. (2.12) in the following way, $\mathcal{X}_{u,d} = c_2^{u,\,d}\,\mathcal{X}_a$ (where the charge of the axion can be set to $\mathcal{X}_a = 1$).

This Lagrangian has a reparametrization invariance [44],[17] that corresponds to making the usual axion dependent quark field rotations,

$$\begin{aligned}c_1^{u,d} &\longrightarrow c_1^{u,d} + \alpha_{u,d},\\ c_2^{u,d} &\longrightarrow c_2^{u,d} - 2\,\alpha_{u,d},\\ c_3 &\longrightarrow c_3 + 2\,\alpha_u + 2\,\alpha_d,\\ g_{a\gamma\gamma} &\longrightarrow g_{a\gamma\gamma} - \frac{\alpha}{2\pi f_{\rm PQ}}\left(12\alpha_u\,q_u^2 + 12\alpha_d\,q_d^2\right).\end{aligned} \tag{C.2}$$

In the body of the paper we are considering $c_1^{u,d} = 0$, when computing the axion mass and mixings. This is general due to the reparametrization invariance.

When QCD confines and the chiral symmetry is broken by the quark condensate, the couplings in Eq. (C.1) translate into effective operators involving mesons. Defining the π and η_0-fields in terms of the currents:

$$\begin{aligned}j_3^\mu &= \frac{1}{2}\left(\bar{u}\,\gamma_\mu\,\gamma_5\,u - \bar{d}\,\gamma_\mu\,\gamma_5\,d\right) \equiv f_\pi\,\partial_\mu\pi_3,\\ j_0^\mu &= \frac{1}{2}\left(\bar{u}\,\gamma_\mu\,\gamma_5\,u + \bar{d}\,\gamma_\mu\,\gamma_5\,d\right) \equiv f_\pi\,\partial_\mu\eta_0.\end{aligned} \tag{C.3}$$

The low energy chiral Lagrangian can be decomposed in three terms:

$$\delta\mathscr{L}_a = \delta\mathscr{L}_{a,\,\rm kin} + \delta\mathscr{L}_{a,\,\rm mass} + \delta\mathscr{L}_{a,\,\rm anom}. \tag{C.4}$$

– The derivative couplings $c_1^{u,d}$ generate kinetic mixing between the axion and the mesons,

$$\begin{aligned}\delta\mathscr{L}_{a,\,\rm kin} &= \frac{1}{2}\,\partial_\mu\hat{a}\,\partial^\mu\hat{a} + \frac{1}{2}\,\partial_\mu\pi_3\,\partial^\mu\pi_3 + \frac{1}{2}\,\partial_\mu\eta_0\,\partial^\mu\eta_0\\ &\quad + \left(c_1^u - c_1^d\right)\frac{f_\pi}{f_{\rm PQ}}\,\partial_\mu\hat{a}\,\partial^\mu\pi_3\\ &\quad + \left(c_1^u + c_1^d\right)\frac{f_\pi}{f_{\rm PQ}}\,\partial_\mu\hat{a}\,\partial^\mu\eta_0.\end{aligned} \tag{C.5}$$

– The Yukawa couplings $c_2^{u,d}$ produce mass mixing. In the chiral formulation the effects of these operators can be

[17] Note that this reparametrization invariance differs from that in Ref. [44].

encoded in an axion-dependent mass matrix,

$$M_a = \begin{pmatrix} m_u & 0 \\ 0 & m_d \end{pmatrix} \begin{pmatrix} e^{i\, c_2^u\, \hat{a}/f_{\rm PQ}} & 0 \\ 0 & e^{i\, c_2^d\, \hat{a}/f_{\rm PQ}} \end{pmatrix}. \tag{C.6}$$

So that the chiral Lagrangian induced at low energies contains the term

$$\begin{aligned} \delta\mathscr{L}_{a,\,\rm mass} &= B_0 \frac{f_\pi^2}{2}\, {\rm Tr}\left(\Sigma M_a^\dagger + M_a \Sigma^\dagger\right) \\ &= B_0 f_\pi^2 \left[m_u \cos\left(\frac{\pi_3}{f_\pi} + \frac{\eta_0}{f_\pi} - c_2^u\, \frac{\hat{a}}{f_{\rm PQ}}\right) \right. \\ &\quad \left. + m_d \cos\left(\frac{\pi_3}{f_\pi} - \frac{\eta_0}{f_\pi} - c_2^d\, \frac{\hat{a}}{f_{\rm PQ}}\right)\right]. \end{aligned} \tag{C.7}$$

– The coupling to gluons generates an effective potential that is responsible for the bulk of the mass of the η' and can be parametrized at low energies as,

$$\begin{aligned} \delta\mathscr{L}_{a,\,\rm anom} &= -\frac{\alpha_s}{8\,\pi}\left(2\frac{\eta_0}{f_\pi} + c_3\, \frac{\hat{a}}{f_a}\right) G\,\tilde{G} \longrightarrow \\ &\quad -\frac{1}{2}\, K\, \left(2\frac{\eta_0}{f_\pi} \;\; + c_3\, \frac{\hat{a}}{f_a}\right)^2. \end{aligned} \tag{C.8}$$

Altogether, the relevant chiral Lagrangian reads,

$$\begin{aligned} \delta\mathscr{L}_a = &\frac{1}{2}\,\partial_\mu\hat{a}\,\partial^\mu\hat{a} \,+\, \frac{1}{2}\,\partial_\mu\pi_3\,\partial^\mu\pi_3 \,+\, \frac{1}{2}\,\partial_\mu\eta_0\,\partial^\mu\eta_0 \\ &+\alpha_\pi\,\partial_\mu\hat{a}\,\partial^\mu\pi_3 \,+\, \alpha_\eta\,\partial_\mu\hat{a}\,\partial^\mu\eta_0 \\ &+ B_0 f_\pi^2 \left[m_u \cos\left(\frac{\pi_3}{f_\pi} + \frac{\eta_0}{f_\pi} - c_2^u\, \frac{\hat{a}}{f_{\rm PQ}}\right)\right. \\ &\left. +m_d \cos\left(\frac{\pi_3}{f_\pi} - \frac{\eta_0}{f_\pi} - c_2^d\, \frac{\hat{a}}{f_{\rm PQ}}\right)\right] \\ &-\frac{1}{2}\, K\, \left(2\frac{\eta_0}{f_\pi} + c_3\, \frac{\hat{a}}{f_a}\right)^2. \end{aligned} \tag{C.9}$$

The coefficients $\alpha_\pi\,,\ \alpha_\eta$ parametrizing the kinetic mixing are

$$\alpha_\pi = \left(c_1^u - c_1^d\right)\frac{f_\pi}{f_{\rm PQ}}; \qquad \alpha_\eta = \left(c_1^u + c_1^d\right)\frac{f_\pi}{f_{\rm PQ}}. \tag{C.10}$$

In order to obtain the mass matrix and ultimately the mass eigenvalues and mixings, the kinetic terms have to be diagonalized first. This can be done by the following transformations:

$$\begin{aligned} \hat{a} \;&\longrightarrow\; \frac{\hat{a}}{\sqrt{1-\alpha_\pi^2-\alpha_{\eta'}^2}} \simeq \hat{a}\,, \\ \pi_3 \;&\longrightarrow\; \pi_3 - \frac{\alpha_\pi\,\hat{a}}{\sqrt{1-\alpha_\pi^2-\alpha_{\eta'}^2}} \simeq \pi_3 - \left(c_1^u - c_1^d\right)\frac{f_\pi}{f_{\rm PQ}}\,\hat{a}\,, \\ \eta_0 \;&\longrightarrow\; \eta_0 - \frac{\alpha_\eta\,\hat{a}}{\sqrt{1-\alpha_\pi^2-\alpha_{\eta'}^2}} \simeq \eta_0 - \left(c_1^u + c_1^d\right)\frac{f_\pi}{f_{\rm PQ}}\,\hat{a}\,. \end{aligned} \tag{C.11}$$

The Lagrangian Eq. (C.9) becomes,[18]

$$\begin{aligned} \delta\mathscr{L}_a = &\frac{1}{2}\,\partial_\mu\hat{a}\,\partial^\mu\hat{a} \,+\, \frac{1}{2}\,\partial_\mu\pi_3\,\partial^\mu\pi_3 \,+\, \frac{1}{2}\,\partial_\mu\eta_0\,\partial^\mu\eta_0 \\ &+ B_0 f_\pi^2 \left[m_u \cos\left(\frac{\pi_3}{f_\pi} + \frac{\eta_0}{f_\pi} - \bar{c}_2^u\, \frac{\hat{a}}{f_{\rm PQ}}\right)\right. \\ &\left. +m_d \cos\left(\frac{\pi_3}{f_\pi} - \frac{\eta_0}{f_\pi} - \bar{c}_2^d\, \frac{\hat{a}}{f_{\rm PQ}}\right)\right] \\ &-\frac{1}{2}\, K\, \left(2\frac{\eta_0}{f_\pi} + \bar{c}_3\, \frac{\hat{a}}{f_{\rm PQ}}\right)^2, \end{aligned} \tag{C.12}$$

where $\bar{c}_2^u$, $\bar{c}_2^d$ and $\bar{c}_3$ are given by

$$\begin{aligned} \bar{c}_2^u &= 2\,c_1^u + c_2^u, \\ \bar{c}_2^d &= 2\,c_1^d + c_2^d, \\ \bar{c}_3 &= c_3 - 2\,c_1^u - 2\,c_1^d. \end{aligned} \tag{C.13}$$

As expected, these coefficients are invariant under the reparametrization invariance in Eq. (C.2). Therefore, the squared mass matrix coming from Eq. (C.12) is completely general,

$$M^2_{\{\pi_3,\,\eta_0,a\}} = \begin{pmatrix} B_0\,(m_u+m_d) & B_0\,(m_u-m_d) & -B_0\,\frac{f_\pi}{f_{\rm PQ}}\left(m_u\,\bar{c}_2^u - m_d\,\bar{c}_2^d\right) \\ B_0\,(m_u-m_d) & \frac{4K}{f_\pi}+B_0(m_u+m_d) & \frac{2\,\bar{c}_3\,K}{f_\pi\,f_{\rm PQ}}+B_0\,\frac{f_\pi}{f_{\rm PQ}}\left(m_u\,\bar{c}_2^u + m_d\,\bar{c}_2^d\right) \\ -B_0\,\frac{f_\pi}{f_{\rm PQ}}\left(m_u\,\bar{c}_2^u - m_d\,\bar{c}_2^d\right) & \frac{2\,\bar{c}_3\,K}{f_\pi\,f_{\rm PQ}}+B_0\,\frac{f_\pi}{f_{\rm PQ}}\left(m_u\,\bar{c}_2^u + m_d\,\bar{c}_2^d\right) & \bar{c}_3^2\,\frac{K}{f_{\rm PQ}^2}+B_0\,\frac{f_\pi^2}{f_{\rm PQ}^2}\left(m_u\,(\bar{c}_2^u)^2 + m_d\,(\bar{c}_2^d)^2\right) \end{pmatrix}. \tag{C.14}$$

This matrix can be diagonalized analytically in the limit $f_{\rm PQ} \gg B_0,\ m_{u,d},\ f_\pi$. We find that the physical axion corresponds to the combination:

$$a \simeq \hat{a} + \theta_{a\pi}\,\pi_3 + \theta_{a\eta'}\,\eta_0, \tag{C.15}$$

where all mixing angles are assumed small and

$$\theta_{a\pi} \simeq -\frac{f_\pi}{2\,f_{\rm PQ}}\,\frac{\left(\bar{c}_3 + 2\bar{c}_2^d\right)m_d - \left(\bar{c}_3 + 2\bar{c}_2^u\right)m_u}{m_u + m_d},$$

[18] The same Lagrangian can be obtained by making use of the reparametrization invariance in Eq. (C.2) and choosing $\alpha_u = c_1^u$ and $\alpha_d = c_1^d$.

$$\theta_{a\eta'} \simeq -\frac{f_\pi}{2 f_{\rm PQ}}\,\bar{c}_3. \tag{C.16}$$

Note that this gives the physical axion in terms of the fields whose kinetic terms are already diagonalized. In order to express it in terms of the *flavour* meson fields (as defined in Eq. (C.3)), the transformation in Eq. (C.11) needs to be taken into account. The final mixings read,

$$\begin{aligned}\theta_{a\pi} &\simeq -\frac{f_\pi}{2 f_{\rm PQ}}\left(c_2^d - c_2^u + \left(c_3 + c_2^u + c_2^d\right)\frac{m_d - m_u}{m_u + m_d}\right),\\ \theta_{a\eta'} &\simeq -\frac{f_\pi}{2 f_{\rm PQ}}\,c_3,\end{aligned} \tag{C.17}$$

expressed in terms of the couplings of the starting Lagrangian in Eq. (C.1). It is worth noting that the physical mixing parameters do not depend on the coefficient $c_1^{u,\,d}$ of the derivative operator, since it is PQ invariant and therefore it has no impact on the masses and the mixings.

Now we are ready to study the effect of these two diagonalizations in the coupling of the axion to photons,

$$g_{a\gamma\gamma} = g^0_{a\gamma\gamma} + \theta_{a\pi}\, g_{\pi\gamma\gamma} + \theta_{a\eta'}\, g_{\eta'\gamma\gamma}. \tag{C.18}$$

Taking into account that the coupling of the mesons to photons are given by

$$g_{\pi\gamma\gamma} \equiv -\frac{3\,\alpha}{\pi\, f_\pi}\left(q_u^2 - q_d^2\right), \quad g_{\eta'\gamma\gamma} \equiv -\frac{3\,\alpha}{\pi\, f_\pi}\left(q_u^2 + q_d^2\right), \tag{C.19}$$

where q_u and q_d are the electromagnetic charges of the up and down quarks, we find,

$$\begin{aligned}g_{a\gamma\gamma} &= g^0_{a\gamma\gamma} + \frac{\alpha}{2\pi f_{\rm PQ}}\\ &\times\left(-6\,c_2^u\,q_u^2 - 6\,c_2^d\,q_d^2 - 6\left(c_3 + c_2^u + c_2^d\right)\frac{q_d^2\,m_u - q_u^2\,m_d}{m_u + m_d}\right).\end{aligned} \tag{C.20}$$

Recalling that the coefficients $c_2^{u,\,d}$ correspond to the PQ charges, the combinations that appear in the above equation can be identified as the electromagnetic and QCD anomaly coefficients for the up and down quarks,

$$\begin{aligned}E_{u,\,d} &= \sum_{\psi=u,\,d} 2\,\mathcal{X}_\psi\, q_\psi^2 = -6\,c_2^u\,q_u^2 - 6\,c_2^d\,q_d^2\,,\\ N &= c_3 + c_2^u + c_2^d.\end{aligned} \tag{C.21}$$

Redefining the axion decay constant as usual $f_a = f_{\rm PQ}/N$, we can express

$$g_{a\gamma\gamma} = g^0_{a\gamma\gamma} + \frac{\alpha}{2\pi f_a}\left(\frac{E_{u,\,d}}{N} - \frac{2}{3}\frac{m_u + 4\,m_d}{m_u + m_d}\right). \tag{C.22}$$

To sum up, from the most general mass matrix we have obtained the same result of Eq. (2.55) taking into account that in the E/N we have to sum over all fermions transforming under the PQ symmetry, that means including the up and down quarks $E = E_{\rm heavy} + E_{u,\,d}$,

$$g_{a\gamma\gamma} = \frac{\alpha}{2\pi f_a}\left(\frac{E_{\rm heavy}}{N} + \frac{E_{u,\,d}}{N} - \frac{2}{3}\frac{m_u + 4\,m_d}{m_u + m_d}\right). \tag{C.23}$$

References

1. R.D. Peccei, H.R. Quinn, CP conservation in the presence of instantons. Phys. Rev. Lett. **38**, 1440–1443 (1977). [,328(1977)]
2. S. Weinberg, A new light Boson? Phys. Rev. Lett. **40**, 223–226 (1978)
3. H. Georgi, D.B. Kaplan, L. Randall, Manifesting the invisible axion at low-energies. Phys. Lett. B **169**, 73–78 (1986)
4. J.E. Kim, Weak interaction singlet and strong CP invariance. Phys. Rev. Lett. **43**, 103 (1979)
5. M.A. Shifman, A.I. Vainshtein, V.I. Zakharov, Can confinement ensure natural CP invariance of strong interactions? Nucl. Phys. B **166**, 493–506 (1980)
6. A.R. Zhitnitsky, On possible suppression of the axion hadron interactions (In Russian). Sov. J. Nucl. Phys. **31**, 260 (1980). [Yad. Fiz.31,497(1980)]
7. M. Dine, W. Fischler, M. Srednicki, A simple solution to the strong CP problem with a harmless axion. Phys. Lett. **104B**, 199–202 (1981)
8. L. Di Luzio, F. Mescia, E. Nardi, P. Panci, R. Ziegler, Astrophobic axions. Phys. Rev. Lett. **120**(26), 261803 (2018). arXiv:1712.04940
9. L. Di Luzio, F. Mescia, E. Nardi, Redefining the axion window. Phys. Rev. Lett. **118**(3), 031801 (2017). arXiv:1610.07593
10. D.B. Kaplan, Opening the axion window. Nucl. Phys. B **260**(1), 215–226 (1985)
11. M. Srednicki, Axion couplings to matter: (i). CP-conserving parts. Nucl. Phys. B **260**(3), 689–700 (1985)
12. W.A. Bardeen, R.D. Peccei, T. Yanagida, Constraints on variant axion models. Nucl. Phys. B **279**, 401–428 (1987)
13. G. Grilli di Cortona, E. Hardy, J. Pardo Vega, G. Villadoro, The QCD axion, precisely. JHEP **01**, 034 (2016). arXiv:1511.02867
14. G.G. Raffelt, Astrophysical axion bounds. Lect. Notes Phys. **741**, 51–71 (2008). arXiv:hep-ph/0611350. [,51(2006)]
15. J.H. Chang, R. Essig, S.D. McDermott, Supernova 1987A constraints on sub-GeV dark sectors, Millicharged particles, the QCD axion, and an axion-like particle. JHEP **09**, 051 (2018). arXiv:1803.00993
16. I.G. Irastorza, J. Redondo, New experimental approaches in the search for axion-like particles. Progr. Part. Nucl. Phys. **102**, 89–159 (2018). arXiv:1801.08127
17. L.D. Luzio, F. Mescia, E. Nardi, Window for preferred axion models. Phys. Rev. D **96**(7), 075003 (2017). arXiv:1705.05370
18. D.S.M. Alves, N. Weiner, A viable QCD axion in the MeV mass range. JHEP **07**, 092 (2018). arXiv:1710.03764
19. J. Jaeckel, M. Spannowsky, Probing MeV to 90 GeV axion-like particles with LEP and LHC. Phys. Lett. B **753**, 482–487 (2016). arXiv:1509.00476
20. K. Mimasu, V. Sanz, ALPs at colliders. JHEP **06**, 173 (2015). arXiv:1409.4792
21. M. Bauer, M. Neubert, A. Thamm, Collider probes of axion-like particles. JHEP **12**, 044 (2017). arXiv:1708.00443
22. M. Bauer, M. Heiles, M. Neubert, A. Thamm, Axion-like particles at future colliders. arXiv:1808.10323

23. C. Frugiuele, E. Fuchs, G. Perez, M. Schlaffer, Relaxion and light (pseudo)scalars at the HL-LHC and lepton colliders. JHEP **10**, 151 (2018). arXiv:1807.10842
24. I. Brivio, M.B. Gavela, L. Merlo, K. Mimasu, J.M. No, R. del Rey, V. Sanz, ALPs effective field theory and collider signatures. Eur. Phys. J. C **77**(8), 572 (2017). arXiv:1701.05379
25. N. Craig, A. Hook, S. Kasko, The photophobic ALP. JHEP **09**, 028 (2018). arXiv:1805.06538
26. E. Izaguirre, T. Lin, B. Shuve, Searching for axionlike particles in flavor-changing neutral current processes. Phys. Rev. Lett. **118**(11), 111802 (2017). arXiv:1611.09355
27. M. Freytsis, Z. Ligeti, J. Thaler, Constraining the axion portal with $B \to K l^+ l^-$. Phys. Rev. D **81**, 034001 (2010). arXiv:0911.5355
28. V.A. Rubakov, Grand unification and heavy axion. JETP Lett. **65**, 621–624 (1997). arXiv:hep-ph/9703409
29. H. Fukuda, K. Harigaya, M. Ibe, T.T. Yanagida, Model of visible QCD axion. Phys. Rev. D **92**(1), 015021 (2015). arXiv:1504.06084
30. Z. Berezhiani, L. Gianfagna, M. Giannotti, Strong CP problem and mirror world: the Weinberg–Wilczek axion revisited. Phys. Lett. B **500**, 286–296 (2001). arXiv:hep-ph/0009290
31. S.D.H. Hsu, F. Sannino, New solutions to the strong CP problem. Phys. Lett. B **605**, 369–375 (2005). arXiv:hep-ph/0408319
32. A. Hook, Anomalous solutions to the strong CP problem. Phys. Rev. Lett. **114**(14), 141801 (2015). arXiv:1411.3325
33. C.-W. Chiang, H. Fukuda, M. Ibe, T.T. Yanagida, 750 GeV diphoton resonance in a visible heavy QCD axion model. Phys. Rev. D **93**(9), 095016 (2016). arXiv:1602.07909
34. S. Dimopoulos, A. Hook, J. Huang, G. Marques-Tavares, A collider observable QCD axion. JHEP **11**, 052 (2016). arXiv:1606.03097
35. T. Gherghetta, N. Nagata, M. Shifman, A visible QCD axion from an enlarged color group. Phys. Rev. D **93**(11), 115010 (2016). arXiv:1604.01127
36. A. Kobakhidze, Heavy axion in asymptotically safe QCD. arXiv:1607.06552
37. P. Agrawal, K. Howe, Factoring the strong CP problem. JHEP (2017). arXiv:1710.04213
38. P. Agrawal, K. Howe, A flavorful factoring of the strong CP problem. arXiv:1712.05803
39. M. K. Gaillard, M. B. Gavela, R. Houtz, P. Quilez, R. Del Rey, Color unifed dynamical axion. arXiv:1805.06465
40. S. Knapen, T. Lin, H.K. Lou, T. Melia, Searching for axionlike particles with ultraperipheral heavy-ion collisions. Phys. Rev. Lett. **118**(17), 171801 (2017). arXiv:1607.06083
41. X. Cid Vidal, A. Mariotti, D. Redigolo, F. Sala, K. Tobioka, New axion searches at flavor factories. arXiv:1810.09452
42. K. Choi, K. Kang, J.E. Kim, Effects of η' in low-energy axion physics. Phys. Lett. B **181**, 145–149 (1986)
43. A. Salvio, A. Strumia, W. Xue, Thermal axion production. JCAP **1401**, 011 (2014). arXiv:1310.6982
44. J.E. Kim, G. Carosi, Axions and the strong CP problem. Rev. Mod. Phys. **82**, 557–602 (2010). arXiv:0807.3125
45. P. Di Vecchia, G. Veneziano, Chiral dynamics in the large n limit. Nucl. Phys. B **171**, 253–272 (1980)
46. P. Di Vecchia, G. Rossi, G. Veneziano, S. Yankielowicz, Spontaneous CP breaking in QCD and the axion potential: an effective Lagrangian approach. JHEP **12**, 104 (2017). arXiv:1709.00731
47. P. Di Vecchia, F. Sannino, The physics of the θ-angle for composite extensions of the standard model. Eur. Phys. J. Plus **129**, 262 (2014)
48. D. Aloni, Y. Soreq, M. Williams, Coupling QCD-scale axion-like particles to gluons. arXiv:1811.03474
49. BNL-E949 Collaboration, A. V. Artamonov et. al., Study of the decay $K^+ \to \pi^+ \nu \bar{\nu}$ in the momentum region $140 < P_\pi < 199$ MeV/c. Phys. Rev. D **79**, 092004 (2009). arXiv:0903.0030
50. ATLAS Collaboration, T. A. collaboration, Search for new light resonances decaying to jet pairs and produced in association with a photon or a jet in proton–proton collisions at $\sqrt{s} = 13$ TeV with the ATLAS detector. http://inspirehep.net/record/1650592?ln=en
51. CAST Collaboration, V. Anastassopoulos et. al., New CAST limit on the axion–photon interaction. Nat. Phys. **13**, 584–590 (2017). arXiv:1705.02290
52. E. Armengaud et al., Conceptual design of the international axion observatory (IAXO). JINST **9**, T05002 (2014). arXiv:1401.3233
53. A. Payez, C. Evoli, T. Fischer, M. Giannotti, A. Mirizzi, A. Ringwald, Revisiting the SN1987A gamma-ray limit on ultralight axion-like particles. JCAP **1502**(02), 006 (2015). arXiv:1410.3747
54. J. Jaeckel, P.C. Malta, J. Redondo, Decay photons from the axion-like particles burst of type II supernovae. Phys. Rev. D **98**(5), 055032 (2018). arXiv:1702.02964
55. J. Blümlein, J. Brunner, New exclusion limits on dark gauge forces from proton bremsstrahlung in beam-dump data. Phys. Lett. B **731**, 320–326 (2014). arXiv:1311.3870
56. J.D. Bjorken, S. Ecklund, W.R. Nelson, A. Abashian, C. Church, B. Lu, L.W. Mo, T.A. Nunamaker, P. Rassmann, Search for neutral metastable penetrating particles produced in the SLAC beam dump. Phys. Rev. D **38**, 3375 (1988)
57. E.M. Riordan et al., A search for short lived axions in an electron beam dump experiment. Phys. Rev. Lett. **59**, 755 (1987)
58. B. Döbrich, J. Jaeckel, F. Kahlhoefer, A. Ringwald, K. Schmidt-Hoberg, ALPtraum: ALP production in proton beam dump experiments. JHEP **02**, 018 (2016). arXiv:1512.03069. [JHEP 02, 018 (2016)]
59. L3 Collaboration, O. Adriani et. al., Isolated hard photon emission in hadronic Z0 decays.Phys. Lett. B **292**, 472–484 (1992)
60. BaBar Collaboration, J. P. Lees et. al., Search for hadronic decays of a light Higgs boson in the radiative decay $\Upsilon \to \gamma A^0$. Phys. Rev. Lett. **107**, 221803 (2011). arXiv:1108.3549
61. S. Benson, A. Puig Navarro, Triggering $B_s^0 \to \gamma\gamma$ at LHCb. Tech. Rep. LHCb-PUB-2018-006. CERN-LHCb-PUB-2018-006, CERN, Geneva (2018). https://cds.cern.ch/record/2314368?ln=en
62. J. Jaeckel, M. Jankowiak, M. Spannowsky, LHC probes the hidden sector. Phys. Dark Univ. **2**, 111–117 (2013). arXiv:1212.3620
63. A. Mariotti, D. Redigolo, F. Sala, K. Tobioka, New LHC bound on low-mass diphoton resonances. Phys. Lett. B **783**, 13–18 (2018). arXiv:1710.01743
64. CHARM Collaboration, F. Bergsma et. al., Search for axion like particle production in 400-GeV proton–copper interactions. Phys. Lett. B **157**, 458–462 (1985)
65. J.D. Clarke, R. Foot, R.R. Volkas, Phenomenology of a very light scalar (100 MeV $< m_h <$ 10 GeV) mixing with the SM Higgs. JHEP **02**, 123 (2014). arXiv:1310.8042
66. B. Döbrich, F. Ertas, F. Kahlhoefer, T. Spadaro, Model-independent bounds on light pseudoscalars from rare B-meson decays. arXiv:1810.11336
67. SLD Electroweak Group, DELPHI, ALEPH, SLD, SLD Heavy Flavour Group, OPAL, LEP Electroweak Working Group, L3 Collaboration, S. Schael et. al., Precision electroweak measurements on the Z resonance. Phys. Rept. **427**, 257–454 (2006). arXiv:hep-ex/0509008
68. J. F. de Troconiz et al., Work in progress

Part III

Dark matter and inflation

Chapter 7

Lightish but clumpy: scalar dark matter from inflationary fluctuations

Authors:
Gonzalo Alonso-Álvarez and Joerg Jaeckel

Published in *JCAP 10 (2018) 022*,
also available at arXiv:1807.09785

Gonzalo Alonso-Álvarez is the principal author of this article. The original idea for the project was conceived by Joerg Jaeckel and Gonzalo Alonso-Álvarez. All the calculations were performed by Gonzalo Alonso-Álvarez and all figures were produced by Gonzalo Alonso-Álvarez. The article was originally written by Gonzalo Alonso-Álvarez, and it received corrections and improvements by Joerg Jaeckel. Both authors participated equally in the review process.

Journal of Cosmology and Astroparticle Physics
An IOP and SISSA journal

Lightish but clumpy: scalar dark matter from inflationary fluctuations

Gonzalo Alonso-Álvarez and Joerg Jaeckel

Institut für Theoretische Physik, Universität Heidelberg,
Philosophenweg 16, 69120 Heidelberg, Germany

E-mail: alonso@thphys.uni-heidelberg.de, jjaeckel@thphys.uni-heidelberg.de

Received August 15, 2018
Accepted October 3, 2018
Published October 15, 2018

Abstract. It has recently been shown [1] that light vector particles produced from inflationary fluctuations can give rise to the dark matter in the Universe. A similar mechanism has been discussed in [2] for a non-minimally coupled scalar enjoying a Higgs portal interaction. We discuss in detail how such a generation of dark matter works in a minimal setup of a massive scalar non-minimally coupled to gravity. For suitable values of the non-minimal coupling any initial constant value of the field is suppressed during inflation. At the same time, the quantum fluctuations acquired during inflation give rise to a peaked energy density power spectrum. Isocurvature constraints can be avoided since nearly all of the energy is concentrated in fluctuations too small to be observed in the CMB. For masses $\gtrsim$ eV and sufficiently high inflation scale the energy contained in these fluctuations is sufficient to account for the cold dark matter of the Universe. At small scales $\ell_{\rm today} \sim 10^4\,{\rm km}\sqrt{m/{\rm eV}} \sim 10^{-4}\,{\rm AU}\sqrt{m/{\rm eV}}$ fluctuations are large and we therefore expect a rather clumpy nature of this form of dark matter.

Keywords: dark matter theory, inflation

ArXiv ePrint: 1807.09785

https://doi.org/10.1088/1475-7516/2018/10/022

JCAP10(2018)022

Contents

JCAP10(2018)022

1 Introduction

Bosonic fields are interesting and well motivated candidates for the dark matter in the Universe. Both new heavy particles as well as fields in the intermediate and low mass ranges are phenomenologically viable possibilities.

Heavy new degrees of freedom in the GeV and TeV mass range have traditionally been very popular, as a relic density compatible with the observed dark matter abundance may in a natural way be thermally produced through a freeze-out process [3–6]. Direct detection experiments, indirect observations and limits coming from colliders (see [7, 8] and [9], respectively, for recent reviews on these areas) are able to strongly constrain this paradigm. It is therefore timely to study alternative scenarios that could generate dark matter in this mass range and, perhaps even more importantly, to explore different mass regimes.

Prominent examples of light bosons as dark matter candidates are axions, axion-like particles (ALPs) and hidden photons [10–16]. A significant number of direct detection experiments are currently underway, while novel ideas and setups are being developed at an astonishing rate (see [17] for a recent review). Until recently, most efforts were concentrated

on relatively low masses where the coherence and de Broglie wavelengths of the bosonic fields are macroscopic. However, new ideas for the detection of meV − keV mass particles via absorption in superconductors, semiconductors as well as other materials are being brought forward [18, 19] (see also [20] and references therein). This nicely complements absorption signals for masses $\gtrsim 10\,\mathrm{eV}$ which can be searched for in large scale WIMP dark matter detectors [21–24] or neutrinoless double beta decay experiments [25].

While the observational situation is not yet fully clear, the 3.5 keV line provides an interesting hint for a dark matter particle in the keV mass range [26, 27]. Possible explanations include sterile neutrinos [26, 27] but interestingly also scalars [28] and axion-like particles [29].

The standard production mechanism for light bosons in the early Universe is the misalignment mechanism [10–14]. For the paradigmatic example of pseudo-Goldstone bosons, the combination of a weak coupling (i.e. high symmetry breaking scale) and masses $\gtrsim 1\,\mathrm{eV}$ requires a significant amount of fine tuning to avoid producing an overabundance of dark matter [29].[1] At the same time, thermal production is in conflict with structure formation for masses $\lesssim$ keV and may also be problematic for larger masses if interactions with the Standard Model particles are very weak. This motivates the search for new production mechanisms.[2]

For vector particles, it has recently been shown in [1] that a sufficient abundance of dark matter can be produced from the quantum fluctuations of the vector field present during inflation for masses $\gtrsim 10^{-5}\,\mathrm{eV}$. The main goal of the present paper is to show that scalar and pseudoscalar particles non-minimally coupled to gravity are subject to a similar production mechanism and can provide the correct dark matter abundance for masses in the range $\gtrsim$ eV. The scenario is also viable for much larger masses depending on the inflationary scale, but for very heavy fields other production mechanisms [33–43] might dominate over the one presented in this work. The inflationary production of scalar dark matter with intermediate masses has been studied by various authors [2, 44–46], focusing on the "Higgs portal" scenario. We provide a more minimal setup where neither self-interactions nor direct couplings to Standard Model fields are assumed. This already leads to a different cosmological evolution and a modified range of masses and inflation scales that yield the correct dark matter abundance. Moreover, we carefully follow the evolution of the power spectrum of fluctuations and consider the particularities of the behaviour of the higher momentum modes. We find significant qualitative and quantitative differences between our formalism and a treatment of the field as quasi-homogeneous.

It is a well known fact that light fields present during inflation can be excited coherently [47–49]. This phenomenon can be understood as arising from the fact that an observer in de Sitter space will feel a thermal bath at the Hawking temperature $T_\mathrm{H} = H/2\pi$ [50]. Small scale modes acquire quantum fluctuations which are stretched and grow in amplitude as the Universe expands. Eventually, these fluctuations transition into a classical regime when they leave the horizon.

If such field excitations survive the evolution until present time, they can contribute to the energy budget of the Universe. In particular, if we are dealing with a sufficiently weakly interacting particle that is cosmologically stable, it is possible that these particles make up the dark matter that we observe today. For vectors this has been realized in [1]. Here, we will show that such a mechanism is also viable for scalars.

[1] For a recent modification of the minimal pseudo-Goldstone boson setup, breaking the usual relation between the naturally produced dark matter abundance and the coupling to other fields see [30].

[2] An interesting mechanism for a potentially less tuned production of very light $\lesssim \mu$eV bosons has recently been discussed in [31, 32].

JCAP10(2018)022

The main issue with this scenario has to do with the generation of isocurvature perturbations. In general, the quantum fluctuations induced in the inflaton field are uncorrelated with the ones acquired by other light fields. In the cosmological standard model, the inflaton is responsible for the generation of the curvature (or *adiabatic*) perturbations whose spectrum perfectly matches the one imprinted in the cosmic microwave background (CMB). As the inflaton decays during reheating, these fluctuations are passed on to the different fluids that populate the Universe. However, if dark matter is not produced from the decay of the inflation but rather is already present during inflation, its fluctuations will not match the ones that the rest of the fluids have: they are isocurvature rather than adiabatic. This mismatch in the spectrum of fluctuations would leave an imprint in the CMB which has not been observed by the Planck mission [51].

The consequence is that the amplitude of isocurvature fluctuations in the dark matter field has to be very small compared to the adiabatic one. There is however a caveat: this statement only holds for the very large scales that are observed by the Planck satellite. It is perfectly allowed by observations that the dark matter field enjoys isocurvature fluctuations as long as they are "hidden" at low scale modes. This is possible, for instance, if the power spectrum of the dark matter field is peaked at some intermediate scale much below the ones probed by CMB observables. Such a possibility was studied in [1] in the context of a massive vector field. In this paper we see that this is also the case for a scalar field non-minimally coupled to gravity. This is in line with the findings of [2, 46], who discussed a suppression of the isocurvature perturbations of a scalar field which during inflation acquires a large mass from couplings to other fields, such as the inflaton, and a non-minimal coupling, respectively. In this work, we investigate the cosmological evolution in more detail and keep track of the wavelength-dependent evolution of fluctuations during the different eras. In short, the very long-range fluctuations accessible in CMB measurements are suppressed during inflation because of the presence of a $\mathcal{O}(H_I)$ effective mass arising from the non-minimal coupling. During radiation domination the Ricci scalar drops to $R \simeq 0$, stopping the suppression of the superhorizon modes and thus avoiding a further dilution of the energy density stored in shorter wavelength modes. The result at late times is a peaked power spectrum with order one fluctuations on very small scales.

Throughout this work, we only deal with gravitational interactions of a non-minimally coupled scalar field, without assuming the existence of any further couplings to the inflaton or to standard model fields. This is motivated by the fact that the only current evidence for the existence of dark matter comes from the gravitational sector. Indeed, the misalignment mechanism that is usually employed to produce low mass bosonic fields also does not rely on any interactions with other particles. Further scenarios where dark matter is produced gravitationally and where it only interacts through the metric have been considered in the past. So far, studies have focused on the production at the end of inflation or during reheating [33–39], and were concerned primarily with very heavy scalar fields. The possibility that dark matter was produced thermally through graviton-mediated processes has been considered in [39–43], again for heavy scalar fields with masses above ~ 1 TeV. Our approach is essentially different, as we focus on the production purely due to the expansion during inflation and deal with lighter masses.

We would like to stress that similar to the misalignment mechanism, the production mechanism considered here is independent of additional (weak) interactions of the field with Standard Model particles. The resulting dark matter can therefore be equipped with a wide variety of very weak interactions with the Standard Model, e.g. two-photon couplings,

JCAP10(2018)022

derivative couplings to fermions and many others, opening a wide range of phenomenological possibilities (see [14, 17, 52, 53] for some examples). Another natural example would be the dimension 4 coupling to the Higgs field, usually known as the Higgs portal coupling, whose implications for the inflationary or misalignment produced dark matter have been studied in [2].[3]

Moreover, we note that this mechanism is generic and not necessarily only relegated to dark matter production.[4] Indeed, any scalar field with a non-minimal coupling to gravity present during inflation is bound to acquire the spectrum of fluctuations predicted in this work, even the ones that are not stable on cosmological time scales. This may have interesting implications in cosmology when applied, for instance, to the Higgs boson. In what follows, we focus on the generation of dark matter and leave the study of this possibility for future work.

The paper is structured as follows. In section 2 we present the essential phenomenological results. We discuss the relevant features of the evolution of non-minimally coupled scalar fields as well as their fluctuations (sketched in figure 1)). From this we compute the power spectrum (cf. figure 2) and the relic abundance and see how isocurvature perturbations can be suppressed at large scales resulting in the viable parameter space for the scalar fields to be the dark matter of the Universe (shown in figure 3). In section 3, we give a more in depth discussion of the generation of the fluctuations based on methods of quantum field theory in curved spacetimes. Finally, section 4 is devoted to the conclusions and discussion about the potential phenomenological implications of this scenario.

JCAP10(2018)022

2 Generating dark matter from inflationary fluctuations

In this section we discuss the main features of the generation of dark matter from inflationary fluctuations of non-minimally coupled scalar fields.

After introducing the model we first study the evolution of the homogeneous field. For a suitable range of the non-minimal coupling the homogeneous field is completely suppressed, ensuring independence of the results from the initial conditions.

We then turn to the evolution of the fluctuations that give rise to the dark matter. We develop the power spectrum and the energy density it contains and discuss the features that allow to avoid isocurvature constraints.

During this whole section we will treat the evolution of the field with classical equations of motion. As the fluctuations arise from the quantum fluctuations of the field during inflation that turn classical only later on, one may wonder if this is correct. The upshot is that as long as the evolution is linear, the mode functions of the creation and destruction operators follow the classical equations of motion. For appropriate quantities such as the power spectrum, the evolution can then be directly extracted from these mode functions and hence from the classical evolution. We provide more details on this in section 3.

2.1 Model setup

Our starting point is the action of a scalar field ϕ non-minimally coupled to gravity in the following way

$$S = \int \mathrm{d}^4x \sqrt{-g} \left(\frac{1}{2} \left(M^2 - \xi\phi^2 \right) R - \frac{1}{2}\partial_\mu\phi\partial^\mu\phi - \frac{1}{2}m^2\phi^2 + \mathcal{L}_{\mathrm{back}}\left(\sigma_i\right) \right). \tag{2.1}$$

[3] Higgs portal dark matter from thermal production [54–56] is an entire field on its own.

[4] See [57] for a construction where baryogenesis is achieved via a non-minimally coupled scalar.

Here, M corresponds to the Planck mass in the non-minimally coupled frame and $\mathcal{L}_{\rm back}(\sigma_i)$ refers to the action of any other field(s) σ_i present in the Universe. At early times they may dominate its energy density. For simplicity we take them into account by specifying a FRW background with the metric $\mathrm{d}s^2 = -\mathrm{d}t^2 + a^2(t)\mathrm{d}\mathbf{x}^2$ (t being the physical time) and setting the Hubble scale to an appropriate value. The normalisation of the coupling constant ξ is chosen such that $\xi = 1/6$ corresponds to the case of a conformal coupling. For the purposes of the present paper we will focus on $\xi \geq 0$.

Due to the non-minimal coupling our action is strictly speaking in the *Jordan frame*, as opposed to the *Einstein frame*, where all the couplings to gravity are canonically normalised. In the Jordan frame, the Einstein equations and thus the backround evolution of the Universe are modified by the non-minimal coupling to ϕ. In appendix A we study this modification by analysing the dynamics in both frames. We find that for the purposes of this paper, we can safely study our system in the Jordan frame without taking into account backreaction effects, knowing that they remain small. The reason is that we are dealing with a positive coupling ξ and field values that will always remain way below the Planck scale. The same logic also allows us to safely identify the value of the Planck mass in both frames and fix $M \simeq M_{\rm Pl}$. With this we can now proceed to analysing the evolution of the field.

2.2 Classical evolution of the homogeneous field

Let us start with the evolution of the homogeneous field. Its equation of motion is

$$\ddot{\phi} + 3H\dot{\phi} + \left(m^2 + \xi R\right)\phi = 0. \tag{2.2}$$

The effect of the non-minimal coupling is that of a background-dependent mass term. The Ricci scalar in the FRW background is given by $R = 3(1-3\omega)H^2$, where H is the Hubble parameter and $\omega = p/\rho$ is the equation of state of the fluid that dominates the expansion. Its value varies depending on the era according to

- Inflation: $R = 12H^2$, $\quad (H \simeq H_{\rm I} = \text{ const})$.
- Radiation domination: $R \simeq 0$, $\quad (H \sim 1/(2t))$.
- Matter domination: $R = 3H^2$, $\quad (H \sim 2/(3t))$.

We expect that the positive contribution to the mass coming from the Ricci scalar will dominate during inflation and force the field to evolve towards smaller values. During radiation domination, however, the dependence on R vanishes and the field will be constant because of the Hubble friction until we reach the time when $3H \simeq m$ and damped oscillations start. By the time of matter-radiation equality, the R-term will be negligible compared to the mass, as $H_{\rm eq} \simeq 2 \cdot 10^{-28}$ eV, and observations require $m \gg 10^{-28}$ eV.

The interesting regime is the inflationary one. If we assume that $\sqrt{12\xi}H_{\rm I} \gg m$, the solution to the equation of motion is

$$\phi(t) = \frac{\phi_0}{2}\left(\mathrm{e}^{-\frac{\alpha_+}{2}H_{\rm I}t} + \mathrm{e}^{-\frac{\alpha_-}{2}H_{\rm I}t}\right), \tag{2.3}$$

where

$$\alpha_\pm = 3 \pm \sqrt{9 - 48\xi}. \tag{2.4}$$

JCAP10(2018)022

For $0 < \xi < 3/16$, the solution decays exponentially and if $\xi > 3/16$, there will be oscillations with an exponentially damped amplitude. In both cases, we can relate the amplitude of the field at the end of inflation $\phi_{\rm E}$ to its preinflationary value by

$$\phi_{\rm E} \simeq \phi_0 \ {\rm e}^{-\frac{{\rm Re}(\alpha_-)}{2}N}, \tag{2.5}$$

where N is the number of e-folds of inflation.

This shows that for $\xi > 0$ any possible initial homogeneous value for the field will be quickly damped away by inflation (unless ξ is very small), and the contribution to the energy density of the Universe of the homogeneous mode is totally negligible. We are interested in a situation where the dark matter arises from fluctuations and not from the misalignment mechanism, which justifies why in the following we will only consider values $\xi > 0$. We also find that in most of the region where the fluctuations are sufficient to produce the full dark matter density and isocurvature constraints are avoided, ξ will be sufficiently large such that ${\rm Re}(\alpha_-)N/2 \gg 1$ and contributions from initially non-vanishing field values are small.

2.3 Evolution of fluctuations and dark matter density

The goal of this section is twofold. First, we obtain the present-day field power spectrum by tracking the evolution of the primordial one through the different eras of expansion of the Universe. Then, we compute the energy density in the field ϕ and compare it with the observed dark matter abundance. With this, we find that in this scenario the non-minimally coupled field can account for all of the dark matter in our Universe.

The central quantity to describe fluctuations is their power spectrum. To set our conventions, throughout this work we will use the following definition for the power spectrum of a homogeneously and isotropically distributed random field Ψ:

$$\langle \Psi^\star(\mathbf{k},t)\ \Psi(\mathbf{k}',t)\rangle \equiv (2\pi)^3\delta^{(3)}(\mathbf{k}-\mathbf{k}')\frac{2\pi^2}{k^3}\mathcal{P}_\Psi(k,t). \tag{2.6}$$

Note that the power spectrum $\mathcal{P}_\Psi$ can only depend on the magnitude of the momentum, $k = |\mathbf{k}|$. With this definition, the variance of a field is given by,

$$\langle \Psi^2\rangle = \int {\rm d}(\log k)\ \ \mathcal{P}_\Psi(k,t). \tag{2.7}$$

If Ψ is Gaussian-distributed, then it is completely determined by its variance (assuming it has zero mean).

For modes that are already classical, the effect of the evolution on the power spectrum of the field at any point in time is given by,[5]

$$\mathcal{P}_\phi(k,t) = \mathcal{P}_\phi(k,t_0)\left(\frac{\phi({\rm k},t)}{\phi({\rm k},t_0)}\right)^2, \tag{2.8}$$

where $\phi({\rm k},t)$ is a solution of the classical equation of motion

$$\left(\partial_t^2 + 3H\partial_t + \frac{k^2}{a^2} + m^2 + \xi R\right)\phi(k,t) = 0, \tag{2.9}$$

[5] At late times $\phi(k,t)$ will be oscillating quickly. In most of our calculations we will not keep track of these oscillations (e.g. by using a different symbol) but instead consider the envelope of the oscillations for which we find simple power law behaviors. When calculating the energy density from the power spectrum this is actually correct because it accounts for both potential and kinetic energy contributions according to the virial theorem, as we will explain in section 3.2.

with initial condition $\phi(\mathrm{k}, t_0)$ at t_0. But even in the quantum regime the power spectrum is given in terms of the mode functions $f_{\mathbf{k}}$ of the creation and annihilation operators that evolve according to the classical equations of motion,

$$\mathcal{P}_\phi(k,\tau) = \frac{1}{a^2(\tau)}\frac{k^3}{2\pi^2}\left|f_k(\tau)\right|^2. \tag{2.10}$$

We will discuss this in more detail in section 3. Here it suffices to say that the most important input from the quantum calculation is the proper choice of initial conditions for the evolution. In addition, the quantum formalism also provides us with a way to treat the UV-divergences that arise due to the small-scale fluctuations and obtain a finite expression for the energy density of the field.

For now let us plow ahead and understand the relevant phenomenological features. In what follows, we solve the classical equation of motion (2.9) analytically in the different regimes of the history of the Universe, similar to the procedure used in [1]. The relevant features of this evolution can be understood by looking at figure 1, which summarises the evolution of the different Fourier modes through those regimes, represented by different colours in that figure.

(0) **Sub-horizon inflationary regime and horizon exit.** This is the regime where quantum fluctuations are amplified by the effect of the time-evolving gravitational background until they transition into a regime when they can be treated classically. This is a crucial process that provides the appropriate initial conditions and which we will study in more detail in the next section 3. The bottom line is that after horizon exit the field can be described in terms of classical Fourier modes, each of them evolving independently according to (2.9). The initial condition at horizon exit that we obtain in section 3 is that $\phi_0(\mathbf{k})$ is Gaussian-distributed with power spectrum

$$\mathcal{P}_{\phi_0}(k) = \left(\frac{H_{\rm I}}{2\pi}\right)^2 F(\alpha_-); \qquad F(\alpha_-) \equiv \frac{2^{2-\alpha_-}}{\pi}\Gamma^2\left(\frac{3-\alpha_-}{2}\right). \tag{2.11}$$

This is readily obtained from (3.24). We see that the primordial power spectrum right at horizon exit is scale invariant, only differing from the one of a minimally coupled, massless field by the $\mathcal{O}(1)$ factor $F(\alpha_-)$.

(I) **Super-horizon inflationary regime $H \simeq H_{\rm I} \gg k/a,\ m$.** We can drop both the k/a and the m terms from the equation of motion (2.9), which then reads

$$\left(\partial_t^2 + 3H_{\rm I}\partial_t + 12\xi H_{\rm I}^2\right)\phi \simeq 0 \quad \longleftrightarrow \quad \left(\partial_a^2 + \frac{4}{a}\partial_a + \frac{12\xi}{a^2}\right)\phi \simeq 0. \tag{2.12}$$

The solution is

$$\phi = C_+ a^{-\frac{\alpha_+}{2}} + C_- a^{-\frac{\alpha_-}{2}}, \tag{2.13}$$

with, as in (2.3), $\alpha_\pm = 3 \pm \sqrt{9-48\xi}$. Its real part ranges from $\mathrm{Re}(\alpha_-) = 0$ for $\xi = 0$ to $\mathrm{Re}(\alpha_-) = 3$ for $\xi \geq 3/16$. For $\xi > 0$, the dominant term is the second one, so after a short time the solution will approach $\phi \propto a^{-\alpha_-/2}$. In the overlapping region, this is in agreement[6] with the quantum result (3.23). This result makes explicit that, after horizon exit, the effect of the non-minimal coupling quickly becomes important and suppresses the amplitude of the modes.

[6] Note that α_- used here is related to ν used in section 3 by $\alpha_- \simeq 3 - 2\nu$.

JCAP10(2018)022

(II) **Super-horizon radiation era relativistic regime $H \gg k/a \gg m$.** This regime is similar to the previous one except that during radiation domination, the Ricci scalar vanishes and the Hubble parameter is not constant. We are then left with the equation of motion

$$\left(\partial_t^2 + 3H\partial_t\right)\phi \simeq 0 \quad \longleftrightarrow \quad \left(\partial_a^2 + \frac{2}{a}\partial_a\right)\phi \simeq 0, \tag{2.14}$$

which has the solution

$$\phi = C_1 + C_2 a^{-1}. \tag{2.15}$$

The second term dies off and we find that in this regime $\phi \simeq$ const and the field is frozen.

(III) **Super-horizon radiation era non-relativistic regime $H \gg m \gg k/a$.** The equation of motion is the same as the one in (II), so we conclude that the field is also frozen, $\phi \simeq$ const.

(IV) **Sub-horizon radiation era relativistic regime $k/a \gg H,\ m$.** The modes behave in this region as pure radiation. The equation of motion in physical and conformal time reads

$$\left(\partial_t^2 + 3H\partial_t + \frac{k^2}{a^2}\right)\phi \simeq 0 \quad \longleftrightarrow \quad \left(\partial_\tau^2 + 2aH\partial_\tau + k^2\right)\phi \simeq 0. \tag{2.16}$$

Treating the Hubble friction term as a small perturbation, one can find the approximate solution

$$\phi \simeq \frac{1}{a}\left(C_1 \mathrm{e}^{ik\tau} + C_2 \mathrm{e}^{-ik\tau}\right). \tag{2.17}$$

The amplitude of the field decreases as $\phi \propto a^{-1}$, while the energy density

$$\rho \simeq \frac{k^2}{a^2}\phi^2 \propto a^{-4}, \tag{2.18}$$

as expected for a relativistic fluid.

(V) **Non-relativistic massive regime $m \gg H,\ k/a$.** The equation of motion is now

$$\left(\partial_t^2 + 3H\partial_t + m^2\right)\phi \simeq 0. \tag{2.19}$$

In this region, the mass has overcome the Hubble friction and the field performs the well-known oscillations (cf., e.g., [13]) by which it acquires a pressureless matter-like equation of state $\omega \simeq 0$. We can find an analytical expression for the solution of the equation of motion using the WKB approximation,

$$\phi \simeq a^{-\frac{3}{2}}\left(C_1 \mathrm{e}^{imt} + C_2 \mathrm{e}^{-imt}\right). \tag{2.20}$$

The energy density in this regime redshifts as matter,

$$\rho \sim \frac{1}{2}m^2\phi^2 \propto a^{-3}. \tag{2.21}$$

All these solutions are summarised in figure 1. The results obtained here for the non-minimally coupled scalar present similarities with the ones obtained in [1] for the vector, but differ in several key aspects. Firstly, the behaviour of the modes within the horizon and

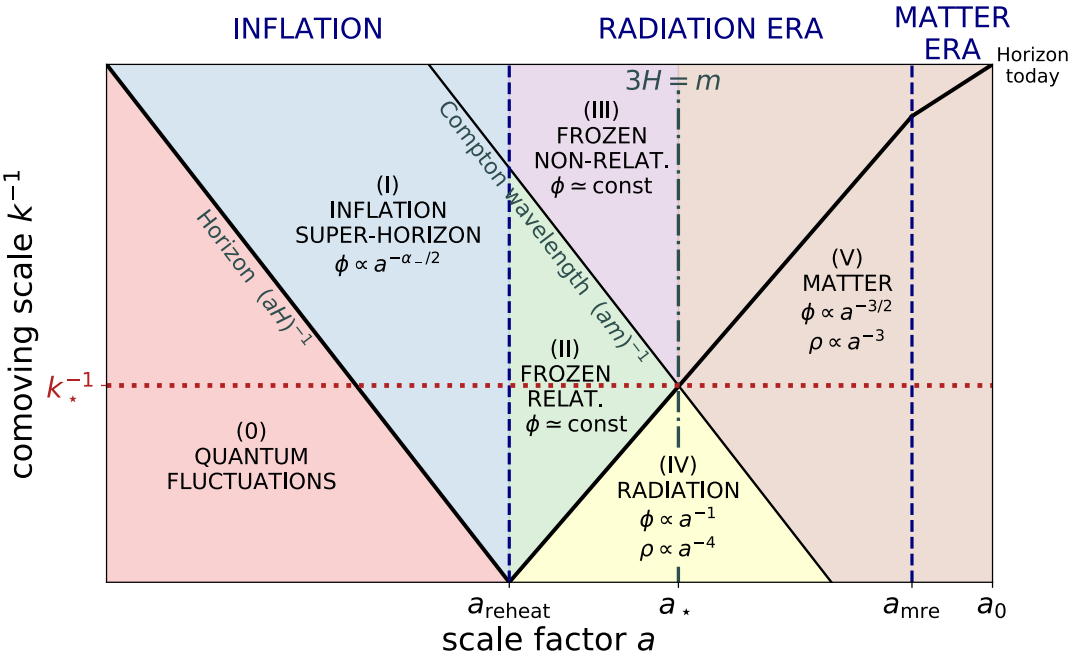

Figure 1. Cosmological evolution of the amplitude of the Fourier modes as a function of their comoving wavelength k^{-1}. The various regions for which we have analytically solved the evolution are shaded in different colours and labelled by roman numerals. The thick black line labelled "Horizon" represents the comoving Hubble radius $(aH)^{-1}$, which shrinks during inflation and grows during the radiation and matter eras. The thin black line depicts the Compton wavelength of the vector $(am)^{-1}$, which dictates when a mode becomes non-relativistic. A mode of fixed comoving wavenumber k evolves from left to right in a horizontal line, starting deep within the horizon during inflation as a quantum fluctuation and eventually behaving as a massive matter-like scalar at present times. In between, the field amplitude behaves as depicted. Modes around $k_\star$, defined as the one that becomes non-relativistic at the same time that it leaves the horizon, are suppressed the least and dominate the energy density.

at horizon exit is in our scenario different to the standard massless case, due to the presence of the non-minimal coupling to gravity. This requires us to study this quantum regime in detail, which we do in section 3, together with a careful treatment of the divergencies that we encounter in the energy density of the UV modes. Secondly, the suppression of the amplitude of the large scale modes happens in our case during inflation, when the gravitation-induced effective mass is large. This can be seen in (2.13) and is also calculated in section 3, where we perform the full quantum computation all the way through inflation and through the inflation-radiation era transition. In contrast, for the vector case this suppression happens later in the evolution after the modes become non-relativistic, and is due to the particularities of the equation of motion for vectors, as discussed in [1]. Regarding the total energy density, we find that due to the evolution in the super-horizon regime we have effectively an extra suppression compared to the vector case, resulting in a preference for somewhat higher masses.

In general, at the boundaries of each of these regimes (0)-(V), the parameters entering the equation change gradually and smoothly so that it is a good approximation to just "glue" together the solutions that we have obtained in each of the regions. However, there is one transition that needs special attention: reheating. Between inflation and radiation

JCAP10(2018)022

domination, the Ricci scalar drops from $R \simeq 12H^2$ to $R \simeq 0$. The exact dynamics of reheating will dictate how exactly this transition happens. In this work we assume that reheating proceeds quickly enough that we can take it to be instantaneous and thus there is a sudden drop in the Ricci scalar. Assuming that this transition is fast allows us to neglect any potential change in the field amplitude during reheating. We look at this in detail in section 3 and confirm that this approximation is justified within our assumptions.

More generally, gravitational particle production can occur during preheating and reheating. This has been studied extensively in [33–39]. In particular, the authors of [38] study dark matter production through tachyonic resonance during reheating in the same non-minimally coupled setup as ours. This effect depends on the precise model of inflation assumed, but occurs quite generically after inflation if the inflaton coherently oscillates around the minimum of its potential. In that case, the Ricci scalar R will oscillate about zero and the $\xi\phi^2 R$ term will periodically give rise to a tachyonic mass for the dark matter particle. As shown in detail in [58], this can result in significant particle creation. Following the same strategy as [38] but for small ξ, the amount of dark matter generated in this way in our setup during reheating is

$$\frac{\Omega_{\rm reh}}{\Omega_{\rm DM}} \lesssim \xi^{3/8} \left(\frac{m}{10\,\text{GeV}}\right) \left(\frac{T_{\rm reh}}{10^{15}\,\text{GeV}}\right)^3 \left(\frac{H_{\rm osc}}{H_{\rm reh}}\right)^{3/4} \exp\left(0.73\,\frac{\sigma_{\rm osc}}{M_{\rm Pl}}\right) \tag{2.22}$$

$$\ll 1 \qquad \text{for} \quad \xi \lesssim 1,\ m \lesssim 10\,\text{GeV}.$$

Here, $T_{\rm reh}$ and $H_{\rm reh}$ denote the temperature and Hubble parameter at the end of reheating, while $H_{\rm osc}$ and $\sigma_{\rm osc}$ are the Hubble scale and the field value of the inflaton when it starts oscillating around the minimum of its potential (for most models, $\sigma_{\rm osc} \lesssim M_{\rm Pl}$). Eq. (2.22) shows that this contribution to the energy density is always small if $\xi \lesssim 1$ or $m \lesssim 10\,\text{GeV}$, both of which are satisfied in the parameter region of interest for this work, as can be seen in figure 3. It is thus justified to neglect the contribution to the particle production from preheating and reheating.

2.3.1 Field power spectrum

With this information we are able to compute the power spectrum of the field amplitude at late times. By late times, we mean a time when all the relevant modes are non-relativistic, so that they are behaving like matter. In order not to spoil the correct procedure of structure formation, all modes contributing significantly to the energy density need to be non-relativistic before matter-radiation equality. We have checked that this is indeed the case in this scenario. The power spectra obtained in what follows are valid for all the modes that have entered region (V) (cf brown region in figure 1) and are applicable from matter-radiation equality onwards.

A simple inspection of figure 1 can give a good qualitative idea of the field power spectrum. All modes start with the same amplitude given by (2.11) when they exit the horizon during inflation. Then, they evolve differently depending on how much time they spend in each of the regions (I) - (V). By visual inspection, it is easy to understand that $k_\star$ is the mode whose amplitude is the least suppressed (at least as long as α_- is not too large, we will shortly quantify this). On the one hand, modes with large comoving wavelength (above $k_\star^{-1}$ in figure 1) leave the horizon earlier during inflation and spend extra time being suppressed in that era. On the other hand, modes with comoving wavelength shorter than $k_\star^{-1}$ experience a stronger suppression while behaving like radiation in region (IV).

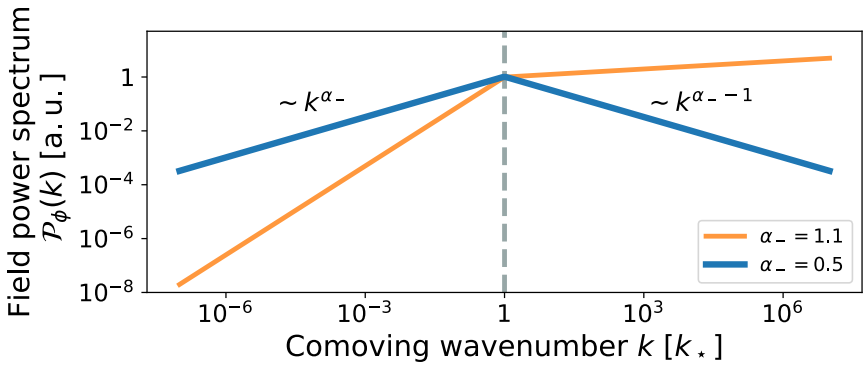

Figure 2. Field power spectrum generated by inflationary fluctuations of a scalar field non-minimally coupled to gravity (normalized to 1 at $k_\star$). The solid blue line shows the behaviour of the power spectrum for small non-minimal couplings $\alpha_- < 1$ and has a peaked structure at the critical scale $k_\star$ (marked by the grey dashed line), which is a very small scale in cosmological terms. The solid orange line corresponds to stronger couplings $\alpha_- > 1$ and is dominated by the power at very small scales (UV modes).

This behaviour is confirmed by our calculations (see appendix B for the details), resulting in the field power spectrum presented in figure 2. At scales larger than the critical wavelength $k_\star^{-1}$, the power spectrum is suppressed by $(k/k_\star)^{\alpha_-}$, while at smaller scales its amplitude scales as $(k/k_\star)^{1-\alpha_-}$. Thus, we find that $\alpha_- = 1$ (i.e $\xi = 5/48$) is the critical value for which the power spectrum changes from being dominated by the $k_\star$ mode to being dominated by ultraviolet modes. We restrict our study to the regime where $\alpha_- < 1$ featuring a peaked power spectrum. Though potentially interesting, the scenario with $\alpha_- > 1$ is dominated by the UV modes and would require a careful treatment of the divergencies with a full regularisation scheme.

These arguments agree with the result obtained from the quantum computation in section 3. Indeed, for adequate values of the non-minimal coupling, the field power spectrum in figure 5 already exhibits a peaked structure at some intermediate scale, while it is suppressed at both very large and very small scales. Note that the power spectrum of figure 5 corresponds to much earlier times than those of figure 2. This explains why the slope in both figures does not match: figure 5 still has to be evolved through the full radiation era.

The mode with critical comoving wavenumber $k_\star$ reenters the horizon during the radiation era precisely when it becomes non-relativistic, as can be seen in figure 1. Phenomenologically, $k_\star^{-1}$ is a very small scale, much below the cosmological scales that play the key roles in structure formation or can be observed with the CMB. It is defined by $k_\star = a_\star m$, where $a_\star$ is the scale factor at the time when the Hubble parameter equals one third of the mass of the scalar field, $3H(a_\star) = m$. The comoving scale associated with this critical wavenumber can be given as a function of the mass as

$$\frac{1}{k_\star} \simeq 4.1 \cdot 10^7 \text{ km } \sqrt{\frac{\text{eV}}{m}}. \tag{2.23}$$

The last thing we need to completely determine the field power spectrum is to compute its overall dimensionful normalisation (note that $\mathcal{P}_\phi$ has mass dimension 2). To do this, we obtain the power at the critical wavenumber $k_\star$. We refer the reader to appendix B for the

JCAP10(2018)022

details of the calculation. Here we just give the final result

$$\mathcal{P}_\phi(t,k_\star) \simeq \mathcal{P}_{\phi_0}(k_\star)\; H_{\rm I}^{-\frac{\alpha_-}{2}}\; m^{-\frac{1}{2}(3-\alpha_-)}\; H_{\rm eq}^{\frac{3}{2}}\; \left(\frac{a(t)}{a_{\rm eq}}\right)^{-3}. \tag{2.24}$$

Here, $H_{\rm I}$ is the Hubble scale of inflation, while the subscript "eq" refers to quantities evaluated at the time of matter-radiation equality. For the sake of clarity, in this expression we have removed some $\mathcal{O}(1)$ factors. The full version of the result is given in (B.3). The primordial power spectrum at horizon exit $\mathcal{P}_{\phi_0}$ is given in (2.11). As was stressed before, this expression is only applicable at late times for modes that are already redshifting as matter.

2.3.2 Dark matter abundance

Once we have the power spectrum of the field, we move on to compute the dark matter abundance. The full expression for the energy density of the field is given in next section's eq. (3.18). At late times when H is negligible and all relevant modes are non relativistic we have,[7]

$$\rho(t) = \int \mathrm{d}(\log k)\; \frac{1}{2} m^2 \mathcal{P}_\phi(k,t). \tag{2.25}$$

This result is independent of the regularisation scheme that has to be applied to cure the Hubble scale-dependent divergences. The integral can be easily carried out analytically for any value of α_-. Here we will focus on the regime $\alpha_- < 1$, and we refer to appendix B for the computation and the results for other choices of α_-. We can now compare the energy density in the non-minimally coupled scalar field with the observed dark matter abundance, finding the result

$$\frac{\Omega_\phi}{\Omega_{\rm DM}} \simeq \frac{3^{\frac{1}{2}(1+\alpha_-)}}{2^{\frac{11}{4}}\pi^2}\; \frac{F(\alpha_-)}{\alpha_-\,(1-\alpha_-)}\; \frac{[\mathcal{F}(T_\star)]^{1+\frac{1}{3}\alpha_-}}{[\mathcal{F}(T_{\rm r})]^{\frac{1}{3}\alpha_-}}\; \frac{1}{M_{\rm Pl}^2}\; H_{\rm eq}^{-\frac{1}{2}}\; H_{\rm I}^{\frac{1}{2}(4-\alpha_-)}\; m^{\frac{1}{2}(\alpha_-+1)}. \tag{2.26}$$

Here, $\mathcal{F}(T)$ is a function encoding the dependence on the number of degrees of freedom, defined in [13] and eq. (B.4). It is typically of order 1. The total abundance depends, as expected, on the Hubble scale of inflation, the scalar mass and the non-minimal coupling ξ through the parameter $\alpha_- = 3 - \sqrt{9-48\xi}$. If we want to explain the observed dark matter abundance, we need to require $\Omega_\phi = \Omega_{\rm DM}$. This requirement, together with a choice of the Hubble scale of inflation, gives a one to one correspondence between the mass of the scalar particle and its non-minimal coupling to gravity, as can be seen in figure 3.

2.4 Density power spectrum and isocurvature fluctuations

In this subsection we will compute the power spectrum of the energy density fluctuations of the non-minimally coupled field ϕ. It is clear that these fluctuations are produced independently of the inflaton ones, and we thus expect both to be uncorrelated. As the inflaton is responsible for setting the curvature (or *adiabatic*) perturbations that affect the metric, the ones generated in the non-minimally coupled scalar will be of purely entropic (or *isocurvature*) nature.

This is not a problem while the non-minimally coupled field remains a subdominant contribution to the energy density of the Universe. Things change when the field's contribution to the energy budget becomes appreciable, which is of course the case in the scenario

[7] We note that the $\mathcal{P}_\phi(k,t)$ at this point denotes the envelope of the oscillating power spectrum as explained in section 3.2.

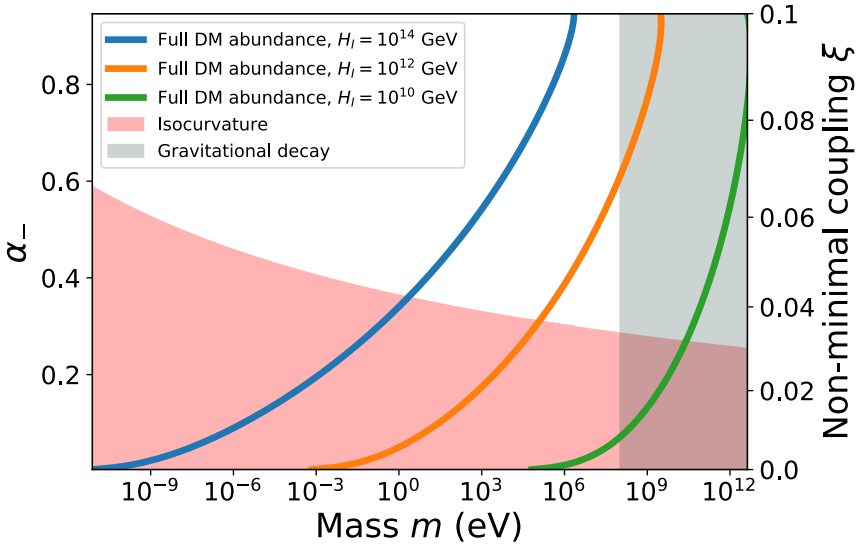

Figure 3. Parameter space of our scenario, composed of the mass of the scalar field and the strength of its non-minimal coupling to gravity. Additionally, our predictions depend on the Hubble scale of inflation $H_{\rm I}$. The lines represent the combination of masses and couplings that give the correct dark matter abundance, plotted for various values of $H_{\rm I}$. The upper limits on the scale of inflation make it impossible to generate enough dark matter to the left of the blue line. The region shaded in red is excluded because our setup generates too much isocurvature power at the scales probed by the Planck satellite (note that this limit assumes that all the dark matter originates from the scalar field fluctuations and effectively only applies to the right of the blue line). The grey-shaded area is disfavoured if we assume that the $\mathbb{Z}_2$ symmetry $\phi \to -\phi$ of the field is broken by quantum gravity effects, inducing gravity-mediated decays of the dark matter particles, as discussed in section 4.

where ϕ makes up the dark matter. Then, isocurvature perturbations leave their imprint in observables like the cosmic microwave background (CMB) and the structure formation dynamics. The lack of observation of such an imprint in the CMB by the Planck mission sets the strongest constraints on the amplitude of isocurvature perturbations [51]. The Planck collaboration gives the name "cold dark matter isocurvature (CDI)" to the scenario where the dark matter fluid has a contribution of isocurvature fluctuations. In this setting, the power in isocurvature fluctuations is observed to be much smaller than the power in adiabatic ones.

This may seem like a nail in the coffin of our setup, as all the power in the non-minimally coupled field energy density is generated as isocurvature. However, the key point is that the bulk of the energy density in our scenario is stored in the fluctuations at the very small scales around $k_\star^{-1}$ given in (2.23) to be $k_\star^{-1} \sim 1.3 \times 10^{-12}\,\text{Mpc}\sqrt{\text{eV}/m}$. This scale is orders of magnitude below the typical scales that the CMB and other cosmological observables probe, which typically lie in the $k^{-1} \sim 10 - 1000$ Mpc range. At those very large scales, the energy density of ϕ acquires the adiabatic fluctuations of the metric, as argued in section 2.5. The isocurvature power at the scales probed by Planck can in this way be suppressed below the observed limits provided.

Let us then compute the power spectrum of the energy overdensities of the field ϕ. We define the density contrast field, that describes the deviations from the mean energy density,

JCAP10(2018)022

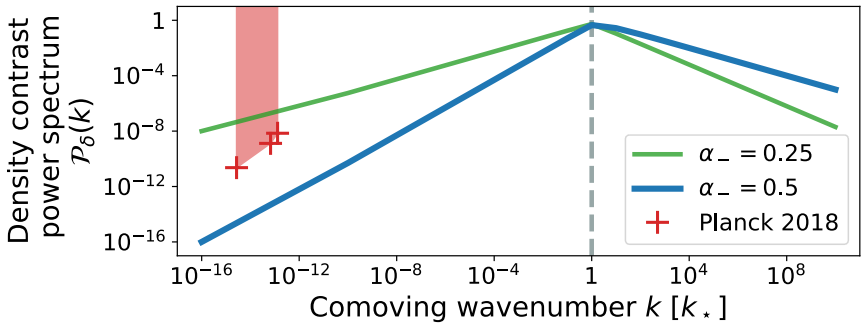

Figure 4. Power spectrum of the density contrast δ of the non-minimally coupled scalar field ϕ. The general shape is valid for all values of the coupling $\alpha_- < 1$. For this plot we have chosen $m = 1$ eV, $\alpha_- = 0.5$ (solid blue line) and $\alpha_- = 0.25$ (solid green line). As the field power spectrum, the density contrast power spectrum is peaked at the scale $k_\star^{-1}$ (highlighted by the grey dashed line), which is orders of magnitude smaller than the ones probed by the CMB. The red crosses correspond to the upper limits on isocurvature perturbations (CDI) set by the Planck satellite [51]. Note that for a large enough α_-, the amplitude of the isocurvature perturbations at the CMB scales is strongly suppressed.

by

$$\rho(\mathbf{x}) \equiv \langle\rho\rangle\,(1+\delta(\mathbf{x}))\,. \tag{2.27}$$

Its Fourier transform can be computed as

$$\delta(\mathbf{k}) = \frac{1}{\langle\phi^2\rangle}\int \frac{\mathrm{d}^3\mathbf{q}}{(2\pi)^3}\phi(\mathbf{q})\phi(\mathbf{k}-\mathbf{q}). \tag{2.28}$$

The mean of the density contrast of course vanishes, and the two point function is given by

$$\langle\delta^\star(\mathbf{k})\delta(\mathbf{k}')\rangle = 8\pi^4\delta^{(3)}(\mathbf{k}-\mathbf{k}')\frac{1}{\langle\phi^2\rangle^2}\int\frac{\mathrm{d}^3\mathbf{q}}{(2\pi)^3}\,\frac{1}{q^3}\frac{1}{|\mathbf{k}-\mathbf{q}|^3}\mathcal{P}_\phi(q)\mathcal{P}_\phi(|\mathbf{k}-\mathbf{q}|). \tag{2.29}$$

The details of this and the following calculations can be found in appendix B (carrying out steps similar to [1]). From this we can easily extract the power spectrum of δ, which can be expressed as a function of the power spectrum of the field as

$$\mathcal{P}_\delta(k) = \frac{k^2}{\langle\phi^2\rangle^2}\int_{|k-q|<p<k+q}\mathrm{d}q\;\mathrm{d}p\;\frac{1}{q^2}\frac{1}{p^2}\mathcal{P}_\phi(q)\mathcal{P}_\phi(p). \tag{2.30}$$

This integral can be carried out numerically resulting in the density contrast power spectrum presented in figure 4. In the parameter region of interest $\alpha_- < 1$, the density power spectrum has the same peaked structure as the field power spectrum of figure 2, and thus the energy density is dominated by overdensities of size $\sim k_\star^{-1}$, which corresponds to the cosmologically small scale given in (2.23). At scales smaller than $k_\star^{-1}$ the power spectrum is suppressed by $(k/k_\star)^{(\alpha_- - 1)}$, whereas for large scales the suppression goes with $(k/k_\star)^{2\alpha_-}$ and is thus stronger than for the field power spectrum.

We can now compute the amplitude of isocurvature perturbations at large scales and compare them with the Planck observations to constrain our scenario. At scales larger than the critical scale $k_\star^{-1}$, we have

$$\mathcal{P}_\delta(k) \simeq \left(\frac{k}{k_\star}\right)^{2\alpha_-}\mathcal{P}_\delta(k_\star), \tag{2.31}$$

k_i	$\beta_{\rm iso}(k_i)$	$\mathcal{P}_{\mathcal{I}}(k_i)$
$k_{\rm low} = 0.002$ Mpc^{-1}	0.011	$2.3 \cdot 10^{-11}$
$k_{\rm mid} = 0.05$ Mpc^{-1}	0.38	$1.3 \cdot 10^{-9}$
$k_{\rm high} = 0.1$ Mpc^{-1}	0.77	$7.0 \cdot 10^{-9}$

Table 1. Planck 2018 limits on the cold dark matter isocurvature (CDI) scenario [51]. More precisely we take the "axion II" scenario of that paper which is appropriate for our case.

where the power at the critical scale $\mathcal{P}_\delta(k_\star)$ also depends on α_- and can be computed using (2.30). We have checked that for the values that interest us, $\mathcal{P}_\delta(k_\star) = \mathcal{O}(1)$ is an order one number.

The absence of observed isocurvature fluctuations in the CMB puts an upper limit on their amplitude. Planck gives constraints on the CDI scenario at three different scales k_i (see table 1), as upper limits for the *primordial isocurvature fraction* defined as

$$\beta_{\rm iso}(k_i) = \frac{\mathcal{P}_{\mathcal{I}}(k_i)}{\mathcal{P}_{\mathcal{I}}(k_i) + \mathcal{P}_{\mathcal{R}}(k_i)}, \tag{2.32}$$

where $\mathcal{P}_{\mathcal{I}}$ and $\mathcal{P}_{\mathcal{R}}$ are the isocurvature and adiabatic power spectra, respectively. Using the Planck normalisation for the curvature power spectrum, $\mathcal{P}_{\mathcal{R}} = 2.1(9) \cdot 10^{-9}$, approximately valid for all the scales of interest k_i, we can translate the bound on $\beta_{\rm iso}$ into a bound on $\mathcal{P}_{\mathcal{I}}$. The values are given in table 1. We can see that the bounds get weaker at smaller scales.

Putting everything together, we can obtain the following bound on the non-minimal coupling to gravity:

$$\alpha_- > \frac{1}{2} \log\left(\frac{\beta_{\rm iso}(k_i)}{1-\beta_{\rm iso}(k_i)} \frac{\mathcal{P}_{\mathcal{R}}(k_i)}{\mathcal{P}_\delta(k_\star)}\right) \left[\log\left(\frac{k_i}{7.5 \cdot 10^{11}\ \text{Mpc}^{-1}} \sqrt{\frac{\text{eV}}{m}}\right)\right]^{-1}, \tag{2.33}$$

which assumes that the scalar makes up all of the dark matter in the Universe. This rules out the region of parameter space shaded in red in figure 3. As expected, a minimum value of the non-minimal coupling ξ is required to suppress the isocurvature perturbations at large scales.

2.5 Acquisition of adiabatic fluctuations

In order for the scenario to agree with cosmological observations, it is not enough that the isocurvature perturbations are sufficiently small at large scales. It is also necessary that the dark matter presents the observed adiabatic spectrum of fluctuations at those scales. Here we will reason that this is indeed the case.

Because of the strongly peaked structure of the power spectrum, the energy density of the scalar field is stored in clumps of typical comoving size $k_\star^{-1}$. As we have argued, this is a scale orders of magnitude smaller than the ones relevant for the CMB and structure formation. At those large scales the inhomogeneities of size $k_\star^{-1}$ are indistinguishable from a true continuum, and the energy density of the field looks very homogeneous. The situation is similar to other scenarios where dark matter has substructure at very small scales like, for instance, primordial black holes [59] or axion miniclusters [60, 61].

At cosmological scales, the energy density of the field is primordially homogeneous (except for the very suppressed component of isocurvature fluctuations). After inflation ends, the fluctuations of the inflaton are imprinted in the metric in the form of curvature

JCAP10(2018)022

perturbations. At that time, the energy density of the scalar field is subdominant and will thus follow the metric fluctuations sourced by the dominant species, which at those early times are the relativistic decay products of the inflaton. This is the reason why the scalar field acquires the adiabatic perturbations at large scales, even if it did not have them originally. At the same time, the small isocurvature component at large scales does not experience such a growth and becomes subdominant to the adiabatic mode. This effect is analogous to other dark matter scenarios like axions [62, 63] and other coherently oscillating scalar fields [64, 65], vectors [1, 13, 66], and further non-thermal mechanisms of dark matter production.

3 Generation of fluctuations in a curved background

So far we have argued mostly based on the classical equations of motion, which is essentially correct for the description of the evolution of the field after its quantum fluctuations have been amplified during inflation. Importantly, however, the initial conditions for this evolution are set by the quantum nature of the particle production due to the time-dependent gravitational background during the inflationary epoch. Moreover, the quantum description also leads to UV divergencies that need to be treated. In this section we will discuss both of these aspects to complement and justify some of the claims made in section 2.

3.1 Quantum behaviour during inflation

We use the tools of quantum field theory in classical curved spacetimes, following [47, 49] to obtain the power spectrum of the field arising from inflationary quantum fluctuations. The action for the non-minimally coupled scalar field is given in (2.1). We specify to a FRW background but this time using conformal time τ, defined by $\mathrm{d}t = a\,\mathrm{d}\tau$. The discussion is simplified by using the field redefinition

$$f(\tau, \mathbf{x}) = a(\tau)\phi(\tau, \mathbf{x}). \tag{3.1}$$

Focusing only on the terms in (2.1) with dependence on the field ϕ, the action becomes

$$S = \int \mathrm{d}\tau\, \mathrm{d}^3\mathbf{x}\, \frac{1}{2}\left(f'^2 - |\nabla f|^2 - \mu^2 f^2\right), \tag{3.2}$$

where the prime denotes a derivative with respect to conformal time and we have defined the effective mass

$$\begin{aligned} \mu^2 &\equiv a^2 m^2 - \left(\frac{1}{6} - \xi\right) a^2 R \\ &= a^2 m^2 - (1 - 6\xi)\,\frac{a''}{a} \\ &= a^2 m^2 - (1 - 6\xi)\left(\mathcal{H}' + \mathcal{H}^2\right). \end{aligned} \tag{3.3}$$

Here, $\mathcal{H}$ denotes the conformal Hubble parameter (we specify to inflation later in (3.12)),

$$\mathcal{H} = \frac{a'}{a}. \tag{3.4}$$

The equation of motion for the field is

$$f'' - \nabla^2 f + \mu^2 f = 0. \tag{3.5}$$

We now quantise the theory. In the canonical quantisation formalism, we promote both f and its conjugate momentum π to operators and impose equal-time commutation relations

$$\begin{aligned}\left[\hat{f}(\tau,\mathbf{x}),\ \hat{\pi}(\tau,\mathbf{x}')\right] &= i\delta^{(3)}(\mathbf{x}-\mathbf{x}'),\\ \left[\hat{f}(\tau,\mathbf{x}),\ \hat{f}(\tau,\mathbf{x}')\right] &= 0,\\ \left[\hat{\pi}(\tau,\mathbf{x}),\ \hat{\pi}(\tau,\mathbf{x}')\right] &= 0.\end{aligned} \tag{3.6}$$

The conjugate momentum for our field is

$$\pi(\mathbf{x}) = \frac{\delta\mathcal{L}}{\delta f'(\mathbf{x})} = f'(\mathbf{x}). \tag{3.7}$$

We can then perform expansions of both operators in Fourier space,

$$\begin{aligned}\hat{f}(\tau,\mathbf{x}) &= \int \frac{d^3k}{(2\pi)^3}\left(\hat{a}(\mathbf{k})f_k(\tau)\mathrm{e}^{i\mathbf{k}\cdot\mathbf{x}} + \hat{a}^\dagger(\mathbf{k})f_k^\star(\tau)\mathrm{e}^{-i\mathbf{k}\cdot\mathbf{x}}\right)\\ \hat{\pi}(\tau,\mathbf{x}) &= \int \frac{d^3k}{(2\pi)^3}\left(\hat{a}(\mathbf{k})f_k'(\tau)\mathrm{e}^{i\mathbf{k}\cdot\mathbf{x}} + \hat{a}^\dagger(\mathbf{k})f_k'^\star(\tau)\mathrm{e}^{-i\mathbf{k}\cdot\mathbf{x}}\right).\end{aligned} \tag{3.8}$$

Here, $\hat{a}^\dagger,\ \hat{a}$ are creation and annihilation operators. Because of isotropy, the mode functions f_k only depend on $k = |\mathbf{k}|$, and f being real further requires that $f_k = f_{-k}$. The creation and annihilation operators are time-independent and satisfy commutation relations

$$\begin{aligned}\left[\hat{a}(\mathbf{k}),\ \hat{a}^\dagger(\mathbf{k}')\right] &= (2\pi)^3\delta^{(3)}(\mathbf{k}-\mathbf{k}'),\\ \left[\hat{a}(\mathbf{k}),\ \hat{a}(\mathbf{k}')\right] &= 0,\\ \left[\hat{a}^\dagger(\mathbf{k}),\ \hat{a}^\dagger(\mathbf{k}')\right] &= 0.\end{aligned} \tag{3.9}$$

This expansion and our convention for the creation and annihilation operators put a constraint on the mode functions in the form of a Wronskian normalisation,

$$f_k(\tau)f_k'^\star(\tau) - f_k^\star(\tau)f_k'(\tau) = i. \tag{3.10}$$

As f_k and $f_k^\star$ are linearly independent (this can be seen from the fact that the Wronskian is nonzero), the mode functions satisfy the same equation of motion as the classical fields. Namely,

$$f_k'' + \omega_k^2\, f_k = 0, \qquad \omega_k^2(\tau) = k^2 + \mu^2(\tau). \tag{3.11}$$

This is the Mukhanov-Sasaki [67–69] equation for f. The time dependence of the curved background induces a time-dependent frequency for the field. As a consequence, the vacuum state can have a non-trivial evolution into an excited state, which can be interpreted as a particle production phenomenon. Indeed, we will see that the field will acquire fluctuations and its modes f_k will be populated.

Let us now specify to the case of an inflationary background. For simplicity, we will assume exact de Sitter expansion with a parametrisation such that the scale factor is given by

$$a(\tau) = \frac{-1}{H_\mathrm{I}\,\tau}, \tag{3.12}$$

JCAP10(2018)022

where we take the scale of inflation $H_{\rm I}$ to be constant and conformal time runs from $\tau \to -\infty$ at the beginning of inflation to $\tau \to -\tau_r$ at the end. Note that, as is customary, in our conventions conformal time is negative during inflation, ensuring that the scale factor is positive, as it should be.

The other ingredient we need to solve the quantum evolution of the field operator is the initial condition for the mode functions, which amounts to choosing a suitable initial vacuum state for our theory. For general time-dependent backgrounds this procedure can be ambiguous, but for an inflationary background there is a preferred choice. The modes start their evolution deep inside the horizon when $\tau \to -\infty$. In this limit, $k/a \gg H_{\rm I}$, which means that the effects of curvature become negligible. Thus, at very early times all the modes start being approximately massless. In this high frequency limit quantisation in de Sitter and Minkowski spaces should be equal. The most common choice of vacuum is to select the positive frequency mode $f_k \propto \mathrm{e}^{-ik\tau}$ as the minimal excitation state. This choice, together with the Wronskian normalisation condition (3.10) sets our initial condition to be

$$f_k(\tau \to -\infty) = \frac{1}{\sqrt{2k}} e^{-ik\tau}. \tag{3.13}$$

In exact de Sitter space, the equation of motion (3.11) for the mode functions together with the initial condition (3.13) has the following solution,

$$f_k(\tau) = \mathrm{e}^{i\frac{\pi}{4}(2\nu+1)} \frac{1}{\sqrt{2k}} \sqrt{\frac{\pi}{2}(-k\tau)}\, H_\nu^{(1)}(-k\tau), \qquad \nu^2 = \frac{9}{4} - 12\xi - \frac{m^2}{H^2}. \tag{3.14}$$

This solution applies as long as $\nu \notin \mathbb{N}$ and agrees with the result in [70]. For the range of values on which we focus in this work, the mass is much smaller than the Hubble scale of inflation, so that we can safely take $\nu^2 \simeq \frac{9}{4} - 12\xi$.

We can now compute the quantum statistics of the field operator. As expected, the expectation value of the field vanishes, $\langle \hat{f} \rangle = 0$. However, the variance of the field receives non-zero quantum fluctuations

$$\langle |\hat{f}|^2 \rangle = \int \frac{\mathrm{d}^3\mathbf{k}}{(2\pi)^3} \left| f_k(\tau) \right|^2 . \tag{3.15}$$

This variance is commonly expressed as a power spectrum for the field.

With the definition (2.6), we can compute the power spectrum of the original field ϕ during inflation, and we obtain

$$\begin{aligned} \mathcal{P}_\phi(k,\tau) &= \frac{1}{a^2(\tau)} \frac{k^3}{2\pi^2} \left| f_k(\tau) \right|^2 \\ &= \left(\frac{H_{\rm I}}{2\pi} \right)^2 (-k\tau)^3 \frac{\pi}{2} \left| H_\nu^{(1)}(-k\tau) \right|^2 . \end{aligned} \tag{3.16}$$

Before we can correctly interpret our results, we have to deal with one usual problem that arises in quantum field theory in curved space-time: the power spectrum (3.16) is UV divergent. Indeed, the variance of the field is dominated by the very small scales, where the power spectrum grows as k^2. However, we expect that modes that are deep inside the horizon are very close to the vacuum state and thus should not dominate the fluctuations. In order to solve this issue, we should look carefully at the energy density of the field and find a suitable regularisation scheme.

3.2 Energy density and regularisation of the power spectrum

As we have a non-minimal coupling to the metric, we have to be careful when deriving the energy density of the field. We start by computing the full stress-energy tensor of ϕ, which is given by

$$\begin{aligned} T^{\phi}_{\mu\nu} &= \frac{-2}{\sqrt{-g}} \frac{\delta\left(\mathcal{L}_{\phi}\sqrt{-g}\right)}{\delta g^{\mu\nu}} \\ &= \xi\phi^2 G_{\mu\nu} + \partial_\mu\phi\partial_\nu\phi - \frac{1}{2}\partial_\alpha\phi\partial^\alpha\phi g_{\mu\nu} - \frac{1}{2}m^2\phi^2 g_{\mu\nu}. \end{aligned} \tag{3.17}$$

Here, $G_{\mu\nu} = R_{\mu\nu} - 1/2\, R\, g_{\mu\nu}$ is the Einstein tensor and $\partial_0 \equiv \partial_t$ is the derivative with respect to physical time. We define the energy density through $\rho_\phi = T^{\phi}_{00}$, and thus

$$\rho_\phi = \frac{1}{2}\left(\partial_t\phi\right)^2 + \frac{1}{2}\frac{1}{a^2}\left|\nabla\phi\right|^2 + \frac{1}{2}m^2\phi^2 + \xi G_{00}\phi^2. \tag{3.18}$$

Let us rewrite this result in terms of the Fourier modes of the field f and using conformal time, so that we can more easily apply our previous results.

$$a^4\rho_\phi = \int \frac{\mathrm{d}^3\mathbf{k}}{(2\pi)^3}\frac{1}{2}\left[\left|f_k'\right|^2 + \left(k^2 + a^2m^2 + (1-6\xi)\,\mathcal{H}^2\right)|f_k|^2 - \mathcal{H}\left(f_k' f_k^\star + f_k'^\star f_k\right)\right]. \tag{3.19}$$

It is possible to substitute the mode function for the field during inflation (3.14) in this expression. We focus on the short wavelength modes. If we place an arbitrary UV cutoff scale Λ, after expanding the Hankel function for large arguments [71] we find

$$a^4\rho_\phi = C_0\Lambda^4 + C_2\mathcal{H}^2\Lambda^2 + C_4\mathcal{H}^4\log\Lambda + \mathcal{O}\big(\Lambda^{-2}\big), \tag{3.20}$$

where C_i are some numerical coefficients that only depend on ν (and m). Each one of these divergences in the energy density can be removed by adjusting the constant term, the Planck mass and the coefficient of the R^2 term in the action, respectively [48]. We can extract a meaningful result for the energy density and the variance of the field after removing the UV divergences in this way.[8] To properly do this, one would need to define a consistent renormalisation scheme including the perturbative expansion of gravity. This task is (of course) beyond the scope of this work. Fortunately, for the purposes of this paper, a simpler regularisation will suffice.

What is observable and relevant for the purposes of dark matter production is the energy density of the field at late times. Deep into the radiation and matter eras, the effect of the gravitational background (the expansion) is weaker, which is made explicit by the fact that $\mathcal{H} \to 0$ in the far future. Thus, when computing the energy density at late times, we can safely neglect the terms that depend on $\mathcal{H}$, which are the ones that can be affected by the regularisation scheme chosen to cure the $\mathcal{H}^2\Lambda^2$ and $\mathcal{H}^4\log\Lambda$ divergences.

Because of this, the one divergence that we really have to care about is the Λ^4 one. As is well know, this one is related to the energy of the quantum vacuum and can be regularised away by a redefinition of the cosmological constant in the action. A computation yields $C_0 = 1/(4\pi^2)$, which corresponds to the usual $k/2$ vacuum energy of each mode in Fourier space. The regularisation is then achieved by subtracting this quantity for every mode at

[8] Of course, this is only a tree-level statement. Including loop corrections would lead to the well-known fact that an infinite number of counterterms are needed. This is the usual result that perturbative quantisation of gravity fails due to the loss of predictivity, and not in any way a particularity of our scenario.

JCAP10(2018)022

the level of the energy density in (3.19). However, we will approach this subtraction from a slightly different perspective. We cure this divergence by removing the corresponding term at the level of the power spectrum[9] of the field with the shift

$$\mathcal{P}_\phi(k,t) \to \mathcal{P}_\phi(k,t) - \frac{1}{2\pi^2}\frac{k^2}{a^2}. \tag{3.21}$$

With this, we can safely write the regularised energy density at late times as

$$\rho(t) = \int \mathrm{d}(\log k)\, \frac{1}{2}\left(\mathcal{P}^{(\mathrm{reg})}_{\partial_t\phi}(k,t) + \left(\frac{k^2}{a^2}+m^2\right)\mathcal{P}^{(\mathrm{reg})}_{\phi}(k,t)\right), \tag{3.22}$$

where the regularised power spectra are obtained by performing the subtraction (3.21) and then dropping all the terms proportional to powers of $\mathcal{H}$. This procedure of regularising the field power spectrum is effectively equivalent to the direct subtraction of the vacuum energy, as the only observable consequence of the power spectrum of the field is precisely its contribution to the energy density.

The regularised power spectrum at the end of inflation is shown in figure 5. The fact that we have not removed the Hubble scale-dependent divergences explains why the power stays constant at small scales. Figure 5 also shows how the power in those UV modes decreases as H^2 after the end of inflation, as expected. This shows that we can obtain a power spectrum and an energy density which are free of divergences at late times.

After being reassured that our quantum computation leads to well-defined observables at late times, we can safely extract the required initial conditions for the classical evolution computed in section 2. For modes well outside the horizon that satisfy $-k\tau \ll H_{\mathrm{I}}$, we can Taylor expand the regularised version of (3.16) to obtain the approximate expression[10]

$$\mathcal{P}^{(\mathrm{reg})}_{\phi}(k,t) \simeq \mathcal{P}^{(\mathrm{reg})}_{\phi_0}(k)\ \left(\frac{k}{a(t)H_{\mathrm{I}}}\right)^{3-2\nu}, \tag{3.23}$$

where

$$\mathcal{P}^{(\mathrm{reg})}_{\phi_0}(k) = \left(\frac{H_{\mathrm{I}}}{2\pi}\right)^2 \frac{2^{2\nu-1}\Gamma^2(\nu)}{\pi} \tag{3.24}$$

is the power spectrum at horizon exit. This is precisely the initial condition that we use for the classical evolution of the field in section 2. Moreover, note that the result (3.23), valid in the region labelled (I) in figure 1, matches the classical result obtained in (2.13) (we remind the reader that $\alpha_- = 3-2\nu$).

From now on, we drop the superscript (reg) and it should be understood that we are always dealing with regularised power spectra. Of course, it should also be understood that all the quantities with which we deal in section 2 are regularised and free of divergencies.

A further comment is in order. As mentioned in section 2.3 we usually do not account for the rapid oscillations of ϕ and in consequence $\mathcal{P}_\phi(k)$, but instead only consider the envelope (for which we use the same symbol). Moreover, in section 2 we use the simpler eq. (2.25) instead of eq. (3.22) to calculate the energy density, where the former only includes the last

[9] Note that this transformation leaves $\mathcal{P}_{\partial_t\phi}$ unchanged up to factors proportional to powers of $\mathcal{H}$, which we drop at late times.

[10] Note that regularisation has a negligible effect in the power spectrum for superhorizon modes, as required.

term of the latter. At late times this follows from the virial theorem. Averaging the energy density over (at least) one oscillation we have

$$\langle\dot{\phi}^2\rangle = \langle(m^2+k^2)\phi^2\rangle = \frac{1}{2}(m^2+k^2)\phi^2_{\rm amp}, \tag{3.25}$$

where $\phi_{\rm amp}$ gives the amplitude that is specified by the enveloping function of $\mathcal{P}_\phi(k)$. Inserting this into eq. (3.22) we obtain eq. (2.25).

3.3 End of inflation and radiation domination era

In exact de Sitter expansion, the solution (3.14) holds exactly. However, inflation is only an approximate de Sitter era.

Firstly, we know that, at least during the epoch when the scales observable in the CMB leave the horizon, the Hubble parameter varies slightly with time. We nevertheless ignore this effect in our derivation, the reason being that we are particularly interested in modes around $k_\star$ that exit the horizon much later than the ones observable in the CMB. There is very little observational guidance to how the Hubble parameter behaves at the epoch relevant for those modes. Rather than extrapolating the value of the spectral index orders of magnitude away from the region where it is measured, we opt for the simplest assumption of a constant Hubble scale of inflation. In section 4 we will nevertheless discuss how this effect could be incorporated into our results.

Secondly, inflation has to end at some point so that the Universe can be reheated. As a first approximation, we will assume that this process happens very quickly when the inflating Universe reaches a size a_r. After that moment, we assume that the Universe enters an era where the relativistic decay products of the inflation dominate the background energy density. In our parametrisation, inflation ends at conformal time $-\tau_r$, with $\tau_r = 1/(a_r H_{\rm I})$, and the equation of state of the Universe suddenly changes from $\omega = -1$ to $\omega = 1/3$.

The solution (3.14) is thus only valid for $\tau < -\tau_r$. For $\tau > -\tau_r$, we have to solve the mode equation (3.11) for a radiation dominated expansion. Then, the time-dependent frequency simplifies to $\omega_k^2 = k^2 + a^2 m^2$, as the Ricci scalar is zero in the radiation era. If we assume that the modes are relativistic at that time (this assumption is justified *a posteriori*), then $\omega_k^2 \simeq k^2$ becomes time-independent and we can easily solve the mode equation to obtain the outgoing vacuum mode function

$$v_k^{(\rm out)}(\tau) = \frac{1}{\sqrt{\omega_k}} {\rm e}^{i(\tau+\tau_r)\omega_k}, \qquad \tau > -\tau_r. \tag{3.26}$$

The incoming wave function can thus be expanded after reheating via a Bogolyugov transformation as

$$\begin{aligned} f_k(\tau) &= \alpha_k^\star v_k^{(\rm out)}(\tau) + \beta_k^\star v_k^{\star(\rm out)}(\tau) \\ &= \frac{1}{\sqrt{\omega_k}}\left(\alpha_k^\star {\rm e}^{i(\tau+\tau_r)\omega_k} + \beta_k^\star {\rm e}^{-i(\tau+\tau_r)\omega_k}\right), \qquad \tau > -\tau_r. \end{aligned} \tag{3.27}$$

We can extract the Bogolyugov coefficients by requiring continuity of the mode function and its first derivative at $\tau = -\tau_r$. The result is

$$\begin{aligned} \alpha_k^\star &= {\rm e}^{i\frac{\pi}{4}(2\nu+1)}\frac{\sqrt{2\pi}}{4}\sqrt{k\tau_r}\left[\left(1 - i\frac{(\nu+1/2)}{k\tau_r}\right)H_\nu^{(1)}(k\tau_r) + iH_{\nu+1}^{(1)}(k\tau_r)\right], \\ \beta_k^\star &= {\rm e}^{i\frac{\pi}{4}(2\nu+1)}\frac{\sqrt{2\pi}}{4}\sqrt{k\tau_r}\left[\left(1 + i\frac{(\nu+1/2)}{k\tau_r}\right)H_\nu^{(1)}(k\tau_r) - iH_{\nu+1}^{(1)}(k\tau_r)\right]. \end{aligned} \tag{3.28}$$

JCAP10(2018)022

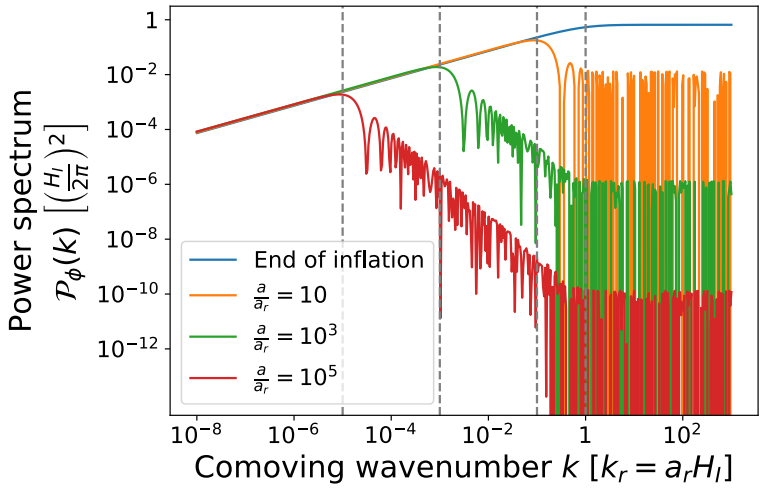

Figure 5. Power spectrum of the field while the modes are still relativistic, as a function of the wavenumber normalised to the Hubble radius at the end of inflation, $k_r^{-1} = (a_r H_\mathrm{I})^{-1}$ (note that this normalisation is different to the one in figures 2 and 4). The solid lines depict the power spectrum right at the end of inflation and at different moments during radiation domination. The dashed vertical lines depict the comoving Hubble radius at the end of inflation and each later moment, respectively from right to left. A value of $\nu = 5/4$ (equivalently $\alpha_- = 1/2$) is chosen here, corresponding to a non-minimal coupling $\xi \simeq 0.06$.

The fact that $|\alpha_k|^2 - |\beta_k|^2 = 1$ ensures that the normalisation condition (3.10) is still satisfied. The mode function that we have derived is valid while radiation domination lasts and as long as the modes are relativistic.

The power spectrum in the radiation era can then be expressed[11] as

$$\mathcal{P}_\phi(k,a) = 2\left(\frac{H_\mathrm{I}}{2\pi}\right)^2\left(\frac{a_r}{a}\right)^2\left(\frac{k}{a_r H_\mathrm{I}}\right)^2\left[2\,|\beta_k|^2 + 2\mathrm{Re}\left(\alpha_k^\star\,\beta_k\,\mathrm{e}^{2i\frac{k}{a_r H_\mathrm{I}}\left(\frac{a}{a_r}+1\right)}\right)\right]. \tag{3.29}$$

This power spectrum is depicted in figure 5 at different moments of the radiation dominated era, starting right after inflation. Wavelengths larger than $k_r^{-1} \equiv (a_r H_\mathrm{I})^{-1}$ exit the horizon at some point during inflation and are excited, while shorter wavelengths that stay inside the horizon do not receive large fluctuations. The power decreases at very large scales because of the suppression arising from the effective mass during inflation due to the non-minimal coupling. This means that right after inflation, the power spectrum is peaked at the scale k_r^{-1}. Later on, as modes reenter the horizon during radiation domination, they start to oscillate and their amplitude is damped, while superhorizon modes are still frozen. The consequence is that the peak in the power spectrum shifts towards larger scales. This will continue as long as all the modes involved are relativistic, which means that the final position of the peak will be at the scale which reenters the horizon at the same time as it becomes non-relativistic, which happens when $H(a_\star) = m$. Note that the suppression for small-scale modes in figure 5 is steeper than in figure 2. This is due to the fact that figure 5 depicts the power spectrum at early times $a \ll a_\star$, and thus the modes inside the Hubble radius are still relativistic. After

[11] In this expression we have already removed the contribution of the vacuum energy, as discussed in section 3.2.

$a_\star$, these subhorizon small-scale modes start becoming non-relativistic and the final shape figure 2 is attained (this becomes clearer by looking at the evolution outlined in figure 1).

It is possible to make analytical approximations of the power spectrum (3.29) for the modes with $k \ll k_r$, that is, modes that were well outside the Hubble radius at the end of inflation. We can distinguish two regimes, depending on wether the modes have already reentered the horizon during radiation domination or not. If they have, we can average out the oscillating terms and find

$$\mathcal{P}_\phi(k,\tau) \simeq \left(\frac{H_\mathrm{I}}{2\pi}\right)^2 \frac{1}{\pi}\, 2^{2(\nu-1)}\Gamma^2(\nu)\,(\nu-1/2)^2 \left(\frac{k}{a_r H_\mathrm{I}}\right)^{1-2\nu} \left(\frac{a_r}{a(\tau)}\right)^2 , \tag{3.30}$$

which is valid if $k \gg aH$. In this expression, the damping of the power with the scale factor is manifest in the last factor and matches the result (2.17) corresponding to region (IV) in figure 1. In the opposite limit, $k \ll aH$, the modes are still superhorizon and an expansion of the oscillating functions for small arguments gives

$$\mathcal{P}_\phi(k,\tau) \simeq \left(\frac{H_\mathrm{I}}{2\pi}\right)^2 \frac{1}{\pi}\, 2^{2\nu-1}\Gamma^2(\nu)\,(\nu-1/2)^2 \left(\frac{k}{a_r H_\mathrm{I}}\right)^{3-2\nu} , \tag{3.31}$$

confirming that the amplitude of these long wavelength modes is constant as long as they remain superhorizon (regions (II) and (III) in figure 1).

Let us recapitulate: in this section we have seen how a light scalar field which is non-minimally coupled to gravity acquires quantum fluctuations that can grow large during inflation. We have been careful to study the UV divergences that arise and we have extracted a regularised, physically meaningful power spectrum. Interestingly, the existence of the non-minimal coupling suppresses the magnitude of superhorizon modes during inflation, meaning that the amplitude of the power spectrum decreases on very large scales. We have seen that when the modes reenter the horizon after inflation, they start to oscillate and their amplitude is also damped. These effects result in a power spectrum which is peaked at some intermediate scale. This quantum analysis complements the classical study done in section 2, in particular giving the right initial conditions for the classical evolution. It also justifies the phenomenological results in section 2, showing that they are firmly grounded and independent of the particular UV physics that is necessary to make sense of the full quantum theory.

4 Conclusions

4.1 Summary

In this work, we have shown that in one of the simplest extensions of general relativity, i.e. general relativity plus a non-minimally coupled scalar field, the scalar field can acquire a relic density sufficient to account for the totality of the dark matter observed in our Universe. In our scenario, dark matter is produced during inflation by purely gravitational means independently of any couplings to other fields that could be present. As shown in figure 3, for small values of the non-minimal coupling constant $\xi \lesssim 0.1$ together with masses above ~ 1 eV, high-scale inflation naturally yields the right relic abundance. For lower inflation scales and similar non-minimal couplings significantly higher masses are viable, e.g. $m \sim 10\,\mathrm{keV}$ for $H_\mathrm{I} \sim 3 \cdot 10^{12}\,\mathrm{GeV}$.

This scenario does not rely on any initial conditions, and the only necessary requirement is for the field to be present during the inflationary era. The reason for this is that the energy density is entirely produced from the quantum fluctuations of the scalar field, which are

JCAP10(2018)022

amplified during inflation due to the strong time dependence of the scale factor. Such fluctuations are suppressed on the largest scales due to the presence of the non-minimal coupling. In the regime that we consider, the non-minimal coupling essentially acts as an effective mass term for the field of the order of the Hubble parameter during inflation. At a later stage of the evolution during radiation domination, the fluctuations on small scales are also suppressed due to the fact that the modes are still relativistic when they reenter the horizon and oscillate with damped amplitude. The interplay of these two effects can be intuitively understood by looking at figure 1. The resulting energy density power spectrum is depicted in figure 4. The main feature is that it is peaked at some intermediate scale $k_\star^{-1}$ given by (2.23), which means that the energy density is mainly stored in clumps of typical comoving size $k_\star^{-1}$. Compared to a treatment of the field as quasi-homogeneous [2, 46] there are two implications. The first is the presence of additional small scale substructure (similar to the vector case [1]). Secondly, the suppression of the relativistic higher momentum modes during the radiation dominated era leads to an overall reduction in the dark matter density for a given mass and inflation scale. In consequence, sufficient dark matter production requires somewhat higher masses.

An important observation is that this scenario predicts that the density perturbations of the dark matter are of isocurvature type, as they are uncorrelated with the perturbations in the other fluids. However, these fluctuations are only large at intermediate scales close to $k_\star^{-1} \sim 4 \times 10^7\,\mathrm{km}$, while their amplitude is suppressed at the very large scales relevant for cosmological observables such as the CMB (cf. [1, 2, 46]). Indeed, this suppression can be large enough for the power spectrum to fall below the stringent constraints set by the Planck satellite, as computed in section 2.4 and summarised in figure 3.

While the quantum fluctuations lead to UV divergences, we have argued that they can be absorbed into the parameters of the Lagrangian such as the cosmological constant. We have provided a definition of the energy density that is compatible with this regularisation and thus free of divergences. The amount of dark matter is finite.

4.2 Discussion

In this paper, we have focused on the basics of the mechanism and the generation of dark matter, leaving the study of the interesting phenomenology associated with the scenario for future work. However, we would like to briefly comment on some interesting points.

As was stated in section 3.3, in our derivation we have assumed a constant Hubble parameter during inflation. It is nevertheless easy to see that our results remain qualitatively unchanged if we allow for a small time variation of it. In particular, a slowly decreasing H, as a constant spectral index $n_s < 1$ hints, amounts to a constant tilt of the power spectrum, increasing towards larger scales. This can be compensated with a slight shift towards larger values of the non-minimal coupling ξ, after which all of our conclusions remain valid. Of course, there is no reason to assume that the spectral index remains constant beyond the scales probed by the Planck satellite. However, without observational guidance that could provide a preference for any particular behaviour, this issue, though potentially very rich in terms of physical consequences, lies beyond the scope of this work.

A natural question that arises has to do with the detectability and stability of the dark matter in this scenario. It is in principle possible to consider direct couplings of the scalar to other fields. This opens up many possibilities and would require an extensive study. Also note that in principle the action (2.1) allows for a $\mathbb{Z}_2$ symmetry $\phi \to -\phi$ which would forbid decay-inducing couplings. We may nevertheless assume that gravity does not preserve this

$\mathbb{Z}_2$ symmetry.[12] In such a case ϕ could undergo gravity-mediated decay. The most relevant decay channels for the mass range discussed in this paper are decays to photons or light fermions. For the decay to two photons, mediated by the operator $\frac{\phi}{M_{\rm Pl}}F_{\mu\nu}F^{\mu\nu}$, the rate can be estimated as $\Gamma \sim m^3/64\pi M_{\rm Pl}^2$. If we require that the lifetime of the dark matter is longer than the age of the Universe, we get the limit $m \lesssim 0.1$ GeV. The decay to two fermions can arise from the operator $\frac{\phi}{M_{\rm Pl}}\bar{f}Hf$, where after electroweak symmetry breaking the Higgs is replaced by its vacuum expectation value $v \simeq 246$ GeV. With this, we estimate the decay rate as $\Gamma \sim N_{\rm c} v^2 m/16\pi M_{\rm Pl}^2$, assuming that the scalar is much heavier than the fermions. This can give a much larger decay rate than the one to two photons. In particular, any scalar heavier than ~ 1 eV would be cosmologically unstable due to the decay to neutrinos. However, the operator that we wrote down for the decay to two fermions is probably too simplistic. For instance, it seems plausible that the operator comes with an appropriate Yukawa factor (for all we know, the fermions always couple to the Higgs this way).[13] This would mean that the rate would go as $m_f^2\, m$ instead of $v^2\, m$, thus suppressing the decay to the lighter fermions. In this case, it is easy to see that a potential decay to two photons becomes the dominant one for any scalar mass. This stability estimate is shown in figure 3 but should only be taken as an indication and not as a strong bound, given the arguments presented above.

In contrast to the lack of precise predictions regarding the non-gravitational interactions, the mechanism has potentially interesting cosmological signatures. A first feature is the potential presence of a small component of isocurvature fluctuations also at large scales. This could be detectable[14] in the vicinity of the boundary of the red region in figure 3. The main feature is that the bulk of the energy density is contained in substructures whose characteristic comoving size, as long as they follow the Hubble flow, is $k_\star^{-1}$. However, as these overdensities are very large (the value of the power spectrum at the peak is close to $\mathcal{O}(1)$), it is likely that they decouple from the expansion and form bound structures very early. Indeed, the authors of [80] (see also [81]) showed that this decoupling can happen around matter-radiation equality. The characteristic size of these bound structures is then

$$\ell_{\rm today} \simeq \frac{1}{z_{\rm eq}} k_\star^{-1} \simeq 10^4\,{\rm km}\,\sqrt{\frac{\rm eV}{m}}. \tag{4.1}$$

These small-scale overdensities are similar to the ones described in [1] and also present some resemblance with the *axion miniclusters* that are predicted to form (under some assumptions) if a cosmological population of QCD axions exists in our Universe [60, 61]. Although they are probably too small to affect the formation of large scale structures in any significant way, they could have interesting signatures in gravitational lensing [82, 83], astrophysical processes [84, 85] and in direct [86] and indirect detection experiments, in the case where additional couplings to Standard Model fields exist. In particular, at larger masses, indirect detection signatures, e.g. coming from an annihilation of dark matter particles, could be enhanced due to the clumpiness.

[12] It is conjectured that gravity breaks all continuous global symmetries [72–75], but discrete symmetries can remain unbroken [76, 77].

[13] This is exactly the case if the decay is induced by a linear coupling of ϕ to the Ricci scalar, as was considered in [78, 79].

[14] In the most recent Planck analysis [51], the collaboration has studied a scenario (called "axion II") that is applicable to our isocurvature spectrum. Intriguingly the data seems to have a very slight preference for the presence of non-vanishing isocurvature fluctuations.

JCAP10(2018)022

Acknowledgments

The authors would like to thank J. Berges, A. Chatrchyan, J. Rubio and G. Ballesteros for interesting discussions. This project has received funding from the European Union's Horizon 2020 research and innovation programme under the Marie Sklodowska-Curie grant agreement No 674896 (ITN ELUSIVES).

A Einstein and Jordan frame dynamics

The action in the form presented in (2.1) is written in the Jordan frame where the Planck mass depends on the value of the scalar field. This is in contrast to the Einstein frame, where all the couplings to gravity are canonically normalised. Both frames are related by a conformal transformation of the metric (cf., e.g., [87]). Starting from the Jordan frame metric g, we can get to the Einstein frame one $\tilde{g}$ by means of the transformation

$$g_{\mu\nu} \to \tilde{g}_{\mu\nu} = \Omega^2(x) g_{\mu\nu}, \quad \text{where} \quad \Omega^2(x) = \frac{1}{M_{\rm Pl}^2}\left(M^2 - \xi\phi^2\right). \tag{A.1}$$

Under such a transformation, we have that

$$\begin{aligned} g^{\mu\nu} &\to \tilde{g}^{\mu\nu} = \Omega^{-2} g_{\mu\nu} \\ \sqrt{|g|} &\to \sqrt{|\tilde{g}|} = \Omega^4 \sqrt{|g|} \\ R &\to \tilde{R} = \Omega^{-2} R - 6\Omega^{-3}\Box\Omega. \end{aligned} \tag{A.2}$$

Our action then becomes

$$\begin{aligned} S = \int \mathrm{d}^4x \sqrt{|\tilde{g}|} \Bigg(& \frac{1}{2} M_{\rm Pl}^2 \tilde{R} + \frac{1}{\Omega^4} \tilde{\mathcal{L}}_{\rm back}\left(\phi, \sigma_i\right) \\ & - \frac{1}{2}\left(\frac{1}{\Omega^2} - \frac{6\xi^2\phi^2}{M_{\rm Pl}^2\Omega^4}\right) \tilde{g}^{\mu\nu}\partial_\mu\phi\partial_\nu\phi - \frac{1}{2\Omega^4} m^2\phi^2 \Bigg), \end{aligned} \tag{A.3}$$

where $\tilde{\mathcal{L}}_{\rm back}$ is the transformed version of the background Lagrangian accounting for all the other fields, including the Standard Model ones. It may now also depend on ϕ due to the form of the transformation (A.1).

This shows that in the Einstein frame, where the coupling to gravity is minimal, non-canonical kinetic terms for the fields ϕ and σ_i arise. We can nevertheless canonically normalise the field ϕ by performing a field redefinition to a new field φ, given by

$$\frac{\mathrm{d}\varphi}{\mathrm{d}\phi} = \sqrt{\frac{1}{\Omega^2} - \frac{6\xi^2\phi^2}{M_{\rm Pl}^2\Omega^4}}. \tag{A.4}$$

In terms of φ, the action reads

$$S = \int \mathrm{d}^4x \sqrt{|\tilde{g}|} \left(\frac{1}{2} M_{\rm Pl}^2 \tilde{R} + \frac{1}{\Omega^4} \tilde{\mathcal{L}}_{\rm back}\left(\varphi, \sigma_i\right) - \frac{1}{2}\partial_\mu\varphi\partial^\mu\varphi - \frac{1}{2\Omega^4} m^2\phi^2(\varphi) \right). \tag{A.5}$$

In general we cannot neglect the backreaction of the non-minimal coupling on the metric. However, if we are dealing with a not too large coupling constant ξ and subplanckian field

values $\phi \ll M_{\rm Pl}$, then these effects are expected to be small. Indeed, in this regime we have that $M \simeq M_{\rm Pl}$ and we can approximate

$$\begin{aligned} \Omega^2 &\simeq 1 - \xi \left(\frac{\phi}{M_{\rm Pl}}\right)^2, \\ \varphi &= \phi \left[1 + \frac{3}{2}(1-6\xi)\xi \left(\frac{\phi}{M_{\rm Pl}}\right)^2 + \mathcal{O}\left(\left(\frac{\phi}{M_{\rm Pl}}\right)^4\right)\right]. \end{aligned} \tag{A.6}$$

This shows that backreaction effects on the metric appear at higher orders in the $\phi/M_{\rm Pl}$ expansion. To first order only the dynamics of the non-minimally coupled field ϕ will be affected. One may wonder where the effect on the field φ is encoded. As will become clear in the example below, this arises from the second term in (A.6). Expanding the action in φ, an additional mass term for the field appears that is proportional to the density. For sufficiently high density/Hubble scale this term can be bigger than m^2, significantly altering the evolution of the field.

Let us now study a specific example for the background Lagrangian $\mathcal{L}_{\rm back}$. We set our metric to be a flat FLRW one,

$$\mathrm{d}s^2 = -\mathrm{d}t^2 + a^2(t)\left(\mathrm{d}x^2 + \mathrm{d}y^2 + \mathrm{d}z^2\right). \tag{A.7}$$

With this particular choice of geometry, the Ricci scalar reads

$$R = 6\left(\dot{H} + 2H^2\right) = 3\left(1 - 3\omega\right)H^2, \tag{A.8}$$

where the dot denotes a time derivative, $H = \dot{a}/a$ is the Hubble parameter and the last equality is valid if the Universe is dominated by a perfect fluid with equation of state $\omega = P/\rho$, being P and ρ its pressure and energy density, respectively.

A.1 Background dominated by a cosmological constant

We assume that the background is dominated by some form of vacuum energy or cosmological constant Λ, which we parametrise as usual by

$$\mathcal{L}_{\rm back} = -\Lambda M_{\rm Pl}^2. \tag{A.9}$$

(a) *Jordan frame:* it is well known that a cosmological constant makes the Universe expand exponentially fast,

$$a(t) = a_0 \mathrm{e}^{Ht}, \quad \text{with} \quad H^2 = \frac{\Lambda}{3} = \text{const.} \tag{A.10}$$

The curvature in this scenario is $R = 12H^2$, and the equation of motion for ϕ reads

$$\ddot{\phi} + 3H\dot{\phi} + \left(m^2 + 12\xi H^2\right)\phi = 0. \tag{A.11}$$

We see that in this frame the non-minimal coupling introduces an effective mass term for the scalar field, $m_{\rm eff}^2 = m^2 + 4\xi\Lambda$. The solution to the equation of motion is

$$\phi(t) = C_+ \mathrm{e}^{-\frac{\alpha_+}{2}Ht} + C_- \mathrm{e}^{-\frac{\alpha_-}{2}Ht}, \tag{A.12}$$

where

$$\alpha_\pm = 3 \pm \sqrt{9 - 48\xi - 4\left(\frac{m}{H}\right)^2}. \tag{A.13}$$

JCAP10(2018)022

If $C_- \neq 0$, the second term in (A.12) dominates at late times. The condition to have a growing mode is

$$\alpha_- < 0 \quad \Leftrightarrow \quad \xi < -\frac{m^2}{4\Lambda}. \tag{A.14}$$

If this is satisfied, the field value grows exponentially. The reason is that in this range of negative couplings the effective mass $m^2_{\rm eff}$ becomes negative and we have a runaway potential for the field ϕ. In the main text we are interested in $\xi > 0$ so this does not happen there.

(b) *Einstein frame:* after the conformal transformation $g_{\mu\nu} \to \hat{g}_{\mu\nu} = \Omega^2 g_{\mu\nu}$ and the field redefinition $\phi \to \varphi$ that have already been described, we get to the Einstein frame action, where the coupling to gravity is minimal and the scalar field is canonically normalised. Next we expand the action only keep leading terms in the $\varphi/M_{\rm Pl}$ expansion, as we are assuming that the field is subplanckian. The resulting action is

$$S = \int {\rm d}^4x\sqrt{|\tilde{g}|}\left[\frac{1}{2}M^2_{\rm Pl}\tilde{R} - \Lambda M^2_{\rm Pl} - \frac{1}{2}\partial_\mu\varphi\partial^\mu\varphi - \frac{1}{2}\left(m^2 + 4\xi\Lambda\right)\varphi^2 + \mathcal{O}\left(\varphi^4\right)\right]. \tag{A.15}$$

Identifying $\Lambda = 3H^2$ we recover the same equation of motion that we had in the Jordan frame. Of course, if φ takes values close to the Planck scale our expansion in terms of $\varphi^2/M^2_{\rm Pl}$ breaks down and an exact treatment is required.

This example shows that it is reasonable to ignore backreaction effects and work directly in the Jordan frame without modifying the Einstein's equations, as long as we are only dealing with subplanckian field values. We have explicitly checked that this also holds for a background energy dominated by an additional scalar field.

B Power spectra

B.1 Field power spectrum

In this appendix, we present the calculations of the power spectra in a bit more detail. The most useful tool for this will be figure 1, where the solution of the equation of motion for the modes in each regime is summarised. Tracking the evolution of the modes in horizontal lines from left to right in that figure, we can obtain the late-times power spectrum as

$$\mathcal{P}_\phi(k,t_0) = \begin{cases} \mathcal{P}_{\phi_0}\left(\dfrac{a_{\rm r}}{k/H_{\rm I}}\right)^{-\alpha_-}\left(\dfrac{a_0}{k_\star/m}\right)^{-3}, & k < k_\star, \\ \mathcal{P}_{\phi_0}\left(\dfrac{a_{\rm r}}{k_\star/H_{\rm I}}\right)^{-\alpha_-}\left(\dfrac{a_0}{k_\star/m}\right)^{-3}, & k = k_\star, \\ \mathcal{P}_{\phi_0}\left(\dfrac{a_{\rm r}}{k/H_{\rm I}}\right)^{-\alpha_-}\left(\dfrac{k/m}{H_{\rm I}a^2_{\rm r}/k}\right)^{-2}\left(\dfrac{a_0}{k/m}\right)^{-3}, & k > k_\star, \end{cases} \tag{B.1}$$

with $k_\star$ as defined in (2.23). To obtain this, we have assumed a standard cosmology with an instantaneous transition from inflation to radiation domination. We can use the mode $k_\star$ as a reference and write the amplitude of the other modes with respect to it,

$$\mathcal{P}_\phi(k,t_0) = \begin{cases} \mathcal{P}_\phi(k_\star,t_0)\cdot\left(\dfrac{k}{k_\star}\right)^{\alpha_-}, & k \leq k_\star, \\ \mathcal{P}_\phi(k_\star,t_0)\cdot\left(\dfrac{k}{k_\star}\right)^{\alpha_- - 1}, & k \geq k_\star. \end{cases} \tag{B.2}$$

This confirms that, as long as $0 < \alpha_- < 1$, the power spectrum is peaked at the scale $k_\star^{-1}$, as shown in figure 2. The next step is to evaluate the overall normalisation of the power spectrum, which we do by computing the amplitude of the mode $k_\star$. For that, we make use of the definition $k_\star = a_\star m$, together with the fact that during the radiation era, $H \propto a^{-2}$. We find

$$\begin{aligned}\mathcal{P}_\phi(k_\star, t_0) &= \mathcal{P}_{\phi_0} \left(\frac{H_\mathrm{I}}{m}\right)^{-\alpha} \left(\frac{a_\mathrm{r}}{a_\star}\right)^{-\alpha} \left(\frac{a_\mathrm{eq}}{a_\star}\right)^{-3} \left(\frac{a_0}{a_\mathrm{eq}}\right)^{-3} \\ &= \frac{3^{\frac{1}{2}(3+\alpha_-)} F(\alpha_-)}{2^{\frac{11}{4}}\pi^2} \frac{[\mathcal{F}(T_\star)]^{1+\frac{1}{3}\alpha_-}}{[\mathcal{F}(T_\mathrm{r})]^{\frac{1}{3}\alpha_-}} H_\mathrm{I}^{\frac{1}{2}(4-\alpha_-)} m^{-\frac{1}{2}(3-\alpha_-)} H_\mathrm{eq}^{\frac{3}{2}} \left(\frac{a_0}{a_\mathrm{eq}}\right)^{-3}.\end{aligned} \tag{B.3}$$

Here, we have used the result of the primordial power spectrum (2.11) at the time when the mode leaves the horizon. We have also assumed that the comoving entropy $s = a^3 S$ is conserved since the beginning of the radiation era and until present time. This results in the presence of the function [13]

$$\mathcal{F}(T) = \left(\frac{g_\star(T)}{3.36}\right)^{\frac{3}{4}} \cdot \left(\frac{g_{\star S}(T)}{3.91}\right)^{-1}, \tag{B.4}$$

which depends on the number of relativistic degrees of freedom and is always of order $\mathcal{O}(1)$ within the temperature range of interest, assuming Standard Model degrees of freedom.

B.2 Relic abundance

We now move to the computation of the dark matter abundance. We can substitute the result eq. (B.3) into the expression for the energy density at late times (2.25) to find (using $\mathrm{d}(\log k) = \mathrm{d}k/k$),

$$\rho_\phi(t_0) = \frac{1}{2} m^2 \mathcal{P}_\phi(k_\star, t_0) \left(\int_{\frac{k_\mathrm{min}}{k_\star}}^{1} \mathrm{d}x\, x^{\alpha_- - 1} + \int_1^{\frac{k_\mathrm{max}}{k_\star}} \mathrm{d}x\, x^{\alpha_- - 2} \right). \tag{B.5}$$

Here we have explicitly kept the limits of integration. These are essentially set by the duration of inflation. The largest scale corresponds to the size of the Universe, $k_\mathrm{min} \sim a_0 H_0$, which would be undistinguishable from a homogeneous contribution.[15] The smallest scale is determined by the Hubble radius at the end of inflation, $k_\mathrm{max} \sim a_\mathrm{r} H_\mathrm{I}$, where we cut off the power spectrum. In general, we have that $k_\mathrm{min} \ll k_\star \ll k_\mathrm{max}$. In the main text we consider $0 < \alpha_- < 1$ where the integral is convergent on both ends and we can safely put the lower integration limit to 0 and the upper one to ∞. Let us nevertheless have a brief look at all possible cases.

It is more useful and illuminating to express the result in terms of the density parameter $\Omega_\phi \equiv \rho_\phi / \rho_\mathrm{crit}$, and compare it with the observed dark matter density. Depending on the value of α_-, we have different regimes:

- If $\alpha = 0 \Leftrightarrow \xi = 0$, we recover the minimally coupled case, where the power spectrum is flat at large scales. The energy density is dominated by the lower limit of the integral, that is, the homogeneous mode:

$$\frac{\Omega_\phi}{\Omega_\mathrm{CDM}} \simeq \frac{m^2 \mathcal{P}_\phi(k_\star, t_0)}{3 H_\mathrm{eq}^2 M_\mathrm{Pl}^2} \left(1 - \log\left(\frac{k_\mathrm{min}}{k_\star}\right)\right). \tag{B.6}$$

[15] See [31, 32] for a way to use this as the actual source of dark matter.

JCAP10(2018)022

- If $0 < \alpha < 1 \Leftrightarrow 0 < \xi \lesssim 0.1$, the power spectrum is peaked at the intermediate scale $k_\star^{-1}$. The result is in this case independent of both lower and upper cutoffs of the power spectrum:

$$\frac{\Omega_\phi}{\Omega_{\rm CDM}} \simeq \frac{m^2 \mathcal{P}_\phi(k_\star, t_0)}{3H_{\rm eq}^2 M_{\rm Pl}^2} \frac{1}{\alpha_-(1-\alpha_-)}. \tag{B.7}$$

- If $\alpha = 1 \Leftrightarrow \xi \simeq 0.1$, the power spectrum is flat for large momenta above $k_\star$, and the energy density is logarithmically sensitive to the UV cutoff:

$$\frac{\Omega_\phi}{\Omega_{\rm CDM}} \simeq \frac{m^2 \mathcal{P}_\phi(k_\star, t_0)}{3H_{\rm eq}^2 M_{\rm Pl}^2} \left(1 + \log\left(\frac{k_{\rm max}}{k_\star}\right)\right). \tag{B.8}$$

- If $\alpha > 1 \Leftrightarrow \xi \gtrsim 0.1$, the power spectrum is dominated by large momenta, and most of the energy is stored at the UV cutoff:

$$\frac{\Omega_\phi}{\Omega_{\rm CDM}} \simeq \frac{m^2 \mathcal{P}_\phi(k_\star, t_0)}{3H_{\rm eq}^2 M_{\rm Pl}^2} \frac{1}{(\alpha_- - 1)} \left(\frac{k_{\rm max}}{k_\star}\right)^{\alpha_- - 1}. \tag{B.9}$$

In the main text we focus on the second of these four cases, corresponding to a power spectrum peaked at intermediate scales. The observable results being independent of the details of the beginning and the end of inflation is particularly appealing and allows us to make statements that do not rely on the specific choice of inflationary model.

B.3 Energy density power spectrum

In the previous section we have computed the mean energy density in the field ϕ, but we are also interested in the statistics of its spatial distribution. The spatial fluctuations of the energy density with respect to the mean value can be encoded in the density contrast δ, defined by

$$\rho(\mathbf{x}) = \langle\rho\rangle\,(1 + \delta(\mathbf{x}))\,. \tag{B.10}$$

The density contrast is a random field, and as such we can compute its power spectrum. In momentum space, we can write

$$\delta(\mathbf{k}) = \frac{1}{\langle\phi^2\rangle} \int \frac{{\rm d}^3\mathbf{q}}{(2\pi)^3} \phi(\mathbf{q})\phi(\mathbf{k}-\mathbf{q}). \tag{B.11}$$

As expected, we can check that its expectation value vanishes,

$$\begin{aligned} \langle\delta(\mathbf{k})\rangle &= \frac{1}{\langle\phi^2\rangle} \int \frac{{\rm d}^3\mathbf{q}}{(2\pi)^3} \langle\phi(\mathbf{q})\phi(\mathbf{k}-\mathbf{q})\rangle \\ &= \frac{2\pi^2}{\langle\phi^2\rangle} \int \frac{{\rm d}^3\mathbf{q}}{q^3} \mathcal{P}_\phi(q)\delta^{(3)}(\mathbf{k}) \\ &= 0 \qquad \text{if } k \neq 0. \end{aligned} \tag{B.12}$$

To get to the second line, we have used the definition of the power spectrum and the fact that $\phi(\mathbf{x})$ is real, and thus $\phi^\star(\mathbf{k}) = \phi(-\mathbf{k})$. The two point function does not vanish. We can

compute it using Wick's theorem in the following way

$$\begin{aligned}
\langle\delta(\mathbf{k})\delta(\mathbf{k}')\rangle &= \frac{1}{\langle\phi^2\rangle^2}\int\frac{\mathrm{d}^3\mathbf{q}}{(2\pi)^3}\frac{\mathrm{d}^3\mathbf{q}'}{(2\pi)^3}\langle\phi(\mathbf{q})\phi(\mathbf{k}-\mathbf{q})\phi(\mathbf{q}')\phi(\mathbf{k}'-\mathbf{q}')\rangle \\
&= \frac{1}{\langle\phi^2\rangle^2}\int\frac{\mathrm{d}^3\mathbf{q}}{(2\pi)^3}\frac{\mathrm{d}^3\mathbf{q}'}{(2\pi)^3}\begin{bmatrix}\langle\phi(\mathbf{q})\phi(\mathbf{k}-\mathbf{q})\rangle\langle\phi(\mathbf{q}')\phi(\mathbf{k}'-\mathbf{q}')\rangle \\ +\langle\phi(\mathbf{q})\phi(\mathbf{q}')\rangle\langle\phi(\mathbf{k}-\mathbf{q})\phi(\mathbf{k}'-\mathbf{q}')\rangle \\ +\langle\phi(\mathbf{q})\phi(\mathbf{k}'-\mathbf{q}')\rangle\langle\phi(\mathbf{q}')\phi(\mathbf{k}-\mathbf{q})\rangle\end{bmatrix} \\
&= 0+\frac{4\pi^2}{\langle\phi^2\rangle^2}\int\mathrm{d}^3\mathbf{q}\,\mathrm{d}^3\mathbf{q}'\,\frac{\delta^{(3)}(\mathbf{q}+\mathbf{q}')}{q^3}\mathcal{P}_\phi(q)\frac{\delta^{(3)}(\mathbf{q}-\mathbf{k}-\mathbf{k}'+\mathbf{q}')}{|\mathbf{q}-\mathbf{k}|^3}\mathcal{P}_\phi(|\mathbf{q}-\mathbf{k}|) \\
&\quad+\frac{4\pi^2}{\langle\phi^2\rangle^2}\int\mathrm{d}^3\mathbf{q}\,\mathrm{d}^3\mathbf{q}'\,\frac{\delta^{(3)}(\mathbf{q}+\mathbf{k}'-\mathbf{q}')}{q^3}\mathcal{P}_\phi(q)\frac{\delta^{(3)}(\mathbf{q}'+\mathbf{k}-\mathbf{q})}{q'^3}\mathcal{P}_\phi(q') \\
&= (2\pi)^3\delta^{(3)}(\mathbf{k}+\mathbf{k}')\frac{2\pi^2}{k^3}\frac{4\pi^2k^3}{\langle\phi^2\rangle^2}\int\frac{\mathrm{d}^3\mathbf{q}}{(2\pi)^3}\frac{\mathcal{P}_\phi(q)}{q^3}\frac{\mathcal{P}_\phi(|\mathbf{q}-\mathbf{k}|)}{|\mathbf{q}-\mathbf{k}|^3}.
\end{aligned} \tag{B.13}$$

From here, we can read off the power spectrum

$$\begin{aligned}
\mathcal{P}_\delta(k) &= \frac{k^3}{\langle\phi^2\rangle^2}\int\mathrm{d}q\,\mathrm{d}\cos\theta\,\frac{1}{q^3}\frac{1}{|\mathbf{q}-\mathbf{k}|^3}\mathcal{P}_\phi(q)\mathcal{P}_\phi(|\mathbf{q}-\mathbf{k}|) \\
&= \frac{k^3}{\langle\phi^2\rangle^2}\int_{|q-k|<p<q+k}\mathrm{d}q\,\mathrm{d}p\,\frac{1}{q^2}\frac{1}{p^2}\mathcal{P}_\phi(q)\mathcal{P}_\phi(p).
\end{aligned} \tag{B.14}$$

To get to the second line, we have performed a change of variables $\cos\theta \to p \equiv |\mathbf{k}-\mathbf{q}|$.

References

[1] P.W. Graham, J. Mardon and S. Rajendran, *Vector dark matter from inflationary fluctuations*, *Phys. Rev.* **D 93** (2016) 103520 [arXiv:1504.02102] [INSPIRE].

[2] C. Cosme, J.G. Rosa and O. Bertolami, *Scale-invariant scalar field dark matter through the Higgs portal*, *JHEP* **05** (2018) 129 [arXiv:1802.09434] [INSPIRE].

[3] B.W. Lee and S. Weinberg, *Cosmological lower bound on heavy neutrino masses*, *Phys. Rev. Lett.* **39** (1977) 165 [INSPIRE].

[4] J.R. Ellis, J.S. Hagelin, D.V. Nanopoulos, K.A. Olive and M. Srednicki, *Supersymmetric relics from the big bang*, *Nucl. Phys.* **B 238** (1984) 453 [INSPIRE].

[5] H. Goldberg, *Constraint on the photino mass from cosmology*, *Phys. Rev. Lett.* **50** (1983) 1419 [*Erratum ibid.* **103** (2009) 099905] [INSPIRE].

[6] E.W. Kolb and M.S. Turner, *The early universe*, *Front. Phys.* **69** (1990) 1 [INSPIRE].

[7] T. Marrodán Undagoitia and L. Rauch, *Dark matter direct-detection experiments*, *J. Phys.* **G 43** (2016) 013001 [arXiv:1509.08767] [INSPIRE].

[8] T.R. Slatyer, *Indirect detection of dark matter*, in *Proceedings, Theoretical Advanced Study Institute in Elementary Particle Physics: anticipating the next discoveries in particle physics (TASI* 2016*)*, Boulder, CO, U.S.A., 6 June–1 July 2016, World Scientific, Singapore, (2018), pg. 297 [arXiv:1710.05137] [INSPIRE].

[9] F. Kahlhoefer, *Review of LHC dark matter searches*, *Int. J. Mod. Phys.* **A 32** (2017) 1730006 [arXiv:1702.02430] [INSPIRE].

[10] J. Preskill, M.B. Wise and F. Wilczek, *Cosmology of the invisible axion*, *Phys. Lett.* **B 120** (1983) 127 [INSPIRE].

JCAP10(2018)022

[11] L.F. Abbott and P. Sikivie, *A cosmological bound on the invisible axion*, *Phys. Lett.* **B 120** (1983) 133 [INSPIRE].

[12] M. Dine and W. Fischler, *The not so harmless axion*, *Phys. Lett.* **B 120** (1983) 137 [INSPIRE].

[13] P. Arias, D. Cadamuro, M. Goodsell, J. Jaeckel, J. Redondo and A. Ringwald, *WISPy cold dark matter*, *JCAP* **06** (2012) 013 [arXiv:1201.5902] [INSPIRE].

[14] J. Jaeckel, *A family of WISPy dark matter candidates*, *Phys. Lett.* **B 732** (2014) 1 [arXiv:1311.0880] [INSPIRE].

[15] A. Ringwald, *Exploring the role of axions and other WISPs in the dark universe*, *Phys. Dark Univ.* **1** (2012) 116 [arXiv:1210.5081] [INSPIRE].

[16] D.J.E. Marsh, *Axion cosmology*, *Phys. Rept.* **643** (2016) 1 [arXiv:1510.07633] [INSPIRE].

[17] I.G. Irastorza and J. Redondo, *New experimental approaches in the search for axion-like particles*, *Prog. Part. Nucl. Phys.* **102** (2018) 89 [arXiv:1801.08127] [INSPIRE].

[18] Y. Hochberg, T. Lin and K.M. Zurek, *Detecting ultralight bosonic dark matter via absorption in superconductors*, *Phys. Rev.* **D 94** (2016) 015019 [arXiv:1604.06800] [INSPIRE].

[19] Y. Hochberg, T. Lin and K.M. Zurek, *Absorption of light dark matter in semiconductors*, *Phys. Rev.* **D 95** (2017) 023013 [arXiv:1608.01994] [INSPIRE].

[20] M. Battaglieri et al., *U.S. cosmic visions: new ideas in dark matter* 2017 — *community report*, arXiv:1707.04591 [INSPIRE].

[21] XENON100 collaboration, E. Aprile et al., *First axion results from the XENON*100 *experiment*, *Phys. Rev.* **D 90** (2014) 062009 [*Erratum ibid.* **D 95** (2017) 029904] [arXiv:1404.1455] [INSPIRE].

[22] XENON100 collaboration, E. Aprile et al., *Search for bosonic super-WIMP interactions with the XENON*100 *experiment*, *Phys. Rev.* **D 96** (2017) 122002 [arXiv:1709.02222] [INSPIRE].

[23] LUX collaboration, D.S. Akerib et al., *First searches for axions and axionlike particles with the LUX experiment*, *Phys. Rev. Lett.* **118** (2017) 261301 [arXiv:1704.02297] [INSPIRE].

[24] I.M. Bloch, R. Essig, K. Tobioka, T. Volansky and T.-T. Yu, *Searching for dark absorption with direct detection experiments*, *JHEP* **06** (2017) 087 [arXiv:1608.02123] [INSPIRE].

[25] MAJORANA collaboration, N. Abgrall et al., *New limits on bosonic dark matter, solar axions, Pauli exclusion principle violation and electron decay from the Majorana demonstrator*, *Phys. Rev. Lett.* **118** (2017) 161801 [arXiv:1612.00886] [INSPIRE].

[26] E. Bulbul, M. Markevitch, A. Foster, R.K. Smith, M. Loewenstein and S.W. Randall, *Detection of an unidentified emission line in the stacked X-ray spectrum of galaxy clusters*, *Astrophys. J.* **789** (2014) 13 [arXiv:1402.2301] [INSPIRE].

[27] A. Boyarsky, O. Ruchayskiy, D. Iakubovskyi and J. Franse, *Unidentified line in X-ray spectra of the Andromeda galaxy and Perseus galaxy cluster*, *Phys. Rev. Lett.* **113** (2014) 251301 [arXiv:1402.4119] [INSPIRE].

[28] C. Cosme, J.G. Rosa and O. Bertolami, *Scalar field dark matter with spontaneous symmetry breaking and the* 3.5 *keV line*, *Phys. Lett.* **B 781** (2018) 639 [arXiv:1709.09674] [INSPIRE].

[29] J. Jaeckel, J. Redondo and A. Ringwald, 3.55 *keV hint for decaying axionlike particle dark matter*, *Phys. Rev.* **D 89** (2014) 103511 [arXiv:1402.7335] [INSPIRE].

[30] G. Alonso-Álvarez and J. Jaeckel, *Exploring axionlike particles beyond the canonical setup*, *Phys. Rev.* **D 98** (2018) 023539 [arXiv:1712.07500] [INSPIRE].

[31] P.W. Graham and A. Scherlis, *Stochastic axion scenario*, *Phys. Rev.* **D 98** (2018) 035017 [arXiv:1805.07362] [INSPIRE].

JCAP10(2018)022

[32] F. Takahashi, W. Yin and A.H. Guth, *QCD axion window and low-scale inflation*, *Phys. Rev.* **D 98** (2018) 015042 [arXiv:1805.08763] [INSPIRE].

[33] L.H. Ford, *Gravitational particle creation and inflation*, *Phys. Rev.* **D 35** (1987) 2955 [INSPIRE].

[34] D.J.H. Chung, E.W. Kolb and A. Riotto, *Superheavy dark matter*, *Phys. Rev.* **D 59** (1999) 023501 [hep-ph/9802238] [INSPIRE].

[35] D.J.H. Chung, P. Crotty, E.W. Kolb and A. Riotto, *On the gravitational production of superheavy dark matter*, *Phys. Rev.* **D 64** (2001) 043503 [hep-ph/0104100] [INSPIRE].

[36] Y. Ema, R. Jinno, K. Mukaida and K. Nakayama, *Gravitational effects on inflaton decay*, *JCAP* **05** (2015) 038 [arXiv:1502.02475] [INSPIRE].

[37] Y. Ema, R. Jinno, K. Mukaida and K. Nakayama, *Gravitational particle production in oscillating backgrounds and its cosmological implications*, *Phys. Rev.* **D 94** (2016) 063517 [arXiv:1604.08898] [INSPIRE].

[38] T. Markkanen and S. Nurmi, *Dark matter from gravitational particle production at reheating*, *JCAP* **02** (2017) 008 [arXiv:1512.07288] [INSPIRE].

[39] Y. Ema, K. Nakayama and Y. Tang, *Production of purely gravitational dark matter*, *JHEP* **09** (2018) 135 [arXiv:1804.07471] [INSPIRE].

[40] M. Garny, M. Sandora and M.S. Sloth, *Planckian interacting massive particles as dark matter*, *Phys. Rev. Lett.* **116** (2016) 101302 [arXiv:1511.03278] [INSPIRE].

[41] Y. Tang and Y.-L. Wu, *Pure gravitational dark matter, its mass and signatures*, *Phys. Lett.* **B 758** (2016) 402 [arXiv:1604.04701] [INSPIRE].

[42] Y. Tang and Y.-L. Wu, *On thermal gravitational contribution to particle production and dark matter*, *Phys. Lett.* **B 774** (2017) 676 [arXiv:1708.05138] [INSPIRE].

[43] M. Garny, A. Palessandro, M. Sandora and M.S. Sloth, *Theory and phenomenology of Planckian interacting massive particles as dark matter*, *JCAP* **02** (2018) 027 [arXiv:1709.09688] [INSPIRE].

[44] S. Nurmi, T. Tenkanen and K. Tuominen, *Inflationary imprints on dark matter*, *JCAP* **11** (2015) 001 [arXiv:1506.04048] [INSPIRE].

[45] K. Kainulainen, S. Nurmi, T. Tenkanen, K. Tuominen and V. Vaskonen, *Isocurvature constraints on portal couplings*, *JCAP* **06** (2016) 022 [arXiv:1601.07733] [INSPIRE].

[46] O. Bertolami, C. Cosme and J.G. Rosa, *Scalar field dark matter and the Higgs field*, *Phys. Lett.* **B 759** (2016) 1 [arXiv:1603.06242] [INSPIRE].

[47] A.D. Linde, *Inflation and string cosmology*, *Prog. Theor. Phys. Suppl.* **163** (2006) 295 [hep-th/0503195] [INSPIRE].

[48] N.D. Birrell and P.C.W. Davies, *Quantum fields in curved space*, Cambridge University Press, Cambridge, U.K., (1982) [INSPIRE].

[49] V. Mukhanov and S. Winitzki, *Introduction to quantum effects in gravity*, Cambridge University Press, Cambridge, U.K., (2007) [INSPIRE].

[50] G.W. Gibbons and S.W. Hawking, *Cosmological event horizons, thermodynamics and particle creation*, *Phys. Rev.* **D 15** (1977) 2738 [INSPIRE].

[51] Planck collaboration, Y. Akrami et al., *Planck* 2018 *results. X. Constraints on inflation*, arXiv:1807.06211 [INSPIRE].

[52] J. Jaeckel and A. Ringwald, *The low-energy frontier of particle physics*, *Ann. Rev. Nucl. Part. Sci.* **60** (2010) 405 [arXiv:1002.0329] [INSPIRE].

[53] P.W. Graham and S. Rajendran, *New observables for direct detection of axion dark matter*, *Phys. Rev.* **D 88** (2013) 035023 [arXiv:1306.6088] [INSPIRE].

JCAP10(2018)022

[54] V. Silveira and A. Zee, *Scalar phantoms*, *Phys. Lett.* **B 161** (1985) 136 [INSPIRE].

[55] C.P. Burgess, M. Pospelov and T. ter Veldhuis, *The minimal model of nonbaryonic dark matter: a singlet scalar*, *Nucl. Phys.* **B 619** (2001) 709 [hep-ph/0011335] [INSPIRE].

[56] M.C. Bento, O. Bertolami and R. Rosenfeld, *Cosmological constraints on an invisibly decaying Higgs boson*, *Phys. Lett.* **B 518** (2001) 276 [hep-ph/0103340] [INSPIRE].

[57] D. Bettoni and J. Rubio, *Quintessential Affleck-Dine baryogenesis with non-minimal couplings*, *Phys. Lett.* **B 784** (2018) 122 [arXiv:1805.02669] [INSPIRE].

[58] J.F. Dufaux, G.N. Felder, L. Kofman, M. Peloso and D. Podolsky, *Preheating with trilinear interactions: tachyonic resonance*, *JCAP* **07** (2006) 006 [hep-ph/0602144] [INSPIRE].

[59] B. Carr, F. Kuhnel and M. Sandstad, *Primordial black holes as dark matter*, *Phys. Rev.* **D 94** (2016) 083504 [arXiv:1607.06077] [INSPIRE].

[60] C.J. Hogan and M.J. Rees, *Axion miniclusters*, *Phys. Lett.* **B 205** (1988) 228 [INSPIRE].

[61] E.W. Kolb and I.I. Tkachev, *Axion miniclusters and Bose stars*, *Phys. Rev. Lett.* **71** (1993) 3051 [hep-ph/9303313] [INSPIRE].

[62] M.S. Turner, F. Wilczek and A. Zee, *Formation of structure in an axion dominated universe*, *Phys. Lett.* **B 125** (1983) 35 [*Erratum ibid.* **B 125** (1983) 519] [INSPIRE].

[63] M. Axenides, R.H. Brandenberger and M.S. Turner, *Development of axion perturbations in an axion dominated universe*, *Phys. Lett.* **B 126** (1983) 178 [INSPIRE].

[64] L. Iliesiu, D.J.E. Marsh, K. Moodley and S. Watson, *Constraining supersymmetry with heavy scalars: using the CMB*, *Phys. Rev.* **D 89** (2014) 103513 [arXiv:1312.3636] [INSPIRE].

[65] J.A.R. Cembranos, A.L. Maroto and S.J. Núñez Jareño, *Cosmological perturbations in coherent oscillating scalar field models*, *JHEP* **03** (2016) 013 [arXiv:1509.08819] [INSPIRE].

[66] A.E. Nelson and J. Scholtz, *Dark light, dark matter and the misalignment mechanism*, *Phys. Rev.* **D 84** (2011) 103501 [arXiv:1105.2812] [INSPIRE].

[67] M. Sasaki, *Gauge invariant scalar perturbations in the new inflationary universe*, *Prog. Theor. Phys.* **70** (1983) 394 [INSPIRE].

[68] H. Kodama and M. Sasaki, *Cosmological perturbation theory*, *Prog. Theor. Phys. Suppl.* **78** (1984) 1 [INSPIRE].

[69] V.F. Mukhanov, *Quantum theory of gauge invariant cosmological perturbations*, *Sov. Phys. JETP* **67** (1988) 1297 [*Zh. Eksp. Teor. Fiz.* **94N7** (1988) 1] [INSPIRE].

[70] A. Riotto, *Inflation and the theory of cosmological perturbations*, *ICTP Lect. Notes Ser.* **14** (2003) 317 [hep-ph/0210162] [INSPIRE].

[71] *DLMF: NIST Digital Library of Mathematical Functions*, https://dlmf.nist.gov/.

[72] L.F. Abbott and M.B. Wise, *Wormholes and global symmetries*, *Nucl. Phys.* **B 325** (1989) 687 [INSPIRE].

[73] S.R. Coleman and K.-M. Lee, *Wormholes made without massless matter fields*, *Nucl. Phys.* **B 329** (1990) 387 [INSPIRE].

[74] S.B. Giddings and A. Strominger, *Axion induced topology change in quantum gravity and string theory*, *Nucl. Phys.* **B 306** (1988) 890 [INSPIRE].

[75] R. Kallosh, A.D. Linde, D.A. Linde and L. Susskind, *Gravity and global symmetries*, *Phys. Rev.* **D 52** (1995) 912 [hep-th/9502069] [INSPIRE].

[76] L.M. Krauss and F. Wilczek, *Discrete gauge symmetry in continuum theories*, *Phys. Rev. Lett.* **62** (1989) 1221 [INSPIRE].

JCAP10(2018)022

[77] J.E. Kim, *Abelian discrete symmetries Z_N and Z_{nR} from string orbifolds*, *Phys. Lett.* **B 726** (2013) 450 [arXiv:1308.0344] [INSPIRE].

[78] O. Catà, A. Ibarra and S. Ingenhütt, *Dark matter decays from nonminimal coupling to gravity*, *Phys. Rev. Lett.* **117** (2016) 021302 [arXiv:1603.03696] [INSPIRE].

[79] O. Catà, A. Ibarra and S. Ingenhütt, *Dark matter decay through gravity portals*, *Phys. Rev.* **D 95** (2017) 035011 [arXiv:1611.00725] [INSPIRE].

[80] J. Enander, A. Pargner and T. Schwetz, *Axion minicluster power spectrum and mass function*, *JCAP* **12** (2017) 038 [arXiv:1708.04466] [INSPIRE].

[81] E.W. Kolb and I.I. Tkachev, *Large amplitude isothermal fluctuations and high density dark matter clumps*, *Phys. Rev.* **D 50** (1994) 769 [astro-ph/9403011] [INSPIRE].

[82] M. Fairbairn, D.J.E. Marsh and J. Quevillon, *Searching for the QCD axion with gravitational microlensing*, *Phys. Rev. Lett.* **119** (2017) 021101 [arXiv:1701.04787] [INSPIRE].

[83] M. Fairbairn, D.J.E. Marsh, J. Quevillon and S. Rozier, *Structure formation and microlensing with axion miniclusters*, *Phys. Rev.* **D 97** (2018) 083502 [arXiv:1707.03310] [INSPIRE].

[84] K.M. Zurek, C.J. Hogan and T.R. Quinn, *Astrophysical effects of scalar dark matter miniclusters*, *Phys. Rev.* **D 75** (2007) 043511 [astro-ph/0607341] [INSPIRE].

[85] J. Peñarrubia, *Fluctuations of the gravitational field generated by a random population of extended substructures*, *Mon. Not. Roy. Astron. Soc.* **474** (2018) 1482 [arXiv:1710.06443] [INSPIRE].

[86] D.M. Grabowska, T. Melia and S. Rajendran, *Detecting dark blobs*, arXiv:1807.03788 [INSPIRE].

[87] C. Wetterich, *Cosmologies with variable Newton's 'constant'*, *Nucl. Phys.* **B 302** (1988) 645 [INSPIRE].

JCAP10(2018)022

Chapter 8

Misalignment & Co.: (Pseudo-)scalar and vector dark matter with curvature couplings

Authors:
Gonzalo Alonso-Álvarez, Thomas Hugle, and Joerg Jaeckel

Published in *JCAP 02 (2020) 014*,
also available at arXiv:1905.09836

Principal authorship of this article is shared on an equal footing by Thomas Hugle and Gonzalo Alonso-Álvarez. The original idea for the project was conceived by Joerg Jaeckel and was further developed by the three authors. The calculations in Section II were performed predominantly by Gonzalo Alonso-Álvarez. Gonzalo Alonso-Álvarez produced Figures 1, 2, 3, 4, 7, and 8. Section II was written predominantly by Gonzalo Alonso-Álvarez, and Sections I and IV were written with equal participation from the three authors. All three authors contributed with corrections and suggestions to the manuscript, as well as with improvements during the review process.

Journal of Cosmology and Astroparticle Physics
An IOP and SISSA journal

Misalignment & Co.: (pseudo-)scalar and vector dark matter with curvature couplings

Gonzalo Alonso-Álvarez,[a] **Thomas Hugle**[b] **and Joerg Jaeckel**[a]

[a]Institut für theoretische Physik, Universität Heidelberg,
Philosophenweg 16, 69120 Heidelberg, Germany
[b]Max-Planck-Institut für Kernphysik,
Saupfercheckweg 1, 69117 Heidelberg, Germany

E-mail: alonso@thphys.uni-heidelberg.de, thomas.hugle@mpi-hd.mpg.de,
jjaeckel@thphys.uni-heidelberg.de

Received July 3, 2019
Accepted January 29, 2020
Published February 13, 2020

Abstract. Motivated by their potential role as dark matter, we study the cosmological evolution of light scalar and vector fields non-minimally coupled to gravity. Our focus is on a situation where the dominant contribution to the energy density arises from the misalignment mechanism. In addition, we also discuss the possibility that dark matter is generated in a stochastic scenario or from inflationary fluctuations. Even small deviations in the non-minimal couplings from the standard scenarios lead to significant qualitative and quantitative changes. This is due to the curvature-coupling driven superhorizon evolution of the homogeneous field and the non-zero momentum modes during inflation. Both the relic density yield and the large-scale density fluctuations are affected. For the misalignment mechanism, this results in a weakening of the isocurvature constraints and opens up new viable regions of parameter space.

Keywords: dark matter theory, inflation, quantum field theory on curved space

ArXiv ePrint: 1905.09836

JCAP02(2020)014

 https://doi.org/10.1088/1475-7516/2020/02/014

Contents

JCAP02(2020)014

1 Introduction

Light scalars or vectors very weakly coupled to the Standard Model are phenomenologically and experimentally interesting dark matter candidates [1–7] (cf. also [8] for a recent review). Over recent years a sizeable experimental program has developed to search for their signatures [9–20][1] (see [29, 30, 33–35] for some overviews).

Their low mass and very small couplings make them automatically stable even on cosmological time scales, without the need to completely forbid their decay by an additional symmetry. Furthermore, they are naturally produced via the misalignment mechanism [1–3, 5–7] and as such they generally contribute to at least a fraction of the observed dark matter density. The initial (homogeneous) field value in our observable Universe can simply correspond to the initial misalignment of the field away from the vacuum, or it can arise "stochastically" [36–41] from the accumulated effect of fluctuations during a long phase of inflation. Additional contributions may arise from production via inflationary fluctuations [42–47] as well as from decays of precursor particles [48–53]. Modifications to the usual misalignment mechanism have been for example explored in [54, 55].

So far, most studies of the misalignment mechanism for (pseudo-)scalars have concentrated on the case of minimal coupling to gravity [1–3]. For vectors, this case typically only

[1]While not searching directly for dark matter, experiments like ALPS [21–23], CAST [24, 25] and IAXO [26–28] are searching for suitable light candidates (see also [29–32]).

yields a small amount of dark matter in today's Universe. In order to enhance the relic abundance, an option is to introduce a curvature coupling which has to be set close to a specific value that makes the evolution equivalent to that of a scalar [6, 56]. In this paper, we broaden this perspective by considering more general couplings of (pseudo-)scalar and vector fields to the Ricci scalar. Our main aim is to study their effects on the misalignment mechanism, but we also consider the impact of the curvature couplings on the stochastic scenario [38, 39] and the contribution of inflationary fluctuations [42, 47] to the dark matter density.

The starting point of our discussion is the usual Einstein-Hilbert action, which is extended to allow for direct couplings of the fields to the Ricci scalar R. In particular, for the scalar case we consider the action

$$S = \int \mathrm{d}^4x\,\sqrt{-g}\left(\frac{1}{2}\left(M_{\rm pl}^2 - \xi\phi^2\right)R - \frac{1}{2}\partial_\mu\phi\partial^\mu\phi - \frac{1}{2}m_\phi^2\phi^2\right), \tag{1.1}$$

where we allow for both positive and negative values of ξ. Similarly, the action for the vector field is given by

$$S = \int \mathrm{d}^4x\,\sqrt{-g}\left(\frac{1}{2}\left(M_{\rm pl}^2 + \frac{\kappa}{6}X_\mu X^\mu\right)R - \frac{1}{4}X_{\mu\nu}X^{\mu\nu} - \frac{1}{2}m_X^2X_\mu X^\mu\right). \tag{1.2}$$

Note that the non-minimal coupling in the vector model has the opposite sign with respect to the scalar case. Also, this choice for the normalization of κ ensures that the vector field behaves like a minimally coupled scalar for $\kappa = 1$, as we will see in section 3 (such was the convention chosen in [6, 57–59]).

The role of non-minimal couplings to gravity in cosmology has been extensively studied in the literature. The main focus was originally on the construction of inflationary models [60, 61], which attracted particular interest after it was realized that the Higgs boson can play the role of the inflaton [62] if a large value of $\xi \sim 10^4$ is assumed (for a recent review see, e.g. [63]). The possibility of inflation being driven by a non-minimally coupled vector field was also considered in [56]. More recently, increasing attention has been payed to the possibility that the dark matter may also enjoy such couplings. The focus of the studies has been on the generation of dark matter during inflation [42–47] or at preheating and reheating [64–72]. Graviton-mediated thermal production has also been explored [70–76].

Aside from phenomenological reasons, there are theoretical motivations to study the couplings delineated above. Generally, these operators need to be considered if general relativity is viewed as an effective field theory [77]. In addition, the quantization of any scalar field theory in a gravitational background [78] inevitably produces terms like the ones in eq. (1.1). Their presence turns out to be essential for the renormalizability of the energy-momentum tensor in curved backgrounds [79]. We will consider $\mathcal{O}(1)$ (or smaller) dimensionless couplings, which correspond to interactions of strength $1/M_{\rm pl}^2$ after the graviton fields are properly normalized. This is the natural size that is a priori expected in a theory of quantum gravity. As an example, such scalar couplings have been found to generically arise [80–85] in approaches to the quantization of gravity like asymptotic safety [86] (see [87, 88] for recent reviews).

The situation of vectors is somewhat complicated by gauge invariance and the need to involve a Stueckelberg (or Higgs) mechanism. Constructing the appropriate Stueckelberg terms for the couplings to R leads to a naive violation of unitarity[2] already at relatively low energies [48]. A more detailed investigation, e.g. along the lines of [89] would be very

[2]We are indebted to Fuminobu Takahashi for discussions on this issue.

JCAP02(2020)014

interesting but is beyond the scope of this work. Another difficulty for the vector theory is that the sign of the kinetic term of the longitudinal mode becomes negative for a certain range of momenta. This is reminiscent of a scalar particle with a negative kinetic term, i.e. a ghost. As is well known, ghosts are generally dangerous because they destabilize the vacuum of the theory [90, 91]. The situation is however more complex for the vector theory at hand. Firstly, the sign of the kinetic term depends on the size of the momentum, and only becomes negative for a finite range of momenta. Secondly, the sign change appears at all only in situations with sufficiently large spacetime curvature. Thirdly and due to the aforementioned sign flip, the kinetic term becomes singular for certain values of the momentum. These problems have been discussed in [59, 92–94], but no final conclusion regarding the viability of the theory has been reached. This certainly calls for a more exhaustive investigation, which is however not the aim of the present work. Acknowledging this potential issue, we nevertheless consider the vector scenario and treat the non-minimal coupling as a phenomenological $\mathcal{O}(1)$ parameter.

From the point of view of cosmology, the main effect of both scalar and vector non-minimal couplings is that the dark matter fields acquire an additional positive (or negative) mass term during inflation. As a consequence, the superhorizon evolution becomes fast enough so as to strongly suppress (or enhance) the field value and the fluctuations during the inflationary period, typically in an exponential manner. This has important consequences for the initial field values required to produce today's dark matter density, as even relatively small values of the coupling parameters can lead to drastic shifts in the initial scale that "naturally" produces the observed dark matter density. The fluctuations are affected in a similar way, leading to changes in the isocurvature constraints as well as their contribution to the density today. Both effects will be discussed in detail in this work.

Our paper is structured along the following lines. Section 2 discusses the effects of non-minimal couplings on the misalignment, stochastic and fluctuation scenarios for (pseudo-)scalars, whereas section 3 does the same for vectors. For each case, we discuss the amount of dark matter produced as well as constraints from isocurvature fluctuations. Finally, a short summary and conclusions are given in section 4.

Before continuing let us note that, for simplicity, in the following we will simply write scalars instead of (pseudo-)scalars. That said, all of our results equally apply to pseudoscalar particles.

2 Scalars

2.1 Homogeneous scalar field and relic density

The equations of motion (EOMs) for the homogeneous field can be readily derived from the action given in eq. (1.1). Neglecting spatial derivatives, we arrive at

$$\ddot{\phi} + 3H\dot{\phi} + \left(m_\phi^2 + \xi R\right)\phi = 0. \tag{2.1}$$

As already mentioned in the introduction, the presence of the non-minimal coupling to gravity results in a space-time dependent effective mass for the field. Because of the particular cosmological evolution of the Ricci scalar, which is sketched in figure 1, non-negligible effects will only occur during inflation. This means that the post-inflationary evolution of the scalar field can be described by the standard equations used for the misalignment mechanism (cf. [6]).

JCAP02(2020)014

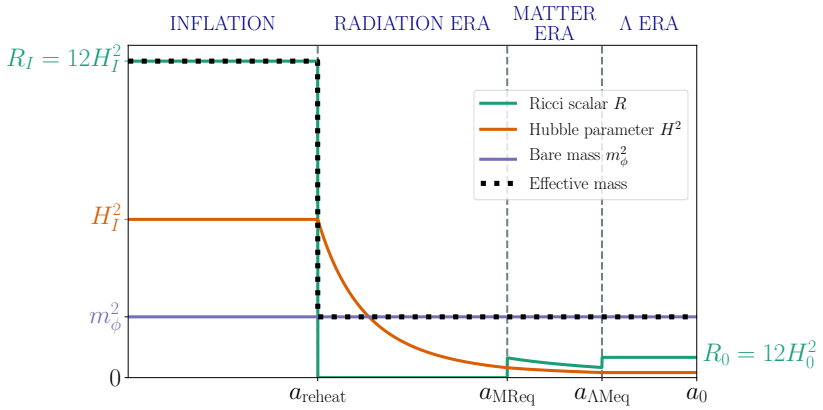

Figure 1. Illustration of the cosmological evolution of the effective mass for the non-minimally coupled scalar (the vector case is analogous). For the purpose of illustration we set $\xi = 1$. The field acquires a large effective mass during inflation, when the Ricci scalar is large. As soon as radiation domination starts, $R = 0$ and the field acquires its late-time mass given by the explicit mass term $m_\phi^2\phi^2/2$. By the time of matter-radiation equality, the Hubble parameter is so small that as long as $m_\phi \gtrsim 10^{-28}\,\mathrm{eV}$, the non-minimal coupling has no significant effect on the effective mass and the evolution any more.

The final relic abundance relative to the observed dark matter one can be expressed as[3]

$$\frac{\Omega_\phi}{\Omega_{\rm DM}} \simeq 5\,\mathcal{F}(T_\star)\left(\frac{\phi_e}{10^{12}\,\mathrm{GeV}}\right)^2\sqrt{\frac{m_\phi}{\mathrm{eV}}}, \tag{2.2}$$

where $\mathcal{F}(T_\star) \equiv (g_\star(T_\star)/3.36)^{3/4}/(g_{\star S}(T_\star)/3.91)$ is an $\mathcal{O}(1)$ function encoding the change in the number of relativistic degrees of freedom between today and the time $t_\star$ when the scalar oscillations start, at $3H(t_\star) \simeq m_\phi$. We have explicitly expressed the result in terms of the field value *at the end of inflation* ϕ_e, to highlight that it is in general different from the initial field value ϕ_s, which can be identified with the field value *at the start of inflation*. This nontrivial evolution is precisely due to the existence of the R-coupling. From now on we assume that the scalar field is responsible for all of the observed dark matter, i.e. $\Omega_\phi = \Omega_{\rm DM}$ is enforced if not explicitly stated otherwise.

During inflation,[4] when $R = 12\,H_I^2$, the EOM eq. (2.1) is that of a damped oscillator with a constant frequency and can easily be solved. Due to the non-minimal coupling $\xi \neq 0$, some care has to be put into selecting the appropriate initial conditions. In the minimally coupled case, one can normally assume that $\dot\phi_s = 0$ (the subscript s denotes the start of inflation). However, this is not necessarily true in the presence of curvature couplings. Allowing for a non-vanishing $\dot\phi_s$ (and assuming that $\phi_s \neq 0$), the general solution is given by

$$\phi(t) = \phi_s\left(c_1\,\mathrm{e}^{-\frac{1}{2}\alpha_- H_I t} + c_2\,\mathrm{e}^{-\frac{1}{2}\alpha_+ H_I t}\right), \tag{2.3}$$

[3] Our result differs slightly from the one in [6] due to the use of the updated value for $\Omega_{\rm DM}$ from [95] and a more careful matching of the initial conditions for the WKB approximation.

[4] We approximate inflation by a purely de Sitter expansion with $H = H_I = \text{const}$. Our results do not change qualitatively if we allow for a small non-vanishing $\dot H_I$. We will briefly discuss this possibility in section 4. We also take reheating to be instantaneous.

JCAP02(2020)014

where c_1 and c_2, which are given in eq. (B.2), satisfy $c_1 + c_2 = 1$ and encode the exact dependence on the initial conditions. Additionally, we have defined

$$\alpha_\pm = 3 \pm \sqrt{9 - 48\xi}. \tag{2.4}$$

As we will see, all our results only depend on the product $c_1\,\phi_s$. As long as $\dot{\phi}_s \sim H_I\phi_s$ and except for fine-tuned choices of initial conditions, the coefficient c_1 is of $\mathcal{O}(1)$. Because of this and for the sake of simplicity, we will henceforth drop it from the equations. For practical purposes, powers of c_1 can be easily reinstated by swapping ϕ_s for $c_1\,\phi_s$ at any point in the discussion. The exact form of the full solution is used for the calculation of the stochastic scenario and can be found in appendix B.

For the parameter range of interest, i.e. $\xi < 3/16$, $\alpha_\pm$ are always real and positive, and satisfy $\alpha_+ > \alpha_-$. Hence, after a long enough time the first term in eq. (2.3) will dominate over the second one and we can approximate the solution by

$$\phi(a) \simeq \phi_s \left(\frac{a}{a_s}\right)^{-\frac{1}{2}\alpha_-} = \phi_s\, \mathrm{e}^{-\frac{1}{2}\alpha_- N(a)}, \tag{2.5}$$

where we use scale factors and number of e-folds instead of time. For small values of the non-minimal coupling ξ, the value of α_- is also small but the product $\alpha_- N(a)$ can be large, resulting in a significant suppression (or enhancement, if $\xi < 0$) of the homogeneous field value. In particular, we can relate the value at the end of inflation to the initial condition by

$$\phi_e \simeq \phi_s \mathrm{e}^{-\frac{1}{2}\alpha_- N_{\mathrm{tot}}}. \tag{2.6}$$

The exponential factor can be enormous depending on the total number of e-folds of inflation N_{tot}, which is observationally only bounded from below. Indeed, some models of inflation predict it to be extremely large [96, 97]. In addition to that and in contrast to the minimally coupled case, the field has a non-vanishing time derivative at the end of inflation,

$$\dot{\phi}_e = -\frac{1}{2}\alpha_- H_I \phi_e. \tag{2.7}$$

When $\xi \ll 1$, this is a small effect, as $\mathrm{d}\log\phi_e/\mathrm{d}t \sim \xi$, but it can have important consequences for the post-inflationary evolution of the fluctuations, as we will see in section 3.

As long as there are no additional stabilizing terms in the potential,[5] a negative value of ξ induces a runaway potential that can drive ϕ into a trans-Planckian field value. Avoiding such a potentially dangerous field excursion sets a limit on the size of the non-minimal coupling. Under the most conservative assumptions of minimal number of inflationary e-folds $N_{\mathrm{tot}} = N_{\mathrm{min}}(H_I)$ (see appendix A for an explicit expression for $N_{\mathrm{min}}(H_I)$) and initial conditions corresponding to de Sitter vacuum fluctuations $\phi_s = H_I/2\pi$, the limit on ξ only depends on the Hubble scale of inflation H_I and is shown in figure 2. This bound is not contingent on the mass of the field or its potential role as dark matter. The bound gets stronger for a longer period of inflation according to eq. (2.6).

[5] For example this could be a self interaction term $\sim \lambda\phi^4$. To avoid trans-Planckian values we would need $\lambda \gtrsim \xi H_I^2/M_{\mathrm{pl}}^2$. Note, however, that for $\lambda\phi^2 \gtrsim m_\phi^2$ the energy density in a homogeneous field dilutes as $\sim a^{-4}$ and the cosmology might be significantly affected (see, e.g., [98–100]). Moreover, stability of the mass under quantum corrections also suggests that self-couplings are severely suppressed, e.g. by a shift symmetry.

JCAP02(2020)014

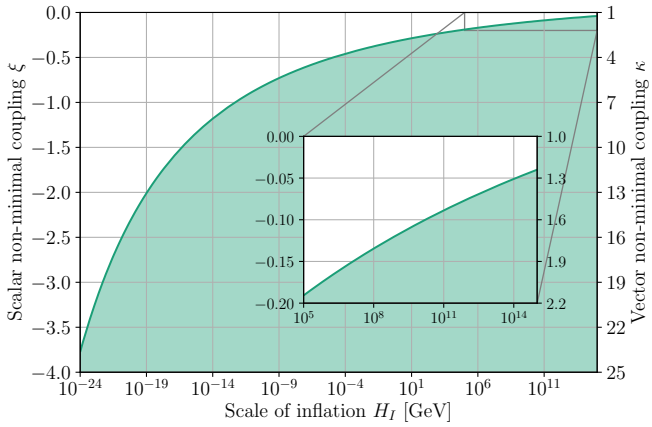

Figure 2. Limit on the size of a negative non-minimal coupling $\xi < 0$ (for scalars, left vertical axis) or $\kappa > 1$ (for vectors, right vertical axis) as a function of the inflation scale H_I, obtained from avoiding a trans-Planckian field excursion (in the absence of extra stabilizing terms in the potential). We make the most conservative assumptions of minimal inflation and initial conditions corresponding to de Sitter vacuum fluctuations, i.e. $\phi_s = H_I/2\pi$ and $\dot{\phi}_s = 0$. The inset zooms into the region of high-scale inflation and small non-minimal couplings.

2.2 Scalar fluctuations and isocurvature perturbations

The evolution of quantum fluctuations produced during inflation is also modified by the presence of the non-minimal coupling to gravity. This was studied in [47], to which we refer for details while presenting here only the main results. The time-evolving gravitational background makes the quantum vacuum transition into an excited state, which can be described as a classical stochastic field on smaller and smaller comoving scales as they leave the horizon during inflation. At that time, each independent Fourier mode becomes a Gaussian-distributed random field with power spectrum (valid for $k \neq 0$)

$$\mathcal{P}_\phi(k, a_k) = \left(\frac{H_I}{2\pi}\right)^2 F(\alpha_-), \tag{2.8}$$

where

$$F(\alpha_-) \equiv \frac{2^{2-\alpha_-}}{\pi}\,\Gamma^2\left(\frac{3-\alpha_-}{2}\right), \tag{2.9}$$

and we denote $a_k = k/H_I$. At this point, the result only deviates from the usual scale invariant power spectrum of a minimally coupled, massless field by the $\mathcal{O}(1)$ factor $F(\alpha_-)$. This is to be expected, as within the horizon where $k \gg aH_I$ the modes are relativistic even with respect to the R-dependent mass. This changes drastically after horizon exit. The modes become non-relativistic due to their large effective mass, and their classical EOM quickly approaches that of the homogeneous field. This means that the field power spectrum is not frozen on superhorizon scales, but rather evolves as

$$\mathcal{P}_\phi(k, a) = \mathcal{P}_\phi(k, a_k)\left(\frac{k}{a\,H_I}\right)^{\alpha_-}. \tag{2.10}$$

By the end of inflation, the power spectrum of an individual mode is suppressed (or enhanced) by

$$\mathcal{P}_\phi(k, a_e) = \mathcal{P}_\phi(k, a_k)\mathrm{e}^{-\alpha_- N(k)}. \tag{2.11}$$

Here $N(k)$ is the number of e-folds (counting from the end of inflation) at which the mode k exits the horizon. A precise expression for it is given in eq. (A.1) in appendix A. The crucial difference to eq. (2.6) is that the evolution of fluctuations only happens while the modes are superhorizon during inflation. As opposed to $N_{\rm tot}$, $N(k)$ can, under some assumptions, be bounded from above using observations, at least for the modes of cosmological interest [101].

The field fluctuations translate into density perturbations which become relevant when the dark matter scalar field composes a significant fraction of the energy density of the Universe. Within the misalignment approximation, the fluctuations are always small compared to the homogeneous field value. As the energy density of the coherently oscillating field is $\rho_\phi \sim \phi^2$, where here ϕ denotes the amplitude of the oscillations rather than the instantaneous field value, we can express the density contrast as

$$\delta_\phi \equiv \frac{\delta\rho_\phi}{\rho_\phi} = 2\frac{\delta\phi}{\phi}, \tag{2.12}$$

so that its power spectrum can be read off the field one,

$$\mathcal{P}_{\delta_\phi}(k) = \frac{4}{\langle\phi\rangle^2}\mathcal{P}_\phi(k,a). \tag{2.13}$$

Being independent of the inflaton ones, these density fluctuations are generically of isocurvature type and thus subject to constraints arising from their non-observation in the Cosmic Microwave Background (CMB). The evaluation of eq. (2.13) at the CMB scales is simple[6] because the evolution of the scalar field is linear at those large scales, which means that $\mathcal{P}_{\delta_\phi}$ stays constant at all times after horizon exit. Taking advantage of this fact, we evaluate it at the time when the relevant mode k leaves the horizon.[7] For the CMB modes, this happens $N_{\rm CMB} \equiv N(k_{\rm CMB})$ e-folds before the end of inflation, and thus

$$\begin{aligned}\mathcal{P}_{\delta_\phi}(k_{\rm CMB}) &= \frac{4}{\phi_s^2\, \mathrm{e}^{-\alpha_-(N_{\rm tot}-N_{\rm CMB})}}\left(\frac{H_I}{2\pi}\right)^2 F(\alpha_-) \\ &= \frac{4}{\phi_e^2\, \mathrm{e}^{\alpha_- N_{\rm CMB}}}\left(\frac{H_I}{2\pi}\right)^2 F(\alpha_-).\end{aligned} \tag{2.14}$$

Note that $N_{\rm CMB} = N_{\rm CMB}(H_I)$ is determined once the scale of inflation is fixed (see appendix A for an explicit formula). We have chosen to display the result both as a function of ϕ_e and ϕ_s to highlight the difference between both expressions, due to the superhorizon evolution of the modes caused by the non-minimal coupling.

The non-observation of an isocurvature mode in the CMB by the Planck satellite [95] sets an upper limit[8] on the size of $\mathcal{P}_{\delta_\phi}(k_{\rm CMB})$. Figure 3 shows the resulting constraints in the (m, H_I) parameter space for some representative values of ξ. A large enough positive non-minimal coupling relaxes the isocurvature bounds, allowing for the misalignment mechanism to produce the observed dark matter density for scales of inflation as high as $\sim 10^{13}\,\mathrm{GeV}$ irrespective of the mass of the scalar field. This is in stark contrast to the minimally coupled

[6] As we are only interested in the amplitude of the oscillations of the background field and the fluctuations, any potential phase difference between the two is irrelevant.

[7] As is commonly done, we use the late time behavior of the fluctuations to evaluate this expression. We estimate that this approximation is valid up to a factor $\lesssim 2$.

[8] The isocurvature power spectrum eq. (2.14) has a nonzero spectral index and is uncorrelated with the adiabatic one. Because of this, we use the limit from the "axion II" case in the Planck 2018 [95] CDI scenario.

JCAP02(2020)014

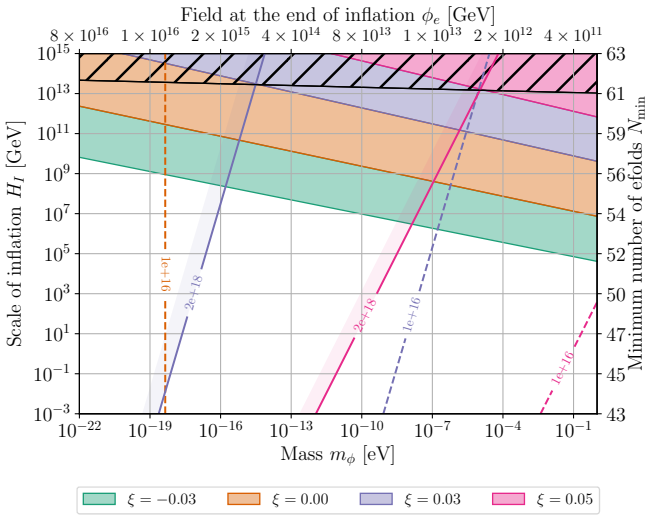

Figure 3. Constraints on the combinations of the inflationary Hubble scale H_I and the mass m_ϕ of the scalar that allow to produce all of the dark matter via the misalignment mechanism. The top axis shows the required field value at the end of inflation whereas the right axis shows the minimal number of e-folds of inflation for a given Hubble scale, as given in eq. (A.2). The colored regions show the exclusions due to isocurvature constraints for some exemplary values of the non-minimal coupling ξ. The lines in the same colors indicate the field value, $\phi_s = M_{\rm pl}$ (solid) and $\phi_s = 10^{16}\,\text{GeV}$ (dashed) at the beginning of inflation under the assumption of minimal inflation. In the black hatched region there exist no values of ξ and $\phi_s < M_{\rm pl}$ for which the misalignment mechanism generates all the dark matter without producing a too large isocurvature component in the CMB.

case, where a low enough inflationary scale is required for the misalignment mechanism to be phenomenologically viable. On the contrary and as expected, a negative ξ strengthens the isocurvature constraints.

2.3 Energy density in fluctuations

In the discussion above we have focused on the production of non-minimally coupled scalar dark matter through the misalignment mechanism. However, as was discussed in [47], inflationary fluctuations of a non-minimally coupled scalar field can also carry a significant energy density. We now briefly review this alternative production mechanism in order to understand the interplay between the misalignment and the fluctuation-based contribution to the dark matter density.

Let us assume that the background homogeneous field value is smaller than the typical fluctuation, in other words, we neglect the energy density generated by misalignment. This is the case if the initial misalignment is too small, or if it gets diluted away by a long period of inflation. To be more precise, any possible initial misalignment is rendered insufficient for dark matter production (cf. eqs. (2.2) and (2.6)) if inflation lasts longer than

$$N_{\rm tot} \gtrsim \frac{1}{\alpha_-}\left(30 + \frac{1}{2}\log\frac{m_\phi}{\text{eV}}\right), \tag{2.15}$$

where we have taken the extreme initial condition $\phi_s \sim M_{\rm pl}$. Looking at figure 3, we see that for non-minimal couplings in the range of interest, $\xi \sim 0.01$, a number of efolds in the 10^2–10^3

JCAP02(2020)014

range is sufficient to effectively dilute any initial homogeneous field value. In this situation and following [47], the energy density stored in the inflationary-generated fluctuations of a non-minimally coupled scalar field is

$$\frac{\Omega_\phi}{\Omega_{\rm DM}} \simeq \frac{3^{\frac{1}{2}(1+\alpha_-)}}{2^{\frac{11}{4}}\pi^2}\,\frac{F(\alpha_-)}{\alpha_-\,(1-\alpha_-)}\,\frac{[\mathcal{F}(T_\star)]^{1+\frac{1}{3}\alpha_-}}{[\mathcal{F}(T_{\rm r})]^{\frac{1}{3}\alpha_-}}\frac{1}{M_{\rm pl}^2}\,H_{\rm eq}^{-\frac{1}{2}}\;H_{\rm I}^{\frac{1}{2}(4-\alpha_-)}\;m^{\frac{1}{2}(\alpha_-+1)}, \tag{2.16}$$

where T_r is the reheating temperature, $H_{\rm eq}$ denotes the Hubble scale at the time of matter-radiation equality and the rest of notation is as described in previous sections. Figure 4 shows the regions of parameter space where this contribution is sizeable, for different values of ξ. It is important to note that the power spectrum of density contrast fluctuations is peaked at the comoving scale

$$k_\star^{-1} \simeq 1.3\cdot 10^{-6}\,{\rm pc}\,\sqrt{\frac{\rm eV}{m_\phi}}, \tag{2.17}$$

which means that the energy density is mainly stored in fluctuations of typical comoving size $k_\star^{-1}$. At larger scales, the power spectrum can be expressed as

$$\mathcal{P}_{\delta_\phi}(k) \simeq \left(\frac{k}{k_\star}\right)^{2\alpha_-}\mathcal{P}_{\delta_\phi}(k_\star), \tag{2.18}$$

which is valid for $0<\alpha_-<1$ and $k<k_\star$. The amplitude of fluctuations at that scale can be computed as

$$\mathcal{P}_{\delta_\phi}(k_\star) \simeq \alpha_-^2(1-\alpha_-)^2\cdot I(\alpha_-), \tag{2.19}$$

where $I(\alpha_-)$ is the integral defined as

$$I(\alpha_-) \equiv \int_{|y-1|<z<y+1}{\rm d}y\,{\rm d}z\,\frac{1}{y^2}\frac{1}{z^2}P(y)P(z), \tag{2.20}$$

with

$$P(x) \equiv \begin{cases} x^{\alpha_-}\,, & x\leq 1 \\ x^{\alpha_--1}\,, & x\geq 1. \end{cases} \tag{2.21}$$

The integral is to be evaluated numerically in order to obtain the size of isocurvature fluctuations at CMB scales using eq. (2.18), which can be confronted with the observational constraints by the Planck satellite [95]. As can be seen in figure 4, a large enough value of the non-minimal coupling $\xi \gtrsim 0.03$ suppresses the large-scales isocurvature fluctuations below the observational limits. One comment is in order: looking at eq. (2.18), one realizes that the isocurvature power spectrum does not directly depend on the scale of inflation. The reason for this is that both the amplitude of field fluctuations and the variance are quadratic in H_I, so the dependence cancels out in the density contrast power spectrum. The apparent dependence on the scale of inflation of figure 4 is only due to the requirement that the relic energy density matches the observed dark matter abundance.

Compared to the production via the misalignement mechanism, dark matter production from fluctuations is typically viable at much larger masses and higher inflationary Hubble scales.

JCAP02(2020)014

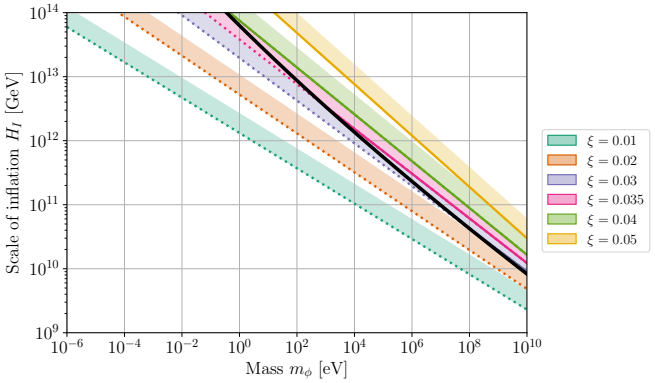

Figure 4. Regions of parameter space where the energy density stored in scalar field fluctuations of inflationary origin makes a sizeable contribution to dark matter. For different choices of the non-minimal coupling ξ, the solid and dotted lines correspond to $\Omega_\phi = \Omega_{\rm DM}$, while in the partially shaded regions to the right (and beyond) dark matter is overproduced. In addition, we show the constraints arising from the non-observation of isocurvature fluctuations at the CMB scales by the Planck satellite [95], the regions to the left of the solid black line (corresponding to the dotted lines) are excluded. Note that this figure assumes no contribution to the relic density from the misalignment mechanism.

2.4 Stochastic scenario

The "stochastic axion" scenario was presented in [38, 39] as a way to generate the dark matter abundance from inflationary fluctuations with wavelengths larger than the current size of the Universe. The accumulation of such fluctuations over a long period of inflation can significantly contribute to the effective homogeneous field in our Hubble patch. This effect can be described as a random walk process of the field value, which receives a "kick" every Hubble time from the modes exiting the horizon during inflation. Working against that is the relaxation of the field towards zero, which is driven by the mass of the scalar. For the following discussion, we take a strict definition of the "stochastic scenario", requiring that equilibrium is reached to a good approximation. In principle, one could also consider situations where equilibrium is not fully attained.

This scenario is also significantly impacted by the inclusion of a non-minimal coupling, which acts as a comparatively large, effective mass during inflation. Our calculation follows along the lines of [39] and generalizes it to be valid for scalars with masses comparable to the scale of inflation. This is important as the effective mass $m_{\rm eff}^2 \equiv m_\phi^2 + \xi R \approx 12\xi H_I^2$ is in general not negligible compared to H_I^2. This fact also requires us to track the evolution of superhorizon modes during the last $N_{\rm min}$ e-folds of inflation. The details of the calculation are presented in appendix B, whereas here we focus on the main results.

Given a long enough inflationary period, the probability distribution of the field value asymptotically approaches a Gaussian distribution with zero mean and variance given by (see eq. (B.9) for the exact expression),

$$\langle \phi_\delta^2 \rangle \simeq \frac{F(\alpha_-)}{\alpha_-} \left(\frac{H_I}{2\pi}\right)^2 \mathrm{e}^{-\alpha_- N_{\rm min}}, \tag{2.22}$$

which is valid for positive ξ. From this, we deduce that the expected typical value of the field at the end of inflation is of order $\sqrt{\langle \phi_\delta^2 \rangle}$. The above expression only sums over the modes

JCAP02(2020)014

which are superhorizon today, as those are the ones that contribute to the homogeneous field value in the observable Universe. The first part of eq. (2.22) accounts for the generation and accumulation of fluctuations, while the last factor describes the evolution of the field during the last $N_{\rm min}$ e-folds of inflation. This late time exponential relaxation towards zero is relevant due to the fast evolution driven by the non-minimal coupling to gravity.

In the stochastic scenario, the field "loses" memory of the preinflationary initial condition and the observable misalignment angle in each Hubble patch is chosen randomly from the distribution described by eq. (2.22). Critically, if the effective mass during inflation is large, equilibrium can be reached much faster than in the minimally coupled scenario studied in [38, 39]. As is shown in appendix B, an extra number of e-folds of inflation $\Delta N \equiv N_{\rm tot} - N_{\rm min} > 1/\alpha_-$ on top of the minimum is necessary for equilibrium to be attained. In addition to this, to reach the purely stochastic regime the variance induced by fluctuations has to become larger than the exponentially decaying field value originating from the initial homogeneous ϕ_s. If we require the induced field value to be a factor of γ larger, we get

$$\Delta N > \frac{1}{\alpha_-} \ln \left[\gamma \frac{2^{2+\alpha_-}\pi^3}{\Gamma^2\left(\frac{3-\alpha_-}{2}\right)} \frac{\alpha_-}{(\alpha_+ - \alpha_-)^2} \left(\frac{\dot{\phi}_s}{H_I^2} + \frac{1}{2}\alpha_+ \frac{\phi_s}{H_I} \right)^2 + 1 \right]. \tag{2.23}$$

The two results in eqs. (2.22) and (2.23) generalize the ones found in [38, 39], allowing for arbitrary initial conditions and large effective masses.

The stochastic scenario is also prone to generating too much isocurvature fluctuations at the CMB scales. From the point of view of subhorizon modes, the homogeneous field value generated in the stochastic regime is indistinguishable from one originating from a homogeneous initial condition. This implies that eq. (2.14) also holds in the stochastic case, which allows us to express the isocurvature component as

$$\mathcal{P}_{\delta_\phi}(k_{\rm CMB}) \simeq 4\alpha_- \, \mathrm{e}^{\alpha_-(N_{\rm min} - N_{\rm CMB})}. \tag{2.24}$$

The exponential factor arises due to the slight difference between the largest observable scale and the ones that are accessible at the CMB, which corresponds to about 7 e-folds (see appendix A). As long as α_- is small, this is a small correction and the result is dominated by the factor in front. It is easy to understand where this factor comes from: comparing eq. (2.22) with eq. (2.8), we see that the accumulated field variance of a large number of superhorizon modes in enhanced by a factor of $1/\alpha_-$ with respect to the amplitude of the fluctuations of an individual mode. Given the Planck [95] constraint on isocurvature fluctuations $\mathcal{P}_I(k_{\rm CMB}) \lesssim 10^{-9}$, we conclude that the stochastic scenario can only be realized for very small values of the non-minimal coupling of order $\xi \lesssim 10^{-10}$. This should apply to any model in which the effective mass is non-negligible compared to H_I, independently of the origin of $m_{\rm eff}$.

3 Vectors

After having discussed the misalignment, stochastic and fluctuations scenario for a scalar field, let us now turn to the vector case and see how these scenarios can be realized there.

3.1 Homogeneous vector field and relic density

Starting from the action eq. (1.2), we derive the EOMs for the homogeneous field [6, 56, 57]

$$\chi_0 = 0 \quad \text{and} \quad \ddot{\chi}_i + 3H\dot{\chi}_i + \left(m_\chi^2 + \frac{1-\kappa}{6} R \right) \chi_i = 0, \tag{3.1}$$

JCAP02(2020)014

which are given in terms of the physical field $\chi_\mu \equiv X_\mu/a$, so that the energy density can (for an approximately homogeneous field) be written as [6, 56, 57]

$$\rho_\chi = \sum_{i=1}^{3} \left[\frac{1}{2}\dot{\chi}_i^2 + \frac{1}{2}m_X^2\chi_i^2 + (1-\kappa)\left(\frac{1}{2}H^2\chi_i^2 + H\dot{\chi}_i\chi_i\right)\right]. \tag{3.2}$$

The advantage of this field redefinition is that the EOM for each of the spatial components coincides with the scalar one, eq. (2.1), after the identification

$$\frac{(1-\kappa)}{6} \longleftrightarrow \xi. \tag{3.3}$$

In particular, a non-minimally coupled vector with $\kappa = 1$ behaves as a scalar with a minimal coupling to gravity ($\xi = 0$). Because of this correspondence, the discussion of the misalignment mechanism made in section 2.1 carries over to the vector case, as do all the evolution equations (cf. eq. (2.3) ff.). Let us then simply rewrite the main results using the notation of this section. The relic density of vectors can be expressed as

$$\frac{\Omega_\chi}{\Omega_{\rm DM}} \simeq 5\,\mathcal{F}(T_\star)\left(\frac{\chi_e}{10^{12}\,\mathrm{GeV}}\right)^2\sqrt{\frac{m_X}{\mathrm{eV}}}, \tag{3.4}$$

where we denote $\chi \equiv |\vec{\chi}|$. As in the scalar case, the field value at the end of inflation χ_e is different than the initial one χ_s due to the superhorizon evolution caused by the coupling to R. Both are related by

$$\chi_e \simeq \chi_s\,\mathrm{e}^{-\frac{1}{2}\beta_- N_{\rm tot}}, \tag{3.5}$$

with an analogous definition[9] to the scalar case,

$$\beta_\pm \equiv 3 \pm \sqrt{1+8\kappa}. \tag{3.6}$$

Note that we are using the conventions described in section 2.1 for the field value at the beginning of inflation. Depending on whether κ is larger or smaller than one, there can be a substantial enhancement or suppression of the homogeneous field value during inflation. As in the scalar case, an absolute limit can be placed on $\kappa > 1$, independently of the dark matter assumption, by avoiding a trans-Planckian field excursion. Using the identification of eq. (3.3), this limit is analogous to the one for scalars. Both are shown simultaneously in figure 2.

3.2 Vector fluctuations and isocurvature perturbations

Like a scalar field, a vector field present during inflation acquires a spectrum of isocurvature perturbations. We now study the role of the non-minimal coupling in the generation and evolution of such fluctuations.

3.2.1 Generation during inflation

For vectors, the situation is similar to the scalar case, albeit a bit more complex due to the multicomponent nature of the field. The best way to deal with the perturbations is to split them into transverse ($\perp$) and longitudinal ($\parallel$) modes and address each polarization separately.

[9] The parameter β_- defined here is related to ν used in [57, 58] by $\beta_- = 3 - 2\nu$, neglecting terms of $\mathcal{O}(m_X/H_I)$.

JCAP02(2020)014

Transverse fluctuations. The EOMs of the fluctuations in momentum space and for the two transverse polarizations $\delta\chi_i^\perp$ read

$$\ddot{\delta\chi_i}^\perp + 3H\dot{\delta\chi_i}^\perp + \left(m_X^2 + \frac{1-\kappa}{6}R + \frac{k^2}{a^2}\right)\delta\chi_i^\perp = 0, \tag{3.7}$$

which is identical to the expression in the scalar case (cf. [47]) with $(1-\kappa)/6 \leftrightarrow \xi$. We can therefore directly translate the results of section 2.2: the power spectrum for non-vanishing momentum modes outside the horizon ($0 \neq k \ll aH_I$) is

$$\mathcal{P}_{\chi_i}^\perp(k,a) = \left(\frac{H_I}{2\pi}\right)^2 F(\beta_-)\left(\frac{k}{aH_I}\right)^{\beta_-}, \tag{3.8}$$

with $F(\cdot)$ as defined in eq. (2.9).

Longitudinal fluctuations. In this case, the discussion is simplified by making use of conformal time τ and of the field redefinition $f \equiv a^2\,\delta\chi^\parallel = a\,\delta X^\parallel$. The full EOM for the mode functions then reads

$$f'' - \frac{2}{\tau}\frac{2\kappa}{k^2\tau^2 - 2\kappa}f' + k^2\left(1 - \frac{2\kappa}{k^2\tau^2} - \frac{2}{k^2\tau^2 - 2\kappa}\right)f = 0 \tag{3.9}$$

where we have assumed that $m_X^2 \ll H_I^2$ so that the bare mass has been neglected. It can easily be reinstated by substituting $\kappa \to \kappa - m_X^2/(12H_I^2)$ at any point in the derivation. Although we are not able to solve eq. (3.9) analytically, we can study its most relevant limits.

- *Subhorizon limit* $|k\tau| \gg 1$. The mode equation simplifies in this limit to

$$f'' + k^2 f = 0. \tag{3.10}$$

  We recognize the equation of motion of a harmonic oscillator in Minkowski space: as expected, the mode functions in the deep subhorizon limit can be described as quantum fluctuations of the vacuum. This allows us to set the initial condition for the evolution,

$$f(\tau \to -\infty) = \frac{1}{\sqrt{2k}}\mathrm{e}^{-ik\tau}, \tag{3.11}$$

  which is the usual Bunch-Davies vacuum. Note that the units of Fourier transformed fields differ from the ones in position space by a factor of $[\text{mass}]^{3/2}$.

- *Superhorizon limit* $|k\tau| \ll 1$. The mode equation now becomes

$$\frac{\mathrm{d}^2 f}{\mathrm{d}y^2} + \frac{2}{y}\frac{\mathrm{d}f}{\mathrm{d}y} - \frac{2\kappa}{y^2}f = 0, \tag{3.12}$$

  where $y \equiv |k\tau|$. This can be solved analytically and we can express the general solution as

$$f = C_1\, y^{\left(-1+\sqrt{1+8\kappa}\right)/2} + C_2\, y^{\left(-1-\sqrt{1+8\kappa}\right)/2}. \tag{3.13}$$

  The second exponent is always smaller that the first one, so the second term dominates at late enough times (for $y \ll 1$). Recovering the physical field and scale factors, we have

$$\delta\chi^\parallel \simeq C_2'\, 2^{1-\frac{1}{2}\beta_-}\frac{H_I}{k^{3/2}}\left(\frac{k}{aH_I}\right)^{\frac{1}{2}\beta_-}. \tag{3.14}$$

JCAP02(2020)014

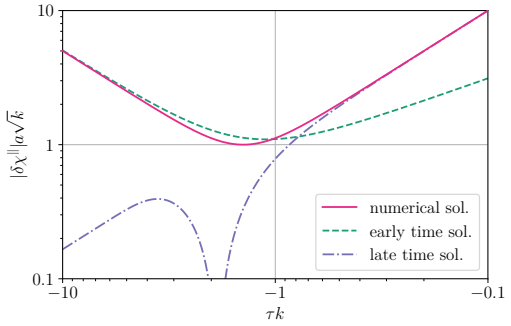

Figure 5. Evolution of the early time, late time and numerical solution to the full mode equation in conformal time (cf. appendix C) for $\kappa = 1$. The value of C_2' is chosen such that for late times the numerical solution agrees with the late time solution.

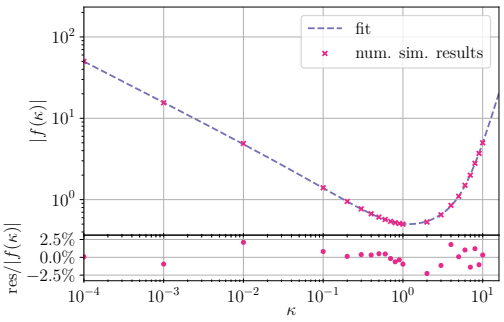

Figure 6. Numerical results (C_2' values), determined from figures similar to figure 5, and corresponding fit function $|f(\kappa)|$ shown together with the relative deviation of the fit function (residuals) from the numerical results underneath. The fit function for $|f(\kappa)|$ is given in eq. (3.15).

The chosen normalization is motivated by the more detailed calculation[10] presented in appendix C. Importantly, this superhorizon solution has the same time dependence as the solution for the homogeneous field and the transverse polarization.

- *Intermediate regime* $|k\tau| \sim 1$. Here we have no choice but to solve the full mode equation. As an analytic solution for it is hard to come by in this regime, we solve it numerically to connect the sub- and superhorizon expressions and determine C_2'. As expected, we find a dependence of C_2' on κ and we use the numerical solution to determine a fitting function $C_2' \equiv |f(\kappa)|$. A particular example for the numerical evaluation and the matching of the analytic asymptotic results in the case of $\kappa = 1$ is shown in the left panel of figure 5 (cf. appendix C for the relevant formulas). Extracting several values of C_2' in the range $\kappa \in [10^{-4}, 10]$, which extensively covers our region of interest, we determine an accurate fit to the numerical results. It is given by

$$|f(\kappa)| = 0.502\kappa^{-0.5} - 0.224 + 0.262\kappa - 0.0411\kappa^2 + 0.00654\kappa^3, \tag{3.15}$$

which is depicted together with the residuals in the right panel of figure 6.

Putting it all together, the expression for the power spectrum of the longitudinal fluctuations can be written as

$$\mathcal{P}_{\chi}^{\parallel}(k,a) \simeq 2^{3-\beta_-}|f(\kappa)|^2 \left(\frac{H_I}{2\pi}\right)^2 \left(\frac{k}{aH_I}\right)^{\beta_-}, \tag{3.16}$$

which is valid for superhorizon modes with $k \neq 0$. Comparing with the expression for the transverse fluctuations eq. (3.8), we find the relation

$$\mathcal{P}_{\chi}^{\parallel} = \frac{2\pi|f(\kappa)|^2}{\Gamma^2\left(\frac{3-\beta_-}{2}\right)}\mathcal{P}_{\chi_i}^{\perp}. \tag{3.17}$$

[10]Note that here we use the redefined field $f = a\delta X^{\parallel}$ to keep the notation as slim as possible, whereas in appendix C, where we present the full detailed calculation, we work with the field $\delta X^{\parallel}$, making it easier to determine the most useful normalization.

JCAP02(2020)014

This generalizes the result found in [58, 59] for $\kappa = 1$, for which the relation $\mathcal{P}_\chi^{\parallel} \simeq 2\,\mathcal{P}_{\chi_i}^{\perp}$ is recovered.

We conclude that the primordial power spectrum of the longitudinal fluctuations is proportional to the one of the transverse fluctuations. In particular, for values of κ close to unity, the proportionality factor is of $\mathcal{O}(1)$. However, as we will now see, the post-inflationary evolution of the two modes can significantly differ.

3.2.2 Evolution after inflation

We now discuss the evolution of the primordial fluctuation power spectrum generated during inflation throughout the different epochs in the history of the Universe until today. As in the previous section, we differentiate between transverse and longitudinal modes.

Transverse fluctuations. The EOMs for the two perpendicularly polarized modes are

$$\ddot{\delta\chi_i}^{\perp} + 3H\dot{\delta\chi_i}^{\perp} + \left(m_X^2 + \frac{1-\kappa}{6}R + \frac{k^2}{a^2}\right)\delta\chi_i{}^{\perp} = 0, \tag{3.18}$$

which after the substitution $\kappa \to 1 - 6\xi$ are the same as for the scalar perturbations: the transverse fluctuations thus evolve in the same way as the fluctuations of a scalar field. We conclude that, for large scales like the CMB ones, the ratio between the transverse fluctuations and the homogeneous field stays constant throughout the cosmological evolution. This implies that the density contrast power spectrum can be evaluated at any point, such as right after horizon exit. Doing so and adding up the two transverse polarizations, we find

$$\mathcal{P}_{\delta_\chi}^{\perp}(k_{\rm CMB}) \simeq \frac{8}{\chi_e^2\,\mathrm{e}^{\beta_- N_{\rm CMB}}}\left(\frac{H_I}{2\pi}\right)^2 F(\beta_-). \tag{3.19}$$

As expected, we encounter the same suppression (for $\kappa < 1$) or enhancement (for $\kappa > 1$) in the isocurvature perturbations as in the scalar case.

Longitudinal fluctuations. The full EOM in this case is more complicated, but it greatly simplifies during the radiation domination epoch when $R = 0$, or whenever we can neglect R, $\dot{R} \ll m_X^2$, yielding

$$\ddot{\delta\chi}^{\parallel} + \left(3 + \frac{2k^2}{k^2 + a^2 m_X^2}\right)H\dot{\delta\chi}^{\parallel} + \left(\frac{2k^2}{k^2 + a^2 m_X^2}H^2 + \frac{k^2}{a^2} + m_X^2\right)\delta\chi^{\parallel} = 0. \tag{3.20}$$

As long as reheating proceeds almost instantaneously, which we assume to be the case, this simplified version of the EOM is adequate to study the full post-inflationary evolution. Comparing eq. (3.20) with eq. (3.18), it becomes clear that the behaviour of longitudinal perturbations can significantly differ from the one of transverse (and scalar) ones. Let us focus on large scale modes that become non-relativistic before they reenter the horizon, as these are the ones relevant for CMB observables. These modes evolve through three distinct regimes:

(i) $H \gg k/a \gg m_X$. In the superhorizon and relativistic limit, eq. (3.20) further simplifies to

$$\ddot{\delta\chi}^{\parallel} + 5H\dot{\delta\chi}^{\parallel} + 2H^2\delta\chi^{\parallel} = 0, \tag{3.21}$$

which is solved by

$$\delta\chi^{\parallel} \simeq c_1' a^{-1} + c_2' a^{-2}. \tag{3.22}$$

The physical field thus redshifts as $1/a$. The modes corresponding to the largest scales might not enter this regime at all if they become non-relativistic before the end of inflation, i.e. if they violate $k/a_r \gg m_X$. Therefore, the condition for the CMB modes to skip this regime is

$$m_X \gtrsim \frac{k_{\rm CMB}}{a_r} \simeq 2 \cdot 10^{-4}\,{\rm eV}\sqrt{\frac{H_I}{6.6 \cdot 10^{13}\,{\rm GeV}}}, \tag{3.23}$$

where $k_{\rm CMB}$ is a typical CMB scale, which we take to be the Plank pivot scale $k_{\rm CMB} = 0.05\,{\rm Mpc}^{-1}$, and a_r is the scale factor at reheating, given by $a_r = {\rm e}^{-N_{\rm min}(H_I)}$ under the assumption of instantaneous reheating. We conclude that if $m \gtrsim 10^{-4}\,{\rm eV}$, the CMB modes do not enter regime (i) if inflation happens at the highest scale compatible with the limit from the non observation of tensor modes [95], $H_I < 6.6 \cdot 10^{13}\,{\rm GeV}$. For lower values of H_I, this condition shifts to lower and lower masses.

(ii) $H \gg m_X \gg k/a$. Modes are superhorizon but already non-relativistic, which allows to approximate eq. (3.20) by

$$\ddot{\delta\chi}^{\parallel} + 3H\dot{\delta\chi}^{\parallel} = 0, \tag{3.24}$$

and to obtain the solution

$$\delta\chi^{\parallel} \simeq c_1'' + c_2'' a^{-1}. \tag{3.25}$$

In principle, it seems that the constant mode would dominate the solution.[11] In the absence of a non-minimal coupling, the authors of [42] argue that this is actually not the case, because $c_1'' \ll c_2''$ and the constant mode can be dropped. The reason for this is that in region (i) the solution becomes $\propto a^{-1}$ to great accuracy, and continuity of the solution and the first derivative imposes a large hierarchy between the two coefficients. This is not necessarily the case when a non-minimal coupling is present, because during inflation the superhorizon modes are not frozen and $\dot{\chi}_e \neq 0$ as eq. (2.7) indicates. As a consequence, the "flattening" of the mode functions is either weakened or not applicable at all depending on how long the CMB modes spend in region (i), if they enter it at all.

On the one hand, if region (i) is skipped, that is, if the CMB modes become non-relativistic before the end of inflation, then there is no suppression. On the other hand, if $m_X \lesssim k_{\rm CMB}/a_r$ and the CMB modes enter region (i), i.e. they are still relativistic once radiation domination starts, then we expect some suppression of the power spectrum at those scales. By carefully matching the field value and its first derivative through the regimes (i) and (ii), we obtain that

$$\delta\chi^{\parallel}(k_{\rm CMB}, a_{\rm (ii)}) \simeq \left(\frac{m_X}{k_{\rm CMB}/a_r}\right)^2 \delta\chi^{\parallel}(k_{\rm CMB}, a_r), \tag{3.26}$$

where $a_{\rm (ii)}$ denotes the scale factor at the end of region (ii).

(iii) $m_X \gg H,\, k/a$. Modes become massive enough to overcome Hubble friction, and we recover the usual pressureless-matter like EOM

$$\ddot{\delta\chi}^{\parallel} + 3H\dot{\delta\chi}^{\parallel} + m_X^2\delta\chi^{\parallel} = 0, \tag{3.27}$$

which is identical to the scalar case, as was already discussed for the homogeneous field and the transverse polarizations.

JCAP02(2020)014

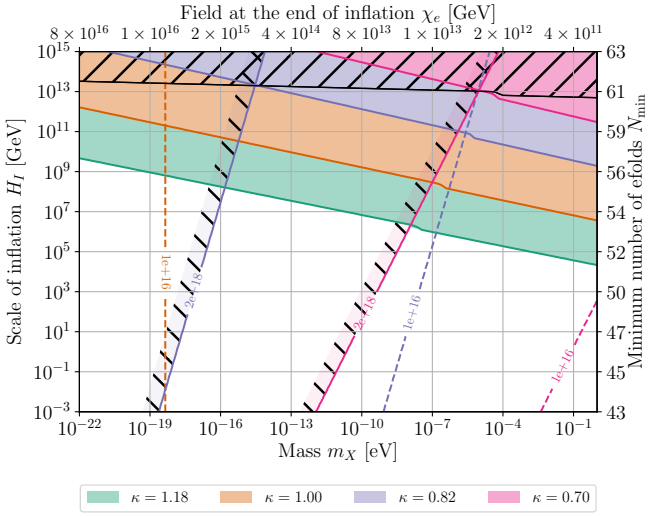

Figure 7. Parameter space showing the ability of a non-minimally coupled vector field to generate the observed dark matter abundance through the misalignment mechanism, as a function of its mass and the Hubble scale of inflation. This figure should be interpreted in the same way as figure 3. The kink in the isocurvature limits is due to the fact that longitudinal modes are only relevant for large enough masses, see eq. (3.28).

We conclude that except for the potential suppression factor of eq. (3.26), the evolution of longitudinal modes is analogous to that of the transverse ones, allowing us to write

$$\mathcal{P}^{\parallel}_{\delta_\chi}(k_{\rm CMB}) \simeq \frac{1}{2}\,\mathcal{P}^{\perp}_{\delta_\chi}(k_{\rm CMB})\cdot\frac{2\pi|f(\kappa)|^2}{\Gamma^2\left(\frac{3-\beta_-}{2}\right)}\cdot\begin{cases}1, & \text{if } m \gtrsim k_{\rm CMB}/a_r\\ \left(\frac{m}{k_{\rm CMB}/a_r}\right)^4, & \text{if } m \lesssim k_{\rm CMB}/a_r.\end{cases} \tag{3.28}$$

The total density contrast is the sum of the contributions from all the polarizations, so that

$$\mathcal{P}_{\delta_\chi}(k_{\rm CMB}) = \mathcal{P}^{\perp}_{\delta_\chi}(k_{\rm CMB}) + \mathcal{P}^{\parallel}_{\delta_\chi}(k_{\rm CMB}). \tag{3.29}$$

In analogy to the scalar case, figure 7 shows the Planck [95] isocurvature constraints in the (m_X, H_I) parameter space for selected values of κ. The conclusion is similar to the scalar case: as long as $H_I \lesssim 10^{13}\,\text{GeV}$, vector dark matter produced from the misalignament mechanism is compatible with isocurvature constraints provided a non-minimal coupling $\kappa \lesssim 1$ is present.

3.3 Energy density in fluctuations

Given the correspondence between transverse vector fluctuations and scalar ones, it is expected that the energy density stored in small scale fluctuations can also be important here. In addition to that and as a particularity of the vector case, the authors of [42] (see [72] as well) showed that longitudinal vector fluctuations can be copiously produced during inflation also for $\kappa = 0$.

As already discussed, the behaviour of the transverse modes is exactly the same as that of a scalar field after the identification $(1-\kappa)/6 \leftrightarrow \xi$. At the same time, when $\kappa \sim 1$, the

[11] Note that in terms of $\delta X_i^{\parallel}$ this would correspond to a growing mode. However, as the physical field is the one that controls the density perturbations, there is no real growth of fluctuations in this regime.

JCAP02(2020)014

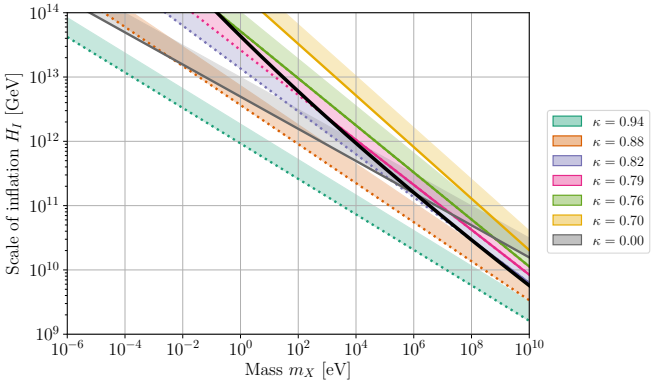

Figure 8. Regions of parameter space where the energy density stored in vector field fluctuations of inflationary origin makes a sizeable contribution to dark matter. This figure should be interpreted in the same way as figure 4, with the addition of the grey line, which corresponds to the contribution of longitudinal fluctuations in the case of a minimal coupling $\kappa = 0$, as was computed in [42] (the presence of a small enough non-minimal coupling as in eq. (3.31) is permitted; in this case the isocurvature constraints are also different and the full grey line is viable). We remind the reader that this figure assumes no contribution to the relic density from the misalignment mechanism.

contribution from longitudinal modes at small scales around the peak at $k_\star^{-1}$ is suppressed due to the particularities of the post inflationary evolution described in the previous section. The easiest way to understand why the suppression at small scales is even stronger than at CMB scales is by replacing $k_{\rm CMB}$ by the much larger $k_\star$ in eq. (3.28). All this means that the discussion in section 3.2 carries over: the inflationary (transverse) fluctuations of a non-minimally coupled vector field can carry enough energy density to reproduce the observed dark matter abundance. As can be seen in figure 8, the region of parameter space where this production is viable corresponds to relatively high-scale inflation, masses above roughly eV and non-minimal couplings κ moderately smaller than 1.

The contribution from longitudinal modes is however relevant for minimally coupled fields, i.e. when $\kappa = 0$, as was discussed in [42, 72]. The relic density that is generated in this case is given by

$$\frac{\Omega_X}{\Omega_{\rm DM}} \simeq \sqrt{\frac{m_X}{3\cdot 10^{-5}\,{\rm eV}}}\left(\frac{H_I}{6.6\cdot 10^{13}\,{\rm GeV}}\right)^2 . \tag{3.30}$$

This is in contrast to misalignment and transverse fluctuations, whose contribution is completely negligible in the minimally coupled case. Longitudinal modes are very strongly suppressed at CMB scales due to the smoothing of the field that occurs during inflation when $\kappa = 0$. However, the presence of even a small non-minimal coupling can significantly weaken this suppression. This is due to the fact that the modes describing the fluctuations have an $\mathcal{O}(\kappa)$ time derivative at the end of inflation, similarly to the homogeneous field value (cf. eq. (2.7)). Taking this into account and carefully matching the solutions of the EOMs in the different regimes, we find that the amplitude of the power spectrum at CMB scales can be approximately computed as

$$\frac{\mathcal{P}_\delta(k_{\rm CMB})}{\mathcal{P}_\delta(k_\star)} \simeq \kappa^2\left(\frac{k_{\rm CMB}}{m_X\cdot a_r}\right)^{2-4\kappa} \simeq 1.7\cdot 10^3\,\kappa^2\left(\frac{6\cdot 10^{-6}\,{\rm eV}}{m_X}\right)^{\frac{9}{4}(1-2\kappa)} , \tag{3.31}$$

JCAP02(2020)014

which is valid for sufficiently small but non-vanishing κ. Taking into account that the power spectrum is of $\mathcal{O}(1)$ at the peak, i.e. $\mathcal{P}_\delta(k_\star) \sim 1$, and applying the Planck constraint [95] on isocurvature perturbations $\mathcal{P}_\delta(k_{\rm CMB}) < 1.3{\cdot}10^{-9}$, we conclude that the non-minimal coupling is bound to be very small if the vector is light. For instance, a mass of $m_X \sim 10^{-6}\,\mathrm{eV}$ requires $\kappa \lesssim 10^{-6}$. If this condition is satisfied, a high inflationary scale allows for generation of sub-eV vector dark matter in this case, as can be seen in figure 8.

3.4 Stochastic scenario

In analogy to the scalar case discussed in section 2.4, the stochastic scenario can also be realized for a vector field with a non-minimal coupling to gravity. Once more, the calculation is simplified by considering the contribution from transverse and longitudinal fluctuations separately. As expected, transverse modes behave like scalar ones with the usual replacements $\alpha_\pm \leftrightarrow \beta_\pm$ and $\xi \leftrightarrow (1-\kappa)/6$. Following appendix B and once equilibrium is reached, the variance of the transverse superhorizon fluctuations is given by

$$\left\langle {\chi_\delta^\perp}^2 \right\rangle \simeq 2\,\frac{F(\beta_-)}{\beta_-}\left(\frac{H_I}{2\pi}\right)^2 \mathrm{e}^{-\beta_- N_{\rm min}}, \tag{3.32}$$

where the factor of 2 accounts for the two transversal polarizations. For the longitudinal fluctuations, we make use of the results of section 3.2 to write the mode functions as

$$\delta\chi^\parallel \simeq |f(\kappa)|\,2^{1-\frac{1}{2}\beta_-}\,\frac{H_I}{k^{3/2}}\left(\frac{k}{aH_I}\right)^{\frac{1}{2}\beta_-}, \tag{3.33}$$

which is valid after horizon exit during inflation. The variance of the Gaussian distribution of the longitudinal field fluctuations can also be found by integrating over the superhorizon contributions.[12] At the end of inflation, both transverse and longitudinal contributions are of the same size. However, the post-inflationary evolution is different for each polarization. Because of the flattening of the wavefunctions described in section 3.2 (cf. also [42]), longitudinal modes will be suppressed unless

$$m_X \gtrsim \frac{k_0}{a_r} \sim 10^{-7}\,\mathrm{eV}\sqrt{\frac{6.6\cdot 10^{13}\,\mathrm{GeV}}{H_I}}, \tag{3.34}$$

where $k_0^{-1} \sim 10\,\mathrm{Gpc}$ is the size of the observable Universe. The variance of superhorizon longitudinal fluctuations is thus

$$\left\langle {\chi_\delta^\parallel}^2 \right\rangle \simeq \frac{1}{2}\left\langle {\chi_\delta^\perp}^2 \right\rangle \cdot \frac{2\pi|f(\kappa)|^2}{\Gamma^2\left(\frac{3-\beta_-}{2}\right)} \cdot \begin{cases} 1, & \text{if } m \gtrsim k_0/a_r \\ \left(\frac{m}{k_0/a_r}\right)^4, & \text{if } m \lesssim k_0/a_r. \end{cases} \tag{3.35}$$

The total variance is obtained by adding up the contributions from both polarizations,

$$\left\langle {\chi_\delta}^2 \right\rangle = \left\langle {\chi_\delta^\perp}^2 \right\rangle + \left\langle {\chi_\delta^\parallel}^2 \right\rangle, \tag{3.36}$$

so that the typical field value is given in the stochastic regime by $\sqrt{\langle {\chi_\delta}^2\rangle}$.

[12] Note that the integral eq. (B.7) is dominated by the upper limit, which means that the variance is dominated by the smallest superhorizon modes.

JCAP02(2020)014

As in the scalar case, the stochastic regime is only reached if inflation lasts for an extra ΔN e-folds in addition to $N_{\rm min}$. On the one hand, $\Delta N > 1/\beta_-$ is required for the random walk process to attain equilibrium. On the other hand, dominance (by a factor of γ) of the variance of the stochastic distribution over any remnant of the initial field value χ_s sets the additional constraint

$$\Delta N > \frac{1}{\beta_-}\ln\left[\gamma\left(\frac{\pi|f(\kappa)|^2}{\Gamma^2\left(\frac{3-\beta_-}{2}\right)}+1\right)^{-1}\frac{2^{1+\beta_-}\pi^3}{\Gamma^2\left(\frac{3-\beta_-}{2}\right)}\frac{\beta_-}{(\beta_+-\beta_-)^2}\left(\frac{\dot{\phi}_s}{H_I^2}+\frac{1}{2}\beta_+\frac{\phi_s}{H_I}\right)^2+1\right]. \quad (3.37)$$

Because the stochastic scenario does not modify the last $N_{\rm min}$ e-folds of inflation, isocurvature constraints can be computed in the same way as for the misalignment mechanism. Using eqs. (3.29), (3.32) and (3.35), we find that the density contrast power spectrum at CMB scales is given by

$$\mathcal{P}_\delta(k_{\rm CMB}) \sim 4\,\beta_-\,{\rm e}^{\beta_-(N_{\rm min}-N_{\rm CMB})}, \quad (3.38)$$

where we have neglected a small effect coming from the different scale dependence (k_0 vs $k_{\rm CMB}$) of the longitudinal power spectrum: see the difference between eq. (3.35) and eq. (3.28). This equation highlights the fact that the accumulated variance is enhanced by a factor of $1/\beta_-$ with respect to that of each individual mode. The need for a strong suppression of the CMB isocurvature makes it hard to realize a stochastic scenario for $\kappa \neq 1$. Indeed, the Planck [95] constraint translates into a limit $1-\kappa \lesssim 10^{-10}$ on the deviation of the non-minimal coupling from the scalar-like value.

4 Conclusions and outlook

In the present paper we have considered light (pseudo-)scalar and vector fields with couplings to the curvature/Ricci scalar as candidates for dark matter. The main impact of these couplings occurs during inflation when they give a contribution to the mass of the fields. The effective mass is then typically of the order of the Hubble scale, leading to a non-trivial evolution of both the field and the fluctuations during inflation. This evolution during inflation impacts all three possible non-thermal scenarios for the production of the dark matter density: misalignment [1–3, 5–7], stochastic [38–41] and fluctuation [42–47] production. After inflation, the Ricci scalar vanishes during radiation domination and the evolution proceeds in the standard way.

For (pseudo-)scalars, even relatively small positive vales of $\xi \lesssim \mathcal{O}(0.1)$ open up sizeable areas in parameter space for the *misalignement* mechanism due to the suppression of isocurvature fluctuations at the CMB scales. In the opposite direction, negative values of $\xi \lesssim -4$ are excluded or require stabilization by an additional term in the potential because the induced tachyonic mass produces trans-Planckian field excursions, even for the smallest possible values of the inflationary Hubble scale (for high-scale inflation, this occurs for much smaller couplings, $\xi \lesssim -0.1$).

For high scale inflation and larger masses above $\sim 1\,{\rm eV}$, the energy density stored in small-scale fluctuations of the scalar field becomes sizeable up to the point where it can account for the entire observed dark matter density. In this situation, dark matter is produced from *fluctuations* of the field generated during inflation, long after the CMB modes exit the horizon. The presence of a non-minimal coupling $\xi \gtrsim 0.03$ suppresses fluctuations at large scales, avoiding the Planck isocurvature constraints and leading to a peaked density contrast power spectrum [47].

JCAP02(2020)014

Finally, assuming that inflation lasts for a sufficiently long time, the accumulation of superhorizon fluctuations with wavelengths larger than the size of the visible Universe can dominate the observable homogeneous field over any initial condition. In this stochastic scenario, the homogeneous field value for the post-inflationary evolution in our Hubble patch is chosen probabilistically from a Gaussian distribution whose variance is controlled by the curvature coupling ξ. In order for the super Hubble variance to grow sufficiently large and avoid isocurvature constraints, the minimal coupling is required to be very small, $\xi \lesssim 10^{-10}$, while the number of e-folds of inflation has to be larger than $\sim 1/(8\xi) \sim 10^9$.

A massive vector can also act as dark matter and is subject to production through the same three mechanisms as a scalar. The cosmological evolution of the homogeneous component of a vector field with curvature coupling κ is found to mimic that of the scalar field after the identification $\kappa \leftrightarrow 1-6\xi$. Consequently, the misalignment mechanism proceeds in the usual way, with the distinction that the minimally coupled scalar corresponds to a non-minimally coupled vector with $\kappa = 1$. It should however be noted that the massive vector acquires a longitudinal polarization whose kinetic term is rendered negative for a finite range of momenta due to the presence of the non-minimal coupling. A detailed study of how this sign flip affects the stability of the vacuum, along the lines of [59, 92–94], is left for future work.

The discussion of vector fluctuations is most easily carried out by considering transverse and longitudinal polarizations separately. As for the homogeneous field and due to their approximate conformal symmetry, transverse fluctuations behave like scalar fluctuations with the identification of curvature couplings mentioned in the previous paragraph. This means that in the misaligned regime, isocurvature constraints are weakened[13] if $\kappa \lesssim 1$. The phenomenologically interesting region where misalignment production is viable even for high scale inflation corresponds to $1-\kappa$ being $\mathcal{O}(0.1)$. The vector DM production from transverse fluctuations and the stochastic scenario are also viable and proceed in a manner analogous to the scalar case.

The longitudinal mode, however, presents a number of particularities with respect to the transverse ones. In the misalignment mechanism and owing to the differences both in its inflationary and post-inflationary evolution, the longitudinal mode is shown to be suppressed if the vector is very light. However, when it is heavier than $10^{-4}\,\mathrm{eV}$ (or less depending on the scale of inflation), the contribution of longitudinal modes to the isocurvature spectrum at CMB scales is of the same size as that of the transverse ones and cannot be neglected. The situation of the production from inflationary fluctuations is also interesting. While small-scale longitudinal fluctuations are always suppressed when $\kappa \sim 1$, in the case of a minimally coupled vector their amplitude can be large enough to contain an energy density comparable to that of the DM, provided inflation occurs at a high scale. We show that the viability of this scenario strictly relies on the almost complete absence of a non-minimal coupling; for instance, a $\kappa \gtrsim 10^{-6}$ spoils the mechanism if $m_X \sim 10^{-6}\,\mathrm{eV}$.

Throughout this paper we have considered the inflationary epoch of our Universe to be a perfect de Sitter expansion with constant H_I. However, the observation of a slight scale dependence in the fluctuation spectrum at CMB scales [95] indicates that H_I is a slowly decreasing function of time. As long as this spectral tilt remains small,[14] the results of this

[13] A tachyonic mass for the vector is generated during inflation if $\kappa > 1$. In analogy to the scalar case, avoiding trans-Planckian field excursions sets strong constraints on the size of the curvature coupling.

[14] The spectral index of adiabatic modes has only been measured around the scales accessible in the CMB. Without more observational guidance, it is reasonable to make the assumption that n_s remains small during most of inflation. A full discussion of the physical consequences of large variations in H_I is an interesting topic, but one that lies beyond the scope of this work.

JCAP02(2020)014

work are not changed qualitatively. Quantitatively, the effect of the spectral tilt can be compensated by a shift to slightly larger (for scalars) or smaller (for vectors) values of the non-minimal coupling.

Non minimal curvature couplings allow for the generation of light (pseudo-)scalar or vector dark matter in a wide range of masses. The three different production mechanisms complement each other in terms of their viability in different regions of parameter space. This opens up exciting possibilities for experiments and potentially interesting interactions between the physics of dark matter and inflation.

Acknowledgments

We would like to thank Fuminobu Takahashi, Manuel Reichert, Tommi Markkanen and Tommi Tenkanen for interesting discussions. The work of G.A. is supported through a "la Caixa" predoctoral grant of Fundación "la Caixa". This project has received funding from the European Union's Horizon 2020 research and innovation programme under the Marie Sklodowska-Curie grant agreement No. 674896 (ITN ELUSIVES).

A Inflation scale and minimal number of e-folds

Being crucial to our calculations, here we give a somewhat exhaustive discussion about how long inflation needs to have lasted, based on observations, the standard cosmology and basic assumptions about the model of inflation and reheating. We will closely follow ref. [101] for this purpose.

Let us denote by $N(k)$ the number of e-folds at which the comoving scale k left the horizon, that is, when $k = aH$ during inflation. Note that the requirement of an accelerated expansion implies that aH is a monotonically increasing function of time. The largest scale to which we have access observationally is the present horizon scale $k_0 = a_0 H_0$. The requirement $N(k_0) \leq N_{\rm tot}$ gives a lower limit on the total number of e-folds of inflation, but it cannot say anything about the actual value of $N_{\rm tot}$, which can (and usually is expected to) be much larger. In order to make numerical statements, we will often make the assumption of *minimal inflation*, which sets $N_{\rm tot}$ to its smallest observationally allowed value $N_{\rm min} = N(k_0)$.

The general expression for $N(k)$ is [101]

$$N(k) = -\ln\left(\frac{k}{a_0 H_0}\right) + \frac{1}{3}\ln\left(\frac{\rho_{\rm reh}}{\rho_{\rm end}}\right) + \frac{1}{4}\ln\left(\frac{\rho_{\rm eq}}{\rho_{\rm reh}}\right) + \ln\left(\frac{H_k}{H_{\rm eq}}\right) + \ln\left(219\,\Omega_0 h\right), \qquad \text{(A.1)}$$

where $\rho_{\rm end}$, $\rho_{\rm reh}$, $\rho_{\rm eq}$ are the energy density at the end of inflation, at reheating and at matter-radiation equality, respectively; and H_k is the Hubble parameter at the time when the scale k exits the horizon during inflation. We can simplify this expression by making two main assumptions:

- $H_k \sim H_{\rm end} \sim H_I$: there is no energy drop during inflation. This amounts to assuming exactly exponential expansion with a constant value of H.
- $\rho_{\rm reh} \sim \rho_{\rm end}$: reheating happens instantaneously when inflation ends.

Under these assumptions and using $\rho = 3m_{\rm pl}^2 H^2$ (with the reduced Planck mass), $H_{\rm eq} \approx 2 \cdot 10^{-27}\,\text{GeV}$, the matter density $\Omega_0 \approx 0.3$ and $h \approx 0.7$, we can obtain a simple expression

JCAP02(2020)014

for the minimum number of e-folds, $N_{\rm min}$, which reads

$$N_{\rm min} = 61.97 + \frac{1}{2}\ln\left(\frac{H_I}{6.6\cdot 10^{13}\,{\rm GeV}}\right). \tag{A.2}$$

We normalize the result to the largest scale of inflation allowed by observations (using the 95% cl limit from [95]). Note that $N_{\rm min}$ becomes smaller for lower inflationary scales. Another quantity that is relevant for us is $N(k_{\rm CMB})$, which is the number of e-folds at which the perturbations accesible in the CMB exited the horizon. Using the Planck pivot scale $k_{\rm CMB} = k_\star = 0.05\,{\rm Mpc}^{-1}$, we obtain that these scales exited the horizon

$$N_{\rm min} - N(k_{\rm CMB}) = 7.26 \tag{A.3}$$

e-folds after the current horizon scale. Finally, let us relax the two former assumptions and give a more general expression for the number of e-folds,

$$N_{\rm min} = 61.97 + \frac{1}{2}\ln\left(\frac{H_I}{6.6\cdot 10^{13}\,{\rm GeV}}\right) + \frac{1}{4}\ln\left(\frac{V_{k_0}}{\rho_{\rm end}}\right) + \frac{1}{12}\ln\left(\frac{\rho_{\rm reh}}{\rho_{\rm end}}\right). \tag{A.4}$$

Here, we use the slow-roll approximation to write $H_k = 8\pi V_k/3M_{\rm pl}^3$ and express the result in terms of the energy scale of inflation instead of the Hubble scale. Note that a longer period of preheating generally implies $\rho_{\rm reh} \leq \rho_{\rm end}$ and leads to a decrease in $N_{\rm min}$, while a deviation from pure de Sitter expansion means that $V_{k_0} \geq \rho_{\rm end}$ and results in a larger value for $N_{\rm min}$.

B Stochastic scenario

One aspect that is relevant to the stochastic scenario is the exact form of the field value evolution during the inflationary period. For arbitrary initial conditions ϕ_s and $\dot\phi_s$, it is given by

$$\phi(t) = \phi_s\left(c_1 {\rm e}^{-\frac{1}{2}\alpha_- H_I t} + c_2 {\rm e}^{-\frac{1}{2}\alpha_+ H_I t}\right), \tag{B.1}$$

with

$$\begin{aligned} c_1 &= \frac{1}{\alpha_+ - \alpha_-}\left(\alpha_+ + \frac{\dot\phi_s}{H_I\,\phi_s}\right), \\ c_2 &= -\frac{1}{\alpha_+ - \alpha_-}\left(\alpha_- + \frac{\dot\phi_s}{H_I\,\phi_s}\right), \end{aligned} \tag{B.2}$$

and identical equations being valid in the vector case for $\chi_i(t)$ only exchanging $\alpha_\pm$ for $\beta_\pm$. Using that $\alpha_+ > \alpha_-$ ($\beta_+ > \beta_-$), we find for late times the expressions

$$\phi(t) \approx \frac{2}{H_I(\alpha_+ - \alpha_-)}\left(\dot\phi_s + \frac{1}{2}\alpha_+ H_I\phi_s\right){\rm e}^{-\frac{1}{2}\alpha_- H_I t} \tag{B.3}$$

$$\dot\phi(t) \approx -\frac{\alpha_-}{\alpha_+ - \alpha_-}\left(\dot\phi_s + \frac{1}{2}\alpha_+ H_I\phi_s\right){\rm e}^{-\frac{1}{2}\alpha_- H_I t}. \tag{B.4}$$

Note that t is defined such that at the end of inflation $H_I t = N_{\rm tot}$. Furthermore, we can see from these expressions that in general

$$\dot\phi(t) = -\frac{1}{2}\alpha_- H_I\phi(t), \tag{B.5}$$

so in terms of initial conditions the assumption $\dot\phi_s \sim H_I\phi_s$ is reasonable as long as $\alpha_- \not\approx 0$.

JCAP02(2020)014

Let us now turn into the stochastic regime, which involves the computation of the variance of the field induced by the non-vanishing momentum modes that describe the fluctuations. As noted in section 2.4, our calculation is done along the lines of [39]. There, the quantity ν appears, which is given by $\alpha_- = 3-2\nu$ in terms of the quantities used throughout this paper, or more directly by $\nu \approx 3/2\sqrt{1-16/3\xi}$, with $0 \leq \xi \leq 3/16$. As in [39], we can also express the Hankel functions that describe the modes in terms of Bessel functions and see that the contribution of $J_{-\nu}(\cdot)$ is the dominant one, leading to

$$|\delta\phi_k|^2 \simeq \frac{H_I^2}{4\pi}\,\Gamma^2\!\left(\frac{3-\alpha_-}{2}\right)\left(\frac{1}{aH_I}\right)^3\left(\frac{2aH_I}{k}\right)^{3-\alpha_-}. \tag{B.6}$$

Here, the subscript "horizon" indicates the quantity at horizon exit. These fluctuations contribute to our Universe's homogeneous field value as long as inflation stretches to scales that are still superhorizon today. The accumulated effect of all the sufficiently long wavelength modes results in a Gaussian distribution for the homogeneous field value, with variance

$$\begin{aligned}\left\langle\phi_\delta^2\right\rangle_{\rm horizon} &= \int_{a(t_i)H_I}^{a(t_{\rm horizon})H_I}\frac{{\rm d}^3\vec{k}}{(2\pi)^3}\,|\delta\phi_k|^2_{a=a_{\rm horizon}} \\ &= \frac{2^{-\alpha}}{\pi^3\alpha_-}\Gamma^2\!\left(\frac{3-\alpha_-}{2}\right)H_I^2\left[1-{\rm e}^{-\alpha_-(N_{\rm tot}-N_{\rm min})}\right].\end{aligned} \tag{B.7}$$

The field value right at horizon exit is randomly drawn from this Gaussian distribution. Assuming that it is centered at the origin, the "typical" result corresponds to $\phi_{\rm horizon} = \sqrt{\left\langle\phi_\delta^2\right\rangle}$. That said, this homogeneous field can vary significantly by the end of inflation due to the potentially fast superhorizon evolution caused by the non-minimal coupling. We can use eq. (B.3) with $\dot{\phi}_{\rm horizon} = 0$ (this assumes that equilibrium has been reached in the sense that is described below) to describe the subsequent evolution after horizon exit by

$$\phi_e \approx \frac{\alpha_+}{\alpha_+-\alpha_-}\,{\rm e}^{-\frac{1}{2}\alpha_- N_{\rm min}}\phi_{\rm horizon}. \tag{B.8}$$

Taking into account this superhorizon evolution during the last $N_{\rm min}$ efolds of inflation, the typical homogeneous field value at the end of inflation in our Hubble patch is

$$\left\langle\phi_\delta^2\right\rangle = \frac{F(\alpha_-)}{\alpha_-}\left(\frac{H_I}{2\pi}\right)^2\left[1-{\rm e}^{-\alpha_-(N_{\rm tot}-N_{\rm min})}\right]\left(\frac{\alpha_+}{\alpha_+-\alpha_-}\,{\rm e}^{-\frac{1}{2}\alpha_- N_{\rm min}}\right)^2. \tag{B.9}$$

The truly stochastic regime, when the distribution is well approximated by a Gaussian, is only reached after a sufficient amount of inflation. This occurs when $\Delta N = N_{\rm tot} - N_{\rm min} > 1/\alpha_-$ so that the integral eq. (B.7) is dominated by the superhorizon modes with the shortest wavelengths. In this regime, the term in the square brackets in eq. (B.9) can be dropped. By also using $\alpha_+/(\alpha_+-\alpha_-) \approx 1$ we get the result given in section 2.4.

The stochastic contribution to the homogeneous field competes with the exponentially decaying contribution from the initial field value at the start of inflation ϕ_s. Determining the extra number of e-folds (before modes dominating eq. (B.7) exit the horizon) that are necessary for the variance in eq. (B.9) to be a factor of γ bigger than the contribution from initial condition, cf. eq. (B.3)) is straightforward. To do so we have to ensure that the remnant of the initially homogeneous field value is a factor of γ smaller than the variance. The result is given in eq. (2.23).

The calculations for the stochastic scenario in the case of a vector field go along the same lines as the ones presented above, with the contributions being split into transverse and longitudinal modes.

JCAP02(2020)014

C Longitudinal fluctuations

The EOMs for the longitudinal modes of the physical field χ in momentum space (cf. [57]) are

$$\begin{aligned} 0 = \ddot{\delta\chi}^{\parallel} &+ \left[3H + \frac{k^2}{k^2 + a^2\left(m_X^2 - \frac{\kappa}{6}R\right)}\left(2H - \frac{\kappa}{6}\frac{\dot{R}}{m_X^2 - \frac{\kappa}{6}R}\right)\right]\dot{\delta\chi}^{\parallel} \\ &+ \left[m_X^2 + \frac{1-\kappa}{6}R + \frac{k^2}{a^2} + \frac{k^2 H}{k^2 + a^2\left(m_X^2 - \frac{\kappa}{6}R\right)}\left(2H - \frac{\kappa}{6}\frac{\dot{R}}{m_X^2 - \frac{\kappa}{6}R}\right)\right]\delta\chi^{\parallel}. \end{aligned} \tag{C.1}$$

When specifying to inflation, it turns out to be advantageous to work with the original field $\delta X^{\parallel} = a\,\delta\chi^{\parallel}$ and to switch to conformal time using $\mathrm{d}t/\mathrm{d}\tau = a$ and $a = -1/(\tau H_I)$. This deviates from the redefinition used in the main text, $f = a\delta X^{\parallel}$, but it allows to more easily obtain more precise analytic approximations of the mode functions. With this, we find (cf. [57])

$$0 = \left[\partial_\tau^2 - \frac{2\tau k^2 H_I^2}{\tau^2 k^2 H_I^2 + m_X^2 - 2\kappa H_I^2}\partial_\tau + \frac{m_X^2 - 2\kappa H_I^2}{\tau^2 H_I^2} + k^2\right]\delta X^{\parallel}. \tag{C.2}$$

This equation can be simplified and analytically solved in the limits of interest to us.

In the subhorizon limit, when $k/(aH_I) = -k\tau \gg 1$, we can approximate eq. (C.2) by

$$0 = \left[\partial_\tau^2 - \frac{2}{\tau}\partial_\tau + \frac{\widetilde{m}^2}{\tau^2 H_I^2} + k^2\right]\delta X^{\parallel}, \tag{C.3}$$

where we introduced the shifted mass $\widetilde{m}^2 \equiv m_X^2 - 2\kappa H_I^2$. As is done in [58], the additional redefinition $\widetilde{\delta X}_i^{\parallel} \equiv -|\widetilde{m}|/(\tau k H_I)\ \delta X_i^{\parallel}$, allows to further simplify the EOM to

$$0 = \left[\partial_\tau^2 + \frac{m_X^2 - 2(\kappa+1)H_I^2}{\tau^2 H_I^2} + k^2\right]\widetilde{\delta X}^{\parallel}. \tag{C.4}$$

This equation allows the Bunch-Davies vacuum as initial condition (cf. [58])

$$\widetilde{\delta X}^{\parallel} \xrightarrow{\tau\to-\infty} \frac{1}{\sqrt{2k}}\mathrm{e}^{-ik\tau}. \tag{C.5}$$

Eq. (C.4) with initial condition eq. (C.5) has the solution [57]

$$\delta X^{\parallel} \equiv -\frac{\tau k H_I}{|\widetilde{m}|}\widetilde{\delta X}^{\parallel} = -\frac{\tau k H_I}{|\widetilde{m}|}\sqrt{-\pi\tau}\frac{\mathrm{e}^{i\frac{\pi}{2}\left(\widetilde{\nu}+\frac{1}{2}\right)}}{1-\mathrm{e}^{2i\pi\widetilde{\nu}}}\left[J_{\widetilde{\nu}}(-k\tau) - \mathrm{e}^{i\pi\widetilde{\nu}}J_{-\widetilde{\nu}}(-k\tau)\right], \tag{C.6}$$

where $J_{\pm\widetilde{\nu}}(\cdot)$ are Bessel functions of the first kind and we introduce $\widetilde{\nu} \equiv 1/2\sqrt{1+8(\kappa+1)-4m_X^2/H_I^2}$. This is the early time solution shown in figure 5.

In the superhorizon limit, i.e. when $-\tau k \ll 1$, eq. (C.2) can be recast as

$$0 = \left[\partial_\tau^2 - \frac{2\tau k^2 H_I^2}{\widetilde{m}^2}\partial_\tau + \frac{\widetilde{m}^2}{\tau^2 H_I^2} + k^2\right]\delta X^{\parallel}. \tag{C.7}$$

This equation can be explicitly solved in terms of confluent hypergeometric functions of the first kind. By making use of relations $m_X^2 \ll 2\kappa H_I^2$ and $-\tau k \ll 1$, the solution can be approximately expressed as

$$\delta X^{\parallel} \approx 2^{-2-\frac{1}{2}\beta_-}(k\tau)^{-1+\frac{1}{2}\beta_-}\left[\widetilde{C}_1\,(k\tau)^{3-\beta_-} + \widetilde{C}_2\,2^{3-\beta_-}\right] \approx \widetilde{C}_2\,2^{1-\frac{1}{2}\beta_-}(k\tau)^{-1+\frac{1}{2}\beta_-}, \tag{C.8}$$

JCAP02(2020)014

where $\widetilde{C}_1$ and $\widetilde{C}_2$ are constants that depend on the initial conditions. The second approximation holds long after horizon exit. This the late time solution that is depicted in figure 5.

The full match of eqs. (C.6) and (C.8) cannot be performed analytically, but it is easy to see that the matching is only possible if the k-dependence of the coefficients is precisely $\widetilde{C}_{1,2} \sim 1/\sqrt{k}$. Using this knowledge, we can extract the momentum dependence and define C_2' such that

$$\delta\chi^{\parallel} \simeq C_2' 2^{1-\frac{1}{2}\beta_-} \frac{H_I}{k^{3/2}} \left(\frac{k}{aH_I}\right)^{\frac{1}{2}\beta_-} , \tag{C.9}$$

in terms of scale factors rather than conformal time. This is precisely the result derived in section 3.2.

References

[1] J. Preskill, M.B. Wise and F. Wilczek, *Cosmology of the Invisible Axion*, *Phys. Lett.* **120B** (1983) 127 [INSPIRE].

[2] L.F. Abbott and P. Sikivie, *A Cosmological Bound on the Invisible Axion*, *Phys. Lett.* **120B** (1983) 133 [INSPIRE].

[3] M. Dine and W. Fischler, *The Not So Harmless Axion*, *Phys. Lett.* **120B** (1983) 137 [INSPIRE].

[4] P. Sikivie, *Axion Cosmology*, *Lect. Notes Phys.* **741** (2008) 19 [astro-ph/0610440] [INSPIRE].

[5] A.E. Nelson and J. Scholtz, *Dark Light, Dark Matter and the Misalignment Mechanism*, *Phys. Rev.* **D 84** (2011) 103501 [arXiv:1105.2812] [INSPIRE].

[6] P. Arias, D. Cadamuro, M. Goodsell, J. Jaeckel, J. Redondo and A. Ringwald, *WISPy Cold Dark Matter*, *JCAP* **06** (2012) 013 [arXiv:1201.5902] [INSPIRE].

[7] J. Jaeckel, *A Family of WISPy Dark Matter Candidates*, *Phys. Lett.* **B 732** (2014) 1 [arXiv:1311.0880] [INSPIRE].

[8] D.J.E. Marsh, *Axion Cosmology*, *Phys. Rept.* **643** (2016) 1 [arXiv:1510.07633] [INSPIRE].

[9] P. Sikivie, *Experimental Tests of the Invisible Axion*, *Phys. Rev. Lett.* **51** (1983) 1415 [*Erratum ibid.* **52** (1984) 695] [INSPIRE].

[10] D. Horns, J. Jaeckel, A. Lindner, A. Lobanov, J. Redondo and A. Ringwald, *Searching for WISPy Cold Dark Matter with a Dish Antenna*, *JCAP* **04** (2013) 016 [arXiv:1212.2970] [INSPIRE].

[11] D. Budker, P.W. Graham, M. Ledbetter, S. Rajendran and A. Sushkov, *Proposal for a Cosmic Axion Spin Precession Experiment (CASPEr)*, *Phys. Rev.* **X 4** (2014) 021030 [arXiv:1306.6089] [INSPIRE].

[12] J. Jaeckel and J. Redondo, *An antenna for directional detection of WISPy dark matter*, *JCAP* **11** (2013) 016 [arXiv:1307.7181] [INSPIRE].

[13] W. Chung, *CULTASK, The Coldest Axion Experiment at CAPP/IBS in Korea*, PoS(CORFU2015)047 (2016) [INSPIRE].

[14] P.W. Graham, D.E. Kaplan, J. Mardon, S. Rajendran and W.A. Terrano, *Dark Matter Direct Detection with Accelerometers*, *Phys. Rev.* **D 93** (2016) 075029 [arXiv:1512.06165] [INSPIRE].

[15] Y. Kahn, B.R. Safdi and J. Thaler, *Broadband and Resonant Approaches to Axion Dark Matter Detection*, *Phys. Rev. Lett.* **117** (2016) 141801 [arXiv:1602.01086] [INSPIRE].

[16] MADMAX Working Group collaboration, *Dielectric Haloscopes: A New Way to Detect Axion Dark Matter*, *Phys. Rev. Lett.* **118** (2017) 091801 [arXiv:1611.05865] [INSPIRE].

JCAP02(2020)014

[17] D. Alesini, D. Babusci, D. Di Gioacchino, C. Gatti, G. Lamanna and C. Ligi, *The KLASH Proposal*, arXiv:1707.06010 [INSPIRE].

[18] A.Á. Melcón et al., *Axion Searches with Microwave Filters: the RADES project*, *JCAP* **05** (2018) 040 [arXiv:1803.01243] [INSPIRE].

[19] ADMX collaboration, *A Search for Invisible Axion Dark Matter with the Axion Dark Matter Experiment*, *Phys. Rev. Lett.* **120** (2018) 151301 [arXiv:1804.05750] [INSPIRE].

[20] D. Carney, S. Ghosh, G. Krnjaic and J.M. Taylor, *Gravitational Direct Detection of Dark Matter*, arXiv:1903.00492 [INSPIRE].

[21] K. Ehret et al., *Production and detection of axion-like particles in a HERA dipole magnet: Letter-of-intent for the ALPS experiment*, hep-ex/0702023 [INSPIRE].

[22] K. Ehret et al., *New ALPS Results on Hidden-Sector Lightweights*, *Phys. Lett.* **B 689** (2010) 149 [arXiv:1004.1313] [INSPIRE].

[23] R. Bähre et al., *Any light particle search II — Technical Design Report*, 2013 *JINST* **8** T09001 [arXiv:1302.5647] [INSPIRE].

[24] CAST collaboration, *First results from the CERN Axion Solar Telescope (CAST)*, *Phys. Rev. Lett.* **94** (2005) 121301 [hep-ex/0411033] [INSPIRE].

[25] CAST collaboration, *New CAST Limit on the Axion-Photon Interaction*, *Nature Phys.* **13** (2017) 584 [arXiv:1705.02290] [INSPIRE].

[26] I.G. Irastorza et al., *Towards a new generation axion helioscope*, *JCAP* **06** (2011) 013 [arXiv:1103.5334] [INSPIRE].

[27] E. Armengaud et al., *Conceptual Design of the International Axion Observatory (IAXO)*, 2014 *JINST* **9** T05002 [arXiv:1401.3233] [INSPIRE].

[28] IAXO collaboration, *Physics potential of the International Axion Observatory (IAXO)*, *JCAP* **06** (2019) 047 [arXiv:1904.09155] [INSPIRE].

[29] J. Jaeckel and A. Ringwald, *The Low-Energy Frontier of Particle Physics*, *Ann. Rev. Nucl. Part. Sci.* **60** (2010) 405 [arXiv:1002.0329] [INSPIRE].

[30] P.W. Graham, I.G. Irastorza, S.K. Lamoreaux, A. Lindner and K.A. van Bibber, *Experimental Searches for the Axion and Axion-Like Particles*, *Ann. Rev. Nucl. Part. Sci.* **65** (2015) 485 [arXiv:1602.00039] [INSPIRE].

[31] J. Beacham et al., *Physics Beyond Colliders at CERN: Beyond the Standard Model Working Group Report*, *J. Phys.* **G 47** (2020) 010501 [arXiv:1901.09966] [INSPIRE].

[32] R. Alemany et al., *Summary Report of Physics Beyond Colliders at CERN*, arXiv:1902.00260 [INSPIRE].

[33] J.L. Hewett et al., *Fundamental Physics at the Intensity Frontier*, DOI [arXiv:1205.2671] [INSPIRE].

[34] R. Essig et al., *Working Group Report: New Light Weakly Coupled Particles*, in *Proceedings, 2013 Community Summer Study on the Future of U.S. Particle Physics: Snowmass on the Mississippi (CSS2013)*, Minneapolis, MN, U.S.A., 29 July–6 August 6, 2013 (2013) [arXiv:1311.0029] [INSPIRE].

[35] I.G. Irastorza and J. Redondo, *New experimental approaches in the search for axion-like particles*, *Prog. Part. Nucl. Phys.* **102** (2018) 89 [arXiv:1801.08127] [INSPIRE].

[36] A.A. Starobinsky and J. Yokoyama, *Equilibrium state of a selfinteracting scalar field in the de Sitter background*, *Phys. Rev.* **D 50** (1994) 6357 [astro-ph/9407016] [INSPIRE].

[37] P.J.E. Peebles and A. Vilenkin, *Noninteracting dark matter*, *Phys. Rev.* **D 60** (1999) 103506 [astro-ph/9904396] [INSPIRE].

[38] P.W. Graham and A. Scherlis, *Stochastic axion scenario*, *Phys. Rev.* **D 98** (2018) 035017 [arXiv:1805.07362] [INSPIRE].

JCAP02(2020)014

[39] F. Takahashi, W. Yin and A.H. Guth, *QCD axion window and low-scale inflation*, *Phys. Rev.* **D 98** (2018) 015042 [arXiv:1805.08763] [INSPIRE].

[40] S.-Y. Ho, F. Takahashi and W. Yin, *Relaxing the Cosmological Moduli Problem by Low-scale Inflation*, *JHEP* **04** (2019) 149 [arXiv:1901.01240] [INSPIRE].

[41] T. Tenkanen, *Dark matter from scalar field fluctuations*, *Phys. Rev. Lett.* **123** (2019) 061302 [arXiv:1905.01214] [INSPIRE].

[42] P.W. Graham, J. Mardon and S. Rajendran, *Vector Dark Matter from Inflationary Fluctuations*, *Phys. Rev.* **D 93** (2016) 103520 [arXiv:1504.02102] [INSPIRE].

[43] S. Nurmi, T. Tenkanen and K. Tuominen, *Inflationary Imprints on Dark Matter*, *JCAP* **11** (2015) 001 [arXiv:1506.04048] [INSPIRE].

[44] K. Kainulainen, S. Nurmi, T. Tenkanen, K. Tuominen and V. Vaskonen, *Isocurvature Constraints on Portal Couplings*, *JCAP* **06** (2016) 022 [arXiv:1601.07733] [INSPIRE].

[45] O. Bertolami, C. Cosme and J.G. Rosa, *Scalar field dark matter and the Higgs field*, *Phys. Lett.* **B 759** (2016) 1 [arXiv:1603.06242] [INSPIRE].

[46] C. Cosme, J.G. Rosa and O. Bertolami, *Scale-invariant scalar field dark matter through the Higgs portal*, *JHEP* **05** (2018) 129 [arXiv:1802.09434] [INSPIRE].

[47] G. Alonso-Álvarez and J. Jaeckel, *Lightish but clumpy: scalar dark matter from inflationary fluctuations*, *JCAP* **10** (2018) 022 [arXiv:1807.09785] [INSPIRE].

[48] P. Agrawal, N. Kitajima, M. Reece, T. Sekiguchi and F. Takahashi, *Relic Abundance of Dark Photon Dark Matter*, *Phys. Lett.* **B 801** (2020) 135136 [arXiv:1810.07188] [INSPIRE].

[49] J.A. Dror, K. Harigaya and V. Narayan, *Parametric Resonance Production of Ultralight Vector Dark Matter*, *Phys. Rev.* **D 99** (2019) 035036 [arXiv:1810.07195] [INSPIRE].

[50] R.T. Co, L.J. Hall and K. Harigaya, *QCD Axion Dark Matter with a Small Decay Constant*, *Phys. Rev. Lett.* **120** (2018) 211602 [arXiv:1711.10486] [INSPIRE].

[51] R.T. Co, A. Pierce, Z. Zhang and Y. Zhao, *Dark Photon Dark Matter Produced by Axion Oscillations*, *Phys. Rev.* **D 99** (2019) 075002 [arXiv:1810.07196] [INSPIRE].

[52] M. Bastero-Gil, J. Santiago, L. Ubaldi and R. Vega-Morales, *Vector dark matter production at the end of inflation*, *JCAP* **04** (2019) 015 [arXiv:1810.07208] [INSPIRE].

[53] A.J. Long and L.-T. Wang, *Dark Photon Dark Matter from a Network of Cosmic Strings*, *Phys. Rev.* **D 99** (2019) 063529 [arXiv:1901.03312] [INSPIRE].

[54] R.T. Co, E. Gonzalez and K. Harigaya, *Axion Misalignment Driven to the Bottom*, *JHEP* **05** (2019) 162 [arXiv:1812.11186] [INSPIRE].

[55] R.T. Co, E. Gonzalez and K. Harigaya, *Axion Misalignment Driven to the Hilltop*, *JHEP* **05** (2019) 163 [arXiv:1812.11192] [INSPIRE].

[56] A. Golovnev, V. Mukhanov and V. Vanchurin, *Vector Inflation*, *JCAP* **06** (2008) 009 [arXiv:0802.2068] [INSPIRE].

[57] T. Hugle, *Hidden photons as dark matter candidates*, ITP MSc Thesis (2015).

[58] K. Dimopoulos, M. Karciauskas, D.H. Lyth and Y. Rodriguez, *Statistical anisotropy of the curvature perturbation from vector field perturbations*, *JCAP* **05** (2009) 013 [arXiv:0809.1055] [INSPIRE].

[59] M. Karciauskas and D.H. Lyth, *On the health of a vector field with $(RA^2)/6$ coupling to gravity*, *JCAP* **11** (2010) 023 [arXiv:1007.1426] [INSPIRE].

[60] D.S. Salopek, J.R. Bond and J.M. Bardeen, *Designing Density Fluctuation Spectra in Inflation*, *Phys. Rev.* **D 40** (1989) 1753 [INSPIRE].

[61] M.P. Hertzberg, *On Inflation with Non-minimal Coupling*, *JHEP* **11** (2010) 023 [arXiv:1002.2995] [INSPIRE].

JCAP02(2020)014

[62] F.L. Bezrukov and M. Shaposhnikov, *The Standard Model Higgs boson as the inflaton*, *Phys. Lett.* **B 659** (2008) 703 [arXiv:0710.3755] [INSPIRE].

[63] J. Rubio, *Higgs inflation*, *Front. Astron. Space Sci.* **5** (2019) 50 [arXiv:1807.02376] [INSPIRE].

[64] L.H. Ford, *Gravitational Particle Creation and Inflation*, *Phys. Rev.* **D 35** (1987) 2955 [INSPIRE].

[65] D.J.H. Chung, E.W. Kolb and A. Riotto, *Superheavy dark matter*, *Phys. Rev.* **D 59** (1998) 023501 [hep-ph/9802238] [INSPIRE].

[66] D.J.H. Chung, P. Crotty, E.W. Kolb and A. Riotto, *On the Gravitational Production of Superheavy Dark Matter*, *Phys. Rev.* **D 64** (2001) 043503 [hep-ph/0104100] [INSPIRE].

[67] Y. Ema, R. Jinno, K. Mukaida and K. Nakayama, *Gravitational Effects on Inflaton Decay*, *JCAP* **05** (2015) 038 [arXiv:1502.02475] [INSPIRE].

[68] T. Markkanen and S. Nurmi, *Dark matter from gravitational particle production at reheating*, *JCAP* **02** (2017) 008 [arXiv:1512.07288] [INSPIRE].

[69] M. Fairbairn, K. Kainulainen, T. Markkanen and S. Nurmi, *Despicable Dark Relics: generated by gravity with unconstrained masses*, *JCAP* **04** (2019) 005 [arXiv:1808.08236] [INSPIRE].

[70] Y. Ema, R. Jinno, K. Mukaida and K. Nakayama, *Gravitational particle production in oscillating backgrounds and its cosmological implications*, *Phys. Rev.* **D 94** (2016) 063517 [arXiv:1604.08898] [INSPIRE].

[71] Y. Ema, K. Nakayama and Y. Tang, *Production of Purely Gravitational Dark Matter*, *JHEP* **09** (2018) 135 [arXiv:1804.07471] [INSPIRE].

[72] Y. Ema, K. Nakayama and Y. Tang, *Production of Purely Gravitational Dark Matter: The Case of Fermion and Vector Boson*, *JHEP* **07** (2019) 060 [arXiv:1903.10973] [INSPIRE].

[73] M. Garny, M. Sandora and M.S. Sloth, *Planckian Interacting Massive Particles as Dark Matter*, *Phys. Rev. Lett.* **116** (2016) 101302 [arXiv:1511.03278] [INSPIRE].

[74] Y. Tang and Y.-L. Wu, *Pure Gravitational Dark Matter, Its Mass and Signatures*, *Phys. Lett.* **B 758** (2016) 402 [arXiv:1604.04701] [INSPIRE].

[75] Y. Tang and Y.-L. Wu, *On Thermal Gravitational Contribution to Particle Production and Dark Matter*, *Phys. Lett.* **B 774** (2017) 676 [arXiv:1708.05138] [INSPIRE].

[76] M. Garny, A. Palessandro, M. Sandora and M.S. Sloth, *Theory and Phenomenology of Planckian Interacting Massive Particles as Dark Matter*, *JCAP* **02** (2018) 027 [arXiv:1709.09688] [INSPIRE].

[77] J.F. Donoghue, *General relativity as an effective field theory: The leading quantum corrections*, *Phys. Rev.* **D 50** (1994) 3874 [gr-qc/9405057] [INSPIRE].

[78] N.D. Birrell and P.C.W. Davies, *Quantum Fields in Curved Space*, Cambridge Monographs on Mathematical Physics, Cambridge University Press, Cambridge, U.K. (1984) [INSPIRE].

[79] C.G. Callan Jr., S.R. Coleman and R. Jackiw, *A New improved energy-momentum tensor*, *Annals Phys.* **59** (1970) 42 [INSPIRE].

[80] G. Narain and R. Percacci, *Renormalization Group Flow in Scalar-Tensor Theories. I*, *Class. Quant. Grav.* **27** (2010) 075001 [arXiv:0911.0386] [INSPIRE].

[81] G. Narain and C. Rahmede, *Renormalization Group Flow in Scalar-Tensor Theories. II*, *Class. Quant. Grav.* **27** (2010) 075002 [arXiv:0911.0394] [INSPIRE].

[82] R. Percacci and G.P. Vacca, *Search of scaling solutions in scalar-tensor gravity*, *Eur. Phys. J.* **C 75** (2015) 188 [arXiv:1501.00888] [INSPIRE].

[83] P. Labus, R. Percacci and G.P. Vacca, *Asymptotic safety in $O(N)$ scalar models coupled to gravity*, *Phys. Lett.* **B 753** (2016) 274 [arXiv:1505.05393] [INSPIRE].

JCAP02(2020)014

[84] Y. Hamada and M. Yamada, *Asymptotic safety of higher derivative quantum gravity non-minimally coupled with a matter system*, *JHEP* **08** (2017) 070 [arXiv:1703.09033] [INSPIRE].

[85] A. Eichhorn, S. Lippoldt and V. Skrinjar, *Nonminimal hints for asymptotic safety*, *Phys. Rev.* **D 97** (2018) 026002 [arXiv:1710.03005] [INSPIRE].

[86] S. Weinberg, *Critical Phenomena for Field Theorists*, in *14th International School of Subnuclear Physics: Understanding the Fundamental Constitutents of Matter*, Erice, Italy, 23 July–8 August 1976, p. 1 (1976) [DOI] [INSPIRE].

[87] A. Eichhorn, *Status of the asymptotic safety paradigm for quantum gravity and matter*, *Found. Phys.* **48** (2018) 1407 [arXiv:1709.03696] [INSPIRE].

[88] A. Bonanno and F. Saueressig, *Asymptotically safe cosmology — A status report*, *Comptes Rendus Physique* **18** (2017) 254 [arXiv:1702.04137] [INSPIRE].

[89] F. Bezrukov, A. Magnin, M. Shaposhnikov and S. Sibiryakov, *Higgs inflation: consistency and generalisations*, *JHEP* **01** (2011) 016 [arXiv:1008.5157] [INSPIRE].

[90] J.M. Cline, S. Jeon and G.D. Moore, *The Phantom menaced: Constraints on low-energy effective ghosts*, *Phys. Rev.* **D 70** (2004) 043543 [hep-ph/0311312] [INSPIRE].

[91] F. Sbisà, *Classical and quantum ghosts*, *Eur. J. Phys.* **36** (2015) 015009 [arXiv:1406.4550] [INSPIRE].

[92] B. Himmetoglu, C.R. Contaldi and M. Peloso, *Instability of anisotropic cosmological solutions supported by vector fields*, *Phys. Rev. Lett.* **102** (2009) 111301 [arXiv:0809.2779] [INSPIRE].

[93] B. Himmetoglu, C.R. Contaldi and M. Peloso, *Ghost instabilities of cosmological models with vector fields nonminimally coupled to the curvature*, *Phys. Rev.* **D 80** (2009) 123530 [arXiv:0909.3524] [INSPIRE].

[94] K. Nakayama, *Vector Coherent Oscillation Dark Matter*, *JCAP* **10** (2019) 019 [arXiv:1907.06243] [INSPIRE].

[95] PLANCK collaboration, *Planck 2018 results. X. Constraints on inflation*, arXiv:1807.06211 [INSPIRE].

[96] G.N. Remmen and S.M. Carroll, *How Many e-Folds Should We Expect from High-Scale Inflation?*, *Phys. Rev.* **D 90** (2014) 063517 [arXiv:1405.5538] [INSPIRE].

[97] P.W. Graham, D.E. Kaplan and S. Rajendran, *Cosmological Relaxation of the Electroweak Scale*, *Phys. Rev. Lett.* **115** (2015) 221801 [arXiv:1504.07551] [INSPIRE].

[98] G. Alonso-Álvarez, J. Gehrlein, J. Jaeckel and S. Schenk, *Very Light Asymmetric Dark Matter*, *JCAP* **09** (2019) 003 [arXiv:1906.00969] [INSPIRE].

[99] T. Markkanen, A. Rajantie and T. Tenkanen, *Spectator Dark Matter*, *Phys. Rev.* **D 98** (2018) 123532 [arXiv:1811.02586] [INSPIRE].

[100] T. Markkanen, A. Rajantie, S. Stopyra and T. Tenkanen, *Scalar correlation functions in de Sitter space from the stochastic spectral expansion*, *JCAP* **08** (2019) 001 [arXiv:1904.11917] [INSPIRE].

[101] A.R. Liddle and S.M. Leach, *How long before the end of inflation were observable perturbations produced?*, *Phys. Rev.* **D 68** (2003) 103503 [astro-ph/0305263] [INSPIRE].

JCAP02(2020)014

Chapter 9

Conclusions

This thesis initially set out to address a relatively specific topic: is the dark matter of the Universe made up of axions or some other light scalar particle? Of course, this innocent-looking question is much deeper than it sounds and a definite answer for it is likely to require a lifetime rather than a single thesis. Even if no conclusive resolution has been reached in this work, many things have been learned in the process that will hopefully contribute to the final "yes" or "no".

In the next few pages of Section 9.1, we summarize the main ideas and results of each of the previous chapters. The goal of this is to provide an overview of the research presented in this thesis without dwelling too much on the details, as the reader is referred back to each chapter for the comprehensive argumentations and calculations. After the summary, the results are discussed and reflected upon in Section 9.2, focussing on the global conclusions reached from the different studies that compose this work and how they embed into the broader picture. Finally, in Section 9.3 we comment on future research directions that are motivated by the results presented in this thesis.

9.1 Summary

This section is intended to be a self-contained presentation of the main findings of this thesis. It is clearly structured in parts and chapters for easy reference back to the respective publications reproduced in Chapters 2 to 8.

Part I - Dark matter and particle asymmetries

The first part of the thesis deals with the cosmological origin of particle-antiparticle asymmetries, and presents novel scenarios of asymmetric dark matter and baryogenesis.

Chapter 2 - Very light asymmetric dark matter. Light scalar fields produced through the misalignment mechanism are well known to be good dark matter candidates. These fields

are usually assumed to be real, or complex enjoying an unbroken $U(1)$ symmetry. In this chapter, we investigate for the first time the possibility that higher-order terms in the potential of a complex scalar dark matter field do not respect the $U(1)$ symmetry. This triggers very rich dynamics involving the angular degree of freedom of the field which play an important role in its cosmological evolution.

In the early Universe, the dark matter field is expected to be displaced away from the origin of its potential. In that way, the field explores the symmetry-breaking self-couplings. At this stage, charge is spontaneously and continuously being created and destroyed through these self-interactions. Later on, the cosmological evolution drives the field towards the minimum of its potential. As long as the symmetry-breaking terms only contain powers of the field higher than 2, the potential is still effectively quadratic and $U(1)$-preserving close to the minimum. Thus, once the charge-generating and -destroying processes freeze out, the complex scalar field is left with a net charge that is comovingly conserved at late times in its cosmological evolution, in a fashion analogous to Affleck-Dine models of baryogenesis [43]. This net charge can be viewed as an excess of particles over antiparticles in the dark matter fluid.

Our calculations show that the energy density stored in the asymmetric part (the excess of particles over antiparticles) can initially be comparable to the one stored in the symmetric part (corresponding to equal amounts of particles and antiparticles). This statement is however very dependent on the initial conditions of the evolution of the field. In fact, the asymmetry can be in excess of 95% for some choices of starting parameters. But even if the initial amount of asymmetric dark matter is subdominant to the symmetric one, there are many effects that can act to deplete the symmetric abundance. As an example, we consider a $U(1)$-symmetric coupling of the dark matter field ϕ to some other species χ, of the form $|\phi^2|\,\chi^2$. This causes a parametric instability by which the symmetric component of the dark matter resonantly decays into χ quanta, in a process that had previously been studied in the context of reheating after inflation [157, 158, 159]. By means of analytic calculations and numerical simulations, we find that the instability only shuts off when the symmetric component is of the same size as the asymmetric one. We therefore conclude that, at late times, the asymmetric part generally constitutes an $\mathcal{O}(1)$ fraction of the dark matter, and for some choices of initial conditions it can significantly dominate over the symmetric part.

The existence of a particle-antiparticle asymmetry makes the phenomenology of this model genuinely distinct to that of other scenarios in which dark matter is made up of a light scalar field. The most important observation is that the asymmetric dark matter component cannot be singly absorbed due to the conservation of particle number. This renders the standard techniques used in direct detection experiments searching for sub-eV dark matter invalid. As a consequence, alternative methods have to be devised in order to probe this dark matter model. As a concrete example, we study constraints on a Higgs portal coupling $|\phi^2||H|^2$ of the asymmetric dark matter field. Firstly, we reinterpret the collider bounds on invisible Higgs decays [160] and find a relatively weak constraint on our model, but one that is robust in the sense that it does not rely on the dark matter assumption. Then, we show how, instead of the oscillatory time-variation of fundamental constants that are normally used to probe this portal,

in the asymmetric scenario such variations only arise due to variations in the dark matter density. The most promising terrestrial search strategies are found to be related to changes in fermion masses, which occur as the Earth travels through small-scale dark matter substructure. These variations can be probed using atomic clocks [161]. Cosmological observables offer even better prospects, as our setup induces redshift variations of the Fermi constant. These can significantly alter Big Bang nucleosynthesis yields [162, 163], and produce deviations in the redshift determination of astrophysical signals using observations in different frequency bands.

After understanding the basic features and requirements for the existence of a particle-antiparticle asymmetry in the dark sector, we move on to explore the possibility that such an asymmetry is connected with a very well established one: the baryon asymmetry of the Universe.

Chapter 3 - A supersymmetric theory of baryogenesis and sterile sneutrino dark matter from B mesons. The most important evidence that particle asymmetries play an important role in nature is the observation of the baryon asymmetry of the Universe. In this chapter, we consider the possibility that the origin of the baryon asymmetry is linked to the production of dark matter, which itself is also (partly) asymmetric [65]. The feature that singles out our scenario is the fact that, in it, baryogenesis proceeds very late in the history of the Universe (at temperature of a few MeV), and directly involves B mesons in the process [164]. We present a complete embedding of the model into a supersymmetric framework, which naturally provides all the necessary ingredients to realize this scenario. Furthermore, such an embedding motivates the identification of the dark matter sector with a right-handed neutrino multiplet.

Low-scale baryogenesis and dark matter production are achieved in this mechanism when neutral B mesons, produced at MeV temperatures in the early Universe, oscillate and subsequently decay into a baryon and dark particles. The three Sakharov conditions outlined in Section 1.2.2 are satisfied as follows.

The first condition, departure from equilibrium, occurs due to the late-time decay of a long-lived scalar with a mass of $\mathcal{O}(10-100)$ GeV. This scalar could be a string modulus or the inflaton in an inflationary model featuring a very low reheating temperature. If the decay produces a large number of b quarks, these quickly hadronize to form B mesons with an abundance that can largely exceed the equilibrium one at such low temperatures.

The second condition, $\mathcal{C}$ and $\mathcal{CP}$ non-conservation, occurs when the neutral B mesons among those produced perform $\mathcal{CP}$-violating particle-antiparticle oscillations, as have been observed to occur in terrestrial experiments [165].

The third condition is baryon number violation, which in this setup is rather *visible* baryon number violation that occurs when a B meson decays into a visible baryon and a dark antibaryon. In this way, global baryon number is exactly conserved, but a net asymmetry created in the ordinary matter that is compensated by an asymmetry with the same magnitude and opposite sign in the dark matter.

The process described above is shown to be able to reproduce the observed baryon asymmetry of the Universe and to generate asymmetric dark matter.

A supersymmetric extension of the Standard Model featuring a continuous $U(1)_R$ symmetry [45] (which is identified with baryon number) and Dirac gauginos [46] provides all the ingredients necessary to implement this baryogenesis mechanism. The mediator between the ordinary and the dark matter is the bino, which as the fermionic superpartner of the B gauge boson is a singlet state. The decay of the B meson is triggered by an R-parity violating transition involving a term of the type $\mathbf{U}^c\mathbf{D}^c\mathbf{D}^c$, which produces a virtual squark that decays into a bino and a quark via a weak interaction. The bino has a mass in the $2-4\,\mathrm{MeV}$ range and carries baryon number -1, so that its Dirac (as opposed to Majorana) nature is crucial to avoid dangerous baryon number violating effects. The bino is assumed to be unstable and decay into a sterile neutrino-sneutrino pair, of which the sneutrino has baryon number -1 and is absolutely stable, constituting the dark matter.

Most of these dynamics occur at the GeV scale and therefore have numerous phenomenological and experimental consequences, which are themselves opportunities to test the mechanism. The most important one is the prediction that neutral B mesons undergo an exotic decay into a baryon and dark particles, which is required to have a branching ratio larger than 10^{-3}. This exotic decay can in principle be looked for at experiments like Belle-II and LHCb. Furthermore, the mechanism requires an enhancement of the $\mathcal{CP}$ violation in B meson oscillations over its predicted Standard Model model value. Such an enhancement is provided in the supersymmetric setup by R-parity violating squark interactions. This manifests in an enhancement of the semileptonic asymmetry in the B meson system, which may be in reach of future experimental setups. In addition to that, the model features a large number of other astrophysical and collider signatures, like dark matter capture in neutron stars, LHC searches for heavy colored scalars and long-lived particles, which can be used to probe the scenario.

The existence of particle asymmetries highlights the importance of discrete symmetries, and in particular of $\mathcal{CP}$, in our theory of nature. When discussing this symmetry, one cannot overlook one of the most pressing puzzles of the Standard Model: the strong CP problem, which motivates the study of axions.

Part II - Dark matter and axions

Axions and axion-like particles are probably the best-known examples of light dark matter candidates. In this part, we study some aspects of their phenomenology in cosmological environments and terrestrial experiments.

Chapter 4 - On the wondrous stability of ALP dark matter. When in a coherent state with a large occupation number, light bosonic particles are prone to suffer parametric instabilities that result in an exponentially fast decay of the system. This is particularly dangerous for cosmological axion populations, which are created in a homogeneous and highly occupied state and could in this way decay into photons through their coupling $g_{\phi\gamma\gamma}\phi F\tilde{F}$ [108,

107]. In this chapter, we scrutinize for the first time the cosmological stability of axion-like particle dark matter with regard to this parametric instability.

We start by studying the equations of motion for the ALP and electromagnetic fields in Minkowski spacetime. In this background, an exponentially growing photon mode is shown to appear. Its characteristic growth rate is given by $\eta \sim g_{\phi\gamma\gamma}\,\phi\,m_\phi$, i.e. it is proportional to the product of the ALP field value, its mass and its coupling to photons. This instability resonantly produces photons with momenta that lie within a thin shell of width $\delta k \sim g_{\phi\gamma\gamma}\,\phi\,m_\phi/2$ around the central value $k = m_\phi/2$. The ALP occupation number consequently diminishes at the same rate. For dark matter axion-like particles, this decay rate is smaller than the age of the Universe only if $g_{\phi\gamma\gamma} \gtrsim 10^{-18}\,\mathrm{GeV}^{-1}$, indicating a potential instability that can affect a large region of parameter space.

The situation however changes when we take into account that our Universe is not static but rather expands with a rate given by the Hubble parameter H. This implies that the wavelength of the photons created through the instability is continuously being redshifted and is "pushed" out of the narrow resonance band described above. If this redshifting occurs in a time-scale that is small compared to the rate of exponential growth of the photon mode, the resonance becomes ineffective and the ALP condensate is stabilized. The expansion of the Universe is shown to alleviate the instability of the most common axion-like particle models, making them good dark matter candidates. On the other hand, axion-like particles that enjoy a photon coupling that is enhanced with respect to the usual Nambu-Goldstone boson expectation (as in e.g. [167, 168, 169, 170, 171, 172]) still exhibit a fast parametric instability.

We then investigate the consequences of the presence of a dense plasma in the early Universe, which severely impacts the propagation properties of photons [91]. The most important effect for our purposes is shown to be linked to the existence of a cutoff frequency below which the medium does not allow photon modes to propagate. This frequency, known as the plasma frequency ω_P, effectively blocks the decay of axion-like particles with a mass $m_\phi < 2\omega_P$, that is, below twice the cutoff. After computing the plasma frequency of the primordial plasma throughout the history of the Universe, we reach two important conclusions. The first one is that the stability of axion-like particles with masses below the present-day plasma frequency in the intergalactic medium, $\omega_P^0 \sim 10^{-14}\,\mathrm{eV}$, is automatically guaranteed. The second one is that the presence of the plasma delays the appearance of the instability for heavier axion-like particles, ultimately making it slower compared to the expansion rate. The final conclusion is that all ALP dark matter models, including those featuring an enhanced photon coupling, are found to be cosmologically stable and therefore constitute viable dark matter candidates.

This chapter has established that axion-like particles with small masses and large decay constants are long-enough lived to be the dark matter of the Universe. However, in the simplest models, axion-like particles with those properties are produced only in vanishingly small amounts by the misalignment mechanism. It is therefore interesting to study the kind of modifications that are necessary for the misalignment mechanism to be more effective in the production of these particles. One such possibility is studied next.

Chapter 5 - Exploring ALPs beyond the canonical. The cosmological evolution of axion-like particles as dark matter is very sensitive to the exact form of their potential. The requirement to act as a pressureless fluid for gravitational processes requires the potential to be quadratic in a sufficiently large region around the minimum. However, deviations can occur for larger field values. For example, the discrete symmetry enjoyed by pseudo Nambu-Goldstone bosons necessarily requires their potential to be periodic. Explicit calculations yield potentials of the form $V(\phi) = \Lambda^4(1 - \cos(\phi/f))$, where f is the ALP decay constant. In this chapter, we explore the phenomenological consequences of the existence of a non-canonical kinetic term for the ALP field, focusing on a kinetic function of the form $(1/\cos(\phi/f)) \cdot \partial_\mu\phi\partial^\mu\phi$, which also respects the $\phi \to \phi + 2\pi$ periodicity. The ALP field redefinition that canonically normalizes this kinetic term results in a flattening of the potential away from the origin, as in α-attractor models of inflation [173, 174, 175]. This leads to very particular cosmological dynamics.

Most importantly, a flatter potential results in a larger dark matter yield for a given choice of initial field value. This can be readily understood in terms of the misalignment mechanism [112]. At early times, the Hubble expansion rate is large and produces an effective friction that "freezes" the field at its original position in the potential. At this stage, the energy density remains constant and the field acts like dark energy. Only when the Hubble parameter becomes sufficiently small compared to the slope of the potential does the field start evolving and behaving like dark matter. At that point, the ALP energy density starts diluting at a rate inversely proportional to the growth of the spatial volume. Given that the non-canonical kinetic term significantly flattens the potential of the axion-like particle, this dark energy-dark matter transition is delayed. This means that the energy density has less time to dilute away and is therefore larger in the late Universe. As a consequence, phenomenologically interesting regions of the parameter space where dark matter is underproduced in other models become viable when a non-canonical kinetic term is considered.

After providing an analytic estimate of the dark matter yield that is backed up with numerical computations, we turn to study the generation of isocurvature perturbations in this scenario. We derive a simple formula that parametrizes the amplitude of fluctuations in terms of an anharmonicity function that encodes the departure from a purely quadratic potential. As expected, a potential which is shallower than quadratic produces larger isocurvature fluctuations and therefore faces stronger constraints from CMB observations.

The case of the QCD axion with a non-canonical kinetic term is studied next. The main difference compared to the axion-like particle case is that the QCD axion potential is time-dependent, as it receives a contribution from the QCD topological susceptibility around the QCD phase transition [176]. In order to incorporate this particularity, we extend our previous formalism to allow for a temperature-dependent anharmonicity function. Making use of it, we identify a strong constraint to this scenario coming from Big Bang nucleosynthesis. The reason for this is that the synthesis of light elements is significantly modified in the presence of a non-vanishing QCD θ angle, as is induced by a QCD axion with a flattened potential.

So far we have focused on axions that can play an important role in our cosmological model, and which are typically very light. However, the solution to the strong CP problem is

largely insensitive to the mass of the axion. It is therefore important to also test the axion paradigm in the large mass region, a task for which terrestrial experiments are better suited than cosmological probes.

Chapter 6 - Axion couplings to electroweak gauge bosons. Collider experiments are very powerful tools to search for axions, particularly those with masses above the MeV scale. In the past, collider searches have focused on a limited set of axion couplings, the most popular one being its coupling to photons [177, 178, 89, 179, 180]. In Chapter 6, we significantly extend the reach of collider experiments as probes for axions by considering their couplings to all other gauge bosons, and by studying the interplays arising from the simultaneous coexistence of multiple couplings.

The focus of this chapter is on the QCD axion, and as such the gluon coupling, $aG\tilde{G}$, is always assumed to be present. This interaction generates an irreducible contribution to the QCD axion mass, which is linked to the non-vanishing QCD topological susceptibility. Aside from this, in our study we allow for additional mass terms that are assumed to arise in ways that do not spoil the solution to the strong CP problem. These constructions are commonly known as *heavy axion* models [106]. As a first step, the most general axion Lagrangian is constructed. Importantly, we account for the non-perturbative QCD contributions to the electroweak gauge boson couplings. These are derived by calculating the mixing angles with the pseudoscalar hadrons, which are obtained using chiral perturbation theory methods. The result is presented for QCD as well as heavy axions. This calculation, together with considerations regarding gauge invariance, showcases the necessity of simultaneously considering more than one axion coupling in phenomenological studies, in contrast to what had previously been considered.

The second half of the chapter is devoted to a phenomenological analysis of heavy axions, including all electroweak interactions and taking into account both tree-level and one-loop effects. Loop-induced couplings to photons, nucleons, and electrons are of particular phenomenological importance given that the most sensitive axion searches rely on the existence of these couplings. The possible decay channels of the axion are compared, finding that the decay to photons tends to dominate in the lower mass region, while hadronic decays induced by the QCD coupling dominate for axion masses above $\mathcal{O}(100)$ MeV. The experimental constraints on the heavy axion parameter space are then presented in a two-operator framework: the axion-gluon coupling and one electroweak gauge coupling are simultaneously considered. For that, the relative interaction strengths are assumed to be proportional to the strong and electroweak fine-structure constants, respectively. At the LHC, the most promising channel to look for heavy axions is found to be the production through strong interactions followed by an electroweak decay. The reason for this is that the QCD production proceeds with a large cross-section, while the electroweak decay results in a final state for which the backgrounds are relatively small.

Part III - Dark matter and inflation

The dynamics of light dark matter candidates in the early Universe is very sensitive to the physics of inflation, as has been exemplified in the previous chapters for the case of axions and isocurvature fluctuations. The final part of this thesis is devoted to a deeper study of the relation between light dark matter and inflation. Importantly, it constitutes a general study as it defocuses from the axion paradigm to consider more general bosonic particles. In particular, we develop new scenarios of dark matter production in the inflationary epoch of the Universe. For the first time, gravitational corrections beyond the minimal coupling are considered. These become relevant in sufficiently curved backgrounds like the inflationary one.

Chapter 7 - Lightish but clumpy: scalar dark matter from inflationary fluctuations. Light scalar fields present during inflation acquire quantum fluctuations that are stretched and become classical statistical fluctuations as spacetime expands [139, 140, 141, 142]. This process can be interpreted as particle production and as such can be an efficient production mechanism for light scalar dark matter. The caveat of this possibility is that it tends to produce too large isocurvature fluctuations, as the fluctuations of the dark matter are in general uncorrelated with the ones of the inflaton. In this chapter, we argue that the existence of a non-minimal coupling of the scalar field to gravity results in a suppression of the isocurvature perturbations at large cosmological scales. This makes production from inflationary fluctuations a viable origin for the dark matter of the Universe.

Non-minimal couplings of scalar fields to gravity are very well-motivated by arguments of quantum field theory in classically curved backgrounds [181, 140, 182]. In particular, a coupling of the form $\xi\phi^2 R$, where ξ is a dimensionless coupling constant and R is the Ricci scalar, results in an effective spacetime dependent mass for the scalar field ϕ. The Ricci scalar vanishes at the background level during radiation domination but is proportional to the Hubble scale of inflation H_I during the inflationary epoch in the early Universe. As a consequence, a scalar field enjoying such non-minimal coupling acquires a large effective mass during inflation, but can be very light in the later stages of the cosmological history.

As opposed to light fields, which acquire a scale-invariant spectrum of fluctuations during inflation, scalar fields with masses of $\mathcal{O}(H_I)$ or larger feature a blue-tilted spectrum. This means that the fluctuations of the field at large spatial scales are suppressed with respect to the ones at small scales. To quantify this effect, we follow the quantum dynamics of the scalar field in the curved inflationary background in order to obtain expressions for the power spectra of field and energy density perturbations. Assuming that the scalar field constitutes the dark matter of the Universe, the power spectra are subsequently evolved through radiation and matter domination until they reach the nonlinear regime of structure formation. The result is a peaked spectrum in which the power is concentrated around a critical comoving wavenumber that is denoted as $k_\star$, while it steeply decreases when moving towards smaller and larger wavenumbers.

There are two main consequences associated with the dynamics delineated above. Firstly,

the amplitude of the dark matter isocurvature density fluctuations at CMB scales is strongly suppressed and can be made compatible with the stringent constraints set by the Planck satellite [156]. Secondly, the peaked structure of the density power spectrum indicates that the majority of the dark matter is stored in overdensities of typical comoving size $k_\star^{-1}$. These overdensities are expected to decouple from the Hubble flow at the time of matter-radiation equality, sourcing rich dark matter substructure at small cosmological scales. The size of this dark matter subhaloes can be linked to the size of the non-minimal coupling to gravity, potentially motivating the study of dark matter substructure as a window to the behavior of gravity in large spacetime curvature regimes.

The finding of such rich dynamics motivates the study of more general scenarios involving light bosonic dark matter candidates and inflation, leading to our final topic of study.

Chapter 8 - Misalignment & Co.: (Pseudo-)scalar and vector dark matter with curvature couplings. This chapter builds up and extends the study of the previous one by considering light scalar and vector dark matter with a non-minimal coupling to gravity. Furthermore, it presents additional production mechanisms which are affected by the existence of such generalized gravitational interactions. As opposed to the scalar case, in which the non-minimal couplings to gravity have been well studied [181, 140, 182], vector fields have been far less explored. We concentrate on a coupling of the form $\kappa X_\mu X^\mu R$, where κ is a dimensionless coupling constant and R is the Ricci scalar, and which has been considered in [190, 191, 192, 193]. As in the scalar case, this coupling induces an effective mass for both transversal and longitudinal polarizations of the vector field.

For the case of scalars, we demonstrate how the Hubble-induced effective mass during inflation results in a modification of the misalignment mechanism. As the field becomes massive during inflation, it naturally slow-rolls towards the minimum of its potential. This ultimately results in a reduction of the dark matter yield and a suppression of isocurvature perturbations for a given initial (preinflationary) field value. In addition, we calculate the contribution to the dark matter energy density arising from quantum fluctuations during inflation, in the spirit of the previous chapter. This production mechanism is shown to be dominant for large field masses, high inflationary scales, and long periods of inflation. Finally, we discuss the "stochastic scenario" [194, 195], in which super-horizon scalar field fluctuations accumulate during a long period of inflation. These super-horizon fluctuations behave like an effective contribution to the homogeneous field value within each separate Hubble patch. We find that this scenario suffers from a severe isocurvature problem unless the non-minimal coupling to gravity is vanishingly small.

The case of a massive vector field is also studied, highlighting the difference between the transversal and longitudinal polarizations. It is well known that the misalignment mechanism is not viable for minimally coupled vector fields because their energy density is diluted as their wavelengths are stretched during inflation [189, 112]. However, we show that the inclusion of a non-minimal coupling of a suitable size can counteract this dilution and enable the misalignment production of vector dark matter. Interestingly, while transversal fluctuations always give a

contribution to the energy density, longitudinal fluctuations are suppressed unless the vector field is sufficiently massive. Furthermore and in parallel to the scalar case, a component of vector dark matter is also produced from inflationary fluctuations, independently of initial conditions. These fluctuations are either predominantly of longitudinal type when the field couples minimally to gravity [196], or of transversal type when a sizable non-minimal coupling is present. Finally, we introduce the stochastic scenario for vectors, for which the energy density is dominated by transverse modes unless the vector field is sufficiently massive.

9.2 Discussion and reflection

The research performed in the course of this thesis is to be framed within the big picture of cosmology and particle physics. Indeed, looking at various open questions in both fields has been our guiding principle in choosing what dark matter scenarios to study. After the main results of this work have been presented, it is time to reflect on the global interpretation of those findings. Each chapter contains an independent discussion detailing the more specific individual conclusions. Because of that, here we rather focus on the aspects that are universal to multiple (or all) of the chapters, and therefore constitute the concluding remarks of the thesis as a whole. There are five main ideas that serve as guiding posts in portraying our conclusions.

A sight of the landscape beyond the Standard Model

In the introduction, we set out to the endeavor of identifying particularly well-motivated dark matter scenarios, in the sense that the theories that produce the dark matter candidate can, at the same time, address open issues in the Standard Models of particle physics or cosmology. This strategy has proven to be very fruitful, resulting in theories of dark matter that do not only address those issues, but also present features that can potentially single them out at the observational and experimental levels. As some examples, we have studied the case of asymmetric dark matter and its potential connection to baryogenesis in Part I, axions and their experimental signatures in Part II, and dark matter of inflationary origin that clumps together at sub-galactic scales in Part III.

In the process, it has become clear that thinking about dark matter as a component of theories beyond the Standard Model is not only useful to infer the properties of the dark matter candidate, but can in addition shed light on the theories themselves. In this way, our initial argumentation is turned upside down: the viability or eventual detection of dark matter with some particular properties can give strong hints of what may lie ahead in our quest for a more complete theory of nature. This way of thinking is not new by itself: various examples can be found in the literature that exploit this approach. In this thesis, we have found novel ways in which this argumentation can be implemented.

A first case of study is the supersymmetric model of Chapter 3, which provides a mechanism for baryogenesis and asymmetric dark matter production. A particularly interesting feature is

that it allows for a very low scale of baryogenesis, essentially as low as possible given the need for it to occur before nucleosynthesis proceeds at a temperature just below 1 MeV [197]. This makes it possible to combine it with models of inflation that have low reheating scales, something that is problematic for many other baryogenesis setups. Incidentally, low-scale baryogenesis scenarios are a necessity of some axion dark matter models, which favor low inflationary scales in order to avoid isocurvature constraints, as discussed in Chapter 5. The achievement of successful baryogenesis in this setup motivates a singular connection with the dark matter problem. Imposing baryon number to be globally conserved leads to the compensating baryon asymmetry being necessarily stored in the dark sector, which consequently contains dark GeV-scale antibaryons that can significantly contribute to the dark matter abundance of the Universe. In a supersymmetric setup in which baryon number is identified with a continuous $U(1)_R$ symmetry, this dark matter component can be identified with a sterile sneutrino, which has the adequate global charge assignments. Similarly, the role of the mediator between the visible and the dark sectors is played by a Dirac bino with a $\mathcal{O}\,(\,\mathrm{GeV})$ mass, which also carries baryon number. In this way, the requirements stemming from successful baryogenesis and dark matter production motivate a very particular supersymmetric extension of the Standard Model with a concrete superpartner spectrum. These arguments can help guide experimental searches to look for non-standard supersymmetric scenarios, as discussed in Section 3.7.

Thinking about the role of axions (and other light scalars) as dark matter can also give an insight about the theory that contains them. One of the cornerstones of our work has been the misalignment mechanism, which very generally predicts the existence of cosmological populations of light scalars that can survive until today, as shown in Chapter 4. The subsequent present-day abundance of axions is only dependent on very fundamental parameters (masses and decay constants), the expansion history of the Universe, and (sometimes) an initial condition. In this sense, for a given mass and decay constant, we can regard the contribution of axions to the dark matter of the Universe as "irreducible". This can either favor some particular combination of parameters like $\mathcal{O}\,(100)$ μeV QCD axions [198, 199, 200, 201], disfavor other combinations on the basis that too much dark matter would be produced, or motivate the existence of non-standard axion models that can generate a large enough density in regions of parameter space that would otherwise underproduce dark matter, in the spirit of Chapter 5. Given this generality, even the *non*-observation of axion dark matter in a given region of parameter space can yield very relevant information about the particle content of theories beyond the Standard Model.

In a more phenomenologically motivated fashion, axions with small masses and large decay constants are appealing dark matter candidates because they are accessible to many proposed (and some projected) experiments, like ABRACADABRA [202], ADMX [203], BRASS [204], CULTASK [205] HAYSTAC [206], KLASH [207], MadMax [208], ORGAN [209], QUAX [210], or RADES [211]. In that regard, the novel findings of Chapter 4 assuring the cosmological stability of axion-like particles with those properties are crucial in assessing the viability and prospects for those experiments. Going further and as exemplified by Chapter 5, a positive detection by one of those experiments in a region where the misalignment mechanism

underproduces dark matter would be solid evidence for the necessity of going beyond the simplest models. An axion could also be found in a setup that does not rely on the dark matter assumption, like a high-energy experiment, as pursued in Chapter 6. Such a potential detection, if compatible with a solution to the strong CP problem but not with dark matter, would constitute a paradigm shift for dark matter searches, perhaps moving the focus away from the QCD axion region into other less explored areas of parameter space.

Finally, this thesis has brought to light the sensitivity of light bosonic dark matter to the physics of inflation. Traditionally, the bounds on the amplitude of isocurvature perturbations have been used to "constrain" the scale of inflation, assuming dark matter to be made of a light scalar field that was present during inflation [212, 213, 214, 215, 216, 217]. This has also been discussed in detail for particular dark matter models throughout this thesis. In Chapters 7 and 8, we have gone beyond that in showing that there are other properties of inflation that can play a key role in the production of light bosons during that epoch. For the same physics model, different mechanisms (misalignment, production from fluctuations, and the stochastic scenario) have different degrees of efficiency in generating dark matter depending not only on the scale of inflation, but also on its duration and how much it departs from an exact de Sitter expansion. Based on these observations, one could even imagine reconstructing the time-evolution of the primordial spectral index through the observation of the present-day power spectrum of (a subcomponent of) dark matter in the form of a light scalar field. What is more, the additional dependence on the non-minimal coupling of the field to gravity can also give information about the inflaton sector. The reason for this is that the Jordan-frame non-minimal coupling leads to a coupling of the dark matter field to the inflaton in the Einstein frame.

All in all, throughout this thesis we have learned that there is a very rich way of thinking about dark matter and physics beyond the Standard Model that is two-way: the former has the ability of telling us as much about the latter as the other way around.

Dark matter is more than just one number

Often when we think about dark matter, we tend to essentially identify it with one single value: its abundance in the Universe, which can be given as a fraction of the critical density as $\Omega_c \simeq 0.26$ [12]. A model of (cold) dark matter is successful if it can reproduce this number, and we usually think there is not much more to worry about. One then tends to focus on potentially detectable interactions of the dark matter particle with the visible sector in order to test the model. In doing that, we are often leaving aside a very powerful tool to distinguish between and probe the different models: the properties of the large- and small-scale distribution of dark matter. In this thesis, this has been a recurrent finding. Repeatedly, we have encountered that the attributes of the dark matter particles and their production mechanisms result in particular features regarding how dark matter is scattered throughout the Universe.

When comparing the clustering properties of dark matter in different scenarios, it is useful to have a well-understood and simple benchmark model against which to contrast. The vanilla

cold dark matter paradigm, in which structure is formed hierarchically from the smallest to the largest scales, is the usual choice for this. Its main properties are a purely adiabatic primordial power spectrum with a slight red tilt and a cutoff occurring at a such small scale that it can be ignored for all practical purposes. Because the distribution of dark matter is relatively well understood and measured on large cosmological scales, it is reasonable to distinguish between deviations of this paradigm that occur at large and small scales[1]. While deviations at large scales have to be tiny, this is not necessarily the case at small scales.

Focusing on large scales first, the distinction between adiabatic and isocurvature fluctuations has proven to be a powerful tool. If dark matter is made up of some light bosonic field that is produced in the very early Universe through the misalignment or some similar mechanism, we have seen that its perturbations at large cosmological scales generally contain some degree of isocurvature. Because observations of the CMB show that the dark matter density power spectrum is adiabatic to a very high accuracy, this prediction has turned out to be extremely useful in constraining the properties of the wide variety of models that has been explored in this thesis. This was particularly relevant in Chapters 5, 7 and 8. What is more, the necessity of suppressing the isocurvature power at CMB scales has been one of the main motivations to develop the scenarios presented in Part III.

That being said, the most important results of this work are related to the clustering behavior of dark matter at scales much below the ones accessible to the CMB. The most striking observation is related to the findings in Chapters 7 and 8, in which the isocurvature power spectrum has a strong blue tilt and features a peak with a large amplitude at some small scale. Two main consequences can be readily derived. The first one is that even if the isocurvature fluctuations are strongly suppressed at CMB scales [156], they can be sizable at intermediate scales and have an impact in the formation of structures. The second one is the presence of a distinguished scale at which the fluctuations are so large that they are expected to decouple from the Hubble flow and form bound structures as early as at matter-radiation equality. Although a more careful study of the formation and survival of these clumps within a cosmological context is warranted, their presence would entail important consequences for astrophysical and direct detection purposes.

Furthermore and as discussed in Chapter 2, self-interactions of light scalar fields can lead to very interesting cosmological phenomenology. On the one hand, a scalar field with a large (repulsive) quartic self-coupling redshifts as radiation and effectively behaves as hot or warm dark matter at different stages of its evolution. This can cause noticeable effects in the CMB power spectrum [110], but also in Lyman-α forest observations [111]. In addition to that, the non-linearities in the potential can cause the fragmentation of the field in a resonant process that produces explosive self-particle production. For attractive self-interaction, this has been shown (see, for instance, [218, 219]) to cause significant deviations in the clustering properties of the dark matter, and lead to the formation of bound objects.

[1] In other words, we distinguish between scales for which linear cosmological perturbation theory is valid and those for which it breaks down due to non-linear effects in structure formation.

Given that, so far, gravity is our only source of information regarding the dark matter properties, it is imperative that we go beyond the single number describing its abundance and explore deeper attributes of its cosmological dynamics. As this thesis shows, even in the most extreme case in which the dark matter has only gravitational interactions, there is a lot that we can learn about its particle nature by studying its clustering properties at large and small cosmological scales. This exemplifies how the distribution of dark matter in the Universe can be a mirror for its particle nature, and it is therefore one that we should carefully inspect.

The discrete importance of discrete symmetries

In this thesis we have studied a number of different topics like dark matter, baryogenesis, axions and inflation, and established possible connections between some of them. At the heart of many of these open questions in physics there is a common origin that has sometimes passed by unnoticed but that should not be overlooked: the discrete symmetries of parity, charge conjugation, time reversal, and combinations thereof. In particular, the degree at which these symmetries are conserved or broken in different processes is of uttermost importance for their outcome. Understanding the possible sources of $\mathcal{C}$, $\mathcal{P}$, and $\mathcal{T}$ violation in the Standard Model and theories beyond it thus deserves careful attention.

An example in which this is particularly manifest is the baryogenesis model discussed in Chapter 3. It is well known that $\mathcal{C}$ and $\mathcal{CP}$ violation are both necessary to produce a baryon number asymmetry, as was discussed in Section 1.2.2. Common lore says that the Standard Model of particle physics does not provide enough $\mathcal{CP}$ violation to produce the observed asymmetry. This fact is linked to the idea that baryogenesis has to proceed at around the electroweak phase transition when baryon number-violating sphaleron process are active. At those high temperatures, the only known source of $\mathcal{CP}$ violation in the Standard Model - complex Yukawa couplings - is suppressed and thus not enough to generate a sufficient asymmetry. In our scenario, thanks to the more relaxed requirement of only needing an effective baryon number violation in the visible sector, baryogenesis proceeds at much lower temperatures when the effects of $\mathcal{CP}$ violation from the CKM matrix are unsuppressed. That said, we find that even in this case, the Standard Model prediction for the quantities measuring the relevant $\mathcal{CP}$ violation - the semileptonic asymmetries in B meson decays - fall a bit short of the values needed to reproduce the observed baryon asymmetry. This is mostly because some of the contributions, though large enough in modulus, come with the sign that acts to erase the baryon asymmetry. However, given that experimental constraints on the semileptonic asymmetries are a factor of ~ 10 looser than the Standard Model predictions [165], there is significant room for new physics to drive the $\mathcal{CP}$ violation in the direction that is necessary in our setup. This makes it especially important to precisely understand how $\mathcal{CP}$ violation behaves in the Standard Model and beyond, both from the theoretical and the experimental perspective.

It is not only baryogenesis that depends on the existence of $\mathcal{C}$ and $\mathcal{CP}$ violation - the dynamical generation of any net global charge requires these discrete symmetries to be broken

as well. An example of this was presented in Chapter 2, in which the global charge translates into a particle-antiparticle imbalance in the dark sector. There, the required $\mathcal{C}$ and $\mathcal{CP}$ violation is generated by the non-vanishing vacuum expectation value of a complex scalar field. This kind of $\mathcal{CP}$ violation only occurs for a short period of time in the early Universe and is qualitatively different from one that is hard-wired into the Lagrangian. Although its origin can be traced back to some explicitly $\mathcal{CP}$-breaking terms in the potential, it is effectively amplified by the motion of the scalar field, and this allows to generate a large charge asymmetry even from a small $\mathcal{CP}$ non-conserving seed. This transient sort of $\mathcal{CP}$ violation has two main practical drawbacks: it is extremely challenging to be tested experimentally given that it was only active in the early Universe, and it features a strong dependence on the initial conditions of the evolution of the field, which somewhat dilutes the predictivity of the scenario.

Finally, it goes without saying that the $\mathcal{CP}$ symmetry is at the very root of axion physics. On one hand, there is experimental evidence for the absence of $\mathcal{CP}$ conservation in the Yukawa couplings. On the other hand, there are indications that $\mathcal{CP}$ needs to be further violated in order to give rise to baryogenesis. In light of these facts, it is extremely surprising that the only other physical $\mathcal{CP}$-violating parameter of the Standard Model, the QCD θ angle, is observed to be vanishingly small. The QCD axion is a very elegant solution to this quandary, but not a completely satisfactory one in the sense that it does not seem to follow a global criterium with respect to the fundamental nature of discrete spacetime symmetries. An argumentation in the lines of the Vafa-Witten theorem [84] assures that minimization of the energy naturally favors the $\mathcal{CP}$-conserving vacuum. Although this is partially satisfactory, the necessary introduction of a Peccei-Quinn symmetry may feel somewhat *ad hoc*. After all, why should nature be provided with the precise tools to switch off $\mathcal{CP}$ violation in the strong interactions, but not in other sectors? The search for axions, in astrophysical setups as well as in terrestrial experiments, as undertaken in Chapter 6, is of crucial importance to shed some light on this quandary.

The task of understanding the role of discrete symmetries in nature is one that sits at the core of many of the questions that we aim to solve in particle physics and cosmology. This is not only a question of theoretical interest, but also one of very direct phenomenological consequences. As we have recurrently encountered in this thesis, the conservation (or absence thereof) of charge conjugation, parity, and time reversal can dictate to a surprisingly large degree what the Universe looks like and what it is made of. Unveiling the transformation properties of the dark matter of the Universe under these symmetries, a goal which this work has contributed to achieve, may constitute a crucial step forward in this direction.

Particle physics and cosmology are symbiotic

Over the past few decades, it has become more evident that particle physics and cosmology are closely intertwined. On the one hand, the former (together with gravity) serves as a language in which to formulate the latter. On the other hand, the latter offers a unique environment in which the theories of the former can be tested. Some of the most interesting findings in this thesis have in fact been obtained by leveraging the interaction between the two fields.

Axions are a paradigmatic example of this interplay, as has been highlighted in many occasions (see Chapters 4 to 6) throughout this work. As a matter of fact, the QCD axion is an inherently cosmological answer to an *a priori* purely particle physics question, that of the strong CP problem. The connection is strengthened by the possibility that QCD axions may serve a double purpose and also constitute the dark matter of the Universe. In fact, this possibility is one of our only "hopes" to eventually find experimental proof for the existence of the QCD axion: to find dark matter axions. Otherwise, this task could be rendered to be virtually impossible, as its extremely weak interactions make the QCD axion very challenging to be both produced and detected in an experimental setup. The dark matter option allows to partially circumvent this difficulty by providing an abundant population of axions with which to experiment.

Chapter 3 constitutes a new instance of how fruitful the combination of cosmological and particle physics considerations can be in developing viable new physics models. Indeed, one of the novelties of the approach presented is the realization of a potential connection between the generation of the baryon asymmetry of the Universe and measurements of $\mathcal{CP}$-violating observables in the B meson system. In this model, the key cosmological observation to reproduce, the baryon-to-photon ratio, is given by a product of two quantities. The first one is the branching ratio of neutral B mesons into a visible baryon-number violating final state, and the second one are the semileptonic $\mathcal{CP}$ asymmetries in flavor-specific B decays. Both are weighted by a temperature-dependent factor that takes into account decoherence effects in the early-Universe plasma. Once the dependencies on the cosmological history have been accounted for, the model yields a very specific prediction for observables accessible in B-factory experiments, which can then directly probe very relevant dynamics of the early Universe. Furthermore, the difficulty of introducing baryon number violation at low energies in the Standard Model, together with the observation of the existence of dark matter, motivates the idea that a compensating baryon asymmetry is stored in the dark sector. Then, the fact that the scalar superpartners of sterile neutrinos naturally carry negative baryon number in the supersymmetric extension of the Standard Model that we consider, ultimately leads to their identification as dark matter candidates.

Another major result of this thesis is the potential connection between the dynamics of dark matter and the behavior of gravity in environments of increasingly large curvature. The understanding of the relationship between gravity and the quantum theory that describes the interactions of particles is one of the milestones of theoretical physics. This is a question that particle physics is very unlikely to be able to address without the input from cosmology, which is one of the very few environments that can produce the extreme conditions in which hypotheses regarding this relationship may be tested. In Chapters 7 and 8, we have demonstrated that the fine sensitivity of the production mechanisms of light scalar dark matter to even slight modifications of gravity has the potential to provide valuable insights on this matter. In this regard, we have shown that observations of the distribution of dark matter in small and intermediate scales can be directly linked to the size of non-minimal interactions of scalar and vector fields with gravity. Such interactions, which are widely expected to be present, become

relevant only in sufficiently curved backgrounds.

Though learning about the reciprocal reliance that particle physics and cosmology display is certainly not a new finding, this lesson is one that has been of singular importance for this thesis. As we strive to test particle physics in more and more extreme regimes, and to probe the history and the contents of the Universe with ever increasing precision, it is only natural that this symbiosis becomes stronger.

Where is the next scale of physics?

The discovery of the Higgs boson at the LHC a few years ago contributed to robustly establish the electroweak scale as the origin of many of the dimensionful parameters in particle physics. With this and neglecting for a moment (pertinent) arguments related to the necessity of perplexingly small parameters, the Standard Model could most likely be consistently extended all the way to the Planck scale, at which point some sort of theory of quantum gravity should take over. Why should we then worry about the existence of any other intermediate scale? The culprit is to a great extent cosmology. Cosmology is surprisingly insensitive to the electroweak scale: the bulk of the mass of the baryonic matter is set by the QCD scale, baryogenesis at the electroweak phase transition does not seem easy to achieve in the Standard Model given the requirement for a first order phase transition, and there exists no known or obvious connection between the electroweak scale and dark matter, dark energy or the physics of inflation. These observations can be interpreted as strong hints in favor of the existence of dimensionful parameters unrelated to the so far well-established scales.

In this thesis, we have considered three different paradigms with respect to this next anchor point of physics after the electroweak scale.

The first one is to assume that there is a new scale "just around the corner", meaning barely out of reach for the current energy-frontier experiments spearheaded by the LHC. This was in fact a very popular take before the LHC began operation, motivated by naturalness arguments regarding the electroweak scale, but is now confronted with the fact that the LHC has failed to find any hints for new physics at the TeV scale. As a consequence, low-scale supersymmetry has fallen out of favor, or at least its minimal implementation has. In fact, well-motivated supersymmetric scenarios with a low supersymmetry-breaking scale, like the one studied in Chapter 3, remain viable, although in some cases only marginally so. If supersymmetry is just around the corner, as supersoft [46] and supersafe [220] as it may be, it tends to produce deviations which are sufficiently large to be phenomenologically relevant. And it may well be the case that these effects have already been observed, if both dark matter and baryogenesis are linked to this scale, as proposed in Chapter 3. Ongoing and future experiments will have the final word regarding this model, so we will not have to wait for long to find out. Another scale that may be in reach of present or future accelerator facilities is the Peccei-Quinn scale. As shown in Chapter 6, these experiments can be powerful tools to look for axions, as long as their decay constant is not too far from the TeV scale.

The second option is that there is indeed some - or multiple - intermediate scales, as

is generally required in many models of leptogenesis and, more importantly for this thesis, axions. Field theory axions appear as pseudo Nambu-Goldstone bosons of spontaneously broken global symmetries, and as such require the existence of a new scale generated by the vacuum expectation value of a complex field[2] that sets the axion decay constant. For the paradigmatic example of the QCD axion that makes up dark matter via the vanilla misalignment mechanism, this scale is expected to be around 10^{12} GeV. Such high scales are out of reach for any conceivable terrestrial high-energy experiment, but leveraging theoretical insights and cosmological and astrophysical data as in Chapters 4 and 5 is a possible way forward to find evidence for those prospective new physics.

Finally, the third possible option is the absence of any new fundamental scale all the way to the Planck scale. This certainly seems like a challenging option with regards to reproducing the Universe as it is observed. That said, in Chapters 7 and 8 we have presented a mechanism by which the dark matter in the Universe can be generated by purely gravitational means, and that therefore contributes to motivate this possibility. One may argue that the mass of the dark matter particles in the models considered is not in principle linked to the Planck scale, but as exemplified in the introduction when discussing axions (Section 1.3), non-perturbative effects can generate small masses for (pseudo)scalar fields without necessarily linking them to any new fundamental scale. The question of whether baryogenesis, dark energy and inflation can be accommodated without introducing any extra scale is perhaps a more intricate one which has not been addressed in this thesis.

So far, we have glanced over hierarchy or naturalness considerations. These are based on the observation that the different scales in physics tend to mix with each other. Without some sort of stabilizing mechanism or fine-tuning of parameters, the largest fundamental scale tends to "raise" the other ones to its level. This is exemplified by the discussion in Section 2.5 regarding the phenomenology of the Higgs portal in that scenario. We find that even a very small mixing with the Higgs field, which is allowed by all the symmetries of the Lagrangian, tends to lift the dark matter mass towards the electroweak scale.

In general, any time that an intermediate scale between the electroweak scale and the Planck scale is introduced, we are prompted to confront questions regarding the naturalness of the electroweak scale. In fact, the existence of the Planck scale is often regarded as the paradigmatic hierarchy problem, although admittedly no final judgment can be pronounced without a complete theory of nature at the Planck scale. Field theory axion models also generally induce a hierarchy problem that is often overlooked. The truth is that outside of the already mentioned low-scale supersymmetry, not many more satisfactory solutions exist for these hierarchy problems. In this situation, an attitude that is becoming more and more common is to leave naturalness considerations out of the spotlight, and either accept fine-tuning as a matter of life or hope that some yet-to-be-discovered mechanism solves this issue. This is

[2]The possibility exists to generate axions "dynamically" as pseudoscalar mesons of extra confining gauge groups, in which case the new scale can be generated via dimensional transmutation, analogously to the QCD scale. Furthermore, open string axions do not introduce any scale beyond the string one, but their decay constants are restricted to lie close to this scale, which typically sits around the Planck scale.

certainly not the most desirable attitude, but it becomes a necessity in the absence of other options. Given that in this thesis we have adopted this pragmatic point of view in a handful of occasions, this brief discussion should serve as an acknowledgment of this decision and what it entails.

9.3 Outlook and future directions

As we have seen so far, understanding the nature of dark matter is one of the most prominent milestones that lay ahead in our search for a complete theory of nature, albeit it is not the only one: the Standard Models of particle physics and cosmology present a number of other shortcomings that to this day wait to be addressed. The ultimate goal of this thesis has been to explore new avenues that connect light scalar dark matter and other open questions in particle physics and cosmology. The results obtained constitute first steps towards the accomplishment of this goal, and therefore motivate further investigation of the models presented in this work and their potential observable signatures. Beyond that, the success of this perspective is an incentive to develop new scenarios that allow for such an interrelation. In these final paragraphs, we suggest some natural directions that can be pursued taking advantage of the advances achieved in this thesis.

In Chapter 3, we have argued that dark matter and the matter-antimatter asymmetry of the universe may originate from particle-antiparticle oscillations and subsequent decay of B mesons in the early Universe. The predictions of this mechanism depend on parameters related to the B meson system which are experimentally accessible at colliders. The next step is therefore to design appropriate search strategies to challenge this paradigm. Indeed, experiments like Belle-II [232] and LHCb [233] are expected to be able to fully test this model in the time span of a few years. If a hint is found, upcoming long-lived particle detectors like Faser [234] or Codex-B [235] would be able to conclusively shed light on the scenario, potentially unveiling the common origin of dark and baryonic matter.

Axions and axion-like particles also offer a wide variety of exciting possibilities to explore. As we have seen in Chapter 6, in addition to their astrophysical phenomenology, axions and axion-like particles can be looked for at high energy experiments. We have concluded that it is advantageous to exploit the complementarity between searches probing different axion couplings to extract all the information that the experimental data encode. Enlarging the scope of Chapter 6, in which a two-coupling-at-a-time strategy was followed, the aim is to perform a global analysis of axion data. This approach has the potential of changing the landscape of axion searches at high energy experiments, similarly to the fields of Higgs [236, 237, 238] and neutrino physics [239, 240, 241].

In Chapters 7 and 8, it has been shown that a generalized gravitational interaction of scalar and vector fields has a dramatic impact on their production in the early Universe, which is particularly relevant if these particles are to constitute dark matter. There are some aspects that need to be better understood regarding this mechanism, in the theoretical side as well as

on the observational one.

The theoretical grounds that motivate the existence of non-minimal couplings to gravity are understood to a significant extent for general scalars [140], but not so much for other particles. Pseudo Nambu-Goldstone bosons are endowed with a shift symmetry that severely restricts the form of the couplings that they can enjoy, but gravitational effects are expected not to respect this symmetry requirement [221, 222]. It would be interesting to study the extent to which non-minimal couplings of pseudoscalar particles to gravity can arise in situations like the one presented in [223], or even in scenarios of quantum gravity like string theory. When applied to the QCD axion, these interactions may have important consequences, in a similar fashion to [224, 225], for the proposed axionic solution to the strong CP problem. For the case of vectors, it has been suggested that direct couplings to the curvature can lead to a ghost-like instability [190], but there are contradicting views on this matter [191, 192, 193] and the debate is far from settled. This certainly warrants an exhaustive investigation, including a study of the generation of non-minimal couplings in scenarios such as Stückelberg-like constructions, in order to explore the behavior of such potential instability in a more complete context.

Perhaps most importantly, gravitational production of dark matter (including mechanisms like the ones discussed in e.g. [196, 226]) leads to predictions related to the statistical properties of the distribution of matter in the Universe. These models generate a component of dark matter isocurvature with a blue spectral index and a degree of non-gaussianity, which can be tested with upcoming observations of the CMB like CMB-S4 [227], but potentially also with large scale structure probes, a possibility that is worth investigating. A blue-tilted spectrum of dark matter density fluctuations can enhance intermediate- and small-scale structure. It may then entail consequences for observables like the abundance of satellite galaxies or the formation and growth of supermassive black holes. At small sub-galactic scales, the existence of dark matter sub-haloes can be probed by direct detection (e.g. [218]), or by studying concrete astronomical effects like tidal disruption of systems [228], stellar dynamics using e.g. Gaia data in the spirit of [229] or lensing events (e.g. [230, 231]).

These complementary theoretical and phenomenological studies would allow to link observational properties of the distribution of dark matter with the behaviour of gravity at large curvature. Evidence for such connection would dramatically improve our understanding of gravitational interactions at scales otherwise not experimentally accessible in other approaches. At the same time, it would provide an explanation for astrophysical observations of small-scale structure that may be challenging to interpret within the standard cold dark matter paradigm.

The specific directions mentioned above are only some instances of the exciting physics that can emerge from the study of theoretical connections between different open problems in particle physics and cosmology. If there is anything to learn from this thesis, it is that scrutinizing these potential links is one of the most fruitful ways of developing well-motivated scenarios that can describe nature beyond what is currently understood. The lesson is thus clear: let us keep an open mind and continue exploring!

Acknowledgments

A thesis, like life, is a path that is not to be travelled alone, and I am very thankful for having enjoyed a wonderful company throughout mine.

First and foremost, I owe incomensurable gratitude to my advisor, Joerg Jaeckel. It is from him that I have learned nearly all of what I now know about physics and, most importantly, what I now know about thinking about physics. Besides him, I have been extremely lucky in having learned from three other "complementary advisors": Belén Gavela, Ann Nelson and Michael Spannowsky. They have been welcoming hosts and altruistic supporters in many aspects, both scientific and personal, of my early career. I am also thankful to Arthur Hebecker for agreeing to review this thesis and to Stephanie Hansmann-Menzemer and Matthias Bartelmann for completing my examination committee.

I gratefully acknowledge support from the European Union's Horizon 2020 research and innovation programme under the Marie Sklodowska-Curie grant agreements 674896/690575, and by the Fundación "la Caixa" via a "la Caixa" postgraduate fellowship.

The work presented here would not have been possible without the cooperation of my collaborators. Beyond the aforementioned "advisory board", it has been a pleasure to work with such dedicated people as Pablo Quílez, Thomas Hugle, Julia Gehrlein, Sebastian Schenck, Gilly Elor, Huangyu Xiao, and Rick Gupta. Furthermore, many others whose names have not appeared alongside mine in any publication (so far) have also contributed to bring this dissertation to life. The Heidelberg colleagues: my seniors Tilman Plehn, Susanne Westhoff, Martin Bauer, Juan González-Fraile, Michael Russell, Jennifer Thompson, Sebastian Bruggisser, and Ilaria Brivio; my predecessors Patrick Foldenauer, Johann Brehmer, Torben Schell, and Anja Butter; my contemporaries Anke Biekötter, Katja Böhnke, Nastya Filimonova, Peter Reimitz, and Ramon Winterhalder; my successors Lennert Thormählen, Marco Bellagente, Sascha Diefenbacher, Michel Luchmann, and Ruth Schäfer; and all other inhabitants of Philosophenweg. The elusiνes family: Álvaro Hernández, Elena Perdomo, Nuno Agostinho, Rupert Coy, Julia Stadler, Andrea Caputo, and all other ESRs and node coordinators.

But all of this would have been void without my most faithful companions: mamá, papá, Paula, and Marta. I cannot imagine a better fellowship for this and all other journeys, past and to come. Thank you for *everything*.

Bibliography

[1] Gonzalo Alonso-Álvarez and Joerg Jaeckel. "Exploring axionlike particles beyond the canonical setup". *Phys. Rev.* D98.2 (2018), 023539. arXiv: 1712.07500 [hep-ph] (cit. on p. v).

[2] Gonzalo Alonso-Álvarez and Joerg Jaeckel. "Lightish but clumpy: scalar dark matter from inflationary fluctuations". *JCAP* 1810.10 (2018), 022. arXiv: 1807.09785 [hep-ph] (cit. on p. v).

[3] G. Alonso-Álvarez, M.B. Gavela, and P. Quilez. "Axion couplings to electroweak gauge bosons". *Eur. Phys. J. C* 79.3 (2019), 223. arXiv: 1811.05466 [hep-ph] (cit. on p. v).

[4] Gonzalo Alonso-Álvarez, Joerg Jaeckel, and Thomas Hugle. "Misalignment & Co.: (Pseudo-)scalar and vector dark matter with curvature couplings". *JCAP* 02 (2020), 014. arXiv: 1905.09836 [hep-ph] (cit. on p. v).

[5] Gonzalo Alonso-Álvarez et al. "Very Light Asymmetric Dark Matter". *JCAP* 09 (2019), 003. arXiv: 1906.00969 [hep-ph] (cit. on p. v).

[6] Gonzalo Alonso-Álvarez et al. "A Supersymmetric Theory of Baryogenesis and Sterile Sneutrino Dark Matter from B Mesons". *JHEP* 03 (2020), 046. arXiv: 1907.10612 [hep-ph] (cit. on p. v).

[7] Gonzalo Alonso-Álvarez et al. "On the Wondrous Stability of ALP Dark Matter". *JCAP* 03 (2020), 052. arXiv: 1911.07885 [hep-ph] (cit. on p. v).

[8] R.H. Dicke et al. "Cosmic Black-Body Radiation". *Astrophys. J.* 142 (1965), 414–419 (cit. on p. 2).

[9] Arno A. Penzias and Robert Woodrow Wilson. "A Measurement of excess antenna temperature at 4080-Mc/s". *Astrophys. J.* 142 (1965), 419–421 (cit. on p. 2).

[10] D.J. Fixsen et al. "The Cosmic Microwave Background spectrum from the full COBE FIRAS data set". *Astrophys. J.* 473 (1996), 576. arXiv: astro-ph/9605054 (cit. on pp. 2, 17).

[11] G. Hinshaw et al. "Nine-Year Wilkinson Microwave Anisotropy Probe (WMAP) Observations: Cosmological Parameter Results". *Astrophys. J. Suppl.* 208 (2013), 19. arXiv: 1212.5226 [astro-ph.CO] (cit. on pp. 2, 17).

[12] N. Aghanim et al. "Planck 2018 results. VI. Cosmological parameters". (2018). arXiv: 1807.06209 [astro-ph.CO] (cit. on pp. 2, 17, 264).

[13] Will J. Percival et al. "Measuring the Baryon Acoustic Oscillation scale using the SDSS and 2dFGRS". *Mon. Not. Roy. Astron. Soc.* 381 (2007), 1053–1066. arXiv: 0705.3323 [astro-ph] (cit. on p. 3).

[14] Daniel J. Eisenstein et al. "SDSS-III: Massive Spectroscopic Surveys of the Distant Universe, the Milky Way, and Extra-Solar Planetary Systems". *AJ* 142.3, 72 (Sept. 2011), 72. arXiv: 1101.1529 [astro-ph.IM] (cit. on p. 3).

[15] T.M.C. Abbott et al. "Dark Energy Survey year 1 results: Cosmological constraints from galaxy clustering and weak lensing". *Phys. Rev. D* 98.4 (2018), 043526. arXiv: 1708.01530 [astro-ph.CO] (cit. on p. 3).

[16] Joop Schaye et al. "The EAGLE project: Simulating the evolution and assembly of galaxies and their environments". *Mon. Not. Roy. Astron. Soc.* 446 (2015), 521–554. arXiv: 1407.7040 [astro-ph.GA] (cit. on p. 3).

[17] Mark Vogelsberger et al. "Introducing the Illustris Project: Simulating the coevolution of dark and visible matter in the Universe". *Mon. Not. Roy. Astron. Soc.* 444.2 (2014), 1518–1547. arXiv: 1405.2921 [astro-ph.CO] (cit. on p. 3).

[18] Matthias Bartelmann and Peter Schneider. "Weak gravitational lensing". *Phys. Rept.* 340 (2001), 291–472. arXiv: astro-ph/9912508 (cit. on p. 3).

[19] F. Zwicky. "On the Masses of Nebulae and of Clusters of Nebulae". *Astrophys. J.* 86 (1937), 217–246 (cit. on p. 3).

[20] Volker Springel et al. "Populating a cluster of galaxies. 1. Results at z = 0". *Mon. Not. Roy. Astron. Soc.* 328 (2001), 726. arXiv: astro-ph/0012055 (cit. on p. 3).

[21] V.C. Rubin, N. Thonnard, and Jr. Ford W.K. "Rotational properties of 21 SC galaxies with a large range of luminosities and radii, from NGC 4605 /R = 4kpc/ to UGC 2885 /R = 122 kpc/". *Astrophys. J.* 238 (1980), 471 (cit. on p. 3).

[22] Kyle A. Oman et al. "The unexpected diversity of dwarf galaxy rotation curves". *Mon. Not. Roy. Astron. Soc.* 452.4 (2015), 3650–3665. arXiv: 1504.01437 [astro-ph.GA] (cit. on p. 3).

[23] P.J.E. Peebles. "Large scale background temperature and mass fluctuations due to scale invariant primeval perturbations". *Astrophys. J.* 263 (1982). Ed. by M.A. Srednicki, L1–L5 (cit. on p. 3).

[24] J.R. Bond, A.S. Szalay, and Michael S. Turner. "Formation of Galaxies in a Gravitino Dominated Universe". *Phys. Rev. Lett.* 48 (1982), 1636 (cit. on p. 3).

[25] George R. Blumenthal, Heinz Pagels, and Joel R. Primack. "GALAXY FORMATION BY DISSIPATIONLESS PARTICLES HEAVIER THAN NEUTRINOS". *Nature* 299 (1982), 37–38 (cit. on p. 3).

[26] George R. Blumenthal et al. "Formation of Galaxies and Large Scale Structure with Cold Dark Matter". *Nature* 311 (1984). Ed. by M.A. Srednicki, 517–525 (cit. on p. 3).

[27] Teresa Marrodán Undagoitia and Ludwig Rauch. "Dark matter direct-detection experiments". *J. Phys.* G43.1 (2016), 013001. arXiv: 1509.08767 [physics.ins-det] (cit. on p. 3).

[28] Tracy R. Slatyer. "Indirect Detection of Dark Matter". *Proceedings, Theoretical Advanced Study Institute in Elementary Particle Physics : Anticipating the Next Discoveries in Particle Physics (TASI 2016): Boulder, CO, USA, June 6-July 1, 2016*. 2018, 297–353. arXiv: 1710.05137 [hep-ph] (cit. on p. 3).

[29] Felix Kahlhoefer. "Review of LHC Dark Matter Searches". *Int. J. Mod. Phys.* A32.13 (2017), 1730006. arXiv: 1702.02430 [hep-ph] (cit. on p. 3).

[30] Maxim Markevitch et al. "Direct constraints on the dark matter self-interaction cross-section from the merging galaxy cluster 1E0657-56". *Astrophys. J.* 606 (2004), 819–824. arXiv: astro-ph/0309303 (cit. on p. 3).

[31] C.S. Wu et al. "Experimental Test of Parity Conservation in β Decay". *Phys. Rev.* 105 (1957), 1413–1414 (cit. on p. 5).

[32] R.L. Garwin, L.M. Lederman, and Marcel Weinrich. "Observations of the Failure of Conservation of Parity and Charge Conjugation in Meson Decays: The Magnetic Moment of the Free Muon". *Phys. Rev.* 105 (1957), 1415–1417 (cit. on p. 5).

[33] J.H. Christenson et al. "Evidence for the 2π Decay of the K_2^0 Meson". *Phys. Rev. Lett.* 13 (1964), 138–140 (cit. on p. 5).

[34] A. Angelopoulos et al. "First direct observation of time reversal noninvariance in the neutral kaon system". *Phys. Lett. B* 444 (1998), 43–51 (cit. on p. 5).

[35] O. W. Greenberg. "Why is CPT fundamental?" *Found. Phys.* 36 (2006), 1535–1553. arXiv: hep-ph/0309309 [hep-ph] (cit. on p. 5).

[36] R. Jost. "A remark on the C.T.P. theorem". *Helv. Phys. Acta* 30 (1957), 409–416 (cit. on pp. 5, 7).

[37] E. P. Wigner. *Gruppentheorie und ihre Anwendung auf die Quanten Mechanik der Atomspektren*. Friedrich Vieweg und Sohn, 1931; E. P. Wigner. *Group Theory and its Application to the Quantum Mechanics of Atomic Spectra*. New York: Academic Press, 1959. ISBN: 978-0-1275-0550-3. Cit. on p. 5.

[38] Steven Weinberg. *The Quantum theory of fields. Vol. 1: Foundations*. Cambridge University Press, June 2005. ISBN: 978-0-521-67053-1 (cit. on p. 6).

[39] Marcus Berg et al. "The Pin Groups in Physics: C, P and T". *Reviews in Mathematical Physics* 13.08 (Aug. 2001), 953?1034. ISSN: 1793-6659. arXiv: math-ph/0012006 [math-ph]. URL: http://dx.doi.org/10.1142/S0129055X01000922.

[40] Makoto Kobayashi and Toshihide Maskawa. "CP Violation in the Renormalizable Theory of Weak Interaction". *Prog. Theor. Phys.* 49 (1973), 652–657 (cit. on pp. 7, 11).

[41] B. Pontecorvo. "Inverse beta processes and nonconservation of lepton charge". *Sov. Phys. JETP* 7 (1958), 172–173 (cit. on p. 7).

[42] Ziro Maki, Masami Nakagawa, and Shoichi Sakata. "Remarks on the unified model of elementary particles". *Prog. Theor. Phys.* 28 (1962), 870–880 (cit. on p. 7).

[43] Ian Affleck and Michael Dine. "A New Mechanism for Baryogenesis". *Nucl. Phys.* B249 (1985), 361–380 (cit. on pp. 7, 254).

[44] F. Gabbiani et al. "A Complete analysis of FCNC and CP constraints in general SUSY extensions of the standard model". *Nucl. Phys.* B477 (1996), 321–352. arXiv: `hep-ph/9604387 [hep-ph]` (cit. on p. 8).

[45] L. J. Hall and Lisa Randall. "U(1)-R symmetric supersymmetry". *Nucl. Phys.* B352 (1991), 289–308 (cit. on pp. 8, 256).

[46] Patrick J. Fox, Ann E. Nelson, and Neal Weiner. "Dirac gaugino masses and supersoft supersymmetry breaking". *JHEP* 08 (2002), 035. arXiv: `hep-ph/0206096 [hep-ph]` (cit. on pp. 8, 256, 269).

[47] A.D. Sakharov. "Violation of CP Invariance, C asymmetry, and baryon asymmetry of the universe". *Sov. Phys. Usp.* 34.5 (1991), 392–393 (cit. on p. 8).

[48] Frans R. Klinkhamer and N.S. Manton. "A Saddle Point Solution in the Weinberg-Salam Theory". *Phys. Rev. D* 30 (1984), 2212 (cit. on p. 9).

[49] Peter Brockway Arnold and Larry D. McLerran. "Sphalerons, Small Fluctuations and Baryon Number Violation in Electroweak Theory". *Phys. Rev. D* 36 (1987), 581 (cit. on p. 9).

[50] Peter Brockway Arnold and Larry D. McLerran. "The Sphaleron Strikes Back". *Phys. Rev. D* 37 (1988), 1020 (cit. on p. 9).

[51] M. Fukugita and T. Yanagida. "Baryogenesis Without Grand Unification". *Phys. Lett.* B174 (1986), 45–47 (cit. on p. 9).

[52] Jeffrey A. Harvey and Michael S. Turner. "Cosmological baryon and lepton number in the presence of electroweak fermion number violation". *Phys. Rev. D* 42 (1990), 3344–3349 (cit. on p. 9).

[53] V. A. Kuzmin, V. A. Rubakov, and M. E. Shaposhnikov. "On the Anomalous Electroweak Baryon Number Nonconservation in the Early Universe". *Phys. Lett.* 155B (1985), 36 (cit. on p. 9).

[54] Glennys R. Farrar and M.E. Shaposhnikov. "Baryon asymmetry of the universe in the minimal Standard Model". *Phys. Rev. Lett.* 70 (1993). [Erratum: Phys.Rev.Lett. 71, 210 (1993)], 2833–2836. arXiv: `hep-ph/9305274` (cit. on p. 9).

[55] C. Jarlskog. "Commutator of the Quark Mass Matrices in the Standard Electroweak Model and a Measure of Maximal CP Violation". *Phys. Rev. Lett.* 55 (1985), 1039 (cit. on p. 9).

[56] M.B. Gavela et al. "Standard model CP violation and baryon asymmetry". *Mod. Phys. Lett. A* 9 (1994), 795–810. arXiv: hep-ph/9312215 (cit. on p. 9).

[57] M.B. Gavela et al. "Standard model CP violation and baryon asymmetry. Part 1: Zero temperature". *Nucl. Phys. B* 430 (1994), 345–381. arXiv: hep-ph/9406288 (cit. on p. 9).

[58] M.B. Gavela et al. "Standard model CP violation and baryon asymmetry. Part 2: Finite temperature". *Nucl. Phys. B* 430 (1994), 382–426. arXiv: hep-ph/9406289 (cit. on p. 9).

[59] Georges Aad et al. "Observation of a new particle in the search for the Standard Model Higgs boson with the ATLAS detector at the LHC". *Phys. Lett.* B716 (2012), 1–29. arXiv: 1207.7214 [hep-ex] (cit. on p. 9).

[60] Serguei Chatrchyan et al. "Observation of a New Boson at a Mass of 125 GeV with the CMS Experiment at the LHC". *Phys. Lett. B* 716 (2012), 30–61. arXiv: 1207.7235 [hep-ex] (cit. on p. 9).

[61] K. Kajantie et al. "Is there a hot electroweak phase transition at m(H) larger or equal to m(W)?" *Phys. Rev. Lett.* 77 (1996), 2887–2890. arXiv: hep-ph/9605288 (cit. on p. 9).

[62] F. Csikor, Z. Fodor, and J. Heitger. "Endpoint of the hot electroweak phase transition". *Phys. Rev. Lett.* 82 (1999), 21–24. arXiv: hep-ph/9809291 (cit. on p. 9).

[63] Stephen M. Barr, R. Sekhar Chivukula, and Edward Farhi. "Electroweak Fermion Number Violation and the Production of Stable Particles in the Early Universe". *Phys. Lett.* B241 (1990), 387–391 (cit. on p. 9).

[64] Stephen M. Barr. "Baryogenesis, sphalerons and the cogeneration of dark matter". *Phys. Rev.* D44 (1991), 3062–3066 (cit. on p. 9).

[65] David B. Kaplan. "A Single explanation for both the baryon and dark matter densities". *Phys. Rev. Lett.* 68 (1992), 741–743 (cit. on pp. 9, 255).

[66] David E. Kaplan, Markus A. Luty, and Kathryn M. Zurek. "Asymmetric Dark Matter". *Phys. Rev.* D79 (2009), 115016. arXiv: 0901.4117 [hep-ph] (cit. on p. 9).

[67] Steven Weinberg. "A New Light Boson?" *Phys. Rev. Lett.* 40 (1978), 223–226 (cit. on pp. 10, 12).

[68] Frank Wilczek. "Problem of Strong P and T Invariance in the Presence of Instantons". *Phys. Rev. Lett.* 40 (1978), 279–282 (cit. on pp. 10, 12).

[69] R. D. Peccei and Helen R. Quinn. "CP Conservation in the Presence of Instantons". *Phys. Rev. Lett.* 38 (1977). [,328(1977)], 1440–1443 (cit. on pp. 10, 12).

[70] C. Abel et al. "Measurement of the permanent electric dipole moment of the neutron". *Phys. Rev. Lett.* 124.8 (2020), 081803. arXiv: 2001.11966 [hep-ex] (cit. on pp. 10, 11).

[71] Maxim Pospelov and Adam Ritz. "Theta induced electric dipole moment of the neutron via QCD sum rules". *Phys. Rev. Lett.* 83 (1999), 2526–2529. arXiv: hep-ph/9904483 [hep-ph] (cit. on pp. 10, 11).

[72] A.A. Belavin et al. "Pseudoparticle Solutions of the Yang-Mills Equations". *Phys. Lett. B* 59 (1975). Ed. by J.C. Taylor, 85–87 (cit. on p. 10).

[73] Gerard 't Hooft. "Computation of the Quantum Effects Due to a Four-Dimensional Pseudoparticle". *Phys. Rev.* D14 (1976). [,70(1976)], 3432–3450 (cit. on pp. 10, 11, 13).

[74] Gerard 't Hooft. "Symmetry Breaking Through Bell-Jackiw Anomalies". *Phys. Rev. Lett.* 37 (1976). Ed. by Mikhail A. Shifman, 8–11 (cit. on pp. 10, 13).

[75] Stefan Vandoren and Peter van Nieuwenhuizen. "Lectures on instantons". (Feb. 2008). arXiv: 0802.1862 [hep-th] (cit. on p. 10).

[76] Michael Dine et al. "Some Remarks on Anthropic Approaches to the Strong CP Problem". *JHEP* 05 (2018), 171. arXiv: 1801.03466 [hep-th] (cit. on p. 11).

[77] David B. Kaplan and Aneesh V. Manohar. "Current Mass Ratios of the Light Quarks". *Phys. Rev. Lett.* 56 (1986), 2004 (cit. on p. 12).

[78] Tom Banks, Yosef Nir, and Nathan Seiberg. "Missing (up) mass, accidental anomalous symmetries, and the strong CP problem". *Yukawa couplings and the origins of mass. Proceedings, 2nd IFT Workshop, Gainesville, USA, February 11-13, 1994*. 1994, 26–41. arXiv: hep-ph/9403203 [hep-ph] (cit. on p. 12).

[79] S. Aoki et al. "FLAG Review 2019". *Eur. Phys. J.* C80.2 (2020), 113. arXiv: 1902.08191 [hep-lat] (cit. on p. 12).

[80] Jihn E. Kim. "A COMPOSITE INVISIBLE AXION". *Phys. Rev. D* 31 (1985), 1733 (cit. on p. 12).

[81] Gia Dvali and Lena Funcke. "Domestic Axion". (Aug. 2016). arXiv: 1608.08969 [hep-ph] (cit. on p. 12).

[82] R. D. Peccei and Helen R. Quinn. "Constraints Imposed by CP Conservation in the Presence of Instantons". *Phys. Rev.* D16 (1977), 1791–1797 (cit. on p. 12).

[83] Sidney Coleman. *Aspects of Symmetry*. Cambridge, U.K.: Cambridge University Press, 1985. ISBN: 0521318270 (cit. on p. 12).

[84] Cumrun Vafa and Edward Witten. "Parity Conservation in QCD". *Phys. Rev. Lett.* 53 (1984), 535 (cit. on pp. 12, 267).

[85] P. Di Vecchia and G. Veneziano. "Chiral Dynamics in the Large n Limit". *Nucl. Phys.* B171 (1980), 253–272 (cit. on p. 13).

[86] Giovanni Grilli di Cortona et al. "The QCD axion, precisely". *JHEP* 01 (2016), 034. arXiv: 1511.02867 [hep-ph] (cit. on p. 13).

[87] Zhen-Yan Lu et al. "QCD θ-vacuum energy and axion properties". (2020). arXiv: 2003.01625 [hep-ph] (cit. on p. 13).

[88] Luca Di Luzio et al. "The landscape of QCD axion models". (2020). arXiv: 2003.01100 [hep-ph] (cit. on p. 13).

[89] Martin Bauer, Matthias Neubert, and Andrea Thamm. "Collider Probes of Axion-Like Particles". *JHEP* 12 (2017), 044. arXiv: 1708.00443 [hep-ph] (cit. on pp. 13, 259).

[90] Igor G. Irastorza and Javier Redondo. "New experimental approaches in the search for axion-like particles". *Prog. Part. Nucl. Phys.* 102 (2018), 89–159. arXiv: 1801.08127 [hep-ph] (cit. on pp. 13, 15).

[91] G. G. Raffelt. *Stars as laboratories for fundamental physics*. Chicago Univ. Pr., 1996. ISBN: 9780226702728. URL: http://wwwth.mpp.mpg.de/members/raffelt/mypapers/199613.pdf (cit. on pp. 13, 15, 257).

[92] Yoichiro Nambu. "Quasiparticles and Gauge Invariance in the Theory of Superconductivity". *Phys. Rev.* 117 (1960). Ed. by J.C. Taylor, 648–663 (cit. on p. 13).

[93] J. Goldstone. "Field Theories with Superconductor Solutions". *Nuovo Cim.* 19 (1961), 154–164 (cit. on p. 13).

[94] Jeffrey Goldstone, Abdus Salam, and Steven Weinberg. "Broken Symmetries". *Phys. Rev.* 127 (1962), 965–970 (cit. on p. 13).

[95] R. Jackiw and C. Rebbi. "Vacuum Periodicity in a Yang-Mills Quantum Theory". *Phys. Rev. Lett.* 37 (1976). Ed. by J.C. Taylor, 172–175 (cit. on p. 13).

[96] Jr. Callan Curtis G., R.F. Dashen, and David J. Gross. "The Structure of the Gauge Theory Vacuum". *Phys. Lett. B* 63 (1976). Ed. by J.C. Taylor, 334–340 (cit. on p. 13).

[97] Th. Kaluza. "Zum Unitätsproblem der Physik". *Int. J. Mod. Phys. D* 27.14 (2018), 1870001. arXiv: 1803.08616 [physics.hist-ph] (cit. on p. 14).

[98] Oskar Klein. "Quantum Theory and Five-Dimensional Theory of Relativity. (In German and English)". *Z. Phys.* 37 (1926). Ed. by J.C. Taylor, 895–906 (cit. on p. 14).

[99] O. Klein. "The Atomicity of Electricity as a Quantum Theory Law". *Nature* 118 (1926), 516 (cit. on p. 14).

[100] Edward Witten. "Some Properties of O(32) Superstrings". *Phys. Lett. B* 149 (1984), 351–356 (cit. on p. 14).

[101] K. Becker, M. Becker, and J.H. Schwarz. *String theory and M-theory: A modern introduction*. Cambridge University Press, Dec. 2006. ISBN: 978-0-511-25486-4 (cit. on p. 14).

[102] P. Candelas et al. "Vacuum Configurations for Superstrings". *Nucl. Phys. B* 258 (1985), 46–74 (cit. on p. 14).

[103] Peter Svrcek and Edward Witten. "Axions In String Theory". *JHEP* 06 (2006), 051. arXiv: hep-th/0605206 [hep-th] (cit. on p. 14).

[104] David J. E. Marsh. "Axion Cosmology". *Phys. Rept.* 643 (2016), 1–79. arXiv: 1510.07633 [astro-ph.CO] (cit. on pp. 14, 15).

[105] Asimina Arvanitaki et al. "String Axiverse". *Phys. Rev.* D81 (2010), 123530. arXiv: 0905.4720 [hep-th] (cit. on p. 15).

[106] V. A. Rubakov. "Grand unification and heavy axion". *JETP Lett.* 65 (1997), 621–624. arXiv: hep-ph/9703409 [hep-ph] (cit. on pp. 15, 259).

[107] L. F. Abbott and P. Sikivie. "A Cosmological Bound on the Invisible Axion". *Phys. Lett.* 120B (1983), 133–136 (cit. on pp. 15, 16, 257).

[108] John Preskill, Mark B. Wise, and Frank Wilczek. "Cosmology of the Invisible Axion". *Phys. Lett.* 120B (1983), 127–132 (cit. on pp. 15, 16, 256).

[109] Michael Dine and Willy Fischler. "The Not So Harmless Axion". *Phys. Lett.* 120B (1983), 137–141 (cit. on pp. 15, 16).

[110] Steen Hannestad et al. "Neutrino and axion hot dark matter bounds after WMAP-7". *JCAP* 08 (2010), 001. arXiv: 1004.0695 [astro-ph.CO] (cit. on pp. 15, 265).

[111] Matteo Viel et al. "Constraining warm dark matter candidates including sterile neutrinos and light gravitinos with WMAP and the Lyman-alpha forest". *Phys. Rev.* D71 (2005), 063534. arXiv: astro-ph/0501562 [astro-ph] (cit. on pp. 15, 265).

[112] Paola Arias et al. "WISPy Cold Dark Matter". *JCAP* 1206 (2012), 013. arXiv: 1201.5902 [hep-ph] (cit. on pp. 16, 258, 261).

[113] P. Sikivie and Q. Yang. "Bose-Einstein Condensation of Dark Matter Axions". *Phys. Rev. Lett.* 103 (2009), 111301. arXiv: 0901.1106 [hep-ph] (cit. on p. 16).

[114] Alan H. Guth, Mark P. Hertzberg, and C. Prescod-Weinstein. "Do Dark Matter Axions Form a Condensate with Long-Range Correlation?" *Phys. Rev. D* 92.10 (2015), 103513. arXiv: 1412.5930 [astro-ph.CO] (cit. on p. 16).

[115] Pierre Sikivie and Elisa M. Todarello. "Duration of classicality in highly degenerate interacting Bosonic systems". *Phys. Lett. B* 770 (2017), 331–334. arXiv: 1607.00949 [hep-ph] (cit. on p. 16).

[116] Gia Dvali and Sebastian Zell. "Classicality and Quantum Break-Time for Cosmic Axions". *JCAP* 07 (2018), 064. arXiv: 1710.00835 [hep-ph] (cit. on p. 16).

[117] Erik W. Lentz, Thomas R. Quinn, and Leslie J. Rosenberg. "Condensate Dynamics with Non-Local Interactions". *Nucl. Phys. B* 952 (2020), 114937. arXiv: 1808.06378 [astro-ph.CO] (cit. on p. 16).

[118] Daniela Saadeh et al. "How isotropic is the Universe?" *Phys. Rev. Lett.* 117.13 (2016), 131302. arXiv: 1605.07178 [astro-ph.CO] (cit. on p. 17).

[119] Y. Akrami et al. "Planck 2018 results. I. Overview and the cosmological legacy of Planck". (July 2018). arXiv: 1807.06205 [astro-ph.CO] (cit. on p. 17).

[120] Robert V. Wagoner, William A. Fowler, and Fred Hoyle. "On the Synthesis of elements at very high temperatures". *Astrophys. J.* 148 (1967), 3–49 (cit. on p. 17).

[121] Alan H. Guth. "The Inflationary Universe: A Possible Solution to the Horizon and Flatness Problems". *Adv. Ser. Astrophys. Cosmol.* 3 (1987). Ed. by Li-Zhi Fang and R. Ruffini, 139–148 (cit. on p. 17).

[122] Alexei A. Starobinsky. "A New Type of Isotropic Cosmological Models Without Singularity". *Adv. Ser. Astrophys. Cosmol.* 3 (1987). Ed. by I.M. Khalatnikov and V.P. Mineev, 130–133 (cit. on p. 17).

[123] D. Kazanas. "Dynamics of the Universe and Spontaneous Symmetry Breaking". *Astrophys. J.* 241 (1980), L59–L63 (cit. on p. 17).

[124] K. Sato. "First Order Phase Transition of a Vacuum and Expansion of the Universe". *Mon. Not. Roy. Astron. Soc.* 195 (1981), 467–479 (cit. on p. 17).

[125] Andrei D. Linde. "A New Inflationary Universe Scenario: A Possible Solution of the Horizon, Flatness, Homogeneity, Isotropy and Primordial Monopole Problems". *Adv. Ser. Astrophys. Cosmol.* 3 (1987). Ed. by Li-Zhi Fang and R. Ruffini, 149–153 (cit. on p. 17).

[126] Andreas Albrecht and Paul J. Steinhardt. "Cosmology for Grand Unified Theories with Radiatively Induced Symmetry Breaking". *Adv. Ser. Astrophys. Cosmol.* 3 (1987). Ed. by Li-Zhi Fang and R. Ruffini, 158–161 (cit. on p. 17).

[127] W. de Sitter. "Einstein's theory of gravitation and its astronomical consequences, Third Paper". *Mon. Not. Roy. Astron. Soc.* 78 (1917), 3–28 (cit. on p. 17).

[128] M. Novello and S.E.Perez Bergliaffa. "Bouncing Cosmologies". *Phys. Rept.* 463 (2008), 127–213. arXiv: 0802.1634 [astro-ph] (cit. on p. 17).

[129] Robert H. Brandenberger and C. Vafa. "Superstrings in the Early Universe". *Nucl. Phys. B* 316 (1989), 391–410 (cit. on p. 17).

[130] Viatcheslav F. Mukhanov and G. V. Chibisov. "Quantum Fluctuations and a Nonsingular Universe". *JETP Lett.* 33 (1981), 532–535 (cit. on p. 17).

[131] Viatcheslav F. Mukhanov and G.V. Chibisov. "The Vacuum energy and large scale structure of the universe". *Sov. Phys. JETP* 56 (1982), 258–265 (cit. on p. 17).

[132] S.W. Hawking. "The Development of Irregularities in a Single Bubble Inflationary Universe". *Phys. Lett. B* 115 (1982), 295 (cit. on p. 17).

[133] Alexei A. Starobinsky. "Dynamics of Phase Transition in the New Inflationary Universe Scenario and Generation of Perturbations". *Phys. Lett. B* 117 (1982), 175–178 (cit. on p. 17).

[134] Alan H. Guth and S.Y. Pi. "Fluctuations in the New Inflationary Universe". *Phys. Rev. Lett.* 49 (1982), 1110–1113 (cit. on p. 17).

[135] James M. Bardeen, Paul J. Steinhardt, and Michael S. Turner. "Spontaneous Creation of Almost Scale - Free Density Perturbations in an Inflationary Universe". *Phys. Rev. D* 28 (1983), 679 (cit. on p. 17).

[136] Antonio Riotto. "Inflation and the theory of cosmological perturbations". *ICTP Lect. Notes Ser.* 14 (2003), 317–413. arXiv: hep-ph/0210162 [hep-ph] (cit. on p. 17).

[137] V. Mukhanov. *Physical Foundations of Cosmology*. Oxford: Cambridge University Press, 2005. ISBN: 0521563984 (cit. on p. 17).

[138] Viatcheslav F. Mukhanov, H.A. Feldman, and Robert H. Brandenberger. "Theory of cosmological perturbations. Part 1. Classical perturbations. Part 2. Quantum theory of perturbations. Part 3. Extensions". *Phys. Rept.* 215 (1992), 203–333 (cit. on p. 18).

[139] G. W. Gibbons and S. W. Hawking. "Cosmological Event Horizons, Thermodynamics, and Particle Creation". *Phys. Rev.* D15 (1977), 2738–2751 (cit. on pp. 18, 260).

[140] N. D. Birrell and P. C. W. Davies. *Quantum Fields in Curved Space*. Cambridge Monographs on Mathematical Physics. Cambridge, UK: Cambridge Univ. Press, 1984. ISBN: 0521278589. URL: http://www.cambridge.org/mw/academic/subjects/physics/theoretical-physics-and-mathematical-physics/quantum-fields-curved-space?format=PB (cit. on pp. 18, 260, 261, 272).

[141] Andrei D. Linde. "Particle physics and inflationary cosmology". *Contemp. Concepts Phys.* 5 (1990), 1–362. arXiv: hep-th/0503203 [hep-th] (cit. on pp. 18, 260).

[142] Viatcheslav Mukhanov and Sergei Winitzki. *Introduction to quantum effects in gravity*. Cambridge University Press, 2007. ISBN: 9780521868341. URL: http://www.cambridge.org/us/catalogue/catalogue.asp?isbn=0521868343 (cit. on pp. 18, 260).

[143] M.C. Guzzetti et al. "Gravitational waves from inflation". *Riv. Nuovo Cim.* 39.9 (2016), 399–495. arXiv: 1605.01615 [astro-ph.CO] (cit. on p. 18).

[144] Richard L. Arnowitt, Stanley Deser, and Charles W. Misner. "The Dynamics of general relativity". *Gen. Rel. Grav.* 40 (2008), 1997–2027. arXiv: gr-qc/0405109 (cit. on p. 19).

[145] David Wands et al. "A New approach to the evolution of cosmological perturbations on large scales". *Phys. Rev.* D62 (2000), 043527. arXiv: astro-ph/0003278 [astro-ph] (cit. on p. 19).

[146] David H. Lyth, Karim A. Malik, and Misao Sasaki. "A General proof of the conservation of the curvature perturbation". *JCAP* 0505 (2005), 004. arXiv: astro-ph/0411220 [astro-ph] (cit. on p. 19).

[147] M. White and W. Hu. "The Sachs-Wolfe effect". *A&A* 321 (1997), 8–9. arXiv: astro-ph/9609105 [astro-ph] (cit. on p. 20).

[148] G. Efstathiou and J.R. Bond. "Isocurvature cold dark matter fluctuations". *Mon. Not. Roy. Astron. Soc.* 218.1 (1986), 103–121 (cit. on p. 20).

[149] Andrew R. Liddle and David H. Lyth. "The Cold dark matter density perturbation". *Phys. Rept.* 231 (1993), 1–105. arXiv: astro-ph/9303019 [astro-ph] (cit. on p. 20).

[150] Martin Bucher, Kavilan Moodley, and Neil Turok. "The General primordial cosmic perturbation". *Phys. Rev.* D62 (2000), 083508. arXiv: astro-ph/9904231 [astro-ph] (cit. on p. 20).

[151] David Langlois and Alain Riazuelo. "Correlated mixtures of adiabatic and isocurvature cosmological perturbations". *Phys. Rev.* D62 (2000), 043504. arXiv: astro-ph/9912497 [astro-ph] (cit. on p. 20).

[152] Wayne Hu and Martin J. White. "A New test of inflation". *Phys. Rev. Lett.* 77 (1996), 1687–1690. arXiv: astro-ph/9602020 [astro-ph] (cit. on p. 20).

[153] Wayne Hu and Martin J. White. "Acoustic signatures in the cosmic microwave background". *Astrophys. J.* 471 (1996), 30–51. arXiv: astro-ph/9602019 [astro-ph] (cit. on p. 20).

[154] Wayne Hu, David N. Spergel, and Martin J. White. "Distinguishing causal seeds from inflation". *Phys. Rev.* D55 (1997), 3288–3302. arXiv: astro-ph/9605193 [astro-ph] (cit. on p. 20).

[155] Anna Mangilli, Licia Verde, and Maria Beltran. "Isocurvature modes and Baryon Acoustic Oscillations". *JCAP* 2010.10, 009 (2010), 009. arXiv: 1006.3806 [astro-ph.CO] (cit. on p. 20).

[156] Y. Akrami et al. "Planck 2018 results. X. Constraints on inflation". (2018). arXiv: 1807.06211 [astro-ph.CO] (cit. on pp. 20, 261, 265).

[157] Lev Kofman, Andrei D. Linde, and Alexei A. Starobinsky. "Reheating after inflation". *Phys. Rev. Lett.* 73 (1994), 3195–3198. arXiv: hep-th/9405187 [hep-th] (cit. on p. 254).

[158] Y. Shtanov, Jennie H. Traschen, and Robert H. Brandenberger. "Universe reheating after inflation". *Phys. Rev.* D51 (1995), 5438–5455. arXiv: hep-ph/9407247 [hep-ph] (cit. on p. 254).

[159] Lev Kofman, Andrei D. Linde, and Alexei A. Starobinsky. "Towards the theory of reheating after inflation". *Phys. Rev.* D56 (1997), 3258–3295. arXiv: hep-ph/9704452 [hep-ph] (cit. on p. 254).

[160] Giorgio Arcadi, Abdelhak Djouadi, and Martti Raidal. "Dark Matter through the Higgs portal". *Phys. Rept.* 842 (2020), 1–180. arXiv: 1903.03616 [hep-ph] (cit. on p. 254).

[161] N. Huntemann et al. "Improved limit on a temporal variation of m_p/m_e from comparisons of Yb^+ and Cs atomic clocks". *Phys. Rev. Lett.* 113.21 (2014), 210802. arXiv: 1407.4408 [physics.atom-ph] (cit. on p. 255).

[162] Edward W. Kolb, Malcolm J. Perry, and T. P. Walker. "Time Variation of Fundamental Constants, Primordial Nucleosynthesis and the Size of Extra Dimensions". *Phys. Rev.* D33 (1986), 869 (cit. on p. 255).

[163] Robert J. Scherrer and David N. Spergel. "How constant is the Fermi coupling constant?" *Phys. Rev.* D47 (1993), 4774–4777 (cit. on p. 255).

[164] Gilly Elor, Miguel Escudero, and Ann Nelson. "Baryogenesis and Dark Matter from B Mesons". (2018). arXiv: 1810.00880 [hep-ph] (cit. on p. 255).

[165] Marina Artuso, Guennadi Borissov, and Alexander Lenz. "CP violation in the B_s^0 system". *Rev. Mod. Phys.* 88.4 (2016), 045002. arXiv: 1511.09466 [hep-ph] (cit. on pp. 255, 266).

[166] Lisa Randall and N. Rius. "The Minimal U(1)-R symmetric model revisited". *Phys. Lett.* B286 (1992), 299–306.

[167] Liam McAllister, Eva Silverstein, and Alexander Westphal. "Gravity Waves and Linear Inflation from Axion Monodromy". *Phys. Rev.* D82 (2010), 046003. arXiv: 0808.0706 [hep-th] (cit. on p. 257).

[168] Joerg Jaeckel, Viraf M. Mehta, and Lukas T. Witkowski. "Monodromy Dark Matter". *JCAP* 1701.01 (2017), 036. arXiv: 1605.01367 [hep-ph] (cit. on p. 257).

[169] Kiwoon Choi, Hyungjin Kim, and Seokhoon Yun. "Natural inflation with multiple sub-Planckian axions". *Phys. Rev.* D90 (2014), 023545. arXiv: 1404.6209 [hep-th] (cit. on p. 257).

[170] Kiwoon Choi and Sang Hui Im. "Realizing the relaxion from multiple axions and its UV completion with high scale supersymmetry". *JHEP* 01 (2016), 149. arXiv: 1511.00132 [hep-ph] (cit. on p. 257).

[171] David E. Kaplan and Riccardo Rattazzi. "Large field excursions and approximate discrete symmetries from a clockwork axion". *Phys. Rev.* D93.8 (2016), 085007. arXiv: 1511.01827 [hep-ph] (cit. on p. 257).

[172] James Halverson et al. "On String Theory Expectations for Photon Couplings to Axion-Like Particles". (2019). arXiv: 1909.05257 [hep-th] (cit. on p. 257).

[173] Renata Kallosh, Andrei Linde, and Diederik Roest. "Superconformal Inflationary α-Attractors". *JHEP* 11 (2013), 198. arXiv: 1311.0472 [hep-th] (cit. on p. 258).

[174] Renata Kallosh and Andrei Linde. "Planck, LHC, and α-attractors". *Phys. Rev.* D91 (2015), 083528. arXiv: 1502.07733 [astro-ph.CO] (cit. on p. 258).

[175] Mario Galante et al. "Unity of Cosmological Inflation Attractors". *Phys. Rev. Lett.* 114.14 (2015), 141302. arXiv: 1412.3797 [hep-th] (cit. on p. 258).

[176] S. Borsanyi et al. "Axion cosmology, lattice QCD and the dilute instanton gas". *Phys. Lett.* B752 (2016), 175–181. arXiv: 1508.06917 [hep-lat] (cit. on p. 258).

[177] Joerg Jaeckel and Michael Spannowsky. "Probing MeV to 90 GeV axion-like particles with LEP and LHC". *Phys. Lett.* B753 (2016), 482–487. arXiv: 1509.00476 [hep-ph] (cit. on p. 259).

[178] Ken Mimasu and Verónica Sanz. "ALPs at Colliders". *JHEP* 06 (2015), 173. arXiv: 1409.4792 [hep-ph] (cit. on p. 259).

[179] Claudia Frugiuele et al. "Relaxion and light (pseudo)scalars at the HL-LHC and lepton colliders". *JHEP* 10 (2018), 151. arXiv: 1807.10842 [hep-ph] (cit. on p. 259).

[180] I. Brivio et al. "ALPs Effective Field Theory and Collider Signatures". *Eur. Phys. J.* C77.8 (2017), 572. arXiv: 1701.05379 [hep-ph] (cit. on p. 259).

[181] John F. Donoghue. "General relativity as an effective field theory: The leading quantum corrections". *Phys. Rev.* D50 (1994), 3874–3888. arXiv: gr-qc/9405057 [gr-qc] (cit. on pp. 260, 261).

[182] Curtis G. Callan Jr., Sidney R. Coleman, and Roman Jackiw. "A New improved energy - momentum tensor". *Annals Phys.* 59 (1970), 42–73 (cit. on pp. 260, 261).

[183] Gaurav Narain and Roberto Percacci. "Renormalization Group Flow in Scalar-Tensor Theories. I". *Class. Quant. Grav.* 27 (2010), 075001. arXiv: 0911.0386 [hep-th].

[184] Gaurav Narain and Christoph Rahmede. "Renormalization Group Flow in Scalar-Tensor Theories. II". *Class. Quant. Grav.* 27 (2010), 075002. arXiv: 0911.0394 [hep-th].

[185] Roberto Percacci and Gian Paolo Vacca. "Search of scaling solutions in scalar-tensor gravity". *Eur. Phys. J.* C75.5 (2015), 188. arXiv: 1501.00888 [hep-th].

[186] Peter Labus, Roberto Percacci, and Gian Paolo Vacca. "Asymptotic safety in $O(N)$ scalar models coupled to gravity". *Phys. Lett.* B753 (2016), 274–281. arXiv: 1505.05393 [hep-th].

[187] Yuta Hamada and Masatoshi Yamada. "Asymptotic safety of higher derivative quantum gravity non-minimally coupled with a matter system". *JHEP* 08 (2017), 070. arXiv: 1703.09033 [hep-th].

[188] Astrid Eichhorn, Stefan Lippoldt, and Vedran Skrinjar. "Nonminimal hints for asymptotic safety". *Phys. Rev.* D97.2 (2018), 026002. arXiv: 1710.03005 [hep-th].

[189] Ann E. Nelson and Jakub Scholtz. "Dark Light, Dark Matter and the Misalignment Mechanism". *Phys. Rev.* D84 (2011), 103501. arXiv: 1105.2812 [hep-ph] (cit. on p. 261).

[190] Burak Himmetoglu, Carlo R. Contaldi, and Marco Peloso. "Instability of anisotropic cosmological solutions supported by vector fields". *Phys. Rev. Lett.* 102 (2009), 111301. arXiv: 0809.2779 [astro-ph] (cit. on pp. 261, 272).

[191] Burak Himmetoglu, Carlo R. Contaldi, and Marco Peloso. "Ghost instabilities of cosmological models with vector fields nonminimally coupled to the curvature". *Phys. Rev.* D80 (2009), 123530. arXiv: 0909.3524 [astro-ph.CO] (cit. on pp. 261, 272).

[192] Mindaugas Karciauskas and David H. Lyth. "On the health of a vector field with $(RA^2)/6$ coupling to gravity". *JCAP* 1011 (2010), 023. arXiv: 1007.1426 [astro-ph.CO] (cit. on pp. 261, 272).

[193] Kazunori Nakayama. "Vector Coherent Oscillation Dark Matter". *JCAP* 1910.10 (2019), 019. arXiv: 1907.06243 [hep-ph] (cit. on pp. 261, 272).

[194] Peter W. Graham and Adam Scherlis. "Stochastic axion scenario". *Phys. Rev.* D98.3 (2018), 035017. arXiv: 1805.07362 [hep-ph] (cit. on p. 261).

[195] Fuminobu Takahashi, Wen Yin, and Alan H. Guth. "QCD axion window and low-scale inflation". *Phys. Rev.* D98.1 (2018), 015042. arXiv: 1805.08763 [hep-ph] (cit. on p. 261).

[196] Peter W. Graham, Jeremy Mardon, and Surjeet Rajendran. "Vector Dark Matter from Inflationary Fluctuations". *Phys. Rev.* D93.10 (2016), 103520. arXiv: 1504.02102 [hep-ph] (cit. on pp. 262, 272).

[197] Brian D. Fields et al. "Big-Bang Nucleosynthesis After Planck". *JCAP* 03 (2020), 010. arXiv: 1912.01132 [astro-ph.CO] (cit. on p. 263).

[198] Masahiro Kawasaki, Ken'ichi Saikawa, and Toyokazu Sekiguchi. "Axion dark matter from topological defects". *Phys. Rev. D* 91.6 (2015), 065014. arXiv: 1412.0789 [hep-ph] (cit. on p. 263).

[199] Guillermo Ballesteros et al. "Standard Model—axion—seesaw—Higgs portal inflation. Five problems of particle physics and cosmology solved in one stroke". *JCAP* 08 (2017), 001. arXiv: 1610.01639 [hep-ph] (cit. on p. 263).

[200] Vincent B.. Klaer and Guy D. Moore. "The dark-matter axion mass". *JCAP* 11 (2017), 049. arXiv: 1708.07521 [hep-ph] (cit. on p. 263).

[201] Marco Gorghetto, Edward Hardy, and Giovanni Villadoro. "Axions from Strings: the Attractive Solution". *JHEP* 07 (2018), 151. arXiv: 1806.04677 [hep-ph] (cit. on p. 263).

[202] Yonatan Kahn, Benjamin R. Safdi, and Jesse Thaler. "Broadband and Resonant Approaches to Axion Dark Matter Detection". *Phys. Rev. Lett.* 117.14 (2016), 141801. arXiv: 1602.01086 [hep-ph] (cit. on p. 263).

[203] T. M. Shokair et al. "Future Directions in the Microwave Cavity Search for Dark Matter Axions". *Int. J. Mod. Phys.* A29 (2014), 1443004. arXiv: 1405.3685 [physics.ins-det] (cit. on p. 263).

[204] http://www.iexp.uni-hamburg.de/groups/astroparticle/brass/brassweb.htm (cit. on p. 263).

[205] Eleni Petrakou. "Haloscope searches for dark matter axions at the Center for Axion and Precision Physics Research". *EPJ Web Conf.* 164 (2017), 01012. arXiv: 1702.03664 [physics.ins-det] (cit. on p. 263).

[206] Alex Droster and Karl van Bibber. "HAYSTAC Status, Results, and Plans". *13th Conference on the Intersections of Particle and Nuclear Physics (CIPANP 2018) Palm Springs, California, USA, May 29-June 3, 2018*. 2019. arXiv: 1901.01668 [physics.ins-det] (cit. on p. 263).

[207] C. Gatti et al. "The Klash Proposal: Status and Perspectives". *14th Patras Workshop on Axions, WIMPs and WISPs (AXION-WIMP 2018) (PATRAS 2018) Hamburg, Germany, June 18-22, 2018*. 2018. arXiv: 1811.06754 [physics.ins-det] (cit. on p. 263).

[208] B. Majorovits et al. "MADMAX: A new road to axion dark matter detection". *15th International Conference on Topics in Astroparticle and Underground Physics (TAUP 2017) Sudbury, Ontario, Canada, July 24-28, 2017*. 2017. arXiv: 1712.01062 [physics.ins-det] (cit. on p. 263).

[209] Ben T. McAllister et al. "The ORGAN Experiment: An axion haloscope above 15 GHz". *Phys. Dark Univ.* 18 (2017), 67–72. arXiv: 1706.00209 [physics.ins-det] (cit. on p. 263).

[210] D. Alesini et al. "Galactic axions search with a superconducting resonant cavity". *Phys. Rev.* D99.10 (2019), 101101. arXiv: 1903.06547 [physics.ins-det] (cit. on p. 263).

[211] Alejandro Álvarez Melcón et al. "Axion Searches with Microwave Filters: the RADES project". *JCAP* 1805.05 (2018), 040. arXiv: 1803.01243 [hep-ex] (cit. on p. 263).

[212] Michael S. Turner and Frank Wilczek. "Inflationary axion cosmology". *Phys. Rev. Lett.* 66 (1991), 5–8 (cit. on p. 264).

[213] D. H. Lyth. "Axions and inflation: Sitting in the vacuum". *Phys. Rev.* D45 (1992), 3394–3404 (cit. on p. 264).

[214] Stephen D. Burns. "Isentropic and isocurvature axion perturbations in inflationary cosmology". (Nov. 1997). arXiv: astro-ph/9711303 (cit. on p. 264).

[215] Patrick Fox, Aaron Pierce, and Scott D. Thomas. "Probing a QCD string axion with precision cosmological measurements". (Sept. 2004). arXiv: hep-th/0409059 (cit. on p. 264).

[216] Maria Beltran, Juan Garcia-Bellido, and Julien Lesgourgues. "Isocurvature bounds on axions revisited". *Phys. Rev.* D75 (2007), 103507. arXiv: hep-ph/0606107 [hep-ph] (cit. on p. 264).

[217] Mark P Hertzberg, Max Tegmark, and Frank Wilczek. "Axion Cosmology and the Energy Scale of Inflation". *Phys. Rev.* D78 (2008), 083507. arXiv: 0807.1726 [astro-ph] (cit. on p. 264).

[218] Asimina Arvanitaki et al. "The Large-Misalignment Mechanism for the Formation of Compact Axion Structures: Signatures from the QCD Axion to Fuzzy Dark Matter". (2019). arXiv: 1909.11665 [astro-ph.CO] (cit. on pp. 265, 272).

[219] Aleksandr Chatrchyan and Joerg Jaeckel. "Gravitational waves from the fragmentation of axion-like particle dark matter". (Apr. 2020). arXiv: 2004.07844 [hep-ph] (cit. on p. 265).

[220] Graham D. Kribs and Adam Martin. "Supersoft Supersymmetry is Super-Safe". *Phys. Rev. D* 85 (2012), 115014. arXiv: 1203.4821 [hep-ph] (cit. on p. 269).

[221] Steven B. Giddings and Andrew Strominger. "Axion Induced Topology Change in Quantum Gravity and String Theory". *Nucl. Phys.* B306 (1988), 890–907 (cit. on p. 272).

[222] L. F. Abbott and Mark B. Wise. "Wormholes and Global Symmetries". *Nucl. Phys.* B325 (1989), 687–704 (cit. on p. 272).

[223] Rodrigo Alonso and Alfredo Urbano. "Wormholes and masses for Goldstone bosons". (2017). arXiv: 1706.07415 [hep-ph] (cit. on p. 272).

[224] Richard Holman et al. "Solutions to the Strong CP Problem in a World with Gravity". *Phys. Lett.* B282 (1992), 132–136. arXiv: hep-ph/9203206 [hep-ph] (cit. on p. 272).

[225] Marc Kamionkowski and John March-Russell. "Planck Scale Physics and the Peccei-Quinn Mechanism". *Phys. Lett.* B282 (1992), 137–141. arXiv: hep-th/9202003 [hep-th] (cit. on p. 272).

[226] Tommi Markkanen, Arttu Rajantie, and Tommi Tenkanen. "Spectator Dark Matter". *Phys. Rev.* D98.12 (2018), 123532. arXiv: 1811.02586 [astro-ph.CO] (cit. on p. 272).

[227] Kevork N. Abazajian et al. "CMB-S4 Science Book, First Edition". (2016). arXiv: 1610.02743 [astro-ph.CO] (cit. on p. 272).

[228] Jorge Peñarrubia. "Fluctuations of the gravitational field generated by a random population of extended substructures". *Mon. Not. Roy. Astron. Soc.* 474.2 (2018), 1482–1498. arXiv: 1710.06443 [astro-ph.GA] (cit. on p. 272).

[229] Ken Van Tilburg, Anna-Maria Taki, and Neal Weiner. "Halometry from Astrometry". *JCAP* 07 (2018), 041. arXiv: 1804.01991 [astro-ph.CO] (cit. on p. 272).

[230] Yashar Hezaveh et al. "Measuring the power spectrum of dark matter substructure using strong gravitational lensing". *JCAP* 11 (2016), 048. arXiv: 1403.2720 [astro-ph.CO] (cit. on p. 272).

[231] Malcolm Fairbairn et al. "Structure formation and microlensing with axion miniclusters". *Phys. Rev.* D97.8 (2018), 083502. arXiv: 1707.03310 [astro-ph.CO] (cit. on p. 272).

[232] W. Altmannshofer et al. "The Belle II Physics Book". (2018). Ed. by E. Kou and P. Urquijo. arXiv: 1808.10567 [hep-ex] (cit. on p. 271).

[233] Jr. Alves A.Augusto et al. "The LHCb Detector at the LHC". *JINST* 3 (2008), S08005 (cit. on p. 271).

[234] Jonathan L. Feng et al. "ForwArd Search ExpeRiment at the LHC". *Phys. Rev.* D97.3 (2018), 035001. arXiv: 1708.09389 [hep-ph] (cit. on p. 271).

[235] Vladimir V. Gligorov et al. "Searching for Long-lived Particles: A Compact Detector for Exotics at LHCb". *Phys. Rev.* D97.1 (2018), 015023. arXiv: 1708.09395 [hep-ph] (cit. on p. 271).

[236] John Ellis et al. "Updated Global SMEFT Fit to Higgs, Diboson and Electroweak Data". *JHEP* 06 (2018), 146. arXiv: 1803.03252 [hep-ph] (cit. on p. 271).

[237] Eduardo da Silva Almeida et al. "Electroweak Sector Under Scrutiny: A Combined Analysis of LHC and Electroweak Precision Data". *Phys. Rev. D* 99.3 (2019), 033001. arXiv: 1812.01009 [hep-ph] (cit. on p. 271).

[238] Anke Biekoetter, Tyler Corbett, and Tilman Plehn. "The Gauge-Higgs Legacy of the LHC Run II". *SciPost Phys.* 6.6 (2019), 064. arXiv: 1812.07587 [hep-ph] (cit. on p. 271).

[239] F. Capozzi et al. "Current unknowns in the three neutrino framework". *Prog. Part. Nucl. Phys.* 102 (2018), 48–72. arXiv: 1804.09678 [hep-ph] (cit. on p. 271).

[240] P.F. de Salas et al. "Status of neutrino oscillations 2018: 3σ hint for normal mass ordering and improved CP sensitivity". *Phys. Lett. B* 782 (2018), 633–640. arXiv: 1708.01186 [hep-ph] (cit. on p. 271).

[241] Ivan Esteban et al. "Global analysis of three-flavour neutrino oscillations: synergies and tensions in the determination of θ_{23}, δ_{CP}, and the mass ordering". *JHEP* 01 (2019), 106. arXiv: 1811.05487 [hep-ph] (cit. on p. 271).